JOURNAL OF THE MECHANICS AND PHYSICS OF SOLIDS

EDITORIAL ADVISORY BOARD

J. F. BAKER—Cambridge W. M. BALDWIN—Cleveland
E. BRANDENBERGER—Zürich G. BUSCH—Zürich
A. H. COTTRELL—Cambridge C. CRUSSARD—Paris M. J. DRUYVESTEYN—Delft
A. KOCHENDÖRFER—Düsseldorf N. F. MOTT—Cambridge
A. NADAI—Pittsburgh, Pa. E. SIEBEL—Stuttgart
V. V. SOKOLOVSKY—Moscow

EDITOR-IN-CHIEF

R. HILL, F.R.S.
University of Nottingham

Volume 9
1961

PERGAMON PRESS · OXFORD · LONDON · NEW YORK · PARIS

Contents of Volume 9

NUMBER 1

Page

J. F. BELL : An experimental study of the unloading phenomenon in constant velocity impact 1

B. JAOUL et D. GONZALEZ : Déformation plastique de monocristaux de fer 16

S. C. HUNTER : Tentative equations for the propagation of stress, strain and temperature fields in viscoelastic solids 39

D. S. BERRY and T. W. SALES : An elastic treatment of ground movement due to mining—II. Transversely isotropic ground 52

S. J. CZYZAK, N. BOW and H. PAYNE : On the tensile stress–strain relation and the Bauschinger effect for polycrystalline materials from Taylor's model 63

Book Reviews

" Progress in Solid Mechanics, Vol. I," edited by I. N. SNEDDON and R. HILL (reviewed by J. D. ESHELBY) 67

" An Introduction to the Physics of Mass, Length and Time," by N. FEATHER (reviewed by M. J. SEWELL) 67

" Mechanics " (2nd Ed.), by K. R. SYMON (reviewed by E. E. JONES) 68

NUMBER 2

B. JAOUL : Consolidation des polycristaux de fer et hypothèses sur l'origine du palier des courbes de traction 69

A. E. GREEN and W. C. EMMERSON : Stresses in a pipe with a discontinuous bend 91

B. E. MILSOM and J. M. ALEXANDER : An experimental determination of the detailed distortion in hot rolling 105

R. HILL : Uniqueness in general boundary-value problems for elastic or inelastic solids 114

L. H. MITCHELL and A. K. HEAD : The buckling of a dislocated plate 131

Book Reviews

" Structural Mechanics," edited by J. N. GOODIER and N. J. HOFF (reviewed by R. HILL) 140

" Crystal Growth " (reviewed by A. J. FORTY) 141

" Moderne Messmethoden der Physik," by F. X. EDER (reviewed by N. DAVY) 141

NUMBER 3

N. E. FROST : A note on the behaviour of fatigue cracks 143

H. H. HILTON and H. G. RUSSELL : An extension of Alfrey's analogy to thermal stress problems in temperature dependent linear viscoelastic media 152

N. CRISTESCU : Spatial motion of elastic–plastic strings 165

J. N. FLAVIN and A. E. GREEN : Plane thermo-elastic waves in an initially stressed medium 179

H. DERESIEWICZ : A note on thermoelastic Rayleigh waves 191

R. W. ARMSTRONG : On size effects in polycrystal plasticity 196

NUMBER 3—*contd.* *Page*

T. H. LIN, S. UCHIYAMA and D. MARTIN : Stress field in metals at initial stage of plastic deformation 200

Book Reviews

" Einführung in die Kontinuumsmechanik," by W. PRAGER (reviewed by R. HILL) 210

" The Mechanics of Vibration," by R. E. D. BISHOP and D. C. JOHNSON (reviewed by H. MCCALLION) 211

" Mechanics," by L. D. LANDAU and E. M. LIFSHITZ, translated by J. B. SYKES and J. S. BELL (reviewed by R. HILL) 212

" Mechanical Waveguides," by M. REDWOOD (reviewed by W. A. GREEN) 213

" Large Elastic Deformations and Non-Linear Continuum Mechanics," by A. E. GREEN and J. E. ADKINS (reviewed by J. L. ERICKSEN) 213

Notice 214

NUMBER 4

F. J. LOCKETT : Interpretation of mathematical solutions in viscoelasticity theory illustrated by a dynamic spherical cavity problem 215

W. A. BASSALI and E. HALIM : Bending of uniformly loaded sectorial plates 230

E. Z. STOWELL and T. S. LIU : On the mechanical behaviour of fibre-reinforced crystalline materials 242

J. F. BELL : Further experimental study of the unloading phenomenon in constant velocity impact 261

A. J. M. SPENCER : Perturbation methods in plasticity—I. Plane strain of non-homogeneous plastic solids 279

Book Reviews

" Plasticity," edited by E. H. LEE and P. S. SYMONDS (reviewed by R. HILL) 289

" Mechanics of Solids and Fluids," by R. R. LONG (reviewed by M. J. SEWELL) 289

" The Stability of Motion," by N. G. CHETAYEV, translated by M. NADLER (reviewed by R. HILL) 290

" An Introduction to the Theory of Vibrating Systems," by W. G. BICKLEY and A. TALBOT (reviewed by R. E. D. BISHOP) 290

" Selected Papers on Stress Analysis " (reviewed by M. L. MEYER) 291

" An Introduction to Applied Anisotropic Elasticity," by R. F. S. HEARMON (reviewed by D. S. BERRY) 291

Notices 293

Author Index

(B) denotes Book Review

ALEXANDER, J. M. p. 105.
ARMSTRONG, R. W. p. 196.
BASSALI, W. A. p. 230.
BELL, J. F. pp. 1, 261.
BERRY, D. S. p. 52; p. 291 (B).
BISHOP, R. E. D. p. 290 (B).
BOW, N. p. 63.
CRISTESCU, N. p. 165.
CZYZAK, S. J. p. 63.
DAVY, N. p. 141 (B).
DERESIEWICZ, H. p. 191.
EMMERSON, W. C. p. 91.
ERICKSEN, J. L. p. 213 (B).
ESHELBY, J. D. p. 67 (B).
FLAVIN, J. N. p. 179.
FORTY, A. J. p. 141 (B).
FROST, N. E. p. 143.
GONZALEZ, D. p. 16.
GREEN, A. E. pp. 91, 179.
GREEN, W. A. p. 213 (B).
HALIM, E. p. 230.
HEAD, A. K. p. 131.
HILL, R. p. 114; pp. 140, 210, 212, 289, 290 (B).
HILTON, H. H. p. 152.
HUNTER, S. C. p. 39.
JAOUL, B. pp. 16, 69.
JONES, E. E. p. 68 (B).
LIN, T. H. p. 200.
LIU, T. S. p. 242.
LOCKETT, F. J. p. 215.
MARTIN, D. p. 200.
MCCALLION, H. p. 211 (B).
MEYER, M. L. p. 291 (B).
MILSOM, B. E. p. 105.
MITCHELL, L. H. p. 131.
PAYNE, H. p. 63.
RUSSELL, H. G. p. 152.
SALES, T. W. p. 52.
SEWELL, M. J. pp. 67, 289 (B).
SPENCER, A. J. M. p. 279.
STOWELL, E. Z. p. 242.
UCHIYAMA, S. p. 200.

J. Mech. Phys. Solids, 1961, Vol. 9, pp. 1 to 15. Pergamon Press Ltd., London. Printed in Great Britain

AN EXPERIMENTAL STUDY OF THE UNLOADING PHENOMENON IN CONSTANT VELOCITY IMPACT

By J. F. Bell
The Johns Hopkins University

(*Received* 1*st July*, 1960)

Summary

The coefficient of restitution, time of contact, and plastic strain distribution are determined experimentally for finite length annealed aluminium rods. These data are found to be in agreement with the strain-rate independent theory of plastic wave propagation in which an elastic wave of a magnitude given by the elastic unloading of the static stress–strain curve is reflected from the free end. The case considered is that of two identical specimens in free flight collision, dynamic plastic strains being determined by the author's diffraction grating technique.

1. Introduction

It is the purpose of this paper to present the results of an experimental study of the unloading phenomenon in finite length annealed aluminium rods subject to constant velocity impact. The situation considered is that of two identical square-ended cylindrical rods in axial collision. During the time in which the measurements are made, both specimens are in free flight. An experimental determination of the coefficient of restitution, the time of contact, and final strain distribution are obtained. Strains are determined from diffraction grating measurements at a large number of positions in the first 8 diameters of specimens whose length is 10 diameters.

It has been found possible to predict the time of contact and coefficient of restitution, as well as the final strain distribution, from a simple interpretation of the characteristics in a Lagrangian diagram, using the strain-rate independent theory of plastic wave propagation. This time of contact is found to be in good agreement at all strain levels with theoretical results computed from the static stress–strain curve. The coefficient of restitution, however, agrees with the static stress–strain curve for strains of 1 per cent and above, but appears to be more in agreement with the dynamic stress–strain curve of Johnson *et al.* (1953) for strains below 0·8 per cent. This result indicates that although all strain levels propagate with velocities agreeing with the slopes of the static stress–strain curve, either higher stress levels are present for the lower strains, or the elastic unloading component is greater than the static stress–strain curve predicts.

The final strain distribution is found to be that of a plastic wave propagating in accordance with the predictions of the strain-rate independent theory and the slopes of the static stress–strain curve. The Lee (1953) velocity for this material, at which an unloading elastic wave will just reach the impact face, is far below the

impact velocities considered here. In the present study, the dispersive plastic wave propagates into the rod undiminished until the energy of deformation equals the available initial kinetic energy. Between 4 and 6 diameters experimental evidence is offered for the absorption of the initial elastic reflected wave front, agreeing with the theoretical predictions of Lee.

2. Experimental Data

In an earlier paper this author (1960a) has shown that the strain-rate independent theory of plastic wave propagation is applicable for annealed aluminium for impact velocities up to at least 80 ft/sec. Furthermore, it was shown that the velocities of propagation at all levels of strain, and the maximum strain amplitude, were very closely predicted from the slopes of the static stress–strain curve of the material. Excess strain, or a mushrooming effect, was found in the first diameter, particularly for the higher velocities. This behaviour in the first diameter has been the subject of a separate study (1960c). Three aspects of that study are relevant in the present instance:

(i) The entire strain–time curve does not proceed from an infinite step at the origin and the initial shape is dependent upon the impact velocity.

(ii) The excess strain in the first diameter, which decreases from a maximum at $\frac{1}{4}$ diameter to the theoretical value of the strain-rate independent theory by 2 diameters, involves the necessity for considering an excess of deformation energy in this region.

(iii) Strains above a level which depends upon the impact velocity are very much more delayed in traversing the first $\frac{1}{4}$ diameter than are the strains below this value.

In any determination of final strain distribution, these effects in the first diameter must be considered.

The diffraction grating method of measuring strain, which was developed by the author for the purpose of investigating plastic wave propagation, has been described in several papers (Bell 1956, 1958, 1959). Using this method of measurement, both strain and surface angle are determined as the plastic wave propagates through a point on the specimen at which a diffraction grating has been located. The gauge length used in all the measurements presented here is 0·005 in., and the accuracy of measurement is of the order of 3 per cent.

Not quite 200 tests have been conducted in annealed aluminium for the purpose of investigating the nature of the plastic wave propagation. In nearly every one, measurements were made of the initial hitter velocity as well as the final specimen velocity. If the collision were sufficiently axial, one would expect that the final velocity of the struck specimen would exceed the mass-centre velocity by the same amount that the hitter specimen was below this velocity, and hence a coefficient of restitution could be determined from these velocity measurements. It was thought desirable, however, to check that this was so in these experiments, and also to determine the time of contact of the two specimens.

A longitudinal beam of light was introduced at the stationary specimen impact face prior to impact. Measurements of total light intensity were made by placing

a 5 in. photomultiplier tube on the opposite side of the specimen from the light source. In order to calibrate the light field, precision spacers were introduced between the hitter and the stationary specimen prior to impact. As may be seen from Fig. 1, when the hitter enters the light field, triggering the oscilloscope, the light decreases until impact takes place, and thus the hitter velocity is determined. This is followed by an interval of no light, during which the specimens remain in contact. The subsequent increase in light is a measure of the relative velocity between the hitter and stationary specimen faces after impact. The final decrease in light occurs after the stationary specimen has left the light field, and is a measure of the final velocity of the hitter specimen.

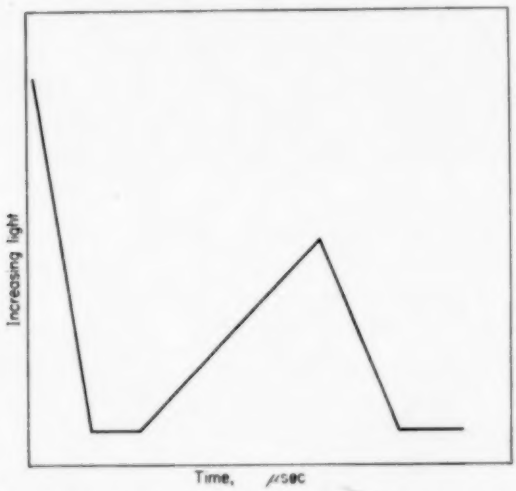

FIG. 1. Variation of light field between specimen faces before, during, and following impact.

In this way it has been possible to verify in these experiments that the hitter final velocity is below the mass-centre velocity by the same amount that the stationary specimen final velocity is above it. Furthermore, these results may be compared with the large number of velocity measurements which were made with chronographs in nearly all earlier tests. The chronograph recorded the time for the hitter specimen to travel between two fine wires spaced an inch apart, and a second chronograph similarly recorded the final velocity of the initially stationary specimen.

The time of contact for a given impact velocity proved to be considerably longer than had been expected from the arrival time of final strain given by the diffraction grating measurements made at a few diameters from the free end of the specimen. In Fig. 2 is shown a series of strain maxima at many different positions in the first 8 diameters. It will be noted that no significant plastic strain was seen to develop in measurements made at 8 diameters in these 10 diameter specimens. Although measurements were made for several impact velocities, those shown in Fig. 2 are for the most thoroughly studied case, with an impact velocity of 66·5 ft/sec.

The time of arrival of maximum strain at positions between 4 and 7 diameters occurs at 200 and 240 μsec respectively. The solid line in Fig. 2 is the theoretical strain at 210 μsec. The experimental time of contact for the impact velocity is 318 μsec, or 80 μsec longer than the longest time at which plastic deformation has been observed.

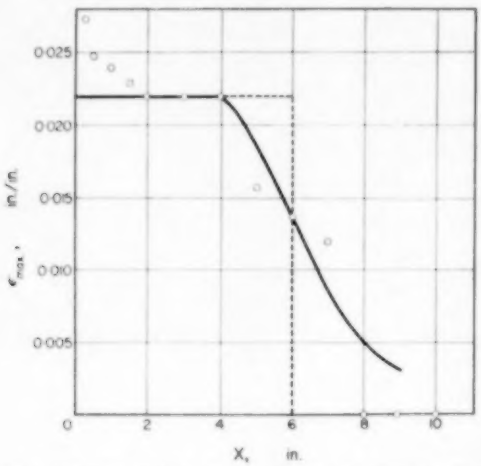

FIG. 2. Experimental maximum strain compared with theoretical distribution (solid line) at 210 μsec.

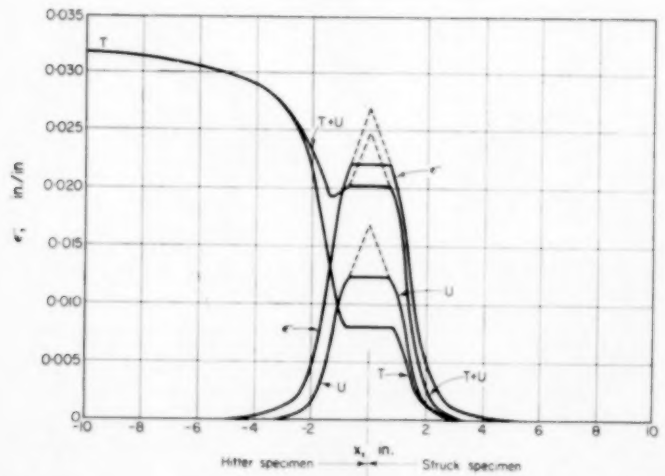

FIG. 3. Strain and energy distributions at 50 μsec when elastic front reaches free end of specimen.

In a recent report (BELL 1960b) it was shown that a very close energy balance could be obtained at 50 μsec, which is the time at which the elastic front reaches the free end of the rod. To obtain this energy balance, the deformation energy distribution and the kinetic energy distribution in both the hitter specimen and the stationary specimen were computed from the strain-rate independent theory

using the static stress–strain curve. The distributions along the specimens were obtained from the strain–space curve, which in turn was experimentally computed from strain–time measurements. These results may be seen in Fig. 3 for specimens of unit area. The actual specimens used in these tests were 0·990 in. in diameter, and the impact velocity for which a comparison is made is 66·5 ft/sec (hitter velocity = 133 ft/sec). Nearly 100 tests were involved in obtaining this energy balance. The difference between the initial total kinetic energy and the sum of the final deformation and kinetic energies was less than 2 per cent.

The significance of this result is that the experimental strain–time curves do not proceed from an infinite step at the origin, and that the deformation energy associated with the mushrooming in the first diameter was included in the calculation. This excess strain energy may be seen in Fig. 3 as the dotted curves in the vicinity of the origin.

In Fig. 4 may be seen a final energy balance for the initially stationary specimen which has been obtained from the final strains at each of many positions shown in Fig. 2. The final kinetic energy is computed from the experimentally determined final velocities. Here, again, an energy balance of closer than 2 per cent is obtained.

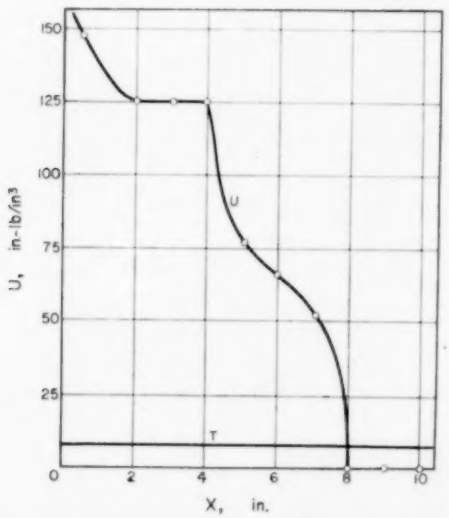

FIG. 4. Final energy distribution from experimental results where T_0 is initial kinetic energy per unit volume, and T and U are final kinetic and deformation energies per unit volume. $V_0 = 66{\cdot}5$ ft/sec. $\Sigma T_0 = \Sigma(T + U) = 800$ in-lb.

It should be emphasized that although diffraction grating results have shown a high order of reproducibility in maximum strains at a given position for a given impact velocity, it is necessary to average large amounts of data due to variations in arrival time. As has been shown elsewhere (BELL 1960c) this effect is due to initial differences in the development of the plastic wave in the first $\frac{1}{8}$ diameter from the impact face.

3. Discussion of Results

The final strain distributions shown in Fig. 2, from which the energy balance of Fig. 4 was obtained, involve the propagation of a plastic wave for a time of 210 μsec for the impact velocity of 66·5 ft/sec. The interesting aspect of this propagation is that each level of strain arrives at 7 diameters, as well as at intervening positions, at a time agreeing with the theoretical velocity of propagation. This includes the theoretical maximum strain which may be seen to propagate to 4 diameters without a decrease in amplitude.

Thus, except for the last 2 diameters where no strain is measured, no visible unloading effects are seen until the plastic wave has arrived at an energy of deformation nearly equal to the initially available kinetic energy. It should be pointed out, however, that the initial elastic front shown in Fig. 5 has a value of approximately 100 μin/in whereas the plastic maximum shown at 4 diameters is a strain of 22,000 μin/in.

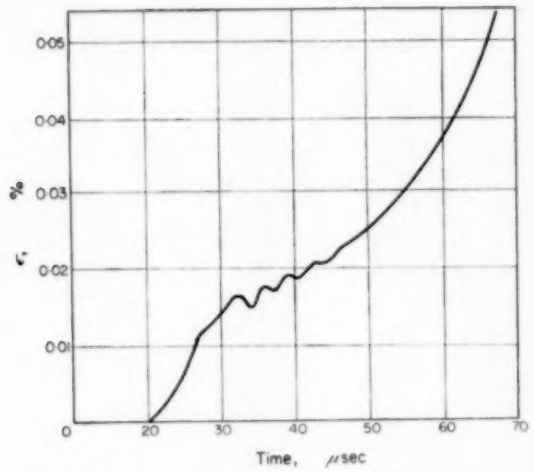

Fig. 5. Initial elastic front at 6 diameters from wire resistance strain measurements.

In order to conduct tests at 8 diameters it was necessary to support the initial stationary specimen at a position between the diffraction grating and the impact face. In all other measurements, including those at 7 diameters, the initial specimen support was located close to the free end. A small amount of strain might be measured at 8 diameters if there were no intervening support. The measurement of specimen diameters following impact has shown zero plastic strain at 9 and 10 diameters, but has indicated the presence of small amounts of strain at 8 diameters. In any event, if the strain at 8 diameters is not zero, it is of very small magnitude, with a correspondingly small contribution to the final energy balance. The absorption of the first reflected elastic front, as suggested by Lee (1953), presumably explains the fact that the maximum strain reaches 4 diameters without unloading.

In Fig. 6 (a) is shown an initial elastic front and the first elastic reflection at a position of 6 diameters from the impact face. Since the specimen was 10 in. long,

the reflection would be expected to arrive at 70 μsec. As may be seen in Fig. 6 (a) the reflection arrives at the predicted time. This elastic reflection which occurs at a plastic strain of 400 μin/in, is the plastic strain level at the time and position predicted by the strain-rate independent theory. The reflected unloading front has the effect of delaying the growth of the plastic wave. If the LEE theory is applied to annealed aluminium, it is found that 80 in/sec is the impact velocity

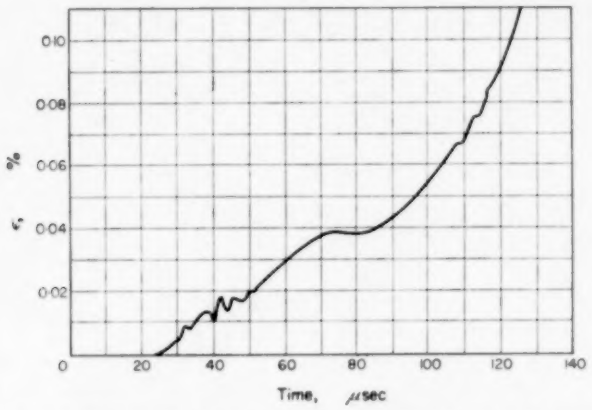

FIG. 6 (a). Initial elastic front and reflected elastic front at 6 diameters.

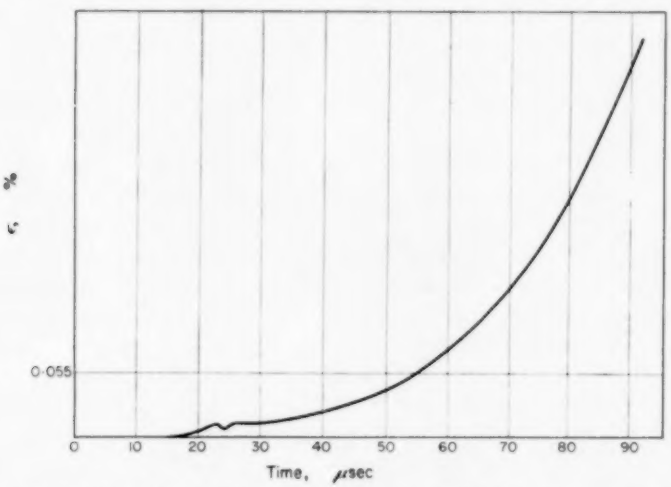

FIG. 6 (b). Initial elastic front and subsequent plastic strain at 4 diameters. No evidence of the initial reflected unloading front is observed at the time of 80 μsec.

at which the elastic wave will just reach the impact face with zero amplitude. The impact velocities of the present study are an order of magnitude higher than this so that it would be expected that the initial elastic reflected front would be absorbed. Using the static stress–strain curve, and assuming a strain-rate independent material, the LEE theory predicts that the absorption will take place between 4 and 5 diameters.

In Fig. 6 (b) at 4 diameters, no evidence of a reflected front is found at the time of 80 μsec. In Fig. 6 (c), however, at 5 diameters, a small reflection front is found at the predicted time of 75 μsec and at a strain level agreeing with the strain rate independent theory. These data of Figs. 5 and 6 (a, b, c) were obtained

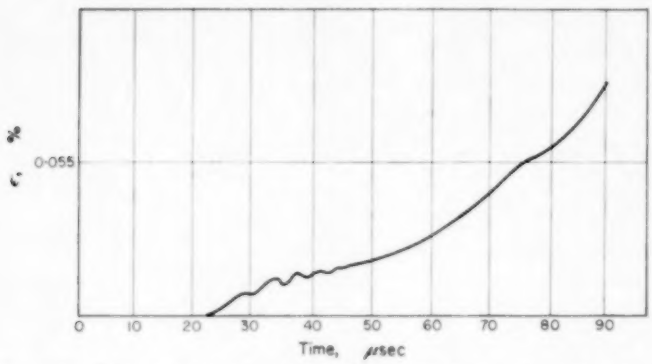

Fig. 6 (c). Initial elastic front and reflected elastic front at 5 diameters.

from $\frac{1}{8}$ in. long wire resistance strain gauges. The arrival times of strain at 4 diameters (Fig. 6 b) are in agreement with propagation velocities of the strain rate independent theory. The 6 diameter results are very reproducible and may be seen in all diffraction grating measurements at this position. On the other hand, the reflexion phenomenon at 5 diameters is very often too small to be delineated. No such reflexion phenomena have ever been observed at 3 or 4 diameters.

These results provide experimental evidence that the reflected elastic front which occurs at 400 μin/in plastic strain at 6 diameters, and 570 μin/in plastic strain at 5 diameters, is indeed absorbed, as predicted by Lee, before reaching much higher plastic strain levels at 3 and 4 diameters. These results hence provide additional evidence, from a different point of view, for the applicability of the strain-rate independent theory to annealed aluminium. The actual absorption effect would appear to be more in the slowing down of the deformation process than in a decrease in the final maximum plastic strain, since the maximum strain level at 6 diameters is unaffected. However, from the results reported below, it would appear that higher levels of reflected elastic strain are able to propagate through the oncoming plastic front without noticeable effect upon the strain–time detail.

It has been found possible to predict the time of contact and coefficient of restitution from a consideration of the characteristics in a Lagrangian diagram. In Fig. 7 such a diagram is shown for a 10 in. specimen, where the characteristics are drawn as as to include the delaying effects of the larger strains in the first diameter. To maintain a zero stress at the free end, it is assumed that each level of strain on arriving at 10 diameters is reflected elastically.

The time of contact is given by the arrival time of that reflected elastic strain whose stress level is half that of the maximum stress for the given impact velocity:

$$T_c = \frac{L}{c_p\,(\sigma_{\max}/2)} + \frac{L}{c_0}, \tag{1}$$

where T_c is the time of contact; L the specimen length; c_0 the elastic velocity; and $c_p\,(\sigma_{max}/2)$ the propagation velocity of that value of strain which has a stress level of $\sigma_{max}/2$. The dashed curve of Fig. 7 is the unloading elastic strain at an impact velocity of 66·5 ft/sec. The plastic wave corresponding to 0·42 per cent strain has a stress level of 4050 lb/in², which is half the maximum stress for this impact velocity of 8100 lb/in². For a Young's modulus of 10×10^6 an elastic

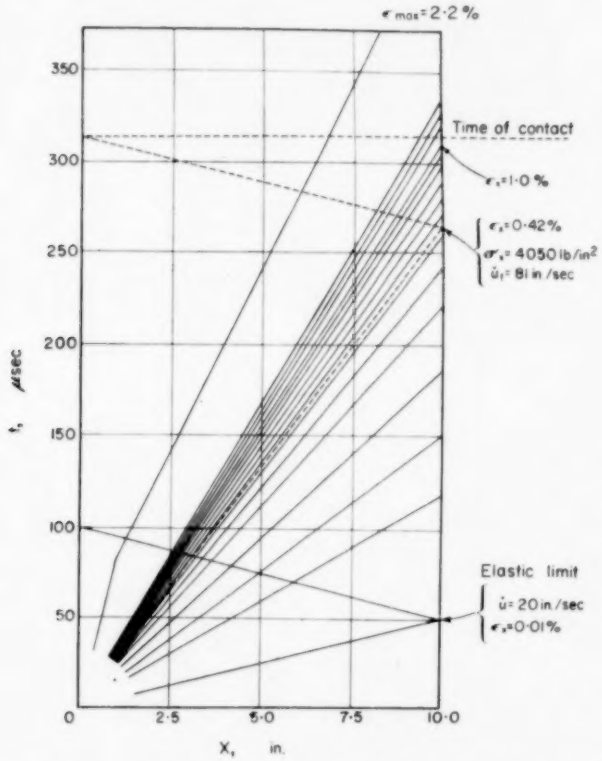

FIG. 7. Lagrangian diagram for 10 diameter specimen where characteristics are determined from slopes of static stress–strain curve and unloading is at elastic velocity. $V_0 = 800$ in/sec. $\sigma_{max} = 8100$ lb/in².

unloading strain of 405 μin/in is obtained. This elastic strain level reaches the impact face at 318 μsec, where, in order to satisfy the boundary condition at the interface, a double unloading takes place and the specimens separate.

The solid line in Fig. 8 is a computation of times of contact calculated from Fig. 7 for several different impact velocities. The circles represent the corresponding experimentally determined contact time. There is a general agreement at all the impact velocities for which such measurements have been made. The cross at 20 in/sec in Fig. 8 is the elastic time of contact obtained by SEARS (1908) in aluminium.

It has been found, further that if the particle velocity of this reflected elastic train, created at the free end, is determined from (2),

$$\dot{u}_f = c_0\,\epsilon, \tag{2}$$

where ϵ is the level of unloading strain arriving at the impact face at the time of contact, and $c_0 = \sqrt{(E/\rho)}$, then the experimental coefficient of restitution may be predicted.

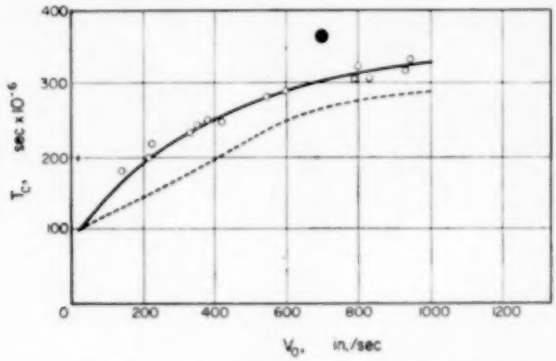

FIG. 8. Experimental time of contact compared with theoretical predictions of static stress–strain curve (solid line) and dynamic stress–strain curve (dashed line).

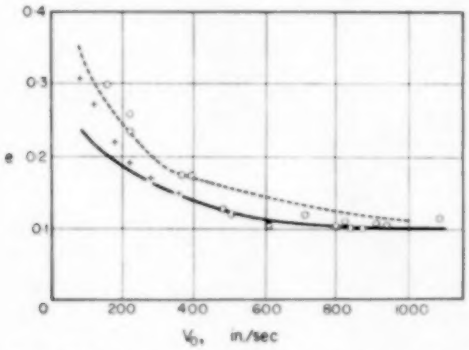

FIG. 9. Experimental coefficient of restitution compared with theoretical predictions of static stress–strain curve (solid line) and dynamic stress–strain curve (dashed line).

Thus, in Fig. 9 the solid curve represents the coefficient of restitution obtained by the ratio of the final particle velocity of (2) to the impact velocity. The circles represent the experimental measurements of this coefficient of restitution. It is found that for velocities above 500 in/sec there is good agreement between the predicted coefficients of restitution and the experimental values where the stress levels of the static stress–strain curve are used in the computation. Below 500 in/sec it is found that the stresses of the static stress–strain curve appear to be lower than those indicated from the experimental data.

The dashed curve in Fig. 9 represents a computation of the coefficient of restitution by means of (2) from the JOHNSON *et al.* (1953) dynamic stress–strain curve. It is seen that the experimental coefficients of restitution are in much better agreement with the dynamic stress–strain curve in this region of lower impact velocity. The 400 in/sec corresponds to a maximum strain level of 0·8 per cent.

A calculation of the time of contact based on the JOHNSON *et al.* dynamic stress–strain curve is shown as the dashed line in Fig. 8. The time of contact is seen to agree with the static stress–strain curve for all impact velocities at all levels of strain.

It should be noted that the number of tests involved in obtaining the experimental values of Fig. 9 varies considerably. For example, the point shown at 800 in/sec, or 66·5 ft/sec, constitutes the averaging of over seventy-five measurements, whereas some of the others involve only two or three measurements.

In the comparison of a number of static stress–strain curves, including the JOHNSON *et al.* static stress–strain curve, differences in stress level are noted from one test to another at the lower strain levels. The crosses in Fig. 9 represent the largest variation observed, which is given by the JOHNSON *et al.* static stress–strain curve. Hence, variations in the static stress–strain curve at low strain levels do not appear to be sufficient to account for the differences in the experimental coefficient of restitution. All earlier diffraction grating studies (BELL 1960a) have shown that the propagation velocities of all strain levels, including the lower

TABLE 1.

Material	*Specimen diameter* (in.)	*Specimen length* (in.)	*Impact velocity* (ft/sec)	*Time of contact*		*Coefficient of restitution*	
				Theoretical (μsec)	*Experimental* (μsec)	*Theoretical*	*Experimental*
Annealed copper	0·990	10	40	564	568	0·21	0·20
Annealed copper	0·990	10	38·9	534	550	0·20	0·17
Annealed aluminium	0·990	5	66·4	159	170	0·105	0·112
Annealed aluminium	0·990	8	66·6	254	250	0·105	0·125
Annealed aluminium	0·990	20	55·2	600	600	0·110	0·132
Annealed aluminium	0·5	10	65	318	310	0·105	0·08

values of strain, are very close to the values predicted from the slopes of the static stress–strain curve. This result is consistent with the time of contact measurements of Fig. 8. The experimental coefficients of restitution, however, suggest a somewhat higher stress level for the lower strains than is given by the static stress–strain curve. Thus the low strain levels propagate in accordance with the slopes of the static stress–strain curve, but have stress levels agreeing with the dynamic stress–strain curve.

In order to examine the general applicability of these results, a few tests were made for different lengths of specimens and for different specimen diameters. In addition, two measurements were made at approximately 40 ft/sec in annealed copper, which has been shown elsewhere (Bell 1960b) also to be strain rate independent. These results are given in Table 1.

Each of the many tests which have been considered in this paper was obtained by ejecting the hitter specimen from a smooth bore air gun, the last foot of which was ported so as to give constant velocity impact. The specimens were optically aligned prior to impact, as described elsewhere (Bell 1960a). At the time of impact, 4 in. of the 10 in. long hitter specimen were still in the bore of the gun. The impact was made with an identical stationary specimen and at the time of measurement both specimens were in free flight. Following impact, both the specimen and hitter were captured in a steel box. Circumferential measurements of the struck specimens after impact have given agreement with the final strain measurements obtained from the diffraction gratings. The aluminium used in this study was 1100 F, annealed for 2 hr at 1100°F, and furnace cooled. The gratings were 30,720 lines per inch, and the light source was the 5461 λ green line of the mercury arc.

4. Summary and Conclusions

A number of theoretical papers in the last few years have dealt with the problem of reflected waves interacting with the initial plastic front. In most of those studies a bi-linear stress–strain curve was assumed, and the amplitude of the elastic front was a significant fraction of the amplitude of the plastic wave front. To the experimentalist two aspects of the results obtained in such studies are of particular interest: one is the prediction of internal reflexions at the intersecting wave fronts, and the other is that the reflected or transmitted loading waves in an already stressed plastic field propagate as plastic waves. Several years ago in a series of experiments in copper which were designed to examine the phenomenon of internal reflexion, this author was unable to obtain experimental evidence of such behaviour. Further, in a series of experiments in 1949–1950 (Bell 1951) this author discovered that incremental loading waves, as well as unloading waves, propagate with elastic velocities in a plastically pre-stressed field. It was shown independently by Riparbelli (1953) and Rubin (1954) that the elastic velocity of the incremental loading wave is consistent with the plastic wave theory of Malvern (1951) for a material possessing strain-rate properties, thus suggesting the necessity for introducing a strain-rate theory. The present paper has shown that there exists a close agreement between the experimental reflexion behaviour and the theoretical predictions of Lee (1953), in that the initial reflected elastic unloading front is absorbed provided the impact velocity is above a critical value. This value depends upon the physical properties of the material. The theory assumes that the plastic wave propagation is strain-rate independent, and the actual static stress–strain curve of the material is used rather than a bi-linear approximation. The fact that the experimental results given in the present paper not only indicate that the initial reflected elastic unloading front is absorbed, but that it is absorbed at the position along the rod predicted by the theory, provides additional evidence of strain-rate independence. Thus, with one exception, all the evidence obtained by the present writer – including propagation velocities, maximum strain

amplitude, time of contact, coefficient of restitution, the absorption of the initial elastic reflected wave, and an energy balance before and after impact – points to a strain-rate independent theory of plastic wave propagation. The only exception is the elastic velocity of the incremental loading wave. It has been the opinion of this author for many years that incremental loading waves in a pre-stressed field might require additional elastic deformation of some unspecified amount in order to trigger further plastic deformation. Preliminary experiments in annealed aluminium, with larger loading increments than have been used before, have indicated that this indeed may be so.

With measurements made with diffraction gratings located at $\frac{3}{32}$ in. or less from the impact face, it has been found that, for impact velocities above a critical value of approximately 48 ft/sec (which is the KARMAN critical velocity for this material), the strains up to a value corresponding to the mean energy do propagate from a nearly infinite step at the origin. Since the characteristic from which the unloading strain is determined always lies in this region, it is possible to predict the time of contact and the coefficient of restitution directly from the strain-rate independent theory without reference to the delay in the formation of the larger strains at the origin.

The prediction of final strain distribution, however, requires the experimental detail of the shape of the strain–time front upon emergence from the first diameter. Experimental results have shown that this final strain distribution may be determined by computing the distance which the dispersive plastic front must propagate until the distributed energy of deformation is equal to the available energy. For the situation studied, this plastic wave propagates without modification, except for the very low strains within 2 diameters of the free end of the specimen.

In Fig. 2 was seen a comparison of the theoretical and experimental final strain distributions. These results are for a 66·5 ft/sec impact velocity for which the maximum plastic strain is 2·2 per cent, involving an energy deformation per unit volume of 124 in-lb. This is, of course, a dispersive wave.

The kinetic energy per unit volume prior to impact is 80 in-lb, so that the final deformation energy of the 124 in-lb per unit volume is approximately $\frac{3}{2} \times$ the initial kinetic energy. The final strain energy distribution may be computed empirically from the observation (shown as the dotted line in Fig. 2) that, if a straight-fronted plastic wave with the amplitude and deformation energy of the maximum strain is allowed to propagate with the velocity of the strain, ϵ_1, corresponding to the value at half the total energy of deformation, it will reach a position corresponding to the distance travelled by ϵ_1 at a time when the total deformation energy equals the total initial kinetic energy. Thus, for the case shown, ϵ_1 is equal to 0·0135 in/in, having an energy level of 62 in-lb per unit volume and a velocity of propagation of approximately 30,000 in/sec. Considered in this fashion, when this strain reaches 6 diameters, as shown, the total energy of deformation behind this apparent non-dispersive wave front exactly equals the total available energy. It has been necessary to subtract the 5 per cent of excess deformation energy due to the mushrooming in the first diameter.

It has been shown empirically that for annealed aluminium cylindrical rods in axial, free flight collision, the coefficient of restitution, time of contact, and final strain distributions may be determined from the introduction of a simple elastic

reflexion from the free end. The strain-time detail, time of contact, and, for higher strain levels, the coefficient of restitution, are all given by the strain-rate independent theory using the detail of the static stress–strain curve. For lower strain levels, the coefficient of restitution appears to be in better agreement with the stress levels of the dynamic stress–strain curve. The velocity dividing these two cases is of the order of 500 in/sec, which is somewhat below the Karman critical velocity of 581 in/sec determined from static tension tests for this annealed aluminium. These static tension tests and the calculation of the critical velocity are from data obtained by Professor ROBERT POND of the Johns Hopkins University (personal communication).

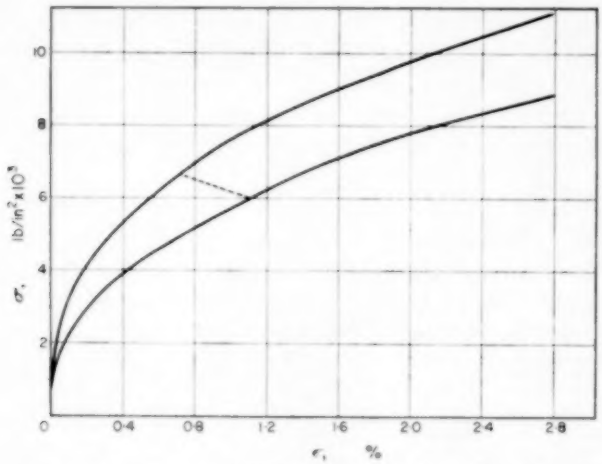

FIG. 10. Dynamic stress–strain curve (after JOHNSON *et al.*) and static stress–strain curve.

In Fig. 10 the dynamic stress–strain curve of JOHNSON *et al.* and the author's static stress–strain curve are compared. The dashed curve connecting these two is that given from the experimental measurements of the coefficient of restitution. It should be remembered that the velocities of propagation and times of contact are not given from either the slopes of the dynamic stress–strain curve or this dashed connexion, but by the slopes of the lower static stress–strain curve.

The results reported here, together with the earlier studies of the strain rate independent behaviour in annealed aluminium (BELL 1960a) and the study of the initial behaviour (BELL 1960c), provide, from the solid mechanics point of view, a detailed description of the total behaviour of the axial collision of annealed aluminium rods for impact velocities up to 80 ft/sec at room temperatures.

Studies are currently in progress to extend this impact velocity to 500 ft/sec and to extend the temperature to within 50° of the melting point of the metal. In as yet unpublished work it has been found that these results are independent of specimen diameters up to 1 in. diameter specimens, and appear to apply also to annealed copper. These results are not to be universally expected, since the large number of experiments conducted in lead and magnesium have indicated significant departures from the strain-rate independent behaviour.

Acknowledgments

The author wishes to acknowledge the sponsorship of the United States Air Force, Office of Scientific Research. He wishes to thank his research assistants, John Suckling, and Patricia Jones ; and to thank again Dr. Joseph Krafft of the United States Naval Research Laboratory for the continued loan of the air gun used in these tests. He would like to express his appreciation to J. Wenig of the Ballistics Research Laboratory, United States Army, Aberdeen Proving Ground, for his help with the electronics.

References

Bell, J. F.	1951	Tech. Report No. 5, U.S. Navy Contract No. 6-ONR-243, Task Order VIII (NR 035-215).
	1956	*J. Appl. Phys.* **27**, 10.
	1958	*Proc. 3rd. U.S. Nat. Congr. Appl. Mech.*, p. 489.
	1959	*Proc. Soc. Exp. Stress Anal.* **17**, 2.
	1960a	*J. Appl. Phys.* **31**, 2.
	1960b	Tech. Report No. 5, U.S. Army, OOR Contract No. DA–36–034–ORD–2366.
	1960c	*J. Appl. Phys.* **31**, 12.
Johnson, J. E., Wood, D. S. and Clark, D. S.	1953	*J. Appl. Mech.* **20**, 4.
Lee, E. H.	1953	*Quart. Appl. Math.* **10**, 4.
Malvern, L. E.	1951	*J. Appl. Mech.* **18**, 203.
Riparbelli, C.	1953	*Proc. 1st Midwestern Conf. on Solid Mechanics*, p. 148.
Rubin, R. J.	1954	*J. Appl. Phys.* **25**, 528.
Sears, J. E.	1908	*Proc. Camb. Phil. Soc.* **14**, 257.

J. Mech. Phys. Solids, 1961, Vol. 9, pp. 16 to 38. Pergamon Press Ltd., London. Printed in Great Britain

DÉFORMATION PLASTIQUE DE MONOCRISTAUX DE FER

Par B. Jaoul et D. Gonzalez
Centre de Recherches Métallurgiques de l'École des Mines de Paris

(*Received 4th August*, 1960)

Sommaire

L'étude des mécanismes géométriques de la déformation de monocristaux de fer à la température ambiante montre l'importance du phénomène de consolidation sur les systèmes latents ; le glissement unique, qui peut se poursuivre jusqu'à de grandes déformations, se développe sur des surfaces dont l'orientation moyenne correspond au maximum de contrainte de cission. La consolidation reste généralement faible, sauf pour certaines orientations particulières où deux systèmes peuvent apparaître sous forme de bandes ; mais, même dans ce cas, le durcissement est moins important que dans les cristaux de structure cubique à faces centrées.

A la température de l'azote liquide, le maclage intervient en premier. Le glissement apparaît pour une contrainte beaucoup plus élevée, mais la consolidation reste encore relativement faible. Les systèmes de maclage actifs ne sont pas les mêmes suivant l'orientation de la traction ; notamment, si l'axe de traction est voisin d'une direction $< 100 >$, le maclage sur deux plans conjugués entraine le clivage.

1. Introduction

Le Mecanisme géométrique de la déformation des cristaux de structure cubique à faces centrées a fait l'objet d'un grand nombre d'études ; les éléments de glissement qui interviennent, ainsi que les hétérogénéités de déformation, sont relativement bien connus et il est possible d'en déduire la consolidation, à partir de la théorie des dislocations imparfaites (Friedel 1956).

Dans le cas des cristaux cubiques centrés, par contre, les mécanismes de la déformation sont moins bien définis. Depuis Taylor et Elam (1928), qui ont proposé le ' Pencil glide,' surface de glissement en " tôle ondulée," de nombreux expérimentateurs ont cherché à définir quels plans de glissement intervenaient. La direction de glissement étant toujours $< 111 >$, des plans du type $\{110\}$, $\{112\}$, $\{123\}$ ont été proposés, tandis que certains auteurs étaient partisans du glissement sur une surface non cristallographique. Ces divergences pourraient être liées soit à la température des essais, soit à la teneur en carbone des échantillons, soit à l'amplitude de la déformation (Allen 1959).

Nous avons nous-mêmes effectué un certain nombre d'essais dans le but de déterminer le taux de consolidation des cristaux de fer ; mais, les variations observées nous ont conduit à rechercher quels mécanismes géométriques pouvaient intervenir au cours de la déformation.

2. Preparation des Echantillons et Conduite des Essais

Le métal utilisé était un fer Armco de composition : C/0·030* – Mn/0·025 – Ni/0·12 – Cu/0·15 – S/0·016 – P/0·007. La tôle, initialement épaisse de 3 mm, a été laminée à froid jusqu'à des

*Les traitements effectués ultérieurement ont entraîné une décarburation importante : $C < 0{\cdot}001\,\%$.

épaisseurs variant entre 2 mm et 0·5 mm, puis, des éprouvettes de 2 mm de large et de 10 mm de longueur utile, avec des congés de raccordement de 3 mm de diamètre, (Fig. 1) ont été découpées par matriçage.

Les échantillons ont alors subi un traitement thermique sous vide de 20 h à 950°C, suivi d'un refroidissement à l'air, puis un écrouissage critique de 3·75 pour cent à vitesse lente* ; enfin, un traitement thermique à 880°C sous hydrogène purifié, variant de 3 à 8 jours, avec une montée en température relativement rapide (environ une heure) a entraîné un grossissement du grain, en même temps que la décarburation : l'analyse chimique a révélé une teneur en carbone inférieure à 0·001 pour cent.

Nous avons ainsi obtenu près de quatre-vingt cristaux occupant toute la portion utile des éprouvettes ainsi qu'une partie des congés (Fig. 1) ; cette condition est nécessaire pour assurer une déformation régulière, notamment à basse température où la décohésion intergranulaire intervient avant la déformation plastique (Fig. 1). L'axe de traction de ces éprouvettes occupait dans le réseau cristallin des orientations couvrant à peu près toute la surface du triangle stéréographique élémentaire (Fig. 2), la normale à la surface des éprouvettes étant également au hasard

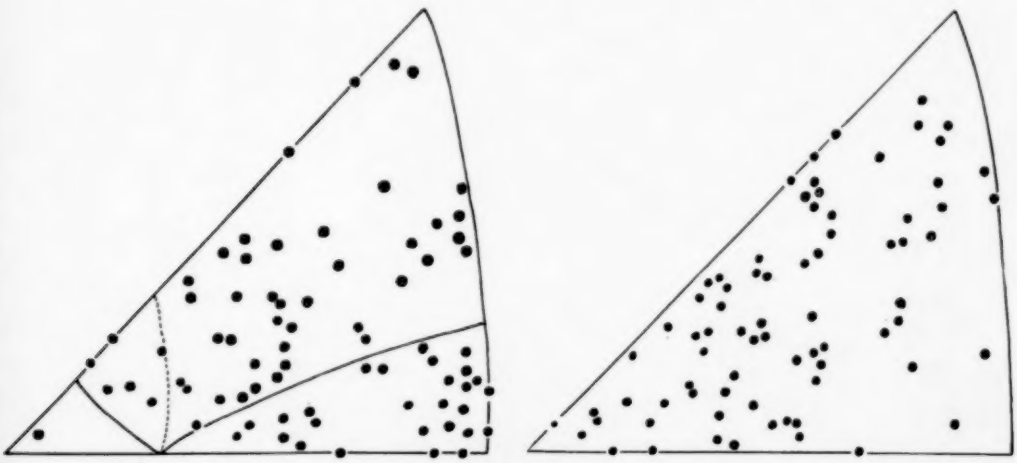

FIG. 2. Orientations de l'axe (à gauche) et de la normale à la surface des monocristaux.

(sans avoir cependant de surface voisine d'un plan {110}). Les taches des diagrammes de Laue étaient généralement fines, sauf pour trois cristaux qui présentaient une polygonisation nette. Les éprouvettes ont été polies électrolytiquement, soit dans leur ensemble dans un bain acéto-perchlorique à 5 pour cent, soit sur une seule face au Disa Electropol avec une fente couvrant toute la section utile des éprouvettes et une partie des congés.

Ces cristaux ont été étirés à des températures variant entre − 195 °C et + 400 °C, à des vitesses d'allongement comprises entre 3×10^{-5} et 3×10^{-2} sec^{-1}. L'appareil utilisé était une machine Chevenard pour traction de fils, munie d'un dispositif d'amarrage spécial pour ces éprouvettes : celles-ci étaient prises par les congés entre deux ergots de même rayon, solidaires d'un support monté sur un axe, permettant ainsi la rotation des mordaches avec la rotation du cristal (Fig. 3) ; sur cette machine pouvaient être montés, soit un petit four pour les essais à chaud, soit une cuvette pour les essais à − 80 °C dans l'acétone ou à − 195 °C dans l'azote liquide.

Le traitement thermique effectué sur les éprouvettes n'a pas donné seulement des monocristaux ; nous avons également obtenu une série de polycristaux de grosseur moyenne de grain très variable, jusqu'à un diamètre de l'ordre de 25 μ. Ces éprouvettes, ayant subi le même traitement que les monocristaux, donc la même décarburation, nous ont permis d'étudier l'influence des joints, que nous analyserons dans un prochain article.

*Les courbes de traction présentant un palier, l'allongement a été arrêté généralement peu après la fin du palier.

3. GEOMETRIE DE LA DEFORMATION DES MONOCRISTAUX

La vitesse de traction s'est révélée sans influence sur l'aspect micrographique des éprouvettes déformées ; par contre de nouveaux phénomènes peuvent apparaître si l'on fait varier la température.

(i) *Déformations à la température ambiante*

Des cristaux de diverses orientations ont été soumis à des allongements compris entre 5 pour cent et la rupture, certains progressivement par sauts de 5 pour cent environ, avec observation de la structure après chaque déformation.

D'une manière générale, *les cristaux se sont déformés jusqu'à la rupture par glissement dans une seule direction.* Ce n'est que dans certains cas particuliers, que nous étudierons plus loin, qu'un second système est apparu.

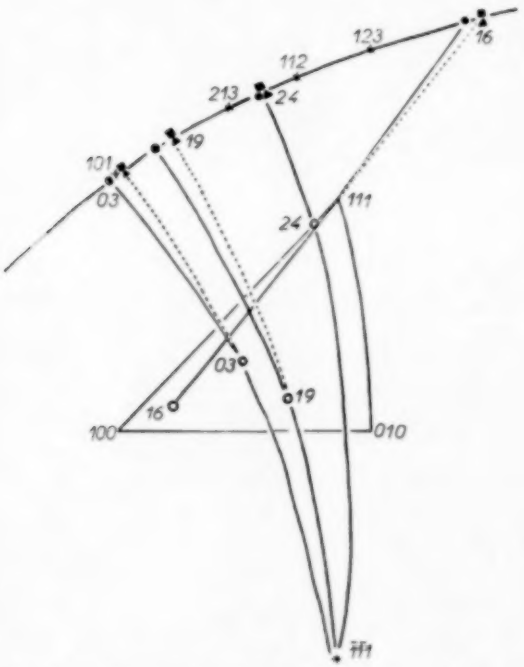

FIG. 4. **Résultats des déterminations du plan de glissement par deux méthodes. ■ calcul, ● RX, ▲ mesures au microscope.**

Les glissements sont toujours sinueux, même après de faibles déformations. Observés à très fort grossissement, au microscope électronique, sur réplique au carbone, ils présentent les mêmes sinuosités, sans avoir tendance à se localiser dans certains plans privilégiés. Celà ne permet pas de définir un plan de glissement, mais seulement la direction moyenne d'une surface de glissement, surface réglée qui contient la direction de glissement.

Cette direction unique est $[\bar{1}11]$ (Fig. 4), sauf pour les cristaux d'orientation voisine de [100] où le glissement se développe dans la direction [111] qui est alors

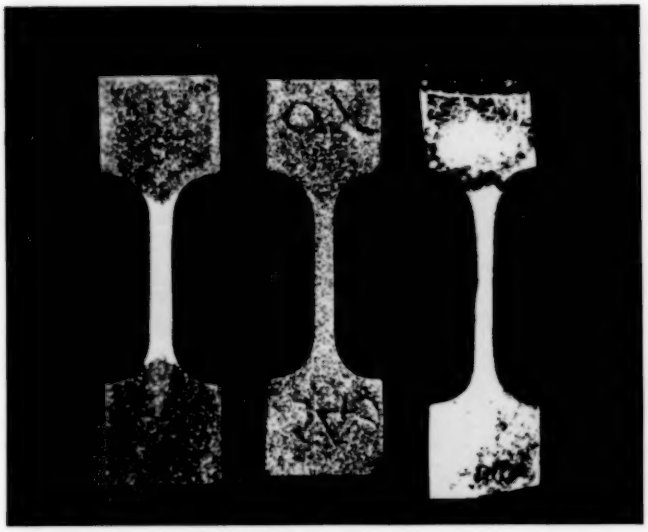

FIG. 1. Forme des éprouvettes de traction, (échelle 1.8). A gauche : monocristal ; au centre : polycristal ; à droite : monocristal rompu dans le congé, puis déformé jusqu'à la striction.

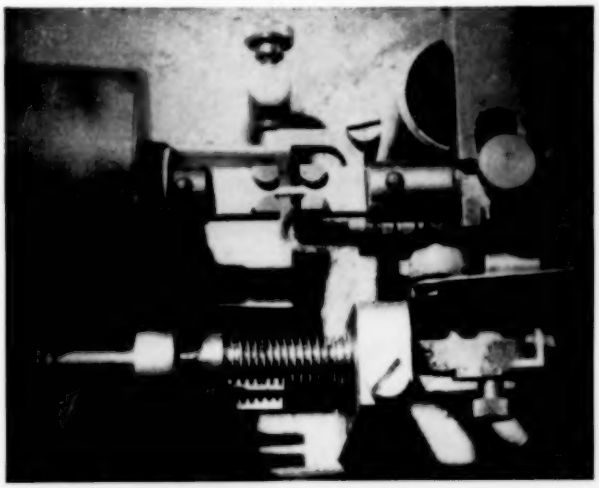

FIG. 3. Montage des éprouvettes sur la machine. On aperçoit le four servant aux essais à chaud.

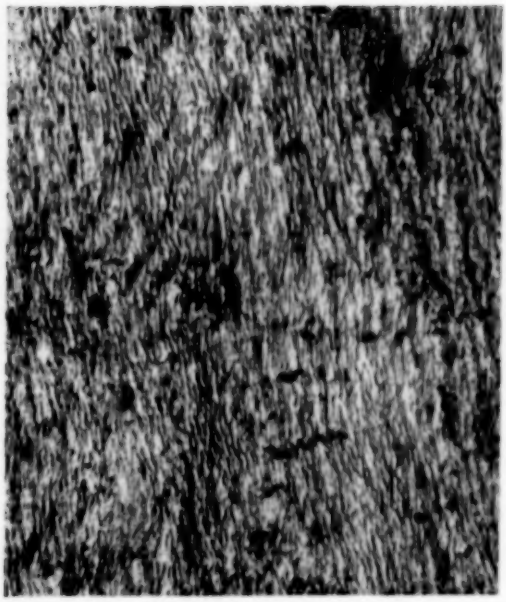

FIG. 6. Surface du cristal No. 16 allongé de 76 pour cent à l'ambiante. × 150.

FIG. 7. Formation de micropliages sur une éprouvette déformée de 15 pour cent. × 150.

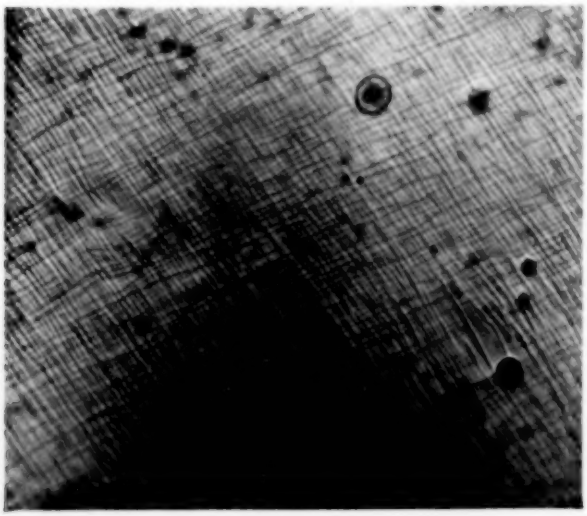

FIG. 9. Développement de deux systèmes. × 300.

mieux favorisée. Cette direction a été déterminée par la rotation du réseau accompagnant la déformation ; on sait en effet que pour un allongement $d\epsilon$, l'angle λ entre la direction de glissement et l'axe de traction varie de $d\lambda$ tel que

$$d\lambda = -d\epsilon \operatorname{tg} \lambda.$$

La comparaison des orientations cristallines avant et après déformation permet donc de déterminer la direction de glissement ; la nouvelle orientation obtenue par un diagramme de Laue correspond à celle que l'on peut calculer par la relation ci-dessus à 2° près.

L'orientation moyenne de la surface de glissement a été déterminée par trois méthodes :

(a) par les traces des glissements sur la surface et sur la tranche des éprouvettes ;

(b) par les modifications de la forme extérieure des échantillons, qui étaient initialement de section rectangulaire ;

(c) par une méthode moins directe, basée sur l'orientation de l'axe des rotations créant l'astérisme, cet axe définissant, avec la direction de glissement, la surface de glissement.

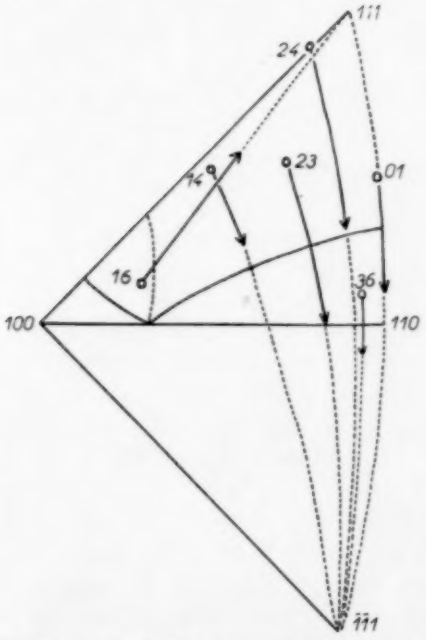

FIG. 5. Déplacement de l'axe de traction au cours de l'allongement. La zone figurée en pointillé autour de la direction [100] correspond à la limite où les directions [111] et [$\bar{1}\bar{1}\bar{1}$] sont également disposées.

Le plan moyen de glissement, déterminé par ces trois méthodes, est, dans tous les cas, à 2° près, *le plan dans lequel la cission a la valeur maximale*. La Fig. 4 représente les résultats des déterminations pour quelques éprouvettes : la normale au plan

moyen de glissement est située dans le plan défini par la direction de traction et l'axe de l'éprouvette. Dans ces conditions, la composante de cission créant le glissement ne dépend plus que de l'angle λ ; le triangle stéréographique peut alors être décomposé en deux zones (Fig. 5) correspondant aux orientations de cristaux pour lesquelles le glissement se développe soit dans la direction $[\bar{1}\bar{1}1]$, soit dans la direction $[111]$.

Le système reste unique, même quand la déformation devient importante et qu'un autre système se trouve mieux favorisé. La Fig. 5 représente le déplacement de l'axe de traction par rapport au réseau cristallin pour quelques éprouvettes fortement déformées ; ces déplacements, déterminés par diagramme de Laue, correspondent toujours à la rotation que l'on peut calculer, ce qui montre que s'il s'est développé des glissements secondaires non observables au microscope, ils n'ont jamais pris une grande extension. Le cas de l'éprouvette No. 16 est très caractéristique : sur la zone en pointillé les deux directions de glissement $[111]$ et $[\bar{1}\bar{1}1]$ sont également favorisées et le cristal a commencé à glisser conformément à son orientation initiale ; quand la zone symétrique a été traversée, le second système n'est pas intervenu et le glissement s'est pousuivi jusqu'à un allongement de 76 pour cent, correspondant à l'apparition de la striction : l'angle entre l'axe et la direction de glissement $[111]$ était alors de 21°*, alors que la direction $[\bar{1}\bar{1}1]$ était orientée à 60° ; la cission dans cette dernière direction était de 30 pour cent supérieure à la composante dans la direction active. La Fig. 6 montre l'aspect de cette éprouvette après l'allongement de 76 pour cent.

Hétérogénéités de déformation. La déformation n'est cependant pas un cisaillement pur ; dans tous les cas, il se développe un astérisme appréciable dont la plus grande dimension est généralement dirigée vers la direction de glissement. L'astérisme correspond donc à des zones qui ont plus tourné que l'ensemble du cristal ; les taches sont continues et l'on ne voit aucune ponctuation apparaître au cours de la déformation. Par micrographie, on observe dans tous les cas des petits pliages (Fig. 7) analogues aux micropliages qui se développent dans les cristaux d'aluminium et qui, eux aussi, correspondaient à une rotation vers la direction de glissement (Jaoul *et al.* 1957). Mais, sur aucun cristal nous n'avons observé des pliages larges ; les seules bandes de déformation importantes font intervenir des glissements secondaires.

Glissements secondaires. Un deuxième système de glissement n'apparaît que si l'orientation initiale est très voisine d'une zone symétrique ; ce second système se développerait donc dès le début de la déformation. Il n'apparaît pas si le premier a déjà pris une extension notable et nous avons vu que l'axe peut, au cours de la rotation, traverser largement une zone symétrique.

On peut considérer, dans le triangle stéréographique, trois zones symétriques par rapport aux directions de glissement : la zone $[100]$–$[110]$ qui est une zone stable, c'est à dire que, si le point figuratif de l'axe de traction quitte cette zone, le glissement favorisé a tendance à l'y ramener, la zone $[100]$–$[111]$ qui est 'instable' et la zone indiquée en pointillé sur la Fig. 8 où les deux directions $[111]$ et $[\bar{1}\bar{1}1]$ sont également favorisées.

Les éprouvettes dont l'axe était situé au voisinage de cette dernière zone se

*La nouvelle orientation par un diagramme de Laue donne un angle de 20°, tandis que le calcul de la rotation à partir de la déformation conduit à un angle de 22°, l'angle initial étant de 41°.

sont déformées avec un seul système ; la zone est ' instable,' cependant, sa traversée ne modifie pas beaucoup le rapport des composantes de cission relatives aux deux directions ; nous avons vu que l'éprouvette No. 16 (Fig. 5) avait toujours glissé dans la même direction.

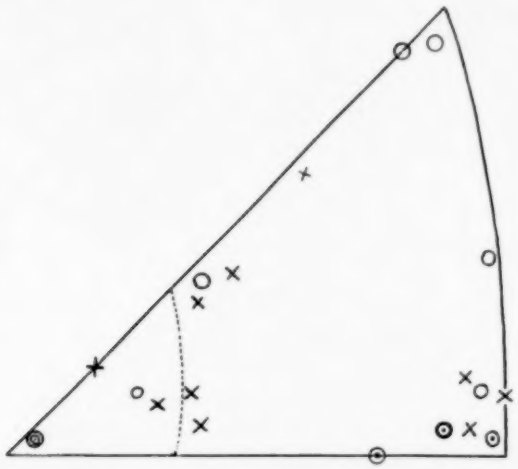

FIG. 8. Nombres de systèmes étant intervenus dans les éprouvettes voisines des zones symétriques. × 1 système de glissements, ⊙ 2 systèmes de glissements, ○ deuxième système local.

Sur les deux autres zones symétriques, l'aspect des glissements secondaires est totalement différent :

Sur la zone [100]–[110], ils se développent simultanément en se croisant (Fig. 9) et le point figuratif de l'axe reste sur la zone. Il est à remarquer que les glissements sont alors moins sinueux. Si l'axe est un peu plus éloigné de la zone, il n'apparaît que de fins glissements secondaires pour de grandes déformations, quand l'axe est bien au delà de la zone ; l'apparition de ces fins glissements précède d'ailleurs de peu la rupture, mais leur formation n'est pas systématique (Fig. 10).

Les cristaux orientés initialement sur la zone [100]–[111] présentent *des bandes de glissement secondaire*, ces bandes étant très développées et visibles à l'oeil sur l'éprouvette. Les variations d'orientation, par suite des rotations différentes sont importantes et la désorientation déterminée par les figures de corrosion peut atteindre 15° après un allongement de 25 pour cent. Celà est dû à ce que, initialement, les deux systèmes sont apparus chacun en divers points de l'éprouvette et que, la déformation se poursuivant, chacune de ces zones a continué à se déformer avec un seul système. Pour de plus grandes déformations, de véritables cassures se forment, la limite de la bande étant alors très nette (Fig. 11). Une éprouvette orientée initialement très près de [100] s'est déformée avec quatre systèmes de glissement (Fig. 12) ayant chacun tendance à se localiser dans des zones particulières. Il est à remarquer que les glissements secondaires sont assez droits, tandis que le glissement principal reste sinueux.

La Fig. 8 résume les résultats obtenus avec les éprouvettes dont l'orientation initiale était voisine des zones symétriques ; on voit que la proportion d'éprouvettes présentant deux systèmes reste faible.

Nous avons recherché, par observation au microscope électronique, comment les glissements pouvaient se croiser dans le fer et nous avons constaté deux types d'intersection : ou bien les deux systèmes se sont développés simultanément, les deux bandes de glissement se trouvant chacune décalée par l'autre (Fig. 13), ou bien les deux glissements se recombinent : dans le cas de la Fig. 14, le glissement principal, qui est le plus sinueux a pour direction $[\bar{1}\bar{1}1]$ et le glissement secondaire $[111]$; la portion rectiligne à l'intersection des deux glissements définit, avec l'intersection des deux surfaces de glissement, un plan qui contient la direction $[001]$ résultant de la recombinaison :

$$a\sqrt{\tfrac{3}{4}}\,[\bar{1}\bar{1}1] + a\sqrt{\tfrac{3}{4}}\,[111] \rightarrow a\,[001]$$

qui correspond au gain d'énergie :

$$\tfrac{3}{4}a^2 + \tfrac{3}{4}a^2 = \tfrac{3}{2}a^2 \rightarrow a^2.$$

Souvent les glissements ne se croisent pas réellement, mais semblent se réfléchir l'un sur l'autre (Fig. 15).

Enfin, il faut signaler que les glissements présentent parfois de brusques décrochements (Fig. 16) correspondant probablement à un obstacle que doit contourner la ligne de dislocations.

(*ii*) *Déformations à température supérieure à l'ambiante*

Les essais effectués à des températures supérieures à l'ambiante présentent les mêmes caractéristiques ; les glissements sont toujours sinueux et ramifiés mais cependant plus gros et plus nets. Aucune observation n'a été faite après déformation à une température supérieure à 300°C, par suite de l'oxydation.

(iii) *Déformations à basse température*

Par traction à $-80°$, les glissements sont très fins et difficilement observables au microscope optique ; ils sont cependant beaucoup moins sinueux qu'à la température ambiante.

A la température de l'azote liquide, trois phénomènes peuvent intervenir : le glissement, le maclage et le clivage, selon l'orientation de l'axe de traction par rapport au réseau (Fig. 17).

(a) *Glissement.* Si l'axe de traction fait avec la normale à un plan $\{100\}$ un angle supérieur à 30°, l'éprouvette se déforme par glissement jusqu'à striction ; les glissements sont courts et moins ramifiés qu'après déformation à la température ambiante ; ils sont généralement plus droits (Fig. 18), mais présentent encore de nombreux décrochements brusques. Ils semblent avoir tendance à se localiser dans certains plans (Fig. 19) qui sont du type $\{123\}$ d'après les traces observées sur la surface.

(b) *Maclage.* Trois éprouvettes seulement se sont déformées par glissement seul, sans maclage ; leurs orientations initiales étaient voisines de $[111]$, de $[112]$ et $[110]$ (Fig. 17). Toutes les autres se sont maclées, généralement sur de nombreux plans, mais chaque famille n'a qu'un développement très limité (Fig. 20). Nous

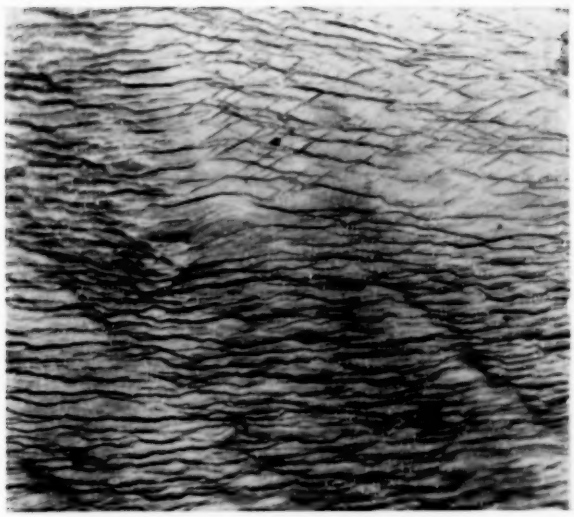

FIG. 10. Glissements secondaires se développant après la traversée d'une zone symétrique. × 300.

FIG. 11. Bande de glissement secondaire après forte déformation (22 pour cent). × 150.

FIG. 12. Glissements multiples dans une éprouvette voisine de [100]. × 150.

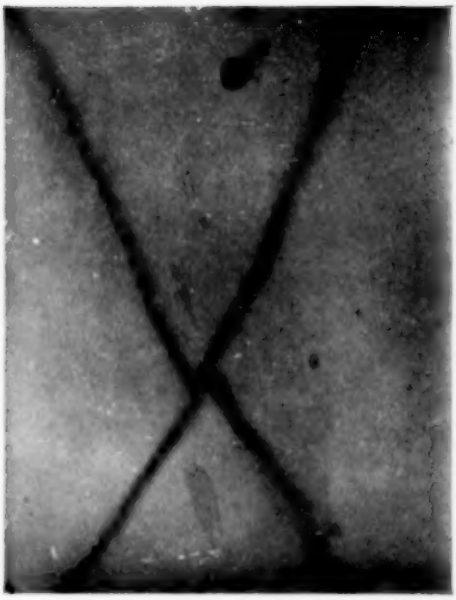

FIG. 13. Intersection de deux bandes de glissement chacune étant décalée par l'autre. × 60,000.

FIG. 14. Recombinaison de deux glissements. × 60,000.

FIG. 15. Décomposition des glissements près d'une intersection. × 60,000.

FIG. 16. Aspect d'un décrochement d'un glissement. × 60,000.

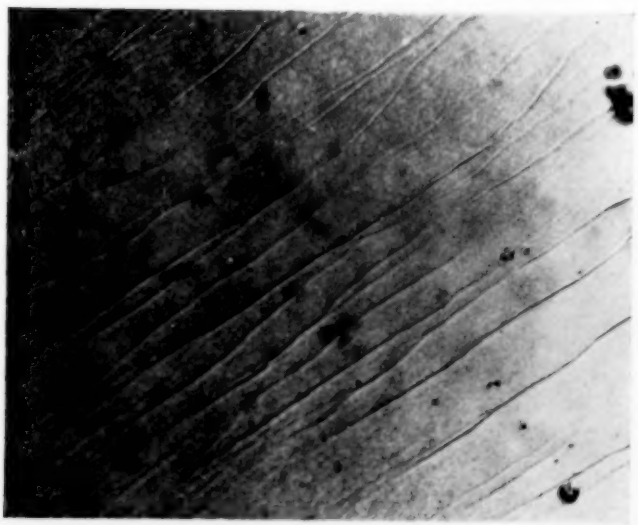

FIG. 18. Aspect des glissements après déformation à — 195 °C. × 400.

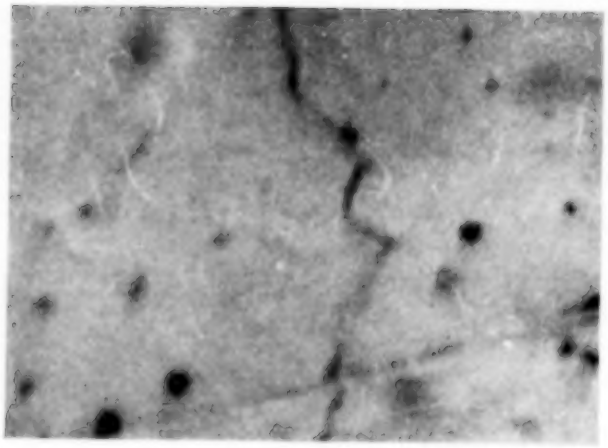

FIG. 19. Tendance des glissements à se stabiliser dans des plans {123}. × 4000.

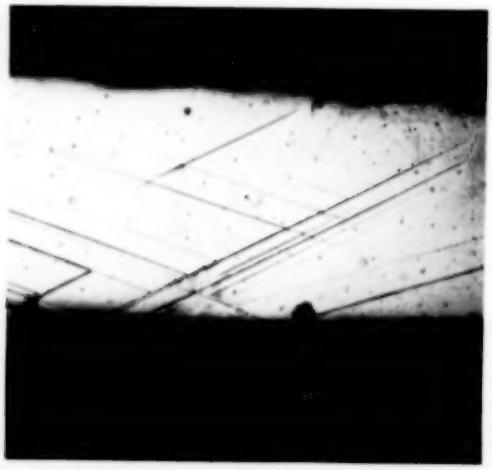

FIG. 20. Macles, ou bandes de Neumann, visibles sur la surface d'une éprouvette (No. 21). Ces macles se sont formées sous une tension de 43 kg/mm² et leur développement est resté limité quoique le glissement ne soit apparu que pour une tension axiale de 56 kg/mm².

avons observé jusqu'à sept systèmes de maclage sur une même éprouvette, l'allongement dû à la formation d'un seul système étant de l'orde de 0·2 pour cent*. Les macles sont souvent très fines, mais elles ne peuvent cependant pas être confondues avec des glissements droits, car elles réapparaissent après polissage électrolytique ; les plus importantes que nous ayons observées avaient une largeur, comptée

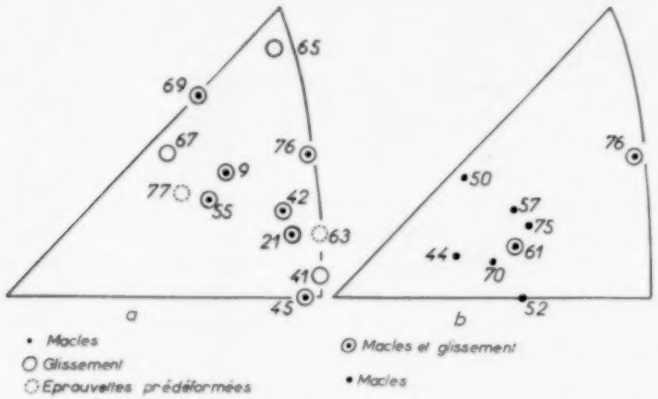

FIG. 17. Mécanisme de déformation à basse température en fonction de l'orientation. (a) Eprouvettes strictionnées. (b) Eprouvettes rompues par clivage. Deux éprouvettes (Nos. 61 et 76) ont présenté, après glissement, une rupture sur un plan de clivage.

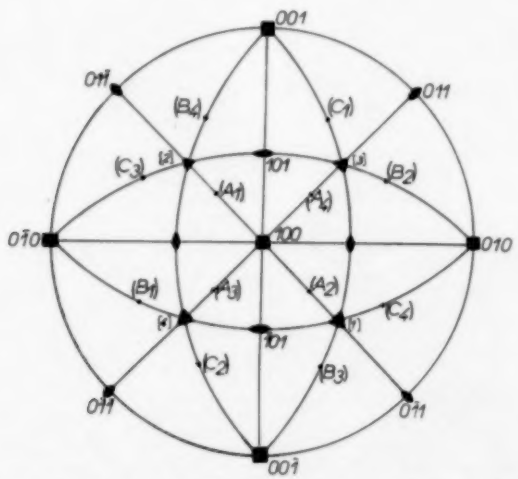

FIG. 21. Positions des douze plans de maclage ; entre crochets sont indiquées les quatre directions.

normalement au plan de maclage, de 30 μ. Elles se forment généralement avant le glissement, le développement de celui-ci gênant le maclage ; les deux éprouvettes Nos. 77 et 63 (en pointillé sur la Fig. 17), qui avaient été prédéformées de 2 pour cent

*Nous avons observé, dans un cas, un décrochement de 2 pour cent sur la courbe de traction, lors de la formation d'une famille de macles, mais la tension était alors suffisante pour que du glissement ait pu intervenir simultanément.

à la température ambiante, se sont allongées, à — 195°, par simple glissement, sans que le maclage apparaisse.

Les éléments de maclage ont été déterminés, pour les plus grosses macles, par leurs traces sur deux faces orthogonales, ou par les figures de corrosion (Fig. 25). Pour les macles fines et très localisées, l'orientation d'une seule trace sur la surface ne permet de les identifier qu'en faisant une hypothèse sur la direction de maclage.

Les macles sont du système $<111>\{112\}$*. Il existe douze telles familles qui sont repérées par leur plan sur la Fig. 21, le chiffre indiquant la direction de maclage correspondante ; des macles appartenant à trois systèmes portant le même numéro ont donc la même orientation. En déterminant les traces des plans conjugués qui coupent le triangle stéréographique de référence, on peut déterminer, en fonction de l'orientation de l'axe de traction, quels sont les systèmes de maclage qui donnent une contraction (SCHMID et BOAS 1935) (Fig. 22) et qui, par suite, ne doivent pas intervenir. Seuls les systèmes *A* donnent un allongement pour toutes les orientations ; aussi, ce n'est pas le système *C*1, qui est le mieux favorisé par la cission, qui intervient en premier, mais le système *A*1. Sur les limites des domaines de la Fig. 22, deux systèmes de maclage conduisent à un allongement nul.

Le tableau 1 suivant indique les systèmes de maclage observés sur quatorze éprouvettes, les macles qui ne semblent pas correspondre à des plans $\{112\}$ n'étant pas indiquées.

TABLEAU 1. *Systèmes de maclage observés*

Nos.					
44	*A*1	*A*2	*A*3	*A*4	Clivage sans glissement
70	*A*1	*A*2			
52	*A*1	*A*2	*A*3		
50	*A*1	*A*2–*C*2*	*A*3–*B*3*		
75	*A*1–*C*1*	*A*2	*A*3	*A*4	
61	*A*1			*B*4*–*C*4	Clivage après glissement
76	*A*1–*B*1				
9	*A*1–*B*1	*A*2	*A*3–*B*3*		Glissement et striction
45	*A*1–*B*1				
55	*A*1–*B*1		*A*3		
21	*A*1–*B*1				
69	*A*1–*B*1			*B*4	
73	*A*1–*B*1				Eprouvettes non rompues
74	*A*1–*B*1	*A*2	*C*3		

*Les systèmes marqués d'un astérisque donnent une contraction.

On remarque que le système le mieux favorisé, *A*1 est toujours entré en action, le système conduisant à la même orientation, *B*1, se développant également quand il donne un allongement, quoiqu'il soit généralement peu favorisé par la contrainte; *B*1 se développerait donc comme un maclage ' d'accommodation.' Pour les orienta-

*Les nombreuses macles observées sur quinze éprouvettes ne correspondent cependant pas toujours à des plans $\{112\}$. Certaines, très faibles, n'appartiennent pas à ce système ; ne pouvant les observer sur deux faces orthogonales de l'éprouvette, nous n'avons pas pu définir le plan avec certitude, mais la zone contenant la normale au plan de maclage passe par une direction $<123>$ et non une direction $<112>$.

tions telles que $B1$ donne une contraction, ou un allongement très faible, ce qui est le cas des cinq premières éprouvettes, divers plans A interviennent.

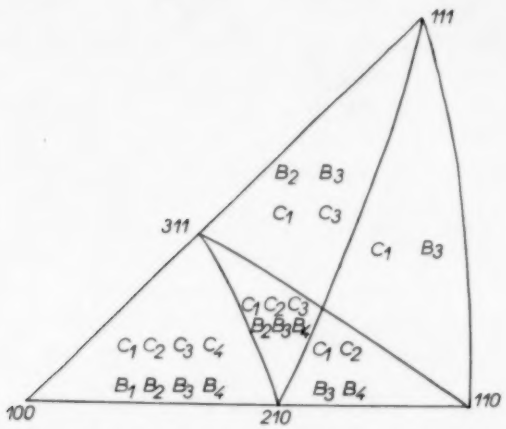

FIG. 22. Systèmes de maclage conduisant à une contraction, en fonction de l'orientation.

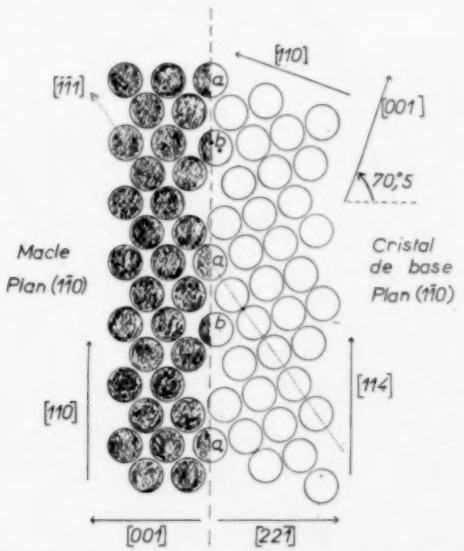

FIG. 26. Accolement de la macle et du cristal de base dans un plan perpendiculaire à une face d'une dent ; la direction perpendiculaire au plan de la figure est $[1\bar{1}0]$ commune aux deux cristaux.

Les atomes marqués a sont communs aux deux réseaux.

Les atomes marqués b ont été légèrement déplacés de leurs positions, marquées d'un point dans chacun des réseaux.

En pointillé est figurée la direction de maclage $[\bar{1}\bar{1}1]$, commune aux deux réseaux.

Un certain nombre de macles correspondent à des contractions ; leur trace ayant été observée après rupture, il est difficile de dire s'il s'agit de macles d'accommodation ou de macles créées par le choc dû au retour du dynamomètre de la

machine de traction au moment de la rupture. Dans le cas des macles dont nous n'avons pas pu définir le plan, il est vraisemblable qu'elles se sont développées pour accommoder des déformations, car elles partent souvent de l'intersection de deux autres macles (Fig. 23).

Aspect des macles. Les macles les plus épaisses présentent généralement un bord droit et l'autre dentelé (Fig. 24), comme si la macle s'élargissait progressivement et que son développement était arrêté en certains points. HULL (1960) a étudié ce phénomène sur des cristaux de fer-silicium très minces (0·05 mm d'épaisseur). Les décrochements correspondant aux faces dents, et qui peuvent atteindre 5 μ sont toujours sur des *plans* $\{100\}$ *de la zone maclée* (Fig. 25) ; dans le cristal non maclé, les plans correspondants sont $\{221\}$; ces deux plans ont une direction commune $< 110 >$, qui est parallèle à la surface dans le cas de la Fig. 25; dans la direction perpendiculaire, il y a accolement le long de directions $< 110 >$ de la macle et $< 114 >$ du cristal ; La Fig. 26 représente l'accolement des deux cristaux qui doit correspondre à un joint de faible énergie. DUNN et LIONETTI (1949) ont mesuré l'énergie de joints analogues dans le fer silicium, c'est à dire de cristaux désorientés par une rotation autour d'une direction $< 110 >$, et ont effectivement observé un minimum d'énergie pour une rotation de 70° 32′, correspondant à la position de macle. Il est à remarquer que l'amorce de fissures créées au joint est dans un plan $\{110\}$ qui n'est pas le plan de clivage.

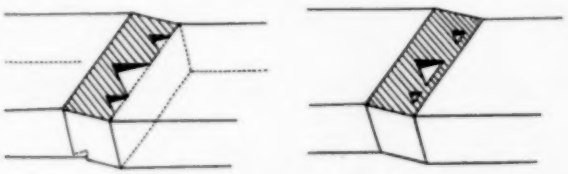

FIG. 27. Schéma d'une macle dentelée : à droite, aspect après un léger polissage.

Mais, en réalité ce joint ne traverse pas toute l'éprouvette : non seulement on n'observe pas la même configuration des dents sur l'autre face mais on s'aperçoit que le bord droit et le bord dentelé de la macle sont inversés, ainsi que l'avait déjà observé HULL. La formation d'une macle créant sur la surface un angle saillant et un angle rentrant, le bord dentelé est, le plus souvent, du côté de l'angle rentrant, conformément à la Fig. 27. Le défaut à la limite de la macle n'intéresse donc pas toute l'épaisseur : si l'on effectue un polissage électrolytique léger, on voit rapidement apparaître le bord extrême de la macle, avant même que l'épaisseur enlevée ait atteint la profondeur du déchaussement (Fig. 27). Il ne s'agit donc que d'un effet de surface et il doit y avoir un autre plan d'accolement entre les cristaux, ou peut-être deux autres plans, le défaut formant un coin sous la surface. Il pourrait alors s'agir des deux autres plans de macle, ayant la même direction de maclage que le système principal, mais nous n'avons pas encore pu le définir. Pour un polissage plus long, le défaut disparaît complètement (Fig. 27 bis.).

A plus grande distance de la surface, les macles ne sont cependant pas limitées par des plans rigoureux : la limite présente encore de nombreux décrochements qui ne semblent pas être fixés par des conditions cristallographiques (Fig. 28).

FIG. 23. Naissance de macles aux intersections de deux autres familles. × 1200.

FIG. 24. Bord dentelé des macles. × 400.

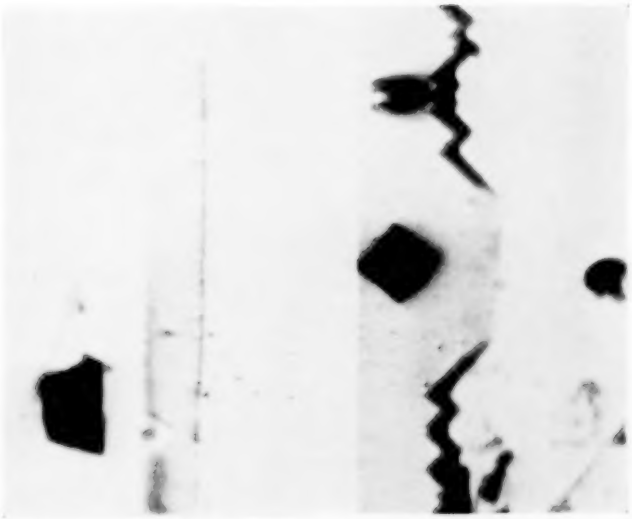

FIG. 25. Figures de corrosion sur une éprouvette maclée : les dents sont parallèles au bord de la figure. × 600.

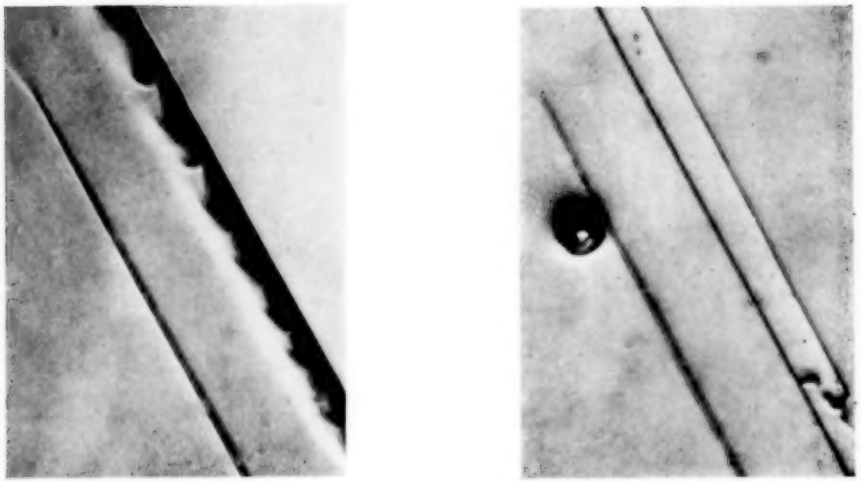

FIG. 27 bis. Macle dentelée; à droite, aspect après polissage. × 700.

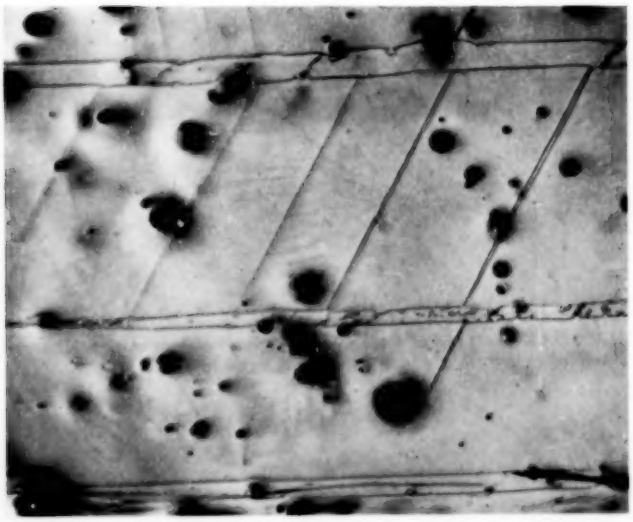

FIG. 28. Discontinuité des macles à l'intérieur de l'éprouvette. × 150.

FIG. 29. Déviation de macles parallèlement à des plans (112) ayant même direction de glissement. × 400.

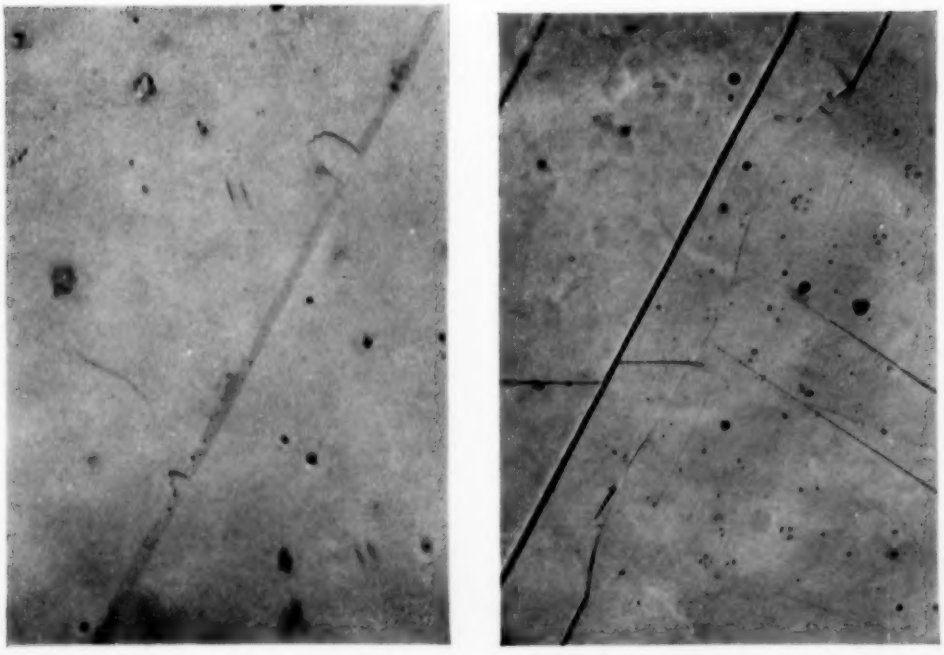

(a) (b)

FIG. 30. Aspects particuliers des irrégularités sur les macles.
(a) × 400 (b) × 300

Enfin, il faut signaler que l'existence de trois systèmes de maclage conduisant à la même orientation fait que l'on peut observer des macles qui changent de plan, en prenant un aspect sinueux (Fig. 29). En plus des décrochements, les macles présentent souvent des aspects très particuliers, dont nous n'avons pas pu définir l'origine (Fig. 30).

(c) *Clivage.* Les cristaux orientés de telle manière que l'axe de traction fasse avec la normale à un plan $\{100\}$ un angle inférieur à 30° se sont rompus par clivage sur ce plan, sans déformation par glissement.

Il faut remarquer que pour ces orientations, le système de maclage $B1$ donne un allongement très faible, ou même négatif, et que l'accommodation des macles principales se fait par maclage sur d'autres plans de la famille A, qui n'ont donc pas la même direction $< 111 >$, ces plans étant les seuls qui donnent un allongement.

L'intersection de ces macles crée des joints de macle du second ordre qui sont responsables du clivage. L'intersection des systèmes $A1$ et $A2$ ou $A3$ et $A4$ est une direction $< 110 >$ du plan de clivage, tandis que les autres types d'intersection donnent une direction commune $< 210 >$ qui n'est pas dans le plan de clivage.

On remarque que tous les cristaux qui se sont clivés étaient maclés sur les deux plans conjugués $A1$ et $A2$. La limite théorique des orientations conduisant au clivage serait donc la zone $[210]\,[311]$ (Fig. 21) ; pratiquement, elle est un peu plus éloignée de $[100]$ (Fig. 17), la contribution du plan $B1$ à la déformation étant nulle sur cette zone. Cette limite est cependant beaucoup moins éloignée que celle donnée par Biggs et Pratt (1958).

Certaines éprouvettes ont un comportement anormal : les Nos. 61 et 76 ont donné une rupture parallèlement au plan (100) après avoir subi respectivement des déformations de 2·5 et 7 pour cent par glissement ; l'orientation particulière du cristal No. 76, près de la zone $[111]\,[110]$ laisse cependant supposer qu'un mécanisme différent est intervenu pour le clivage.

Les éprouvettes Nos. 9 et 74 ont révélé des macles des systèmes $A1$ et $A2$, sans s'être clivées. Dans le cas du No. 9, les macles se sont développées successivement, alors que le glissement était déjà actif ; sur la surface du cristal No. 74, on n'observe pas d'intersection des systèmes $A1$ et $A2$.

Nous reviendrons sur ces mécanismes de maclage et de clivage avec l'étude des contraintes correspondantes.

4. Courbes de Consolidation des Cristaux

(i) *Courbes de cisaillement*

Les cristaux se déformant par glissement sur une surface pour laquelle la cission a la valeur maximale, l'angle moyen de cette surface avec l'axe de traction est le même que l'angle λ entre la direction de glissement et l'axe. La composante de cission effective τ doit alors être reliée à la contrainte de traction σ, corrigée de la réduction de section, par la relation*:

$$\tau = \tfrac{1}{2} \sin 2\lambda.$$

*On peut d'ailleurs voir que si l'orientation moyenne de la surface de glissement change de quelques degrés, le rapport τ/σ ne varie pas sensiblement.

A la limite élastique la cission critique est

$$\tau_0 = \tfrac{1}{2}\,\sigma_0 \sin 2\lambda_0.$$

Dans le domaine plastique, par suite du mécanisme de glissement dans une seule direction, le réseau tourne par rapport à l'axe de traction de telle manière que celui-ci se rapproche de la direction de glissement :

$$d\lambda = -\operatorname{tg}\lambda \cdot \frac{dl}{l}$$

dl/l étant l'allongement. Dans le domaine plastique, le rapport τ/σ ne reste donc pas constant, mais varie suivant la relation :

$$\alpha = \frac{\tau}{\sigma} = \frac{\sin\lambda_0}{1 + (\Delta l/l_0)} \cdot \sqrt{\left\{1 - \frac{\sin^2\lambda_0}{[1 + (\Delta l/l_0)]^2}\right\}}$$

$\Delta l/l_0$ étant alors l'allongement total.

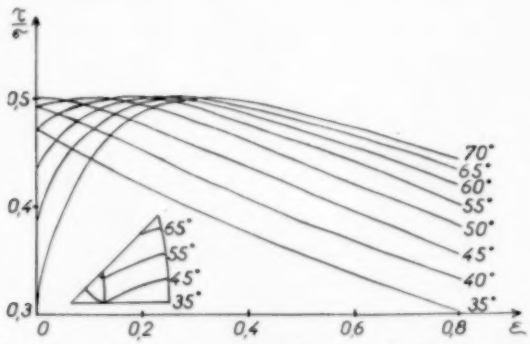

FIG. 31. Variations du rapport de la cission effective à l'effort de traction en fonction de l'allongement, pour diverses valeurs de l'angle initial entre l'axe de la traction et la direction de glissement.

La Fig. 31 représente la variation de α en fonction de l'allongement pour diverses valeurs de l'angle initial λ_0. On remarque que, si λ_0 est supérieur à 45°, le rapport présente un maximum, tandis que s'il est inférieur, la courbe décroît régulièrement.

De même le glissement γ doit être relié à l'allongement, à chaque instant de la déformation, par la relation :

$$d\gamma = \frac{2}{\sin 2\lambda} \cdot \frac{dl}{l}$$

et le glissement total pour un allongement fini $\Delta l/l_0$, rapporté à la longueur initiale du cristal, l_0, est :

$$\gamma = \frac{1}{\sin\lambda_0}\left\{\sqrt{\left[\left(1 + \frac{\Delta l}{l_0}\right)^2 - \sin^2\lambda_0\right]} - \cos\lambda_0\right\}^{*}.$$

L'ensemble de ces deux conditions peut modifier notablement la forme des courbes, en passant des coordonnées effort de traction – allongements aux co-

*Il est à remarquer qu'il n'intervient pas de logarithme népérien dans cette relation qui donne cependant la déformation rationnelle de cisaillement. En effet, les cisaillements simples ne font pas varier la longueur prise pour référence.

ordonnées cission – cisaillement. Notamment, si l'éprouvette est étirée initialement suivant une direction $< 111 >$, qui correspond à $\lambda_0 = 70°$, le rapport $\alpha = \tau/\sigma$ qui est initialement égal à 0·31 passe à la valeur 0·40 pour un allongement

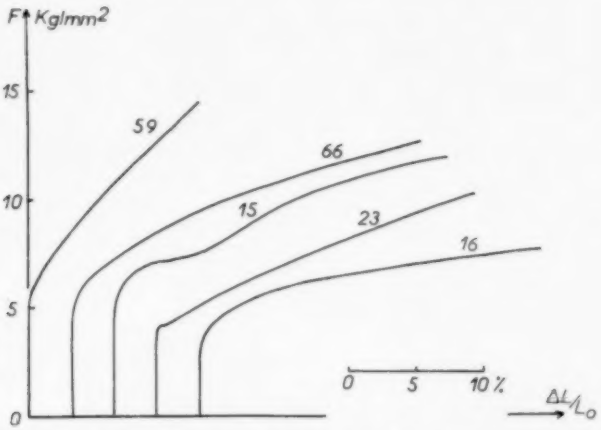

FIG. 32. Forme des courbes de traction à l'ambiante de quelques monocristaux. Les orientations des éprouvettes sont indiquées sur la Fig. 34.

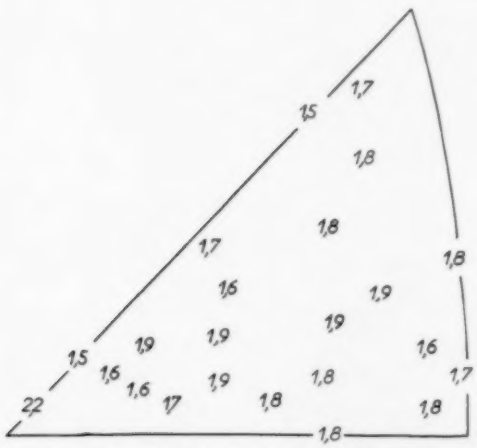

FIG. 33. Valeur de la cission critique à température ambiante pour diverses orientations.

de 5 pour cent. C'est ainsi que les courbes de traction (Fig. 32) peuvent présenter un palier et que l'anomalie disparaît si l'on considère les courbes de cisaillement.

(ii) *Déformations à la température ambiante*

(a) *Cission critique.* La valeur de la cission critique, à la température ambiante, est assez bien définie et l'on peut écrire :

$$\tau_0 = 1{\cdot}7 \pm 0{\cdot}2 \text{ kg/mm}^2.$$

Elle ne varie pas systématiquement avec l'orientation (Fig. 33) ; seule l'éprouvette située près de $< 100 >$ et qui a présenté quatre systèmes de glissement a une limite élastique plus élevée.

Cette valeur est faible relativement à celles qui ont été observées par d'autres expérimentateurs et qui sont indiquées dans le tableau ci-dessous :

TABLEAU 2. *Valeurs de cission critique à 20°C*

Impuretés autre que le carbone (%)	*Carbone* (%)	*Vitesse d'allongement* (%/min)	τ_0 (kg/mm^2)	*Auteur*
~ 0·04	0·0030	0·2	2·1*	PAXTON et CHURCHMAN (1953)
	0·0027		4·1	ALLEN, HOPKINS et MCLENNAN (1956)
	0·0023	1	2·7	STEIJN et BRICK (1954)
	0·0005	0·2	1·5*	PAXTON et CHURCHMAN (1953)
~ 0·18	0·003	0·06	2·1*	PAXTON et BEAR (1955)
	< 0·001	1·5	1·7	Présente étude
~ 0·80	Décarburé sous H_2	0·5	2·8	COX, HORNE et MEHL (1957)
Non précisé		1	4·2	VOGEL et BRICK (1953)

*Valeur relevée sur une seule courbe publiée.

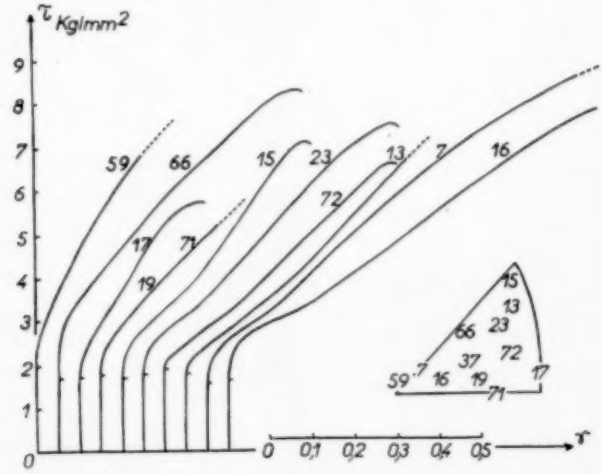

FIG. 34. Courbes de cisaillement de monocristaux de diverses orientations, à température ambiante.

La valeur de la cission critique n'est donc pas seulement affectée par la composition du métal ; il est vraisemblable que le degré de perfection des cristaux, par suite du mode de préparation, varie largement. Les diagrammes de Laue obtenus avec nos cristaux présentaient généralement des taches fines et sans distorsion ; accidentellement, nous avons obtenu des cristaux polygonisés : la cission critique peut alors atteindre 3 kg/mm^2, ce qui montre la forte influence des sous joints sur la limite élastique.

Il faut aussi signaler que la cission critique varie avec la vitesse de déformation. Nous avons utilisé généralement une vitesse d'allongement plastique de 1·5 pour cent/min* ; pour une vitesse 4 fois plus rapide, nous avons obtenu $\tau_0 = 2{\cdot}2$ et pour une vitesse 160 fois plus rapide, (250 pour cent/min), nous avons obtenu, pour trois essais, les valeurs : 2·75, 3·20 et 3·50 kg/mm^2.

Les courbes n'ont jamais présenté de décrochement à la limite élastique, celle-ci correspondant toujours à une lente inflexion à partir du régime élastique.

(b) *Courbes de consolidation plastique.* Après transformation des coordonnées (effort de traction – allongement) en coordonnées (cission – cisaillement dans la direction de glissement), les courbes de déformation des cristaux de fer présentent des aspects comparables.

Après une portion parabolique correspondant à un glissement de l'ordre de 0·05 (Fig. 34) les courbes deviennent sensiblement rectilignes. On remarque cependant qu'elles peuvent être classées en deux groupes : celles qui se trouvent sur les zones symétriques $< 100 > < 111 >$ et $< 100 > < 110 >$ peuvent être considérées comme composées d'une seule droite, tandis que les autres peuvent être décomposées en deux droites, comme les courbes des monocristaux cubiques à faces centrées qui présentent le phénomène du glissement facile. Dans le premier cas, la pente de la courbe varie entre 9 et 16 kg/mm^2 ; dans le second, les pentes sont en moyenne de 6 et 8·5 kg/mm^2.

Il faut remarquer que ces consolidations sont très faibles ; si on les rapporte au module de cission dans la direction de glissement, qui est égal à 6000 kg/mm^2, les plus fortes valeurs correspondent à $\mu/400$, les plus faibles à $\mu/1000$, soit des valeurs beaucoup plus faibles que celles que l'on observe dans le cas des métaux cubiques à faces centrées. Dans ces derniers, en effet, la consolidation est égale à $\mu/200$ dans le cas où il se développe deux systèmes de glissement (Friedel 1955) ; s'il n'y en a qu'un seul, ce qui correspond au glissement facile à l'origine des courbes, la pente est sensiblement moitié, soit $\mu/400$ (Jaoul et Bricot 1955). Le taux de consolidation des cristaux de fer est donc toujours inférieur à celui des cristaux cubiques à faces centrées et si l'on compare le fer à l'aluminium, en se plaçant à des températures équivalentes vis à vis de la température de fusion, on s'aperçoit que ce dernier, qui a une limite beaucoup plus basse, devient par écrouissage relativement plus résistant que le premier (Fig. 35).

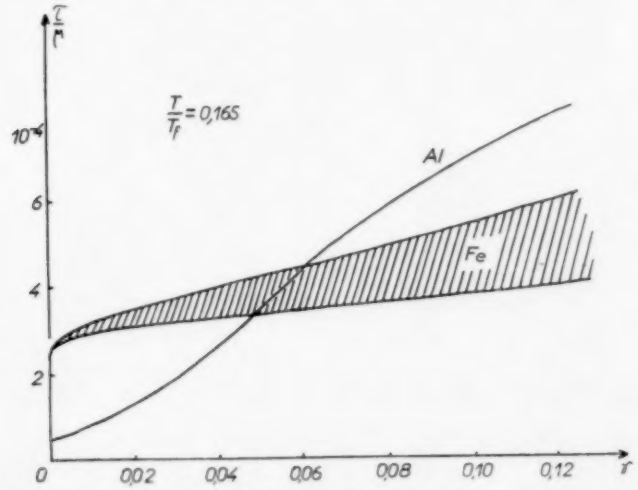

Fig. 35. Comparaison des courbes de traction de monocristaux de fer et d'aluminium à des températures équivalentes.

Les variations du taux de consolidation, représentées sur la Fig. 34 peuvent être interprétées pour les éprouvettes voisines de la zone $< 100 > < 111 >$; nous avons vu en effet que, dans ce cas, deux systèmes intervenaient sous forme de bandes et qu'à la limite de ceux-ci se créait pro-

*Celà ne définit pas la vitesse d'allongement dans le domaine élastique, car le déplacement d'une mordache de la machine est à la vitesse constante imposée, tandis que l'autre est solidaire d'un ressort qui, lui aussi, se déplace.

gressivement un véritable joint par suite des rotations différentes. Par contre, les autres variations sont difficilement explicables : les éprouvettes orientées initialement près de [100] et qui glissent dans la direction [111] ont une consolidation nettement plus faible que les éprouvettes situées au centre du triangle et qui glissent dans la direction $[\bar{1}11]$, ainsi que le montre la comparaison des courbes des éprouvettes Nos. 16 et 23 ; toutes deux se sont déformées avec un seul système dans des conditions géométriques équivalentes, si ce n'est que dans l'éprouvette No. 16 ce n'était pas le système le mieux favorisé qui était actif.

D'autre part, au voisinage de l'orientation [110], les résultats sont très dispersés : des éprouvettes voisines qui, micrographiquement, ont réagi de la même manière ont donné des consolidations variant du simple au double. Celà peut être attribué au développement, dans un cas, de fins glissements secondaires qui gêneraient le glissement principal. Mais, on peut remarquer que l'éprouvette No. 71, située sur la zone $< 100 > < 110 >$ et qui s'est déformée avec deux systèmes ne donne qu'une consolidation de 9 kg/mm^2.

On ne sait donc pas associer les variations de la consolidation avec le développement plus ou moins important de glissements secondaires venant couper le système de glissement principal. Seules les éprouvettes présentant deux systèmes sous forme de bandes subissent une consolidation appréciable ; les autres, en mettant à part des cas inexplicables, ne subissant qu'une consolidation très faible, en moyenne de l'ordre de $\mu/700$.

(c) *Rupture.* Tous les monocristaux déformés suffisamment à la température ambiante ont donné une striction, correspondant à l'instabilité de déformation. Dans certains cas, au cours de l'amincissement localisé, l'éprouvette a subi une rupture brusque, probablement par clivage, sans que celà puisse être défini avec précision, la surface de rupture étant de trop petites dimensions.

(d) *Influence de la vitesse de déformation.* Si la vitesse d'allongement a une influence sur la limite élastique, elle ne semble pas en avoir sur la consolidation : une variation de vitesse en cours de déformation entraîne une modification de la tension appliquée, mais la pente de la courbe n'est pas sensiblement affectée. La Fig. 36 représente la courbe de traction obtenue avec une éprouvette soumise successivement à des allongements aux vitesses de 2·5 et 25 pour cent/min. La courbe oscille entre deux courbes parallèles qui correspondraient chacune à l'une des vitesses réalisées.

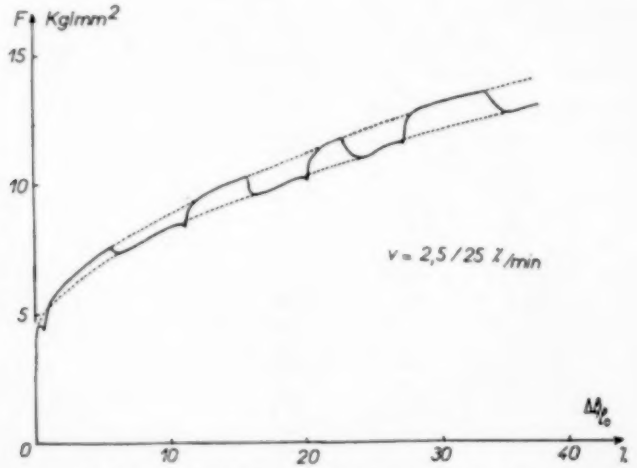

FIG. 36. Influence de la variation de la vitesse au cours de la traction d'un monocristal.

(iii) *Déformations à températures supérieures à l'ambiante*

La cission critique ne varie pas beaucoup quand on augmente la température, par suite des phénomènes de vieillissement (Fig. 37). Le taux de consolidation également ne semble pas être affecté notablement.

Nous avons effectué sur certaines éprouvettes des essais en faisant varier la température de déformation : après un premier allongement à 400 °C, la température était diminuée à 200 °C sans enlever la charge, puis l'essai poursuivi un certain temps avant de passer à 20 °C. Les courbes présentent exactement la même pente après la baisse de température (Fig. 38).

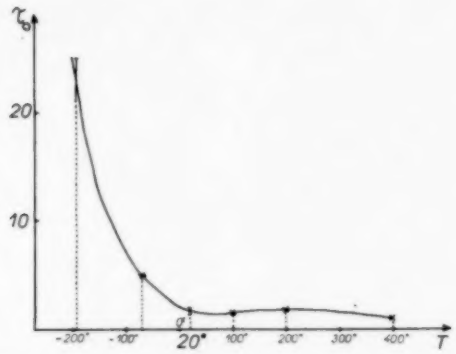

FIG. 37. Variation de la cission critique en fonction de la température.

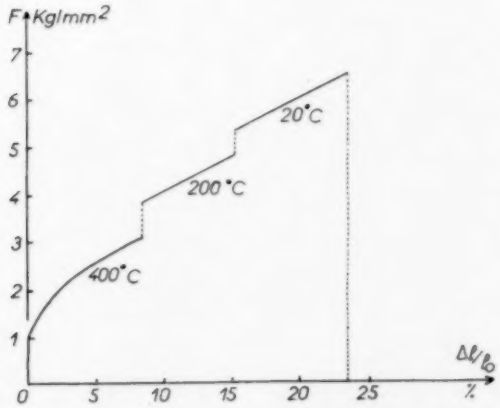

FIG. 38. Influence de la variation de la température sur la forme de la courbe de traction d'un monocristal.

(iv) *Déformations à basse température*

A la température de la glace carbonique, — 80 °C, la cission critique se trouve notablement augmentée, puisqu'elle passe à 5·1 kg/mm². Le taux de consolidation est de l'ordre de 15 kg/mm²*, alors qu'une éprouvette de même orientation étirée à la température ambiante donne 8 kg/mm².

A la température de l'air liquide trois phénomènes interviennent, qui se traduisent par les anomalies que l'on peut observer sur la Fig. 39 représentant les courbes de traction d'éprouvettes ayant subi le maclage et le clivage (No. 50), le maclage et le glissement (No. 9), enfin le glissement seul (No. 41).

*Les glissements observés sur cette éprouvette sont très fins et il est possible qu'un second système de glissement soit intervenu.

Le tableau ci-après réunit les résultats relevés sur les courbes.

TABLEAU 3. *Tensions et cissions critiques à* 195°C

Eprouvette No.	*Rupture*	*Tension de rupture*	*Tensions de maclage*	*Tension critique de glissement*	*Contrainte de clivage sur* (100)	*Cission critique de glissement*	*Cission critique de maclage**
9	Striction	80	44/66/53/57	58	/	24·8	14·5
21	Striction	60	43	56	/	25·1	14
41	Striction	70	/	30	/	21·5	/
42	Non rompue	/	?	45·5	/	23	?
44	Clivage	31	31	/	30	/	15
45	Dans congé	62	28/46/51/53	53	/	25	9
50	Clivage	47	26/30/31	/	41	/	10
52	Clivage	30	22/26/27/28	/	28	/	10
55	Striction	57	39/45/50	49	/	24	13·5
57	Clivage	44	44	/	39	/	20
58	Dans congé	39	39	/	/	/	17
61	Clivage	42	28/34	40	37	20	11·5
62	Dans congé	/	39	/	/	/	13
65	Striction	54	/	49	/	24	/
67	Striction	53	/	46	/	20	/
69	Striction clivage	45	32·5	?	32		10
70	Clivage	35	35	/	31·5	/	16
73	Non rompue	/	50	/	/	/	?
74	Non rompue	/	?	/	/	/	?
75	Clivage	35	35	/	31·5	/	14
76	Striction clivage	49	48	48	34	22	13

*Le premier décrochement observé sur la courbe de traction est supposé correspondre à un maclage sur le plan A_1

La contrainte de clivage, normale au plan (100), varie pour les divers essais entre 28 et 41 kg/mm^2. On peut cependant remarquer que les plus fortes valeurs correspondent aux éprouvettes Nos. 50, 57 et 61, qui se différenciaient des autres par les faits que la première était beaucou p plus épaisse que les autres, la seconde n'avait pas été polie électrolytiquement et la troisième avait

subi un allongement de 2·5 pour cent par glissement. En considérant que la valeur relative à l'éprouvette No. 76 qui s'était déformée par glissement est également un peu forte, on peut définir une contrainte critique de clivage égale à :

$$\sigma_c = 30 \pm 2 \text{ kg/mm}^2$$

normalement au plan (100).

Mais nous avons vu que le clivage était toujours lié à un maclage ; la composante de cission sur le système $A1$ étant environ 0·4 fois la contrainte appliquée, pour les cristaux s'étant clivés, on pourrait aussi dire qu'il existe une contrainte critique de maclage de l'ordre de $(\tau_0)_m = 12 \text{ kg/mm}^2$.

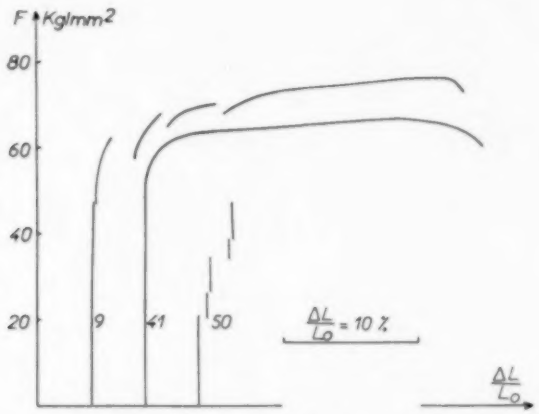

Fig. 39. Forme des courbes de traction à − 195 °C.

Cependant, on remarque que la cission critique de maclage peut varier notablement d'une éprouvette à l'autre : de 9 kg/mm² (ép. No. 45) à 20 kg/mm² (ép. No. 57) ou, en mettant à part les éprouvettes présentant une anomalie, de 10 à 16 kg/mm². Des variations du même ordre ont été observées par Biggs et Pratt (1958) qui ont trouvé des cissions critiques de maclage variant entre 10 et 21 kg/mm².

Il semble donc difficile de pouvoir définir une contrainte critique de maclage. Par contre, la cission critique de glissement varie dans des limites plus étroites :

$$(\tau_0)_g = 22{\cdot}5 \pm 2{\cdot}5 \text{ kg/mm}^2$$

cette valeur étant très élevée par rapport à celle que nous avons observée à la température ambiante : 1·7 kg/mm².

Nous pouvons donc conclure en disant qu'il existe à basse température une cission critique de glissement, mais que la contrainte nécessaire au maclage et, par suite au clivage qui semble en être une conséquence, peut varier dans de plus larges limites. Celà pourrait être dû au fait qu'il existe dans les cristaux des petits germes en position de macle qui peuvent se développer en fonction de leur nombre (puisque les macles d'un même système sont très limitées) et de leur taille (puisque la cission peut varier notablement). Pour les orientations les plus éloignées de [100] où le système $B1$ est possible en traction, ces germes peuvent se développer dans deux directions, tandis que si l'axe de traction est trop voisin de [100], ils ne se développent que dans une direction ; l'accommodation des déformations nécessite alors un second système et celui qui intervient préférentiellement entraîne le clivage. Les tensions pour lesquelles ces germes peuvent se développer sont comprises entre 10 et 16 kg/mm².

La Fig. 39 représente la forme des courbes de consolidation des éprouvettes qui se sont déformées par glissement à la température de l'azote liquide. Comme pour la déformation à 20 °C, les anomalies sur les courbes de traction disparaissent quand on passe en cisaillement (Fig. 40). Après une région parabolique très courte, les courbes sont encore assimilables à des droites, mais la pente est plus élevée qu'à la température ambiante, quoiqu'il ne se soit généralement développé qu'un

seul système de glissement. Le cristal No. 9 qui présente une consolidation nettement plus forte avait subi, avant le glissement un important maclage sur un plan sensiblement perpendiculaire aux glissements qui viennent s'arrêter contre les macles.

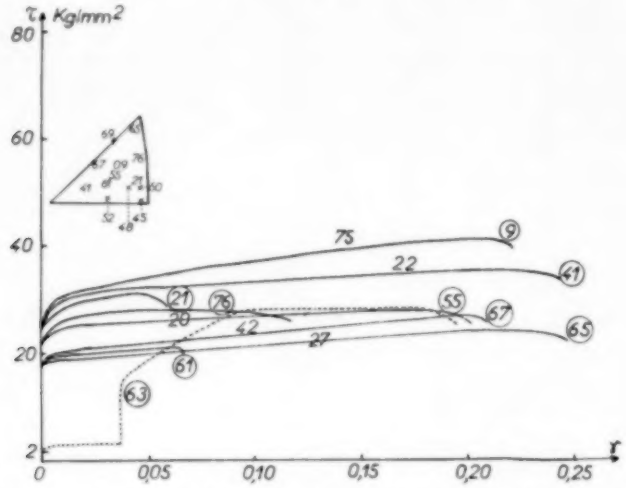

FIG. 40. Forme des courbes de cisaillement à — 195 °C. Sur certaines courbes, la valeur de la pente a été portée.

La striction apparait par instabilité de forme pour des déformations relativement faibles; la tension appliquée étant élevée et la consolidation peu importante, la condition que la pente de la courbe de traction soit égale à la tension appliquée est rapidement atteinte.

5. CONCLUSIONS

L'absence de décomposition des dislocations dans le fer ne permet pas le développement des deux phénomènes responsables de la consolidation dans les cristaux de structure cubique à faces centrées: stabilité des dislocations dans un plan et formation de barrières de Cottrell aux intersections de dislocations.

Effectivement, les glissements sont sinueux et leur orientation moyenne correspond, à la précision de nos mesures, au plan de cission maximale, la direction de glissement étant toujours du type $< 111 >$.

L'absence de formation de barrières aux intersections de glissements ne devrait pas empêcher le développement simultané de deux systèmes de glissement; or, pratiquement, nous n'avons observé un deuxième système que pour des orientations initiales très proches d'une zone symétrique. La rotation du réseau au cours de la déformation n'entraîne pas de glissements secondaires et l'axe du cristal peut traverser largement une zone de symétrie en conservant toujours le même mécanisme de déformation. Il existe donc une consolidation très importante sur les systèmes latents, phénomène probablement dû aux impuretés, comme dans le laiton α ou les alliages d'aluminium.

En fonction de l'orientation, l'aspect micrographique des glissements change peu, à part les cristaux d'orientation voisine de la zone $< 100 > < 111 >$ où deux systèmes se développent sous forme de bandes; l'absence d'intersection

des deux systèmes crée à la limite des bandes des désorientations brusques quis peuvent devenir de véritables joints pour les grandes déformations.

Nous n'avons jamais observé de larges pliages comme dans l'aluminium, mais presque toujours des micropliages correspondant à des zones ayant plus tourné que le cristal : la queue d'astérisme est en effet généralement dirigée vers la direction de glissement

La cission critique est relativement élevée : 1·7 kg/mm², mais le passage du domaine élastique est bien continu et sans décrochement ; par contre, la consolidation reste faible : on peut assimiler grossièrement la courbe de cisaillement à une droite dont la pente est de l'ordre de 8 à 9 kg/mm², soit $\mu/700$, ce qui est inférieur à la consolidation dans le glissement facile de l'aluminium. La consolidation est plus forte pour les cristaux ayant donné des glissements de deux systèmes répartis en bandes (de 13 à 16 kg/mm²), mais ne semble pas augmenter systématiquement quand deux systèmes se développent simultanément. Cette faible pente se conserve jusqu'à l'apparition de la striction due à l'instabilité de forme.

Il est à remarquer qu'une variation de vitesse ou une augmentation de température (jusqu'à 400°) reste sans influence sur la valeur de la consolidation.

A basse température (— 195°C), les glissements présentent toujours beaucoup de sinuosités, mais ont cependant parfois tendance à se stabiliser dans des plans $\{123\}$. A part trois cristaux étirés suivant des orientations voisines, respectivement de $[110]$, $[111]$ et $[112]$, qui se sont déformés par glissement, toutes les éprouvettes se sont toujours maclées sur au moins deux systèmes. Le système principal contient la direction $< 111 >$ la mieux favorisée, et le plan d'accolement est le plan $\{112\}$ tel que la macle corresponde toujours à un allongement ; le second système admet la même direction, quoique la composante de cission pouvant le créer soit très faible, si l'orientation est telle que ce système conduise à un allongement. Il donne, en effet, une contraction si l'axe de traction est proche d'une direction $< 100 >$; c'est alors sur le plan conjugué du système principal que se développent les macles secondaires ; la rencontre de deux macles crée alors un joint du second ordre et, simultanément, apparaît la rupture par clivage sur le plan $\{100\}$ qui passe par une direction $< 110 >$ commune aux deux macles et au cristal. Ce mécanisme se développe si l'éprouvette est étirée suivant un axe faisant moins de 30° avec une direction $< 100 >$.

Chacun de ces systèmes de maclage n'a qu'un développement très limité, quoique les tensions atteintes aient été bien supérieures à celle à laquelle elles se sont formées. D'autre part, on observe souvent un grand nombre de systèmes de maclage, certains correspondant à des plans très peu favorisés par la cission, ou même entraînant une contraction ; il semble donc que les systèmes secondaires doivent être considérés comme des macles d'accomodation et que les portions maclées croissent à partir de germes, pouvant se développer parallèlement à plusieurs plans contenant la même direction $< 111 >$ si le maclage correspondant entraîne un allongement.

Les macles présentent généralement un bord droit (plans $\{112\}$ des cristaux accolés) et un bord dentelé où peuvent se former d'importants déchaussements le long d'un plan $\{110\}$ de la macle et d'un plan $\{221\}$ du cristal, tous deux ayant une direction commune $< 110 >$. Ce type de joint a une énergie relativement faible. Il ne s'agit cependant que d'un phénomène de surface, les dents disparaissant

après un très léger polissage ; d'autre part, ce mécanisme est sans rapport avec le clivage. La cission critique de glissement à $-195°$ est très élevée : 22 kg/mm² et le maclage se développe généralement avant. On ne peut pas définir une cission critique de maclage ; la valeur la plus courante est de 10 à 12 kg/mm², mais des variations importantes sont observées. La contrainte critique de clivage serait de l'ordre de 30 kg/mm², mais sa définition est délicate si l'on admet que le clivage résulte du maclage sur deux plans conjugués.

La consolidation par glissement est plus forte qu'à la température ambiante, mais elle doit être fortement influencée par le maclage antérieur. Par suite du clivage ou de la striction, qui se développe très tôt, la limite élastique étant élevée et la consolidation relativement faible, on ne peut pas atteindre des déformations de grande amplitude par traction.

Les mécanismes de déformation des monocristaux de fer sont donc caractérisés par le petit nombre de systèmes de glissement entrant en action et la faible valeur de la consolidation. Des phénomènes analogues sont observés avec les aggrégats de cristaux ; l'étude de leur consolidation, ainsi qu'une hypothèse sur le mécanisme de formation des bandes de Piobert-Lüders, correspondant au palier des courbes de traction feront l'objet d'un prochain article.

BIBLIOGRAPHIE

ALLEN, N. P.	1959	*J. Iron Steel Inst.* **191**, 1.
ALLEN, N. P., HOPKINS, B. E. et MCLENNAN, J. E.	1956	*Proc. Roy. Soc.* A **234**, 221.
BIGGS, W. D. et PRATT, P. L.	1958	*Acta Met.* **6**, 694.
COX, J. J., HORNE, G. I. et MEHL, R. F.	1957	*Trans. Amer. Soc. Metals* **49**, 118.
DUNN, C. G. et LIONETTI, F.	1949	*J. Met. Trans.* **1**, 125.
FRIEDEL, J.	1955	*Les Dislocations* (Gauthier-Villars, Paris).
	1956	*Phil. Mag.* **46**, 1169.
HULL, D.	1960	*Acta Met.* **8**, 11.
JAOUL, B. et BRICOT, I.	1955	*Rev. Métall.* **52**, 629.
JAOUL, B., BRICOT, I. et LACOMBE, P.	1957	*Rev. Métall.* **54**, 756.
PAXTON, H. W. et BEAR, I. J.	1955	*J. Met. Trans.* **7**, 989.
PAXTON, H. W. et CHURCHMAN, A. T.	1953	*Acta Met.* **1**, 473.
SCHMID, E. et BOAS, W.	1935	*Kristallplastizität* (Springer, Berlin).
STEIJN, R. J. et BRICK, R. M.	1954	*Trans. Amer. Soc. Metals* **46**, 1406.
TAYLOR, G. I. et ELAM, C. F.	1928	*Proc. Roy. Soc.* A **118**, 1.
VOGEL, F. L. et BRICK, R. M.	1953	*Trans. AIME* **197**, 700.

J. Mech. Phys. Solids, 1961, Vol. 9, pp. 39 to 51. Pergamon Press Ltd., London. Printed in Great Britain

TENTATIVE EQUATIONS FOR THE PROPAGATION OF STRESS, STRAIN AND TEMPERATURE FIELDS IN VISCOELASTIC SOLIDS

By S. C. Hunter
Brown University, Providence, R.I.

(*Received 22nd September*, 1960)

Summary

A thermodynamic analysis of the 'thermo-rheologically simple' solid proposed by Schwarzl and Staverman (1952) leads to a set of thermomechanically coupled equations for the propagation of stress, strain and temperature fields in viscoelastic solids. The propagation of harmonic dilational waves is investigated in a linear approximation whose range of validity is ascertained; thermomechanical coupling effects appear to be more severe than for elastic solids.

1. Introduction

The phenomenological theory of linear isothermal viscoelasticity is a rapidly developing field whose current status has been evaluated in a recent monograph by Bland (1960). The present paper is an attempt to remove the isothermal limitation and to obtain a set of equations governing transient stress, strain and temperature fields in viscoelastic solids. The analogous equations for elastic solids have been known for may years and have been the subject of much discussion in the literature; a recent review of dynamic thermoelasticity has been given by Chadwick (1960).

The objects of the present paper entail extending the phenomenological theory of viscoelasticity to include the effects of variation in temperature on the mechanical properties of viscoelastic solids. For this purpose we have adopted the simplest form of the 'thermo-rheologically simple' solid whose compatibility with the experimental characteristics of a wide range of polymeric materials has been amply demonstrated (e.g. see Staverman and Schwarzl 1956, Payne 1958).

The plan of the paper is as follows. A brief review of some pertinent features of isothermal viscoelasticity is given in Section 2(a) while Section 2(b) is concerned with the thermo-rheologically simple solid. The thermo-viscoelastic equations are derived for a single spatial dimension in Section 3 and appropriately generalized in Section 4. Finally, in Section 5, the equations are used to discuss thermomechanical coupling effects in the propagation of periodic disturbances.

2. The Linear Solid

(*a*) *Isothermal behaviour*

We adopt the notation of Hunter (1960a). Measuring strain from a reference equilibrium state at a fixed temperature T, the relation connecting (tensile)

stress, strain and time may be written in either of the forms

$$\sigma = E_D\left(\epsilon - \int_{-\infty}^{t} \dot{\epsilon}\,(t')\,\phi\,(t-t')\,dt'\right), \tag{2.1}$$

$$\epsilon = E_D^{-1}\left(\sigma + \int_{-\infty}^{t} \dot{\sigma}\,(t')\,\psi\,(t-t')\,dt'\right), \tag{2.2}$$

where E_D is the instantaneous dynamic modulus while ϕ and ψ denote respectively normalized relaxation and creep functions. Internal consistency of (2.1), (2.2) is guaranteed by the auxiliary relation

$$\left[1 - s\,\bar{\phi}\,(s)\right]\left[1 + s\,\bar{\psi}\,(s)\right] = 1 \tag{2.3}$$

where $\bar{\phi}$, $\bar{\psi}$ denote Laplace transforms,

$$\text{e.g.} \qquad \bar{\phi}\,(s) = \int_0^\infty e^{-st}\,\phi\,(t)\,dt, \text{ etc.} \tag{2.4}$$

If the viscoelastic behaviour is attributable to a number of relaxation mechanisms, the mechanical properties may be modelled by a (possibly continuous) distribution of springs and dashpots. Under these circumstances ϕ admits the integral representation

$$\phi\,(t) = \int_0^\infty g\,(\tau)\,(1 - e^{-t/\tau})\,d\tau \tag{2.5}$$

where $g > 0$ and where (HUNTER 1960a)

$$\phi\,(\infty) = \int_0^\infty g\,(\tau)\,d\tau \leqslant 1. \tag{2.6}$$

With ϕ given by (2.5) it may be shown that ψ admits a similar representation with the possible addition of a linear creep term,

$$\psi\,(t) = \eta^{-1}\,t + \int_0^\infty f\,(\tau)\,(1 - e^{-t/\tau})\,d\tau \tag{2.7}$$

where

$$\begin{aligned} &\eta^{-1} = 0, \qquad \phi\,(\infty) < 1\,; \\ &\eta^{-1} \neq 0, \qquad \phi\,(\infty) = 1. \end{aligned} \tag{2.8}$$

For the given integral representations (2.5), (2.7), there are infinitely many equivalent spring and dashpot representations.

Less familiar formulae are those for the stored elastic energy and rate of energy dissipation. Defining W as the energy stored by all the springs in any of the spring and dashpot models, and similarly defining Q as the rate of energy dissipation in the dashpots, we have

$$\begin{aligned} W &= (E_D/2)\left[\epsilon^2 - \int_{-\infty}^{t}\int_{-\infty}^{t} \dot{\epsilon}\,(t')\,\dot{\epsilon}\,(t'')\,\phi\,(2t - t' - t'')\,dt'\,dt''\right] \\ &\equiv \sigma\,\epsilon - (2E_D)^{-1}\left[\sigma^2 + \int_{-\infty}^{t}\int_{-\infty}^{t} \dot{\sigma}\,(t')\,\dot{\sigma}\,(t'')\,\psi\,(2t - t' - t'')\,dt'\,dt''\right] > 0, \end{aligned} \tag{2.9}$$

$$\begin{aligned} Q &= E_D \int_{-\infty}^{t}\int_{-\infty}^{t} \dot{\epsilon}\,(t')\,\dot{\epsilon}\,(t'')\,\phi'\,(2t - t' - t'')\,dt'\,dt'' \\ &\equiv E_D^{-1} \int_{-\infty}^{t}\int_{-\infty}^{t} \dot{\sigma}\,(t')\,\dot{\sigma}\,(t'')\,\psi'\,(2t - t' - t'')\,dt'\,dt'' > 0. \end{aligned} \tag{2.10}$$

Essentially equivalent formulae were derived originally by STAVERMAN and SCHWARZL (1952) and were rediscovered independently by BLAND (1960) and the author (1960b). The equivalence of the two forms given for W and Q devolves on the compatibility relation (2.3).

An important feature of (2.9) and (2.10) is that, although their derivation rests on the use of models, the formulae themselves are entirely expressed in terms of the observable quantities ϕ and ψ. In other words, mechanically equivalent spring and dashpot representations are energetically equivalent. This is discussed more fully in the author's paper (1960b).

The energy conservation equation

$$\partial W/\partial t + Q = \sigma\, \dot{\epsilon}\,(t)$$

is readily verified.

The stored energy W defines a (Helmholtz) free energy of deformation (STAVERMAN and SCHWARZL 1952). If we consider a thermodynamic system comprising all the springs but excluding the dashpots in any of the spring and dashpot representations, W is a free energy in the sense of classical thermodynamics, i.e. during an isothermal deformation, the work done on the springs is equal to the increase in W. However, this does not imply that the stored energy can all be turned into useful work since during the extraction process some of the energy is inevitably dissipated in the dashpots.

Energy dissipation is characteristic of viscoelastic solids; thus for any real material we expect to encounter temperature variations during dynamic loading. Under these circumstances we require an extension of the isothermal model discussed immediately above. The simplest extension, consistent with experimental evidence, is that of a thermo-rheologically simple solid proposed by SCHWARZL and STAVERMAN (1952) and discussed in some detail below.

(*b*) *The thermo-rheologically simple solid*

This was introduced to account for the observed mechanical behaviour of polymer materials at different fixed temperatures. Suppose, in any of the spring and dashpot representations discussed in Section 2(a), we assume temperature independent spring moduli but allow all the dashpot viscosities to depend on temperature through a common law

$$\eta\,(T) = \eta\,(T_1) \exp\left[x\,(T_1) - x\,(T)\right] \equiv \eta\,(T_1)\, e^{-\Gamma} \tag{2.12}$$

where

$$\Gamma = x\,(T) - x\,(T_1). \tag{2.13}$$

Then, it is easily seen that the isothermal creep and relaxation functions at different temperatures satisfy the relations

$$\psi\,(T, t) = \psi\,(T_1, te^{\Gamma}), \qquad \phi\,(T, t) = \phi\,(T_1, te^{\Gamma}),$$

while the complex modulus for circular frequency ω satisfies

$$E\,(i\omega, T) = E\,(i\,\omega\, e^{-\Gamma}, T_1). \tag{2.14}$$

In particular, (2.14), leading to the concept of a shift factor Γ on a logarithmic frequency scale (FERRY 1950) is in striking agreement with the experimental evidence (PAYNE 1958).

[We have somewhat oversimplified the theoretical and experimental evidence. There are theoretical reasons, based on the kinetic theory of rubber elasticity, to suppose that, at least for low circular frequencies ω, (2.14) is more correctly written

$$E(i\omega, T) = \frac{\rho(T)\,T}{\rho(T_1)\,T_1} E(i\,\omega\,e^{-\Gamma}, T_1) \tag{2.15}$$

where $\rho(T)$ is the equilibrium density. Whether (2.15) is empirically superior to (2.14) is still a matter of some debate (STAVERMAN and SCHWARZL 1956); in any event $\rho(T)\,T/\rho(T_1)\,T_1$ is a much less temperature sensitive factor than $e^{-\Gamma}$. It is possible to introduce the factor $\rho(T)\,T/\rho(T_1)\,T_1$ into the spring and dashpot models by assuming precisely this temperature dependence for the springs. However, this considerably complicates the ensuing analysis, both in the derivation of the stress – strain – temperature – time relation and in the thermodynamic treatment of the model. For this reason, and because of the relative insignificance and uncertain validity of the factor $\rho(T)\,T/\rho(T_1)\,T_1$, we prefer the simpler model leading to (2.14)].

Following the arguments of LEE and MORLAND (1959), the equations analogous to (2.1), (2.2), but for a thermo-rheologically simple solid subject to temperature variations, take the form

$$\sigma = E_D\left(\epsilon - \int_{-\infty}^{t} \dot{\epsilon}(t')\,\phi(q - q')\,dt'\right), \tag{2.16}$$

$$\epsilon = E_D^{-1}\left(\sigma + \int_{-\infty}^{t} \dot{\sigma}(t')\,\psi(q - q')\,dt'\right), \tag{2.17}$$

where $q(t)$ is a single valued monotonic function of time,

$$q(t) = \int_0^t e^{\Gamma[T(t')]}\,dt' \quad \text{and} \quad q' \equiv q(t')$$

and where $\phi(t)$, $\psi(t)$ denote the relaxation and creep functions at the base temperature T_1.

So far we have neglected the thermal expansion of the solid; in this context it is to be remembered that in the isothermal experimental observations confirming (2.14), the strain is measured from a reference temperature T. In considering different temperatures T it is more convenient to refer the strain to an equilibrium state at a fixed temperature T_1. With $T - T_1 = \theta$, and assuming a linear expansion law, (2.16) and (2.17) become

$$\sigma = E_D\left(\epsilon - \beta\theta - \int_{-\infty}^{t} \left[\dot{\epsilon}(t') - \beta\,\dot{\theta}(t')\right]\phi(q - q')\,dt'\right), \tag{2.18}$$

$$\epsilon - \beta\theta = E_D^{-1}\left(\sigma + \int_{-\infty}^{t} \dot{\sigma}(t')\,\psi(q - q')\,dt'\right), \tag{2.19}$$

where β is the coefficient of linear expansion.

In writing down (2.18), (2.19) it is assumed that in the absence of stress (and stress history), the material strain responds instantaneously with temperature, viz. $\epsilon = \beta\,\theta$.

If the thermal expansion arises from the scattering of phonons by the anharmonic components of an internal potential field (PEIERLS 1955), the assumption seems

not unreasonable for all realistic frequencies lying below the Debye limit. Within the phenomenological framework it is implied that the dashpots are inoperative in respect of thermal strain. If the dashpots are to be associated with frictional forces overcome by the applied stress, again this seems a not unreasonable assumption.

We can calculate the elastically stored energy and energy dissipation rate exactly as in Section 2 (a); the formulae are obvious modifications of (2·9), (2·10):

$$W = (E_D/2)\left[(\epsilon - \beta\theta)^2 - \int_{-\infty}^{t}\int_{-\infty}^{t}\left[\dot{\epsilon}\,(t') - \beta\dot{\theta}\,(t')\right]\left[\dot{\epsilon}\,(t'') - \beta\dot{\theta}\,(t'')\right]\phi\,(2q - q' - q'')\,dt'\,dt''\right]$$

$$\equiv \sigma\,(\epsilon - \beta\theta) - (2E_D)^{-1}\left[\sigma^2 + \int_{-\infty}^{t}\int_{-\infty}^{t}\dot{\sigma}\,(t')\,\dot{\sigma}\,(t'')\,\psi\,(2q - q' - q'')\,dt'\,dt''\right], \tag{2.20}$$

$$Q = E_D\,e^{\Gamma(\theta)}\int_{-\infty}^{t}\int_{-\infty}^{t}\left[\dot{\epsilon}\,(t') - \beta\dot{\theta}\,(t')\right]\left[\dot{\epsilon}\,(t'') - \beta\dot{\theta}\,(t'')\right]\phi'\,(2q - q' - q'')\,dt'\,dt''$$

$$\equiv E_D^{-1}\,e^{\Gamma(\theta)}\int_{-\infty}^{t}\int_{-\infty}^{t}\dot{\sigma}\,(t')\,\dot{\sigma}\,(t'')\,\psi'\,(2q - q' - q'')\,dt'\,dt''. \tag{2.21}$$

From (2.20), (2·21), we have

$$\partial W/\partial t + Q = \sigma\left[\dot{\epsilon}\,(t) - \beta\dot{\theta}\,(t)\right] \tag{2.22}$$

analogous to (2.11).

Subsequently we shall require an expression for the specific internal energy of a viscoelastic solid. We obtain this as follows. It is assumed that the total free energy is given by the stored energy (2.20) (divided by the density) together with a term dependent only on temperature; thus

$$F = W/\rho + A\,(T) \tag{2.23}$$

where $A\,(T)$ measures the free energy in the stress history free state and where the density is a function of the strain i.e. $\rho = \rho\,(\epsilon)$.

For a solid whose free energy is expressed as a function of temperature and strain, we have the formula (Landau and Lifschitz 1958)

$$U = F - T\,\partial F/\partial T \tag{2.24}$$

determining the internal energy per unit mass. However, the first of (2.20) and (2.23) define F as a functional rather than function of strain and temperature and this poses some difficulty in interpreting the derivative $\partial F/\partial T$ appearing in (2.24). If, tentatively, we interpret $\partial F/\partial T$ in the sense

$$\frac{\partial F}{\partial T} = \mathrm{Lt.}_{\Delta\theta\to 0}\frac{\Delta F}{\Delta\theta}$$

where $\Delta\theta$ is an instantaneous increment in temperature (i.e. occurring in such a short time interval that the strain remains constant), we obtain

$$U = W/\rho + \beta T\,\sigma/\rho + G\,(\theta) \tag{2.25}$$

where $$G\,(\theta) = A\,(T) - TA'\,(T)$$

and where we have made use of the constitutive equation (2.18).

Equation (2.25) may be put on a firmer foundation by appeal to the spring and dashpot models. Details of the calculations are given in the author's paper (1960b). Essentially the internal energy of each spring is calculated using (2.24) and the resulting contributions summed; here there is no difficulty in taking the derivative $\partial/\partial T$, since for each spring the free energy is given as a function of temperature and strain in the spring. In the calculation it is assumed that each spring contributes to the thermal expansion; thus the springs are conceived as very real elements with the property of spatial extension.

In the absence of stress history, the internal energy (2.25) reduces to the temperature term $G(\theta)$. For sufficiently small θ we assume the expansion

$$G(\theta) = \text{const.} + s\theta$$

where s, the specific heat at zero pressure, is taken as constant.

3. The Equations for Transient Disturbances

The isothermal propagation of stress and strain in viscoelastic solids is governed by the equation of motion, the strain-displacement relation and either of the constitutive equations (2.1), (2.2)*. These three equations, together with the pertinent boundary conditions, suffice to determine the three unknowns σ, ϵ, u (displacement). With the advent of transient temperature fields into the analysis, (2.1), (2.2) are replaced by (2.18) and (2.19) and we require a fourth equation to accommodate the new variable θ. For many purposes, the additional equation may be taken as the heat conduction equation

$$m\,\partial^2\theta/\partial x^2 = \rho s\dot{\theta} \tag{3.1}$$

where m is the thermal conductivity. Where the use of (3.1) is admissible, $\theta(x, t)$ determined from (3.1), is a known function which when substituted into either of (2.18), (2.19) reduces the problem to solving three equations for the three unknowns σ, ϵ, u.

However, it is known that even for elastic solids (3.1) is not exact and that an improved linear approximation is given by (e.g. see Chadwick 1960)

$$m\,\partial^2\theta/\partial x^2 = \rho s\dot{\theta} + \beta T_1\,\dot{\sigma} \tag{3.2}$$

where the additional term, arising out of a detailed thermodynamic treatment of thermoelasticity, couples the thermal and mechanical modes of behaviour. The quantity $\beta T_1\,\dot{\sigma}$, commonly known as the thermodynamic coupling term, is for most purposes insignificant (see Chadwick and Sneddon 1958, Chadwick 1960).

For viscoelastic solids the situation is more complicated in that deformation is always accompanied by a positive energy dissipation rate Q. The object of the present section is to derive the viscoelastic analogue of (3.2). The relevant equation is provided by the first law of thermodynamics in the form (e.g. see Chadwick 1960)

$$\rho\,DU/Dt = \sigma\,D\epsilon/Dt - \partial H/\partial x \tag{3.3}$$

*For a review of isothermal wave propagation see Hunter (1960a).

where H is the heat flow vector and D/Dt denotes a convective derivative. With the usual laws of heat conduction

$$-\partial H/\partial x = m\,\partial^2\theta/\partial x^2. \tag{3.4}$$

Finally, combining (2.22), (2.25), (3.3) and (3.4) yields

$$m\,\partial^2\theta/\partial x^2 = \rho s\,D\theta/Dt + \beta T\dot{\sigma} - Q \tag{3.5}$$

together with higher order terms. These latter are either cubic functions and functionals in σ, ϵ, u, θ, (and their derivatives) or else quadratic functions multiplied by the (small) parameter βT_1. Within the stated assumptions, (3.5) is correct to the (included) second order terms for a thermo-rheologically simple solid.

Equation (3.5) differs from (3.2) in the appearance of the convective derivative $D\theta/Dt$ (which is readily understandable) and the positive energy dissipation rate Q. In the absence of the thermodynamic coupling term, (3.5) is susceptible to an elementary physical derivation. For, the heat dissipated per unit time in an element dx is $Q dx$ while the heat transferred by conduction out of the element is $-m\,(\partial^2\theta/\partial x^2)\,dx$; the difference of these two quantities is the rate of heat accumulation in the element, i.e. $\rho s\,(D\theta/Dt)\,dx$.

Because of the positive definite nature of the second order functional Q, this term is on a somewhat different footing to the remaining second order terms in (3.5). Indeed in the long run Q may be more significant than the linear terms. For consider the limiting case of a solid with negligible thermal conductivity; an approximate integration of (3.5) for $m = 0$ leads to

$$\rho s\theta = -\beta T_1\,\sigma + \int_0^t Q\,(t')\,dt'$$

and for bounded stress levels (e.g. for periodic stresses), the integral may attain an indefinitely large value.

4. Generalization to Three Dimensions

Generalization of the previous analysis to three dimensions is not difficult. We assume a solid isotropic in respect of both its mechanical and thermal expansion properties. We define the isothermal creep and relaxation functions in shear and dilation as in Hunter (1960a) at a fixed temperature T_1, viz.

$$\psi_s\,(t) \quad \phi_s\,(t), \quad \psi_d\,(t) \quad \phi_d\,(t)$$

and further suppose identical shift factors in shear and dilation*. The constitutive equations take the form

$$s_{ij} = 2\mu_D\,(\gamma_{ij} - \int_{-\infty}^{t} \dot{\gamma}_{ij}\,(t')\,\phi_s\,(q - q')\,dt'), \tag{4.1}$$

$$\sigma_{ii} = (3\lambda_D + 2\mu_D)\,[\epsilon_{ii} - 3\beta\theta - \int_{-\infty}^{t} [\dot{\epsilon}_{ii}\,(t') - 3\beta\dot{\theta}\,(t')]\,\phi_d\,(q - q')\,dt'], \tag{4.2}$$

where s_{ij} and γ_{ij} denote respectively the stress and strain deviators

$$s_{ij} = \sigma_{ij} - \tfrac{1}{3}\,\sigma_{ii}\,\delta_{ij}, \quad \gamma_{ij} = \epsilon_{ij} - \tfrac{1}{3}\,\epsilon_{ii}\,\delta_{ij}.$$

*For present purposes this is not an essential assumption; however, if different shift factors obtain for shear and dilation, the tensile properties do not conform to a simple shift law except in the limiting case where the dilation response is purely elastic.

while λ_D, μ_D are the instantaneous Lamé moduli. Equations (4.1), (4.2) may be inverted to express γ_{ij}, ϵ_{ii} in terms of s_{ij}, ψ_s and σ_{ii}, ψ_d.

The total energy dissipation rate is given by

$$Q = Q_s + Q_d$$

where Q_s is the energy dissipation in shear

$$Q_s = 2\mu_D e^{\Gamma} \int_{-\infty}^{t} \int_{-\infty}^{t} \dot{\gamma}_{ij}(t') \dot{\gamma}_{ij}(t'') \phi_s'(2q - q' - q'')\, dt'\, dt'',$$

and Q_d the energy dissipation in dilation

$$Q_d = (\lambda_D + 2\mu_D/3) e^{\Gamma} \int_{-\infty}^{t} \int_{-\infty}^{t} [\dot{\epsilon}_{ii}(t') - 3\beta\dot{\theta}(t')][\dot{\epsilon}_{ii}(t'') - 3\beta\dot{\theta}(t'')] \phi_d'(2q - q' - q'')\, dt'\, dt''.$$

Formulae for the stored energy W, of no immediate interest, follow similarly.

Finally the modified heat conduction equation is given by

$$m \nabla^2 \theta = \rho s\, D\theta/Dt + \beta T \dot{\sigma}_{ii} - Q. \tag{4.3}$$

5. Stress Wave Propagation in a Linear Approximation

If quadratic functions and functionals are neglected in the constitutive equations (4.1), (4.2), the heat conduction equation (4.3) and in the equations of motion, there remains a linear coupled problem analogous to that for elastic solids (e.g. see Chadwick and Sneddon 1958). In as much that the steady build up of temperature, arising from the dissipative term Q, is neglected in this approximation, the resulting periodic steady state eigenfunctions are not realizable in principle; nevertheless, in practice, for the small stress levels encountered in ultrasonic work, the eigenfunction solutions could be reproduced experimentally for a finite period of time. The eigenfunction solutions are also of interest in the analysis of transient disturbances by the methods of Fourier analysis.

In the absence of thermal effects the general wave problem in viscoelastic solids is solvable in terms of the damped periodic eigenfunctions

$$\xi e^{\pm \alpha(\omega) x + i\omega[t \pm x/c(\omega)]}$$

where the attenuation factor $\alpha(\omega)$ and phase velocity $c(\omega)$ are defined by the equations (Hunter 1960a).

$$\omega/c(\omega) - i\alpha = [\rho\omega^2/M(i\omega)]^{\frac{1}{2}} \equiv k_0(\omega), \tag{5.1}$$

or

$$\alpha c/\omega = \tan(\delta/2), \quad c = (|M|/\rho)^{\frac{1}{2}} \sec(\delta/2), \tag{5.2}$$

where

$$\tan\delta = M_2/M_1.$$

Here M is an appropriate complex modulus with real and imaginary parts M_1 and M_2; for shear waves $M = \mu(i\omega)$, for dilatational waves $M = \lambda(i\omega) + 2\mu(i\omega)$ while for longitudinal waves in bars of small cross section $M = E(i\omega)$. The displacement vector ξ is parallel to the direction of propagation for dilational and longitudinal waves, perpendicular for shear waves.

Solutions of the linearized thermo-viscoelastic equations may be effected similarly; we assume solutions of the form

$$\mathbf{u} = \boldsymbol{\xi}\, e^{i\omega t \pm i\mathbf{k}\cdot\mathbf{r}}, \quad \theta = \theta_0\, e^{i\omega t \pm i\mathbf{k}\cdot\mathbf{r}},$$

and arrive at an algebraic equation for the magnitude of the complex propagation vector $\mathbf{k}$. ($\mathbf{k}$ is complex in the sense that $\mathbf{k} = V\mathbf{a}$ where $\mathbf{a}$ is a real unit vector and V a complex number, e.g. see CHADWICK and SNEDDON 1958).

The dynamics of viscoelastic bodies are still describable in terms of shear and dilational waves and as in the corresponding elastic problem the shear waves are propagated without modification by the thermal coupling. For dilational waves the complex magnitude of $\mathbf{k}$ is determined by the equation

$$J\left[\rho\omega^2 - (\lambda + 2\mu)\,k^2\right]\left[m\,k^2 + i\omega\left\{\rho s - 3\beta^2\,T_1\,(3\lambda + 2\mu)/J\right\}\right] - i\beta^2\,T_1\,(3\lambda + 2\mu)^2\,\omega k^2 = 0 \tag{5.3}$$

in which J is the mechanical equivalent of heat and m, s are measured in conventional units. In this equation λ and μ denote frequency dependent complex moduli.

Equation (5·3) is a quartic in k. Of the four roots, two represent thermal modifications of the mechanical modes described in (5·1) while the remaining pair, which we shall not consider further, describe mechanical modifications of thermal modes of the heat conduction equation. (This point is discussed in detail for elastic solids by CHADWICK 1960).

For reasonable values of the parameters

$$\rho s \gg 3\beta^2\,T_1\,|3\lambda + 2\mu|/J$$

and accordingly we approximate (5.3) by

$$J\left[\rho\omega^2 - (\lambda + 2\mu)\,k^2\right]\left[mk^2 + i\omega\rho s\right] - i\beta^2\,T_1\,(3\lambda + 2\mu)^2\,\omega k^2 = 0. \tag{5.4}$$

If the thermodynamic coupling term $\beta T_1\,\dot{\sigma}_{ii}$ is expressed as a functional of $\epsilon_{ii} - 3\beta\theta$, the approximation is equivalent to neglecting $3\beta\theta$ in comparison with ϵ_{ii}.

We anticipate solutions of (5.4) of the type

$$k = k_0\,(1 + \eta), \quad |\eta| \ll 1, \quad k_0^2 = \rho\omega^2/(\lambda + 2\mu). \tag{5.5}$$

Substituting (5.5) into (5.4) and neglecting terms in η^2 yields

$$\eta = -\frac{\beta^2\,T_1\,(3\lambda + 2\mu)^2}{2\,(\lambda + 2\mu)\,J\rho s\left[1 - im\omega/(\lambda + 2\mu)\,s\right]} \tag{5.6}$$

For all reasonable frequencies $m\omega/|\lambda + 2\mu|\,s \ll 1$; typically for polymethylmethacraylate at room temperature

$$m \simeq 4 \times 10^{-4}\,(\text{cal}/^\circ\text{C cm}) \qquad s \simeq 0{\cdot}5\,(\text{cal}/^\circ\text{C})$$
$$|\lambda + 2\mu| \sim 5 \times 10^{10}\,(\text{dyn/cm}^2) \tag{5.7}$$
$$\text{and} \qquad |\lambda + 2\mu|\,s/m \sim 5 \times 10^{13}\,(\text{sec})^{-1},$$

which is at least of the order of the atomic vibration frequencies. In writing down (5.7) we have made use of the result

$$\lambda + 2\mu = K + 4\mu/3$$

where K, the bulk modulus, is unlikely to vary by more than a small factor over the entire frequency range. Expanding (5.6) gives finally

$$\eta = -\frac{\beta^2 T_1 (3\lambda + 2\mu)^2}{2(\lambda + 2\mu) J\rho s}\left[1 + im\omega/(\lambda + 2\mu)\, s\right] \tag{5.8}$$

for all practically attainable frequencies.

For an elastic solid, where λ and μ are real constants, finite attenuation obtains only by virtue of the term $im\omega/(\lambda + 2\mu)\, s$. For viscoelastic solids however, the quantity $(1 + \eta)$ multiplies an existing complex quantity

$$k_0 = \omega/c - i\alpha$$

and even in the absence of the term $im\omega/(\lambda + 2\mu)\, s$, the isothermal attenuation factor α is modified. In fact, for most frequencies, this modification of the existing α is much more important than the attenuation introduced by $im\omega/(\lambda + 2\mu)\, s$.

As an example, we consider a solid whose dilational behaviour is purely elastic with a real bulk modulus

$$K = \lambda + 2\mu/3$$

independent of frequency. It is convenient to re-write $\lambda + 2\mu$ as

$$\lambda + 2\mu = (K + 4\mu_1/3)(1 + i \tan \delta)$$

where μ_1 and μ_2 are the real and imaginary parts of the shear modulus and where δ is the loss angle appearing in (5.2), i.e. for dilational waves

$$\tan \delta = (4\mu_2/3)/(K + 4\mu_1/3) \ll 1.$$

The above inequality is based on experimental evidence for cross-linked polymers.

In terms of the relatively insensitive real functions of ω

$$Z = 9\beta^2 T_1 K^2/2J\rho s\,(K + 4\mu_1/3) \sim 2 \times 10^{-2}, \tag{5.9}$$

$$\Omega = (K + 4\mu_1/3)\, s/m \sim 5 \times 10^{13}\,(\text{sec})^{-1},$$

equations (5.1), (5.5) and (5.8) lead to the complex propagation vector

$$k = \omega/c^1 - i\alpha^1$$

where the modified phase velocity and attenuation are given by

$$c^1 = c\left\{1 - Z\left[1 + 5 \tan(\delta/2)\, \omega/\Omega\right]\right\}^{-1} + \text{higher order terms in } Z,\ \delta,\ \omega/\Omega,$$

$$\alpha^1 = \alpha\left\{1 - 3Z\left[1 + 8 \tan(\delta/2)\, \omega/3\Omega\right]\right\} + \omega^2 Z/c\,\Omega + \text{higher order terms.}$$

Since $Z \ll 1$, $\delta \ll 1$, while for all reasonable frequencies $\omega/\Omega \ll 1$, these equations are well approximated by

$$c^1 = c(1 + Z),$$

$$\alpha^1 = \alpha(1 - 3Z) + \omega^2 Z/c\Omega, \tag{5.10}$$

so that the effects of thermomechanical coupling in viscoelastic solids are (a) to increase the phase velocity in the ratio $(1 + Z)$, (b) to decrease the existing attenuation in the ratio $(1 - 3Z)$ and (c) to introduce an additional attenuation analogous to that obtaining for an elastic solid. Since

$$\alpha = (\omega/c) \tan(\delta/2)$$

we see that the additional attenuation, in any event small for experimentally realisable values of ω, is negligible compared with $3\alpha Z$ provided

$$\omega/\Omega \ll \tan(\delta/2)$$

which is almost certainly true in the frequency ranges for which most real polymers exhibit significant viscoelastic behaviour. We are led therefore to the curious result that for viscoelastic solids with elastic dilational behaviour, the effects of thermomechanical coupling are to reduce the isothermal attenuation.

This conclusion is verifiable directly since neglecting the second term in (5.10) is tantamount to assuming a vanishing thermal conductivity ; the resulting linearized heat conduction equation is directly integrable and yields

$$\theta = -(3\beta T_1 K/J\rho s)\,\epsilon_{ii}.$$

On substituting this result into the Fourier transform of the constitutive equation relating stress in the direction of propagation to the associated strain, viz.

$$\bar{\sigma} = \lambda(i\omega)(\bar{\epsilon} - 3\beta\bar{\theta}) + 2\mu(i\omega)(\bar{\epsilon} - \beta\bar{\theta}),$$

it is seen that the approximation is entirely equivalent to replacing the complex moduli λ and μ by

$$\lambda(1 + 9\beta^2 T_1 K/J\rho s), \qquad \mu(1 + 3\beta^2 T_1 K/J\rho s).$$

We may now re-work the derivation of the propagation vector directly using equation (5.1). If we remember that the imaginary part of the bulk modulus vanishes, we arrive at

$$c' = c(1 + Z), \qquad \alpha' = \alpha(1 - 3Z),$$

in agreement with the previous results.

Since Z is of order 2×10^{-2}, the effects of thermomechanical coupling are rather more severe than in the corresponding elastic case ; in particular a 6 per cent underestimation of $\alpha \equiv (\omega/c)\tan(\delta/2)$ appears possible.

There is an essential difference for the behaviour of longitudinal waves in bars of small cross section. In an approximation corresponding to that discussed immediately above, we find an increase for both the phase velocity and attenuation,

$$c' = c(1 + Z), \qquad \alpha' = \alpha(1 + Z),$$

where now

$$Z = E_1 \beta^2 T_1/2J\rho s.$$

It remains to investigate the limits of validity of the linear approximation. Over long periods of time the dominant error arises from neglect of the dissipative term Q in the heat conduction equation. For the periodic eigenfunctions under consideration, the persistent generation of heat entails a gradual increase in temperature and limits the number of cycles for which the linear analysis is valid. An inequality for the limiting number of cycles is obtained as follows.

Over long periods of time, the heat conduction equation predicts a temperature

$$\theta = (J\rho s)^{-1} \int_0^t Q dt' \tag{5.11}$$

together with oscillatory terms. For periodic disturbances, the maximum mean value of Q is

$$\bar{Q} \simeq \omega E_2(\omega)\,\epsilon_0^2/2 \tag{5.12}$$

where ϵ_0 is the maximum strain amplitude and where E_2 is defined at the base temperature T_1. From (5.11) and (5.12) the maximum value of θ (averaged over a number of cycles) is

$$\bar{\theta} = \frac{\omega E_2 \epsilon_0^2}{2J\rho s} t \tag{5.13}$$

where t is the duration. The corresponding variation in the real part of the complex modulus is

$$\Delta E_1/E_1 = \left[E_1(\omega e^{\Gamma(\bar{\theta})}) - E_1(\omega)\right]/E_1(\omega)$$

or, since for small values of $\bar{\theta}$ we may write $\Gamma(\bar{\theta}) = \gamma\bar{\theta}$,

$$\Delta E_1/E_1 \simeq \gamma\bar{\theta}\frac{d(\log E_1)}{d(\log \omega)} \simeq \frac{2\gamma\bar{\theta}}{\pi}\tan\delta \tag{5.14}$$

on using a well known approximation (STAVERMAN and SCHWARZL 1956).

For the linear approximation to be valid we require the variation (5.14) to be small compared with the variation implied by the thermomechanical coupling:

$$\frac{2\gamma\bar{\theta}}{\pi}\tan\delta < 2Z. \tag{5.15}$$

Combining (5.9), (5.13) and (5.15) yields for the limiting number of cycles N,

$$N < \frac{\beta^2 T_1}{2\gamma\epsilon_0^2\tan^2\delta}.$$

For polymethylmethacrylate at room temperature $\gamma \simeq 0{\cdot}5\,(°C)^{-1}$, $\beta \simeq 4 \times 10^{-4}\,(°C)^{-1}$, and

$$N < \frac{5 \times 10^{-5}}{\epsilon_0^2\tan^2\delta}.$$

Typically $\tan\delta \sim 10^{-2}$ and the inequality leads to

$$N < 5 \times 10^7$$

for a maximum strain amplitude of $\epsilon = 10^{-4}$ and to

$$N < 5 \times 10^5$$

for $\epsilon = 10^{-3}$.

ACKNOWLEDGMENTS

It is a pleasure to acknowledge the interest and helpful comments of Dr. A. J. STAVERMAN. I am also indebted to the Commonwealth Fund of New York for the award of a Harkness Fellowship during the tenure of which the present work was undertaken.

REFERENCES

BLAND, D. 1960 *Theory of Linear Viscoelasticity* (Pergamon Press, London).

CHADWICK, P. 1960 *Progress in Solid Mechanics*, Vol. 1. (North Holland Publishing Co., Amsterdam).

CHADWICK, P. and SNEDDON, I. N. 1958 *J. Mech. Phys. Solids* **6**, 223.

FERRY, J. D. 1950 *J. Amer. Chem. Soc.* **72**, 3746.

HUNTER, S. C.	1960a	*Progress in Solid Mechanics*, Vol. 1. (North Holland Publishing Co., Amsterdam).
	1960b	Brown University Report NOrd 18594/2.
LANDAU, L. D. and LIFSCHITZ, E. M.	1958	*Statistical Physics* (Pergamon Press, London).
LEE, E. H. and MORLAND, L. W.	1959	Brown University Report NOrd 18594/1.
PAYNE, A. R.	1958	*The Rheology of Elastomers* (Pergamon Press, London).
PEIERLS, R. E.	1955	*Quantum Theory of Solids* (Clarendon Press, Oxford).
SCHWARZL, F. and STAVERMAN, A. J.	1952	*J. Appl. Phys.* **23**, 838.
STAVERMAN, A. J. and SCHWARTZL, F.	1952	*Nederl. Akad. Wetensch. Proc.* **55**, 474.
	1956	*The Physics of High Polymers*, Vol. 4 (Springer, Berlin).

J. Mech. Phys. Solids, 1961, Vol. 9, pp. 32 to 62. Pergamon Press Ltd., London. Printed in Great Britain

AN ELASTIC TREATMENT OF GROUND MOVEMENT DUE TO MINING—II. TRANSVERSELY ISOTROPIC GROUND

By D. S. Berry and T. W. Sales
Department of Mining Engineering, University of Nottingham

(*Received 27th October*, 1960)

Summary

The convergence of roof and floor in an infinitely long excavation is treated as a displacement discontinuity in a transversely isotropic medium. The non-closure, partial and complete closure solutions are found for the infinite medium, and the corresponding results for the semi-infinite medium are derived (the complete closure solution exactly, but the other two only approximately). For a deep enough excavation, the shape of the subsidence curve depends upon only two parameters, functions of the four elastic constants involved. A method of deducing these parameters from a graph of measured subsidence is given, and is illustrated by an example. Good correspondence between measured and theoretical curves is found.

The theory is applicable to the problem of closure of a slit in a large plate.

1. Introduction

In the first paper of this series (Berry 1960) reasons were given for supposing that a treatment based on an identification of an excavation with a discontinuity in displacement (or dislocation) might bear sufficient relation to reality to be useful. In the earlier paper the ground was supposed to be homogeneous and isotropic, but it was shown that as the excavation closed, the ensuing vertical surface displacement tended to a limit which was usually less than that found in actual subsidence in British coalfields. It was concluded that the basic assumptions were not good enough approximations to the truth.

The ground is clearly inhomogeneous, but the difficulties of treating it as such are great. Moreover, not only do the type and degree of inhomogeneity vary from site to site, but it is laborious to discover the constituent strata at any point and even harder to determine their elastic properties. A generally applicable treatment would be impossible. However, if the scale of mining operations is large compared with the thickness of strata and there is comparatively regular stratification, the ground may be looked upon as a *laminated* material which is homogeneous in the large, although inhomogeneous in small portions. It would be reasonable to suppose such a material to have elastic coefficients invariant under rotations about an axis normal to the plane of a lamina, but not under any other rotation: a material of this kind is *transversely isotropic* and is indistinguishable from an *hexagonally aeolotropic* medium under classically small deformations.

In the present paper the plane strain solution is found for partial closure of an infinitely long excavation (considered as a dislocation) lying in a plane normal

to the axis of symmetry of an infinite transversely isotropic medium, using the complex variable formulation given by GREEN and ZERNA (1954). From this result the non-closure and complete closure solutions are easily deduced in the same way as in the isotropic problem. The solution for a half-plane with boundary parallel to the line of the excavation is then given. This solution is exact for complete closure but only approximate otherwise, since the traction condition at the excavation is violated.

For complete closure the surface displacement depends on the four elastic constants of two-dimensional transverse isotropy by way of only two parameters. A method is found for deducing values of these parameters appropriate to a given subsidence curve, on the assumption that closure is nearly complete. The method does not of course lead to the determination of all four elastic constants, but for some purposes it may be sufficient to know the two parameters only.

The parameters have been determined for an actual example, and good correspondence between the theoretical curve and the subsidence profile has been obtained. Further investigation has shown that this particular observed profile is attributable to any degree of closure of the excavation: the choice of the two parameters is virtually unaffected by the state of closure assumed. The calculated convergence of roof and floor is less than two-fifths of the thickness of extraction. It is unlikely that the excavation has remained actually unclosed, but rather that the *effective* convergence is diminished by packing and, even more, by large quantities of broken rock between the nearest undamaged strata above and below the excavation. In an elastic model it is the convergence of these undamaged strata which decide the displacement of the rocks beyond.

The results of this paper have an application outside the present context. The closure of a suitably oriented slit in a large transversely isotropic or orthotropic *plate* is essentially the same problem, varying only in the relations between the elastic constants and the parameters appearing in the solution.

2. General Solution for Plane strain

The stress–strain relations for transverse isotropy with the x_2-axis as the axis of symmetry can be written

$$\left.\begin{aligned} E_1 e_{11} &= t_{11} - \nu_2 t_{22} - \nu_1 t_{33}, \\ E_1 e_{22} &= -\nu_2 t_{11} + (E_1/E_2)\, t_{22} - \nu_2 t_{33}, \\ E_1 e_{33} &= -\nu_1 t_{11} - \nu_2 t_{22} + t_{33}, \\ 2Me_{23} &= t_{23}, \\ E_1 e_{13} &= (1+\nu_1)\, t_{13}, \\ 2Me_{12} &= t_{12}, \end{aligned}\right\} \qquad (1)$$

where $e_{ij} = \frac{1}{2}(\partial u_i/\partial x_j + \partial u_j/\partial x_i)$, E_1 and E_2 are Young's moduli, ν_1 and ν_2 are Poisson's ratios, and M is a shear modulus, defined as in Fig. 1.

For the discussion of plane strain in the $x_1 x_2$ plane, we put $e_{33} = e_{13} = e_{23} = 0$ in (1) and eliminate t_{33}. The result may be expressed in suffix notation in the form

$$e_{\alpha\beta} = s_{\alpha\beta}^{\lambda\mu}\, t_{\lambda\mu}, \qquad \alpha, \beta, \lambda, \mu = 1, 2, \qquad (2)$$

where

$$\left.\begin{aligned} s_{11}^{11} &= (1-\nu_1^2)/E_1, & s_{22}^{22} &= 1/E_2 - \nu_2^2/E_1, \\ s_{11}^{22} &= -\nu_2(1+\nu_1)/E_1, & s_{12}^{12} &= 1/4\,M, \\ & & s_{11}^{12} &= s_{22}^{12} = 0, \end{aligned}\right\} \tag{3}$$

with the usual relations of the form $s_{\alpha\beta}^{\lambda\mu} = s_{\alpha\beta}^{\mu\lambda} = s_{\beta\alpha}^{\lambda\mu} = s_{\beta\alpha}^{\mu\lambda} = s_{\lambda\mu}^{\alpha\beta}$. The plane-strain equations for an *orthotropic* material having the $x_1\,x_2$ plane as a plane of elastic symmetry take the same form as those of transverse isotropy, although the non-zero $s_{\alpha\beta}^{\lambda\mu}$ cannot be expressed in terms of the moduli and Poisson's ratios appropriate to transverse isotropy, as in (3). This similarity permits the use of some results on orthotropic materials given by GREEN and ZERNA (1954).

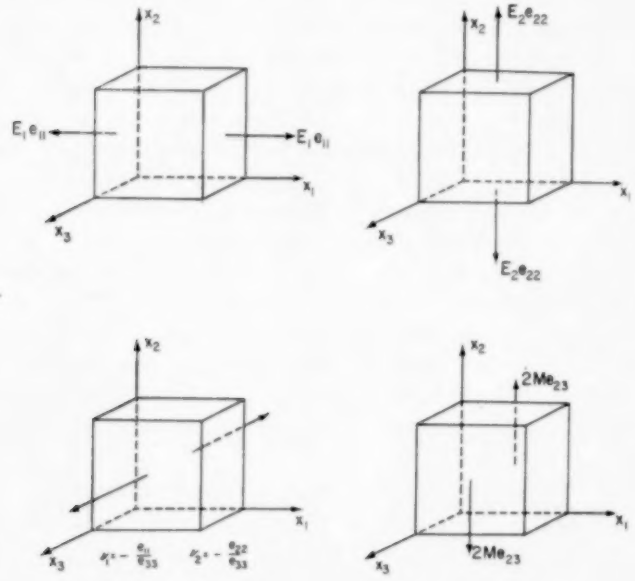

FIG. 1. Definitions of E_1, E_2, ν_1, ν_2, M.

The general plane strain solution for any aeolotropic material can be expressed in terms of analytic functions of two complex variables as follows:

$$\left.\begin{aligned} u + iv &= \delta_1\,\Omega'(z_1) + \rho_1\,\bar{\Omega}'(\bar{z}_1) + \delta_2\,\omega'(z_2) + \rho_2\,\bar{\omega}'(\bar{z}_2), \\ \sigma_x + \sigma_y &= 4\gamma_1\,\Omega''(z_1) + 4\bar{\gamma}_1\,\bar{\Omega}''(\bar{z}_1) + 4\gamma_2\,\omega''(z_2) + 4\bar{\gamma}_2\,\bar{\omega}''(\bar{z}_2), \\ \sigma_x - \sigma_y + 2i\tau_{xy} &= -4\gamma_1^2\,\Omega''(z_1) - 4\bar{\Omega}''(\bar{z}_1) - 4\gamma_2^2\,\omega''(z_2) - 4\bar{\omega}''(\bar{z}_2), \end{aligned}\right\} \tag{4}$$

where (x, y) replaces (x_1, x_2). (u, v) are the corresponding components of displacement, and

$$z_j = 2(\alpha_j x + i\,y)/(\alpha_j + 1), \qquad j = 1, 2. \tag{5}$$

The constants α_i, γ_i, δ_i, ρ_i $(j = 1, 2)$ are functions of the elastic constants, which,

for orthotropy and transverse isotropy are given by

$$\left.\begin{aligned} &\delta_j = \frac{2(\alpha_j \beta_k - \beta_j)}{\alpha_j + 1}, \qquad \bar{\rho}_j = \frac{2(\alpha_j \beta_k + \beta_j)}{\alpha_j + 1}, \qquad k \neq j; \\ &\gamma_j = (\alpha_j - 1)/(\alpha_j + 1), \qquad \beta_j = s_{11}^{22} - s_{22}^{22} \alpha_j^2; \end{aligned}\right\} \tag{6}$$

and those two roots, α_j, of

$$s_{22}^{22} \alpha^4 - 2(s_{11}^{22} + 2s_{12}^{12}) \alpha^2 + s_{11}^{11} = 0 \tag{7}$$

which are either (i) complex conjugates with positive real parts or (ii) real and positive. The conditions imposed on the $s_{\alpha\beta}^{\lambda\mu}$ by the positive definite character of the strain energy are such that (7) always has roots of one of these two types. In equations (4)–(7) the notation is that of GREEN and ZERNA, but some of the definitions have been expressed differently.

3. INFINITE MEDIUM

In partial closure the roof and floor are supposed to meet over the part $|x| \leqslant b$ of an excavation occupying the interval $|x| < a$ of the line $y = 0$. If the normal component of primitive stress is $-p$, the induced stress must exert a normal traction p in the intervals $b \leqslant |x| < a$ of $y = 0$. The displacement and induced stress must be zero at infinity. Since we do not require the solution for *adhesive* contact at $z = \pm b$, σ_y must be bounded at those points. On $y = 0$ the conditions of displacement discontinuity and traction are

$$\begin{aligned} &\Delta v = -t, \qquad |x| \leqslant b; \qquad \Delta v = 0, \qquad |x| > a; \\ &\sigma_y = p, \qquad \tau_{xy} = 0, \qquad b \leqslant |x| < a. \end{aligned}$$

The symmetry of the problem ensures, in fact, that $\tau_{xy} = 0$ on the whole of $y = 0$. When that is so the formulation of the problem can be simplified considerably, and we can write

$$\left.\begin{aligned} \Omega(z_1) &= \frac{\alpha_1}{\alpha_1 - \alpha_2} H(\zeta_1), \\ \omega(z_2) &= -\frac{\alpha_2}{\alpha_1 - \alpha_2} H(\zeta_2), \\ \zeta_j &= \frac{\alpha_j + 1}{2\alpha_j} z_j = x + \frac{iy}{\alpha_j}. \end{aligned}\right\} \tag{8}$$

The function $H(\zeta_j)$ will be regular in the ζ_j plane cut along the interval $|x| < a$ of $y = 0$ and its complex conjugate is defined so that $\overline{H}(x) = H(x)$ outside that interval.

By an elaboration of the method of GREEN and ZERNA for linear cracks the solution of the present problem is found to be

$$H'(\zeta) = \tfrac{1}{2} p \int_{\infty}^{\zeta} \left[1 - (q^2 - b^2)^{\frac{1}{2}} (q^2 - a^2)^{-\frac{1}{2}}\right] dq \tag{9}$$

with the condition

$$t/2\, a\, p\, S = E(k) - (b^2/a^2) K(k), \tag{10}$$

$$S = s_{22}^{22} (\alpha_1 + \alpha_2), \tag{11}$$

where $k = (1 - b^2/a^2)^{\frac{1}{2}}$ and $K(k)$, $E(k)$ are the complete elliptic integrals of the first and second kinds respectively. The condition (10) is obtained in the same way as the similar condition in the isotropic problem (Berry 1960) and, in fact, reduces easily to the latter when the extra relations appropriate to isotropy are imposed on the constants of transverse isotropy, giving $S = (1 - \nu)/\mu$.

As in the isotropic treatment the non-closure solution is obtained from (9) by putting $b = 0$, when the integration can be performed with the result

$$H'(\zeta) = \tfrac{1}{2} p \left[\zeta - (\zeta^2 - a^2)^{\frac{1}{2}}\right]. \tag{12}$$

The complete closure solution is found by letting $b \to a$ and hence, from (10), $t/a\,p\,S \to 0$, with the result

$$H'(\zeta) = \frac{t}{4\pi S} \log \frac{\zeta + a}{\zeta - a}, \tag{13}$$

where S is given by (11). There is non-closure or partial closure according as $t/2\,a\,p\,S \gtrless 1$, with point contact at equality.

4. Half-Plane

In Section 3 the function $H(\zeta)$ represented a displacement discontinuity in an infinite medium, located on $y = 0$. In this section we give the complex potentials representing the same discontinuity located on $y = -h$, with a traction-free boundary at $y = 0$. From a more general result given by Green and Zerna there follow the expressions

$$\Omega(z_1) = f(\zeta_1), \qquad \omega(z_2) = g(\zeta_2), \tag{14}$$

where

$$\left.\begin{aligned} f(\zeta) &= \frac{\alpha_1}{\alpha_1 - \alpha_2}\left[H(\zeta + ih_1) - \right. \\ &\qquad \left. - \frac{(\bar{\alpha}_1 + \alpha_2)\,\overline{H}(\zeta - i\bar{h}_1) - (\alpha_2 + \bar{\alpha}_2)\,\overline{H}(\zeta - i\bar{h}_2)}{\bar{\alpha}_1 - \bar{\alpha}_2}\right], \\ g(\zeta) &= -\frac{\alpha_2}{\alpha_1 - \alpha_2}\left[H(\zeta + ih_2) + \right. \\ &\qquad \left. + \frac{(\alpha_1 + \bar{\alpha}_2)\,\overline{H}(\zeta - i\bar{h}_2) - (\alpha_1 + \bar{\alpha}_1)\,\overline{H}(\zeta - i\bar{h}_1)}{\bar{\alpha}_1 - \bar{\alpha}_2}\right], \\ h_j &= h/\alpha_j, \quad j = 1, 2, \end{aligned}\right\} \tag{15}$$

which, with (4), form the solution for a given discontinuity in the half-plane.

As with the isotropic medium this result is not accurate for partial closure or non-closure, with function (9) or (12) respectively, since the introduction of a traction-free boundary has upset the original traction conditions at the discontinuity. Nevertheless, if h/a is large enough, the departure of the calculated traction from the specified value of $\sigma_y + i\,\tau_{xy} = p$ on $b \leqslant |x| < a$ of $y = -h$ will be small in comparison, being of the order of pa^2/h^2. The discrepancy depends upon the elastic constants and an estimate of its size is difficult to make unless they are given numerically.

For complete closure, with the function (13), the half-plane solution given by (4), (14) and (15) is an exact one, since the conditions on $y = -h$ are now $\Delta v = -t$ in $|x| < a$, $\Delta v = 0$ in $|x| > a$ and there is no traction condition.

In the rest of this paper we shall chiefly be concerned with the displacement on $y = 0$. This may be expressed most succinctly in the form

$$(u + iv)_0 = -2s_{22}^{22}\frac{\alpha_1 + \alpha_2}{\alpha_1 - \alpha_2}\left[\alpha_1(\alpha_2 - 1)H'(x + ih_1) + \alpha_1(\alpha_2 + 1)\overline{H}'(x - ih_1) - \right.$$
$$\left. - \alpha_2(\alpha_1 - 1)H'(x + ih_2) - \alpha_2(\alpha_1 + 1)\overline{H}'(x - ih_2)\right]. \quad (16)$$

When the function (13), characteristic of complete closure, is substituted in (16) we find that

$$(u + iv)_0 = -\frac{t}{2\pi(\alpha_1 - \alpha_2)}\left[\alpha_1(\alpha_2 - 1)\log\frac{x + a + ih_1}{x - a + ih_1} + \right.$$
$$+ \alpha_1(\alpha_2 + 1)\log\frac{x + a - ih_1}{x - a - ih_1} - \alpha_2(\alpha_1 - 1)\log\frac{x + a + ih_2}{x - a + ih_2} -$$
$$\left. - \alpha_2(\alpha_1 + 1)\log\frac{x + a - ih_2}{x - a - ih_2}\right]. \quad (17)$$

Here the surface displacement depends upon the elastic constants through the α_j alone. When the $\alpha_j \to 1$, expression (17) tends to the result for an *isotropic* medium given in the previous paper (Berry 1960), where it was noted that the surface displacement is completely independent of the isotropic constants. The condition $\alpha_1 = \alpha_2 = 1$ does not restrict the result to the isotropic medium, since the four relevant elastic constants are thereby subjected to only two restrictions, which by virtue of (7) may be written $s_{11}^{11} = s_{22}^{22} = s_{11}^{22} + 2s_{12}^{12}$.

Greater importance is attached here to the *vertical* displacement since it is the most reliable ground movement measurement. For complete closure we find from (17) that there are two different expressions for v_0 according to whether the α_j are real or complex. In order to avoid complex quantities, two new parameters, k_1 and k_2, are introduced, such that

$$\left.\begin{aligned} k_1 &= \alpha_1\alpha_2 = \bar{\alpha}_1\bar{\alpha}_2 = (s_{11}^{11}/s_{22}^{22})^{\frac{1}{2}} \\ &= (1 - \nu_1^2)^{\frac{1}{2}}(E_1/E_2 - \nu_2^2)^{-\frac{1}{2}}, \\ k_2 &= \tfrac{1}{2}(\alpha_1^2 + \alpha_2^2) = \tfrac{1}{2}(\bar{\alpha}_1^2 + \bar{\alpha}_2^2) = (s_{11}^{22} + 2s_{12}^{12})/s_{22}^{22} \\ &= \left[E_1/2M - \nu_2(1 + \nu_1)\right](E_1/E_2 - \nu_2^2)^{-1}, \end{aligned}\right\} \quad (18)$$

by means of (7) and (3). Thus k_1 is always positive; when the α_j are real $k_2 > k_1$, but when the α_j are complex $-k_1 < k_2 < k_1$. The expressions are

A. $\underline{0 < k_1 < k_2}$

$$-\frac{2\pi}{t}v_0(x) = \left(\frac{k_1 + k_2}{k_2 - k_1}\right)^{\frac{1}{2}}\left\{\tan^{-1}\frac{2^{\frac{1}{2}}(k_2 - k_1)^{\frac{1}{2}}h(a + x)}{h^2 + k_1(a + x)^2} + \right.$$
$$\left. + \tan^{-1}\frac{2^{\frac{1}{2}}(k_2 - k_1)^{\frac{1}{2}}h(a - x)}{h^2 + k_1(a - x)^2}\right\} +$$
$$+ \tan^{-1}\frac{2^{\frac{1}{2}}(k_1 + k_2)^{\frac{1}{2}}h(a + x)}{h^2 - k_1(a + x)^2} + \tan^{-1}\frac{2^{\frac{1}{2}}(k_1 + k_2)^{\frac{1}{2}}h(a - x)}{h^2 - k_1(a - x)^2}; \quad (19)$$

B. $\underline{-k_1 < k_2 < k_1}$

$$-\frac{2\pi}{t}v_0(x) = \tfrac{1}{2}\left(\frac{k_1+k_2}{k_1-k_2}\right)^{\frac{1}{2}}\left\{\log\frac{(k_1+k_2)(a+x)^2+\left[2^{\frac{1}{2}}h+(k_1-k_2)^{\frac{1}{2}}(a+x)\right]^2}{(k_1+k_2)(a+x)^2+\left[2^{\frac{1}{2}}h-(k_1-k_2)^{\frac{1}{2}}(a+x)\right]^2}+\right.$$

$$\left.+\log\frac{(k_1+k_2)(a-x)^2+\left[2^{\frac{1}{2}}h+(k_1-k_2)^{\frac{1}{2}}(a-x)\right]^2}{(k_1+k_2)(a-x)^2+\left[2^{\frac{1}{2}}h-(k_1-k_2)^{\frac{1}{2}}(a-x)\right]^2}\right\}+$$

$$+\tan^{-1}\frac{2^{\frac{1}{2}}(k_1+k_2)^{\frac{1}{2}}h(a+x)}{h^2-k_1(a+x)^2}+\tan^{-1}\frac{2^{\frac{1}{2}}(k_1+k_2)^{\frac{1}{2}}h(a-x)}{h^2-k_1(a-x)^2}. \quad (20)$$

As with the isotropic medium it is possible to find a general expansion for the surface displacement valid for h/a large. If A is the area of the displacement discontinuity in the infinite medium, the expansion may be written

$$(u+iv)_0 = -\frac{2^{\frac{1}{2}}Ah^2(k_1+k_2)^{\frac{1}{2}}(k_1x+ih)}{\pi(k_1^2x^4+2k_2h^2x^2+h^4)}\left[1+O(a^2/h^2)\right]. \quad (21)$$

The value of A increases steadily with $ps_{22}^{22}(k_1+k_2)^{\frac{1}{2}}$ until complete closure is reached, and is given by

(i) Non-closure

$$A = 2^{\frac{1}{2}}\pi pa^2 s_{22}^{22}(k_1+k_2)^{\frac{1}{2}}, \quad (22a)$$

(ii) Partial closure

$$A = 2^{\frac{1}{2}}\pi p(a^2-b^2)s_{22}^{22}(k_1+k_2)^{\frac{1}{2}}, \quad (22b)$$

(iii) Complete closure

$$A = 2at. \quad (22c)$$

In (21) the term of order a^2/h^2 conceals the discrepancy due to the disturbance of the traction condition at the discontinuity by the introduction of a traction-free boundary on $y = 0$.

In the next Section we shall require the expansion for v_0 developed to the second term. The result is

$$v_0(x) = -\frac{2^{\frac{1}{2}}Ah^3(k_1+k_2)^{\frac{1}{2}}}{\pi(k_1^2x^4+2k_2h^2x^2+h^4)}\left[1+\frac{3a^2+b^2}{h^2}\delta(x)+O\left(\frac{a^4}{h^4}\right)\right], \quad (23)$$

where

$$\delta(x) = \frac{5k_1^4h^2x^6+9k_1^2k_2h^4x^4+3(2k_2^2-k_1^2)h^6x^2-k_2h^8}{6(k_1^2x^4+2k_2h^2x^2+h^4)^2}, \quad (24)$$

and $b = 0$ for non-closure, $b = a$ for complete closure. Excluding complete closure, (23) is accurately true only for a prescribed displacement discontinuity on $y = -h$ equal to that found in the *infinite* medium under the original conditions: in the half-plane the second term cannot be expected to be of much value unless closure is nearly complete. The expression (24) is bounded for permissible values of k_1 and k_2; but, if k_2 is allowed to take the limiting value $-k_1$, $\delta(x)$ is infinite at $x = \pm k_1^{-\frac{1}{2}}h$. Hence, if actual bounds are required, they must pertain to a range of values of k_2 excluding the neighbourhood of $-k_1$. As an example, when $k_2 \geqslant 0$, the following inequalities hold:

$$-3^{\frac{1}{2}}k_2 \leqslant 12\,\delta \leqslant 5k_1+2k_2.$$

This is not a best possible result.

5. Determination of the Two Parameters

This Section is concerned with the development and an application of a method of determining k_1 and k_2 from given subsidence curves. It is supposed that h/a is large enough to make the first term of (23) a fair approximation, the second term being used, if necessary, to improve the result, on the assumption that it is reasonably accurate. In any particular application the validity of the results must be tested afterwards.

From (23)

$$v_0(x)/v_0(0) = V(x)\left[1 + O(a^2/h^2)\right] \tag{25}$$

where

$$V(x) = -\left[k_1^2 (x/h)^4 + 2k_2 (x/h)^2 + 1\right]^{-1}. \tag{26}$$

Then, simple calculations show that

$$\left.\begin{aligned} k_1 &= \frac{h^2}{x_1^2}\left[2x\frac{dV}{dx} - 1\right]^{\frac{1}{2}}_{x=x_1}, \\ k_2 &= \frac{h^2}{x_1^2}\left[1 - x\frac{dV}{dx}\right]_{x=x_1}, \end{aligned}\right\} \tag{27}$$

where $\pm x_1$ are the points such that $V(x_1) = \frac{1}{2}V(0) = \frac{1}{2}$. By these formulae estimates of k_1 and k_2 may be made from a suitable curve of $v_0(x)/v_0(0)$ drawn from actual subsidence measurements. If this curve corresponds closely with a graph of $V(x)$ using the estimated k_1 and k_2, it indicates that the rest of the terms in the expansion are probably negligible, but the magnitude of the second term of (23) should be investigated in any event. However, if the two curves do not nearly coincide, the estimates of k_1 and k_2 must certainly be modified.

It is convenient to proceed at first on the supposition that closure is practically complete, so that expressions (19) or (20), and (23) and (24) hold. From (19) or (20) a graph of $v_0(x)/v_0(0)$ may be drawn assuming the estimated k_1 and k_2. Comparison with the original curve would show in which respects the theoretical curve required modifying to produce reasonable correspondence. The modes of varying k_1 and k_2 in order to improve the fit are probably better investigated with the aid of the first term of (23), so long as it dominates the second term. If it were found impossible to obtain a good fit in this way, the possibility of doing so on the assumption of a lesser degree of closure would have to be examined, starting with the easiest case, non-closure: this would involve correcting for the discrepancy in the traction at the excavation when a free surface is introduced. Even if close correspondence of the curves were found by assuming complete closure, it is possible that a comparable result would be obtained assuming a much smaller extent of closure; and this possibility should be explored. The example which is considered at the end of this Section is of the latter type.

If it is concluded that the practical curve is best interpreted by the complete closure model, then all the parameters in the expression for $v_1(x)$ are determined except t. This quantity cannot necessarily be equated to the seam thickness because the presence of broken rock at the excavation has probably diminished the convergence of the *intact* strata adjacent to roof and floor, thus decreasing the effective value of t. This value may be deduced by comparing the measured surface

displacement at $x = 0$ with that given by (19) or (20) using the final values of k_1 and k_2.

A suitable graph* (Fig. 2) by which the method may be illustrated, has been made from measurements of vertical surface displacement due to extraction of a panel of coal from the top hard seam in the N. Notts. coalfield. The depth (h) is 1973 ft, the width (2a) 550 ft and the thickness 48 in. The overlying coal measures are composed of thin shales and sandstones, except for a sandstone bed 75 ft thick about 1140 ft above the seam. Above the coal measures are the Permo-Triassic series consisting of 150 ft of a Lower Limestone series, 210 ft of interbedded sandstones and marls, and finally 240 ft of massive jointed sandstone, all the thicknesses being approximate. The value of $h/2a$, 3·59, is not very large, but proves to be enough to justify the use of the methods already discussed. Since the curve is not quite symmetrical, the estimation of k_1 and k_2 has been based on averages of the two sides. The displacement at the centre is 180 mm.

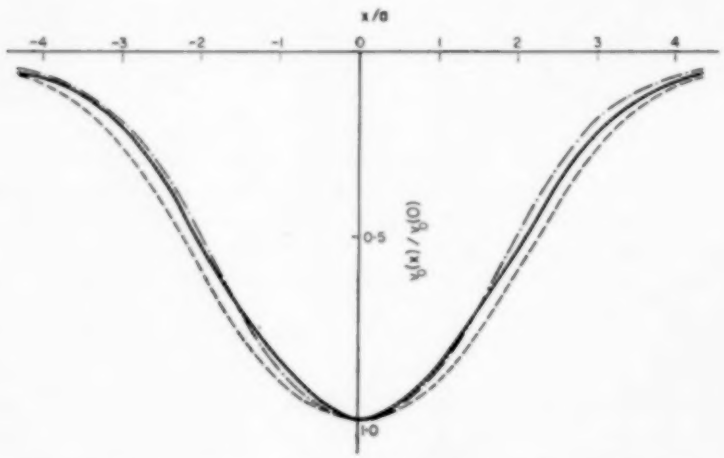

Fig. 2. Measured subsidence (——) compared with theoretical curves for $k_1 = 11$, $k_2 = 0$ (– – –) and $k_1 = 14$, $k_2 = 0$ (– · – · –), assuming complete closure.

From (27), first estimates of $k_1 = 11$, $k_2 = 0$ (to the nearest integer) were made. A graph of (20) for these values is compared, in Fig. 2, with the measured vertical displacement. The correspondence is not bad but improvement is evidently possible. This can be effected with the aid of the first term of (23) since the magnitude of $(4a^2/h^2)\,\delta(x)$ is not more than 0·23 when $k_1 = 11$, $k_2 = 0$. In this way second estimates of $k_1 = 14$, $k_2 = 0$ were made and a better correspondence found (Fig. 2). It is doubtful if any appreciable improvement can be made by varying k_1 and k_2 further, while a variation of as much as a unit in either parameter would certainly make the fit worse.

The possibility of non-closure being an equally valid model of the situation was tested, using the second estimates of k_1 and k_2. Computations were made of the vertical displacement at the surface given by substituting (12) in (16). The

*The authors' thanks are due to Mr. K. Wardell (Mining Consultant) for permission to use this graph, based upon an extremely thorough survey.

resulting curve was practically identical with the theoretical curve for $k_1 = 14$, $k_2 = 0$ (Fig. 2) which was obtained from the complete closure expression. From (4), (14) and (15) the components σ_y and τ_{xy} of the induced stress were computed at points in the interval $|x| < a$ of $y = -h$ for $H'(\zeta)$ given by (12). Fig. 3 shows

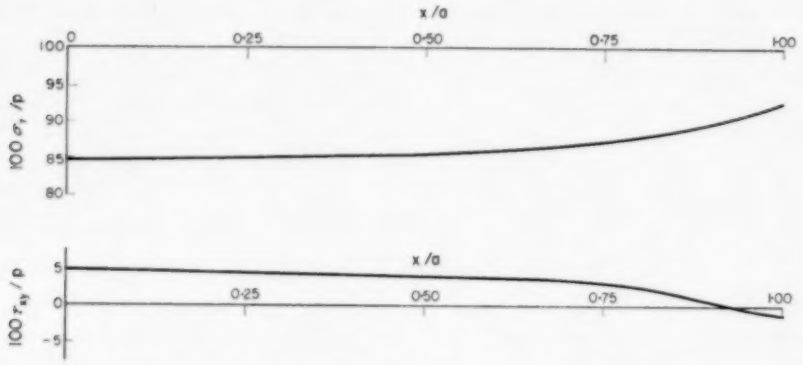

FIG. 3. Distribution of traction at excavation which produces in a semi-infinite medium the same convergence of roof and floor as would be produced in an infinite medium by a uniform pressure p; $k_1 = 14$, $k_2 = 0$, $h/a = 7{\cdot}18$.

that, although it is smaller than p, σ_y does not vary a great deal, while τ_{xy} remains quite small. If cp (where $c = 1{\cdot}15$, say) were substituted for p in (12), that expression, with (14) and (15), would give a solution satisfying the conditions of the non-closure problem to a good approximation. The partial closure solution has not been investigated in this way: the results would vary with the extent of closure, but there is no reason to suppose that the subsidence curve would not always lie close to that for complete closure. In this example any of the states of closure appears to be equally consistent with the subsidence profile, and the determination of k_1 and k_2 does not depend on the assumption of any particular state. Equally, the subsidence curve gives no evidence of the degree of closure of the excavation.

The expression (23) may be used for non-closure if cp is substituted for p. Without this correction the second term is inaccurate to an extent depending upon the discrepancy in the traction at the excavation due to the introduction of the free surface. However, the discrepancy largely disapppears when the function (12) is corrected by means of the factor c, and the error in the second term of (23) becomes correspondingly small. When $k_2 = 0$, $\delta(0) = 0$ and, to a very close approximation,

$$v_0(0) = (2k_1)^{\frac{1}{2}} A/\pi h. \tag{28}$$

From (28) and (22a), with cp in place of p, may be obtained the equation

$$s_{22}^{22} = h\, v_0(0)/2k_1\, c\, p\, a^2. \tag{29}$$

Now (29) holds only if there is no closure: if there is partial closure it must be due to the ground being 'weaker' than it would be for non-closure; that is, s_{22}^{22} must be greater than the value given by (29). When p is given the accepted approximate

value of h lb/in^2 and the other parameters their known values, this argument leads to the inequality $s_{22}^{22} \geqslant 2{\cdot}4 \times 10^{-7}$ (lb wt)$^{-1}$ in^2.

It is clear that A, the area of discontinuity (or volume closure per unit length of panel), is of some importance in this example. The value of A obtained when actual values are substituted in (28) is 690 ft^2. If closure were complete this figure would imply an effective convergence of roof and floor of 15 in., which is less than a third of the actual thickness of coal extracted, namely, 48 in. If there were no contact of roof and floor the convergence would have a maximum of 19 in. at $x = 0$ and diminish to zero at $x = \pm a$. For partial closure the maximum convergence would lie between 15 and 19 in. This bears out the expectation that the effective convergence would be considerably less than the thickness of extraction because of the presence of broken rock.

Acknowledgments

The authors are grateful to their colleagues Dr. P. Hackett, Professor F. B. Hinsley and Professor R. Hill for helpful discussions. The work described is part of an extended investigation on strata control undertaken for the National Coal Board, to whom the authors are indebted for financial support.

References

Berry, D. S. 1960 *J. Mech. Phys. Solids* **8**, 280.

Green, A. E. and Zerna, W. 1954 *Theoretical Elasticity* (Oxford University Press).

J. Mech. Phys. Solids, 1961, Vol. 9, pp. 63 to 66. Pergamon Press Ltd., London. Printed in Great Britain

ON THE TENSILE STRESS–STRAIN RELATION AND THE BAUSCHINGER EFFECT FOR POLYCRYSTALLINE MATERIALS FROM TAYLOR'S MODEL*

By S. J. Czyzak, N. Bow and H. Payne
Physics Department, University of Detroit

(*Received 4th November*, 1960)

Summary

An extension of Taylor's theoretical model has been used to investigate the behaviour of a polycrystalline material subjected to a fully plastic tensile strain first in one sense of displacement and then in the opposite sense. Some agreement with experimental results has been obtained.

Taylor's model (1938) for calculating the stress–strain relation for a crystalline aggregate in the plastic region has been extended by Lin (1957) so as to include the elastic strain component. It is the purpose of this paper to report the predictions of this extended model for the problem in which a large plastic strain is developed in a face-centred cubic polycrystalline material first in simple tension (or compression) and then in simple compression (or tension). The mathematical procedure has been previously described (Payne 1959) and applied to the problem of a torsion following a plastic extension (Payne and Czyzak 1960).

The deviator of the total strain tensor – assumed to be the same for each crystal in the Taylor model – may be represented in the notation of Payne (1959) by

$$\epsilon = \lambda\left(-\tfrac{1}{2}, -\tfrac{1}{2}, 1, 0, 0, 0\right)\frac{\tau_c}{2\mu}$$

where τ_c is the critical stress and μ is the shear modulus of elasticity. Here the third Cartesian coordinate axis is chosen parallel to the lines of action of the forces providing the simple tensile stress.

The problem consisted in determining the deviator of the elastic strain tensor $\bar{\epsilon}(\lambda)$ for each of the forty-four crystal orientations proposed by Taylor as λ was first increased, beginning at $\lambda = 0$, until it assumed the value λ_m (which would be infinite for a continuous distribution of crystal orientations) at or before which a vertex on the yield surface is reached in each crystal, and then decreased until the fully plastic state was again attained. For each selected value of λ the $\bar{\epsilon}$ were averaged over the crystal orientations, using the procedure described by Payne and Czyzak (1960). The tensile stress was then derived from the average elastic strain in accordance with elasticity theory.

*Research supported by the Office of Scientific Research, Air Research and Development Command, U.S. Air Force under Contract No. AF 18(600)–1466.

Representing ϵ for a particular λ in a given crystal by a point in strain space, one may imagine the point moving along the straight line $\epsilon(\lambda)$ as λ increases from zero until the yield surface is encountered. Then the point moves along the yield surface, as additional slip systems become active, and away from the line $\epsilon(\lambda)$ until it reaches a vertex. There it remains for further increases in λ.

If λ is now decreased, the point ϵ will move from the vertex. For some crystal orientations it will move from the yield surface along a line parallel to $\epsilon(\lambda)$, indicating a purely elastic strain increment. In any event it is apparent that the path of the point ϵ for decreasing λ will differ from the one it traversed during the increase of λ. Thus, it is not surprising that the stress-strain curve for the aggregate according to this model exhibits a characteristic for decreasing λ different from that for increasing λ and, moreover, shows a foreshortening of the elastic portion of the curve for $\lambda < 0$ in accordance with observation, the Bauschinger effect.

Table 1. *The function $f(\lambda)$*

Increasing λ		*Decreasing* λ	
λ	f	λ	f
0–4/3	λ	λ_m	2·055
1·5	1·449	$\lambda_m - 1$	1·075
1·75	1·571	$\lambda_m - 2$	0·089
2	1·622	$\lambda_m - 3$	− 0·792
2·5	1·740	$\lambda_m - 4$	− 1·142
3	1·826	$\lambda_m - 5$	− 1·339
4	1·919	$\lambda_m - 6$	− 1·405
5	1·960	$\lambda_m - 7$	− 1·439
6	1·980	$\lambda_m - 8$	− 1·454
8	2·004	$\lambda_m - 9$	− 1·465
10	2·016	$\lambda_m - 10$	− 1·473
λ_m	2·055		

Since the distribution of crystal orientations gives an essentially isotropic specimen, symmetry demands that the averaged $\epsilon(\lambda)$ assume the form

$$\bar{\epsilon}_{ap}(\lambda) = f(\lambda)\left(-\tfrac{1}{2}, -\tfrac{1}{2}, 1, 0, 0, 0\right)\frac{\tau_c}{2\mu}.$$

After including the hydrostatic component of the strain tensor one relates the tensile stress S and the tensile strain s to λ and $f(\lambda)$ through

$$S = \tfrac{3}{2}\,\tau_c f(\lambda), \tag{1}$$

$$s = \left[\lambda + \frac{(1-2\rho)}{2(1+\rho)} f(\lambda)\right]\frac{\tau_c}{2\mu}, \tag{2}$$

where ρ is Poisson's ratio. The calculated $f(\lambda)$ is given in Table 1 and plotted in Fig. 1.

The elastic limit for increasing λ is represented by $\lambda = 4/3$, the point at which the yield surface is reached in that crystal most favourably oriented for this to occur. For decreasing λ, however, the point at which the plot of f assumes a nonlinear

characteristic is not so well defined since for some orientations the point ϵ, in departing from the vertex, does not leave the yield surface. This means that the linear portion does not represent a purely elastic strain and thus has a slightly smaller slope than the linear portion of the curve for increasing λ.

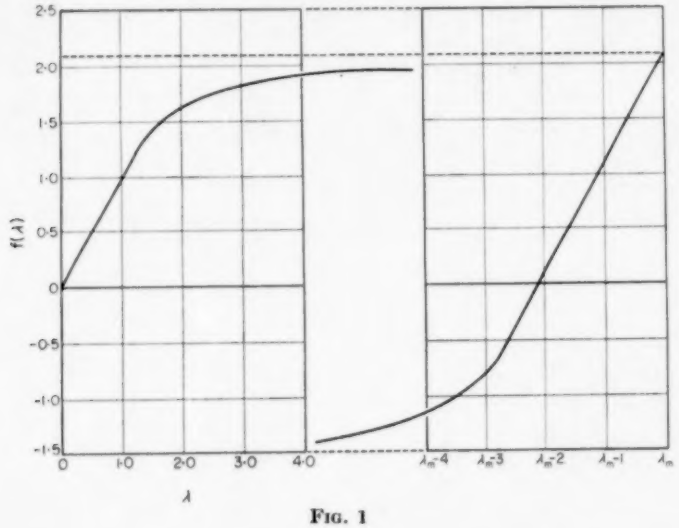

FIG. 1

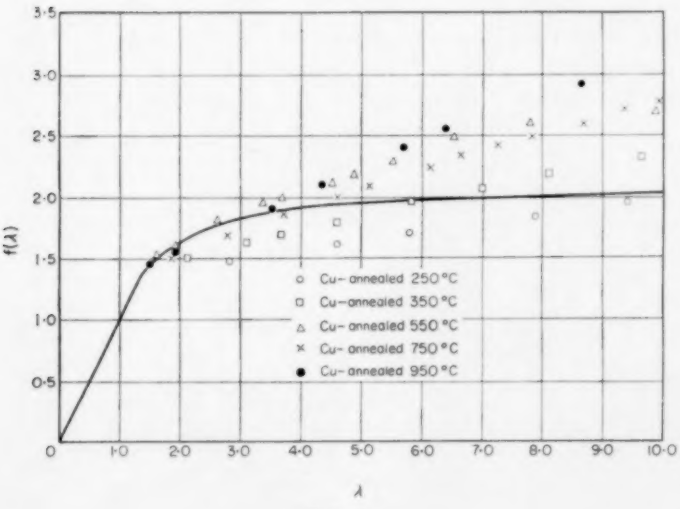

FIG. 2

Since in an experiment one would not expect to attain the state represented by $\lambda \geqslant \lambda_m$, the observed Bauschinger effect should be less pronounced than that depicted in Fig. 1.

In Figs. 2 and 3 are presented comparisons between the calculated f and corresponding values derived from stress–strain measurements on copper and silver

as reported by Carreker and Hibbard (1953) and Carreker (1957). For obtaining the experimental points τ_c was treated as a constant equal to one half the value of S at the elastic limit, as may be verified by setting $f(\lambda) = 4/3$ in equation (1). The experimental value for μ was determined from equation (2) by inserting the values of S and s at the elastic limit and for ρ assigning the values 0·32 for copper

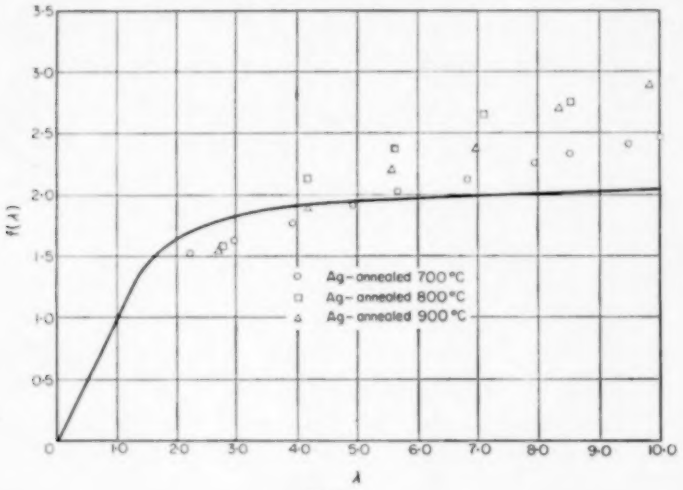

Fig. 3

and 0·37 for silver. This procedure assured that the experimental and theoretical curves coincided for $\lambda \leqslant 4/3$. It is seen from Figs. 2 and 3 that in order to achieve better agreement between the predictions of this model and the experimental results the constant τ_c must be withdrawn in favour of one which increases with λ.

References

Carreker, R. P., Jr.	1957	*Trans. A.I.M.M.E.* **209**, 112.
Carreker, R. P., Jr. and Hibbard, W. R., Jr.	1953	*Acta Met.* **1**, 654.
Lin, T. H.	1957	*J. Mech. Phys. Solids* **5**, 143.
Payne, H.	1959	*J. Mech. Phys. Solids* **7**, 126.
Payne, H. and Czyzak, S. J.	1960	*J. Mech. Phys. Solids* **8**, 39.
Taylor, G. I.	1938	*J. Inst. Metals* **62**, 307.

BOOK REVIEWS

Progress in Solid Mechanics, Vol. 1. Edited by I. N. SNEDDON and R. HILL. North-Holland Publishing Company, Amsterdam, 1960, 448 pp., 100*s*.

THIS is the first volume of a new addition to the publishers' 'Progress' series. Three of the eight articles deal with elastic boundary-value problems. MARGUERRE's 'Matrices of transmission in beam problems' is concerned with the use of matrices which relate conditions at one end of a beam to those at the other. The title of W. A. GREEN's article, 'Dispersion relations for elastic waves in bars,' refers to the various approximate wavelength–velocity relations which have been derived, and not to dispersion relations as commonly understood in modern physics. Using the language of dislocation theory, we might describe the latter as Peierls–Nabarro equations in frequency–space; there is an example on p. 14 of HUNTER's article in the volume under review. MUKI's article on 'Asymmetric problems of the theory of elasticity for a semi-infinite solid and a thick plate' presents a generalization of methods already worked out for the axisymmetric case. One may question the usefulness of presenting detailed solutions of highly specific problems, but it is certainly convenient to have recorded solutions of fair generality which can be applied to special problems as they arise. For instance, from MUKI's equations (21) and (22) one could quickly find the stress-field of an edge dislocation in a semi-infinite solid.

Some aspects of CHADWICK's subject 'Thermoelasticity. The dynamic problem' received the attention of physicists before the war. Zener and Päsler, for example, found the rate of thermoelastic damping in vibrating solids of various shapes. CHADWICK is concerned with more recent work by applied mathematicians, mostly on thermoelastic waves. It is perhaps worth noting that the characteristic length l^* which he introduces, being equal to the thermal diffusivity divided by the velocity of sound is, in a non-metal, practically the mean free path of the carriers (phonons) responsible for heat conduction. In metals also, as it happens, l^* is about the mean free path of the appropriate carriers (electrons). Thus the results presented for waves of length less than l^* should not be taken too seriously. In 'Viscoelastic waves' HUNTER applies Laplace and Fourier transforms to the propagation of waves in rods, compares theory and experiment, and indicates what progress has been made with the three-dimensional problem. H. G. HOPKINS' 'Dynamical expansion of spherical cavities in metals' successfully combines physical considerations with the theories of elasticity and plasticity.

The remaining two articles are more philosophical. In KOITER's 'General theorems for elastic–plastic solids' it is fascinating to see such a wealth of results derived from very modest premisses. BILBY's 'Continuous distributions of dislocations' is a thorough treatment by one of the founders of the theory. For the reviewer, at least, the continuum theory of dislocations has thrown much light on higher differential geometry. No doubt when the subject is further advanced the converse will also be true.

J. D. ESHELBY

N. FEATHER: **An Introduction to the Physics of Mass, Length and Time.** Edinburgh University Press, 1959, pp. x + 358, 18*s*.

THE SCOPE of this book is essentially the Mechanics and Properties of Matter which is covered by a good sixth form course in England. The treatment, however, is unusual, in that it is explicitly aimed at providing an understanding of the concepts and principles of the subject matter, and gives no account of techniques. Such a book might expect a wide potential audience in view of what must be a common experience among teachers and students, namely that the ability to reproduce a set of techniques in an examination by no means implies a thorough grasp of the principles involved.

The author's approach commends itself in two aspects. One is the attempt to convey an 'historical awareness' of the evolution of the ideas. Each topic is presented against a much stronger background of the historical facts than is commonly found in formal textbooks with the same scope. For example, much space is devoted to the problem of defining arbitrary and natural standards of length and time.

The other aspect is the way in which the concepts themselves, and their derived notions, are discussed. This is done by implicit insistence on the importance of being able to interpret an equation in words, in terms of the physical concepts involved. The significant equations are quoted where they cannot be deduced simply (the calculus is eschewed), and they are used to illustrate rather than to express the physical relationships. This important viewpoint is not new – what is unusual is the present attempt to apply it systemmatically in one volume to each topic in turn. It is on the whole successful, if occasionally lacking in conviction in respect of unproved generalization and quotation. The mathematical limitation is presumably imposed for the benefit of the 'humanist' to whom the book is rather boldly addressed on the flyleaf. More informed readers may disagree on points of emphasis; the reviewer cannot accept the argument on p. 130 that Newton's Second Law is 'certainly not a law of nature.' The author regards a law of nature as a general statement which tells us that 'the universe has this particular character – not that possible one.' Thus he appears to regard it as obvious *a priori* that momentum should be the particular quantity whose rate of change provides a quantitative measure of the intuitive concept of force.

However, the book should make interesting, and at times illuminating, reading for anyone concerned with the subject at this level.

M. J. SEWELL

K. R. SYMON: **Mechanics** (2nd Ed.). Addison-Wesley, Reading, Mass., 1960, 537 pp., $10.50.

THIS TEXTBOOK has been written mainly for physicists, and forms a basis for an undergraduate course of study. Interest is centred on the introduction and understanding of the basic principles of mechanics, and not in the detailed methods of solving individual problems. The examples used to emphasize the theory are of an essentially physical nature, and these are supplemented by problems included at the end of each chapter.

The first nine chapters are substantially the same as in the first edition, and introduce the fundamental laws and definitions, particle motion in one, two and three dimensions, statics and dynamics of rigid bodies, gravitation theory, moving axial systems, mechanics of wave propogation and kinematics of fluid motion, and the Lagrange and Hamilton equations of motion. Vector algebra has been used consistently in developing the theory, and a summary of the main results appears in Chapter 3.

The remaining three chapters contain more advanced material which does not appear in the first edition. Chapter 10 gives a detailed account of the algebra of second order tensor quantities, and the inertia tensor and tensors associated with the state of stress in fluid and elastic media are defined. The motion of a rigid body about a fixed point is considered in Chapter 11 based on Euler's equations of motion, with particular reference to the motion of a symmetrical top under gravity. Tensor algebra is utilized in Chapter 12 to give an elegant method of investigating the stability of an equilibrium configuration of a dynamical system. The stability of the Lagrange three-body configuration is discussed in detail.

E. E. JONES

J. Mech. Phys. Solids, 1961, Vol. 9, pp. 69 to 90. Pergamon Press Ltd., London. Printed in Great Britain

CONSOLIDATION DES POLYCRISTAUX DE FER ET HYPOTHÈSES SUR L'ORIGINE DU PALIER DES COURBES DE TRACTION

Par B. JAOUL
Centre de Recherches Métallurgiques, École des Mines, Paris

(*Received* 15*th October*, 1960)

SOMMAIRE

L'ÉTUDE de la déformation plastique de polycristaux de fer décarburé montre que peu de systèmes de glissement interviennent dans chaque grain et que la consolidation n'est pas affectée par la présence des joints.

Ces caractéristiques conduisent à des hypothèses permettant de déterminer l'amplitude de la déformation correspondant au palier des courbes de traction. Le développement des bandes de Piobert-Lüders serait dû à une instabilité limitée créée par la rotation des cristaux au cours de la déformation. Un certain nombre de résultats expérimentaux vérifient ces hypothèses.

L'ÉTUDE des propriétés plastiques de monocristaux de fer (JAOUL et GONZALEZ 1961) avait révélé deux caractéristiques importantes :

(a) le fait que le second système de glissement ne se développe que rarement, la consolidation sur les systèmes latents semblant élevée.

(b) la faible valeur de la consolidation, qui est de l'ordre de $\mu/700$, μ étant le module de cission, sauf dans des cas exceptionnels (glissements dans des positions symétriques) où elle peut s'élever à $\mu/400$.

Nous avons recherché si des particularités comparables pouvaient se retrouver dans la déformation d'aggrégats de cristaux et quelle serait leur influence sur la consolidation. Ces essais ont porté sur le même métal que l'étude précédente, c'est à dire un fer Armco décarburé ($C < 0{\cdot}001$ pour cent). Le palier apparaissant sur les courbes de traction pour les grains les plus fins, mais avec un développement assez limité, l'étude de l'origine de ce phénomène nous a conduit également à faire des essais sur un acier doux, non décarburé.

1. INFLUENCE DES JOINTS SUR LA DEFORMATION DES POLYCRISTAUX

1. *Glissements dans les grains des polycristaux*

Dans la déformation d'un monocristal par traction, où seul un allongement dans une direction est imposé, les contractions transversales sont seulement fonction des mécanismes de glissement qui interviennent. Dans un aggrégat de cristaux, par contre, un grain n'est plus soumis à une sollicitation simple, mais à un ensemble complexe de déformations dû aux compatibilités entre les grains voisins.

Dans un métal cubique à faces centrées, les cinq paramètres à satisfaire pour réaliser une déformation quelconque sont les amplitudes des glissements sur cinq systèmes, bien définis cristallographiquement.

Une ligne de glissement visible à la surface correspond à un plan de glissement dans lequel sont situées trois directions de glissement ; en réalité on peut toujours décomposer un glissement dans une direction en deux glissements suivant les deux autres, ce qui revient à considérer, géométriquement, qu'il n'y a que deux systèmes indépendants par plan. L'apparition d'une famille de glissements sur la surface satisfait deux paramètres et on doit donc voir se développer dans les polycristaux cubiques à faces centrées, en moyenne, au moins 2·5 familles de glissements par grain ; c'est effectivement ce que l'on observe.

Dans le cas du fer, où une famille de lignes de glissement ne se développe pas sur des plans cristallographiques simples, il n'intervient qu'une seule direction de glissement ; mais le choix du plan moyen de glissement pourra lui-même satisfaire un paramètre et le développement d'une famille de glissements remplit deux conditions. Donc, on devrait voir se développer, en moyenne, au plus 2·5 systèmes de glissement par grain.

Pratiquement, on en observe moins ; La Fig. 1 représente l'aspect de la surface d'un polycristal de fer poli électrolytiquement et allongé de 10 pour cent. On remarque, dans plusieurs grains, un seul système de glissement ; dans certains, on en observe deux, le second étant souvent seulement localisé dans une partie d'un grain. D'autre part, nous n'avons jamais observé, à l'intérieur des grains, le développement d'hétérogénéités de déformation comme des pliages ou des bandes de glissement secondaire qui étaient, dans les monocristaux, responsables d'une consolidation importante. Ce n'est que dans le cas d'un bicristal avec un joint sinueux en moyenne parallèle à la direction de traction que nous avons observé de tels phénomènes (Fig. 3) ; ceux-ci disparaissent quand le diamètre moyen des grains devient petit par rapport aux dimensions des éprouvettes.

La continuité aux joints ne peut donc pas être respectée et il s'ensuit de fortes distorsions qui sont visibles sur les micrographies. Si l'on trace une rayure droite, avant déformation sur la surface d'un polycristal de fer, les distortions de cette ligne repère sont localisées près des joints où un mécanisme de déformation très complexe intervient (Fig. 3). Dans le cas d'un polycristal de structure cubique à faces centrées, il n'apparaît pas de déchaussement aux joints pour les mêmes déformations, sauf cependant si le métal est impur (Fig. 4) ; en effet, les impuretés augmentant la consolidation sur les systèmes latents (SCHMID et BOAS 1935) font qu'un moins grand nombre de systèmes intervient. Les particularités de la déformation du fer peuvent donc être attribuées aux impuretés présentes qui, pouvant être en insertion, jouent un rôle très actif.

On peut considérer, en simplifiant, que chaque grain se déforme par glissement sur la famille de surfaces la mieux favorisée et que, le long des joints, sur une épaisseur de l'ordre d'une dizaine de microns, la déformation est beaucoup plus importante, faisant intervenir plusieurs systèmes ainsi, vraisemblablement, qu'une déformation d'un type visqueux.

En dessous d'une certaine température, cette déformation n'est plus possible et la rupture intervient le long des joints.* Si l'on augmente la température de

*La teneur en oxygène du fer est en effet de l'ordre de 0·012 pour cent, proportion suffisante pour diminuer fortement la cohésion intergranulaire à basse température (REES et HOPKINS 1952).

FIG. 1. Aspect de la surface d'un polycristal après déformation de 10 pour cent à l'ambiante × 700.

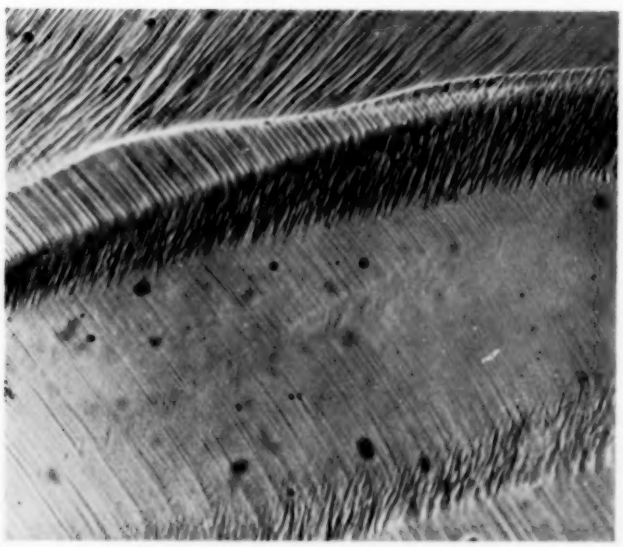

FIG. 2. Hétérogénéité de déformation au voisinage du joint d'un bicristal de fer × 300.

FIG. 3. Distorsion d'une rayure au voisinage d'un joint × 300.

FIG. 4. Surface d'une éprouvette d'aluminium-silicium à 0·2 pour cent après déformation à température ambiante de 6 pour cent × 75.

FIG. 5. Glissements dans un polycristal de fer déformé à 300 C × 600.

déformation, l'aspect des glissements change peu, ils deviennent seulement plus gros et plus marqués (Fig. 5) et les déchaussements aux joints sont plus nets. Une variation de vitesse a également un effet sur ces déformations aux joints et, à partir d'une vitesse d'allongement de 15 pour cent par minute, on voit apparaître le maclage.

2. *Limite élastique*

Les déformations par glissement à l'intérieur des grains, sans que les déplacements aux joints interviennent, sont de très faible amplitude, aussi le seuil de plasticité doit-il être fortement affecté par la grosseur du grain. La Fig. 6 reproduit une série de courbes de traction effectuées à la température ambiante sur des éprouvettes à diverses grosseurs de grain.

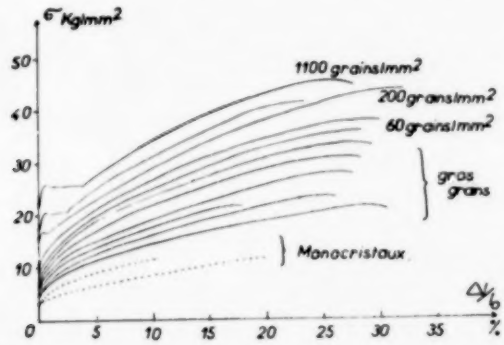

FIG. 6. Courbes de traction d'une série d'éprouvettes de diverses grosseurs de grain. En pointillé sont représentées les limites des courbes de traction de monocristaux.

On remarque que la limite élastique varie dans de très larges limites entre le monocristal et les éprouvettes à grains les plus fins. Dans l'aluminium, elle varie seulement dans un rapport de 2 à 2·5; dans le fer, elle passe de 3·5 à 25 Kg/mm², ce qui montre le très important effet durcissant des joints.

On remarque que les éprouvettes à gros grains ne présentent pas de palier, celui-ci n'apparaissant que quand la limite élastique atteint environ 15 kg/mm². Il intervient alors un phénomène, lié au mécanisme cristallographique de la déformation, que nous étudierons plus loin.

3. *Forme des courbes de traction*

Mais, si les joints ont une forte influence sur la limite élastique, on remarque que la consolidation, c'est à dire la pente de la courbe est peu affectée. Les courbes de traction, enregistrées phctographiquement, étant assez fines pour qu'une analyse précise de leur forme puisse être faite, nous avons recherché, sur une centaine de courbes, la variation de la pente de la courbe, $d\sigma/d\epsilon$ en fonction de l'allongement ϵ. Cette méthode revient au même que celle que nous avions appliquée dans l'étude des courbes de traction de l'aluminium (CRUSSARD et JAOUL 1950). En portant sur un graphique, en coordonnées logarithmiques, les valeurs de la pente en fonction de l'allongement, on observe que les points s'alignent sur deux droites,

c'est à dire que les courbes de traction sont formées de deux paraboles successives (Fig. 7).

En fonction de la grosseur du grain, de la vitesse et de la température de déformation, nous n'avons trouvé aucune variation systématique de la courbe traduisant la variation de la pente. Notamment, le point où la courbe s'infléchit correspond à un allongement compris entre 7 et 9 pour cent et une pente variant entre 85 et 110 kg/mm²*; σ_0 étant la limite élastique la tension correspondant à ce point varie

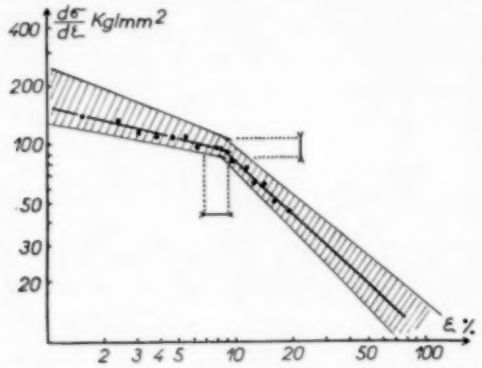

FIG. 7. Variation de la pente des courbes de traction en fonction de l'allongement. La zone hachurée représente le domaine dans lequel se sont placées toutes nos courbes.

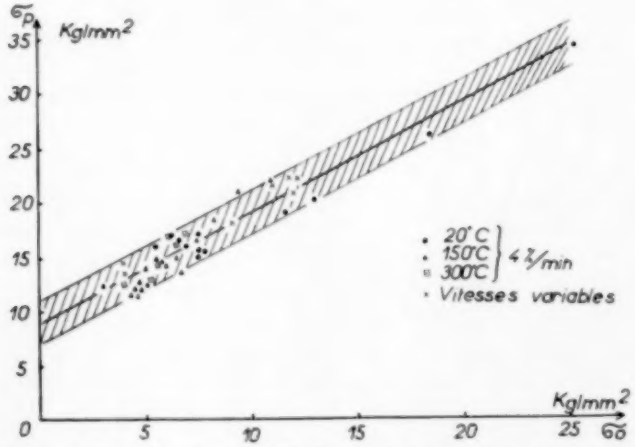

FIG. 8. Variation de la tension au point d'inflexion de la courbe de traction en fonction de la limite élastique.

elle-même entre $(\sigma_0 + 7)$ et $(\sigma_0 + 11)$ kg/mm² (Fig. 8). A partir de ce point, les deux branches rectilignes peuvent être définies par leur coefficient qui varie entre — 0·2 et — 0·4 pour les faibles déformations et entre — 0·8 et — 1 pour les fortes

*Nous avions indiqué précédemment (JAOUL 1957) une pente plus forte. Mais les essais avaient porté sur des polycristaux à grains très fins que nous avions trempés pour éliminer le palier. Le point d'inflexion se trouvait alors à 4 pour cent et la pente correspondante était de l'ordre de 200 kg/mm². D'autre part, ces polycristaux n'avaient pas été décarburés et, nous verrons plus loin que la présence de carbone a pour effet de diminuer l'allongement correspondant à l'inflexion.

déformations ; les courbes de déformation de ces polycristaux de fer peuvent donc, en moyenne, être représentées par les deux équations :

$$\begin{cases} \sigma = \sigma_0 + 60\,\epsilon^{0{\cdot}7} & \text{pour} \quad 0 < \epsilon < 8\ \%, \\ \sigma = \sigma_0' + 60\,\epsilon^{0{\cdot}2} & \text{pour} \quad \epsilon > 8\% \end{cases}$$

σ_0', ordonnée à l'origine de la seconde parabole étant égale à $(\sigma_0 - 26)$ kg/mm²; il est à remarquer que, pour les grains les plus fins ($d \sim 25\ \mu$), σ_0' est nul et que la seconde parabole part de l'origine ; il y aurait peut-être là un rapprochement à faire entre la largeur de la zone très perturbée près du joint et le diamètre des grains.

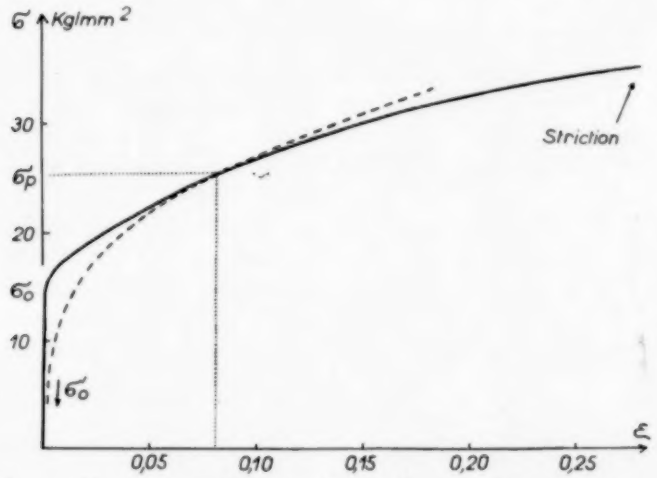

Fig. 9. Décomposition de la courbe de traction en deux paraboles tangentes au point de transition. La courbe supérieure, d'exposant 0·7, correspond aux allongements inférieurs à 8 pour cent ; la courbe inférieure, d'exposant 0·2, aux grands allongements.

La Fig. 9 représente la forme de la courbe de traction d'une éprouvette de fer. Une variation de grosseur de grain modifie de la même quantité les valeurs de σ_0 et σ_0'. Dans le cas où σ_0' devient nul, on obtient un résultat comparable à ceux de Truszkowski (1958) qui a observé que, pour les grains très fins, la courbe de traction, après un certain allongement était une parabole passant par l'origine ; cet auteur en concluait, par analogie, que le métal était alors ' homogène.'

Quand le grain devient très gros, les résultats sont encore trop dispersés pour que l'on puisse définir une variation conduisant aux courbes des monocristaux. D'ailleurs, la comparaison entre les courbes des monocristaux et des polycristaux est difficile ; en effet, dans le premier cas, on doit considérer le cisaillement pour que la courbe ait un sens, tandis que dans le deuxième, il faudrait faire un calcul de l'orientation moyenne des grains et connaître, dans chacun l'orientation moyenne de la surface de glissement. On ne peut donc que comparer approximativement les pentes des courbes, en admettant un coefficient moyen permettant de passer de l'allongement au glissement et de la tension normale à la cission. En utilisant un coefficient de l'ordre de celui de Taylor pour les cristaux cubiques à faces centrées, soit 3·1, la pente au point d'inflexion qui est comprise entre 85 et 110

kg/mm², correspond à un taux de consolidation des cristaux approximativement égal à 10 kg/mm², ce qui est bien l'ordre de grandeur de la pente des courbes de cisaillement.

Si l'on fait varier la vitesse de traction ou la température de l'essai, on observe des variations de limite élastique, mais la consolidation n'est pas affectée, comme dans les monocristaux. Il n'a pas été possible d'effectuer des essais à basse température, la décohésion intergranulaire intervenant avant la limite élastique.

Nous pouvons donc conclure que la consolidation qui se développe au cours de la déformation plastique du fer reste un phénomène purement intracristallin et que le rôle des joints n'est que d'augmenter la limite élastique et d'élever l'ensemble de la courbe parallèlement à elle-même.

4. *Inflexion des courbes*

Dans le cas des métaux de structure cubique à faces centrées, il avait été observé que l'inflexion de la courbe, que nous avions appelée le point de transition, était accompagnée de l'apparition de glissements déviés* (CRUSSARD et JAOUL 1950) et correspondait à un début de fragmentation des grains : elle était alors liée à l'écrouissage critique de recristallisation (JAOUL 1952). Plus récemment, SEEGER et ses collaborateurs (1957) ont observé que dans le cuivre, le mécanisme correspondant à l'inflexion des courbes était la déviation des glissements. Le même phénomène ne peut pas être pris en considération dans le cas du fer, puisque, les glissements ne se développant pas sur un plan cristallographiquement défini, les déviations des glissements apparaissent dès le début de la déformation.

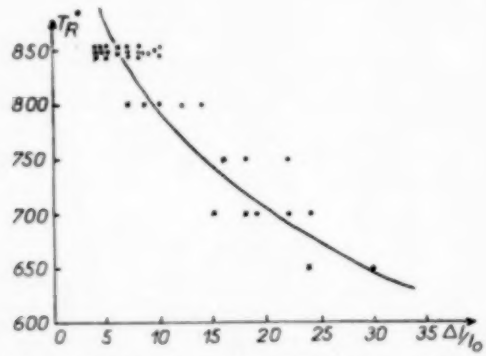

FIG. 10. Variation de l'écrouissage critique de recristallisation en fonction de la température de traitement thermique. ● Recristallisé ; × Non recristallisé.

Une hypothèse de fragmentation des grains, par réarrangement des dislocations paraîtrait plus vraisemblable. Nous n'avons pu observer le phénomène directement par les rayons X, l'astérisme étant trop important ; mais, par contre, on peut constater que l'inflexion des courbes correspond à l'écrouissage critique de recristallisation. La Fig.10 représente, pour diverses températures de traitement thermique après écrouissage, la limite d'allongement séparant les éprouvettes qui ont re-

*Dans le cas d'alliages comme l'acier inoxydable 18/10 ou les laitons 70/30, le point de transition est rejeté vers de très grands allongements et ces métaux ne présentent effectivement pas de glissements déviés (JAOUL et GONZALEZ 1959).

cristallisé de celles qui sont simplement restaurées ; on remarque que pour les traitements aux températures les plus élevées, l'écrouissage critique correspond à l'allongement au point d'inflexion des courbes.

Il faut signaler d'autre part, que des traitements thermiques en haut de la phase α du fer n'ont pas permis la recristallisation des monocristaux, même après forte déformation ; les phénomènes correspondant au point d'inflexion ne sont donc pas atteints avec les monocristaux. Nous avions observé avec l'aluminium que les germes de recristallisation pouvaient, dans les monocristaux, être aux intersections des glissements où se forment des empilements de dislocations (Jaoul *et al.* 1957). Dans le cas du fer, les germes de recristallisation ne pourraient donc apparaître que dans les zones fortement distordues au voisinage des joints.

Enfin, nous rappellerons que pour préparer nos monocristaux, nous avons effectué sur les éprouvettes, avant décarburation, un écrouissage de 3·75 pour cent* ; après décarburation, l'écrouissage critique s'élèverait à 7 ou 8 pour cent. Le rôle du carbone dans le fer serait donc inverse de celui que nous avions observé avec l'aluminium (Jaoul 1957) ; mais là intervient peut-être le mécanisme particulier des bandes de Piobert-Lüders.

2. Hypotheses sur Le Mecanisme de Developpement des Bandes de Piobert-Luders†

Le phénomène du palier des courbes de traction du fer et des aciers doux est dû à une déformation hétérogène du métal : dès que la limite élastique est atteinte, il se développe dans une zone de l'éprouvette, généralement près d'un congé,

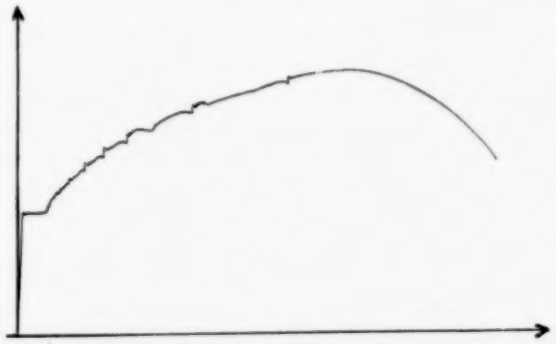

Fig. 11. Reproduction d'une courbe de traction enregistrée à la machine Chevenard ; traction d'une éprouvette de fer Armco à vitesse très lente. $v = 4 \times 10^{-5}$/sec.

une bande dans laquelle la déformation a une valeur finie; puis, la tension appliquée restant sensiblement constante, cette zone déformée s'étend et gagne toute l'éprouvette. Le mécanisme de déformation change alors et la courbe de traction reprend une allure normale.

*Qui correspond d'ailleurs à l'inflexion des courbes, observée dans une étude précédente (Jaoul 1957).

†La découverte des bandes de déformation dans les polycristaux de fer est généralement attribuée à Lüders (1860) En réalité, celles-ci avaient été observées et parfaitement bien décrites vingt ans plus tôt par Piobert (1842 ; cf. Jaoul 1959).

Il s'agit donc d'un mécanisme de déformation limitée mais d'amplitude bien définie : il arrive que les bandes apparaissent en deux points de l'éprouvette et s'étendent l'une vers l'autre ; quand elles se rejoignent, elles se réunissent sans qu'un défaut subsiste à la limite. La déformation est exactement la même dans les deux bandes.

C'est ce fait que l'amplitude ait une valeur caractéristique que nous allons chercher à expliquer ; nous ne considérerons pas ici le phénomène des limites élastiques supérieures et inférieures, correspondant au décrochement de la contrainte, phénomène lié à la présence d'atomes étrangers en insertion dans le réseau. Nos observations ont d'ailleurs porté en partie sur un fer Armco décarburé (teneur en carbone inférieure à 0·001 pour cent). La Fig. 11 représente une courbe de traction effectuée à vitesse très lente sur un fer extra doux, mais contenant encore assez d'impuretés pour que les phénomènes de vieillissement soient appréciables ; on remarque, sur la reproduction de la courbe enregistrée photographiquement sur une machine Chevenard, la différence entre les aspects du palier et des décrochements ultérieurs, dus aux impuretés.

L'absence de décrochement à la limite élastique des éprouvettes de fer décarburé pourrait être attribuée à des efforts parasites de flexion au cours de l'allongement ; mais, pratiquement, nos essais de traction ont été effectués avec un dispositif à rotules assurant une bonne axialité de l'effort.

Déformation dans les bandes

En jouant sur l'état de cristallisation d'un acier doux, et les conditions de déformation, nous sommes arrivés à développer des bandes dans lesquelles la déformation correspondait à un allongement de 15 pour cent. Si l'on arrête la traction, tout en maintenant l'effort appliqué, le développement de la bande s'arrête et l'on peut observer que le front est formé par une ligne nette, ainsi que HALL (1951) l'a déjà fait remarquer. On peut donc se poser la question : comment ces deux zones, l'une non déformée et l'autre déformée de 15 pour cent peuvent-elles se raccorder sans qu'il existe à la limite une importante concentration de contraintes qui devrait entraîner un développement très rapide de la bande formée ou, plutôt, empêcher cette déformation hétérogène ? Deux hypothèses sont possibles :

(i) Dans la déformation normale par traction, l'allongement longitudinal ϵ_1 est compensé par deux contractions transversales $\epsilon_2 = \epsilon_3 = -\frac{1}{2}\epsilon_1$, c'est à dire que si l'on tourne, à partir de l'axe, vers une direction transversale, on passe par une direction où la dilatation est nulle ; parallèlement à cette direction, le raccordement d'une zone déformée et d'une zone non déformée est possible. On calcule facilement* que cette direction est inclinée à 55° sur l'axe.

(ii) La deuxième hypothèse serait que la déformation dans la bande soit un cisaillement pur ; mais l'une des déformations transversales serait alors nulle et la bande devrait être inclinée à 45° sur l'axe.

Cette hypothèse de cisaillement pur avait été retenue par FELL (1935) ; d'après HALL (1951), la déformation serait due à un cisaillement simple à l'avant de la

*A partir des cercles de Mohr des déformations. La condition $\epsilon_2 = \epsilon_3 = -\frac{1}{2}\epsilon_1$ n'est cependant pas toujours vérifiée ; nous avions observé que dans la traction de tubes minces (JAOUL 1952) on avait $\epsilon_3 = 2\epsilon_2$. CRUSSARD *et al.* (1960) ont fait de nombreux essais sur des tôles de diverses épaisseurs et ont observé que $\epsilon_3 = k\,\epsilon_2$, k étant différent de un pour de fortes déformations. Dans ces conditions, l'angle entre l'axe et la direction de dilatation nulle est :

$$\phi = \tan^{-1}\sqrt{(1+k)}.$$

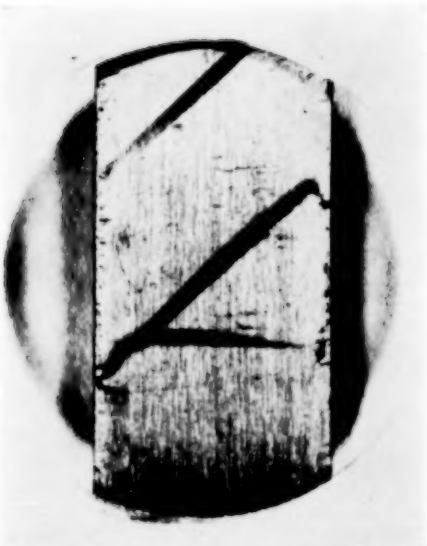

FIG. 12. Bandes de Piobert-Lüders formées sur une éprouvette présentant deux entailles situées sur une ligne inclinée à 55° sur l'axe. (Bandes révélées par photoélasticité) × 2.

FIG. 13. Lignes de PIOBERT développées sur une éprouvette d'acier doux de grandes dimensions sollicitée par l'intermédiaire de mordaches à rotules × $\frac{1}{3}$.

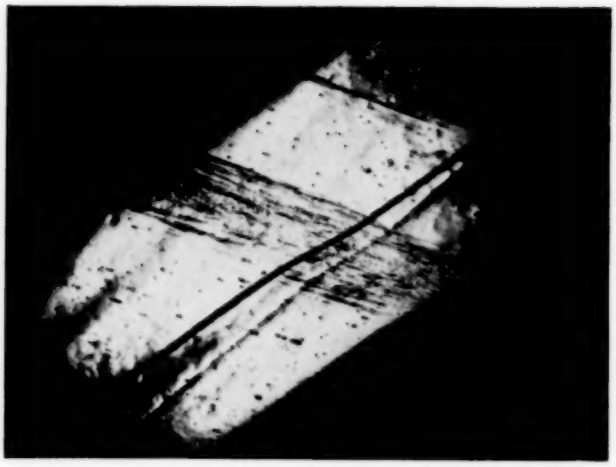

FIG. 14. Désorientation d'une ligne repère tracée sur une éprouvette avant déformation. Acier doux à grain très fin × 20.

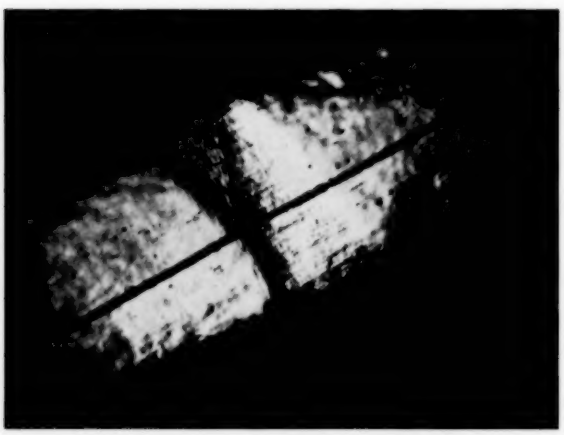

FIG. 15. Cas du développement simultané de deux bandes ; la déformation de la ligne repère disparaît, les deux rotations se compensant × 15.

bande, suivi d'un écoulement qui n'est pas nécessairement un cisaillement pur ; LOMER (1952) a observé que le cisaillement ne rendait compte que de la moitié de la déformation. On pourrait, dans ces conditions, admettre que l'angle d'inclinaison des bandes sur l'axe ait une valeur intermédiaire entre 45° et 55°, soit environ 50°.

HALL et SYLWESTROVICZ (1951) ont indiqué que l'angle entre le front de la bande et l'axe de traction était égal à $48° \pm 1{\cdot}5°$, ce qui est en accord avec les valeurs données par NADAI (1950). Nous avons nous-mêmes observé des angles un peu supérieurs, de l'ordre de 50°. Un grand nombre d'essais effectués par PLATEAU (1960) a conduit à des angles variant entre 50° et 51°. Un de ces essais (Fig. 12) est d'ailleurs assez caractéristique ; la traction a été effectuée sur une éprouvette présentant deux entailles dont les fonds sont sur une direction à 55° de l'axe : la bande n'est pas parallèle à cette ligne, mais s'est développée à 50°, malgré les concentrations de contrainte. On remarque, sur la même figure, une autre bande, normale à l'axe ; en réalité, celle-ci fait un angle de 50° avec l'axe si on l'observe sur la tranche de l'éprouvette. Le développement des bandes est en effet initialement affecté par l'axialité de la traction et c'est à l'extrémité du grand côté que la limite élastique est généralement atteinte en premier, mais si le défaut d'axialité est à 90°, la bande fait alors l'angle de 50° dans l'épaisseur. La Fig. 13 est relative à une large éprouvette plate faiblement étirée avec un dispositif à rotules permettant une très bonne axialité de l'effort. On remarque que les deux familles de bandes se sont développées. Dans une éprouvette ronde, la trace des bandes est une ellipse dont le grand axe est incliné à 50° sur l'axe.

On se trouve donc dans le cas intermédiaire entre les deux possibilités que nous avions indiquées, qui conduisaient respectivement à 45 et 55°. Celà serait alors en accord avec le résultat de LOMER (1952) qui avait observé, sur des éprouvettes à section pentagonale, que l'allongement correspondait pour moitié à un cisaillement simple.

Ce n'est cependant pas ce que nous avons observé sur nos éprouvettes plates. La Fig. 14 représente la surface d'une microéprouvette de fer sur laquelle avait été tracée une rayure ; après traction de telle manière que la déformation ne se développe que sur une portion de la longueur utile, on remarque que la ligne repère est cassée aux limites de la bande, comme si le métal avait subi un cisaillement pur dans la direction de la bande. De l'angle ϕ d'inclinaison de la bande sur l'axe et de l'angle α correspondant au décalage du repère, on peut déduire la valeur de l'allongement correspondant à la bande dans l'hypothèse du cisaillement pur par :

$$\epsilon_p \neq \tan \alpha/(\tan \phi - \tan \alpha).$$

Dans le cas de la figure, on a donc, avec $\phi = 51°$ et $\alpha = 7{\cdot}5 \pm 0{\cdot}5$, un allongement ϵ_p dû au cisaillement qui serait compris entre 11 et 13 pour cent. Or, l'allongement correspondant à la longueur du palier de la courbe de traction enregistrée est de 12 pour cent. La déformation n'est donc formée que d'un cisaillement.

On ne peut faire cette mesure que si la bande a son front perpendiculaire au grand côté et si elle est unique. Il arrive en effet que deux systèmes de bandes se développent simultanément dans deux directions (Fig. 15) ; la désorientation de la ligne repère disparaît alors.

B. Hypothèses sur l'origine des bandes

Cette déformation limitée et par cisaillement simple conduit à supposer que chaque grain subit lui-même un cisaillement simple dans une direction voisine de celle de la bande. Si l'on suppose que cette déformation entraîne la rotation des grains liée au glissement simple (JAOUL et GONZALEZ 1961) les orientations des surfaces de glissement actives changeront au cours du développement d'une bande ; la modification de la composante de cission dans la direction de glissement peut alors être responsable d'une déformation localisée due à une instabilité. Ce mécanisme comporte deux hypothèses :

(a) Il ne doit se développer, dans chaque grain, qu'un seul système ; on sait en effet que l'action simultanée de plusieurs systèmes limite généralement les phénomènes de rotation. Cette condition semble assez bien vérifiée par toutes les observations micrographiques que nous avons pu faire : dans la plus grande partie des grains, même après des déformations assez fortes, il n'apparaît qu'une seule famille de lignes. Nous avons cherché à observer les lignes de glissement qui se forment dans les bandes ; elles sont excessivement fines et, dans les zones où nous avons pu les apercevoir, elles étaient d'orientation sensiblement parallèle à la limite de la bande. Les zones déformées se marquent beaucoup plus par les déchaussements aux joints.

(b) L'influence des joints est négligée, chaque grain étant supposé pouvoir tourner librement. Nous avons vu qu'une fois la limite de plasticité des joints dépassée, ils ne concouraient plus à la consolidation, leur comportement ayant un caractère visqueux ; leur effet principal est donc de modifier la valeur de la limite élastique, mais leur rôle, dans la suite de la déformation n'apparaît pas.

Un raisonnement sur les modifications macroscopiques de l'état des contraintes n'est pas suffisant pour expliquer la formation rapide des bandes : dans le cas de la Fig. 14, l'inclinaison moyenne des glissements sur l'axe de traction passe de 51° à 44° par suite de la rotation, c'est à dire que l'augmentation de cission effective n'est que de l'ordre de 2 pour cent. Or, la consolidation, pour un allongement de 13 pour cent, est appréciable (JAOUL et GONZALEZ 1961). Il ne faut donc pas considérer la simple rotation d'ensemble, mais la rotation de chacun des cristaux, ce qui rend nécessaires les deux hypothèses précédentes.

Dans chaque grain, le glissement a lieu dans une direction cristallographique $< 111 >$ et, pour les divers cristaux, l'angle entre cette direction la plus favorisée et l'axe varie entre 35° et 70°. Si l'on fait la moyenne de toutes les orientations de l'espace, on trouve un angle moyen égal à $\lambda_m = 50°8$. C'est la direction moyenne d'un glissement qui cheminerait à travers les grains d'un aggrégat ne présentant pas d'orientation préférentielle. Or, c'est également l'angle que font les bandes avec la direction de traction.

Nous allons maintenant chercher à déterminer quelles modifications de contrainte effective entraîne le mécanisme de rotation des cristaux et en déduire, compte tenu de la consolidation des cristaux, l'allongement correspondant au développement d'une bande.

C. Calcul de la longueur du palier

Si la tension appliquée à l'éprouvette est σ, la composante de cission créant le glissement est, dans chaque grain,

$$\tau = \sigma \sin \chi \cos \lambda,$$

x et λ étant les angles que font avec la direction de traction, le plan moyen de glissement et la direction de glissement. Dans les monocristaux, les glissements se développent sur une surface qui est sensiblement celle pour laquelle la cission est maximale, c'est à dire que $\lambda = x$. Dans les polycristaux, cette condition n'est plus parfaitement remplie, mais une variation d'orientation de la surface de glissement a peu d'influence sur la valeur du coefficient liant la tension appliquée à la cission effective. On peut donc écrire, comme nous l'avions fait pour les monocristaux,

$$\tau = \sigma \times \tfrac{1}{2} \sin 2\lambda = \rho\,\sigma.$$

Le coefficient $\rho = \tau/\sigma$ est égal à $\frac{1}{2}$ pour $\lambda = 45°$, mais il peut varier entre 0·5 et 0·3. La Fig. 16 représente cette variation en fonction de l'orientation de l'axe pour une portion du réseau cubique.

Un glissement cristallographique n'est pas une déformation pure, car il fait intervenir une rotation ; il peut être décomposé en deux cisaillements et une rotation. Celle-ci est telle que l'axe de traction se rapproche de la direction de glissement et l'angle λ varie, pour un allongement $d\epsilon$, suivant :

$$d\lambda = \tan\lambda \,.\, d\epsilon.$$

Pour des cristaux étirés suivant une direction voisine de $< 111 >$, cette rotation est très importante :

$$d\lambda = 2{\cdot}8\, d\epsilon, \qquad \text{soit } (d\lambda)^0 = 1{\cdot}6\,(d\epsilon)\ \%.$$

La variation de l'angle λ entraine, bien entendu, une variation de coefficient $\rho = \tau/\sigma$:

$$d\rho/\rho = (\tan^2\lambda - 1)\, d\epsilon.$$

Elle est nulle pour $\lambda = 45°$, positive pour $\lambda > 45°$ et négative pour $\lambda < 45°$. Pour l'orientation $< 111 >$, on aurait

$$d\rho/\rho \neq 7\, d\epsilon\ ;$$

c'est à dire que pour un effort de traction constant, la cission effective augmente rapidement avec l'allongement. C'est ce phénomène de rotation qui est responsable de certaines courbes de traction anormales que nous avions rencontrées dans l'étude des monocristaux (Jaoul et Gonzalez 1961).

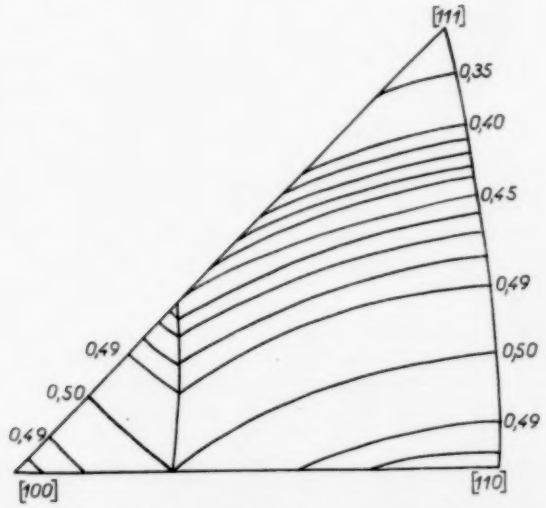

Fig. 16. Valeurs du coefficient $\rho = \sin x \cos\lambda$ en fonction de la direction suivant laquelle est étiré un cristal de fer. Les courbes 0·50 correspondent à $\lambda = 45°$, la zone située en dessous à $\lambda < 45°$.

Donc, tous les grains dont la direction $< 111 >$ active fait un angle supérieur à 45° subiront, au cours d'un allongement, cette augmentation de cission sans augmentation de contrainte de traction. On remarque sur la Fig. 16 que c'est le cas de la plus grande partie des orientations.

Nous avons calculé, en considérant toutes les orientations de l'espace la valeur moyenne de $d\rho/\rho$ en fonction de l'allongement effectué. A l'origine, pour $\epsilon = 0$, la majeure partie des cristaux étant au dessus de la courbe $\lambda = 45°$, $d\rho/\rho$ sera positif. Mais, dans la suite de la déformation, les rotations de chacun des cristaux font diminuer l'angle λ et la valeur de $d\rho/\rho$ décroît, pour s'annuler, puis devenir négative. Par le calcul, nous avons obtenu une relation sensiblement linéaire :

$$d\rho_m/\rho_m = 0{\cdot}70 - 9{\cdot}4\,\epsilon.$$

On en déduit la valeur moyenne de la cission effective en fonction de l'allongement :

$$\tau_m = (\tau_m)_0\,[1 + 0{\cdot}70\,\epsilon - 4{\cdot}70\,\epsilon^2]$$

et, en tenant compte de la réduction de section, due à l'allongement, on obtient, en négligeant le 3ème degré :

$$\tau_m = (\tau_m)_0\,[1 + 1{\cdot}70\,\epsilon - 4{\cdot}0\,\epsilon^2].$$

On peut donc tracer la variation de la cission effective moyenne au cours du développement d'une bande sous un effort de traction constant (Fig. 17). Si le métal ne subissait aucune consolidation, la déformation se poursuivrait donc jusqu'à 40 pour cent avant que la cission ait retrouvé sa valeur initiale.

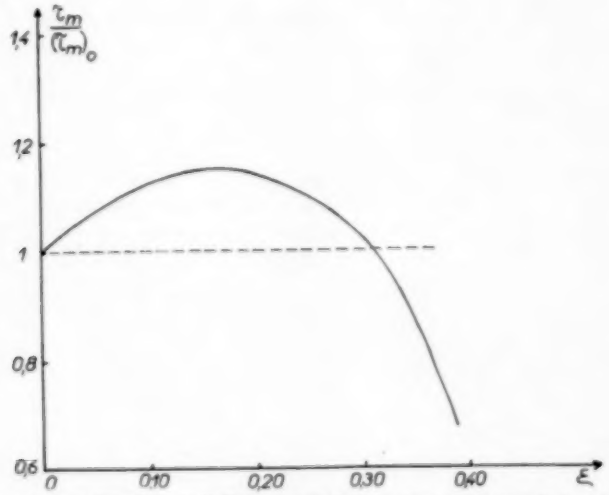

FIG. 17. Variation, en fonction de l'allongement de la valeur moyenne de la cission effective créant le glissement, la contrainte de traction restant constante.

Mais, pratiquement, le métal subit un durcissement et l'instabilité se développera jusqu'à ce que le phénomène de baisse de tension due à la rotation soit compensé par la consolidation, ce que l'on peut écrire, puisque l'on est toujours dans un état d'équilibre au cours d'une traction :

$$(d\,\tau_m/d\,\epsilon)_R = (d\,\tau/d\,\epsilon)_C \neq 2\,d\,\tau/d\,\gamma,$$

$d\,\tau/d\,\gamma$ étant la consolidation des cristaux dans la direction de glissement. Cette condition se traduit par

$$2\,d\,\tau/d\,\gamma = (1{\cdot}70 - 8\,\epsilon_p)\,\tau_0$$

d'où l'amplitude des bandes, ou l'allongement correspondant au palier :

$$\epsilon_p = 0{\cdot}21 - (d\,\tau/d\,\gamma)/4\,\tau_0$$

et, en remplaçant la cission τ_0 par la valeur de la limite élastique σ_0 :

$$\epsilon_p = 0{\cdot}21 - (d\,\tau/d\,\gamma)/2\,\sigma_0.$$

Cette formule ne peut cependant être appliquée qu'aux faibles valeurs de longueur de palier, car nous avons pris des relations simplifiées. Plus rigoureusement, la longueur du palier en fonction de $(d\tau/d\gamma)/2\sigma_0$ est donnée sur la Fig. 18 ; on voit que si la longueur du palier est supérieure à 8 pour cent, la relation ci-dessus conduit à des valeurs trop fortes et que la longueur maximale du palier, dans un échantillon isotrope, peut être de 17 pour cent.

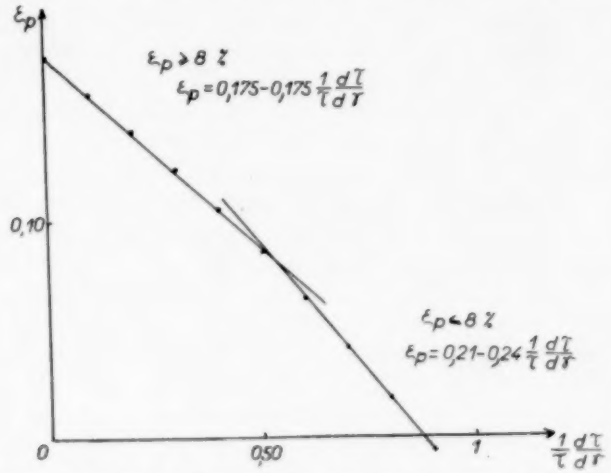

FIG. 18. Variation de la longueur du palier en fonction du rapport de la consolidation des cristaux à la cission critique.

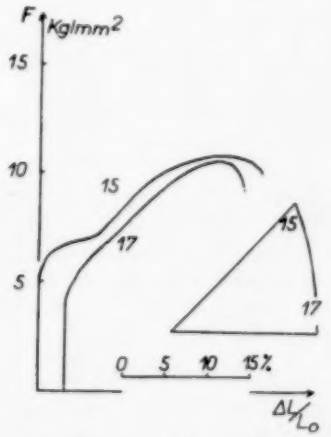

FIG. 19. Courbes de traction de deux monocristaux de fer ayant des orientations telles que λ soit supérieur ou inférieur à 45°. Dans le premier cas, un palier se dessine.

D. Comparaison avec les résultats expérimentaux

Nous avons recherché des vérifications expérimentales de cette relation et, par suite, des hypothèses que nous avons été amené à faire.

La longueur du palier doit donc dépendre de la limite élastique σ_0, du taux de consolidation des cristaux $d\tau/d\gamma$, et également de la texture, puisque des orientations préférentielles viendraient à l'encontre de nos calculs, basés sur l'isotropie du métal.

Ce rôle de la texture peut être observé dans le cas extrême, qui est celui des monocristaux. La Fig. 19 représente les courbes de traction de deux monocristaux étirés suivant $< 111 >$, direction pour laquelle $\lambda_0 = 70°$, et suivant $< 110 >$, où l'on a : $\lambda = 35°$. Dans le premier cas, le phénomène de rotation du réseau doit entraîner une baisse de consolidation, dans le second une augmentation ; c'est ce que l'on observe effectivement. Mais, si l'on trace les courbes de cission en fonction du glissement, en tenant compte de la rotation du réseau, on retrouve deux courbes normales (JAOUL et GONZALEZ 1960), le taux de consolidation des deux cristaux étant de l'ordre de 13 kg/mm². Cette forte valeur est due à des mécanismes particuliers de déformation pour ces orientations ; normalement, le taux de consolidation $d\tau/d\gamma$ dans le fer Armco est de l'ordre de 8 à 9 kg/mm² (JAOUL et GONZALEZ 1961). Avec cette valeur de $d\tau/d\gamma$ et des limites élastiques relativement faibles, comme celles des monocristaux ou des éprouvettes à gros grains, la formule donnerait $\epsilon_F < 0$, ce qui explique qu'il n'y ait pas de palier.

Une méthode pour faire varier seulement la texture est de prélever des éprouvettes suivant diverses orientations dans des tôles laminées. Après un fort laminage à froid et un court recuit à température assez basse, la tôle présente une majorité de grains dont une direction $< 110 >$ est sensiblement parallèle à la direction de laminage. En prélevant des éprouvettes de traction de telle manière que leur axe soit dans la direction de laminage ou incliné à 45°, on aura des textures $< 110 >$ ou $< 100 >$, c'est à dire de part et d'autre de la courbe $\lambda = 45°$. Le palier doit

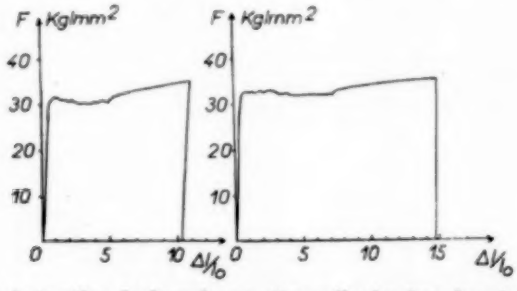

FIG. 20. Courbes de traction de deux éprouvettes prélevées dans la même tôle de manière que la texture majeure dans la direction de traction soit $< 110 >$ (courbe de gauche) ou $< 100 >$ (courbe de droite).

donc être plus long dans le second cas; La Fig. 20. représente les courbes de traction d'éprouvettes d'acier doux prélevées suivant deux directions dans une même tôle ; les longueurs de palier sont nettement différentes :

parallèle à la direction de laminage ($< 110 >$) : $\epsilon_p = 4{\cdot}0$ pour cent ;

à 45° de la direction de laminage ($< 100 >$) : $\epsilon_p = 6{\cdot}5$ pour cent.

Sur le même métal nous avons effectué, après écrouissage à froid des recuits à diverses températures pour avoir une grosseur de grain variable et, par suite une variation de la limite élastique. Sur la Fig. 21, nous avons porté la longueur du palier en fonction de l'inverse de la limite élastique. Les équations des deux droites tracées, pour les éprouvettes prélevées longitudinalement ou à 45°, encadrent la relation théorique. Le taux de consolidation des cristaux serait de 9 à 10 kg/mm²,

soit une valeur un peu plus forte que celle que nous avions observée avec les monocristaux de fer Armco.

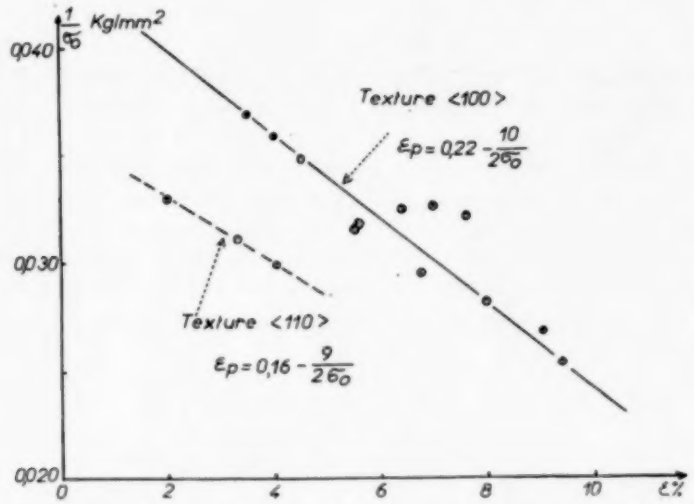

FIG. 21. Variation de la longueur du palier en fonction de l'inverse de la limite élastique d'éprouvettes d'acier doux prélevées dans la direction de laminage et à 45°.

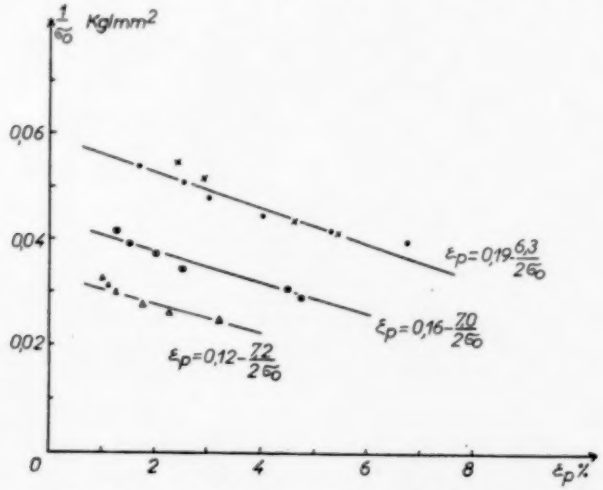

FIG. 22. Variation de la longueur du palier en fonction de l'inverse de la limite élastique (essais de Winlock). Les valeurs repérées par des croix sont tirées d'anciens essais de Winlock et Leiter. ● 0·06 pour cent C ; ○ 0·21 pour cent C ; △ 0·34 pour cent C.

Il est à remarquer, d'autre part, que le palier des courbes de traction doit disparaître si la limite élastique tombe en dessous d'une certaine valeur :

$$\sigma_0 < 2{\cdot}3\,(d\,\tau/d\,\gamma).$$

Dans le cas du fer Armco, nous n'avons jamais observé de palier pour des limites élastiques inférieures à 16 kg/mm², ce qui correspondrait à un taux de consolidation

$d\tau/d\gamma = 7$ kg/mm². Ce ne sont que les éprouvettes ayant les grains les plus fins (Fig. 6) qui ont donné un palier d'autant plus grand que la limite élastique était plus élevée.

WINLOCK (1953) a publié une série de courbes de traction d'aciers à diverses teneurs en carbone, les essais ayant été effectués à plusieurs vitesses. Sur la Fig. 22, sont portées, à partir de ces résultats, les longueurs du palier en fonction de l'inverse de la limite élastique. On voit qu'une équation du type de celle que nous avons proposée se trouve assez bien vérifiée. Cependant, la longueur maximale du palier diminue quand la teneur en carbone croît ; si l'on considère que les phénomènes ne se développent pas dans la perlite, la longueur réelle du palier afférent à la ferrite est supérieure à celle que l'on mesure effectivement sur les courbes de traction ; en effectuant une correction sur les coefficients des relations, on trouve que le premier est égal à 0·20 dans les trois cas, tandis que le terme contenant la consolidation croît avec la teneur en carbone.

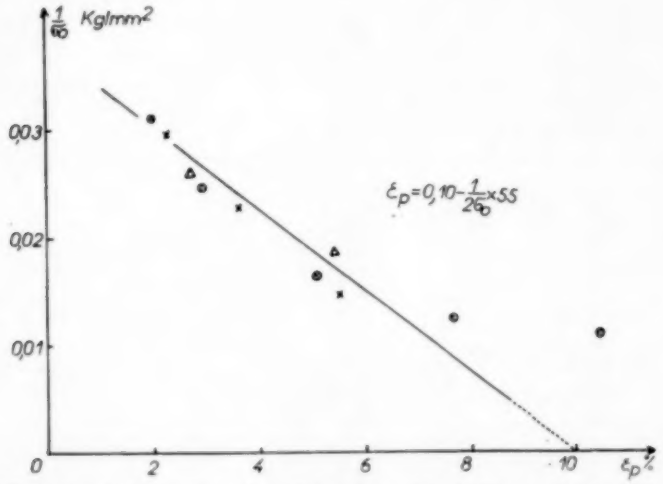

FIG. 23. Variation de la longueur du palier en fonction de l'inverse de la limite élastique (essais de Lean, Plateau et Crussard). Les essais ont été effectués à trois vitesses différentes et à des températures variant entre — 183° et l'ambiante.

Enfin, les valeurs portées sur la Fig. 23 sont tirées d'essais à diverses vitesses et températures de LEAN *et al.* (1959) ; les valeurs des coefficients sont nettement plus faibles que pour les essais précédents. Ceci montre à nouveau l'influence de la texture : en effet, les échantillons utilisés avaient été laminés, puis vieillis deux ans et étirés sans recuit ; la forte texture $< 110 >$ développée entraîne une baisse des deux coefficients.

Ces résultats expérimentaux semblent donc confirmer les hypothèses que nous avons été amené à faire. Il est à remarquer que dans les divers essais, sauf les derniers (Fig. 23), les valeurs du taux de consolidation des cristaux restent sensiblement les mêmes ; celà est dû à ce qu'il s'agit toujours de la consolidation de la ferrite, ainsi que le montre l'interprétation des résultats de WINLOCK. Il faut cependant rappeler que les polycristaux de fer ne présentent jamais de mécanisme

de déformation pouvant entraîner un durcissement important. Un monocristal qui subit une déformation comparable a, dans le domaine des déformations relativement faibles, une consolidation de l'ordre de 6 à 7 kg/mm², ce qui est bien en accord avec les résultats des essais de WINLOCK et aussi avec les nôtres sur fer Armco. Par contre, nos essais sur acier doux (Fig. 21) ont été effectués sur des tôles contenant, notamment, 0·35 pour cent de manganèse ; d'autre part, ces éprouvettes ont des textures peu favorables au développement d'un grand palier, ce qui peut être une raison de l'augmentation apparente de $d\tau/d\gamma$.

Le fait que le fer ait une limite élastique élevée est un facteur favorisant la déformation hétérogène par bandes. En effet, le mécanisme d'adoucissement du métal, dû aux phénomènes de rotation entraîne une variation absolue de cission effective qui est proportionnelle à la contrainte appliquée, tandis que la consolidation des cristaux garde une valeur constante. Il faut donc atteindre une certaine valeur de limite élastique pour que le palier apparaisse, et tous les facteurs diminuant la résistance du métal (grossissement du grain, décarburation, diminution de vitesse . . . .) seront défavorables aux grands paliers.

Connaissant donc les caractéristiques du fer qui facilitent la formation des bandes :

(a) haute limite élastique

(b) faible consolidation plastique

(c) glissements sinueux et peu de systèmes

nous allons chercher à déterminer si des bandes de Piobert peuvent se développer dans d'autres métaux.

E. Possibilités de bandes de Piobert dans d'autres métaux

A première vue, les deux conditions (a) et (b) sont en contradiction avec les propriétés des métaux cubiques à faces centrées, dont la limite élastique est assez basse et la consolidation relativement élevée ; on peut rappeler que le taux de consolidation à l'origine de la déformation de monocristaux (JAOUL et GONZALEZ 1961) est, relativement aux coefficients élastiques, environ deux fois plus fort dans un métal cubique à faces centrées que dans le cas du fer. Il faudrait donc, pour se trouver dans les mêmes conditions, des limites élastiques deux fois plus élevées ; celle des polycristaux de fer Armco étant de l'ordre de $E/1{,}000$, il faudrait, pour un aluminium, par exemple, une limite élastique de l'ordre de 15 kg/mm². C'est ce que l'on peut obtenir, ainsi que nous le verrons plus loin, avec des alliages aluminium-magnésium, par exemple.

Mais il est un autre facteur plus important : est-ce que la rotation du réseau peut conduire, dans d'autres structures à une augmentation de la cission effective moyenne pour une tension constante ? Nous avons vu que c'était le cas pour le fer, étant données les valeurs du coefficient $\rho = \sin x \cos \lambda$ (Fig. 16). Mais les conditions sont différentes, si le plan de glissement est bien défini ; La Fig. 24 donne les valeurs de ρ pour le système cubique à faces centrées, les éléments de glissement étant $< 110 > \{111\}$; la rotation ayant lieu vers la direction [101] quand un seul système de glissement se développe, on voit que, pour aucune orientation, elle ne peut entraîner de variation appréciable de ρ ; notamment, près de [111] où ρ varie rapidement, la rotation déplace l'axe à peu près parallèlement aux courbes $\rho =$ cte.

Mais il est cependant des cas où le glissement ne se fait plus nécessairement sur un plan $\{111\}$ bien défini ; c'est encore le cas des alliages aluminium-magnesium ; on sait (JAOUL 1952) en effet que le magnésium augmente peu la dissociation des dislocations, donc ne gêne pas la déviation des glissements ; on observe d'ailleurs par micrographie, de nombreuses déviations de glissements qui font que le plan

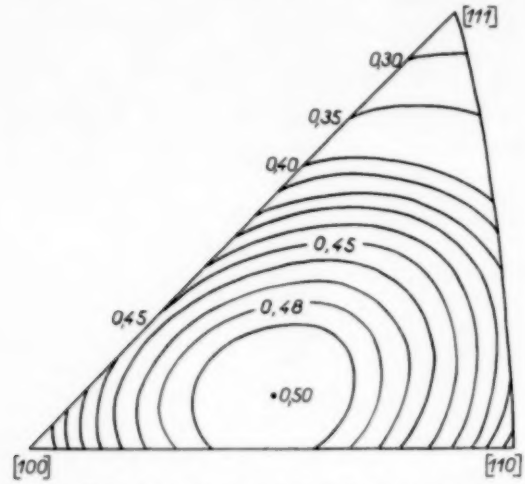

FIG. 24. Valeurs du coefficient $\rho = \sin \chi \cos \lambda$ dans le système cubique à faces centrées. Ces valeurs correspondent également au système cubique centré si le glissement a lieu sur le plan (110).

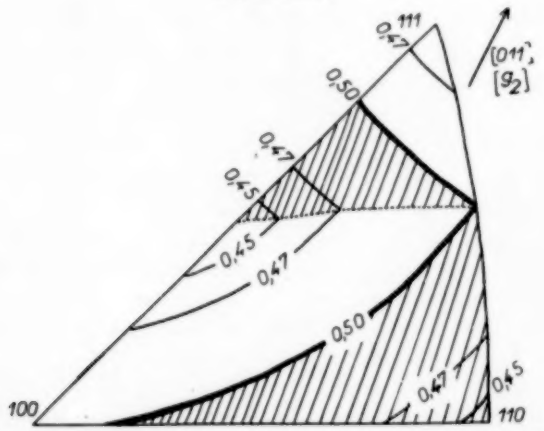

FIG. 25. Valeurs du coefficient $\rho = \sin \chi \cos \lambda$ dans les cristaux cubiques à faces centrées, dans l'hypothèse que le plan de glissement n'est pas défini cristallographiquement, mais corresponde au plan de cission maximale.

moyen de glissement n'est plus $\{111\}$. D'autre part, comme dans tous les alliages, les impuretés ont pour effet de diminuer le nombre de systèmes de glissement actifs. Enfin, les aluminium-magnésium ayant une limite élastique assez élevée, il semble que les conditions nécessaires pour qu'il y ait un palier puissent être remplies. Or, précisément, ces alliages donnent ce phénomène dans certains cas,

avec développement de déformations hétérogènes (stretcher strains). Mais, pratiquement, il ne s'agit plus du même mécanisme d'instabilité ; considérons, en effet la Fig. 25, qui représente les variations du coefficient ρ en supposant un glissement dans la direction $< 110 >$ la mieux favorisée, sur la surface où le cisaillement a en moyenne la valeur maximale. L'augmentation de cission effective par suite de la rotation n'a lieu que pour des cristaux étirés suivant une direction située dans une zone hachurée et l'on remarque que les variations du coefficient ρ restent faibles. Le calcul montre qu'elles peuvent difficilement expliquer le développement d'une instabilité de déformation.

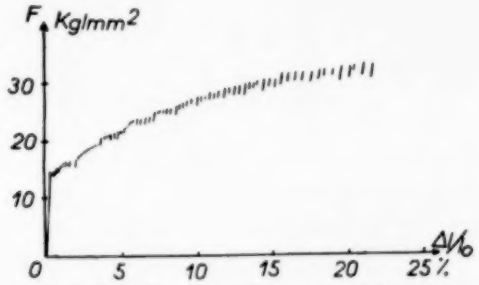

FIG. 26. Courbe de traction d'un alliage aluminium-magnésium à 5 pour cent. Les paliers successifs correspondent au développement des bandes.

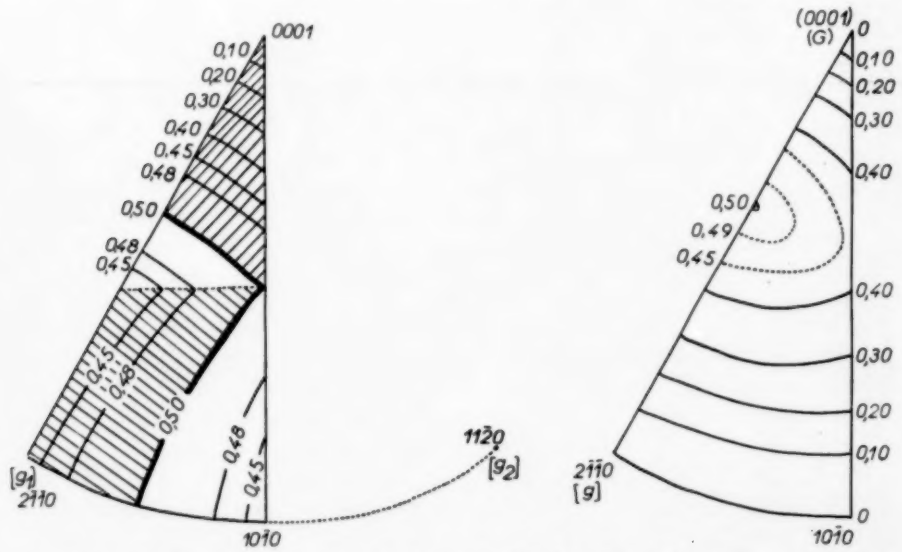

FIG. 27. Valeurs du coefficient : $\rho = \sin x \cos \lambda$ dans les cristaux hexagonaux ; à droite avec glissement sur le plan de base ; à gauche avec glissement sur le plan de cission maximale.

Nous n'avons d'ailleurs pas retrouvé avec les alliages aluminium-magnésium des propriétés du palier analogues à celles que nous avions observées sur le fer. Notamment, les bandes visibles sur la surface, et sur la tranche des éprouvettes plates, ne font pas un angle bien défini avec la direction de traction : nous avons

mesuré 64° dans un cas, 76° dans un autre, alors que la direction de traction fait avec les directions de glissement de chaque grain des angles compris entre 30° et 60°. D'autre part, en jouant sur le vieillissement et la vitesse de traction, nous avons pu faire varier la limite élastique de 20 pour cent, sans variation concomitante de la longueur de palier qui est toujours comprise entre 0·8 et 1·2 pour cent d'allongement. Enfin, la Fig. 26 montre que le palier est un phénomène qui se reproduit tout au long de la déformation, chaque portion à tension constante correspondant au balayage de l'éprouvette par une bande.

Les Fig. 27 sont relatives au cas de la structure hexagonale où le glissement a lieu suivant une direction du type $[11\bar{2}0]$. A droite est représenté le cas où le plan de glissement est bien défini et parallèle au plan de base (0001) ; à gauche sont données les valeurs de ρ dans le cas où le plan de glissement ne serait pas défini ; dans les deux cas l'augmentation de cission effective n'est pas prépondérante.

Il ne reste donc, parmi les structures les plus courantes, que la structure cubique à corps centré qui puisse donner lieu à un palier, même si le plan de glissement est défini, la rotation des grains étirés suivant une direction voisine de $< 111 >$ entraînera un effet important (Fig. 24). C'est ainsi que pour les alliages fer-silicium à 3 pour cent qui présentent des glissements droits, on observe un palier, cependant beaucoup plus faible que le fer si l'on considère la valeur très élevée de la limite élastique.

Le palier apparaît sur les courbes de traction de la plupart des métaux cubiques centrés. Nous l'avons observé avec le vanadium, la variation de longueur du palier avec la limite élastique étant très comparable à celle du fer :

$$\text{Va} : \epsilon_p = 0{\cdot}16 - 12/2\,\sigma_0.$$

Il existe aussi sur les courbes de Tantale (BECHTOLD 1955), de molybdène (BECHTOLD 1953), de Niobium (DYSON *et al.* 1959) et de Tungstène (BECHTOLD et SHEWMON 1954) avec, toujours, une amplitude d'autant plus grande que la limite élastique est plus élevée.

CONCLUSIONS

La déformation des aggrégats de cristaux de fer se caractérise par le fait que peu de systèmes de glissement interviennent dans chaque grain, une grande partie de ceux-ci ne révélant, au microscope, qu'une seule famille de lignes. Un tel type de déformation ne peut être que très limité, si la continuité aux joints doit être respectée. Pratiquement, des déchaussements importants apparaissent entre les grains et une déformation très complexe se développe dans une zone dont l'épaisseur est de l'ordre d'une dizaine de microns.

Ce type de déformation nécessite des tensions élevées, aussi la limite élastique croît-elle rapidement quand le diamètre des grains diminue : elle passe d'une valeur de l'ordre de 3·5 kg/mm² pour les monocristaux à 25 kg/mm² pour des polycristaux dont le diamètre moyen est de l'ordre de 25 μ.

Par contre, la consolidation dans le domaine plastique ne semble pas affectée par les joints. Les courbes d'éprouvettes à diverses grosseurs de grain ont sensiblement la même pente et l'on n'observe aucune variation systématique de forme. Le rôle des joints est donc seulement de déplacer la courbe parallèlement à elle-même. Ce déplacement pouvant être également réalisé par une variation de vitesse

de déformation, on est conduit à supposer que les joints se comporteraient comme le solide "idéalement plastique" de Saint Venant pour lequel la déformation se développe sous tension constante.

Comme dans le cas des cristaux cubiques à faces centrées, les courbes ont initialement une allure parabolique (d'exposant variant entre 0·6 et 0·8) puis s'infléchissent à partir d'une déformation de l'ordre de 8 pour cent, la courbe se poursuivant par une parabole à faible exposant. Il est à remarquer que, pour les grains très fins, cette deuxième parabole extrapolée passe par l'origine. L'inflexion des courbes ne peut pas être attribuée à un mécanisme identique à celui qui a été observé dans les métaux cubiques à faces centrées, puisque les déviations de glissement existent dès le début de la déformation ; elle correspond cependant toujours à l'écrouissage critique de recristallisation et doit donc être liée à une réorganisation des dislocations bloquées.

Les caractéristiques de déformation du fer (peu de systèmes de glissement, comportement quasi-visqueux des joints, forte limite élastique) permettent une interprétation du mécanisme de développement des déformations hétérogènes que sont les bandes de Piobert-Lüders. Si l'on suppose, en simplifiant à l'extrême, que chaque grain se déforme par glissement sur une seule surface, la rotation de ces grains est, en moyenne, telle que la composante de cission créant le glissement augmente pour un effort de traction constant. La consolidation étant faible, si elle ne peut pas compenser cette augmentation de cission effective, il pourra se développer une déformation limitée par instabilité.

La variation de cission due à la rotation étant proportionnelle à la contrainte appliquée, elle croît avec la limite élastique, tandis que la consolidation est indépendante de la grosseur du grain. Donc les facteurs augmentant la limite élastique favoriseront le développement de grands paliers sur les courbes de traction ; par contre, si la limite élastique est diminuée (par décarburation, grossissement du grain, ou faible vitesse de traction), le palier peut disparaître.

Le calcul de la longeur du palier conduit à une relation théorique qui se trouve bien vérifiée par les résultats expérimentaux. Ce mécanisme n'est possible que dans la structure cubique centrée.

Enfin, il faut rappeler que ces hypothèses ne font pas intervenir le rôle des impuretés, qui sont responsables des décrochements, mais ont seulement pour but de donner une interprétation de l'amplitude des déformations dans les bandes, qui a, pour une même éprouvette, une valeur bien définie, mais peut cependant, selon les conditions, varier entre 0 et 15 pour cent d'allongement.

Bibliographie

Bechtold, J. H.	1953	*J. Metals, N.Y.* **5**, 1471.
	1955	*Acta Met.* **3**, 249.
Bechtold, J. H. et Shewmon, P. G.	1954	*Trans. A.S.M.* **46**, 349.
Crussard, C. et Jaoul, B.	1950	*Rev. Métall.* **47**, 589.
Crussard, C., Lajeunesse, D. et Pomey, G.	1960	*Colloque sur la Mise en Forme des Tôles Minces* (Paris).
Dyson, B. F., Jones, R. B. et Tegart, W. J. McG.	1959	*J. Inst. Met.* **87**, 340.

FELL, E. W.	1935	*J. Iron. St. Inst.* **132**, 75.
HALL, E. O.	1951	*Proc. Phys. Soc. Lond.* B **64**, 742.
HALL, E. O. et SYLWESTROVICZ, W.	1951	*Proc. Phys. Soc. Lond.* B **64**, 495.
JAOUL, B.	1952	Thèse, Pub. Sc. et Tech. Ministère Air, No. 290.
	1957	*J. Mech. Phys. Solids* **5**, 95.
	1959	*Rev. Métall.* **56**, 98.
JAOUL, B., BRICOT, I. et LACOMBE, P.	1957	*Rev. Métall.* **54**, 81.
JAOUL, B. et GONZALEZ, D.	1959	*C.R. Acad. Sci., Paris* **248**, 2066.
	1961	*J. Mech. Phys. Solids* **9**, 16.
LEAN, J. B., PLATEAU, J. et CRUSSARD, C.	1959	*Rev. Métall.* **56**, 427.
LOMER, W. M.	1952	*J. Mech. Phys. Solids* **1**, 64.
LUDERS, W.	1860	*Dingler's Polytechnisches* **155**, 18.
NADAI, A.	1950	*Plasticity of Metals* (McGraw-Hill, New York).
PIOBERT, A.	1842	*Mém. de l'Artillerie* **5**, 525.
PLATEAU, J.	1960	Résultats non publiés.
REES, W. P. et HOPKINS, B. E.	1952	*J. Iron St. Inst.* **173**, 403.
SCHMID, E. et BOAS, W.	1935	*Kristallplastizität* (Springer, Berlin).
SEEGER, A., DIEHL, J., MADER, S. et REBSTOCK, H.	1957	*Phil. Mag.* **2**, 323.
TRUSZKOWSKI, W.	1958	*Rev. Métall.* **55**, 716.
WINLOCK, J.	1953	*J. Metals* **5**, 797.
WINLOCK, J. et LEITER, R. W.	1937	*Trans. A.S.M.* **25**, 163.

J. Mech. Phys. Solids, 1961, Vol. 9, pp. 91 to 104. Pergamon Press Ltd., London. Printed in Great Britain

STRESSES IN A PIPE WITH A DISCONTINUOUS BEND

By A. E. Green and W. C. Emmerson
King's College, Newcastle upon Tyne

(*Received 24th October*, 1960)

Summary

Analysis is developed for stress systems in two long straight circular cylindrical pipes which are rigidly joined together over a plane section of each pipe to form one pipe with a discontinuous bend. The analysis is restricted to pipes with a small angle between normal sections of either straight part and the plane of join. In particular, stresses are evaluated at the bend when the pipe is closed at its ends and is under uniform normal internal pressure, or when the pipe is acted on by a pure symmetrical couple.

1. Introduction and Statement of Problem

Elasticity problems concerned with stresses in circular cylindrical pipes containing smooth bends have been examined both theoretically and experimentally by many writers. We consider here pipes containing a 'mitred' or discontinuous bend. During the course of the present work the writers became aware of a paper presented by van der Neut at the Symposium on the theory of thin elastic shells in Delft and subsequently published in the proceedings of the Symposium (1960). In this paper van der Neut examined the stresses in a closed pipe with a number of discontinuous bends, under uniform internal pressure, by a method which was different from that of the present writers. In addition, although the problem considered here is slightly different from van der Neut's problem, the main features should be the same and some of van der Neut's predictions do not correspond with results obtained by Emmerson in an experimental investigation.† In view of this it seems that an alternative discussion of the problem is of value. Also, one new problem is examined.

We consider two long straight circular cylindrical pipes which are rigidly joined together over a plane (elliptical) section of each pipe to form one pipe with a discontinuous bend (see Fig. 1). The angle of inclination of the plane of join to normal sections of either part is $\alpha\,(0 \leqslant \alpha < \frac{1}{2}\pi)$. We suppose that the pipe is subjected to a system of stresses which are symmetrical about the plane of join and about the plane which contains the axis of each part of the pipe. By symmetry the shear stresses in the plane of join, and the displacement normal to this plane, are zero. We develop analysis for a long circular cylindrical pipe which has an oblique end section, and by applying suitable end conditions over this section, we can solve problems for a pipe with a discontinuous bend.

†This work, when completed, will be presented elsewhere, but some of the experimental results will be referred to here as a check on the main predictions of the theory.

The theory for a circular cylindrical pipe with an oblique end section given by van der NEUT was based on shell theory equations. The special case of the clamped end section has also been considered by KORNECKI (1957). Here we base our discussions on the equations of three-dimensional elasticity by using and extending an idea due to JOHNSON and REISSNER (1959)†. This work is contained in Sections

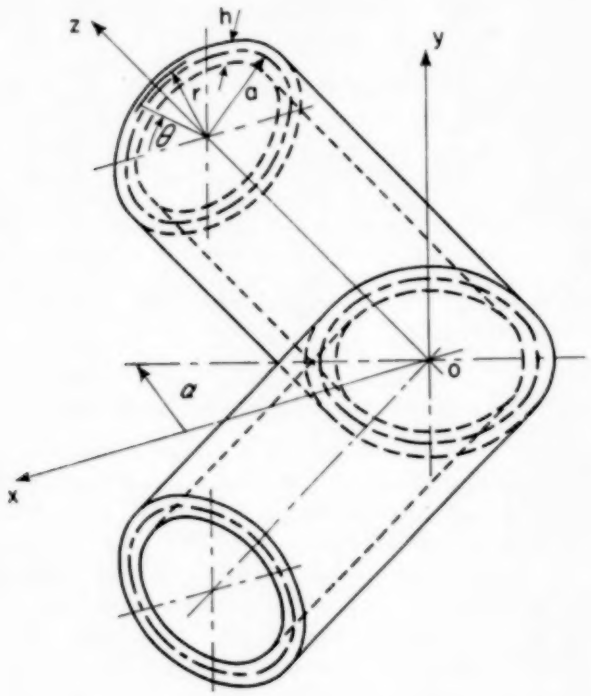

FIG. 1.

2–5. Two applications of the theory are given in Sections 6, 7. The first deals with stresses at an unreinforced discontinuous bend due to uniform internal pressure in the pipe whose ends at large distances from the bend are closed. The second is concerned with stresses at the bend when the pipe is under pure symmetrical flexure.

2. BASIC EQUATIONS

We start with the three-dimensional equations of the linear theory of elasticity expressed in cylindrical polar coordinates r, θ, z. With a usual notation the stress-strain relations for an isotropic body are

†See also E. L. REISS, in a forthcoming paper in the *Comm. Pure App. Math.*

$$
\left.\begin{aligned}
E\frac{\partial u_r}{\partial r} &= \sigma_r - \nu(\sigma_\theta + \sigma_z),\\
E\left(\frac{1}{r}\frac{\partial u_\theta}{\partial \theta} + \frac{u_r}{r}\right) &= \sigma_\theta - \nu(\sigma_r + \sigma_z),\\
E\frac{\partial u_z}{\partial z} &= \sigma_z - \nu(\sigma_r + \sigma_\theta),\\
E\left(\frac{\partial u_r}{\partial z} + \frac{\partial u_z}{\partial r}\right) &= 2(1+\nu)\,\tau_{rz},\\
E\left(\frac{1}{r}\frac{\partial u_z}{\partial \theta} + \frac{\partial u_\theta}{\partial z}\right) &= 2(1+\nu)\,\tau_{\theta z},\\
E\left(\frac{\partial u_\theta}{\partial r} - \frac{u_\theta}{r} + \frac{1}{r}\frac{\partial u_r}{\partial \theta}\right) &= 2(1+\nu)\,\tau_{r\theta},
\end{aligned}\right\} \qquad (2.1)
$$

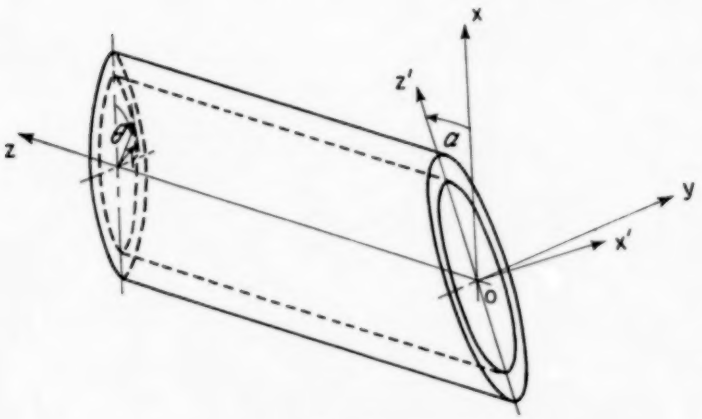

FIG. 2.

and the equations of equilibrium, in the absence of body forces, are

$$
\left.\begin{aligned}
\frac{\partial \sigma_r}{\partial r} + \frac{1}{r}\frac{\partial \tau_{r\theta}}{\partial \theta} + \frac{\partial \tau_{rz}}{\partial z} + \frac{\sigma_r - \sigma_\theta}{r} &= 0,\\
\frac{\partial \tau_{r\theta}}{\partial r} + \frac{1}{r}\frac{\partial \sigma_\theta}{\partial \theta} + \frac{\partial \tau_{\theta z}}{\partial z} + \frac{2\tau_{r\theta}}{r} &= 0,\\
\frac{\partial \tau_{rz}}{\partial r} + \frac{1}{r}\frac{\partial \tau_{\theta z}}{\partial \theta} + \frac{\partial \sigma_z}{\partial z} + \frac{\tau_{rz}}{r} &= 0.
\end{aligned}\right\} \qquad (2.2)
$$

We now consider a long circular cylindrical shell of radius a and constant thickness h bounded at one end by a plane section whose angle of inclination to a normal section of the shell is α (see Fig. 2). The equation of the plane end is

$$z = x \tan\alpha = r\cos\theta \tan\alpha. \qquad (2.3)$$

The origin of coordinates 0 is at the centre of the (elliptical) end section, $0z$ is along the axis of the cylindrical shell and $0y$ is along the minor axis of the elliptical

section. We make a change of variable and also introduce dimensionless coordinates ρ, β by an extension of a method used by JOHNSON and REISSNER (1959) for symmetrical deformations of long circular cylindrical shells. Thus

$$\rho = \frac{r-a}{\frac{1}{2}h}, \qquad \beta = \frac{z - r\cos\theta\tan\alpha}{(ah/2)^{\frac{1}{2}}}, \tag{2.4}$$

or

$$r = a(1+\lambda\rho), \quad z - r\cos\theta\tan\alpha = \beta a\lambda^{\frac{1}{2}}, \quad \lambda = \frac{h}{2a}. \tag{2.5}$$

In addition we define non-dimensional components of displacement and stress by the formulae

$$Eu_r = (1-\nu^2)\sigma a v_r, \quad Eu_\theta = (1-\nu^2)\sigma a\lambda^{\frac{1}{2}} v_\theta, \quad Eu_z = (1-\nu^2)\sigma a\lambda^{\frac{1}{2}} v_z, \tag{2.6}$$

and

$$\left.\begin{aligned} &\sigma_z = \sigma s_z, && \sigma_\theta = \sigma s_\theta, && \sigma_r = \lambda\sigma s_r, \\ &\tau_{\theta z} = \sigma s_{\theta z}, && \tau_{rz} = \sigma\lambda^{\frac{1}{2}} s_{rz}, && \tau_{r\theta} = \sigma\lambda^{\frac{1}{2}} s_{r\theta}. \end{aligned}\right\} \tag{2.7}$$

The quantity σ, which has the dimensions of stress, will be determined later.

Using (2.5)–(2.7), equations (2.1) become

$$\left.\begin{aligned} (1-\nu^2)\left(\frac{\partial v_r}{\partial\rho} - \lambda^{\frac{1}{2}}\frac{\partial v_r}{\partial\beta}\cos\theta\tan\alpha\right) &= \lambda^2 s_r - \nu\lambda(s_\theta + s_z), \\ (1-\nu^2)\left[v_r + \lambda^{\frac{1}{2}}\frac{\partial v_\theta}{\partial\theta} + (1+\lambda\rho)\frac{\partial v_\theta}{\partial\beta}\sin\theta\tan\alpha\right] &= (1+\lambda\rho)(s_\theta - \nu s_z - \nu\lambda s_r), \\ (1-\nu^2)\frac{\partial v_z}{\partial\beta} &= s_z - \nu s_\theta - \nu\lambda s_r, \end{aligned}\right\} \tag{2.8}$$

$$\left.\begin{aligned} \frac{\partial v_r}{\partial\beta} + \frac{\partial v_z}{\partial\rho} - \lambda^{\frac{1}{2}}\frac{\partial v_z}{\partial\beta}\cos\theta\tan\alpha &= 2\lambda s_{rz}/(1-\nu), \\ \lambda^{\frac{1}{2}}\frac{\partial v_z}{\partial\theta} + (1+\lambda\rho)\left(\frac{\partial v_\theta}{\partial\beta} + \frac{\partial v_z}{\partial\beta}\sin\theta\tan\alpha\right) &= 2(1+\lambda\rho)s_{\theta z}/(1-\nu), \\ \lambda^{\frac{1}{2}}\frac{\partial v_r}{\partial\theta} - \lambda v_\theta + (1+\lambda\rho)\left(\frac{\partial v_\theta}{\partial\rho} + \frac{\partial v_r}{\partial\beta}\sin\theta\tan\alpha - \lambda^{\frac{1}{2}}\frac{\partial v_\theta}{\partial\beta}\cos\theta\tan\alpha\right) &= 2\lambda(1+\lambda\rho)s_{r\theta}/(1-\nu), \end{aligned}\right\} \tag{2.9}$$

and equations (2.2) become

$$\left.\begin{aligned} (1+\lambda\rho)\left(\frac{\partial s_r}{\partial\rho} + \frac{\partial s_{r\theta}}{\partial\beta}\sin\theta\tan\alpha + \frac{\partial s_{rz}}{\partial\beta} - \lambda^{\frac{1}{2}}\frac{\partial s_r}{\partial\beta}\cos\theta\tan\alpha\right) + \\ + \lambda^{\frac{1}{2}}\frac{\partial s_{r\theta}}{\partial\theta} + \lambda s_r - s_\theta = 0, \\ (1+\lambda\rho)\left(\frac{\partial s_{r\theta}}{\partial\rho} - \lambda^{\frac{1}{2}}\frac{\partial s_{r\theta}}{\partial\beta}\cos\theta\tan\alpha + \frac{\partial s_\theta}{\partial\beta}\sin\theta\tan\alpha + \frac{\partial s_{\theta z}}{\partial\beta}\right) + \\ + \lambda^{\frac{1}{2}}\frac{\partial s_\theta}{\partial\theta} + 2\lambda s_{r\theta} = 0, \end{aligned}\right\} \tag{2.10}$$

$$(1 + \lambda\rho)\left(\frac{\partial s_{rz}}{\partial \rho} - \lambda^{\frac{1}{2}}\frac{\partial s_{rz}}{\partial \beta}\cos\theta\tan\alpha + \frac{\partial s_{\theta z}}{\partial \beta}\sin\theta\tan\alpha + \frac{\partial s_z}{\partial \beta}\right) + \\ + \lambda^{\frac{1}{2}}\frac{\partial s_{\theta z}}{\partial \theta} + \lambda s_{rz} = 0.$$

The next step is to seek a solution of equations (2.8)–(2.10) by assuming that, for sufficiently small λ, all dimensionless components of displacement and stress can be expanded for each value of ρ, θ and β in a power series in $\lambda^{\frac{1}{2}}$. The equations corresponding to the first approximation can be integrated and are found to provide a completely satisfactory solution for the problem of a long closed cylinder under uniform internal pressure when the oblique end section ($\beta = 0$) is *clamped*. This solution, however, is equivalent to that given by KORNECKI (1957) so will not be presented in detail here. When the boundary conditions at the oblique end correspond to those for the pipe with a free ' mitred ' joint the first approximation does not provide an adequate solution and it is necessary to proceed to a second approximation. The conditions at the oblique end section, together with the condition that the shear stresses at a plane at a large distance from the end vanish, force the conclusion that the membrane forces (per unit length) along the cylinder at large distances from the end has the form

$$\tfrac{1}{2}\,pa\,(1 + \tan^2\alpha\cos 2\,\theta), \tag{2.11}$$

where p is the internal pressure. This agrees with the prediction of van der NEUT and shows that, particularly for large values of $\tan\alpha$, there should be a great variation in membrane forces around any section sufficiently far from the mitred end. Van der NEUT makes the comment that ' this type of redistribution (of membrane stresses) is contrary to what would be expected ' but he does in fact accept it. The present writers feel that in the problem considered here, as well as in van der NEUT's problem, the result should be the usual value $\frac{1}{2}\,pa$ occuring in a single long closed circular cylinder under internal pressure p. Since there seemed to be no obvious mathematical reason for rejecting (2.11), the result required experimental confirmation. A number of experiments have now been undertaken by one of the present writers (W.C.E.) for different values of α up to 45°. In all cases so far studied the experiments reveal no variation of membrane force of the form (2.11) but they yield a constant value $\frac{1}{2}\,pa$. If $\alpha = 45°$ then $\tan\alpha = 1$, so that (2.11) varies from 0 to pa; and there is some variation of membrane force whatever value α has, so it is clear that (2.11) must be rejected, at least for our problem. This is not conclusive evidence that the same is true in van der NEUT's problem but the present writers believe that this is so.

One further drawback to van der NEUT's results emerges from equations (2.8)–(2.10), even if (2.11) is accepted. It is found that the hoop stress at the oblique end section cannot be evaluated to the order of magnitude required in λ without proceeding to a third approximation. This would be an extremely heavy piece of algebra and has not been undertaken, but the partial results of the second approximation suggest that the hoop stresses given by van der NEUT may not be complete to the order of magnitude stated†.

Problems of stress distribution in continuously curved pipes have been studied theoretically on the assumption that the radius of curvature of the pipe was large

†The discussion in Section 6 indicates, however, that these results are correct when $\tan\alpha$ is small.

compared with the cross section of the pipe.† This suggests that in the problem of a discontinuous bend it might be necessary to restrict the analysis to small values of the angle α. Further, an examination of (2.11) shows that when α is small the membrane force takes the expected value $\frac{1}{2}\,pa$ approximately at large distances from the bend. An examination of equations (2.8)–(2.10), together with the end conditions at the oblique end section, leads one to put

$$\tan\alpha = \epsilon\,\lambda^{\frac{1}{2}}, \tag{2.12}$$

and to replace v_θ, $s_{\theta z}$, $s_{r\theta}$ in (2.6) and (2.7) by $\lambda^{\frac{1}{2}} v_\theta$, $\lambda^{\frac{1}{2}} s_{\theta z}$, $\lambda^{\frac{1}{2}} s_{r\theta}$ respectively. Thus equations (2.6) and (2.7) are replaced by

$$Eu_r = (1-\nu^2)\,\sigma a\, v_r, \quad Eu_\theta = (1-\nu^2)\,\sigma a\,\lambda v_\theta, \quad Eu_z = (1-\nu^2)\,\sigma a\,\lambda^{\frac{1}{2}} v_z, \tag{2.13}$$

and

$$\left.\begin{aligned} \sigma_z &= \sigma s_z, & \sigma_\theta &= \sigma s_\theta, & \sigma_r &= \lambda\sigma\, s_r,\\ \tau_{\theta z} &= \sigma\lambda^{\frac{1}{2}}\, s_{\theta z}, & \tau_{rz} &= \sigma\lambda^{\frac{1}{2}}\, s_{rz}, & \tau_{r\theta} &= \sigma\lambda\, s_{r\theta}. \end{aligned}\right\} \tag{2.14}$$

Also equations (2.8)–(2.10) become

$$\left.\begin{aligned} (1-\nu^2)\left(\frac{\partial v_r}{\partial\rho} - \epsilon\lambda\frac{\partial v_r}{\partial\beta}\cos\theta\right) &= \lambda^2 s_r - \nu\lambda\,(s_\theta + s_z),\\ (1-\nu^2)\left[v_r + \lambda\frac{\partial v_\theta}{\partial\theta} + \epsilon\lambda\,(1+\lambda\rho)\frac{\partial v_\theta}{\partial\beta}\sin\theta\right] &= (1+\lambda\rho)\,(s_\theta - \nu s_z - \nu\lambda\, s_r),\\ (1-\nu^2)\frac{\partial v_z}{\partial\beta} &= s_z - \nu s_\theta - \nu\lambda\, s_r, \end{aligned}\right\} \tag{2.15}$$

$$\left.\begin{aligned} \frac{\partial v_r}{\partial\beta} + \frac{\partial v_z}{\partial\rho} - \epsilon\lambda\frac{\partial v_z}{\partial\beta}\cos\theta &= 2\lambda\, s_{rz}/(1-\nu),\\ \frac{\partial v_z}{\partial\theta} + (1+\lambda\rho)\left(\frac{\partial v_\theta}{\partial\beta} + \epsilon\frac{\partial v_z}{\partial\beta}\sin\theta\right) &= 2\,(1+\lambda\rho)\, s_{\theta z}/(1-\nu),\\ \frac{\partial v_r}{\partial\theta} - \lambda v_\theta + (1+\lambda\rho)\left(\frac{\partial v_\theta}{\partial\rho} - \epsilon\lambda\frac{\partial v_\theta}{\partial\beta}\cos\theta + \epsilon\frac{\partial v_r}{\partial\beta}\sin\theta\right) &= 2\lambda\,(1+\lambda\rho)\, s_{r\theta}/(1-\nu), \end{aligned}\right\} \tag{2.16}$$

and equations (2.2) become

$$\left.\begin{aligned} (1+\lambda\rho)\left(\frac{\partial s_r}{\partial\rho} - \epsilon\lambda\frac{\partial s_r}{\partial\beta}\cos\theta + \frac{\partial s_{rz}}{\partial\beta} + \epsilon\lambda\frac{\partial s_{r\theta}}{\partial\beta}\sin\theta\right) + \\ + \lambda\frac{\partial s_{r\theta}}{\partial\theta} + \lambda s_r - s_\theta = 0,\\ (1+\lambda\rho)\left(\frac{\partial s_{r\theta}}{\partial\rho} - \epsilon\lambda\frac{\partial s_{r\theta}}{\partial\beta}\cos\theta + \frac{\partial s_{\theta z}}{\partial\beta} + \epsilon\frac{\partial s_\theta}{\partial\beta}\sin\theta\right) + \\ + \frac{\partial s_\theta}{\partial\theta} + 2\lambda\, s_{r\theta} = 0, \end{aligned}\right\} \tag{2.17}$$

†Pipes with small curvatures have, however, been considered by a mixture of empirical and experimental methods.

$$(1+\lambda\rho)\left(\frac{\partial s_{rz}}{\partial\rho}-\epsilon\lambda\frac{\partial s_{rz}}{\partial\beta}\cos\theta+\frac{\partial s_z}{\partial\beta}+\epsilon\lambda\frac{\partial s_{\theta z}}{\partial\beta}\sin\theta\right)+ \\ +\lambda\frac{\partial s_{\theta z}}{\partial\theta}+\lambda s_{rz}=0.$$

3. Expansions in Powers of λ

We assume that for sufficiently small λ all dimensionless components of displacements and stress can be expanded for each value of ρ, θ and β in a power series in λ:

$$\left.\begin{aligned} v &= v^{(0)}(\rho,\theta,\beta)+\lambda v^{(1)}(\rho,\theta,\beta)+\ldots,\\ s &= s^{(0)}(\rho,\theta,\beta)+\lambda s^{(1)}(\rho,\theta,\beta)+\ldots, \end{aligned}\right\} \tag{3.1}$$

We then substitute these expansions in equations (2.15) to (2.17) and equate to zero the coefficients of powers of λ, assuming that ϵ is a parameter independent of λ. The coefficients of λ^0 yield

$$\left.\begin{aligned} &\frac{\partial v_r^{(0)}}{\partial\rho}=0,\\ &\frac{\partial v_z^{(0)}}{\partial\rho}=-\frac{\partial v_r^{(0)}}{\partial\beta},\\ &\frac{\partial v_\theta^{(0)}}{\partial\rho}=-\epsilon\frac{\partial v_r^{(0)}}{\partial\beta}\sin\theta-\frac{\partial v_r^{(0)}}{\partial\theta}, \end{aligned}\right\} \tag{3.2}$$

and

$$\left.\begin{aligned} &s_{\theta z}^{(0)}=\frac{1-\nu}{2}\left(\frac{\partial v_\theta^{(0)}}{\partial\beta}+\epsilon\frac{\partial v_z^{(0)}}{\partial\beta}\sin\theta+\frac{\partial v_z^{(0)}}{\partial\theta}\right),\\ &s_z^{(0)}=\frac{\partial v_z^{(0)}}{\partial\beta}+\nu v_r^{(0)},\\ &s_\theta^{(0)}=v_r^{(0)}+\nu\frac{\partial v_z^{(0)}}{\partial\beta},\\ &\frac{\partial s_{rz}^{(0)}}{\partial\rho}=-\frac{\partial s_z^{(0)}}{\partial\beta},\\ &\frac{\partial s_{r\theta}^{(0)}}{\partial\rho}=-\frac{\partial s_{\theta z}^{(0)}}{\partial\beta}-\epsilon\frac{\partial s_\theta^{(0)}}{\partial\beta}\sin\theta-\frac{\partial s_\theta^{(0)}}{\partial\theta},\\ &\frac{\partial s_r^{(0)}}{\partial\rho}=-\frac{\partial s_{rz}^{(0)}}{\partial\beta}+s_\theta^{(0)}. \end{aligned}\right\} \tag{3.3}$$

Further equations, obtained by equating coefficients of higher powers of λ to zero, can be obtained without difficulty but we restrict attention here to the equations (3.2) and (3.3). These equations have been written in an order which makes integration with respect to ρ possible step by step. Introducing functions $V_r^{(0)}(\theta,\beta)$ etc., which are independent of ρ, and using the notation

$$\frac{\partial(\ )}{\partial\beta}=(\ )',\qquad \frac{\partial(\ )}{\partial\theta}=(\ )^*, \tag{3.4}$$

equations (3.2) and (3.3) yield

$$\left.\begin{aligned} v_r^{(0)} &= V_r^{(0)},\\ v_z^{(0)} &= V_z^{(0)}-\rho V_r^{(0)\prime},\\ v_\theta^{(0)} &= V_\theta^{(0)}-\epsilon\rho\,V_r^{(0)\prime}\sin\theta-\rho V_r^{(0)*}, \end{aligned}\right\} \tag{3.5}$$

$$
\left.\begin{aligned}
s_{\theta z}^{(0)} &= \frac{1-\nu}{2}\,(V_\theta^{(0)\prime} + \epsilon V_z^{(0)\prime}\sin\theta + V_z^{(0)\bullet} - 2\rho\, V_r^{(0)\prime\bullet} - 2\rho\, V_r^{(0)\prime\prime}\,\epsilon\sin\theta),\\
s_z^{(0)} &= V_z^{(0)\prime} + \nu V_r^{(0)} - \rho V_r^{(0)\prime\prime},\\
s_\theta^{(0)} &= V_r^{(0)} + \nu V_z^{(0)\prime} - \nu\rho\, V_r^{(0)\prime\prime},\\
s_{rz}^{(0)} &= S_{rz}^{(0)} - \rho\,(V_z^{(0)\prime\prime} + \nu V_r^{(0)\prime}) + \tfrac{1}{2}\rho^2 V_r^{(0)\prime\prime\prime},\\
s_{r\theta}^{(0)} &= S_{r\theta}^{(0)} - \rho\left(\frac{1-\nu}{2}\,V_\theta^{(0)\prime\prime} + V_r^{(0)\prime}\,\epsilon\sin\theta + \frac{1+\nu}{2}\,V_z^{(0)\prime\prime}\,\epsilon\sin\theta + \right.\\
&\qquad \left. + \frac{1+\nu}{2}\,V_z^{(0)\prime\bullet} + V_r^{(0)\bullet}\right) + \tfrac{1}{2}\rho^2\,(V_r^{(0)\prime\prime\prime}\,\epsilon\sin\theta + V_r^{(0)\prime\prime\bullet}),\\
s_r^{(0)} &= S_r^{(0)} + \rho\,(-S_{rz}^{(0)\prime} + V_r^{(0)} + \nu V_z^{(0)\prime}) + \tfrac{1}{2}\rho^2\, V_z^{(0)\prime\prime\prime} - \tfrac{1}{6}\rho^3\, V_r^{(0)\mathrm{IV}}.
\end{aligned}\right\} \tag{3.6}
$$

Since we are only considering the first approximation we can omit the upper sign (0) on quantities $V_r^{(0)}$ etc. for the rest of this paper without confusion.

4. Surface Conditions and Solution of Equations

We suppose that there are zero applied shear stresses at the surfaces $\rho = \pm 1$ of the shell, zero normal applied stress at the outer surface $\rho = 1$ and a normal pressure p at the inner surface $\rho = -1$, where p may depend on θ but not on β. Hence

$$
\left.\begin{aligned}
s_{rz}^{(n)} = s_{r\theta}^{(n)} &= 0, && (n \geqslant 0,\ \rho = \pm 1),\\
s_r^{(n)} &= 0, && (n \geqslant 0,\ \rho = 1),\\
s_r^{(0)} = -P = \frac{-p}{\lambda\sigma}, \qquad s_r^{(n)} &= 0, && (n \geqslant 1,\ \rho = -1).
\end{aligned}\right\} \tag{4.1}
$$

Satisfaction of (4.1) for $n = 0$ by the stresses (3.6) leads, after some manipulation, to

$$
\left.\begin{aligned}
&V_z'' + \nu V_r' = 0,\\
&\frac{1-\nu}{2}\,V_\theta'' + \frac{1+\nu}{2}\,(V_z''\,\epsilon\sin\theta + V_z'^{\bullet}) + V_r'\,\epsilon\sin\theta + V_r^{\bullet} = 0,
\end{aligned}\right\} \tag{4.2}
$$

$$
\left.\begin{aligned}
S_{rz} &= -\tfrac{1}{2}\,V_r''',\\
S_{r\theta} &= -\tfrac{1}{2}\,(V_r'''\,\epsilon\sin\theta + V_r''^{\bullet}),\\
S_r &= -\tfrac{1}{2}\,(P + V_z'''),
\end{aligned}\right\} \tag{4.3}
$$

$$
-S_{rz}' + V_r + \nu V_z' - \tfrac{1}{6}\,V_r^{\mathrm{IV}} = \tfrac{1}{2}\,P. \tag{4.4}
$$

The first of equations (4.2) can be integrated to yield

$$
V_z' = -\nu V_r + B, \tag{4.5}
$$

where B is a function of θ. Using (4.3) and (4.5) equation (4.4) becomes

$$
V_r^{\mathrm{IV}} + 3\,(1-\nu^2)\,V_r = \tfrac{3}{2}\,P - 3\nu B. \tag{4.6}
$$

Since P and B are functions of θ and independent of β we can integrate (4.6) in the form

$$
V_r = \frac{P}{2\,(1-\nu^2)} - \frac{\nu B}{1-\nu^2} + (K\cos k\beta + L\sin k\beta)\,e^{-k\beta}, \tag{4.7}
$$

if we omit the solutions which tend to infinity with β. In (4.7)

$$
k = \left[\frac{3\,(1-\nu^2)}{4}\right]^{\frac{1}{4}}, \tag{4.8}
$$

and K, L are functions of θ. Returning to (4.5) we find, with the help of (4.7),

$$V_z' = -\frac{\nu P}{2(1-\nu^2)} + \frac{B}{1-\nu^2} - \nu(K\cos k\beta + L\sin k\beta)\,e^{-k\beta}, \tag{4.9}$$

and one further integration gives

$$V_z = C + \beta\left[\frac{B}{1-\nu^2} - \frac{\nu P}{2(1-\nu^2)}\right] + \frac{\nu}{2k}\left[(K+L)\cos k\beta + (L-K)\sin k\beta\right]e^{-k\beta}, \tag{4.10}$$

where C is a function of θ. Using (4.7) and (4.10) we can integrate the second of equations (4.2) to get

$$\begin{aligned} V_\theta' = A - \frac{(2+\nu)\,\epsilon P\sin\theta}{2(1-\nu^2)} + \frac{(2+\nu)\,\nu\epsilon\, B\sin\theta}{1-\nu^2} - \beta\left[\frac{B^*}{1-\nu^2} + \frac{(2+\nu)\,P^*}{2(1-\nu^2)}\right] - \\ - (2+\nu)\,\epsilon\,(K\cos k\beta + L\sin k\beta)\,e^{-k\beta}\sin\theta + \\ + \frac{2+\nu}{2k}\left[(K^*+L^*)\cos k\beta + (L^*-K^*)\sin k\beta\right]e^{-k\beta}, \end{aligned} \tag{4.11}$$

where A is a function of θ.

For convenience in later parts of the paper we record the following results:

$$V_z' + \nu V_r = B, \tag{4.12}$$

$$V_r + \nu V_z' = \tfrac{1}{2}P + (1-\nu^2)(K\cos k\beta + L\sin k\beta)\,e^{-k\beta}, \tag{4.13}$$

$$\begin{aligned} V_\theta' + V_z'\,\epsilon\sin\theta + V_z^* = A + C^* - \frac{P\epsilon\sin\theta}{1-\nu} + \frac{(1+\nu)\,B\epsilon\sin\theta}{1-\nu} - \frac{(1+\nu)\,\beta P^*}{1-\nu} - \\ - 2(1+\nu)\,\epsilon\,(K\cos k\beta + L\sin k\beta)\,e^{-k\beta}\sin\theta + \\ + \frac{1+\nu}{k}\left[(K^*+L^*)\cos k\beta + (L^*-K^*)\sin k\beta\right]e^{-k\beta}. \end{aligned} \tag{4.14}$$

5. Edge Conditions

We now consider edge conditions in the plane $\beta = 0$ and for this purpose we require components of stresses across this plane and also the component of normal displacement. It is convenient to make a change of rectangular axes x, y, z to x', y, z' (see Fig. 2) where

$$z' = x\cos\alpha + z\sin\alpha, \qquad x' = x\sin\alpha - z\cos\alpha. \tag{5.1}$$

When $\beta = 0$ we have

$$z' = \frac{r\cos\theta}{\cos\alpha}, \qquad y = r\sin\theta, \tag{5.2}$$

and using (2.5) and (2.12) these become

$$\left.\begin{aligned} \frac{z'}{a} &= \cos\theta + \lambda(\rho + \tfrac{1}{2}\epsilon^2)\cos\theta + \ldots, \\ \frac{y}{a} &= \sin\theta + \lambda\rho\sin\theta. \end{aligned}\right\} \tag{5.3}$$

Also from (5.2), we see that an element of area in the plane $\beta = 0$ is

$$dz'\,dy = \frac{r\,.\,dr\,.\,d\theta}{\cos\alpha} = \frac{a^2\lambda(1+\lambda\rho)\,d\rho\,.\,d\theta}{\cos\alpha}, \tag{5.4}$$

Components of stress $\sigma_{x'}$, $\tau_{x'y}$, $\tau_{x'z}$ across the plane $\beta = 0$ or $x' = 0$ are obtained by using the usual formulae for transformation of stress. Thus

$$\left.\begin{aligned} \sigma_{x'} &= \sigma_x \sin^2\alpha + \sigma_z \cos^2\alpha - 2\tau_{xz} \sin\alpha \cos\alpha, \\ \tau_{x'y} &= \tau_{xy} \sin\alpha - \tau_{zy} \cos\alpha, \\ \tau_{x'z'} &= (\sigma_x - \sigma_z) \sin\alpha \cos\alpha + (\sin^2\alpha - \cos^2\alpha)\, \tau_{xz}, \end{aligned}\right\} \tag{5.5}$$

$$\left.\begin{aligned} \sigma_x &= \sigma_r \cos^2\theta + \sigma_\theta \sin^2\theta - 2\,\tau_{r\theta} \sin\theta \cos\theta, \\ \sigma_y &= \sigma_r \sin^2\theta + \sigma_\theta \cos^2\theta + 2\,\tau_{r\theta} \sin\theta \cos\theta, \\ \tau_{xy} &= (\sigma_r - \sigma_\theta) \sin\theta \cos\theta + \tau_{r\theta} \cos 2\theta, \end{aligned}\right\} \tag{5.6}$$

$$\left.\begin{aligned} \tau_{xz} &= \tau_{rz} \cos\theta - \tau_{\theta z} \sin\theta, \\ \tau_{yz} &= \tau_{rz} \sin\theta + \tau_{\theta z} \cos\theta. \end{aligned}\right\} \tag{5.7}$$

With the help of (2.12), (2.14), (3.1), (5.6) and (5.7) the stresses (5.5) across the plane $\beta = 0$ can be expressed in powers of λ. Here we are only concerned with the major terms in each stress component which are found to be

$$\sigma_{x'} = \sigma\, s_z^{(3)}, \tag{5.8}$$

$$\left.\begin{aligned} \frac{\tau_{x'y}}{\sigma\lambda^{\frac{1}{2}}} &= -\epsilon s_\theta^{(0)} \sin\theta \cos\theta - s_{rz}^{(0)} \sin\theta - s_{\theta z}^{(0)} \cos\theta, \\ \frac{\tau_{x'z'}}{\sigma\lambda^{\frac{1}{2}}} &= \epsilon\,(s_\theta^{(0)} \sin^2\theta - s_z^{(0)}) - s_{rz}^{(0)} \cos\theta + s_{\theta z}^{(0)} \sin\theta. \end{aligned}\right\} \tag{5.9}$$

With the help of (3.6), (4.7) and (4.12) to (4.14) the shear stresses (5.9) over the plane $\beta = 0$ become

$$\begin{aligned} \frac{\tau_{x'y}}{\sigma\lambda^{\frac{1}{2}}} = &-\frac{1-\nu}{2}(A + C^*)\cos\theta - \frac{1+\nu}{2} B\epsilon \sin\theta\cos\theta - \\ &- \frac{1-\nu^2}{2k}(K^* + L^*)\cos\theta + (1-\rho^2)k^3(K+L)\sin\theta + \\ &+ \rho\left[-2k^2 L\epsilon \sin\theta + k(1-\nu)(L^* - K^*)\right]\cos\theta, \end{aligned} \tag{5.10}$$

$$\begin{aligned} \frac{\tau_{x'z'}}{\sigma\lambda^{\frac{1}{2}}} = &\frac{1-\nu}{2}(A + C^*)\sin\theta + \frac{1+\nu}{2} B\epsilon \sin^2\theta - B\epsilon + \\ &+ \frac{1-\nu^2}{2k}(K^* + L^*)\sin\theta + (1-\rho^2)k^3(K+L)\cos\theta - \\ &- \rho\left[2k^2 L\epsilon \cos^2\theta + k(1-\nu)(L^* - K^*)\sin\theta\right]. \end{aligned} \tag{5.11}$$

In applications of the theory we require shear stresses over the plane $\beta = 0$ to be zero. It is not, however, possible to satisfy this condition exactly; instead we require that shearing stress resultants over the plane should be zero†. Since we are only concerned here with the first term in the expansions with respect to λ we can impose the conditions

$$\int_{-1}^{1} \tau_{x'y}\, d\rho = 0, \qquad \int_{-1}^{1} \tau_{x'z'}\, d\rho = 0, \tag{5.12}$$

where $\tau_{x'y}$, $\tau_{x'z'}$ are given respectively by (5.10) and (5.11). Substituting from (5.10) and (5.11) in (5.12), and making use of (4.8), we obtain the edge conditions

†Strictly speaking the tangential component of the stress resultant is zero and the normal component modified in the usual way by a contribution from the derivative of the torsional couple resultant is zero, but to our order of approximation in λ this latter contribution does not affect the result. In view of (5.19), however, the torsional couple is actually zero.

$$\left.\begin{aligned}(K+L)\sin\theta-(K^*+L^*)\cos\theta-\frac{k(A+C^*)\cos\theta}{1+\nu}-\frac{kB\epsilon\sin\theta\cos\theta}{1-\nu}=0,\\(K+L)\cos\theta+(K^*+L^*)\sin\theta+\frac{k(A+C^*)\sin\theta}{1+\nu}+\frac{kB\epsilon\sin^2\theta}{1-\nu}-\frac{2Bk\epsilon}{1-\nu^2}=0.\end{aligned}\right\}\tag{5.13}$$

Equations (5.13) may be solved to yield

$$\left.\begin{aligned}K+L&=\frac{2Bk\epsilon\cos\theta}{1-\nu^2},\\K^*+L^*&=\frac{2Bk\epsilon\sin\theta}{1-\nu^2}-\frac{kB\epsilon\sin\theta}{1-\nu}-\frac{k(A+C^*)}{1+\nu},\end{aligned}\right\}\tag{5.14}$$

so that

$$A+C^*=\frac{4B\epsilon\sin\theta}{1-\nu}-\frac{(1+\nu)B\epsilon\sin\theta}{1-\nu}-\frac{2B^*\epsilon\cos\theta}{1-\nu}.\tag{5.15}$$

The component of displacement normal to the plane $\beta=0$ can be obtained by simple resolution of components. Thus

$$u_{x'}=(u_r\cos\theta-u_\theta\sin\theta)\sin\alpha-u_z\cos\alpha.\tag{5.16}$$

Using (2.12) and (2.13), and retaining only the first terms in λ, this gives

$$u_{x'}=\frac{(1-\nu^2)\sigma a\,\lambda^{\frac{1}{2}}}{E}\left[\epsilon v_r^{(0)}\cos\theta-v_z^{(0)}\right].\tag{5.17}$$

Hence, with the help of (3.5), (4.7) and (4.10), equation (5.17) becomes

$$\frac{Eu_{x'}}{(1-\nu^2)\sigma a\,\lambda^{\frac{1}{2}}}=\frac{P\epsilon\cos\theta}{2(1-\nu^2)}-\frac{\nu B\epsilon\cos\theta}{1-\nu^2}-C+K\epsilon\cos\theta-\frac{\nu(K+L)}{2k}+\rho k(L-K).\tag{5.18}$$

If this is to be zero for all values of ρ then

$$L=K,\tag{5.19}$$

$$C=\frac{P\epsilon\cos\theta}{2(1-\nu^2)}-\frac{\nu B\epsilon\cos\theta}{1-\nu^2}-\frac{\nu(K+L)}{2k}+K\epsilon\cos\theta.\tag{5.20}$$

Finally in this Section we require stress components $\sigma_{z'}$, $\tau_{z'y}$, σ_y in planes $\beta=$ constant, and we only record values corresponding to the terms in λ considered here. A straightforward calculation yields

$$\sigma_{z'}=\sigma s_\theta^{(0)}\sin^2\theta,\ \tau_{z'y}=-\sigma s_\theta^{(0)}\sin\theta\cos\theta,\ \sigma_y=\sigma s_\theta^{(0)}\cos^2\theta,\tag{5.21}$$

and in view of (5.3) this is equivalent to a hoop stress $\sigma s_\theta^{(0)}$ in planes $\beta=$ constant, i.e.

$$\sigma\left[\tfrac{1}{2}P+(1-\nu^2)(K\cos k\beta+L\sin k\beta)e^{-k\beta}+2\nu k^2\rho(L\cos k\beta-K\sin k\beta)e^{-k\beta}\right],\tag{5.22}$$

if we use (3.6), (4.7) and (4.13). Also the stress normal to planes $\beta=$ constant is

$$\sigma s_z^{(0)}=\sigma\left[B+2k^2\rho(L\cos k\beta-K\sin k\beta)e^{-k\beta}\right].\tag{5.23}$$

6. Pressure Problem

Here we consider the problem of a circular cylindrical pipe, closed at its ends, under uniform internal pressure p, the pipe having a sharp bend at its middle section which is assumed to be at a large distance from either end. By symmetry the shearing stresses over the plane elliptical section of the pipe at its bend are zero as also is the normal displacement provided we allow free displacements at the ends

of the pipe. The analysis developed in this paper can be applied at once to this problem, provided we replace the stress condition at $\beta = 0$ by the approximate condition that shearing stress resultants vanish there. In addition, for large values of β, we should obtain the classical values for the stresses so that

$$s_\theta \to \frac{P}{2}, \qquad s_z \to \frac{P}{4}, \qquad s_{\theta z} \to 0, \qquad P = \frac{p}{\lambda\sigma}, \tag{6.1}$$

when $\beta \to \infty$.

From (3.6) and (4.13) we see that the first condition in (6.1) is satisfied. From (3.6) and (4.12) the second condition is satisfied if

$$B = \frac{P}{4}. \tag{6.2}$$

Equation (5.15) then gives

$$A + C^* = \frac{(3 - \nu)\, P\epsilon \sin\theta}{4\,(1 - \nu)}, \tag{6.3}$$

and the last condition in (6.1) is automatically satisfied in view of (3.6) and (4.14), if we remember that $P^* = 0$. Next, from (5.14), (5.19) and (6.2), we have

$$K = L = \frac{Pk\,\epsilon \cos\theta}{4\,(1 - \nu^2)}. \tag{6.4}$$

Equation (5.20) then gives C, and A can be found from (6.3), but these are not required here.

Using (6.4) and (5.22) we see that the hoop stress in the plane of join $\beta = 0$ is

$$\frac{pa}{h}\left\{1 + \frac{k\epsilon}{2}\left(1 + \frac{2\nu k^2 \rho}{1 - \nu^2}\right)\cos\theta\right\}. \tag{6.5}$$

The hoop stress for large values of β is pa/h so that the ratio of the hoop stress in the plane $\beta = 0$ to that for large β is

$$1 + \frac{k\epsilon}{2}\left(1 + \frac{2\nu k^2 \rho}{1 - \nu^2}\right)\cos\theta. \tag{6.6}$$

Also, from (5.23), (6.2) and (6.4), we see that the normal stress across the plane $\beta = 0$ is

$$\frac{pa}{2h}\left(1 + \frac{2k^3\,\epsilon\rho\cos\theta}{1 - \nu^2}\right). \tag{6.7}$$

As pointed out earlier the present writers have suggested that the results given by van der NEUT (1960) are not satisfactory for the present problem for arbitrary values of α. However, if in his work all terms involving $\tan^2\alpha$ and higher powers of $\tan\alpha$ are neglected, then his results become identical with those of the present paper. The method of solution adopted here suggests that the results may only be reliable for small values of α.

As an example of the magnitude of the factor (6.6) we consider values of a, h, α and ν used in experimental work by EMMERSON†

$$2a = 4 \text{ in.}, \qquad h = 0{\cdot}1 \text{ in.}, \qquad \alpha = 15^\circ, \qquad \nu = \tfrac{1}{2}. \tag{6.8}$$

†Frozen-stress photo-elastic technique is used on a material which is virtually incompressible.

The corresponding values of λ, k and ϵ are

$$\lambda = 0{\cdot}025, \qquad k = (\tfrac{3}{4})^{\frac{1}{2}}, \qquad \epsilon = 1{\cdot}696, \tag{6.9}$$

and hence (6.6) becomes

$$1 + 0{\cdot}735\,(1 + \rho)\cos\theta. \tag{6.10}$$

This has a maximum value 2·47 at the inside of the bend and on the outer surface of the pipe ($\theta = 0$, $\rho = 1$). Preliminary results indicate that (6.10) is in reasonable agreement with experiment.†

From (6.7) we see that the normal stress resultant across $\beta = 0$ is $\frac{1}{2}\,p\,a$ and this seems to be in agreement with experiment. It is clear, however, that (6.7) cannot be completely accurate for all values of ρ since, when $\rho = 1$, the normal stress should vanish when $\theta = 0$ or π, which, in general, is contrary to the formula (6.7). This is, perhaps, not very surprising in view of the fact that boundary conditions have not been satisfied at $\beta = 0$ for all values of ρ, as far as shearing stresses are concerned.

It is unlikely that the stress factor (6.6) will remain completely satisfactory for larger values of α, e.g. for values of α near 45°, but further discussion of this must await the completion of the experimental work.

7. Pure Flexure

We now suppose that the pipe has zero pressure on its faces so that $p = 0$ and suppose that it is bent symmetrically about the plane at the sharp bend, and about a plane containing the axes of both sections of the pipe, by pure couples applied at the ends of the pipe which are at large distances from the bend. Again, by symmetry, the shearing stresses and the normal displacement over the plane elliptical section at the bend are zero and we can use the analysis of previous Sections with the same degree of approximation. To obtain pure flexure we must have

$$s_z^{(0)} \to \frac{M\cos\theta}{2\pi a^3\,\lambda\sigma} = \frac{M\cos\theta}{\pi a^2\,h\sigma}, \qquad (\beta \to \infty), \tag{7.1}$$

where M is a constant couple, so that

$$B = M_0\cos\theta, \qquad M_0 = \frac{M}{2\pi\,a^3\,\lambda\sigma}. \tag{7.2}$$

Equations (5.14) and (5.19) then give

$$K = L = \frac{M_0\,k\epsilon\cos^2\theta}{1 - \nu^2}, \tag{7.3}$$

and hence, from (5.15),

$$A + C^* = \frac{5 - \nu}{1 - \nu}\,\epsilon M_0\sin\theta\cos\theta. \tag{7.4}$$

With the values (7.2) and (7.4) respectively for B and $A + C^*$ we find, from (3.6) and (4.14), that

$$s_{\theta z}^{(0)} \to 3M_0\,\epsilon\sin\theta\cos\theta \qquad (\beta \to \infty). \tag{7.5}$$

†As indicated earlier these results will be published elsewhere when completed and detailed comparison with (6.10) is postponed until then.

This stress component does not appear in the usual flexure problem but since it contributes nothing to the resultant force and couple over the end of the tube it causes no difficulty. Equations (7.4) and (5.20) can be solved for A and C^*. Using (5.22) we see that the hoop stress in the plane $\beta = 0$ is

$$\frac{Mk\epsilon \cos^2 \theta}{\pi a^2 h}\left(1 + \frac{2\nu k^2 \rho}{1 - \nu^2}\right). \tag{7.6}$$

Taking the special values of the constants given in (6.8), the expression (7.6) reduces to

$$\frac{1{\cdot}47\, M\,(1 + \rho)\cos^2 \theta}{\pi a^2 h}. \tag{7.7}$$

This has a maximum value

$$\frac{2{\cdot}94\, M}{\pi a^2 h}, \tag{7.8}$$

at the inside and outside of the bend and on the outer surface of the pipe ($\theta = 0$ or π, $\rho = 1$). The value (7.8) may be compared with a numerical maximum value $M/(\pi a^2 h)$ of the longitudinal stress $\sigma s_z^{(0)}$ when β is large.

Again, from (5.23) and (7.2), we see that the stress *resultant* normal to the plane $\beta = 0$ has the value

$$\frac{M \cos \theta}{\pi a^2 h}, \tag{7.9}$$

and this equals the longitudinal stress resultant when $\beta \to \infty$.

REFERENCES

JOHNSON, M. W. and REISSNER, E. 1959 *J. Math. Phys.* **31**, 371.

KORNECKI, A. 1957 *Rozprawy Inzynierski* **5**, 119.

NEUT, A. VAN DER 1960 *Proc. Symposium on the Theory of Thin Elastic Shells*, p. 247. (North-Holland Publ. Co., Amsterdam).

J. Mech. Phys. Solids, 1961, Vol. 9, pp. 105 to 113. Pergamon Press Ltd., London. Printed in Great Britain

AN EXPERIMENTAL DETERMINATION OF THE DETAILED DISTORTION IN HOT ROLLING

By B. E. Milsom and J. M. Alexander
Department of Mechanical Engineering, Imperial College of Science and Technology

(*Received* 10*th November*, 1960)

Summary

A technique has been developed for measuring the detailed distortion occurring in the arc of contact of a rolling mill, under conditions simulating hot rolling. A single configuration has been considered, typical of the final stages of hot rolling wide strip in industry, and comparison made of the conditions existing on interior and exterior sections of the metal in the arc of contact.

It was not found possible to derive a slip-line field from the experimental results, due to the excessively wavy character of the velocity variation along the streamlines. This is possibly due to the influence of the grain structure of the material used, which was commercially pure aluminium and to an insufficiently precise rolling technique. The experimental technique is described in detail, and proposals for further work put forward.

1. Introduction

A theoretical analysis of the plane strain problem of hot rolling, leading to a slip line field for a single geometry of rolling, has been proposed by Alexander (1955a). In that analysis it was assumed that the material was the hypothetical plastic/rigid material of classical plasticity theory, with infinite Young's modulus and constant yield stress. Also the assumption was made that the yield shear stress was attained along the interface in the arc of contact, not unreasonable for the hot-rolling process. This gives the easily handled boundary condition that the slip-lines meet the roll material interface either tangentially or normally.

Before proceeding with considerations of other geometries of rolling it was decided to try and establish an experimental technique to check the proposed theoretical solution. This would then facilitate extending the solution to other pass geometries, since the approximate shape of the slip-line field could thereby be determined. The theoretical problem is particularly complicated, since it is not statically determined, so that the solution has to be continually modified until all stress and velocity boundary conditions are satisfied. Therefore any means whereby a trial solution can be quickly found would be most valuable. There follows a description of the preliminary experiments which have been undertaken in this project.

2. Experimental Apparatus

The material finally chosen for these experiments was commercially pure aluminium strip. In order to make this material approximate to the hypothetical

plastic/rigid material it was pre-rolled until the stress-strain curve was considered suitable. The basic yield stress curve of the metal was determined in the plane-strain compression sub-press used by Watts and Ford (1955), and all necessary precautions were taken to minimize frictional and other undesirable effects. To maintain the geometry of the theoretical solution it was necessary to use the aluminium in a thickness of 0·086 in., having been rolled from about 0·2 in. in the annealed state.

The rolling mill is of quite rudimentary design but nevertheless adequate for the intended purpose. It is two-high, with rolls 10 in. diameter, 6 in. long, mounted in roller bearings. The mill is driven by a fractional horsepower d.c. motor through V-belt and worm gear reduction, giving a roll speed of about 4 rev/min. The rolls are supported in chocks in housings and the roll gap can be altered by screws in the normal way.

A universal measuring machine, manufactured by Société Genevoise Ltd., designated MU214B, was adapted for scribing and measuring the grids used to determine the distortion. The machine can accommodate a specimen 16 in. long, 4 in. wide and 6 in. high, the principle of measurement being the microscopic observation of standard scales which are graduated at intervals of 0·05 in. The graticule of the microscope head is moved by means of an accurate micrometer screw, the movement being noted on a rotating scale graduated in units of 0·00005 in. A further sub-division by eye enables the reading to be estimated to the nearest 10 μin.

To engrave the grids a tracelet mechanism was attached to the location microscope. The height of the engraving tool can be easily adjusted to bring the engraved line coincident with the focal plane of the microscope. The tool was made of high carbon steel, hardened, and ground to a wedge form of 30° included angle, being held at one end of a lever pivotted in conical bearings carried in the main member. The force between the tool and the specimen can be adjusted by moving a jockey weight along the counter-balance arm of this lever. It was found unnecessary to measure the grid after scribing since the machine setting was sufficiently accurate. A more complete description of the measuring machine and tracelet mechanism is given by Brewer and Alexander (1960).

3. Experimental Procedure

The specimen of commercially pure aluminium was made from strip 0·086 in. thickness, having been pre-rolled by a determined amount. The remaining dimensions of the specimen and its properties were also determined experimentally, as follows.

Firstly, the basic yield-stress curve was established by using the plane-strain compression sub-press in a laboratory testing machine. During the tests the dies were lubricated by a mixture of graphite grease and mineral oil, the ratio of die width to strip thickness being kept in the neighbourhood of 3 : 1 as recommended by Watts and Ford (1955). The specimens for the tests were cut from the stock material to a convenient size and incremental loading employed, the dies being relubricated between each increment of load.

The basic yield-stress curve in plane-strain compression in the annealed state is shown in Fig. 1. It can be seen that the material did not have a sharp yield point and would therefore be unsatisfactory for the experiment if used in the annealed condition. The effect of rolling the strip to give 32·8 and 58 per cent reductions is shown also in Fig. 1, from which it can be seen that such pre-rolling gives a much sharper yield point, followed by a fairly low rate of workhardening. The reduction of 58 per cent was finally chosen, this being the maximum which could be given to the stock material to reduce its thickness to 0·086 in.

It was necessary to ensure that the frictional conditions between the strip and the rolls would correspond to those necessary for 'full' or 'sticking' friction

assumed in the theoretical analysis. Since an analysis of the effect of friction in plane-strain compression had been made by ALEXANDER (1955b), it was possible to use this to assess the effect of various surface treatments on the frictional conditions existing in the plane strain compression test. Having found the conditions necessary to ensure that the full yield shear stress was being attained along the interface in the plane-strain compression test, these conditions could be imposed on the rolls and strip in the knowledge that the desired frictional effects would occur in the rolling experiments.

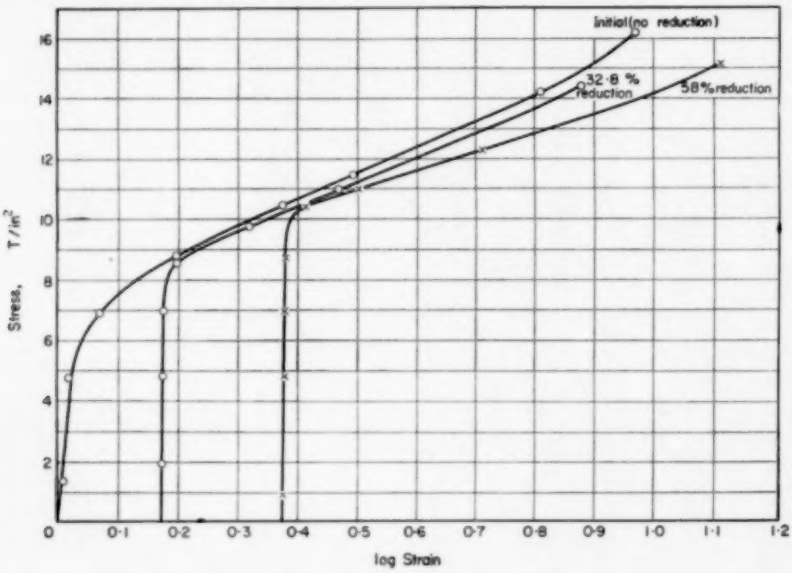

FIG. 1. Yield stress curves in plane-strain compression.

In the analysis for the plane-strain compression test it is shown that for a die width/strip thickness ratio of 3 : 1, the ratio of the mean pressure for ' full ' friction to the yield stress with smooth platens should be approximately 1·5. Both platens and strip were roughened with coarse emery paper before carrying out the plane-strain compression test, and all interfaces thoroughly cleaned with carbon tetrachloride, to remove all particles of dirt and grease, before each incremental loading. The mean pressure from this test, for the material having had 58 per cent reduction from the annealed state, was found to be approximately 1·47 times the yield stress with smooth platens, initially, this ratio falling off slightly during the test, probably due to a slight smoothing of the sperities of the roughened surfaces (Fig. 2). This showed that, although it could not be guaranteed that full friction conditions would be maintained during the whole rolling experiment they would certainly exist initially. In the final analysis the angle of incidence of the experimentally determined slip-lines with the interface would reveal whether or not full friction existed.

The technique used to measure the interior distortion of part-rolled specimens has been described elsewhere (BREWER and ALEXANDER 1960 ; ALEXANDER 1958). It is necessary to scribe a grid on an interior section produced by making the specimen in two halves, these halves being secured together sufficiently strongly to prevent parting during the experiment, but not so strongly that they cannot be parted for examination of the distorted grid.

The first method tried for securing the halves together consisted of rivetting aluminium strips transversely with aluminium rivets (Fig. 3). It was found that, on subsequent rolling, the halves had parted between the transverse strips, as shown diagramatically in Fig. 3 for specimens with

two and three transverse strips. Clearly, it would be necessary to secure the strips together along the whole of their length in order to achieve plane strain conditions during rolling. A technique of pressure welding had been developed with copper specimens,* but it appeared that for aluminium the deformations involved would be too large and cause uneven distortion of the scribed grid. Other methods considered were soldering, welding, and ultrasonic welding, but all these would destroy the scribed grid and were therefore unsuitable.

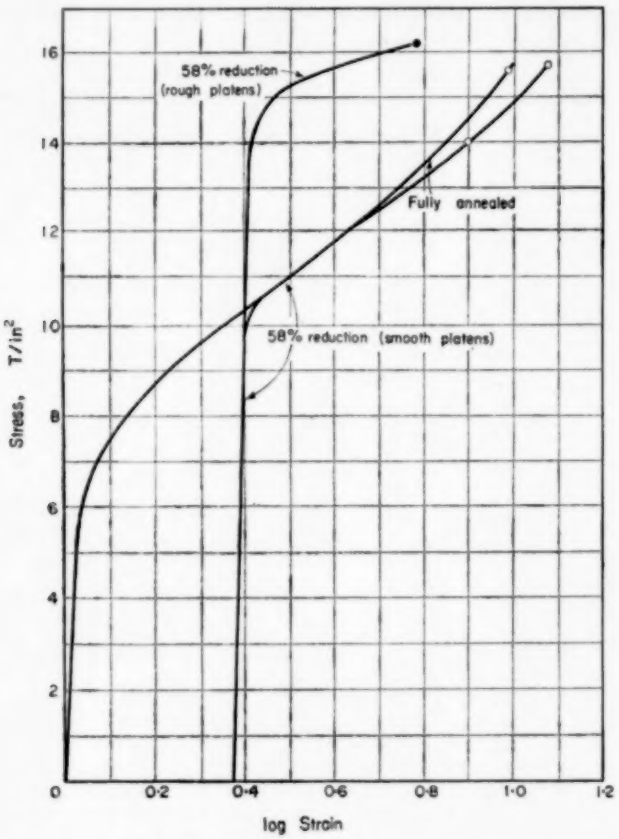

Fig. 2. Effect of interfacial roughness in plane-strain compression.

The final securing technique adopted was to use an adhesive, manufactured by CIBA (Aero-Research Labs.) Ltd., designated Araldite No. 1. This particular adhesive was recommended by the manufacturers as being the most suitable for securing aluminium under the conditions imposed by rolling. The instructions for obtaining a secure joint are briefly as follows:

(a) Degrease surfaces thoroughly with carbon tetrachloride.
(b) Spread adhesive onto the two surfaces and lightly clamp together.
(c) Cure for 1 hr at 180°C.

It was found necessary to secure the halves of the specimen with both the adhesive and the three transverse strips, the strips being rivetted across the ends and middle of the strip (Fig. 3), after the adhesive had been cured. Under these conditions it was found that, after part rolling, plane-strain conditions were apparently obtained at the centre face, and there was no tendency for the Araldite to crack.

*Due to Mr. F. Ellis, Department of Mechanical engineering, City and Guilds College.

A preliminary experiment was next carried out to determine whether there were significant differences between the deformation on the outside edge of the specimen and the interior section. If there were negligible differences, it would mean of course, that a grid scribed on the outside edge of the specimen would suffice, leading to a simplified design of specimen. For this experiment the grids were scribed by holding the scribing tool in the fixed arbor of a milling machine, and moving the specimen over the tool by traversing the machine table to which it was secured. A grid spacing of 0·025 in. was chosen, being accomplished by using the graduated scale on the table control. The two grids were then carefully measured by means of a Vickers tool-makers microscope, and the results noted. Having assembled and glued the specimen it was part-rolled, broken open, and the distorted grids again measured. It was found that the conditions of strain were not the same, so that measurement of the distortion of interior cross sections would have to be made. A more precise measurement of the distortion at the outer edge was eventually made, so that a direct comparison can be made between these two sections, as discussed later.

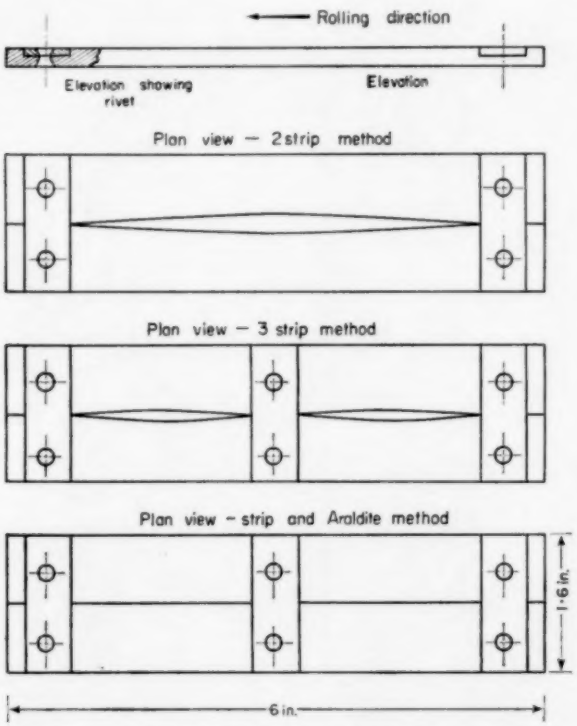

FIG. 3. Details of specimens for part-rolling.

To determine whether or not a small grid would be visible under a layer of Araldite, and also whether refraction or thermal distortion would impair the accuracy of the grid, the following experiment was carried out. A few squares of a grid of 0·007 in. mesh were scribed using the MU214B machine on the polished edge of an aluminium specimen. The specimen was then glued to its counterpart and heated for the requisite period. Then, without any rolling, the specimen was broken apart and the grid remeasured. It was found that, within the accuracy of the measuring machine, no distortion of the grid could be detected and it was easy to distinguish the nodal points of the grid.

Having completed these preliminary experiments, the final specimen to be used for deriving a slip line field for hot rolling was constructed, from commercially pure aluminium 0·086 in. thick, rolled 58 per cent from the annealed state. A rectangular grid of mesh size 0·007 $\times$ 0·0035 in.

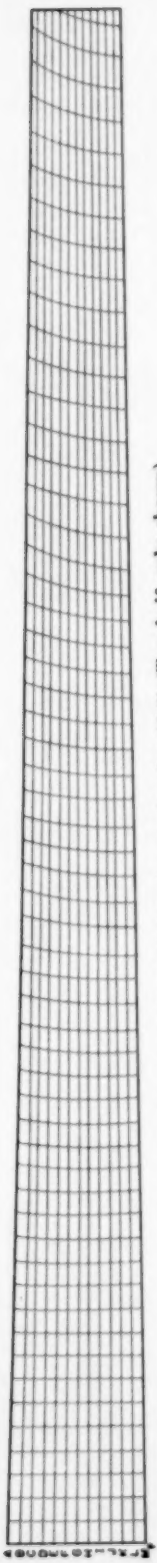

Fig. 5. Distorted interior section (× 17·5) (Top half only shown).

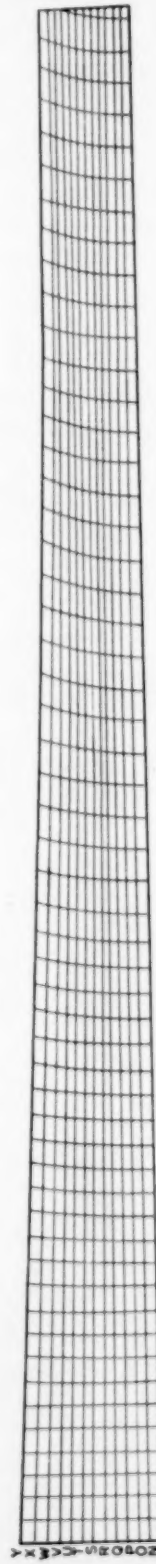

Fig. 6. Distorted exterior section (× 17·5) (Top half only shown).

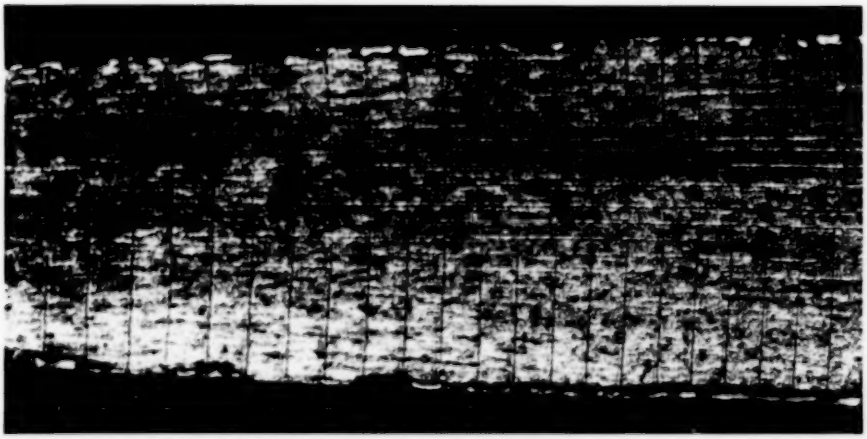

FIG. 4. Enlarged view of exterior edge of a part-rolled specimen. ($\times$ 25)

was scribed on one edge of one strip, and then the two strips secured together using the adhesive and rivetted strips as described previously. The final dimensions chosen are shown in Fig. 3. Finally, a second grid of the same mesh was scribed on the exterior edge of the specimen. Both these grids were scribed using the MU214B measuring machine with the tracelet mechanism.

The specimen was then *part*-rolled in the rolling mill, reduction 33 per cent, the surfaces of the rolls and the specimen having been roughened with coarse emery paper, and thoroughly cleaned with carbon tetrachloride to achieve the desired frictional conditions. The part-rolled specimen was then broken open carefully and the distorted grids, both interior and exterior, measured using the MU214B machine. The measured results were then plotted to give large scale drawings of the distorted grids, on squared graph paper, to facilitate the construction of slip line fields and hodographs for the two planes of distortion.

4. Interpretation of the Results

A photograph of part of the deformed grid on the exterior edge of the specimen is shown in Fig. 4, from which the distortion of the originally vertical lines can be clearly seen. The deformation due to rolling was not symmetrical about the centre

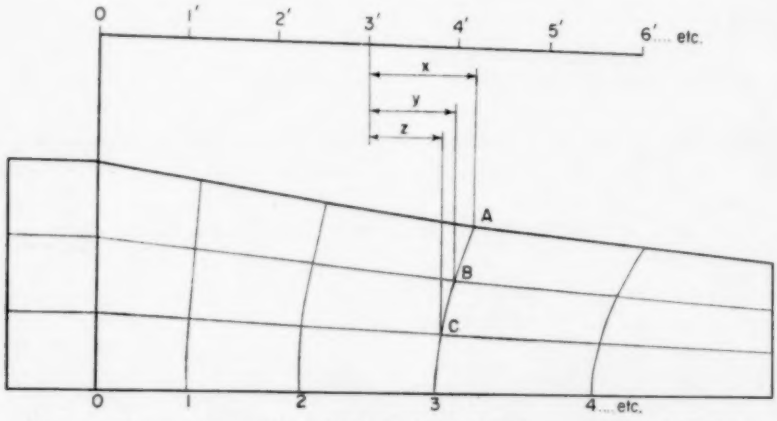

Fig. 7. Diagram illustrating relative horizontal displacement of nodal points.

line, so that it was necessary to correct the grids. This was done by observing the *unsymmetrical* distortion above and below the centre line, finding corresponding nodal points and determining the mean distances of such nodal points from the horizontal centre line and from a vertical datum line in the undistorted material. This then gave the most likely horizontal and vertical coordinates of the nodal points in the corresponding *symmetrical* rolling distortion. The resulting distorted networks are shown to scale in Figs. 5 and 6, Fig. 5 being that for the interior section, under plane-strain conditions, Fig. 6 referring to the distortion of the exterior edge.

The method used to find the velocities of elements in the distorted field under discussion here was as follows. Having obtained the corrected grids, one for the interior, the other for the exterior section, graphs of the relative displacement of nodal points along each streamline were constructed. The procedure is shown diagrammatically in Fig. 7, in which the points 0′, 1′, 2′,

etc., are set off above the grid, such that '0' corresponds to 0 (the initial vertical line chosen as datum) and the spacings $0' - 1'$, $1' - 2'$, etc., each correspond to the length of one undistorted grid (0·007 in.). Then the relative horizontal displacement of the point A will be given by the distance x, of B by y, and of C by z. It is a simple matter to find the relative vertical displacement also, so that graphs of both horizontal and vertical displacement could be constructed. The slopes of these graphs represent the horizontal and vertical components of the velocity of each nodal point relative to the velocity of the ingoing strip.

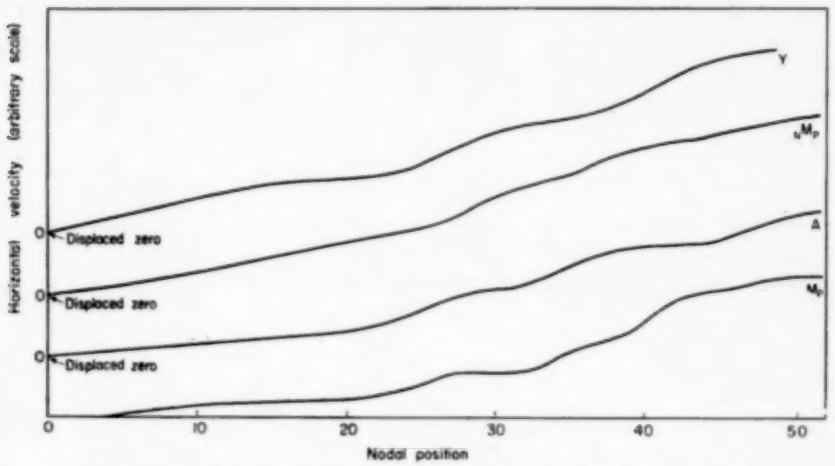

Fig. 8. Typical graphs of horizontal velocity. (See Figs. 5 and 6 for streamline lettering).

In Fig. 8 are shown typical graphs of the horizontal components of velocity along the streamlines, relative to the ingoing strip, from which the undulating character of the variation of velocity may be observed. Attempts to derive a slip line field from this data have not been successful.

5. Discussion

It can be seen from the drawings of the distorted networks in Figs. 5 and 6, for plane-strain and non-plane-strain conditions respectively, that although the distortion is generally similar, some differences do exist. In particular, it appears that the vertical lines have deformed to a slightly greater extent on the exterior section, giving greater velocities at the roll-specimen interface. This may be due to the unrestrained lateral expansion which occurs at the exterior section. It is also clear from these Figures that the originally horizontal stream lines near the centre of the specimen have received little or no vertical displacement. By definition, such streamlines on emerging from the plastic zone should be closer together by an amount proportional to the overall rolling compression. The fact that they are not, and that the velocity curves exhibit unduly 'wavy' characteristics, indicates that the material does not approach the idealized behaviour assumed in slip-line field theory. Thus it is not possible to use the results as they stand for the derivation of a slip-line field.

6. Conclusions and Further Work

Although at first sight somewhat disappointing, the behaviour of the material observed in these experiments must approximate to the behaviour of material during hot rolling. In fact, under the influence of temperature, leading to some recrystallization of the metal, it is likely that even more non-uniform effects will occur in practice. The value of slip-line field theory is to give an overall picture of the deformation process, however, and some means must be sought to give experimental results which will allow the determination of such fields.

There are two possibilities, either to 'smooth' results of the type presented here, probably by ignoring the undulations in the velocity curves, or to continue searching for a material with more homogeneity and also to improve the experimental technique. Preliminary experiments with tellurium lead showed even greater variations, which the use of work hardened aluminium has greatly reduced. There is, of course, the possibility of increasing the specimen size, but this would be costly if the desired geometry of rolling is to be maintained.

Experiments are at present being continued with aluminium, with a view to establishing the repeatability of the results and making a more detailed investigation of the effects of grain size. To establish a meaningful experimental slip-line field it will doubtless be necessary to smooth out the velocity curves. The use of work hardened copper may also be tried, since this metal has been shown to give satisfactory behaviour in other experiments of this type. It is also possible that the rolling mill itself is not behaving in the precise way intended. The combined action of imperfect gears and wobblers may be to cause non-uniform rotation of the rolls, leading to unsymmetrical rolling and undesirable creep recovery of the specimens. In addition to improving these conditions it may be necessary to improve the experimental technique used during part-rolling, possibly by introducing a quick-release mechanism to minimize creep effects.

Acknowledgments

Acknowledgment is made to Professor Hugh Ford, who supervised the earlier work on this project, for helpful discussions and suggestions; to Mr. M. C. Hillier who designed and developed the rolling mill used; to Mr. Bodhidatta, who carried out the preliminary experiments with tellurium lead; and to Mr. F. Ellis for help and encouragement in developing a suitable technique for preparing the necessary specimens.

References

Alexander, J. M. 1955a *Proc. Instn. Mech. Engrs., Lond.* **169**, 1021.
1955b *J. Mech. Phys. Solids* **3**, 233.
1958 *Proc. Conf. on Technology of Engineering Manufacture*, Paper No. 42. (Institution of Mechanical Engineers, London)

Brewer, R. C. and Alexander, J. M. 1960 *J. Mech. Phys. Solids* **8**, 76.

Watts, A. B. and Ford, H. 1953 *Proc. Instn. Mech. Engrs., Lond.* **166**, 1141.

J. Mech. Phys. Solids, 1961, Vol. 9, pp. 114 to 130. Pergamon Press Ltd., London. Printed in Great Britain

UNIQUENESS IN GENERAL BOUNDARY-VALUE PROBLEMS FOR ELASTIC OR INELASTIC SOLIDS

By R. Hill
Department of Mathematics, University of Nottingham

(*Received 25th November*, 1960)

Summary

The class of solids considered is characterized by a linear relation between the stress-rate and strain-rate tensors. The boundary-value problem is set by prescribed surface velocities or nominal traction-rates, the existing state of stress, anisotropy, etc., being regarded as known. Changes in geometry are unrestricted. Various criteria for uniqueness of the solution (Hill 1957 a, b, 1959) are re-derived (Sections 2 and 4), together with a useful new transformation (Section 3) and related extremum principles (Section 6).

The results are specialized for a homogeneous isotropic elastic solid undergoing infinitesimal strains (Section 5), the thermodynamic restriction of positive strain energy being relaxed. For the displacement boundary-value problem Boggio's (1907) extension of the classical uniqueness theorem of Kirchhoff is recovered by an automatic process, together with related extremum principles of Gurtin and Sternberg (1960). The traction boundary-value problem is re-examined. Plane strain and generalized plane stress are also treated in detail.

1. Scope and Objectives

We consider here a class of solids characterized by the following properties:

(a) The mechanical behaviour in isothermal deformation does not depend on time.

(b) The constitutive law is a relation between stress-rate and strain-rate:

$$\mathring{\tau}^{\alpha\beta} = \dot{\sigma}^{\alpha\beta} + \sigma^{\alpha\beta}\epsilon_{\gamma}{}^{\gamma} = \frac{\partial W}{\partial \epsilon_{\alpha\beta}}. \tag{1}$$

In this, $\sigma^{\alpha\beta}$ and $\tau^{\alpha\beta}$ are respectively the true stress and Kirchhoff stress in curvilinear coordinates deforming with the material element, and the dot denotes their instantaneous convected derivatives (Oldroyd 1950). $\epsilon_{\alpha\beta}$ is the strain-rate, $\frac{1}{2}(v_{\alpha,\beta} + v_{\beta,\alpha})$, where v_β is velocity and a comma denotes covariant differentiation.

(c) The 'potential' W is a quadratic form in the components of strain-rate:

$$2W = f^{\alpha\beta\gamma\delta}\epsilon_{\alpha\beta}\epsilon_{\gamma\delta} \tag{2}$$

where the coefficients are supposed symmetrized with respect to interchange of α, β; γ, δ; $\alpha\beta$ and $\gamma\delta$. Then (1) becomes

$$\mathring{\tau}^{\alpha\beta} = f^{\alpha\beta\gamma\delta}\epsilon_{\gamma\delta} \tag{3}$$

and is consistent with (a), since the relations are dimensionally homogeneous in time. The coefficients may depend on the current stress and also on the local state of anisotropy, and thereby on the entire previous strain-history. Consequently, in an extended body at a generic instant, the coefficients must usually vary in space; it is assumed that this variation is continuous.

The structure of the desired theorems becomes particularly suggestive and clear-cut (HILL 1957a) when phrased in terms of the unsymmetric tensor of 'nominal' stress-rate

$$\dot{s}^{\alpha\beta} = \dot{\tau}^{\alpha\beta} + \sigma^{\alpha\gamma} v^{\beta}{}_{,\gamma}.$$

This has the following interpretation: if $d\boldsymbol{S}_\alpha$ is the vector area of an infinitesimal plane element at a considered instant, $\dot{s}^{\alpha\beta}\, d\boldsymbol{S}_\alpha$ is the intrinsic derivative of the load vector: i.e., the rate of change of the load components when these are referred back always to the coordinate configuration at that instant.† (It is $\dot{\tau}^{\alpha\beta}\, d\boldsymbol{S}_\alpha$ that is the *convected* derivative of the load vector). It is apparent that the nominal stress-rate is derivable from a quadratic potential function of velocity gradient:

$$\dot{s}^{\alpha\beta} = \frac{\partial U}{\partial v_{\beta,\alpha}} \qquad \text{where} \qquad U(v_{\beta,\alpha}) = W(\epsilon_{\alpha\beta}) + \tfrac{1}{2}\sigma^{\alpha\gamma} v_{\beta,\alpha} v^{\beta}{}_{,\gamma}. \tag{4}$$

Explicitly,

$$\left.\begin{aligned} \dot{s}^{\alpha\beta} &= c^{\alpha\beta\gamma\delta} v_{\delta,\gamma}, \qquad 2U = \dot{s}^{\alpha\beta} v_{\beta,\alpha} = c^{\alpha\beta\gamma\delta} v_{\beta,\alpha} v_{\delta,\gamma} \\ \text{where} \qquad c^{\alpha\beta\gamma\delta} &= f^{\alpha\beta\gamma\delta} + g^{\beta\delta}\sigma^{\alpha\gamma} \end{aligned}\right\} \tag{5}$$

and is symmetric with respect to interchange of $\alpha\ \beta$ and $\gamma\ \delta$ ($g^{\beta\delta}$ is the metric tensor).

Solids with such a quadratic potential are called 'linear' to distinguish them from solids whose potential is not simply quadratic but a general function homogeneous of degree two, with corresponding non-linear rate equations. Most linear solids behave inelastically, in the following sense. Take a material element in any given mechanical state and under a given stress, and subject it to any cycle of deformation that finally restores its shape. Then it will usually happen that certain *arbitrarily small* cycles can be found that do *not* restore the stress to its initial value. If, however, the stress is recovered on *all* sufficiently small cycles of strain, the solid can appropriately be described as 'resilient' in that state. Particular resilient solids for which

$$\tau^{\alpha\beta} = \frac{\partial E}{\partial e_{\alpha\beta}}, \qquad \text{so that} \qquad f^{\alpha\beta\gamma\delta} = \frac{\partial^2 E}{\partial e_{\alpha\beta}\,\partial e_{\gamma\delta}} \tag{6}$$

(HILL 1959, p. 220), are elastic in the accepted sense, E being the free energy function of the finite strain $e_{\alpha\beta}$, measured with respect to some previous reference configuration of the convected coordinates.*

Still more particularly, the classical elastic solid is obtained when $e_{\alpha\beta}$ is infinitesimal (E being quadratic); to this approximation there is no need to distinguish true stress and Kirchhoff stress, since both are small compared with the bulk modulus. The rate equations (3) become the generalized Hooke's law when $\epsilon_{\alpha\beta}$ is regarded as an infinitesimal increment of strain instead of rate of strain and W is identified with E. If, further, the body dimensions are such that instability

†Or these coordinates can be imagined to move, without deformation or rotation, with the element.

*In (6) use is made of the notable fact that the *convected* derivative of finite strain $e_{\alpha\beta}$ is just the strain-rate $\epsilon_{\alpha\beta}$.

is not in question (so that all displacement gradients are of a similar order of magnitude), U merges into W and $c^{\alpha\beta\gamma\delta}$ into $f^{\alpha\beta\gamma\delta}$. In this way the uniqueness and extremum principles that we shall prove in terms of U (and velocity) for a general linear solid (with no restriction on changes in geometry) can be immediately specialized and re-phrased in terms of E (and displacement) for the linear theory of elasticity (where geometry changes are neglected).

It is, indeed, with the latter, when E is isotropic, that this paper is largely concerned. The wellknown Kirchhoff proof of uniqueness of the general mixed boundary-value problem of the linear theory of elasticity requires that Poisson's ratio is in the range $-1 < \nu < \frac{1}{2}$. This ensures that E is definite, which is of course a thermodynamic characteristic of a real elastic solid. However, these restrictions on ν are by no means *necessary* for uniqueness. This was probably first shown by BOGGIO (1907)* when the displacement is prescribed over the entire surface: uniqueness was established for all ν except $\frac{1}{2} \leqslant \nu \leqslant 1$. Several other independent sources for this theorem have been listed by GURTIN and STERNBERG (1960).

It seems worthwhile, nevertheless, to show that BOGGIO's result follows easily and automatically from a uniqueness criterion for linear solids in general [indicated by HILL (1957a, p. 234) and more explicitly by HILL (1961a)†]. Precisely the same range of ν is also obtained here for the displacement boundary-value problem in plane strain. We examine also the case when traction is prescribed everywhere. In 3 dimensions a best possible result has not been obtained. In plane strain, however, $\nu = 1$ is found to be the only value for which the solution is not unique.

In essence the method involves extremizing a quotient of two functionals, either of the field of stress or of displacement. In this form the method was indicated for linear solids by HILL (1957a, p. 236). Some particular results have also been obtained in this way for certain non-linear solids (HILL 1957b, 1958; HILL and SEWELL 1960), in circumstances where they may be treated as linear.

For convenience we shall recapitulate the proof of this uniqueness criterion, together with that of an associated pair of extremum principles. [These are indeed valid also for non-linear solids (HILL 1959) but this is less easily shown. Two proofs are available (HILL 1958, p. 244; 1961a); the second is more rigorous and is to be preferred]. Another pair of extremum principles is then derived, in conjunction with a useful device for rendering the uniqueness criterion more tractable. By this means some isolated theorems of GURTIN and STERNBERG (1960) for an isotropic elastic solid are brought within the general framework, in a quite natural way.

2. UNIQUENESS CRITERION FOR LINEAR SOLIDS

The rate equations (5) are associated with the following boundary-value problem. At a generic stage in a process of quasi-static distortion the shape of the surface (supposed finite and piecewise smooth), the internal distribution of stress (assumed continuous) and of the coefficients $c^{\alpha\beta\gamma\delta}$ (then also continuous), are regarded as known. The velocity v_β is now prescribed over a part S_v of the surface S, the nominal traction-rate $\dot{t}^\beta = \nu_\alpha \dot{s}^{\alpha\beta}$ over the remainder S_t (ν_α = outward unit normal), and

*I owe this reference to my colleague Dr. R. J. Knops.

†The derivation of BOGGIO's result by this method also appears as a question in the Honours Examination in Mathematics, Part II, in the University of Nottingham (1960, paper on Mechanics of Solids and Fluids).

the nominal body-force rate $\dot{g}^\beta$ per unit volume through the volume V. We enquire in what circumstances the 'mode of deformation' is uniquely determined; that is, a continuous velocity field with continuous first derivatives and at least piecewise continuous second derivatives.

Suppose, if possible, that there could be more than one mode (a bifurcation) and let the prefix Δ indicate the difference of corresponding quantities in any two distinct modes. Then, since each solution satisfies the equations of equilibrium

$$\dot{s}^{\alpha\beta}{}_{,\alpha} + \dot{g}^\beta = 0$$

with the same body-forces, their difference satisfies $\Delta \dot{s}^{\alpha\beta}{}_{,\alpha} = 0$. Using, now, the divergence theorem,

$$\int \Delta\dot{s}^{\alpha\beta}\, \Delta v_{\beta,\alpha}\, dV = \int (\Delta\dot{s}^{\alpha\beta}\, \Delta v_\beta)_{,\alpha}\, dV = \int \Delta\dot{t}^\beta\, \Delta v_\beta\, dS = 0$$

since $\Delta\dot{t}^\beta = 0$ on S_t and $\Delta v_\beta = 0$ on S_v. But, for a *linear* solid, the differences $\Delta\dot{s}^{\alpha\beta}$ and $\Delta v_{\beta,\alpha}$ are themselves related by (5), and so

$$\int U\,(\Delta v_{\beta,\alpha})\, dV = 0.$$

A *sufficient* condition for uniqueness is therefore either (a)

$$\int U\,(v_{\beta,\alpha})\, dV > 0 \tag{7a}$$

for *all* fields with the analytic properties of an actual mode and *vanishing* on S_v (but not identically zero), or (b)

$$\int U\,(v_{\beta,\alpha})\, dV < 0 \tag{7b}$$

for such fields. Requiring the associated traction-rates to vanish on S_t would not strengthen the respective conditions since the range of the functional would be unaltered.

It is quite natural that (7a, b) do not involve the actual boundary values on S (for given S_v and S_t) since these clearly cannot affect the question of uniqueness in a linear solid. For whatever are the inhomogeneous boundary conditions, the difference of two modes is always an eigenfield (i.e. a solution of the homogeneous problem, with zero boundary values and without body force); conversely, if an eigenfield exists, the solution to every inhomogeneous problem is indeterminate to the extent of an arbitrary additive multiple of the eigenfield. Consequently, when the solid is linear, the question of uniqueness is entirely equivalent to that of the existence of eigenstates (the situation is otherwise when the solid is non-linear). Evidently (7a, b) may be read simply as sufficient conditions for the non-existence of eigenfields (which would cause the functional to vanish).

Of course, (7a, b) need by no means be *necessary* for uniqueness. To fix ideas consider the eigenvalues of any single material (or load) parameter. The continuous variation of this parameter, with everything else held fixed (including the geometry), defines a linear sequence of mechanical states. It is immaterial that this sequence cannot generally correspond to any actual process of straining the body (though

it may do so approximately, as in proportional loading of an elastic solid deforming infinitesimally). Now in an elastic solid it is known that the spectrum of eigenvalues is discrete, and yet throughout the interval spanned by the spectrum the functional is indefinite. In other words, there are ranges of the parameter where the solution is unique but (7a, b) do not hold.

Eigenvalues where the functional is just semi-definite (with respect to non-zero fields) are of especial interest. In an elastic solid it is known that such eigenvalues exist and terminate the spectrum (Rayleigh's Principle). Argument by analogy for their existence in a general linear solid seems reasonable since the differential operator in the field equations is still self-adjoint. However, a rigorous existence proof is apparently lacking at the present time. Of course, *if* the functional were known on other grounds to be semi-definite for a certain value of the parameter, the known field causing the functional to vanish would plainly be an eigenfield. For the first variation of the functional must be zero (otherwise the functional would be indefinite) and so, by (4),

$$\delta \int U \, dV = \int \dot{s}^{\alpha\beta} \, \delta v_{\beta,\alpha} \, dV = 0.$$

Transforming:

$$\int \dot{s}^{\alpha\beta}{}_{,\alpha} \, \delta v_\beta \, dV = \int \dot{t}^\beta \, \delta v_\beta \, dS_t$$

for all admissible fields δv_β vanishing on S_v. By the usual argument of the calculus of variations it follows that the stress-rate corresponding to the considered field is in equilibrium with zero body-force rate in V and zero traction-rate on S_t. We have, therefore, an eigenstate. In this restricted sense the uniqueness conditions (7a, b) are critical.

By the preceding analysis applied in reverse it is clear that the first variation of the function in the class of admissible fields vanishes with respect to *any* of the eigenfields. More generally, for any solution of the inhomogeneous problem, unique or not,

$$\delta \left[\int (U - \dot{y}^\beta \, v_\beta) \, dV - \int \dot{t}^\beta \, v_\beta \, dS_t) \right] = 0 \tag{8}$$

in the class of admissible velocity fields taking the prescribed values on S_t (in fact in the much wider class of continuous fields with merely piecewise continuous first derivatives and no conditions on the second derivatives).

Practical applications of (7a, b) follow in Section 5. It will usually be found convenient, where possible, to select a parameter that enters algebraically into the coefficients in U in such a way that (7a, b) can be re-arranged as direct inequalities for a Rayleigh quotient of two functionals [for a previous example see HILL (1958), equation (18)]. It is then a matter of using established techniques to find the extreme values of this quotient, or perhaps approximate bounds to them [for an example in context see HILL and SEWELL (1960)].

Alternatively, when $S_t = 0$, it may be feasible to make use of a rather elegant artifice which involves the introduction of certain special potentials. This method is described in the next Section.

3. Transformed Uniqueness Criterion ($S_t = 0$)

Consider the special class of velocity-gradient potentials (4):

$$2\Theta = \theta^{\alpha\beta\gamma\delta}\, v_{\beta,\alpha}\, v_{\delta,\gamma} \qquad \left.\right\} \tag{9}$$

where $$\theta^{\alpha\beta\gamma\delta} = -\theta^{\gamma\beta\alpha\delta} = -\theta^{\alpha\delta\gamma\beta} = \theta^{\gamma\delta\alpha\beta} \qquad \left.\right\}$$

and the coefficients do not vary with position. Such potentials are expressible as a divergence:

$$2\Theta = (\dot{s}^{\alpha\beta}\, v_\beta)_{,\alpha} \tag{10}$$

since, by virtue of the stipulated antisymmetry (9) with regard to interchange of the first and third indices,

$$\dot{s}^{\alpha\beta}{}_{,\alpha} = \theta^{\alpha\beta\gamma\delta}\, v_{\delta,\gamma\alpha} \equiv 0.$$

From this we see also that the stress-rate corresponding to any velocity field whatever is automatically in equilibrium.

Again, from (10),

$$2\int \Theta\, dV = \int \dot{l}^\beta\, v_\beta\, dS \quad \text{where} \quad \dot{l}^\beta = \nu_\alpha\, \theta^{\alpha\beta\gamma\delta}\, v_{\delta,\gamma}. \tag{11}$$

But this expression for the nominal traction-rate depends only on the *surface distribution* of velocity. For, when this is given, the gradients $v_{\delta,\gamma}$ at a point on the surface are undetermined only to the extend of additive parts $\lambda_\delta\, \nu_\gamma$, where the λ_δ's are arbitrary functions over the surface (the components, in fact, of the undetermined normal derivative of the velocity vector). By (9),

$$\nu_\alpha\, \nu_\gamma\, \theta^{\alpha\beta\gamma\delta} \equiv 0 \qquad \text{for each } \beta, \delta$$

and so the arbitrary parts make no resultant contribution to the traction-rate.* Equally the functional itself is dependent only on the surface values of the velocity field.

Thus, for prescribed velocity all over the surface ($S_t = 0$) the functional is fixed in value and its variation accordingly vanishes in respect of any admissible field whatever; this was already to be expected from the identical satisfaction of the equilibrium equations. Yet again, the general mixed boundary-value problem is highly non-unique, since any distribution of velocity vanishing on the surface is an eigenfield. However, although the internal state is completely undetermined, the complementary values of velocity and traction-rate on S_t and S_v respectively are unique.

In particular, the most general *isotropic* potential (9) is given (apart from an arbitrary scalar factor) by

$$\theta^{\alpha\beta\gamma\delta} = g^{\alpha\delta}\, g^{\beta\gamma} - g^{\alpha\beta}\, g^{\gamma\delta}, \qquad \left.\right\} \tag{12}$$

$$2\Theta = \epsilon^{\alpha\beta}\, \epsilon_{\alpha\beta} - \epsilon^{\alpha}{}_{\alpha}\, \epsilon^{\beta}{}_{\beta} - \omega^{\alpha\beta}\, \omega_{\alpha\beta}, \qquad \left.\right\}$$

where $\omega_{\alpha\beta}$ is the antisymmetric spin tensor, $\frac{1}{2}(v_{\alpha,\beta} - v_{\beta,\alpha})$. Correspondingly,

$$\dot{s}^{\alpha}{}_{.\beta} = \dot{v}^{\alpha}{}_{,\beta} - \delta^{\alpha}{}_{\beta}\, \dot{\epsilon}^{\gamma}{}_{\gamma}, \qquad \dot{\sigma}^{\alpha}{}_{\beta} = 2\, \dot{\epsilon}^{\alpha}{}_{\beta}, \qquad \left.\right\} \tag{13}$$

$$\dot{v}^{\alpha}{}_{,\beta} = \dot{s}^{\alpha}{}_{.\beta} - \tfrac{1}{2}\, \delta^{\alpha}{}_{\beta}\, \dot{s}^{\gamma}{}_{.\gamma}, \qquad \dot{l}_\beta = \nu_\alpha\, \dot{v}^{\alpha}{}_{,\beta} - \nu_\beta\, \dot{\epsilon}^{\gamma}{}_{\gamma}. \qquad \left.\right\}$$

*Its dependence on surface values of velocity can, if desired, be exhibited explicitly [e.g. Hill 1961b, Section 3(i)].

The existing stress everywhere in the body is a unit hydrostatic pressure, i.e. $\sigma^{\alpha}{}_{\beta} = -\delta^{\alpha}{}_{\beta}$, and moreover the time-variation of surface traction is as though the body continued to be immersed in a fluid of constant unit pressure. (One can easily verify from first principles that $-\dot{l}_{\beta}\,dS$ here is just the intrinsic derivative of the vector area $dS_{\beta} = \nu_{\beta}\,dS$). This interpretation exemplifies the previously mentioned dependence of traction-rate on the surface distortion alone.

We leave aside, now, this interesting question of (9) as potentials, in their own right, of solids real or imagined. Only their formal analytic properties are relevant to the present objective, namely to transform the criteria (7a, b). The following method is applicable where the *velocity is given everywhere on the surface* ($S_t = 0$). In this event, by (11),

$$\int \bar{U}\,dV = \int U\,dV \qquad \text{when} \qquad \bar{U} = U + \Theta, \tag{14}$$

for admissible fields vanishing on S. Thus, for any choice of Θ in the class (9), we can replace

$$\text{(7a) by} \qquad \int \bar{U}\,dV > 0 \tag{15a}$$

$$\text{and (7b) by} \qquad \int \bar{U}\,dV < 0 \tag{15b}$$

for admissible fields vanishing on S and not identically zero. By suitable choice the functionals in the corresponding Rayleigh quotient might be simplified. Even better, it might be obvious that the functional of some $\bar{U}$ as it stands is definite over a certain interval of the varied parameter in U, and semi-definite at the terminal values; the best possible result is then obtained at once. An example is given later in connexion with the classical elastic solid.

Furthermore, since $\int \Theta\,dV$ is constant for prescribed velocities over S, (8) can be replaced by

$$\delta \int (\bar{U} - \dot{y}^{\beta} v_{\beta})\,dV = 0. \tag{16}$$

4. Another Uniqueness Criterion

When (4) admits a unique inverse relation this can be written

$$v_{\beta,\alpha} = \frac{\partial U}{\partial \dot{s}^{\alpha\beta}} \tag{17}$$

when $2U = \dot{s}^{\alpha\beta} v_{\beta,\alpha}$ is expressed entirely in terms of the components of stress-rate. With the Δ notation of Section 2

$$\int U\,(\Delta \dot{s}^{\alpha\beta})\,dV = 0$$

if there are two or more distinct solutions to the general boundary-value problem. Consequently, another sufficient condition for uniqueness is either (a)

$$\int U\,(\dot{s}^{\alpha\beta})\,dV > 0 \tag{18a}$$

for all continuous stress-rate fields in equilibrium with zero body-force rate in V and zero traction-rate on S (and not identically zero), or (b)

$$\int U(\dot{s}^{\alpha\beta})\, dV < 0 \tag{18b}$$

for such fields. Unless, trivially, U is a definite form, conditions (18a, b) usually differ from (7a, b), respectively, in that they need not be simultaneously satisfied. As a general rule one might expect (7a, b) to be stronger than (18a, b) when $S_v \gg S_t$ (and vice versa), the former conditions taking more account of the boundary conditions. Subsequent results for elastic solids conform to this expectation.

For any solution, unique or not, we have a variation principle complementary to (8):

$$\delta\left[\int U(\dot{s}^{\alpha\beta})\, dV - \int \dot{l}^{\beta}\, v_{\beta}\, dS_v\right] = 0 \tag{19}$$

in the class of continuous stress-rate fields in equilibrium with the given body-force rates in V and the given nominal traction-rates on S_t. In particular, for an eigenfield,

$$\delta \int U(\dot{s}^{\alpha\beta})\, dV = \int v_{\beta,\,\alpha}\, \delta\dot{s}^{\alpha\beta}\, dV$$

in the class of continuous stress-rate fields in equilibrium with zero body-force rate in V and zero traction-rate on S_t. This variation also vanishes in a state where the functional in (18a, b) is semi-definite with respect to the stress-rate fields admissible there. However, in general one cannot immediately conclude that the stress-rate field causing the functional to vanish is an eigenfield; i.e. that it is associated through (17) with a continuous velocity distribution vanishing on S_v. For infinitesimal elasticity (even non-linear) such a converse to the variation principle (19) has been elegantly proved by Budiansky and Pearson (1956). For alternative proofs see Sokolnikoff (1956, pp. 389–390).

5. Isotropic Elastic Solid

Application of the preceding techniques is now illustrated by re-examining the two principal boundary-value problems of the linear theory of elasticity, the material being isotropic and homogeneous. The thermodynamic requirement of a positive-definite strain energy is discarded, and so the extensions obtained to Kirchhoff's uniqueness theorem have no physical relevance for the classical elastic solid. They are nonetheless of considerable methodological interest for studies of uniqueness in other solids.

For convenience, the shear modulus μ will be regarded as positive and fixed, while the Lamé constant λ, or equivalently Poisson's ratio ν, is allowed all real values. The $(\lambda/\mu, \nu)$ relation is best remembered and visualized when arranged as

$$(1 + \lambda/\mu)(1 - 2\nu) = 1, \tag{20}$$

which is the equation of a rectangular hyperbola with asymptotes $\nu = \frac{1}{2}$ and $\lambda/\mu = -1$. The values $(\lambda/\mu, \nu) = (-\frac{2}{3}, -1)$ and $(-2, 1)$ will also have special significance in the sequel.

As explained in Section 1 we can take over (7a, b), etc., by replacing velocity by displacement (u_β), strain-rate by infinitesimal strain (retaining the same notation $\epsilon_{\alpha\beta}$), stress-rate by stress ($\sigma^{\alpha\beta}$), and the potential U by the strain-energy density:

$$2U = \lambda \epsilon^\alpha{}_\alpha \, \epsilon^\beta{}_\beta + 2\mu \, \epsilon^{\alpha\beta} \, \epsilon_{\alpha\beta} \qquad (\nu \neq \tfrac{1}{2}). \tag{21}$$

The classical linear theory is of course valid only where the displacement gradients are all of the same order of infinitesimals; true and nominal stress (or traction) need not then be distinguished.

(*a*) 3 *dimensions*

(*i*) *Displacement boundary-value problem* ($S_t = 0$). We can either apply (7a) re-arranged as

$$-\frac{\lambda}{2\mu} = \frac{\nu}{2\nu - 1} < g.l.b. \left\{ \int \epsilon^{\alpha\beta} \, \epsilon_{\alpha\beta} \, dV \Big/ \int \epsilon^\alpha{}_\alpha \, \epsilon^\beta{}_\beta \, dV \right\} \tag{22}$$

and then transform, or immediately apply (15a) with $\bar{U} = U - 2\mu \, \Theta$ where U is given by (21) and Θ by (12). Then

$$2\bar{U} = (\lambda + 2\mu) \, \epsilon^\alpha{}_\alpha \, \epsilon^\beta{}_\beta + 2\mu \, \omega^{\alpha\beta} \, \omega_{\alpha\beta}. \tag{23}$$

This is a positive semi-definite form in the displacement gradients when $\lambda/\mu > -2$; i.e., when

$$-\infty < \nu < \tfrac{1}{2}, \qquad 1 < \nu < \infty.$$

Moreover, for the admissible fields vanishing on S, $\int \bar{U} \, dV$ is clearly positive-definite, since (by a familiar theorem of Helmholtz in vector analysis) the dilatation and rotation can only vanish everywhere in the body when the displacement is identically zero. In this range of ν, therefore, the displacement solution is unique.

The expression (23) appears also in BOGGIO's (1907) proof. Still earlier KELVIN (1888) had noticed it, in connexion with the elastic aether and not in the context of uniqueness. KELVIN's work was utilized by ERICKSEN and TOUPIN (1956) in an independent re-derivation of BOGGIO's result (by implication).

When $\nu = \frac{1}{2}$ the strain is equal to the stress deviator/2μ. The hydrostatic part of the stress is undetermined by the strain, and no potential of the type (4) exists. Moreover the material is incompressible and only deviatoric strains are possible. Condition (7a) remains valid with U standing for the energy density $\mu \, \epsilon^{\alpha\beta} \, \epsilon_{\alpha\beta}$. This condition is automatically satisfied and so the displacement solution is unique; the stress, however, is determined only to within an arbitrary uniform hydrostatic component. Of course, the surface displacement can not be prescribed entirely arbitrarily since the total volume is invariable:

$$\int u^\beta \, \nu_\beta \, dS = 0.$$

When $(\lambda/\mu, \nu) = (-2, 1)$, $\bar{U}$ and its integral are both semi-definite, vanishing for irrotational fields zero on S (and only then). It follows by the remarks in Section 2 that we have an eigenstate. To construct the eigenfields take any twice continuously differentiable function ϕ whose vector gradient vanishes on S and put

$$u_\beta = \phi_{,\beta}.$$

Then (in rectangular coordinates for simplicity)

$$\sigma_{\alpha\beta}/2\mu = \epsilon_{\alpha\beta} - \delta_{\alpha\beta}\,\epsilon_{\gamma\gamma} = \phi_{,\,\alpha\beta} - \delta_{\alpha\beta}\,\phi_{,\,\gamma\gamma}. \tag{24}$$

Since $\sigma_{\alpha\beta,\,\beta} \equiv 0$ the stress distribution is automatically in equilibrium without body-force, verifying that all such irrotational displacements are eigenfields for $S_t = 0$. Moreover, on S $\epsilon_{\alpha\beta} = \phi_{,\,\alpha\beta} = c\nu_\alpha\,\nu_\beta$, where c is a function of position, and so $t_\beta = \nu_\alpha\,\sigma_{\alpha\beta} = 0$ there.

Since the surface traction vanishes, these are eigenfields also for any $S_t \neq 0$ when $\nu = 1$. Again, for the inhomogeneous problem without body-force, any irrotational field satisfying the boundary conditions is a solution. These results naturally parallel the properties of the potential (12) since U in (21) coincides with it when $\bar{U} \equiv 0$.

There remains the range $\frac{1}{2} < \nu < 1$. For every such value an eigenfield vanishing on S can be constructed for a body of special shape, namely an ellipsoid of revolution with axes in the ratio $\sqrt{(1-\nu)}:\sqrt{(2\nu-1)}$ (Ericksen 1957). The question is still open whether this range of ν contains eigenvalues when the body is arbitrary.*

No further information is obtained from (7b) which is violated by any solenoidal field vanishing on S, since this makes the functional positive for any λ/μ. As for (18a), its counterpart here is

$$\left.\begin{aligned} &\int\left(\sigma^{\alpha\beta}\,\sigma_{\alpha\beta} - \frac{\nu}{1+\nu}\,\sigma^{\alpha}{}_{\alpha}\,\sigma^{\beta}{}_{\beta}\right)dV > 0 \\ \text{or}\qquad &\frac{\nu}{1+\nu} < g.l.b.\left\{\int\sigma^{\alpha\beta}\,\sigma_{\alpha\beta}\,dV \Big/ \int\sigma^{\alpha}{}_{\alpha}\,\sigma^{\beta}{}_{\beta}\,dV\right\} \end{aligned}\right\} \tag{25}$$

for all equilibrated stress fields not identically zero, with unrestricted surface traction ($S_t = 0$). Now $\sigma^{\alpha\beta}\,\sigma_{\alpha\beta} \geqslant \frac{1}{3}\,\sigma^{\alpha}{}_{\alpha}\,\sigma^{\beta}{}_{\beta}$ and so the Rayleigh quotient is certainly never less than $\frac{1}{3}$, and it actually attains this value for any uniform distribution of pure hydrostatic stress (and only then). Therefore $\nu/(1+\nu) < \frac{1}{3}$ or $-1 < \nu < \frac{1}{2}$. Thus Kirchhoff's result is not improved, and so (18a) is here inferior to (7a). No information is gained from (18b) since any equilibrated deviatoric field makes the functional positive.

(ii) *Traction boundary-value problem* ($S_u = 0$). In (7a) or its equivalent (22) the surface values of the displacement are now unrestricted. But, as with (25), the quotient has a minimum value of $\frac{1}{3}$, obtained with a field of pure dilatation. Therefore $\lambda/\mu > -\frac{2}{3}$ or $-1 < \nu < \frac{1}{2}$, and Kirchhoff's result is not bettered. Nothing is learned from (7b).

In (25) the equilibrated fields must now produce no surface traction ; in particular a hydrostatic state is inadmissible. Consequently, the Rayleigh quotient does not take the value $\frac{1}{3}$, and the solution for $\nu = \frac{1}{2}$ is unique. It remains possible that the greatest lower bound may be in excess of $\frac{1}{3}$. On the other hand, it can not exceed $\frac{1}{2}$, since $\nu = 1$ has already been shown to be an eigenvalue for any S_u, S_t. Indeed, for the stress fields (24),

$$\int(\sigma^{\alpha\beta}\,\sigma_{\alpha\beta} - \tfrac{1}{2}\,\sigma^{\alpha}{}_{\alpha}\,\sigma^{\beta}{}_{\beta})\,dV = 4\mu^2\int(\epsilon^{\alpha\beta}\,\epsilon_{\alpha\beta} - \epsilon^{\alpha}{}_{\alpha}\,\epsilon^{\beta}{}_{\beta})\,dV = 0$$

*The ellipsoid fields can not simply be surrounded by an unstressed rigid region, since the traction would be discontinuous across the interface, violating equilibrium.

as shown before, and so

$$\int \sigma^{\alpha\beta}\,\sigma_{\alpha\beta}\,dV \Big/ \int \sigma^{\alpha}{}_{\alpha}\,\sigma^{\beta}{}_{\beta}\,dV = \tfrac{1}{2}.$$

The conclusion is, then, that the traction problem has a unique solution when

$$-1 < \nu \leqslant \tfrac{1}{2} + n, \qquad 0 \leqslant n < \tfrac{1}{2}.$$

n would be zero if there existed a sequence of stress states, in equilibrium and without surface traction, having vanishingly small ratios of shear strain energy to dilatational energy.

We turn next to (18b). If the least upper bound of the Rayleigh quotient in (25) were finite, the previous range of ν would be extended. However, it seems probable that in 3 dimensions (*not* in 2) an equilibrated deviatoric stress field can always be found that produces no traction on an arbitrary surface. Should this be true, (18b) cannot be satisfied for any ν.

When $\nu = 1$ the stress is equal to $2\mu \times$ the strain deviator. The dilatation is undetermined by the stress, and no potential of type (17) exists. Moreover, only deviatoric stresses are possible. Condition (18a) remains valid with U standing for the energy density $\sigma^{\alpha\beta}\,\sigma_{\alpha\beta}/4\mu$. This condition is automatically satisfied. Consequently the stress is unique even though the strain and displacement are not. It should be observed that, even apart from the necessary conditions of overall equilibrium, the traction vector $\mathbf{t}$ cannot be prescribed arbitrarily here: we must also have

$$\int \mathbf{t}\,dS = \int \sigma^{\alpha}{}_{\alpha}\,dV = 0$$

where $\mathbf{r}$ is the position vector relative to an arbitrary origin.

(*b*) *Plane strain*

This will be treated *ab initio* as a general boundary-value problem in two independent variables over a plane area. It could, however, also be regarded as a particular mixed boundary-value problem in three variables for a right cylinder of uniform section: the displacement or traction prescribed along any generator is constant and perpendicular to it, while the normal displacement and tangential traction over the ends are given zero. When the solution is unique it must necessarily also be the unique solution of the 2-dimensional problem. Uniqueness of the latter, on the other hand, does not guarantee uniqueness of the 3-dimensional problem since this might also have a non-planar solution. This possibility is not examined here.

We take rectangular coordinates (x, y) in the plane, and let (u, v), $(\sigma_x, \sigma_y, \tau)$, and $(\epsilon_x, \epsilon_y, \gamma)$ be the x, y components of the displacement, stress, and strain tensor, respectively. Then the relations for stress in terms of strain are ($\nu \neq \frac{1}{2}$, all λ/μ)

$$(\sigma_x, \sigma_y)/2\mu = \begin{pmatrix} 1 + \lambda/2\mu & \lambda/2\mu \\ \lambda/2\mu & 1 + \lambda/2\mu \end{pmatrix} (\epsilon_x, \epsilon_y), \qquad \tau/2\mu = \gamma. \tag{26}$$

The relations for strain in terms of stress are ($\lambda/\mu \neq -1$, all ν)

$$(\epsilon_x, \epsilon_y) = \begin{pmatrix} 1 - \nu & -\nu \\ -\nu & 1 - \nu \end{pmatrix} (\sigma_x, \sigma_y)/2\mu, \qquad \gamma = \tau/2\mu. \tag{27}$$

The energy density is

$$\mu\left[(1+\lambda/2\mu)(\epsilon_x+\epsilon_y)^2+2(\gamma^2-\epsilon_x\epsilon_y)\right]=$$
$$=\left[(1-\nu)(\sigma_x+\sigma_y)^2+2(\tau^2-\sigma_x\sigma_y)\right]/4\mu. \tag{28}$$

(*i*) ***Displacement problem.*** The procedure exactly parallels the 3-dimensional treatment of (7a) and leads again to (22) and (23), except that the indices now take two values only and the integration extends over the section area. The range of ν for which the planar solution is unique is therefore as before:

$$-\infty<\nu<\tfrac{1}{2}. \qquad 1<\nu<\infty.$$

In place of (25), however, we now have

$$(1-2\nu)+g.l.b.\left\{\iint\left[(\sigma_x-\sigma_y)^2+4\tau^2\right]dx\,dy\Big/\iint(\sigma_x+\sigma_y)^2\,dx\,dy\right\}>0. \tag{29}$$

A uniform hydrostatic field is admissible and yields $1-2\nu>0$ or $-\infty<\nu<\frac{1}{2}$. This is a larger range than was obtained in 3 dimensions by this method. No information is furnished by the (7b) or (18b) procedures.

The situation when $\nu=\frac{1}{2}$ or 1 is similar to that in 3 dimensions. Some further discussion of $\nu=1$ follows under (ii).

(*ii*) ***Traction problem.*** The 2-dimensional form of (22) can be re-arranged as

$$1/(1-2\nu)+g.l.b.\left\{\iint\left[(\epsilon_x-\epsilon_y)^2+4\gamma^2\right]dx\,dy\Big/\iint(\epsilon_x+\epsilon_y)^2\,dx\,dy\right\}>0$$

for displacement fields with unrestricted boundary values. Whence $-\infty<\nu<\frac{1}{2}$. $\nu=\frac{1}{2}$, however, is here just a singularity of (26) and not an eigenvalue (as we shall see). Nothing is learned from (7b).

In (29) the traction must now vanish on the boundary. For such a field of stress it is proved below that

$$\iint(\sigma_x\sigma_y-\tau^2)\,dx\,dy=0 \tag{30}$$

and so

$$\iint\left[(\sigma_x-\sigma_y)^2+4\tau^2\right]dx\,dy=\iint(\sigma_x+\sigma_y)^2\,dx\,dy. \tag{31}$$

The Rayleigh quotient in (29) therefore has the constant value unity, and the condition on ν is just $1-\nu>0$. Similarly, from the counterpart of (29) stemming from (18b), $1-\nu<0$. Uniqueness has therefore been proved for

$$\nu\neq 1.$$

Alternatively, this can be seen directly from the basic requirement that the functional of the strain energy (28) should be definite, in conjunction with (30). Notice, from (31), that no admissible field is deviatoric.

Eigenfields with displacements and traction both vanishing on the boundary have already been demonstrated in (24) for $\nu=1$.

It remains to prove (30). The equilibrium equations without body-force are equivalent to

$$\sigma_x=\frac{\partial P}{\partial y}, \qquad \sigma_y=-\frac{\partial Q}{\partial x}, \qquad \tau=-\frac{\partial P}{\partial x}=\frac{\partial Q}{\partial y},$$

where (P, Q) are the resultant force components transmitted across any interior curve linking (x, y) to an arbitrary origin O. Then

$$\iint (\sigma_x \sigma_y - \tau^2)\, dx\, dy = \iint \left[\frac{\partial}{\partial x}\left(P \frac{\partial Q}{\partial y} \right) - \frac{\partial}{\partial y}\left(P \frac{\partial Q}{\partial x} \right) \right] dx\, dy$$

$$= \oint P dQ = - \oint Q dP$$

taken round the section perimeter. The integral vanishes if the traction is everywhere in one direction (P/Q constant) and *a fortiori* if the boundary is traction-free. Notice that $\sigma_x \sigma_y - \tau^2$ is an invariant, equal to the product of the principal stresses.

In terms of an Airy stress function, ϕ say,

$$P = -2\mu \frac{\partial \phi}{\partial y}, \qquad Q = 2\mu \frac{\partial \phi}{\partial x}.$$

The stresses themselves are given in terms of ϕ by the 2-dimensional form of (24). The strain compatibility relation is $(1 - \nu)\, \nabla^2 (\sigma_x + \sigma_y) = 0$, which is satisfied when ϕ is biharmonic, or exceptionally for any ϕ when $\nu = 1$.

In the latter case

$$(P, Q) = 2\mu\, (-v, u) \tag{32}$$

when the displacement is reckoned relative to the particle at O.* The unique relation between the boundary values of traction and displacement for the solution family (24) therefore takes this particularly simple form in 2 dimensions. In a multiply connected region this implies that the traction prescribed on the boundaries must be such that the resultant force vanishes on *each*.

(*c*) *Generalized plane stress*

By the well-known transformation, results in plane strain are convertible into ones for generalized plane stress by replacing ν by $\nu/(1 + \nu)$ (μ being unaltered). In this way we deduce that the *displacement problem* has a unique solution when

$$-\infty < \nu < 1,$$

and the *traction problem* when

$$\nu \neq -1.$$

When $\nu = -1$ only deviatoric states of stress are possible, and the dilatation is undetermined.

6. Extremum Principles

(i) For the rate equations (5) the basis of all the extremum principles is an elementary quadratic identity consequent on the linearity and on the symmetry of the coefficients (with respect to interchange of $\alpha\ \beta$ and $\gamma\ \delta$). Let $\mathbf{v}$ and $\mathbf{v}^*$ be any two velocity fields, continuous and at least piecewise continuously differentiable. Write $\Delta \mathbf{v} = \mathbf{v}^* - \mathbf{v}$, and similarly for the difference of any other dependent quantities in the two fields. Then

$$\Delta U \equiv U(\Delta \mathbf{v}) + \dot{s}^{\alpha\beta}\, \Delta v_{\beta, \alpha} \tag{33}$$

where $\dot{s}^{\alpha\beta}$ is related to $v_{\beta, \alpha}$ through the rate equations.

*This is somewhat akin to the theorem (HILL 1955) that if (P, Q, u, v) is an *incompressible* elastic state so is $(2\mu u, 2\mu v, -P/2\mu, -Q/2\mu)$.

Now suppose that the uniqueness condition (7a) is satisfied in the specified class, and let $\mathbf{v}$ denote the actual mode and $\mathbf{v}^*$ any 'kinematically admissible' field: i.e. it takes the values prescribed on S_v, but the associated stress-rate need not be in equilibrium with $\dot{\mathbf{g}}$ in V or with $\dot{\mathbf{t}}$ on S_t. Then

$$\int U(\Delta \mathbf{v})\, dV > 0.$$

Integration of (33) and use of the divergence theorem then gives (HILL 1957a, p. 233)

$$\Delta\left[\int (U - \dot{\mathbf{g}}\mathbf{v})\, dV + \int \dot{\mathbf{t}}\mathbf{v}\, dS_t\right] > 0 \qquad \text{(if 7a)} \tag{34}$$

with equality only if the starred field is the unique solution. In view of the variation principle (8) the extremum is analytic. When (7b) is satisfied the inequality in (34) is reversed.

Similarly, for the inverse relations (17) we have the identity

$$\Delta U \equiv U(\Delta \dot{s}^{\alpha\beta}) + v_{\beta,\alpha}\, \Delta \dot{s}^{\alpha\beta} \tag{35}$$

for any pair of stress-rate fields. Suppose (18a) is satisfied in the specified class, and let the starred stress-rate be any 'statically admissible' field: i.e., it is in equilibrium with $\dot{\mathbf{g}}$ in V and $\dot{\mathbf{t}}$ on S_t, but is not necessarily associated with a continuous velocity. Then (HILL 1959, p. 215)

$$\Delta\left[\int \dot{\mathbf{t}}\mathbf{v}\, dS_v - \int U\, dV\right] < 0 \qquad \text{if (18a)} \tag{36}$$

with equality only if the starred field is the unique solution. When (18b) is satisfied the inequality in (36) is reversed.

For the actual solution the bracketed expressions in (34) and (36) both become equal to

$$\tfrac{1}{2}\left[\int \dot{\mathbf{t}}\mathbf{v}\, dS_v - \int \dot{\mathbf{t}}\mathbf{v}\, dS_t - \int \dot{\mathbf{g}}\mathbf{v}\, dV\right]. \tag{37}$$

When either of the pairs of conditions (7a, 18a) or (7b, 18b) are *simultaneously* satisfied, the corresponding pair of extremum principles are also valid and form a continued inequality bounding the quantity (37) from opposite sides.

(ii) Consider, in particular, the situation in the isotropic *linear theory of elasticity*, when (34) and (36) have as their counterparts the familiar minimum principles of potential energy and complementary energy, respectively.

From the results in Section 5 for $S_u = 0$ or $S_t = 0$ in 3 dimensions we see that (7b, 18b) are never simultaneously valid, while (7a, 18a) are so only for $-1 < \nu < \frac{1}{2}$. Consequently, there is no extension of the known range of validity of the continued inequality. But when $S_t = 0$ the potential energy principle is also valid *by itself* when $|\nu| > 1$ as indicated by HILL (1957a, pp. 233–234); an independent proof has been given recently by GURTIN and STERNBERG (1960, Section 4).

In plane strain (7b, 18b) are never valid together, but (7a, 18a) are for all $\nu < \frac{1}{2}$ when either $S_u = 0$ or $S_t = 0$. Additionally, when $S_t = 0$ (34) holds by itself when $\nu > 1$; and when $S_u = 0$ (36) holds when $\nu < 1$ and with the inequality reversed when $\nu > 1$.

(iii) Among the kinematically admissible fields are some which have an associated stress-rate in equilibrium with $\dot{\mathbf{g}}$ in V and also satisfy on S_t the integral condition

$$\int \mathbf{v}^* \, \Delta\dot{\mathbf{t}} \, dS_t = 0. \tag{38}$$

It is supposed here that $S_t \neq 0$, otherwise the sub-class contains only the solution itself when this is unique. For these particular fields the functional of velocity in (34) is actually equal in value to the functional of stress-rate in (36). The latter then bounds (37) from above, when (7a) holds for (equilibrated) velocity fields vanishing on S_v. This follows easily by the usual transformation:

$$2\int U^* \, dV - \int \dot{\mathbf{g}}\mathbf{v}^* \, dV = \int \dot{\mathbf{t}}^* \mathbf{v}^* \, dS$$

$$= \int \dot{\mathbf{t}}^* \mathbf{v} \, dS_v + \int \dot{\mathbf{t}}\mathbf{v}^* \, dS_t$$

on using (38). By re-arrangement:

$$\int (U^* - \dot{\mathbf{g}}\mathbf{v}^*) \, dV - \int \dot{\mathbf{t}}\mathbf{v}^* \, dS_t = \int \dot{\mathbf{t}}^* \mathbf{v} \, dS_v - \int U^* \, dV$$

and the statement is proved. Alternatively, this bound also follows independently of (34) from the identity obtained by interchanging starred and unstarred variables in (35).

Thus, when (7a) and (18a) are simultaneously valid, the quantity (37) is bounded on both sides by the *same* functional (36). Upper bounds are furnished by the sub-class of kinematically admissible fields and lower bounds by statically admissible fields.

In the dual theorem we consider (when $S_v \neq 0$) those statically admissible fields that are associated with a continuous velocity and satisfy on S_v the integral condition

$$\int \dot{\mathbf{t}}^* \, \Delta\mathbf{v} \, dS_v = 0. \tag{39}$$

By the preceding transformation the functional of stress-rate in (36) for these fields is equal in value to the functional of velocity in (34). The latter then bounds (37) from below, when (18a) holds for equilibrated (velocity) fields with zero traction-rate on S_t. Alternatively, this bound also follows independently of (36) from the identity obtained by interchanging starred and unstarred variables in (33).

Thus, when (7a) and (18a) are simultaneously valid, the quantity (37) is bounded on both sides by the same functional (34). Upper bounds are furnished by kinematically admissible fields and lower bounds by the sub-class of statically admissible fields.

Similar theorems with inequalities reversed apply when (7b) and (18b) are simultaneously valid.

Even in the linear theory of elasticity these results do not seem well known in their full generality. The method of Trefftz-Weinstein for the harmonic equation is a familiar special case (e.g. SOKOLNIKOFF 1956, pp. 425–429).

(iv) We examine, finally, the implications of Section 3 in regard to extremum principles. Let U be the potential of the given solid under consideration. Introduce

the associated group of solids having potentials $\bar{U} = U + \Theta$, where Θ is any of the special potentials (9). The velocity boundary-value problem ($S_t = 0$) has a unique solution when (15a or b) is satisfied. Since this is equivalent to (7a or b), for any Θ, the group of solutions are then simultaneously unique. Moreover, the field equations for velocity are the same, since the Θ field equations without body-force vanish identically. Consequently, the unique mode of deformation is common to all solids in the group, although the unique stress-rate solutions differ.

The required mode for U could therefore be characterized by any of the relevant extremum principles for any solid in the group. Thus, from (34) with $\bar{U}$ written in place of U,

$$\Delta \int (\bar{U} - \dot{\mathbf{g}}\mathbf{v})\, dV > 0 \tag{40}$$

for kinematically admissible fields, when the functional of $\bar{U}$ is positive for fields *vanishing* on S. The extremum is analytic in view of (16). Alternatively, to obtain (40) from a purely formal standpoint, simply combine (34) for U itself with the property that the functionals of U and any one $\bar{U}$ differ in value by a mere constant for admissible fields.

Again, in relation to (39) there is a complementary principle characterising the actual mode:

$$\Delta \int (\bar{U} - \dot{\mathbf{g}}\mathbf{v})\, dV < 0 \tag{41}$$

for velocity distributions satisfying the field equations and the integral condition

$$\int v_\alpha \left(c^{\alpha\beta\gamma\delta} + \theta^{\alpha\beta\gamma\delta}\right)\left(v^*{}_\beta - v_\beta\right) v^*{}_{\delta,\gamma}\, dS = 0. \tag{42}$$

This principle holds when the functional of $\bar{U}$ is positive for equilibrated velocity fields *unrestricted* on S.

In particular, when the group of solids contains a $\bar{U}$ which is positive definite, (40) and (41) are simultaneously valid for that $\bar{U}$.

In the isotropic linear theory of elasticity the group of solids is associated with (21), and for these (40) is valid in 3 dimensions when $-\infty < \nu < \frac{1}{2}$, $1 < \nu < \infty$ (Section 5a). Thus, for example, the substitution of (21) itself for $\bar{U}$ yields again the potential energy principle, while the substitution (23) yields a result of Gurtin and Sternberg (1960, Section 3) proved on its merits with the help of certain vector operator identities. Corresponding to (23) the condition (42) reduces to

$$\int v_\alpha \left\{(\lambda + 2\mu)\, \epsilon^\gamma{}_\gamma\, g^{\alpha\beta} - 2\mu\, \omega^{\alpha\beta}{}_{,\gamma}\right\}\left(v^*{}_\beta - v_\beta\right) dS = 0. \tag{43}$$

However, the functional of this $\bar{U}$ is only positive semi-definite in the above range of ν, vanishing for any solenoidal irrotational field. Consequently, only a weak form of (41) holds, the extremum being attained for other fields besides the actual mode. This result is also due to Gurtin and Sternberg (1960, Section 5), (43) being the same as their (57) (note the different use of the asterisk).

References

Boggio, T. 1907 *Atti. d. Accad. dei Lincei* **16**, 248.

Budiansky, B. and Pearson, C. E. 1956 *Quart. Appl. Math.* **14**, 328.

ERICKSEN, J. L. 1957 *Proc. Amer. Math. Soc.* **8**, 521.

ERICKSEN, J. L. and TOUPIN, R. A. 1956 *Canad. J. Math.* **8**, 432.

GURTIN, M. E. and STERNBERG, E. 1960 *Arch. Rat. Mech. Anal.* **6**, 177.

HILL, R. 1955 *J. Mech. Phys. Solids* **4**, 1.

1957a *Ibid.* **5**, 229.

1957b *Ibid.* **5**, 153.

1958 *Ibid.* **6**, 236.

1959 *Ibid.* **7**, 209.

1961a *Bifurcation and Uniqueness in Non-linear Mechanics of Continua*, in Presentation Volume to N.I. MUSKHELISHVILI (U.S.S.R. Acad. Sci.).

1961b *Discontinuity Relations in Mechanics of Solids*, in *Progress in Solid Mechanics* II (N. Holland Publ. Co.).

HILL, R. and SEWELL, M. J. 1960 *J. Mech. Phys. Solids* **8**, 105.

KELVIN, LORD 1888 *Phil. Mag.* **26**, 414.

OLDROYD, J. G. 1950 *Proc. Roy. Soc.* A **200**, 523.

SOKOLNIKOFF, I. S. 1956 *Mathematical Theory of Elasticity* 2nd Ed. (McGraw-Hill, New York).

J. Mech. Phys. Solids, 1961, Vol. 9, pp. 131 to 139. Pergamon Press Ltd., London. Printed in Great Britain

THE BUCKLING OF A DISLOCATED PLATE

By L. H. Mitchell
Aeronautical Research Laboratories, Fishermen's Bend, Melbourne

and A. K. Head
C.S.I.R.O., Division of Tribophysics, University of Melbourne

(*Received 5th December*, 1960)

Summary

The buckling criteria for a thin circular dislocated plate is calculated for three types of dislocation. These are (i) a sector inserted into the plate, (ii) a sector removed from the plate, (iii) the edge dislocation of solid state physics at the centre of the plate. It is concluded that it is most unlikely that edge dislocations observed in thin metal films by electron microscopy can relieve their long range stress field by buckling the film.

1. Introduction

Eshelby and Stroh (1951) have shown that, if a thin plate contains a screw dislocation whose line is normal to the plane of the plate, the stress field of the dislocation is largely confined to the neighbourhood of the dislocation line. Thus two such screw dislocations in a plate will have a short range interaction in contrast to the long range inverse first power interaction between dislocations in an infinite medium. They also showed that the stress field due to an edge dislocation is essentially the same in a thin plate and an infinite body as long as the plate remains flat, but that there is the possibility of the plate buckling with a consequent reduction in the stress field.

In this paper we calculate the buckling conditions for a circular plate which contains an edge dislocation at the centre. On a macroscopic scale such a dislocation can be generated in an initially unstressed plate by first cutting the plate along a radius from circumference to centre, removing from one face of the cut a constant thickness of material, and then rejoining the two faces of the cut. As a preliminary, we also consider the buckling of a circular plate when a sector is inserted into or removed from the plate. The latter is, of course, familiar as the method of making a cone from a circle of paper although it is not usually thought of as a buckling process.

2. Buckling of circular plate with sector inserted or removed

The critical thickness of a circular plate which has a sector added or subtracted is here calculated approximately by the energy method formulated, for example, by Timoshenko (1936). In addition the plate with a sector subtracted is considered

by means of the differential equation of bending of thin plates, these two methods yield upper and lower bounds for the critical thickness.

From the plane stress solution given by COKER and FILON (1931) for an annulus which has a sector removed, the stresses can be shown to be

$$\sigma_{rr} = \frac{E\alpha}{4\pi}\left[\frac{K^2(1-1/r^2)\log K + (1-K^2)\log r}{1-K^2}\right],$$

$$\sigma_{\theta\theta} = \frac{E\alpha}{4\pi}\left[1 + \frac{K^2(1+1/r^2)\log K + (1-K^2)\log r}{1-K^2}\right],$$

$$\sigma_{r\theta} = 0,$$

where E is Young's modulus, α the angle of the sector subtracted, K the ratio of inner to outer radii of the annulus and r the radial distance to any point divided by the outer radius R. Addition of a sector is obtained by merely changing the sign of α. Since only a very small inner radius is of interest, i.e. $K \ll 1$, the stresses are approximately given by

$$\left.\begin{aligned} \sigma_{rr} &= E\alpha\,(r^2\log r - K^2\log K)/4\pi r^2, \\ \sigma_{\theta\theta} &= E\alpha\,(r^2 + r^2\log r + K^2\log K)/4\pi r^2, \\ \sigma_{r\theta} &= 0. \end{aligned}\right\} \qquad (1)$$

The stability of a plate having this stress distribution will now be examined.

(a) *Energy solution*

Since there are no external forces applied to the plate, a lower bound for the critical thickness can be obtained by equating the work done by the initial stresses during an assumed plate deflexion to the corresponding work absorbed in bending. The work done by the stresses during a deflexion $w(r, \theta)$ satisfying the boundary conditions is

$$tE\alpha\, U_s = -\frac{t}{2}\int_0^{2\pi}\int_K^1\left[\sigma_{rr}\left(\frac{\partial w}{\partial r}\right)^2 + \sigma_{\theta\theta}\left(\frac{1}{r}\frac{\partial w}{\partial \theta}\right)^2 + 2\sigma_{r\theta}\frac{1}{r}\frac{\partial w}{\partial \theta}\frac{\partial w}{\partial r}\right] r\,dr\,d\theta. \qquad (2)$$

The bending energy of the deflected plate is given by

$$Et^3\, U_b/R^2 = \frac{Et^3}{24(1-\nu^2)R^2}\int_0^{2\pi}\int_K^1\left[\left(\frac{\partial^2 w}{\partial r^2} + \frac{1}{r}\frac{\partial w}{\partial r} + \frac{1}{r^2}\frac{\partial^2 w}{\partial \theta^2}\right)^2\right.$$

$$\left. - 2(1-\nu)\left\{\frac{\partial^2 w}{\partial r^2}\left(\frac{1}{r^2}\frac{\partial^2 w}{\partial \theta^2} + \frac{1}{r}\frac{\partial w}{\partial r}\right) - \left(\frac{1}{r}\frac{\partial^2 w}{\partial r\,\partial \theta} - \frac{1}{r^2}\frac{\partial w}{\partial \theta}\right)^2\right\}\right] r\,dr\,d\theta \qquad (3)$$

By equating these two energies a lower bound for the critical thickness can be obtained from

$$t^2\, U_b = \alpha\, R\, U_s. \qquad (4)$$

The assumed deflexion is of the form

$$w = \sum_{i=0}^{n} a_i\, w_i(r, \theta)$$

where the w_i are desirably part of a complete set of functions. Provided that the w_i can represent quite general boundary conditions, (4) will give a lower bound for the critical thickness of a plate with free boundaries and this bound can be maximized with respect to the a_i. It is convenient to find this maximum value by solving for the maximum value of $\beta = t^2/\alpha R^2$ for which the set of $(n+1)$ homogeneous equations

$$\beta \frac{\partial U_b}{\partial a_i} - \frac{\partial U_s}{\partial a_i} = 0, \qquad i = 0 \ldots n \tag{5}$$

yields a non-trivial solution for the a_i. If the w_i are part of a complete set of functions then it is well known that this lower bound for the critical thickness can be made arbitrarily close to the true value by making n large enough.

If the set of equations (5) is determined for the deflexion

$$w = \sum_{i=0}^{m} \sum_{j=-n}^{n} a_{ij} r^j \cos i\theta \tag{6}$$

it can be shown that the set can be written as m independent sets, each corresponding to one value of i, and that values of $j < 2$ need not be considered if K is small. It also follows that the critical thickness is not dependent on whether or not there is a very small hole at the centre of the plate. Hence the expression for the deflexion can be simplified to

$$w = \cos i\theta \sum_{j=2}^{n} a_j r^j$$

and with $K = 0$ the set of equations (5) becomes

$$\left.\begin{aligned} \pi\beta \sum_{k=2}^{n} \left[\frac{(j^2-1)(k^2-i^2)}{j+k-2} - (1-\nu)\{jk - i^2(j+k-1)\} \right] a_k \\ + 3(1-\nu^2) \sum_{k=2}^{n} \frac{i^2(j+k-1) - jk}{(j+k)^2} a_k = 0, \qquad j = 2 \ldots n. \end{aligned}\right\} \tag{7}$$

Values of β found from (7) are given for $\nu = 0{\cdot}3$ and various values of i and n. It can be seen

TABLE 1. *Values of* β *for* $\nu = 0{\cdot}3$

n \ i	0	1	2	3
2	0·042	0·014	− 0·078	− 0·044
3	0·073	0·022	− 0·094	− 0·045

that for the case of removal of a sector the plate buckles into a ' conical ' shape and that the critical value of $\beta > 0{\cdot}073$. The flat plate is unstable if the parameter β divided by its critical value is less than unity. For the case of the addition of a sector the deflected form is likely to depend on $\cos 2\theta$ and the critical value of $\beta < -0{\cdot}094$.

(b) *Differential equation solution for removal of sector*

The differential equation of equilibrium of a thin plate using polar co-ordinates is

$$\frac{Et^2}{12\,(1-\nu^2)\,h^2}\,\nabla^4 w = \sigma_{rr}\frac{\partial^2 w}{\partial r^2} + \sigma_{\theta\theta}\left(\frac{1}{r^2}\frac{\partial^2 w}{\partial \theta^2} + \frac{1}{r}\frac{\partial w}{\partial r}\right) + 2\,\sigma_{r\theta}\left(\frac{1}{r}\frac{\partial^2 w}{\partial r\,\partial \theta} - \frac{1}{r^2}\frac{\partial w}{\partial \theta}\right).$$

Since $\sigma_{r\theta} = 0$ it follows immediately that solutions for w can be expressed as $\cos i\theta$ multiplied by a function of r. Here we will only consider the solution independent of θ and by using the stresses (1) this differential equation can be reduced to

$$r^2\frac{d^3 w}{dr^3} + r\frac{d^2 w}{dr^2} - \left[1 + \frac{3\,(1-\nu^2)}{\pi\beta}\,(r^2\log r - K^2\log K)\right]\frac{dw}{dr} = 0$$

if no transverse shear load is applied at the boundaries. If K is very small then this equation is approximately

$$r^2\frac{d^2\phi}{dr^2} + r\frac{d\phi}{dr} - \left[1 + \frac{3\,(1-\nu^2)}{\pi\beta}\,r^2\log r\right]\phi = 0 \qquad (8)$$

where $\phi = dw/dr$.

By putting $\phi = \sum_{\mu=0}^{\infty}\phi_\mu\,\delta^\mu$ in (8), equating coefficients of powers of $\delta = 3\,(1-\nu^2)/\pi\beta$ and solving the resulting differential equations for ϕ_μ, the following results can be obtained:

$$\left.\begin{aligned}\phi = c_1\Bigg[r - \frac{r^3}{8}\left(\frac{3}{4} - \log r\right)\delta + \frac{r^5}{192}\left(\frac{83}{144} - \frac{19}{12}\log r + \log^2 r\right)\delta^2 \\ - \frac{r^7}{9216}\left(\frac{1031}{2304} - \frac{181}{48}\log r + \frac{59}{24}\log^2 r - \log^3 r\right)\delta^3 + \dots\Bigg]\end{aligned}\right\} \qquad (9)$$

or

$$\phi = c_2\left[\frac{1}{r} + \dots\right].$$

It can be shown that with K very small only the first of these solutions is needed and that the necessary boundary condition is that the bending moment is zero at $r = 1$; i.e.

$$\frac{d^2 w}{dr^2} + \frac{\nu}{r}\frac{dw}{dr} = \frac{d\phi}{dr} + \frac{\nu}{r}\phi = 0 \quad \text{at} \quad r = 1.$$

Using this condition and the first four terms of (9) with $\nu = 0{\cdot}3$ we find $\delta = 11{\cdot}0$. Because (9) yields an alternating series it follows that the critical value of β is less than 0·079. Hence, with the result from the energy solution,

$$0{\cdot}073 < \beta_{\text{crit.}} < 0{\cdot}079$$

for a sector removed from a plate with free boundaries.*

3. Buckling of circular plates with edge dislocations

Coker and Filon (1931) give the plane stress solution for a plate containing an edge dislocation of Burgers' vector b along the line $\theta = -\frac{1}{2}\pi$, i.e. a plane of width b inserted along $\theta = 0$. The stresses in a circular plate with a small hole at the centre are

$$\frac{\sigma_{rr}}{\cos\theta} = \frac{\sigma_{r\theta}}{\sin\theta} = \frac{Eb}{4\pi R}\left[\frac{r}{1+K^2} - \frac{1}{r} + \frac{K^2}{(1+K^2)\,r^3}\right],$$

*The authors subsequently discovered that this case had been previously considered by Willers (1943). By an energy method he found $\beta_{\text{crit.}} > 0{\cdot}076$ (after correction of a numerical error) and by a finite difference approximation $\beta_{\text{crit.}}$ is approximately 0·077.

$$\sigma_{\theta\theta} = \frac{Eb}{4\pi R}\left[\frac{3r}{1+K^2} - \frac{1}{r} - \frac{K^2}{(1+K^2)\,r^3}\right]\cos\theta,$$

and when K is small these reduce to

$$\left.\begin{aligned} \frac{\sigma_{rr}}{\cos\theta} = \frac{\sigma_{r\theta}}{\sin\theta} &= \frac{Eb}{4\pi R}\left[r - \frac{1}{r} + \frac{K^2}{r^3}\right], \\ \sigma_{\theta\theta} &= \frac{Eb}{4\pi R}\left[3r - \frac{1}{r} - \frac{K^2}{r^3}\right]. \end{aligned}\right\} \tag{10}$$

Since the solution of the differential equation given in Section 2(b) is difficult for the stress distribution (10), the critical thickness of a plate containing an edge dislocation was estimated using the energy method already outlined. The deflected form was taken as

$$w = r^2 \sum_{i=0}^{m} \sum_{j=0}^{n} a_{ij}\,(1-r)^j \cos i\theta \tag{11}$$

as it was found that the form (6) led to a badly conditioned set of equations. This form (11) was adopted for the reasons that the coefficients of the set of equations equivalent to (5) are easily calculated and that the solution (9) can be expressed by a convergent series of this form. As in the previous Section it can be shown that it is unnecessary to consider powers of r less than 2 for plates with very small central holes and that K can be put equal to zero in the stress distribution (10). A more general form for w than that given by (11) involves terms in $\sin i\,\theta$ but if these are included an independent set of equations is found. This set happens to be identical with the cosine set if the coefficients a_{0j} are omitted and consequently the critical thickness found from the sine set must be less than or equal to that found using the form (11).

The set of equations equivalent to (5) was found to be

$$\begin{aligned} 0 = {} & \pi\gamma \sum_{\mu=0}^{n} a_{i\mu} \left[\begin{aligned} & A_j\,A_\mu\,K_{j+\mu} - \{\mu\,(2\mu+3)\,A_j + j\,(2j+3)\,A_\mu\}\,K_{j+\mu-1} \\ & + \{j\mu\,(2j+3)\,(2\mu+3) + \mu\,(\mu-1)\,A_j + j\,(j-1)\,A_\mu\}\,K_{j+\mu-2} \\ & - j\mu\,(4j\mu + j + \mu - 6)\,K_{j+\mu-3} + j\mu\,(j-1)\,(\mu-1)\,K_{j+\mu-4} - (1-\nu)\,B_{i\mu} \end{aligned}\right] \\ & - 3\,(1-\nu^2) \sum_{\mu=0}^{n} \left[\begin{aligned} & a_{i-1,\mu}\,(1+\delta_{i1})\,\{i\,(i-1)\,J_{j+\mu} + [(j+2)\,(\mu+i+1) - i\,(\mu+2)]\,I_{j+\mu} \\ & - [j\,(\mu+i+1) + \mu\,(j-i+2)]\,I_{j+\mu-1} + j\mu\,I_{j+\mu-2}\} \\ & + a_{i+1,\mu}\,\{i\,(i+1)\,J_{j+\mu} + [(j+2)\,(\mu-i+1) + i\,(\mu+2)]\,I_{j+\mu} \\ & - [j\,(\mu-i+1) + \mu\,(j+i+2)]\,I_{j+\mu-1} + j\mu\,I_{j+\mu-2}\} \end{aligned}\right] \end{aligned}$$

$$i = 0 \ldots m, \qquad j = 0 \ldots n, \tag{12}$$

where

$$\gamma = \frac{t^2}{Rb},$$

$$A_j = (j+2)^2 - i^2,$$

$$B_{00} = (8 - 6i^2)\,K_0,$$

$$B_{01} = B_{10} = 12\,(1-i^2)\,K_1 - (10 - 6\,i^2)\,K_0,$$

$$B_{11} = (24 - 20\,i^2)\,K_2 - (24 - 16\,i^2)\,K_1 + (8 - 2\,i^2)\,K_0,$$

$$B_{\mu j} = 0 \quad \text{if} \quad \mu > 1 \text{ or } j > 1,$$

$$I_j = \frac{2(j+8)}{(j+2)(j+3)(j+4)(j+5)},$$

$$J_j = \frac{2(j^2+9j-16)}{(j+1)(j+2)(j+3)(j+4)(j+5)},$$

$$K_j = \frac{1}{(j+1)(j+2)},$$

$$\delta_{i1} = 1 \quad \text{if } i = 1, \qquad = 0 \text{ if } i \neq 1,$$

$$a_{i\mu} = 0 \qquad \text{if } i < 0,$$

ν = Poisson's ratio = 0·3.

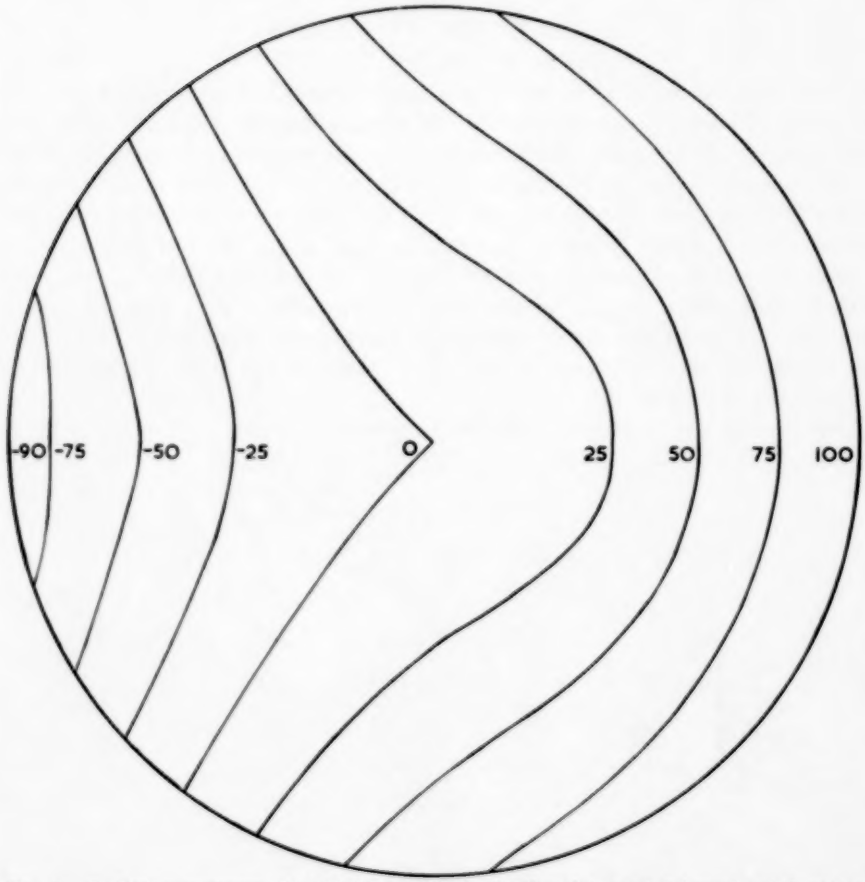

Fig. 1. Deflexion contours of buckled form of thin circular plate containing edge dislocation at centre. Outer edge free.

The eigenvalues of γ were found from equations (12) for three trial functions (11) containing four, nine and sixteen terms. These are given in Table 2 and suggest that the critical value of γ is not likely to be much greater than 0·1.

From the values of a_{ij} found for $m = n = 4$, the buckled form of the plate was calculated from (11) and is shown in Fig. 1, with the maximum deflexion normalized to 100 and zero deflexion and slope at the centre of the plate. This is

TABLE 2

Number of terms	m	n	γ
4	2	2	0·070
9	3	3	0·092
16	4	4	0·096

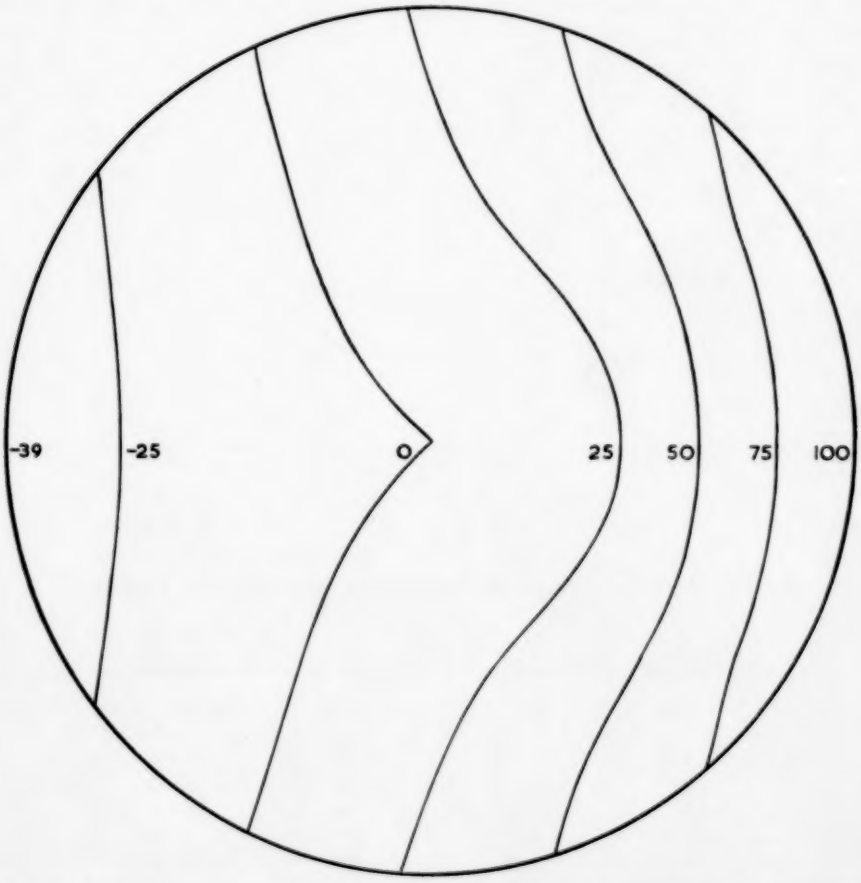

FIG. 2. Deflexion contours of buckled form of thin circular plate containing edge dislocation at centre. Outer edge simply supported.

of course the form of the infinitesimal buckle when γ is just equal to the critical value. However, it was found from paper models that finite buckles had the same general form.

The form (11) assumed for the deflexion has the advantage that a simply supported circular plate can be obtained simply by omitting the terms involving a_{i0}, $i > 1$, from the above calculation. With $m = n = 4$, γ was then found to be 0·086. Thus the critical value of γ for a simply supported circular plate containing an edge dislocation is greater than 0·086. The approximate deflected shape is given in Fig. 2 with maximum deflection normalized to 100, and zero deflexion and slope at the centre of the plate.

4. Magnitude of finite deflexion of buckled plate

The maximum deflexion after buckling of any circular plate containing an edge dislocation should be less than that for a very thin circular plate containing the same dislocation and with a free edge. The very thin plate will deflect until

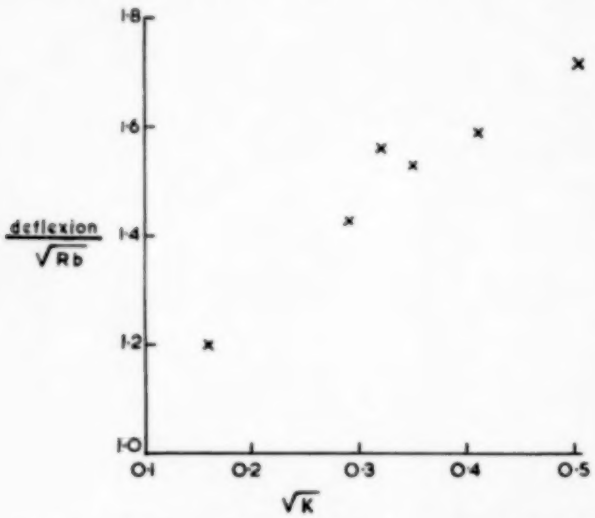

Fig. 3. Maximum deflexion of paper models containing edge dislocation.

Table 3

$\gamma \times 10^5$	K	R/b	*Deflexion*$/\sqrt{(Rb)}$
5·2	0·25	8	1·7
4·2	0·17	15	1·6
3·1	0·13	20	1·5
2·5	0·10	25	1·6
2·1	0·08	30	1·4
0·9	0·03	100	1·2

the outer portions of it are very nearly stress free. In paper models the outer circumference is almost flat for somewhat more than half its length and the remainder deflects roughly in the shape $a\{1 - \cos(2\pi\theta/\theta_0)\}$ over an angle θ_0. For the outer portion to be stress free the difference in length between the length of the

circumference and its projection on a plane must be equal to the Burgers' vector. These considerations suggest that the maximum deflexion depends on $\sqrt{(Rb)}$.

The maximum deflexion for a series of paper models with a central hole is given in Table 3. By approximating the deflected shape with developable surfaces it can be shown that the maximum deflexion divided by $\sqrt{(Rb)}$ should be a linear function of $\sqrt{K}$. These quantities are plotted in Fig. 3. Hence it seems likely that the deflexion of a buckled circular plate containing an edge dislocation will be less than $2\sqrt{(Rb)}$.

5. Discussion

As an application of these results we consider an edge dislocation in a metal film which is sufficiently thin to be used in transmission electron microscopy. The condition for buckling is $R > 10\,t^2/b$ where we can take $t \sim 500$ Å and $b \sim 2{\cdot}5$ Å, giving $R \sim 10^6$ Å. Although no actual thin film specimen will have the simple geometry we have assumed, namely a single dislocation at the centre of a uniform circular film, we can take 10^6 Å as an estimate of the minimum spacing between dislocations of opposite sign. If dislocations are closer than this distance buckling will not occur. This corresponds to the very low dislocation density of $10^4/\text{cm}^2$ and so it may be concluded that the edge dislocations which are observed by the electron microscope have not relieved their long range stress field by buckling the film.

6. Acknowledgment

One of us (L.H.M.) wishes to thank the Chief Scientist, Australian Defence Scientific Service, Department of Supply, for permission to publish this paper.

References

Coker, E. G. and Filon, L. N. G. 1931 *Treatise on Photoelasticity* (Cambridge University Press).

Eshelby, J. D. and Stroh, A. N. 1951 *Phil. Mag.* **42**, 1401.

Timoshenko, S. 1936 *Theory of Elastic Stability* (McGraw-Hill, New York).

Willers, A. 1943 *Z. Angew. Math. Mech.* **23**, 252.

BOOK REVIEWS

Structural Mechanics, Proceedings of the First Symposium on Naval Structural Mechanics: Edited by J. N. Goodier and N. J. Hoff. Pergamon Press, Oxford, 1960. 594 pp., 70s.

This Symposium was held at Stanford University in August 1958. Although sponsored by the U.S. Office of Naval Research, and avowedly designed to 'highlight the Naval orientation of the subject matter,' the authors are not noticeably swayed by this consideration and the articles are almost entirely of broad fundamental interest. Only one deals specifically with problems peculiar to ship design: this is the opening address by J. A. Brown, a fascinating and instructive account of the many complex problems and new thinking in what has been until recently an over-conservative art. The other contributions, seventeen in number, can conveniently be reviewed in four groups, according to content and treatment.

First, there are the theoretical papers for specialists in the respective branches. 'Waves and Vibrations in Elastic Plates' by R. D. Mindlin, and 'Some Problems in Shell Theory' by E. Reissner, are not aimed at a wide audience and are likely to be most useful as sources for equations and formulae. A. H. Flax on 'Aero-Hydro-Elasticity' is a good deal more readable but does not trouble to define technical terms in wing theory for the uninitiated: a pity, because the subject is intrinsically of general interest, drawing on several distinct branches of mechanics. B. A. Boley's article on 'Thermal Stresses' has now been superseded by his recent excellent monograph.

In the second group of papers the treatment makes them generally accessible. Of these, R. S. Rivlin on 'Some Topics in Finite Elasticity' will probably make the widest appeal, because of the previous absence of good elementary accounts. He assumes virtually no previous knowledge of the subject, and handles it so that mathematical difficulties are cut to the minimum. He does not, however, go very deeply into the most recent advances. E. Sternberg on 'Recent Developments in the Linear Theory of Elasticity' is equally successful, though in a totally different way. He assumes a moderate acquaintance with classical elasticity, and gives a mostly verbal account, with relatively few formulae, of the present stand in selected problems of fundamental importance. This should be particularly useful as a guide to young researchers in this field who already have a working knowledge of a restricted part of it. 'Visco-elastic Stress Analysis' by E. H. Lee is handled rather similarly, though covering less ground in more detail. The author emphasizes that theory has now outstripped experiment, particularly as regards behaviour under combined stress, and indicates what should be done to close the gap. D. C. Drucker writes on 'Plasticity,' or actually only on the classical part of it concerned with infinitesimal strain of rigid/plastic solids. (The Second Symposium, just published, is entirely devoted to mechanics of plastic materials in general). The author's approach to the logical foundations of the subject is entirely personal and (as he says) 'has by no means met with general acceptance.' His article will perhaps be mostly valued for its broad survey of plastic limit analysis, of which he is a wellknown exponent. The concluding sentence, however, is curious in its implication: 'Part of the challenge is gone from plasticity if it is true that its essence has been grasped.' The author must be here equating plasticity merely with the theory of the initial flow of a certain highly special hypothetical solid, namely a rigid/plastic solid for which the maximum work inequality and some related attractively simple theorems hold.

The third group is concerned mainly with experimental results and techniques. H. Kolsky writes on 'Wave Propagation in Solids' and M. Hetenyi on 'Photoelasticity and Photoplasticity,' both very informatively. 'Trends in Materials to meet the Problems of Structural Mechanics' is a timely review by J. J. Harwood, N. E. Promisel and J. Maltz, of wide interest, not least to theoreticians. G. R. Irwin on 'Fracture Mechanics' presents once more the two-dimensional elastic stress analysis of cracks and pushes it as far as is reasonable (some might say farther than) in attempts to explain a variety of phenomena. The article is stimulating but a needed corrective to over-confidence is applied by C. Mylonas in the Discussion. A reasoned reply by the author

would have been invaluable: instead, he says, incomprehensibly, 'Applicability of fracture mechanics to any particular fracture experiments is determined not by questions of whether a theory is applicable but rather by questions of applicability of a stress analysis appropriate to the suggested descriptive procedure.'

Special mention is made of a first-rate article combining the best qualities of all three groups: Y. C. FUNG and E. E. SECHLER on 'Instability of Thin Elastic Shells.'

The fourth group is somewhat miscellaneous and is here merely cited by name: H. H. BLEICH, 'Dynamic Interaction between Structures and Fluid'; M. C. JUNGER, 'Structure-Borne Noise'; I. VIGNESS, 'Instrumentation, Analyses, and Problems concerning Shock and Vibration'; H. J. GREENBERG, 'Solving Structural Mechanics Problems on Digital Computers.'

One of the permanently useful features of an invaluable (and reasonably priced) book is the remarkable documentation of most contributions: the average number of references per paper cannot be far from a hundred.

R. HILL

Crystal Growth. Discussions of the Faraday Society, No. 5, 1949. Butterworth, London, 1959. 366 pp., 60*s*.

THE fifth General Discussion of the Faraday Society must surely be ranked as one of the most outstanding and successful of the series. The papers presented at that meeting provided the stimulus for the great burst of activity in studies of the mechanism of crystal growth as a branch of solid state physics which took place in the following 4 or 5 years. Our present knowledge of the intimate relationship between crystal growth and crystal imperfection is due entirely to the sound ideas formulated in those papers.

Many of the papers presented are now standard works in the fields of crystal growth and solid state physics. Those on the spiral mechanism for crystal growth and the disordering of solids by fast massive particles are probably best known, but there are many others which remain as references of authority even after 10 years of development. The Faraday Society and the publishers must be congratulated on their decision to reprint the discussion as a self-contained bound volume. This is a book which should be available for all who are concerned with crystals and imperfections in crystals.

A. J. FORTY

F. X. EDER: **Moderne Messmethoden der Physik.** Teil 1. Zweite, erweiterte Auflage. VEB Deutscher Verlag der Wissenschaften, Berlin, 1960. 696 pp., DM 40.

THIS COMPREHENSIVE and valuable work in German first appeared in 1951, and the present volume is part one of a set of four, forming the second edition. It deals with general physics, mechanics and sound. The book has been considerably extended, and many chapters have been re-written, in view of the growing importance of the more refined methods of investigation now used in research and technology. A new noteworthy feature is the thirty-page preliminary Chapter called Bases of Physical Experimentation, which contains useful considerations about the planning and design of experiments, the most effective use of apparatus, the efficiency of the eye and ear, and errors of apparatus and measurement. Further on, the most modern experimental methods employed in the physics of high vacua, high pressures, semiconductors, the solid state, control technology and supersonic technology are discussed with special care. As one case chosen at random, the attractive treatment of quartz and atomic clocks may be noted. There are four times as many references as before, the range now extending to the end of 1958.

In view of the quickness with which exact, up-to-date information is provided, the book should be of great use in physical laboratories in research and technological establishments, and in universities and colleges, where German is read. Physics masters in schools, who run advanced laboratories, and who can read German, would also benefit. The diagrams and the quality of the printing are excellent.

N. DAVY

J. Mech. Phys. Solids, 1961, Vol. 9, pp. 143 to 151. Pergamon Press Ltd., London. Printed in Great Britain

A NOTE ON THE BEHAVIOUR OF FATIGUE CRACKS

By N. E. Frost
National Engineering Laboratory, East Kilbride

(*Received 24th December*, 1960)

Summary

Published work (Frost 1959, 1960) has suggested that, for a given material, the critical alternating stress σ required to propagate a crack of length l is given by $\sigma^3 l$ = constant. The significance of such a relationship in interpreting several well known fatigue phenomena (notch sensitivity, whether fatigue failure originates at a free surface or at an internal flaw, the effect of environment, etc.) is discussed.

1. Initiation of Surface Cracks

Metallographic examination of the surface of suitably prepared plain fatigue specimens has shown that slip bands form early during the course of testing. Thompson *et al.* (1956), using high purity copper, found that as a test proceeded some bands became more pronounced than others (termed ' persistent slip bands ') and it was such bands that micro-cracks eventually formed. Similar behaviour has been observed with other materials, for example, Hempel (1956) found with mild steel that submicroscopic fissures formed in slip bands even at stresses below the fatigue limit. Wood (1958) suggested that surface micro-cracks may be a geometrical consequence of to-and-fro fine slip movements within the broad slip bands. The formation of extrusions and intrusions on the specimen surface has been reported, for example, by Forsyth (1956) and Hull (1958); intrusions are an obvious source of surface micro-cracks. May (1960) has treated the problem of surface roughening mathematically by assuming that dislocations make return journeys along paths which are shifted in a random fashion with respect to previous paths. Such random distribution of slip will roughen the surface, leading to a redistribution of stress so that later cyclic slip will tend to be concentrated in valleys already formed on the surface. Some valleys will become deeper and May shows that the expected number of stress cycles required to form valleys deep enough to be considered as micro-cracks is of the same order as found experimentally.

Thus, nucleation of surface micro-cracks is associated with the roughening of the surface within broad slip bands as a result of cyclic stressing. Grooves, intrusions, fissures and other surface irregularities form from which surface micro-cracks develop as the test proceeds, one crack eventually predominating and growing across the specimen to cause failure. In a plain fatigue specimen whether such surface phenomena lead to fracture of the specimen depends on whether or not the applied cyclic stress is greater or less than the plain fatigue limit (or fatigue strength at large endurances). As surface markings and micro-cracks are known to form in specimens subjected to a wholly compressive loading cycle, their formation is dependent on the operative cyclic shear stresses.

2. Crack Propagation

When a specimen contains a true crack, the plain fatigue limit is no longer indicative of the cyclic stress required to cause the crack to grow. Frost (1959, 1960), using plate specimens containing edge cracks subjected to reversed direct stress loadings, found that the relationship between the critical alternating stress required to propagate the crack (σ) and crack length or depth (l) was given by the equation $\sigma^3 l = C$, where C was a material constant. The value of C has been determined experimentally for mild steel (Frost 1959) and a $4\frac{1}{2}$ per cent Copper–Aluminium alloy (solution treated and aged) (Frost 1960). Tests are in progress to determine values of C for copper and a nickel–chromium alloy steel; this work will be reported elsewhere. However, sufficient tests have been completed to allow C to be estimated with sufficient accuracy for the purposes of the present note. These values of C are given in Table 1, where σ is in tons/in^2 and l in inches.

Table 1. *Values of C for various materials*

Material	*C*
Mild steel	5·5
Ni–Cr alloy steel	5·5
$4\frac{1}{2}$% Cu aluminium alloy	0·2
Copper	0·5

For a given value of l the crack will propagate if $\sigma^3 > C/l$ and remain dormant if $\sigma^3 < C/l$. The mechanism by which these true cracks propagate does not appear to be surface dependent. For example, the two surface ends of a fatigue crack growing across a sheet specimen show no tendency to grow faster than the crack front at the centre of the thickness of the sheet. On the contrary, the centre of the crack front tends to be bowed slightly ahead of the two surface crack lengths. Also, the front of a true crack growing across a plain round-bar specimen is roughly semi-circular in shape (Fig. 1 shows the markings made by the crack front in a mild steel specimen when the load on the specimen was altered) implying that the crack is growing into the body of the specimen at the same rate as it grows along the surface. If true crack growth was dependent on surface phenomena the crack would find it easier to grow around the surface than to penetrate into the body of the specimen.

Physical theories have, in general, been limited to discussions of surface crack initiation and have tended to neglect the problem of crack propagation. Holden (1960) has, however, suggested that the mechanism of crack propagation may be different from that responsible for the formation of surface cracks. He examined the material at the tip of a growing crack and the fractured faces of the material through which a crack had grown, by means of an X-ray micro-beam technique. For mild steel and pure aluminium the fractured grains were brought to a characteristic state of deformation different from the deformation which may nucleate a surface crack. The structure was found to consist of well-defined sub-grain

FIG. 1. Photograph of crack front in a mild steel specimen. The alternating stress on the specimen was decreased after the initial crack had grown a certain amount so that an outline of the crack front was left on the final fracture faces.

particles. For the aluminium the particle size was about 5 μ and the total misorientation range about 40° (mean angle between particles $\simeq$ 13°), while for mild steel the size was 1–2 μ with a total misorientation range of 30° (mean angle between particles $\simeq$ 10°). Forsyth (1951, 1953) has observed the formation of such sub-grains metallographically in several materials, especially at the tip of a growing crack. Holden found the sub-grain structure reached an extreme condition of size and misorientation on the fracture face, irrespective of stress range, thus being characteristic of the fracture condition and not of any intervening plastic deformation. He suggested that the misorientation of regions of a grain through large angles would cause stresses to develop in adjacent parts of the grain, and the densely packed boundary regions would be expected to be sites of micro-cracks. Such micro-cracks will not propagate immediately after formation, since the material within the sub-grain is still quite ductile. The first micro-cracks serve to cause further local stress concentration and aid the formation of the cyclic sub-structure at the region of the main crack tip. The progress of the main crack front depends on the formation of a sufficient number of independent micro-cracks such that the remaining necks of material between micro-cracks are broken by the maximum tensile stress in the loading cycle. This implies that the main crack cannot propagate under a wholly compressive loading cycle. The model proposed is in accord with the fact that the crack front consists of many small elementary cracks unconnected with the original metallurgical structures known to be effective in brittle and ductile fracture. Holden presents metallographic evidence of small cracks found ahead of the main crack as additional evidence that such cracks are associated with sub-grains.

3. Discussion

It is now interesting to discuss, briefly, some of the more wellknown fatigue phenomena on the assumption that crack initiation and propagation are different processes.

(a) *Plain specimens*

As the relationship $\sigma^3 l = C$ determines whether or not a crack grows, then, if $\sigma^3 l < C$, either the material at the crack tip does not form the characteristic sub-grain structure or, if it does, any micro-cracks which form are unable to join up to the main crack tip and the crack remains dormant. It was argued previously (Frost 1959) that, if this relationship is true for shorter cracks than actually tested, substitution of a stress greater than the plain fatigue limit of the material gives a minimum value of l which must form as an entity for the parameter implies that a shorter crack cannot grow and so fracture the specimen. However, this assumption is no longer necessary for it may now be assumed that this minimum value of l (given by C/σ^3) is the minimum depth of crack which at the given stress is just able to propagate by the particle mechanism.

Table 2 gives values of these minimum crack lengths for stresses equal to the plain fatigue limits of the four materials under consideration.

When a plain fatigue specimen of a given material is tested at a stress greater than the fatigue limit, surface fissures or micro-cracks will spread across the surface and penetrate into the body of the specimen by surface roughening phenomena

until one or more of the surface cracks reaches the critical crack depth for the applied cyclic stress when it can then propagate by the particle mechanism. The higher the nominal alternating stress above the plain fatigue limit, the less will the surface fissures need to penetrate. For similar percentage increases in stress above the plain fatigue limits of the materials in Table 2 the largest critical crack depth occurs with copper. This implies that surface markings will have a longer time to spread across the surface and have greater opportunity to become more numerous and pronounced on copper than with the other materials. Also, as surface fissures in mild steel and copper need to penetrate to a greater depth than in the other two materials, numerous surface cracks should be found in a broken fatigue specimen of the former materials. Metallographic examination has shown that, in addition to the main crack causing failure, many surface cracks may be found in mild steel and copper specimens, but not in aluminium alloy and nickel–chromium alloy steel specimens.

Table 2. *Values of plain fatigue limits and corresponding minimum crack lengths*

Material	*Plain fatigue limit (tons/in²)*	*Minimum crack length $l = C/(\text{plain fatigue limit})^3$ (in.)*
Mild steel	± 13·5	0·0022
Ni–Cr alloy steel	± 32	0·00017
4½ % Cu–aluminium alloy	± 9	0·00027
Copper	± 4	0·0078

The values of C in Table 1 show that, for the two steels, the stress to propagate cracks of equal length is the same in both materials, irrespective of a 2·4 : 1 ratio in plain fatigue limits. Thus, for the two steels, differences in chemical composition and static mechanical properties have no significant effect on crack propagation, although they are known to have a significant effect on cyclic slip processes occurring on the surface, as they indeed do in the case of the static yield point. This suggests that the scatter in results associated with the conventional S/N diagram for a batch of nominally similar steel specimens is essentially related to the number of stress cycles necessary to form surface fissures. It is known that measurements of the rate of growth of fatigue cracks in specimens of a given material exhibit little scatter. As the higher plain fatigue limit of the alloy steel is due to surface slip processes not occurring until much higher cyclic stresses are applied than for the mild steel, then the inhibition of surface slip results in the fatigue properties of the specimen, as a whole, being increased. However, there is a limit to which the fatigue limit can thus be increased. For example, with plain fatigue specimens of very high tensile steels, surface slip processes may be so inhibited that cracks will grow from inherent flaws or micro-cracks at a cyclic stress less than that necessary to cause surface slip. The inherent flaws may be some form of inclusion whilst sub-microscopic cracks may be nucleated by high localized stresses resulting from an austenitic martensitic reaction (Frankel *et al.* 1960b). A further example

occurs in the case of cast-iron, the fatigue strength of which depends on the stress required to propagate inherent flaws present as graphite flakes. The plain fatigue limit of ordinary cast-iron is in the range ± 5 to ± 9 ton/in^2, while the length of a graphite flake probably lies within the range 0·01–0·04 in. Assuming $\sigma^3 l = 5{\cdot}5$ applies to cast-iron, then substitution of these lengths gives a range of fatigue limits of ± 5 to ± 8 ton/in^2. Additional evidence that cast-iron fails in this manner is obtained from combined stress fatigue tests. If failure is determined by surface phenomena then, under combined stress loading, fatigue failure should obey a shear stress failure criterion, while, if determined by the stress to propagate an inherent crack, the material should obey a maximum principal stress criterion. It has been shown (Gough *et al.* 1951) experimentally that mild steel, for example, does obey a shear stress criterion and cast-iron a maximum principal stress criterion.

Thus, fatigue failure is not necessarily a surface phenomenon. Materials which contain inherent flaws or micro-cracks will fail by the propagation of such micro-cracks if their length is sufficient for the propagation stress to be less than that required to cause surface fissures or micro-cracks to penetrate to the critical depth.

(b) *Notch effects*

To break a specimen at a nominal stress less than the plain fatigue limit it is necessary either to introduce a crack of appropriate length or to accentuate the surface roughening process. The latter occurs when the tests are carried out in a corrosive environment or a notch is introduced into the specimen. The alternating stress required to break a notched specimen must lie between the plain fatigue limit and the alternating stress necessary to propagate a crack of length equal to the notch depth. The root radii of machined notches of practical interest are large compared to the radius at the tip of a crack and it is reasonable to postulate that crack initiation in the material at the notch root will be by surface roughening phenomena as on the surface of a plain specimen. Due to the presence of a stress gradient at the notch root, the surface layers of material are not subjected to a uniform stress distribution and the nominal alternating stress required to initiate a crack will be somewhat greater than given by (plain fatigue limit)/K_t (where K_t is the geometric elastic stress concentration factor), the difference increasing as the notch sharpness increases. Once a crack has formed, its effective length will, for the usual Vee-type notch, be increased by the depth of the notch and whether or not it propagates depends on whether $\sigma^3 l_d$ is greater than or less than C (where σ is the nominal alternating stress and l_d is the length of crack plus notch depth). If the notch is sufficiently sharp to initiate cracks at the notch root at a nominal alternating stress σ and $\sigma^3 l_d < C$, then such cracks will not grow and the specimen will remain unbroken. The problem of non-propagating cracks in notched mild steel and aluminium alloy specimens has been discussed by Frost (1959, 1960). The conventional fatigue limit of such sharply notched specimen (i.e. based only on broken and unbroken specimens, irrespective of whether non-propagating cracks are present in unbroken specimens) is given by $\sigma^3 l_d = C$.

If, in a sharply notched specimen, the length of non-propagating crack formed at the conventional fatigue limit is small compared to the notch depth, then the critical alternating stress to break the specimen is given approximately by $\sigma = \sqrt[3]{(C/d)}$ where d is the depth of notch. Consider now a series of Vee-notched

specimens, of the materials given in Tables 1 and 2, having a notch 0·1in. deep and of sufficient sharpness such that non-propagating cracks are present at the conventional fatigue limit then

$$\sigma = \sqrt[3]{(10\,C)}$$

and the strength reduction factor

$$K_f = \frac{\text{plain fatigue limit}}{\sigma} = \frac{\text{plain fatigue limit}}{\sqrt[3]{(10C)}}.$$

Values of σ and K_f are given in Table 3.

Table 3

Material	σ *ton/in*^{2} (*conventional notched*) (*fatigue limit*)	K_f
Mild steel	± 3·9	3·3
Ni–Cr alloy steel	± 3·9	8·2
4½% Cu–aluminium alloy	± 1·25	7·2
Copper	± 1·7	2·3

The values of K_f are the maximum values that can be attained (at zero mean load) for the depth of notch considered, irrespective of the notch root radius. They clearly indicate why ignorance of the presence of non-propagating cracks has led to the nickel chromium steel and the aluminium alloy being termed 'notch sensitive' and the mild steel and copper being termed 'notch insensitive.'

The effect of surface finish on the fatigue strength of plain specimens depends on changes in surface profile, work hardening of the surface layers and the introduction of residual stresses. If the latter two effects are kept to a minimum, the values given in Table 2 indicate why the fatigue strengths of the aluminium alloy and nickel chromium steel are much more dependent on the surface finish (resulting, for example, from either the machining process or from surface scratches) than the mild steel or copper.

(c) *Environment and mean stress*

The initial assumptions imply that the initiation of surface cracks will be more dependent on environment than the subsequent propagation, unless the environment is so corrosive that it dissolves the material away faster than micro-cracks form. If, for some materials, tests in air are, in fact, mild corrosion fatigue tests (i.e. oxygen, moisture, etc., aid the surface roughening processes) then, excluding the atmosphere from the specimen surface, should result in an increased fatigue life. Frankel *et al.* (1960a) found that coating specimens with an oleophobic film resulted in an increased life compared to uncoated specimens tested at the same stress. The largest increase (360 per cent) was with a copper alloy (1¾ per cent Be), the smallest (7 per cent.) with a high-strength aluminium alloy, while a 0·4 per cent C steel gave an increase about mid-way between these two extremes. The authors considered that the increased life obtained with the oleophobic coating,

was largely due to the increase in number of cycles to initiate fatigue cracks. As surface phenomena need to operate for a relatively long time with copper appreciable differences might occur between fatigue tests on copper in air and in a vacuum. WADSWORTH and HUTCHINGS (1958) found the life of a copper specimen tested in vacuum (10^{-5} mm Hg) was 20 times greater than a specimen tested in air at a similar stress. From metallographic observations of the surface of specimens tested in air and vacuum they found that slip bands and small micro-cracks formed after about the same number of cycles, but that for the latter conditions the small surface micro-cracks took much longer to form longer surface cracks and concluded that the difference in life was due to the effect of atmosphere speeding up the rate of crack propagation. It is suggested that their experimental results supplied evidence regarding the development of surface cracks and were not suitable for determining the rate of growth of cracks into the body of the specimen. The specimen used was, in fact, of sheet form 0·033 in. thick tested in plane bending, and for tests carried out at stresses near the fatigue limit Table 2 suggests that the specimen thickness would be roughly halved before the true crack propagation stage occurred.

Different circumstances arise when oils, etc., are used as the working medium to apply a cyclic load to a specimen. MORRISON *et al.* (1960), for example, subjected high strength alloy steel cylinders to pulsating internal oil pressure and determined the fatigue limits of cylinders of various outside to inside diameter ratios. The fatigue limits for all cylinders were in agreement if the maximum cyclic shear stress in the bore was used as a criterion, this value being 0–18½ ton/in² shear stress. The fatigue limit of the material in reversed shear (as obtained from a torsion fatigue test) was about $\pm$ 18 ton/in²; thus, for the cylinder, the presence of a triaxial tension stress (which varied over the range 2–13 ton/in²) appeared to halve the safe range of shear stress. If, however, it is assumed that the combined effect of the surface cyclic shear stresses and fluctuating oil pressure in intimate contact with the material is to initiate and penetrate incipient surface micro-cracks at cyclic stresses less than the plain fatigue limit, then the fatigue limit of the cylinder will be determined by the critical stress required to propagate such cracks. Cracks will propagate in a direction normal to the hoop stress, and the nominal stress causing the crack to open will be the sum of the hoop stress and the internal pressure in the crack. If p = internal pressure, k = ratio of outside to inside diameter, the hoop stress in the bore plus internal pressure is

$$p + \frac{p(1 + k^2)}{k^2 - 1} = 2\frac{k^2 p}{k^2 - 1} = 2 \times \text{maximum shear stress in bore.}$$

The experimental results thus also conform to the hypothesis suggested. The critical nominal stress range acting normal to the cracks will be 0–37 ton/in² and, taking $C = 5{\cdot}5$ for the steel used, the surface micro-cracks need only be about 0·0001 in. deep.

Tensile or compressive mean stresses superimposed on the alternating stress would not be expected to have a pronounced effect on crack nucleation by surface phenomena provided gross yielding of the specimen does not occur. Slip processes will be either accentuated or retarded, depending on whether the static stress normal to the operative slip planes is tensile or compressive. Subsequent propagation

of surface cracks may, however, be profoundly affected ; static normal compressive stresses of sufficient magnitude such that the surface cracks are kept closed will prevent the cracks growing, while normal tensile stresses will tend to open the cracks and thus increase their rate of growth. Similar arguments apply when the mean stresses are present in the form of surface residual stresses. The overall effect of surface residual stresses will, in addition to their magnitude, depend on the depth to which they extend below the surface and the depth to which surface cracks need to penetrate (for the particular material and alternating stress) before they begin to propagate by the particle mechanism.

The presence of fretting corrosion is known to affect the fatigue strength of some materials more than others. Fenner and Field (1958, 1960) determined the fatigue strength of specimens having pads of material clamped against the test section of the specimen. The slight relative movement occurring between the pad and specimen (due to the deformation of the specimen under the cyclic loading) will create surface roughnesses sufficient to lead to micro-cracks at stresses less than those necessary when the pads are absent. As surface micro-cracks are found in the specimen under the pads at alternating stresses insufficient to propagate them across the specimen, the fatigue limit of such specimens is the critical propagation stress. Work on a $4\frac{1}{2}$ per cent Cu-aluminium alloy (similar to that in Tables 1 and 2) showed that, for a particular set of fretting conditions, the fatigue limit was about $\pm 4\frac{1}{4}$ ton/in^2 at zero mean load and $p \pm 2$ ton/in^2 where p varied from 4 to 20 ton/in^2 tensile mean stress. Surface cracks were found in unbroken specimens beneath the pads, their depths varying between 0·002 and 0·006 in. thus substituting in $\sigma^3 l = 0{\cdot}2$ (for zero mean load) or $\sigma^3 l = 0{\cdot}2/8$ (for tensile mean stresses such that the crack is always open) gives values of σ varying between $\pm 3{\cdot}2$ and $\pm 4{\cdot}6$ ton/in^2 or $p \pm 1{\cdot}6$ and $\pm 2{\cdot}3$ ton/in^2. Removing the pads after 20 per cent of the expected life and continuing the test as a normal fatigue test, gave similar lives as for tests in which the pads were present throughout. The pads thus act merely as a roughening agent for creating the initial surface micro-cracks.

(d) *Conclusions*

To conclude, it is suggested that a characteristic feature of fatigue failure which has no analogy in static loading is the propagation of a crack. Experimental evidence suggests that the critical alternating stress required to propagate a crack may be expressed by $\sigma^3 l = C$. In a plain fatigue specimen the initial micro-cracks of length of depth $l = C/\sigma^3$ (where σ is now a stress greater than the plain fatigue limit) may either be inherent flaws in the material or be caused by surface roughening phenomena.

Acknowledgment

This note is published by permission of the Director of the National Engineering Laboratory.

References

Fenner, A. J. and Field, J. E. 1958 *Rev. Métall.* **55**, 475.
1960 *Trans. N.-E. Cst. Instn. Engrs. Shipb.* **76**, 183.

Forsyth, P. J. E.	1951	*J. Inst. Met.* **80**, 181.
	1953	*J. Inst. Met.* **82**, 449.
Forsyth, P. J. E.	1956	*Int. Conf. on Fatigue of Metals*, p. 535, (Inst. Mech. Engrs.).
Frankel, H. E., Bennett, J. A. and Holshouser, W. L.	1960a	*J. Res. Nat. Bur. Stand.* **64C**, 147.
Frankel, H. E., Bennet, J. A. and Pennington, W. A.	1960b	*Trans. A.S.M.* **52**, 257.
Frost, N. E.	1959	*Proc. Instr. Mech. Engrs., Lond.* **173**, 811.
	1960	*J. Mech. Engng. Sci.* **2**, 109.
Gough, H. J., Pollard, H. V. and Clenshaw, W. J.	1951	Aero. Research Council, R. & M. 2522 (H.M.S.O., London).
Hempel, M.	1956	*Int. Conf. on Fatigue of Metals*, p. 543 (Inst. Mech. Engrs.).
Holden, J.	1961	*Phil. Mag.* (in press).
Hull, D.	1958	*J. Inst. Met.* **86**, 425.
May, A. N.	1960	*Nature, Lond.* **185**, 303.
Morrison, J. L. M., Crossland, B. and Parry, J. S. C.	1960	*Trans. A.S.M.E.* **82**, 143.
Thompson, N., Wadsworth, N. J. and Louat, N.	1956	*Phil. Mag.* **1**, 113.
Wadsworth, N. J. and Hutchings, J.	1958	*Phil. Mag.* **3**, 1154.
Wood, W. A.	1958	*Phil. Mag.* **3**, 692.

J. Mech. Phys. Solids, 1961, Vol. 9, pp. 152 to 164. Pergamon Press Ltd., London. Printed in Great Britain

AN EXTENSION OF ALFREY'S ANALOGY TO THERMAL STRESS PROBLEMS IN TEMPERATURE DEPENDENT LINEAR VISCOELASTIC MEDIA*

By H. H. Hilton† and H. G. Russell‡

(*Received 9th January*, 1961)

Summary

The elastic–viscoelastic analogy due to Alfrey (1944, 1948) is extended to incorporate thermal stress problems in nonhomogeneous linear viscoelastic media. It is shown that the thermal stresses in a body possessing temperature-dependent linear viscoelastic properties can be deduced from an equivalent elastic body.

1. Introduction

At elevated temperatures thermal stresses are accompanied by two phenomena which may be neglected at lower temperatures:

(1) The material will exhibit creep and/or relaxation effects;

(2) The material will no longer be homogeneous since its properties will vary with the temperature distributions.

Admittedly, even at low temperatures, while the material may remain essentially elastic, nonhomogeneity may play an important role in the determination of thermal stresses (Hilton 1952a). However, the variations with temperature of the inelastic material properties are much more pronounced than the elastic ones. For instance, in metals, the coefficient of viscosity varies exponentially with the inverse of the temperature while the shear modulus depends upon the square of the temperature. A typical example is that of alpha-iron where Kê (1948) found that for a temperature variation of 1000 °F the coefficient of viscosity decreases by 42 orders of magnitude while the shear modulus is only halved. Similar experimental results have been obtained by Bozajian and Tsao (1957) for QQ–M–44H magnesium alloy where for a temperature difference of 500 °F, the use of a nonlinear viscoelastic relation yielded reductions of 15 orders of magnitude for inelastic properties with a corresponding decrease of but 35 per cent of the elastic ones.

In the case of solid propellant materials, on the other hand, the change of Young's modulus is considerably more pronounced. Typical reductions of one order of magnitude from 60 to 140 °F have been found (Wimpress 1950).

*This analysis was carried out under the sponsorship of the Mechanics Research Branch, Aeronautical Research Laboratory, Wright–Patterson Air Development Center, Contract No. AF 33(616)–291. The authors are grateful to the U.S. Air Force for permission to publish this article.

†Department of Aeronautical Engineering, University of Illinois, Urbana, Illinois.

‡Department of Physics, James Millikin University, Decatur, Illinois.

A viscoelastic stress–strain law with temperature dependent material properties will describe both of the phenomena outlined above. Unfortunately, the non-homogeneity of the medium greatly complicates the analyses. The general three-dimensional viscoelastic thermal stress problem under a known temperature distribution entails the solution of fifteen simultaneous partial differential equations with variable coefficients in four variables and fifteen unknowns. This is a formidable task even when the equations are linear and, consequently, only essentially one-dimensional nonlinear viscoelastic problems have been solved today.

The actual inelastic behaviour of most materials at very large stresses is nonlinear and linear viscoelastic laws do not account for such phenomena. In particular, in instability problems (creep buckling and divergence) the use of linear viscoelastic stress–strain laws has been proved unable to predict the physically observable finite critical times. However, prior to the onset of instability linear viscoelasticity can describe stress–strain behaviour, since there are an unlimited number of coefficients available in the linear stress–strain laws to match experimental creep and relaxation behaviour. If the actual material should have a highly nonlinear response, then one may represent the stress–strain behaviour approximately by piecewise fitting of linear laws over small ranges of stresses and strains and still retain the relative simplicity of linear analysis prior to instability.

Actually, Allen *et al.* (1954) have demonstrated experimentally that some linear viscoelastic stress–strain relationships, such as those of the Maxwell–Kelvin body, can be used to represent actual creep properties under constant temperature. It has been further shown (Hilton 1959) that under constant stress and temperature conditions a Maxwell–Kelvin linear viscoelastic body is analogous to the experimentally determined nonlinear creep law for QQ–M–44 magnesium alloy of Baer (1954)

Alfrey (1944, 1948) was the first to point out the existence of the elastic–viscoelastic analogy in incompressible, isotropic, and homogeneous linear viscoelastic media. He discussed two types of boundary value problems: in the first, the surface forces are prescribed and in the second the displacements are given. In either case, Alfrey finds that the viscoelastic stresses and strains are equivalent to elastic stresses and strains multiplied by a time response function which is obtained from the viscoelastic stress–strain law and the surface force or displacement time function. This important concept has, of course, greatly simplified viscoelastic stress analysis, since, for any case for which the equivalent elastic stresses and strains are known, it is only necessary to determine the time response function in order to obtain the complete solution to the viscoelastic problem.

This analogy has since been extended to photoviscoelasticity in homogeneous media by Mindlin (1949). It has been further extended by Tsien (1950) to take into account material compressibility and body forces. However, Tsien's solution is somewhat restrictive since he assumed the same type of stress–strain relationship for volumetric deformation as for deviatoric deformation. In general, for homogeneous viscoelastic materials, the volumetric deformation differs greatly from the deviatoric one (Freudenthal 1950).

The analogy has been further extended by Read (1950) who treats nonhomogeneous media which have space- but not time-dependent properties. He has demonstrated that under these conditions the Fourier transforms of the visco-

elastic stresses and strains are equivalent to their elastic counterparts. LORSCH and FREUDENTHAL (1954) have treated the mixed boundary-value problem under both steady state and time dependent boundary forces for Maxwell and Kelvin bodies. LEE (1955, 1960) and LEE *et al.* (1959) have developed the analogy for homogeneous bodies in terms of Laplace transforms and have applied the procedure to a variety of problems.

All the previous papers have treated the differential equation representation of the viscoelastic stress–strain relations. BRULL (1953) however, has employed integral representations and has shown another form of the analogy for constant temperature by using the Laplace transform of the Volterra memory function.

Lastly, ALFREY's analogy has been extended by HILTON (1952b, 1957, 1960) to self-excited systems such as creep buckling of columns and creep divergence of viscoelastic lifting surfaces. Recently, HOFF (1954) has made a very important contribution to these similarity laws by making the first departure from the linear analogies and by demonstrating an analogy between certain homogeneous nonlinear viscoelastic laws and corresponding nonlinear elastic ones.

Several papers (FREUDENTHAL 1954a, b, c ; HILTON 1954 ; HILTON *et al.* 1953 ; PRAGER 1956 ; STERNBERG 1958) have been published on thermal stresses in specific structural shapes obeying specific linear viscoelastic stress–strain relations (either homogeneous or nonhomogeneous) and HILTON *et al.* (1953) have treated the general nonhomogeneous case for a viscoelastic deviatoric deformation and an elastic volumetric one. BLEICH (1957) has solved a number of one-dimensional stress problems in a nonhomogeneous, nonlinear Maxwell body. MORLAND and LEE (1960) have treated the case of a nonhomogeneous incompressible thickwall cylinder under radial pressure, but without thermal stresses or expansions.

It is the purpose of this paper to extend Alfrey's analogy to cover the three dimensional case of thermal stresses in arbitrary shapes obeying general, linear, nonhomogeneous (temperature dependent) viscoelastic stress laws for deviatoric and volumetric deformations.

LIST OF SYMBOLS

$a_n, a_n', b_n, b_n', b_n''$ = material property coefficients
E_{ij} = component of strain deviator on i-th face in j-th direction
G = shear modulus
K = bulk modulus
P, P' = differential operators
Q, Q', Q'' = differential operators
q = ratio of Fourier transforms of Q'' and Q'
S_{ij} = component of stress deviator on i-th face in j-th direction
t = time
T = temperature above a certain uniform temperature where no thermal stresses exist
u_i = displacement component in i-th direction
$x = (x_i)$ = Cartesian coordinate (tensor notation, $i = 1, 2, 3$)
α = coefficient of linear thermal expansion
δ_{ij} = Kronecker delta
ϵ = mean strain
ϵ_{ij} = component of strain on i-th face in j-th direction
σ = mean stress
σ_{ij} = component of stress on i-th face in j-th direction

ω = variable in Fourier transforms
Single bars over symbols indicate average values
Double bars over symbols indicate Fourier transforms
Superscript e denotes equivalent elastic quantities.

2. Analysis

(i) *General considerations*

If a body is subjected to a time- and space-dependent temperature distribution, then its material properties are also functions of time and space. It would be most desirable to have an analogy relating the viscoelastic thermal stresses with their elastic equivalents. Under these circumstances the solution to the viscoelastic problem would be simplified, because then one would only need to solve the equivalent elastic problem and then by analogy arrive at the viscoelastic solution. Since the elastic solution represents the initial conditions of most viscoelastic bodies, it must be known in any case.

It has not been possible to formulate an exact analogy for temperature distributions which are both space- and time-dependent. However, two exact cases are considered, namely one for a time-dependent temperature distribution and one for a steady-steady distribution, which are extended to cover the following:

A. The temperature distribution is predominantly time-dependent and the spatial variations are small compared to the time variations;

B. The temperature distribution has time variations which are negligible compared to its spatial variations.

Finally, an approximate analysis for the analogy is presented for both space- and time-dependent temperature distributions. This last analogy may be used for those temperature distributions where space and time variations are of equal importance.

(ii) *Case A. Temperature distributions predominantly time-dependent*

Consider a body in a Cartesian coordinate system $x = (x_i)\,(i = 1, 2, 3)$ subjected to a temperature distribution $\boldsymbol{T} = \boldsymbol{T}(x, t)$ and obeying the general incompressible linear viscoelastic stress–strain relations

$$\epsilon = \alpha\, \boldsymbol{T}, \tag{1}$$

$$\boldsymbol{P}\{\boldsymbol{S}_{ij}\} = 2\,\boldsymbol{Q}\{\boldsymbol{E}_{ij}\}, \tag{2}$$

where the differential operators $\boldsymbol{P}$ and $\boldsymbol{Q}$ are

$$\boldsymbol{P} = \sum_{n=0}^{r} a_n\, \partial^n/\partial t^n, \tag{3}$$

$$\boldsymbol{Q} = \sum_{n=0}^{s} b_n\, \partial^n/\partial t^n, \tag{4}$$

with the material properties* a_n and b_n assumed as

$$a_n = a_n(t), \tag{5}$$

$$b_n = b_n(t). \tag{6}$$

*It is assumed that the time variations of the temperature distributions are large compared to the space variations. The material properties are therefore only taken as time-dependent.

The incompressible medium is defined as one in which volumetric changes take place only due to the thermal expansion or contractions αT, but the mean stress does not influence the dilatation (compare with (34)). Since in the present analysis one is interested only in the effects of thermal stresses, the boundaries of the body are free. The effects of the boundary restraints and/or forces can be handled by the analogies of Alfrey (1944, 1948) and superimposed over the present solution, since the problem is linear.

The strain and stress deviators are defined respectively as

$$E_{ij} = \epsilon_{ij} - \delta_{ij}\,\epsilon, \tag{7}$$

$$S_{ij} = \sigma_{ij} - \delta_{ij}\,\sigma, \tag{8}$$

with the mean strain and stress

$$\epsilon = \epsilon_{ii}/3, \tag{9}$$

$$\sigma = \sigma_{ii}/3. \tag{10}$$

The summation convention of tensor calculus is used throughout. Accordingly, a sum of terms is represented by a repeated index, i.e.

$$\epsilon_{ii} = \epsilon_{11} + \epsilon_{22} + \epsilon_{33}.$$

In the absence of body forces the three equilibrium equations are

$$\sigma_{ij,\,j} = 0 \tag{11}$$

where an index after a comma indicates differentiation.

Differentiating (2) with respect to x_j, and making use of (1) and (7), yields

$$P\{S_{ij,\,j}\} = 2\,Q\{\epsilon_{ij,\,j} - (\alpha T)_{,\,i}\}. \tag{12}$$

The sum of the derivatives of S_{ij} can be evaluated from (8) and (11), such that

$$S_{ij,\,j} + \sigma_{,\,i} = 0, \tag{13}$$

and the strains are defined in terms of the displacements

$$\epsilon_{ij} = \tfrac{1}{2}\,(u_{i,\,j} + u_{j,\,i}). \tag{14}$$

Substituting (13) and (14) into (12) one obtains

$$P\{\sigma_{,\,i}\} = -\,Q\{u_{i,\,jj} + u_{j,\,ij} - 2\,(\alpha T)_{,\,ij}\}. \tag{15}$$

From (1), (9) and (14), it is seen that

$$\epsilon = \epsilon_{jj}/3 = u_{j,\,j}/3 = \alpha T. \tag{16}$$

Therefore (15) becomes

$$P\{\sigma_{,\,i}\} = -\,Q\{u_{i,\,jj} + (\alpha T)_{,\,ij}\}. \tag{17}$$

The displacement in the last equation can be eliminated by differentiating with respect to x_i and using (16), thus

$$P\{\sigma_{,\,ii}\} = -\,4\,Q\{(\alpha T)_{,\,ii}\}. \tag{18}$$

One now differentiates (8) twice with respect to x_k and operates with P, such that

$$\delta_{ij}\,P\{\sigma_{,\,kk}\} = P\{\sigma_{ij,\,kk} - S_{ij,\,kk}\}. \tag{19}$$

Using (18) to eliminate $\sigma_{,kk}$, one obtains

$$P\{\sigma_{ij,kk} - S_{ij,kk}\} = -4\,\delta_{ij}\,Q\{(\alpha T)_{,kk}\}. \tag{20}$$

Equations (1), (2) and (7) yield upon differentiation

$$P\{S_{ij,kk}\} = 2\,Q\{\epsilon_{ij,kk} - \delta_{ij}\,(\alpha T)_{,kk}\}. \tag{21}$$

With the help of (14) and (17), the last equation reduces to

$$P\{S_{ij,kk}\} = -2\,P\{\sigma_{,ij}\} - 2\,Q\{(\alpha T)_{,ij} + \delta_{ij}\,(\alpha T)_{,kk}\}. \tag{22}$$

Substitution of (22) into (20) yields

$$P\{\sigma_{ij,kk} + 2\,\sigma_{,ij}\} = -2\,Q\{(\alpha T)_{,ij} + 3\,\delta_{ij}\,(\alpha T)_{,kk}\}. \tag{23}$$

In the elastic case this equation, of course, reduces to

$$\sigma^e{}_{ij,kk} + 2\,\sigma^e{}_{,ij} = -2\,G(t)\left[(\alpha T)_{,ij} + 3\,\delta_{ij}\,(\alpha T)_{,kk}\right] \tag{24}$$

where $\sigma^e{}_{ij} = \sigma^e{}_{ij}(x, t)$ is the elastic thermal stress in an equivalent body.

Equations (23) and (24) are the governing differential equations respectively for the general linear incompressible viscoelastic, and general linear incompressible elastic, thermal stress problems for time-dependent material properties.

Since the term $\alpha\,T$ always occurs as a product, it is not necessary to impose the same restrictions on the coefficient of thermal expansion α, as were prescribed for the material properties a_n and b_n of (3) and (4). In many heat transfer problems the temperature distribution is a separable function of time and space variables. Consequently, the product αT will be a sum of separable functions since it generally varies parabolically with the temperature, i.e.

$$\alpha T = \left[\alpha_0 + \alpha_1\,T^2\right]T = \alpha_0\,H(t)\,F(x) + \alpha_1\left[H(t)\,F(x)\right]^2. \tag{25}$$

If the temperature distribution is not in a separable form and /or if the coefficient of thermal expansion does not vary with the second power of the temperature, then one may express the product $\alpha\,T$ as an infinite sum of separable functions, such that

$$\alpha T = \sum_{m=0}^{\infty} A_m(x, t) = \sum_{m=0}^{\infty} H_m(t)\,F_m(x) \tag{26}$$

where every $F_m(x)$ has the dimensions of strain and every $H_m(t)$ is dimensionless. For every thermal expansion A_m there corresponds a thermal stress $\sigma_{ij}{}^{(m)}(x, t)$ obtainable in a manner outlined below. The total thermal stress due to the thermal expansion (26) is then the sum of all $\sigma_{ij}{}^{(m)}$, or

$$\sigma_{ij}(x, t) = \sum_{m=0}^{\infty} \sigma_{ij}{}^{(m)}(x, t). \tag{27}$$

Assume that the stress due to the thermal expansion (26) may be written in the form

$$\sigma_{ij}{}^{(m)}(x, t) = g_m(t)\,\sigma_{ij}{}^{*(m)}(x). \tag{28}$$

Upon substitution of (25) and (28) and after performing the necessary divisions, one obtains

$$\frac{P\{g_m(t)\}}{Q\{H_m(t)\}} = -\frac{2\,F_{m,ij} + 6\,\delta_{ij}\,F_{m,kk}}{\sigma_{ij,kk}{}^{*(m)} + 2\,\sigma_{,ij}{}^{*(m)}} = \frac{1}{\lambda_m} \quad \text{(no summation on } i \text{ and } j\text{)} \tag{29}$$

where the λ_m are constants having the dimensions of stress.

Rewriting (29) such that

$$\sigma_{ij,\,kk}{}^{*(m)} + 2\,\sigma,_{ij}{}^{*(m)} = -\,2\,\lambda_m\left[F_{m,\,ij} + 3\,\delta_{ij}\,F_{m,\,kk}\right] \tag{30}$$

and comparing (30) with (24) shows that $\sigma_{ij}{}^{*(m)}$ is the stress of an equivalent elastic body of shear modulus λ_m and subject to thermal expansions $\alpha T = F_m(x)$. It should be noted that the stress $\sigma_{ij}{}^{*(m)}$ is for a homogeneous elastic body. The values of λ_m are determined from the initial conditions of the particular viscoelastic body.

The time response functions $g_m(t)$ are found from the total differential equations

$$\lambda_m\,P\left\{g_m(t)\right\} = Q\left\{H_m(t)\right\} \tag{31}$$

which is obtained from (29).

It can be readily seen from (8), (10) and (28) that

$$S_{ij}(x,t) = \sum_{m=0}^{\infty} g_m(t)\,S_{ij}{}^{*(m)}(x) \tag{32}$$

where $S_{ij}{}^{*(m)}(x)$ is the equivalent elastic stress deviator corresponding to $\sigma_{ij}{}^{*(m)}(x)$.

The thermal strains may be obtained by substitution of (1), (29) and (31) into (2) and by solving the resulting differential equation

$$Q\left\{\epsilon_{ij}(x,t)\right\} = \sum_{m=0}^{\infty}\left[S_{ij}{}^{*(m)}(x)/2\,\lambda_m + \delta_{ij}\,F_m(x)\right]Q\left\{H_m(t)\right\}. \tag{33}$$

It is, therefore, evident that in this case one needs only to know the thermal stress in an equivalent homogeneous elastic body and then find the time response functions $g_m(t)$ from (31) to solve the linear viscoelastic problem. It should be noted that the solution of the equivalent homogeneous elastic body must be known in any event, since it forms the initial conditions of the viscoelastic problem. Thermal stresses in bodies with constant elastic properties are treated by Timoshenko (1934).

(iii) *Case B. Temperature distributions predominantly space-dependent or steady state*

Consider, next, a viscoelastic body in a Cartesian coordinate system $x = (x_i)$ $(i = 1, 2, 3)$, subject to a temperature distribution $T = T(x, t)$ where the time variation of the temperature is small compared with the space variation or steady state, and obeying the general compressible linear viscoelastic stress-strain relations

$$P'\left\{\sigma\right\} = Q'\left\{\epsilon\right\} - Q''\left\{\alpha T\right\}, \tag{34}$$

$$P\left\{S_{ij}\right\} = 2\,Q\left\{E_{ij}\right\}, \tag{35}$$

with the differential operators defined by (3) and (4) and with

$$P' = \sum_{n=0}^{r'} a_n{}'\,\partial^n/\partial t^n, \tag{36}$$

$$Q' = \sum_{n=0}^{s'} b_n{}'\,\partial^n/\partial t^n, \tag{37}$$

$$Q'' = \sum_{n=0}^{s''} b_n'' \, \partial^n / \partial t^n. \tag{38}$$

In most cases the differential operators Q' and Q'' will be equal, but they are included in this analysis as different quantities for the sake of generality and since this inclusion does not unduly complicate the analysis.

Because of the relatively small time variations of the temperatures, the material properties a_n, a_n', b_n, b_n' and b_n'' are assumed as space functions only, i.e.

$$a_n = a_n(x), \quad \text{etc.} \tag{39}$$

It may be noted that the temperature T is retained as $T(x, t)$ and only the material properties are approximated. Equations (39) are exact for a steady state temperature distribution, $T = T(x)$, and are approximate when the temperature is other than steady state.

The strain and stress deviators and the mean strain and stress are defined respectively by (7), (8), (9) and (10).

The time dependence of the stress deviator S_{ij} can be represented by a Fourier integral

$$S_{kl}(x, t) = \int_{-\infty}^{\infty} \bar{S}_{kl}(x, \omega) \, e^{i\omega t} \, d\omega \tag{40}$$

where

$$\bar{S}_{kl}(x, \omega) = (1/2\pi) \int_{-\infty}^{\infty} S_{kl}(x, t) \, e^{-i\omega t} \, dt \tag{41}$$

is the Fourier transform of $S_{kl}(x, t)$. The Fourier transforms $\bar{\epsilon}_{kl}(x, \omega)$ $\bar{\sigma}(x, \omega)$, $\bar{\epsilon}(x, \omega)$ and $\overline{\alpha T}(x, \omega)$ are formed in a similar manner. In addition, due to (36) and (37), one finds that

$$\bar{P}(x, \omega) \, \bar{S}_{kl}(x, \omega) = (1/2\pi) \int_{-\infty}^{\infty} P\{S_{kl}(x, t)\} \, e^{-i\omega t} \, dt, \tag{42}$$

$$\bar{Q}(x, \omega) \, \bar{\epsilon}_{kl}(x, \omega) = (1/2\pi) \int_{-\infty}^{\infty} Q\{\epsilon_{kl}(x, t)\} \, e^{-i\omega t} \, dt, \tag{43}$$

with similar expressions for the operators of (34).

Operating on (34) and (35) with the Fourier transform yields

$$\bar{S}_{ij}(x, \omega) = 2\bar{G}\{\bar{\epsilon}_{ij}(x, \omega) - \delta_{ij}[\bar{q} \, \overline{\alpha T}(x, \omega) + \bar{K}^{-1} \bar{\sigma}(x, \omega)]\} \tag{44}$$

where

$$\bar{G} = \bar{G}(x, \omega) = \bar{Q}(x, \omega)/\bar{P}(x, \omega) = \sum_{n=0}^{s} (i\omega)^n \, b_n(x) / \sum_{n=0}^{r} (i\omega)^n \, a_n(x), \tag{45}$$

$$\bar{K} = \bar{K}(x, \omega) = \bar{Q}'(x, \omega)/\bar{P}'(x, \omega) = \sum_{n=0}^{s'} (i\omega)^n \, b_n'(x) / \sum_{n=0}^{r'} (i\omega)^n \, a_n'(x), \tag{46}$$

$$\bar{\bar{q}} = (x, \omega) = \bar{Q}''(x, \omega)/\bar{Q}'(x, \omega) = \sum_{n=0}^{s''} (i\omega)^n \, b_n''(x) / \sum_{n=0}^{s'} (i\omega)^n \, b_n'(x). \tag{47}$$

An expression similar to (44) has been derived by Read (1950) for $T = 0$ and elastic volumetric deformations ($P' = 1/K$, $Q' = Q'' = 1$).

The linear elastic stress–strain relation can be deduced from (34) and (35) as

$$S_{ij}^{e}(x, t) = 2G(x, t)\{\epsilon_{ij}^{e}(x, t) - \delta_{ij}[\alpha T(x, t) + \sigma^{e}(x, t)/K(x, t)]\}. \tag{48}$$

An inspection of (44) and (48) indicates that they are indeed very similar. In effect it is seen that the Fourier transforms of the viscoelastic stress deviators, strains, etc. due to a steady-state or quasi steady-state temperature distribution are equivalent to their elastic counterparts in an equivalent elastic body possessing a shear modulus $\overline{G}(x, \omega)$, a bulk modulus $\overline{K}(x, \omega)$ and exposed to a volumetric thermal strain $\overline{q}(x, \omega)\,\overline{\alpha T}(x, \omega)$.

The procedure for finding viscoelastic thermal stresses and strains due to steady-state or quasi steady-state temperature distributions is to form first the complex shear and bulk moduli $\overline{G}$ and $\overline{K}$ from (45) and (46) and the Fourier transform product $\overline{q}\,\overline{\alpha T}$. One then calculates the stresses and strains for an equivalent nonhomogeneous elastic body of shear and bulk moduli $\overline{G}$ and $\overline{K}$ subjected to temperature expansions $\overline{q}\,\overline{\alpha T}$. A typical analysis for thermal stresses in a nonhomogeneous elastic body has been given by Hilton (1952a). The dummy variable ω appears as a parameter in the equivalent elastic solution and should be treated as such.

The arbitrary functions resulting from the solution of the equivalent elastic problem are evaluated by taking the Fourier transforms of the viscoelastic boundary conditions and using these as boundary conditions for the equivalent elastic problem. The viscoelastic stresses, strains, etc. are found by taking the inverse Fourier transform of these equivalent elastic stresses, strains, etc. by performing the operations indicated in (40).

(iv) *Case C. Temperature distributions which are mixed functions of time and space*

It is evident from the two special cases considered that in the general case where the temperature distribution and, consequently, the material properties are both time-and space-dependent, no known linear integral operator will produce analogies of the type presented. When the material properties a_n, a_n', b_n, b_n' and b_n'' are both space-and time-dependent, then the stress–strain relations of (34) and (35) are partial differential equations of order one or higher (depending on the highest value of r, r', s, s' or s'') with variable coefficients. The reduction of such an equation by an integral operator to an analogous elastic stress–strain relation is equivalent to solving an n-th order partial differential equation with variable coefficients. Such a solution is not known at the present time and hence the corresponding integral operator is also unknown.

In those instances where the temperature distribution has time and space variations of equal importance each of the two cases considered is a poor approximation. However, it is possible to obtain an elastic-viscoelastic analogy by the following approximate analysis.

Consider the compressible viscoelastic body described under Case B obeying the stress–strain relations (34) and (35) but with

$$a_n = a_n(x, t), \qquad a_n' = a_n'(x, t), \qquad \text{etc.}, \tag{49}$$

since it is subjected to a temperature distribution $T = T(x, t)$ where both space and time variations are of equal orders of magnitude.

The time scale may be divided into a number of intervals and then the material properties may be approximated by step functions, such that

$$a_n(x,t) = \begin{cases} a_n(x,\bar{t}_k), & t_k \leqslant t < t_{k+1} \\ 0, & \text{elsewhere} \end{cases} \tag{50}$$

$$b_n(x,t) = \begin{cases} b_n(x,\bar{t}_k), & t_k \leqslant t < t_{k+1} \\ 0, & \text{elsewhere} \end{cases} \tag{51}$$

etc., where k is an integer and

$$\bar{t}_k = \tfrac{1}{2}(t_k + t_{k+1}). \tag{52}$$

The intervals $t_k \leqslant t < t_{k+1}$ are chosen according to the time variations of a_n, a_n', b_n, b_n' and b_n'' such that in any interval the best approximation is obtained for the a_n or b_n which is the most affected by the time variable in that interval. The smaller these intervals are taken the better the approximation. The barred quantities are essentially the midpoint values of the functions in each interval.

The stress–strain relations (34) and (35) may now be written in an approximate form

$$P'\{\sigma\} = \bar{Q}'\{\epsilon\} - \bar{Q}''\{\alpha T\}, \tag{53}$$

$$P\{S_{ij}\} = 2\,\bar{Q}\{E_{ij}\}, \tag{54}$$

where

$$P = \sum_{n=0}^{r} \bar{a}_n(x,t)\,\partial^n/\partial t^n, \tag{55}$$

$$\bar{Q} = \sum_{n=0}^{s} b_n(x,t)\,\partial^n/\partial t^n, \qquad \text{etc.} \tag{56}$$

In any interval $t_k \leqslant t < t_{k+1}$ the barred quantities are only functions of the space variables. Operating on (53) and (54) with the Fourier transform as defined by (41), and combining, yields over any interval $t_k \leqslant t < t_{k+1}$

$$\bar{S}_{ij}^{\,k}(x,\omega) = 2\,\bar{G}^k\{\bar{\epsilon}_{ij}^{\,k}(x,\omega) - \delta_{ij}[\bar{q}^k\,\overline{\alpha T}^k(x,\omega) + \bar{\sigma}^k(x,\omega)/\bar{K}^k]\} \tag{57}$$

where

$$\bar{G}^k = \bar{G}^k(x,\omega) = \sum_{n=0}^{s}(i\omega)^n\,b_n(x,\bar{t}_k)/\sum_{n=0}^{r}(i\omega)^n\,a_n(x,\bar{t}_k), \tag{58}$$

$$\bar{K}^k = \bar{K}^k(x,\omega) = \sum_{n=0}^{s'}(i\omega)^n\,b_n'(x,\bar{t}_k)/\sum_{n=0}^{r'}(i\omega)^n\,a_n'(x,\bar{t}_k), \tag{59}$$

$$\bar{q}^k = \bar{q}^k(x,\omega) = \sum_{n=0}^{s''}(i\omega)^n\,b_n''(x,\bar{t}_k)/\sum_{n=0}^{s'}(i\omega)^n\,b_n'(x,\bar{t}_k). \tag{60}$$

Equations (57) are of a form similar to (44) and, therefore, the Fourier transform of the viscoelastic thermal stress deviators, strains, etc. over any interval $t_k \leqslant t < t_{k+1}$ are precisely the equivalent elastic thermal stress deviators, strains etc. for $\bar{G}^k$, $\bar{q}^k\,\overline{\alpha T}^k$ and $\bar{K}^k$ defined over the interval. In order to solve the viscoelastic problem it is, therefore, sufficient to know the elastic solution for the equivalent nonhomogeneous elastic body where G, αT and K are replaced in each interval respectively by the appropriate $\bar{G}^k$, $\bar{q}^k$, $\overline{\alpha T}^k$ and $\bar{K}^k$.

The boundary conditions for each time interval are, of course, the same and are the original boundary conditions of the body. The initial conditions for each interval are as follows:

(a) $0 \leqslant t < t_1$, for the first interval the initial conditions at $t = 0$ are the initial conditions of the body;

(b) $t_k \leqslant t < t_{k+1}\,(k \geqslant 1)$, the initial conditions for each subsequent interval are the end-point values of the preceeding interval, or

$$\sigma_{ij}{}^{k}(x, t_k) = \lim_{t \to t_k} \{\sigma_{ij}{}^{k-1}(x, t)\}, \tag{61}$$

with similar conditions imposed on the time derivatives.

In other words the viscoelastic thermal stresses may be found thus:

$0 \leqslant t < t_1$.

$$\sigma_{ij}{}^{0}(x, t) = \int_{-\infty}^{\infty} \sigma_{ij}{}^{e}(x, \bar{G}^0, \bar{q}^0\, \overline{\alpha T}^0, \bar{K}^0)\, e^{i\omega t}\, d\omega \tag{62}$$

with initial conditions at $t = 0$ the same as the initial conditions of the viscoelastic body:

$t_k \leqslant t < t_{k+1} \qquad (k \geqslant 1)$.

$$\sigma_{ij}{}^{k}(x, t) = \int_{-\infty}^{\infty} \sigma_{ij}{}^{e}(x, \bar{G}^k, \bar{q}^k\, \overline{\alpha T}^k, \bar{K}^k)\, e^{i\omega t}\, d\omega \tag{63}$$

with initial conditions for the interval given by (61). The strains may be found in identical fashion by simply interchanging in (61) to (63) $\epsilon_{ij}{}^{k}(x, t)$ for $\sigma_{ij}{}^{k}(x, t)$ and

$$\epsilon_{ij}{}^{e}(x, \bar{G}^k, \bar{q}^k\, \overline{\alpha T}^k, \bar{K}^k) \quad \text{for} \quad \sigma_{ij}{}^{e}(x, \bar{G}^k, \bar{q}^k\, \overline{\alpha T}^k, \bar{K}^k).$$

It should be noted that even though the material properties a_n, b_n, etc., have been treated as step functions in time, the above analysis leads to continuous stresses, strains, etc. which are continuous functions in time.

3. Discussions and Conclusions

The three extensions of Alfrey's elastic–viscoelastic analogy presented here show that the solution to a given linear viscoelastic thermal stress problem with temperature dependent material properties can be obtained by analogy from the equivalent elastic thermal stresses and strains. The extension as covered by Case A is exact for incompressible linear viscoelastic media with time-dependent, but not space-dependent, temperature distributions. Case B is an exact analogy for compressible nonhomogeneous linear viscoelastic media subjected to steady-state temperature distributions. Finally, Case C is an approximate extension of Case B for the same compressible nonhomogeneous medium but with temperature distributions that are functions of space and time variables.

For those problems where no elastic solutions as yet are available in the literature and where nonhomogeneous viscoelastic solutions are desired, it is sufficient to solve the equivalent elastic case and thus by analogy obtain the viscoelastic solution. In most viscoelastic media, except for Kelvin bodies, the initial conditions are the equivalent elastic values and, therefore, one must know the elastic solutions in any event. Consequently, for a given structural shape the analogy offers the solution to any linear nonhomogeneous viscoelastic medium from a single equivalent elastic solution to that particular problem.

It is of interest to note that the analogy is relatively simple for incompressible temperature-dependent viscoelastic media where the temperature is a time function only. Here one can make use of the separation of variable technique and obtain viscoelastic thermal stresses and strains which are equal to their elastic equivalents multiplied by appropriate time response functions. In the case of nonhomogeneous compressible viscoelastic media with steady or nonsteady state spatial dependent temperature distributions one must make use of linear operator transforms.

Throughout the present analysis it has been assumed that Fourier transforms and their inverses exist for viscoelastic thermal stresses and strains. Since the integrability condition for Fourier transforms is rather severe, one may not always be able to satisfy it. In those instances one may resort to the use of Laplace transforms, since the same analogies can be relatively readily established in terms of Laplace transforms as well.

References

Alfrey, T.	1944	*Quart. Appl. Math.* **2**, 113.
	1948	*Mechanical Behaviour of High Polymers*, pp. 557–564 (Interscience, New York).
Allen, H. F., Brull, M. A. and Wilkie, W. J.	1954	*Wright Air Development Center Tech. Rept.* 54–499.
Baer, H. W.	1954	*Proc. 2nd U.S. Nat. Congr. Appl. Mech.*, p. 569.
Bleich, H. H.	1957	*Columbia University Tech. Rept.* 3.
Bozajian, J. M. and Tsao, C. H.	1957	*Hughes Aircraft Co. Tech. Rept. SRSM-7–196.*
Brull, M. A.	1953	*Proc. 1st Midwestern Conf. Solid Mech.*, p. 141.
Freudenthal, A. M.	1950	*The Inelastic Behaviour of Engineering Materials and Structures*, pp. 153–156 (John Wiley, New York).
	1954a	*J. Appl. Phys.* **25**, 1110.
	1954b	*J. Aero. Sci.* **21**, 772.
	1954c	*Studies in Mathematics and Mechanics*, pp. 251–261 (Academic Press, New York).
Hilton, H. H.	1952a	*J. Appl. Mech.* **19**, 350.
	1952b	*J. Aero. Sci.* **19**, 844.
	1954	*Proc. 2nd U.S. Nat. Congr. Appl. Mech.*, p. 547.
	1957	*Proc. 3rd Midwestern Conf. Solid Mech.*, p. 1.
	1959	*J. Aero. Sci.* **26**, 311.
	1960	*Ibid.* **27**, 926.
Hilton, H. H., Hassan, H. A. and Russell, H. G.	1953	*Wright Air Development Center Tech. Rep.* 53–322.
Hoff, N. J.	1954	*Quart. Appl. Math.* **12**, 49.
Kê, T. S.	1948	*Amer. Inst. Mining and Metall. Engrs. Tech. Publ.* 2370.
Lee, E. H.	1955	*Quart. Appl. Math.* **13**, 183.
	1960	*Proc. 1st Symp. Naval Structural Mech.*, p. 456.
Lee, E. H., Radok, J. R. M. and Woodward, W. B.	1959	*Trans. Soc. Rheol.* **3**, 41.
Lorsch, H. G. and Freudenthal, A. M.	1954	*Proc. 2nd U.S. Nat. Congr. Appl. Mech.*, p. 539.
Mindlin, R. D.	1949	*J. Appl. Phys.* **20**, 206.
Morland, L. W. and Lee, E. H.	1960	*Trans. Soc. Rheol.* **4**, 223.
Prager, W.	1956	*Z. angew. Mech. Phys.* **7**, 230.

Read, W. T.	1950	*J. Appl. Phys.* **21**, 671.
Sternberg, E.	1958	*Proc. 3rd U.S. Nat. Congr. Appl. Mech.*, p. 673.
Timoshenko, S.	1934	*Theory of Elasticity*, pp. 203–212, 364–380 (McGraw-Hill, New York).
Tsien, H. S.	1950	*Quart. Appl. Math.* **8**, 104.
Wimpress, R. N.	1950	*Internal Ballistics of Solid Fuel Rockets*, pp. 152, 153 (McGraw-Hill, New York).

J. Mech. Phys. Solids, 1961, Vol. 9, pp. 165 to 178. Pergamon Press Ltd., London. Printed in Great Britain

SPATIAL MOTION OF ELASTIC–PLASTIC STRINGS

By N. Cristescu
Mathematical Institute of the Academy of the Roumanian People's Republic

(*Received 6th February*, 1961)

Summary

The problem of the integration of the equations of motion of an elastic–plastic string, which can move in space, is considered. No restrictions on the initial shape, movement and deformation of the string are imposed. Due to an impact at a point of the string, longitudinal and transverse waves propagate simultaneously in the string. Numerical methods of integration are described.

1. Introduction

The problem of the rapid transverse and longitudinal motion of elastic–plastic strings struck by a point body has been considered by several authors in recent years. Especially, the problem of the movement of a string in a plane has been considered, when the string is initially rectilinear and the longitudinal waves propagate faster than the transverse ones, supposing that these last in fact reduce to a single shock wave (Rakhmatulin 1945b, 1947, 1951 ; Ryabova 1953, Smith *et al.* 1958). Discontinuous solutions were analysed by Craggs (1954), Smith *et al.* (1956), Pavlenko (1959). Experimental verifications, or the experimental establishment of the stress–strain relations, for the case of the transverse impact of strings are due to Rakhmatulin and Shapiro (1955), Smith *et al.* (1956) and Stevens (1957). The particular case when the longitudinal waves propagate behind the transverse ones, when even the shape of the string can be approximated by segments of straight lines, was considered by Smith *et al.* (1958). The transverse impacts of some types of finite strings were theoretically examined by Moroz (1957).

The spatial motion of strings has also been considered. The types of waves propagable, as well as the order of the propagation of perturbations, were considered by Cristescu (1954, 1958) and Pavlenko (1959), and for a particular type of stress–strain relation by Keller (1959). The case when the strain rate also enters in the stress–strain relation was considered by Cristescu (1957). The approximate integration of the equations of motion of the string, when the longitudinal waves propagate before the transverse ones and the string is initially rectilinear, was considered by Cristescu (1960).

In the present paper the motion of a string in space will be considered, supposing that the transverse and longitudinal waves propagate simultaneously in the string. An approximate method of integration is proposed, without any restrictions about the boundary or initial conditions. It is assumed that the stress–strain relation can be approximated by a (finite) number of segments of straight lines.

2. NOTATION AND EQUATIONS

The equations of motion in space of a perfectly flexible string, which is under the action of some external forces, are

$$\left.\begin{aligned} \frac{\partial}{\partial s_0}\left(\frac{T}{1+\epsilon}\frac{\partial x}{\partial s_0}\right) - \rho_0 \frac{\partial^2 x}{\partial t^2} + (1+\epsilon)X = 0, \\ \frac{\partial}{\partial s_0}\left(\frac{T}{1+\epsilon}\frac{\partial y}{\partial s_0}\right) - \rho_0 \frac{\partial^2 y}{\partial t^2} + (1+\epsilon)Y = 0, \\ \frac{\partial}{\partial s_0}\left(\frac{T}{1+\epsilon}\frac{\partial z}{\partial s_0}\right) - \rho_0 \frac{\partial^2 z}{\partial t^2} + (1+\epsilon)Z = 0, \end{aligned}\right\} \tag{1}$$

where ϵ is the strain given by

$$\epsilon = \frac{ds - ds_0}{ds_0} = \sqrt{\left[\left(\frac{\partial x}{\partial s_0}\right)^2 + \left(\frac{\partial y}{\partial s_0}\right)^2 + \left(\frac{\partial z}{\partial s_0}\right)^2\right]} - 1, \tag{2}$$

s being the curvilinear coordinate on the deformed string, and s_0 the Lagrange coordinate on the original string. The two coordinates are connected by relations of the form

$$\frac{\partial x}{\partial s_0} = (1+\epsilon)\frac{\partial x}{\partial s}, \qquad \frac{\partial y}{\partial s_0} = (1+\epsilon)\frac{\partial y}{\partial s}, \qquad \frac{\partial z}{\partial s_0} = (1+\epsilon)\frac{\partial z}{\partial s}. \tag{3}$$

T is the " stress " in the sense of the mechanics of strings, and it is supposed that between T and ϵ there is a given relation of the form

$$T = T(\epsilon). \tag{4}$$

At first we specify about the function in (4) only that is increasing monotonically. In this paper we shall assume that the rate of strain does not enter in (4). In (1) ρ_0 is the initial density, which is connected with the actual density by the relation $\rho_0 = \rho(1+\epsilon)$; X, Y, Z are the components of the resultant of some external forces which act on a portion ds of the string, and it is supposed that these forces are given and continuous functions of s_0 and t. The considerations which follow, however, can be applied to some more general cases when the functions X, Y, Z depend even on the velocities of the particles of the string.

It has been shown (CRISTESCU 1954; CRAGGS 1954) that in strings satisfying the equations (1)–(4) two types of waves are propagable: the transverse waves propagate with the velocity

$$c_{\mathrm{I}} = \pm\sqrt{\left[\frac{T}{\rho_0(1+\epsilon)}\right]} \tag{5}$$

and the longitudinal waves with the velocity

$$c_{\mathrm{II}} = \pm\sqrt{\left[\frac{1}{\rho_0}\frac{dT}{d\epsilon}\right]}. \tag{6}$$

The fronts of the two types of waves correspond respectively to the two families of characteristic lines of the equations (1):

$$\rho_0 \left(\frac{ds_0}{dt}\right)^2 = \frac{T}{1+\epsilon} \tag{7}$$

and to

$$\rho_0 \left(\frac{ds_0}{dt}\right)^2 = \frac{dT}{d\epsilon}. \tag{8}$$

On the lines (7) the relations

$$\left.\begin{aligned} dx_t &= \pm c_1\, dx_{s_0} + \left[(1+\epsilon)\frac{X}{\rho_0} + x_{s_0}\frac{\partial c_1^2}{\partial s_0}\right] dt, \\ dy_t &= \pm c_1\, dy_{s_0} + \left[(1+\epsilon)\frac{Y}{\rho_0} + y_{s_0}\frac{\partial c_1^2}{\partial s_0}\right] dt, \\ dz_t &= \pm c_1\, dz_{s_0} + \left[(1+\epsilon)\frac{Z}{\rho_0} + z_{s_0}\frac{\partial c_1^2}{\partial s_0}\right] dt, \end{aligned}\right\} \tag{9}$$

are satisfied (Cristescu 1960), where for simplicity the notations $x_t = \partial x/\partial t$, $x_{s_0} = \partial x/\partial s_0$ etc. are used. On the lines (8) relations of the form

$$\pm \rho_0 c_{11}(x_{s_0}\, dx_{s_0} + y_{s_0}\, dy_{s_0} + z_{s_0}\, dz_{s_0}) - \rho_0 (x_{s_0}\, dx_t + y_{s_0}\, dy_t + z_{s_0}\, dz_t) + \\ + (1+\epsilon)(Xx_{s_0} + Yy_{s_0} + Zz_{s_0})\, dt = 0 \tag{10}$$

are satisfied. The relation (10) can be written also in the form

$$\pm c_{11}\, d\epsilon - dv + \frac{1+\epsilon}{\rho_0} F\, dt = 0 \tag{11}$$

if one denotes by dv the tangential projection of the increment along the lines (8) of the velocity of the respective particle of the string, and by F the projection on the tangent to the string of the components of external forces:

$$\left.\begin{aligned} dv &= \frac{1}{1+\epsilon}(x_{s_0}\, dx_t + y_{s_0}\, dy_t + z_{s_0}\, dz_t), \\ F &= \frac{1}{1+\epsilon}(Xx_{s_0} + Yy_{s_0} + Zz_{s_0}). \end{aligned}\right\} \tag{12}$$

It is known (Cristescu 1954, 1958) that, depending on the mechanical properties of the material of the string, properties which are reflected in the function in (4), and also depending on the boundary conditions, any order of propagation of the two types of waves in the string is possible. If, initially, the string was rectilinear and if, due to the perturbation produced at $s_0 = 0$, longitudinal waves first propagate in the string and afterward the transverse ones, then it is easy to obtain the solution (Cristescu 1960). In this case, if we have also $F = 0$, then the relation (11) reduces to the well-known relation of the propagation of longitudinal waves in thin rods (Rakhmatulin 1945a). Either in the case $F = 0$, or in the case $F \neq 0$, the equation (11) can be integrated exactly or approximately and therefore the distribution of strains ϵ and of longitudinal velocities v can be obtained. Then the propagation of transverse waves is studied in the same way as the propagation of transverse waves in an inextensible string which is deformed homogeneously or non-homogeneously. This is done by the integration of the equation (1) which is linearized if $\epsilon(s_0, t)$ is a known function.

In almost all the works published up to now there were considered either the cases when the two types of waves propagated in different portions of the string or the cases when (SMITH *et al.* 1958), though the two types of waves propagate simultaneously in the same portion of the string, the shape of the string can be always approximated by segments of straight lines. This last supposition is a very particular model of motion.

Further we shall suppose that the initial motion and strain along the string can be arbitrary and the order of the propagation of the two types of perturbations can be also arbitrary, the shape of the string being deformed continuously.

3. INTERACTION BETWEEN LONGITUDINAL AND TRANSVERSE WAVES

It is known (CRISTESCU 1954) that the longitudinal waves produce only the deformation (extension) of the string, and the transverse ones produce only the variation of its shape. However, each type of wave influences the other. The propagation of transverse waves will be influenced by the strain distribution along the string; even the velocity of propagation (5) of transverse waves is a function of ϵ. The variation of the velocity v is connected with the variation of ϵ by the relation

$$\pm \rho_0 c_1 \, d\epsilon - \rho_0 \, dv + (1 + \epsilon) F \, dt = - \rho_0 (1 + \epsilon) \frac{\partial c_1^2}{\partial s_0} \, dt \tag{13}$$

which can be obtained easily from (9). In the present paper the relation (13) will be used for the calculation of the variation of the velocity of transverse waves due to the concomitant extension of the string. Certainly, (13) holds on the lines (7).

On the other hand, from (10), the velocity of a particle of the string and the external forces which act on it must be projected on the tangent to the string and on a normal direction. Only the tangential components of this velocity and of these forces will produce longitudinal deformations of the string. The normal components will influence the transverse waves only. By crossing the lines which are wave-fronts, the second derivatives $\partial^2 x/\partial s_0^2$, $\partial^2 x/\partial t^2$, etc., are discontinuous. We represent these discontinuities as vectors. Let us project these vectors at the considered point of the string on the tangent to the string and on a normal direction. Then the projections of these discontinuities on the tangent to the string propagate on the longitudinal waves, and the normal projections of discontinuities propagate on the transverse waves. These considerations, together with the relations (9) and (10), are the basis of the approximate method given further.

Therefore, in a string which is not rectilinear initially, are propagable not only longitudinal waves. Even if initially the boundary conditions were given so that only longitudinal waves appeared, during their propagation due to the variation of the shape of the string transverse waves will appear also. This is because the velocities of the particles and the external forces, though initially having only components directed along the tangent to the string, will get also normal components when the string begins to change its shape. Therefore, we could say that the longitudinal waves can generate transverse waves even when the string is not rectilinear.

One can also state that in an extensible string it is impossible to propagate only transverse waves, even if the boundary conditions are such that at the string end only transverse waves appear. The reason is that during the propagation of transverse waves, on certain portions of the string, the velocities of the particles will at a certain moment necessarily have a component directed along the tangent to the string. According to the relation (10) such a component will produce a variation of the longitudinal deformation. Even if previously the string was strongly deformed elastic–plastically, during the propagation of transverse waves the tangential components of the velocities and of external forces, according to (10) will produce at least small elastic variations of the deformations. Certainly, sometimes the longitudinal deformations, which have appeared during the propagation of transverse waves in a string previously strongly deformed, can be neglected. This case was considered by CRISTESCU (1960), and for certain plane motions by the majority of the authors cited in the Introduction.

We also draw attention to the fact that a transverse shock wave, i.e. a discontinuity of the tangent propagable along the string, will also always produce some longitudinal waves. This is because, after crossing the front of a transverse shock wave, particles will move with a velocity which generally is not normal to the string (only in isolated points of the string this velocity does not have a component directed also along the tangent to the string). Then, immediately after crossing the front of the shock wave, the tangential components of the velocity and external forces can be calculated using the relation (12). These components introduced in (10) will give the corresponding variation of the deformation of the string due to the passage of the front of the shock wave. The more sudden the variation of the slope of the string, the more important will be the variation of the deformation. Because the front of a transverse shock wave, which has appeared due to a sudden impact on the string, usually is nothing but a bundle of transverse waves whose fronts 'almost' coincide, it follows that the longitudinal deformations which have appeared will have the tendency to spread (to rarefy) these fronts of transverse waves. Therefore, in extensible strings, the transverse shock waves which have appeared due to certain boundary conditions (impacts), will gradually transform into bundles of continuous transverse waves as they propagate. Certainly, the rigidity of the string plays an important role in these considerations; for the moment we shall not consider it.

In this paper we shall especially examine continuous waves, though many considerations can be applied also to transverse and longitudinal shock waves.

4. Initial and Boundary Conditions

Let us formulate the problem. A string, whose material is arbitrary (the relation (4) is arbitrary), moves according to a given law and is submitted to some given external forces. Therefore it is supposed that, at $t = 0$, the position and the velocity of every particle of the string are known, and the strain distribution $\epsilon(s_0)$ for $t = 0$ is also known. At the time $t = 0$ a rapid motion is applied to a certain point of the string which, by convention, will be considered as the point for which $s_0 = 0$; the string is 'struck' (in a general sense) in that point according to a given law. In these circumstances one seeks to find the motion of the string for

every moment of time and the strain distribution in every point of the string at every moment. We shall suppose that the shock was such that it produces both longitudinal and transverse waves, the two waves being propagable.

In fact the initial conditions must not be known on the straight line $t = 0$, but along the front of the first perturbation propagable in the string. This is because, in the interval of time from $t = 0$ until the front of the first perturbation arrives in the portions of the string farthest from the point of the impact, these portions could be influenced also by other external factors. Therefore, along the front of the first pertubration propagable, the functions $x_t(s_0, t)$, $y_t(s_0, t)$, $z_t(s_0, t)$, $x_{s_0}(s_0, t)$, $y_{s_0}(s_0, t)$, $z_{s_0}(s_0, t)$, $\epsilon(s_0, t)$ and $v(s_0, t)$ must be given.

The boundary conditions will be given in the form: the law of motion of the point on the string, which corresponds to $s_0 = 0$, is known. Therefore both the position of this point and its velocity $x_t(0, t)$, $y_t(0, t)$, $z_t(0, t)$ are known at every moment. Generally the variation of the slope of the tangent in the point $s_0 = 0$ is unknown. If by experiments, for example by the rapid filming of the struck region of the string, the slope of the tangent to the string is known for $s_0 = 0$ and for every moment of time (therefore in addition are known also the functions $x_s(0, t)$, $y_s(0, t)$, $z_s(0, t)$) then with these boundary conditions the approximate integration is easier. In what follows we shall consider the general case when the slope of the tangent to the string in $s_0 = 0$ is *a priori* unknown and must be found by computations. This can be done using an approximate method which is sufficiently laborious. For this reason, if it is possible, it is preferable to avoid it using supplementary conditions given by experiments. Obviously, the slope of the tangent to the string at $s_0 = 0$ cannot be given arbitrarily, because that could lead to an incompatibility between the initial and boundary conditions.

In what follows we assume that the boundary conditions are such that only continuous waves appear in the string. Or, in other words, we shall consider only the case when the velocities x_t, y_t, z_t, given by the boundary conditions on the front of the first perturbation propagable in the string, coincide with those given by the initial conditions in $s_0 = 0$ and $t = 0$.

We shall also mention that both initial and boundary conditions can be given either analytically or numerically at a certain number of points.

5. Approximate Integration

Generally the characteristic curves (7) and (8) form a double net of curves of variable slope. Generally the slopes to the two types of characteristics are different in every point (s_0, t). In certain particular cases, for certain materials and certain domains of variations of ϵ, the slopes of the two families of characteristics are approximately equal: $c_{\mathrm{I}} \simeq c_{\mathrm{II}}$ in a whole domain of the plane (s_0, t). The problem of approximate integration is then easier, because the two families of characteristics coincide, have constant slope, and from (13) it results $\partial c_{\mathrm{I}}^2/\partial s_0 = 0$. This particular case will be considered first.

Secondly, the case when $c_{\mathrm{I}} \neq c_{\mathrm{II}}$ will be considered. There are two possibilities: either $c_{\mathrm{I}} > c_{\mathrm{II}}$ or $c_{\mathrm{I}} < c_{\mathrm{II}}$. It is possible that, in the same problem of impact of a string, the two situations could appear in different domains of the plane (s_0, t). In each of these domains different schemes of integration must then be used.

The approximate integration is imagined in two stages. In the first, the distribution of strains, velocities and slopes of the tangent to the string, for any s_0 and any t must be found. In the second, the shape of the string must be found for any moment of time t.

(i) *The particular case* $c_I \simeq c_{II}$. From the beginning we emphasize that this is a very particular case, but is it found in practice expecially for certain types of artificial strings. In fact it appears only if the deformation has reached a certain magnitude and not from the beginning of the process of deformation ; therefore in the plane (s_0, t) this situation will appear only in a certain domain of this plane.

As follows from (5) and (6), the stress–strain relation is here of the form

$$T = k\,(1 + \epsilon) \tag{14}$$

where k is a constant. This occurs when the tangent to the curve (4) passes through the point $(-1{\cdot}0)$ (Cristescu 1954). Some considerations about the equations of motion of the string in the absence of external forces are due to Keller (1959).

Here the lines (7) and (8) coincide and form a net of straight lines. The problem can be tackled in different ways. Certainly the equations (1), in which the coefficients of the highest derivatives are now constant, could be considered directly. Moreover, if the external forces are absent, the system (1) degenerates into three separate equations of hyperbolic type with constant coefficients which can be integrated by classical methods. In what follows, without neglecting the external forces, we shall prefer a method of approximate integration on the net of characteristics, because it will be applied also to the general case and because this particular case in fact occurs only in a domain of the plane (s_0, t), while in the other domains where $c_I \neq c_{II}$ the solution can be obtained only by approximate integration.

For illustration let us suppose that in the domain ABC (Fig. 1) of the plane (s_0, t) one can consider $c_I \simeq c_{II}$. With the aid of the known and constant value of $dT/d\epsilon$ one draws the net of characteristics so that passing from a vertex to the next one, the increment of Δs_0 is constant. The choice of the value of Δs_0 is arbitrary, but the more sudden the change of slope of the string, the smaller must be the intervals Δs_0.

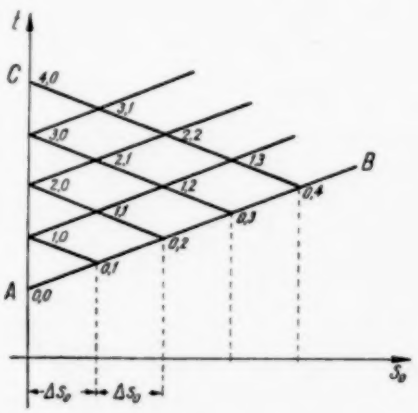

Fig. 1.

Along AB, which is the front of the first wave on which $c_I \simeq c_{II}$, the shape of the string, its motion and its state of deformation are known. Therefore along AB the functions $x_t(s_0, t)$, $y_t(s_0, t)$, $z_t(s_0, t)$, $x_{s_0}(s_0, t)$, $y_{s_0}(s_0, t)$, $z_{s_0}(s_0, t, \epsilon(s_0, t)$ and $v(s_0, t)$ are known. Along AC the motion of the point $s_0 = 0$ is given, therefore its position $x(0, t)$, $y(0, t)$, $z(0, t)$ and its velocity $x_t(0, t)$, $y_t(0, t)$, $z_t(0, t)$ are known. In the whole plane (s_0, t) the functions $X(s_0, t)$, $Y(s_0, t)$ and $Z(s_0, t)$ are supposed known.

On the net of straight lines of Fig. 1 the two groups of relations (9) and (10) are satisfied. Since in this case $\partial c_I^2/\partial s_0 = 0$, the relation (13) coincides with (11), and relations (9) become

$$\left.\begin{aligned} dx_t &= \pm c_1\, dx_{s_0} + \frac{1+\epsilon}{\rho_0} X\, dt, \\ dy_t &= \pm c_1\, dy_{s_0} + \frac{1+\epsilon}{\rho_0} Y\, dt, \\ dz_t &= \pm c_1\, dz_{s_0} + \frac{1+\epsilon}{\rho_0} Z\, dt. \end{aligned}\right\} \tag{15}$$

To integrate relations (11) and (15) on the net of Fig. 1, they will be turned into equations with finite differences. It is advantageous to take into account successively the vertices on a characteristic line parallel to AB, then to pass on the next line and so on. First we must find x_{s_0}, y_{s_0} and z_{s_0} at the point (1,0). In what follows, the round brackets will be reserved to indicate the argument of a function, and to simplify the writing, the indices s_0 and t will be written as superscripts.

The relations (15) become

$$\left.\begin{aligned} x_{0,1}{}^t - x_{1,0}{}^t &= -c_1\left[x_{0,1}{}^{s_0} - x_{1,0}{}^{s_0}\right] + \frac{1+\epsilon_{1,0}}{\rho_0} X_{1,0}\left[t_{0,1} - t_{1,0}\right], \\ y_{0,1}{}^t - y_{1,0}{}^t &= -c_1\left[y_{0,1}{}^{s_0} - y_{1,0}{}^{s_0}\right] + \frac{1+\epsilon_{1,0}}{\rho_0} Y_{1,0}\left[t_{0,1} - t_{1,0}\right], \\ z_{0,1}{}^t - z_{1,0}{}^t &= -c_1\left[z_{0,1}{}^{s_0} - z_{1,0}{}^{s_0}\right] + \frac{1+\epsilon_{1,0}}{\rho_0} Z_{1,0}\left[t_{0,1} - t_{1,0}\right]. \end{aligned}\right\} \tag{16}$$

From (16) one obtains $x_{1,0}{}^{s_0}$, $y_{1,0}{}^{s_0}$ and $z_{1,0}{}^{s_0}$, the other factors being known. To find ϵ and v in the vertex (1,0) one proceeds as follows. From the relations (12) written in the form

$$\left.\begin{aligned} v_{1,0} - v_{0,1} &= \frac{1}{1+\epsilon_{0,1}}\left\{x_{0,1}{}^{s_0}\left[x_{1,0}{}^t - x_{0,1}{}^t\right] + y_{0,1}{}^{s_0}\left[y_{1,0}{}^t - y_{0,1}{}^t\right] + z_{0,1}{}^{s_0}\left[z_{1,0}{}^t - z_{0,1}{}^t\right]\right\}, \\ F_{0,1} &= \frac{1}{1+\epsilon_{0,1}}\left\{X_{0,1}\, x_{0,1}{}^{s_0} + Y_{0,1}\, y_{0,1}{}^{s_0} + Z_{0,1}\, z_{0,1}{}^{s_0}\right\}, \end{aligned}\right\} \tag{17}$$

one obtains $v_{1,0}$ and $F_{0,1}$. Introducing these values in (11) written in the form

$$-c_{11}\left[\epsilon_{1,0} - \epsilon_{0,1}\right] - \left[v_{1,0} - v_{0,1}\right] + \frac{1+\epsilon_{0,1}}{\rho_0} F_{0,1}\left[t_{1,0} - t_{0,1}\right] = 0 \tag{18}$$

one can obtain also $\epsilon_{1,0}$.

We observe that, in this particular case, the transverse waves are influenced in a smaller measure by the longitudinal waves. This influence is represented in (15) by the terms which depend on ϵ. Since c_1 is here a constant, ϵ enters directly only in the last term ; if the external forces are absent, ϵ no longer influences the propagation of the transverse waves.

Further to find $\epsilon_{1,1}$ we shall write (11) in the form

$$\left.\begin{aligned} c_1\left[\epsilon_{1,1} - \epsilon_{1,0}\right] - \left[v_{1,1} - v_{1,0}\right] + \frac{1+\epsilon_{1,0}}{\rho_0} F_{1,0}\left[t_{1,1} - t_{1,0}\right] &= 0, \\ -c_1\left[\epsilon_{1,1} - \epsilon_{0,2}\right] - \left[v_{1,1} - v_{0,2}\right] + \frac{1+\epsilon_{0,2}}{\rho_0} F_{0,2}\left[t_{1,1} - t_{0,2}\right] &= 0. \end{aligned}\right\} \tag{19}$$

The differences $v_{1,1} - v_{1,0}$ and $v_{1,1} - v_{0,2}$ are calculated from (12):

$$\left.\begin{aligned} v_{1,1} - v_{1,0} &= \frac{1}{1+\epsilon_{1,0}}\left\{x_{1,0}{}^{s_0}\left[x_{1,1}{}^t - x_{1,0}{}^t\right] - y_{1,0}{}^{s_0}\left[y_{1,1}{}^t - y_{1,0}{}^t\right] + z_{1,0}{}^{s_0}\left[z_{1,1}{}^t - z_{1,0}{}^t\right]\right\}, \\ v_{1,1} - v_{0,2} &= \frac{1}{1+\epsilon_{0,2}}\left\{x_{0,2}{}^{s_0}\left[x_{1,1}{}^t - x_{0,2}{}^t\right] + y_{0,2}{}^{s_0}\left[y_{1,1}{}^t - y_{0,2}{}^t\right] + z_{0,2}{}^{s_0}\left[z_{1,1}{}^t - z_{0,2}\right]\right\}. \end{aligned}\right\} \tag{20}$$

From (20) one obtains two values of $v_{1,1}$; the arithmetic mean of these two values will be considered in the following computations. Taking into account (20) and (19) two values are obtained for $\epsilon_{1,1}$; in later computations will be considered also the arithmetic mean of these two values.

After that one can pass to the next vertex (1·2) and so on.

(ii) *The general case when* $c_I \neq c_{II}$. From the examination of the expressions (5) and (6), and also of the different types of relations (4) which occur more frequently in practice, it results that the variation of the velocity c_I of transverse waves depends more on the variation of the strain than the variation of the velocity c_{II} of longitudinal waves ; often c_{II} is even constant or almost constant in sufficiently large intervals of variation of ϵ. Further we suppose that the relation (4) can be approximated by a finite number of segments of straight lines. This reduces to the assumption that in different domains of the plane (s_0, t) the velocity c_{II} is constant, or that in these domains the characteristics (8) are a family of straight lines. Certainly, if in certain conditions one can suppose $c_I = \text{const.}$, the situation is inverted. The essential fact is that if in a certain domain of the plane (s_0, t) one of the families of characteristics reduces to a family of straight lines, then an approximate method of integration of the equations can be imagined. The experiments prove, however, that the first supposition is that which is more frequently used.

Since at the beginning of the process of deformation all the material is elastic, and in the elastic domain $c_{II} > c_I$, the first front OA (Fig. 2a) of the bundle of waves will be the front of a longitudinal wave on which $c_{II} = \text{const}$. Along OA the motion and the initial strain of the string are known from the initial conditions, and along OB the motion of the point of the string for which $s_0 = 0$ is known from the boundary conditions.

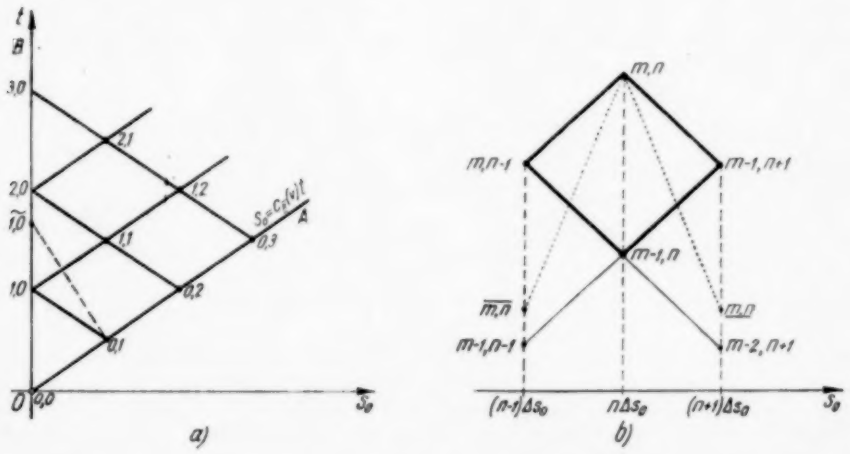

FIG. 2.

For the approximate integration on the line of vertices (1,0), (1,1), (1,2), (1,3), etc., we proceed in two stages. In the first, by a certain algorithm we find the approximate values of the necessary functions at the vertex (1,0). Then, in the second stage, with the aid of another algorithm, we calculate the approximate values of the unknown functions at the vertices (1,1), (1,2), etc. We proceed in the same way on the following line of vertices and so on.

We draw the characteristic (8) of negative slope (0,1)–$(\widetilde{1,0})$, the slope being calculated for $\epsilon = \epsilon_{0,1}$. In this way the point $(\widetilde{1,0})$ is obtained. In $(\widetilde{1,0})$ the values $x_{\widetilde{1,0}}{}^t$, $y_{\widetilde{1,0}}{}^t$, $z_{\widetilde{1,0}}{}^t$ are known from the boundary conditions. With the aid of relations (9) written in the form

$$\left.\begin{aligned} x_{\widetilde{1,0}}{}^t - x_{0,1}{}^t &= -c_I(\epsilon_{0,1})\left[x_{\widetilde{1,0}}{}^{s_0} - x_{0,1}{}^{s_0}\right] + \frac{1+\epsilon_{0,1}}{\rho_0} X_{0,1}\left[t_{\widetilde{1,0}} - t_{0,1}\right], \\ y_{\widetilde{1,0}}{}^t - y_{0,1}{}^t &= -c_I(\epsilon_{0,1})\left[y_{\widetilde{1,0}}{}^{s_0} - y_{0,1}{}^{s_0}\right] + \frac{1+\epsilon_{0,1}}{\rho_0} Y_{0,1}\left[t_{\widetilde{1,0}} - t_{0,1}\right], \end{aligned}\right\} \qquad (21)$$

$$z_{1,0}^{\widetilde{t}} - z_{0,1}{}^{t} = -c_1(\epsilon_{0,1})\left[z_{1,0}^{\widetilde{s_0}} - z_{0,1}{}^{s_0}\right] + \frac{1+\epsilon_{0,1}}{\rho_0} Z_{0,1}\left[t_{1,0}^{\widetilde{}} - t_{0,1}\right]. \qquad \Big]$$

where we have neglected the factor $\partial c_1{}^2/\partial s_0$, the values of $x_{1,0}^{\widetilde{s_0}}$, $y_{1,0}^{\widetilde{s_0}}$, $z_{1,0}^{\widetilde{s_0}}$ are obtained in a first approximation. Then, by interpolation between the vertices (0,0) and $(\widetilde{1,0})$, one obtains in a first approximation $x_{1.0}{}^{s_0}$, $y_{1.0}{}^{s_0}$, $z_{1.0}{}^{s_0}$ and $x_{1.0}{}^{t}$, $y_{1.0}{}^{t}$, $z_{1.0}{}^{t}$. With the aid of (12) considered between the vertices (0,1) and (1,0), one obtains $v_{1.0}$ and $F_{1.0}$ and from (11) one obtains $\epsilon_{1.0}$. By extrapolation one finds $\epsilon_{1,0}^{\widetilde{}}$ and $v_{1,0}^{\widetilde{}}$.

For the second approximation we take again the computations from the beginning, drawing more precisely the characteristic (0,1)–$(\widetilde{1,0})$, its slope being calculated for $\epsilon = \frac{1}{2}(\epsilon_{0.1} + \epsilon_{1,0}^{\widetilde{}})$ and the factor $\partial c_1{}^2/\partial s_0$ is calculated with the aid of (13) in which $\Delta\epsilon = \epsilon_{1,0}^{\widetilde{}} - \epsilon_{0.1}$ etc. After several such series of computations, $\epsilon_{1.0}$, $v_{1.0}$, $x_{1.0}{}^{t}$, $y_{1.0}{}^{t}$, $z_{1.0}$, $x_{1.0}{}^{s_0}$, $y_{1.0}{}^{s_0}$, $z_{1.0}{}^{s_0}$ are obtained with the desired approximation. The above method is rather similar to that recommended by HILL (1950). If by experiments x^s, y^s, z^s are moreover known along $0t$, then these successive approximations can be avoided, as well as the errors which could be introduced in the computations.

To make clear the algorithm used in the second stage, let us consider (Fig. 2b) an arbitrary cell, from those drawn in Fig. 2 (a); the sides of the cell are two characteristics (8) of positive slope and two characteristics (8) of negative slope. In the vertices $(m, n-1)$, $(m-1, n)$ and $(m-1, n+1)$ the values of ϵ, v, x^{s_0}, y^{s_0}, z^{s_0}, x^t, y^t and z^t are known from previous computations or from initial conditions. The strain $\epsilon_{m,n}$ can be obtained in the following way. The magnitude of Δs_0 is conventiently chosen so that the string could be approximated by a segment of straight lines in the interval $(n-1)\,\Delta s_0 < s_0 < (n+1)\,\Delta s_0$. Therefore, in a first approximation, the equation (11) will be integrated on this segment, without taking into account the shape of the string. From (11) one obtains

$$\left.\begin{aligned} &c_{II}\left[\epsilon_{m,n} - \epsilon_{m,n-1}\right] - \left[v_{m,n} - v_{m,n-1}\right] + \\ &\qquad + \frac{1+\epsilon_{m,n-1}}{\rho_0} F_{m,n-1}\left[t_{m,n} - t_{m,n-1}\right] = 0, \\ &-c_{II}\left[\epsilon_{m,n} - \epsilon_{m-1,n+1}\right] - \left[v_{m,n} - v_{m-1,n+1}\right] + \\ &\qquad + \frac{1+\epsilon_{m-1,n+1}}{\rho_0} F_{m-1,n+1}\left[t_{m,n} - t_{m-1,n+1}\right] = 0. \end{aligned}\right\} \tag{22}$$

From (22) one obtains $\epsilon_{m,n}$ and $v_{m,n}$ in a first approximation. Taking into account the value found $\epsilon_{m,n}$ for the calculation of c_1, we can draw the characteristics (7) of positive and negative slope which pass through the vertex (m, n). Intersecting these characteristics with the vertical lines which pass through the vertices $(m, n-1)$ and $(m-1, n+1)$ respectively, we obtain the auxiliary vertices $\overline{m, n}$ and $\underline{m, n}$ respectively. By interpolation between the vertices $(m, n-1)$ and $(m-1, n-1)$ and between the vertices $(m-1, n+1)$ and $(m-2, n+1)$ respectively, one obtains $\epsilon_{\overline{m,n}}$, $\epsilon_{\underline{m,n}}$, $v_{\overline{m,n}}$, and $v_{\underline{m,n}}$ in a first approximation.

With the aid of the formula (13) we calculate now $\partial c_1{}^2/\partial s_0$ between the vertices (m, n) and $\overline{m, n}$ and between (m, n) and $\underline{m, n}$ respectively:

$$\left.\begin{aligned} &c_1(\epsilon_{m,n})\left[\epsilon_{m,n} - \epsilon_{\overline{m,n}}\right] - \left[v_{m,n} - v_{\overline{m,n}}\right] + \frac{1+\epsilon_{\overline{m,n}}}{\rho_0} F_{\overline{m,n}}\left[t_{m,n} - t_{\overline{m,n}}\right] = \\ &\qquad - \left[1+\epsilon_{\overline{m,n}}\right]\frac{\Delta c_1{}^2}{s_{0m,n} - s_{0\overline{m,n}}}\left[t_{m,n} - t_{\overline{m,n}}\right], \\ &-c_1(\epsilon_{m,n})\left[\epsilon_{m,n} - \epsilon_{\underline{m,n}}\right] - \left[v_{m,n} - v_{\underline{m,n}}\right] + \frac{1+\epsilon_{m,n}}{\rho_0} F_{\underline{m,n}}\left[t_{m,n} - t_{\underline{m,n}}\right] = \\ &\qquad - \left[1+\epsilon_{\underline{m,n}}\right]\frac{\Delta c_1{}^2}{s_{0m,n} - s_{0\underline{m,n}}}\left[t_{m,n} - t_{\underline{m,n}}\right]. \end{aligned}\right\} \tag{23}$$

In (23) instead of Δs_0 we have put $s_{0m,n} - s_{0\overline{m,n}}$ and $s_{0m,n} - s_{0\underline{m,n}}$ only in order to indicate between which vertices the respective variation of c_1^2 is considered. The two values $\partial c_1^2/\partial s_0$ given by (23) measure the variation of the velocity c_1 due to the extension of the string between the two considered vertices. Introducing these values in (9) one obtains

$$\left.\begin{aligned} x_{m,n}{}^{t} - x_{\overline{m,n}}{}^{t} &= c_1(\epsilon_{\overline{m,n}})\left[x_{m,n}{}^{s_0} - x_{\overline{m,n}}{}^{s_0}\right] - \\ &- \left(\frac{1+\epsilon_{\overline{m,n}}}{\rho_0} X_{\overline{m,n}} + x_{\overline{m,n}}{}^{s_0}\frac{\Delta c_1^2}{s_{0m,n} - s_{0\overline{m,n}}}\right)\left[t_{m,n} - t_{\overline{m,n}}\right], \\ x_{m,n}{}^{t} - x_{\underline{m,n}}{}^{t} &= -c_1(\epsilon_{\underline{m,n}})\left[x_{m,n}{}^{s_0} - x_{\underline{m,n}}{}^{s_0}\right] - \\ &- \left(\frac{1+\epsilon_{\underline{m,n}}}{\rho_0} X_{\underline{m,n}} + x_{\underline{m,n}}{}^{s_0}\frac{\Delta c_1^2}{s_{0m,n} - s_{0\underline{m,n}}}\right)\left[t_{m,n} - t_{\underline{m,n}}\right]. \end{aligned}\right\} \tag{24}$$

and similar formulae for y and z. The values $x_{m,n}{}^{s_0}$, $y_{m,n}{}^{s_0}$, $z_{m,n}{}^{s_0}$, $x_{m,n}{}^{t}$, $y_{m,n}{}^{t}$, and $z_{m,n}{}^{t}$ result from (24).

For a better approximation of the unknown functions in the vertex (m, n) we shall calculate $v_{m,n}$ in accordance with the formula (12) in two ways:

$$\left.\begin{aligned} v_{m,n} - v_{m,n-1} &= \frac{1}{1+\epsilon_{m,n-1}}\left\{x_{m,n-1}{}^{s_0}\left[x_{m,n}{}^{t} - x_{m,n-1}{}^{t}\right] + \right. \\ &\left. + y_{m,n-1}{}^{s_0}\left[y_{m,n}{}^{t} - y_{m,n-1}{}^{t}\right] + z_{m,n-1}{}^{s_0}\left[z_{m,n}{}^{t} - z_{m,n-1}{}^{t}\right]\right\}, \\ v_{m,n} - v_{m-1,n+1} &= \frac{1}{1+\epsilon_{m-1,n+1}}\left\{x_{m-1,n+1}{}^{s_0}\left[x_{m,n}{}^{t} - x_{m-1,n+1}{}^{t}\right] + \right. \\ &\left. + y_{m-1,n+1}{}^{s_0}\left[y_{m,n}{}^{t} - y_{m-1,n+1}{}^{t}\right] + z_{m-1,n+1}{}^{s_0}\left[z_{m,n}{}^{t} - z_{m-1,n+1}{}^{t}\right]\right\}. \end{aligned}\right\} \tag{25}$$

Taking the arithmetic mean of the two values $v_{m,n}$ which result from (25) we obtain, in a second approximation, the value of $v_{m,n}$. Introducing the differences $v_{m,n} - v_{m,n-1}$ and $v_{m,n} - v_{m-1,n+1}$ from (25) in (23), we obtain $\epsilon_{m,n}$ in a second approximation, making also the arithmetic mean. With this new value $\epsilon_{m,n}$, the computations are continued as before and $x_{m,n}{}^{s_0}$, $y_{m,n}{}^{s_0}$, $z_{m,n}{}^{s_0}$, $x_{m,n}{}^{t}$, $y_{m,n}{}^{t}$ and $z_{m,n}{}^{t}$ are obtained in a second approximation.

In this way the computations can be repeated several times, until the unknown functions in (m, n) are found with the needed approximation. If the intervals Δs_0 are chosen small, the computations must be repeated only a few times. A convenient choice of Δs_0 may cause the first approximation to be sufficient, the second approximation is used only for control, by estimating the error, and also for obtaining a more accurate value of $v_{m,n}$ necessary for the further computations. The value of F in (m, n) is obtained from (12):

$$F_{m,n} = \frac{1}{1+\epsilon_{m,n}}\left[X_{m,n}x_{m,n}{}^{s_0} + Y_{m,n}y_{m,n}{}^{s_0} + Z_{m,n}z_{m,n}{}^{s_0}\right]. \tag{26}$$

With $F_{m,n}$ from (26) and $v_{m,n}$ from (25) one can pass to the calculation in the following vertex $(m, n+1)$.

One proceeds similarly in the whole domain of the plane (s_0, t) where $c_{II} = \text{const}$. Then one considers the neighbouring domain where c_{II}, though constant, has another value corresponding to another portion on the curve (4) which can be approximated by a segment of a straight line.

(iii) *The shape of the string.* By the method indicated above one can obtain approximately the distribution of strain, velocities and slopes of the tangent to the string for every point and every moment of time (in vertices). To obtain the shape of the string at every moment, its shape is approximated by a funicular polygon, formed by the aid of some segments of straight lines. Thus, for a certain $t = \text{const.}$, the portion of the string $(n-1)\Delta s_0 < s_0 < (n+1)\Delta s_0$ included between two successive horizontal vertices, can be approximated by the straight line

$$\frac{x - x_{m,n-1}}{\frac{1}{2}\left(x_{m,n-1}{}^{2} + x_{m-1,n+1}{}^{2}\right)} = \frac{y - y_{m,n-1}}{\frac{1}{2}\left(y_{m,n-1}{}^{2} + y_{m-1,n+1}{}^{2}\right)} = \frac{z - z_{m,n-1}}{\frac{1}{2}\left(z_{m,n-1}{}^{2} + z_{m-1,n+1}{}^{2}\right)}. \tag{27}$$

In the calculations of the denominators from (27) the formulae (3) are also used. Since the position of the point $s_0 = 0$ is known at any moment from the boundary conditions, drawing successively the segments (27) starting from this point and arranging them one next to another, we obtain the shape of the string as a funicular polygon.

The error made by such an approximation to the shape of the string can be estimated. The funicular polygon is drawn from $s_0 = 0$ to the front of the first perturbation propagable in the string. If the approximation is good, the position of the string obtained with the aid of the funicular polygon and the position given by the initial conditions must coincide on this front. The eventual non-concordances can be removed by another choice of the intervals Δs_0 (smaller than before) or by the choice of another method for the approximation of the position of the string at a given moment: approximation by arcs of parabolas, approximation by other segments than those given by (27), etc.

For example, it is sometimes convenient to approximate the portion of the string $(n-1)\,\Delta s_0 < s_0 < (n+1)\,\Delta s_0$ by three segments of a straight line put next to each other. For that we divide the segment $2\,\Delta s_0$ in three equal parts. In the portion $(n-1)\,\Delta s_0 < s_0 < (n-1)\,\Delta s_0 + 2\,\Delta s_0/3$ the string will be approximated by the segment

$$\frac{x - x\left((n-1)\,\Delta s_0, t\right)}{x_{m,n-1}{}^{s}} = \frac{y - y\left((n-1)\,\Delta s_0, t\right)}{y_{m,n-1}{}^{s}} = \frac{z - z\left((n-1)\,\Delta s_0, t\right)}{z_{m,n-1}{}^{s}}. \tag{28}$$

In the portion $(n-1)\,\Delta s_0 + 2\,\Delta s_0/3 < s_0 < (n+1)\,\Delta s_0 - 2\,\Delta s_0/3$, the string will be approximated by the segment

$$\frac{x - x\left((n-1)\,\Delta s_0 + 2\Delta s_0/3, t\right)}{\tfrac{1}{2}\left(x_{m,n-1}{}^{s} + x_{m-1,n+1}{}^{s}\right)} = \frac{y - y\left((n-1)\,\Delta s_0 + 2\Delta s_0/3, t\right)}{\tfrac{1}{2}\left(y_{m,n-1}{}^{s} + y_{m-1,n+1}{}^{s}\right)} =$$

$$\frac{z - z\left((n-1)\,\Delta s_0 + 2\Delta s_0/3, t\right)}{\tfrac{1}{2}\left(z_{m,n-1}{}^{s} + z_{m-1,n+1}{}^{s}\right)}. \tag{29}$$

At last, in the portion $(n+1)\,\Delta s_0 - 2\,\Delta s_0/3 < s_0 < (n+1)\,\Delta s_0$, the string will be approximated by the segment

$$\frac{x - x\left((n-1)\,\Delta s_0 - 2\Delta s_0/3, t\right)}{x_{m-1,n+1}{}^{s}} = \frac{y - y\left((n+1)\,\Delta s_0 - 2\Delta s_0/3, t\right)}{y_{m-1,n+1}{}^{s}} =$$

$$\frac{z - z\left((n+1)\,\Delta s_0 - 2\Delta s_0/3, t\right)}{z_{m-1,n+1}{}^{s}}. \tag{30}$$

6. Some Observations

In the above considerations, as well as in Fig. 2 (b), one supposes that in the considered domain of the plane (s_0, t) the longitudinal waves propagate faster than the transverse ones. Therefore in Fig. (2) b the auxiliary vertices $\overline{m, n}$ and $m, \overline{n}$ are situated between the vertices $(m, n-1)$ and $(m-1, n-1)$ and $(m-1, n+1)$ and $(m-2, n+1)$ respectively. This is the most frequent situation in practice. If in some cases it happened that the transverse waves propagate faster than the longitudinal ones, the considerations are similar to those above with the difference that the auxiliary vertices $\overline{m, n}$ and $m, \overline{n}$ will be situated on a horizontal line between the vertices $(m+1, n-3)$ and $(m, n-1)$ and between $(m-1, n+1)$ and $(m-2, n+3)$ respectively. The computations are similar, except that they are made not between two lines of vertices but between two columns of vertices. The variation of c_1 due to the variation of ϵ will be calculated also with the aid of the formula (13) but written in the form

$$\pm c_I \, d\epsilon - dv + \frac{1+\epsilon}{\rho_0} F \, dt = \mp \frac{1+\epsilon}{c_I} \frac{\partial c_I^2}{\partial t}. \tag{31}$$

It is possible that, during a single experiment, all the three cases $c_I > c_{II}$, $c_I \simeq c_{II}$ and $c_I < c_{II}$ occur in different domains of the plane (s_0, t). In this case, in each of these domains one will proceed accordingly, using eventually the scheme of integration from Section 5 (i) too.

At last, it is possible that $c_I > c_{II}$ or $c_I < c_{II}$. If we refer to the former, this means that the helping vertices are no longer situated on the vertical which joins the vertices $(m, n-1)$ and $(m-1, n-1)$ and respectively $(m-1, n+1)$ and $(m-2, n+1)$. They can be situated on the vertical lines which join more distant vertices, for example between the vertices $(m-1, n-1)$, $(m-2, n-1)$ and $(m-2, n+1)$, $(m-3, n+1)$ respectively, or even between more distant vertices from the vertex (m, n) than these. Depending on the magnitude of the velocities c_I and c_{II}, as depending on the magnitude of the interval Δs_0, one can however specify, in either event, between which vertices (on the vertical or on the horizontal line) will be situated the auxiliary vertices. But all the details of the approximate solution must be established separately for each particular case, knowning the boundary conditions, the relation (4), etc.

If we consider a general situation, when the string was not rectilinear initially, even if due to the boundary conditions only one type of waves appears at the string end, it is necessary to start the computations as if both types of waves had appeared. This is because the second type of waves will appear gradually as the first type of wave propagates in the string which initially was not rectilinear. If, for example, the boundary conditions produce only the appearance of transverse waves, this means that at the string end $dv = 0$ and $F = 0$ in accordance with (12). However, quite soon, during the propagation one gets $dv \neq 0$ and $F \neq 0$. Therefore the string begins to become longer and in accordance with formula (13) the strain will begin to influence the transverse waves. If initially the string was homogeneous, up to those points of the string for which $dv = 0$, we shall put $d\epsilon = 0$ and $\partial c_I^2/\partial s_0 = 0$ in computations. If initially the string was non-homogeneous, then from the beginning $\partial c_I^2/\partial s_0 \neq 0$. In practice it is convenient to cnesider that the string, when it is homogeneous, possesses initially a certain deformation ; the transverse waves will then propagate from the beginning with a certain finite velocity. In this way one avoids at the beginning of the process of deformation very small values of c_I which are sometimes annoying in computations.

We shall also observe that if there are waves which appreciably modify the shape of the string or its extension, the above computations can be applied, but in that portion of the string where this sudden variation occurs the intervals Δs_0 must be chosen much smaller. Therefore the net of characteristics must be made denser in a certain strip of the plane (s_0, t). If, for example, the sudden modification refers to the shape of the string, the strip with the denser net will be chosen between two characteristics (7). The characteristics (7), fronts of transverse waves, can be drawn approximately, in the form of funicular polygon, after the solution is approximately obtained. These polygons are drawn with the aid of some segments of straight lines, portions of characteristics (7), their ends being always put on the vertical (or horizontal) line between two vertices of Fig. 2 (a).

If the impact is not applied at the same point s_0, but at a variable point, the

boundary conditions are given in a similar way, the same equations (9) and (10) being the basis of the solution. The restrictive conditions will enter when the striking body moves along the string with a velocity which is approximately of the same order of magnitude as the velocity of the waves propagable in the string. This problem will not be considered here. Also the problem of reflection of waves and the problem of transverse shock waves, in which the relation (10) gives the connexion between the sudden variation of the shape of the string and the sudden variation of the strain, will not be considered. The unloading problem, when during the decrease of the strain another relation (4) is used instead of that used during the loading, will be considered elsewhere.

Numerical computations along the lines described are now being carried out for various boundary and initial values, and different materials (characterized by a relation (4)).

REFERENCES

CRAGGS, J. W.	1954	*J. Mech. Phys. Solids* **2**, 286.
CRISTESCU, N.	1954	*Prikl. Mat. Mekh.* **18**, 237.
	1957	*Prikl. Mat. Mekh.* **21**, 486.
	1958	*Probleme Dinamice in Teoria Plasticităţii* (Editura Tehnică, Bucuresti).
	1960	*Arch. Mech. Stoss.* **12**, 564.
HILL, R.	1950	*The Mathematical Theory of Plasticity*, p. 148 (Clarendon Press, Oxford).
KELLER, J. B.	1959	*Amer. J. Phys.* **27**, 584.
MOROZ, G. S.	1957	*Prikl. Mat. Mekh.* **21**, 67.
PAVLENKO, A. L.	1959	*Izv. Akad. Nauk. SSSR, Otd. Tekh. Nauk, Mekh. Mash.* **4**, 112.
RAKHMATULIN, H. A.	1945a	*Prikl. Mat. Mekh.* **9**, 91.
	1945b	*Prikl. Mat. Mekh.* **9**, 449.
	1947	*Prikl. Mat. Mekh.* **11**, 379.
	1951	*Uch. zap. Mosk. gos. Univ.* 4.
RAKHMATULIN, H. A. and SHAPIRO, G. S.	1953	*Izv. Akad. Nauk. SSSR, otd. Tekh. Nauk* **2**, 68.
RYABOVA, E. V.	1953	*Vest. Moskovsk. Univ.* **10**, 85.
SMITH, J. C., MCCRACKIN, F. L., SCHIEFER, H. F., STONE, W. R. and TOWNE, K. M.	1956	*Textile Res. J.* **26**, 821.
SMITH, J. C., MCCRACKIN, F. L. and SCHIEFER, H. F.	1958	*Textile Res. J.* **28**, 288.
STEVENS, G. W. H.	1957	*Proc. Conf. on the Properties of Material at High Rates of Strain*, p. 209 (Inst. Mech. Engrs., London).

J. Mech. Phys. Solids, 1961, Vol. 9, pp. 179 to 190. Pergamon Press Ltd., London. Printed in Great Britain

PLANE THERMO-ELASTIC WAVES IN AN INITIALLY STRESSED MEDIUM

By J. N. Flavin and A. E. Green
King's College, Newcastle upon Tyne

(*Received 9th March*, 1961)

Summary

The propagation of plane thermo-elastic waves of small amplitude in an infinite body is studied, the body having been subjected to large uniform extensions, at constant temperature, in three perpendicular directions, two of the extension ratios being equal.

1. Introduction

We consider a homogeneous isotropic elastic body and suppose that it is deformed by uniform large extensions in three perpendicular directions, so that two of the extension ratios are equal, the body remaining at constant temperature. We then study the propagation of plane thermo-elastic waves of small amplitude in an infinite body which is pre-stressed in this way. During the course of this work the authors received a copy of an unpublished paper by Hayes and Rivlin (1960), who consider the propagation of plane waves in an isotropic elastic material subjected to pure homogeneous deformation. Their homogeneous deformation is more general than that considered in the present paper but they do not include thermal effects, so that there is little overlap with the work described here. We first consider a compressible medium. The incompressible medium can then be regarded as a limiting case, but it is found to be more convenient to study this from first principles.

2. Notation and Formulae

Let the points of an undeformed body referred to a rectangular cartesian system of coordinates be x_i and let the corresponding points of the deformed body be y_i referred to the same axes. When the body is initially isotropic the stress tensor σ_{ij} referred to these axes is given by

$$\sigma_{ij} = p\,\delta_{ij} + \Phi\,C_{ij} + \Psi(I_1\,C_{ij} - C_{ik}\,C_{kj}), \tag{2.1}$$

where

$$C_{ij} = \frac{\partial y_i}{\partial x_m}\frac{\partial y_j}{\partial x_m}, \tag{2.2}$$

$$\Phi = \frac{2}{\sqrt{I_3}}\frac{\partial W}{\partial I_1}, \qquad \Psi = \frac{2}{\sqrt{I_3}}\frac{\partial W}{\partial I_2}, \qquad p = 2\sqrt{I_3}\,\frac{\partial W}{\partial I_3}, \tag{2.3}$$

$$I_1 = C_{ii}, \qquad I_2 = \tfrac{1}{2}\,(C_{ii}\,C_{jj} - C_{ij}\,C_{ij}), \qquad I_3 = C = |C_{ij}|. \tag{2.4}$$

In (2.3) W is the Helmholtz function

$$W = W(I_1, I_2, I_3, T) \tag{2.5}$$

where T is temperature and I_i are the three invariants of C_{ij}. Cartesian tensor notation is used throughout.

When the body is incompressible,

$$I_3 = 1, \quad W = W(I_1, I_2, T), \tag{2.6}$$

and

$$\Phi = 2\,\frac{\partial W}{\partial I_1}, \qquad \Psi = 2\,\frac{\partial W}{\partial I_2}. \tag{2.7}$$

The stress tensor is still given by (2.1) but p is now an arbitrary scalar representing a hydrostatic tension.

If body forces are zero the equations of motion are

$$\frac{\partial \sigma_{ij}}{\partial y_i} = \rho f_j, \tag{2.8}$$

where f_j are components of acceleration and ρ, the density of the deformed body, is related to the (constant) density ρ_0 of the undeformed body by

$$\rho \sqrt{I_3} = \rho_0. \tag{2.9}$$

If R_i are the components of the heat conduction vector, per unit area of the deformed body, and S is the entropy, measured per unit volume of the undeformed body, then†

$$S = -\,\frac{\partial W}{\partial T}, \tag{2.10}$$

$$-\,T\,\frac{DS}{Dt} = \frac{\partial R_i}{\partial y_i}\sqrt{I_3}, \tag{2.11}$$

where D/Dt denotes differentiation with respect to t holding x_i fixed. When the body is initially isotropic

$$-\,R_i = (\mathscr{C}_1\,\delta_{ri} + \mathscr{C}_2\,C_{ri}^* + \mathscr{C}_3\,C_{rn}^*\,C_{si}^*)\,\frac{\partial T}{\partial y_r}$$

$$+\,e_{rsi}\,\frac{\partial T}{\partial y_m}\,\frac{\partial T}{\partial y_n}\,C_{ml}^*\,(\mathscr{C}_4\,\delta_{rn}\,\delta_{st} + \mathscr{C}_5\,\delta_{rn}\,C_{st}^* + \mathscr{C}_6\,C_{rn}^*\,C_{st}^*), \tag{2.12}$$

where e_{rsi} is the alternating Cartesian tensor, $\mathscr{C}_1, \ldots, \mathscr{C}_6$ are polynomials in the invariants

$$\left.\begin{aligned} &I_1, I_2, I_3, \frac{\partial T}{\partial y_i}\,\frac{\partial T}{\partial y_i}, \\ &\frac{\partial T}{\partial y_i}\,\frac{\partial T}{\partial y_j}\,C_{ij}^*, \qquad \frac{\partial T}{\partial y_i}\,\frac{\partial T}{\partial y_j}\,C_{jk}^*\,C_{ki}^*, \end{aligned}\right\} \tag{2.13}$$

†See GREEN and ADKINS (1960, Ch. VIII).

with coefficients which are continuous functions of T, and

$$C_{ij}^{*} = \tfrac{1}{2}(C_{ij} - \delta_{ij}). \tag{2.14}$$

Also

$$-R_i \frac{\partial T}{\partial y_i} \geqslant 0. \tag{2.15}$$

The change here to C_{ij}^{*}, defined by (2.14), is so that in the subsequent work the notation will agree with that used by ENGLAND and GREEN (1961) who considered thermo-static problems. There is, however, a formal difference between the present formula (2.12) for R_i and that given by GREEN and ADKINS (1960).

3. Small Deformation Superposed on Uniform Extension

We suppose that the body is deformed by uniform finite extensions with extension ratios (μ, μ, λ), and is held in equilibrium by suitable surface tractions, the temperature throughout the body remaining constant and equal to T. From Section 2 it follows that the stresses σ_{ij} are constants, the entropy S is constant and the components of the heat conduction vector R_i are zero. We now superpose a small deformation on this initial large deformation so that

$$y_1 = \mu x_1 + \epsilon u, \qquad y_2 = \mu x_2 + \epsilon v, \qquad y_3 = \lambda x_3 + \epsilon w, \tag{3.1}$$

with temperature distribution $T + \epsilon T'$, where $\epsilon\,(>0)$ is a small non-dimensional parameter and u, v, w, T' are functions of x_i. It is convenient to write

$$x = \mu x_1, \qquad y = \mu x_2, \qquad z = \lambda x_3, \tag{3.2}$$

so that (x, y, z) are the coordinates of points of the body after the initial large deformation and we regard (x, y, z) as independent variables instead of x_i. We now compute all quantities in Section 2 as far as terms in order ϵ and neglect terms containing powers of ϵ higher than the first.

From (2.2), (2.4), (3.1) and (3.2) we have

$$\left.\begin{aligned} C_{11} &= \mu^2 + 2\epsilon\,\mu^2 u_x, & C_{12} &= \epsilon\,\mu^2 (v_x + u_y),\\ C_{22} &= \mu^2 + 2\epsilon\,\mu^2 v_y, & C_{13} &= \epsilon\,(\mu^2 w_x + \lambda^2 u_z),\\ C_{33} &= \lambda^2 + 2\epsilon\,\lambda^2 w_z, & C_{23} &= \epsilon\,(\mu^2 w_y + \lambda^2 v_z), \end{aligned}\right\} \tag{3.3}$$

and

$$\left.\begin{aligned} I_1 &= (2\mu^2 + \lambda^2) + 2\epsilon\left[\mu^2 (u_x + v_y) + \lambda^2 w_z\right],\\ I_2 &= 2\mu^2\lambda^2 + \mu^4 + 2\epsilon\left[\mu^2 (\mu^2 + \lambda^2)(u_x + v_y) + 2\lambda^2 \mu^2 w_z\right],\\ I_3 &= \mu^4 \lambda^2 + 2\epsilon\,\mu^4 \lambda^2 (u_x + v_y + w_z), \end{aligned}\right\} \tag{3.4}$$

suffices denoting partial differentiation. Also, when the displacements are given by (3.1) and (3.2),

$$\frac{2}{\sqrt{I_3}}\frac{\partial W}{\partial I_1} = \Phi - \epsilon\,\Phi (u_x + v_y + w_z) + \epsilon\,L\,T' + 2\epsilon\,\{A\left[\mu^2 (u_x + v_y) + \lambda^2 w_z\right]$$
$$+ F\left[\mu^2 (\mu^2 + \lambda^2)(u_x + v_y) + 2\lambda^2 \mu^2 w_z\right] + \mu^4 \lambda^2 E (u_x + v_y + w_z)\}, \tag{3.5}$$

$$\frac{2}{\sqrt{I_3}}\frac{\partial W}{\partial I_2} = \Psi - \epsilon\,\Psi (u_x + v_y + w_z) + \epsilon\,M\,T' + 2\epsilon\,\{F\left[\mu^2 (u_x + v_y) + \lambda^2 w_z\right]$$
$$+ B\left[\mu^2 (\mu^2 + \lambda^2)(u_x + v_y) + 2\lambda^2 \mu^2 w_z\right] + \mu^4 \lambda^2 D (u_x + v_y + w_z)\}, \tag{3.6}$$

$$2\sqrt{I_3}\frac{\partial W}{\partial I_3} = p + \epsilon p (u_x + v_y + w_z) + \epsilon\,N\,\mu^4 \lambda^2 T' + 2\epsilon\,\mu^4 \lambda^2 \{E\left[\mu^2 (u_x + v_y) + \lambda^2 w_z\right]$$

$$+ D\left[\mu^2(\mu^2+\lambda^2)(u_x+v_y)+2\lambda^2\mu^2 w_z\right]+C\mu^4\lambda^2(u_x+v_y+w_z)\},\tag{3.7}$$

where

$$\left.\begin{aligned} A &= \frac{2}{\sqrt{I_3}}\frac{\partial^2 W}{\partial I_1^2}, \qquad B = \frac{2}{\sqrt{I_3}}\frac{\partial^2 W}{\partial I_2^2}, \qquad C = \frac{2}{\sqrt{I_3}}\frac{\partial^2 W}{\partial I_3^2},\\ D &= \frac{2}{\sqrt{I_3}}\frac{\partial^2 W}{\partial I_2\,\partial I_3}, \qquad E = \frac{2}{\sqrt{I_3}}\frac{\partial^2 W}{\partial I_3\,\partial I_1}, \qquad F = \frac{2}{\sqrt{I_3}}\frac{\partial^2 W}{\partial I_1\,\partial I_2},\\ L &= \frac{2}{\sqrt{I_3}}\frac{\partial^2 W}{\partial T\,\partial I_1}, \qquad M = \frac{2}{\sqrt{I_3}}\frac{\partial^2 W}{\partial T\,\partial I_2}, \qquad N = \frac{2}{\sqrt{I_3}}\frac{\partial^2 W}{\partial T\,\partial I_3}, \end{aligned}\right\}\tag{3.8}$$

and Φ, Ψ, p are given by (2.3). All derivatives in (2.3) and (3.8) are evaluated at $\epsilon = 0$ and are therefore constants in the present analysis. The components of stress may now be found from (2.1) and (3.4)–(3.8). Denoting these by $\sigma_{ij} + \epsilon\,\sigma'_{ij}$ we have

$$\left.\begin{aligned} \sigma_{11} &= \sigma_{22} = p + \mu^2\Phi + \mu^2(\mu^2+\lambda^2)\Psi,\\ \sigma_{33} &= p + \lambda^2\Phi + 2\mu^2\lambda^2\Psi, \end{aligned}\right\}\tag{3.9}$$

$$\left.\begin{aligned} \sigma'_{11} &= d_{11}u_x + d_{12}v_y + d_{13}w_z + \omega_1 T',\\ \sigma'_{22} &= d_{12}u_x + d_{11}v_y + d_{13}w_z + \omega_1 T',\\ \sigma'_{33} &= d_{31}(u_x+v_y) + d_{33}w_z + \omega_3 T', \end{aligned}\right\}\tag{3.10}$$

$$\left.\begin{aligned} \sigma'_{12} &= \tfrac{1}{2}(d_{11}-d_{12})(u_y+v_x),\\ \sigma'_{13} &= d_{44}u_z + d_{55}w_x,\\ \sigma'_{23} &= d_{44}v_z + d_{55}w_y, \end{aligned}\right\}\tag{3.11}$$

where

$$d_{11} = \sigma_{11} + 2\mu^4\{A + B(\lambda^2+\mu^2)^2 + C\lambda^4\mu^4 + 2D\lambda^2\mu^2(\lambda^2+\mu^2) + 2E\lambda^2\mu^2 + 2F(\lambda^2+\mu^2)\},\tag{3.12}$$

$$d_{12} = -\Phi\mu^2 + \Psi\mu^2(\mu^2-\lambda^2) + p + 2\mu^4\{A + B(\mu^2+\lambda^2)^2 + C\lambda^4\mu^4 + 2D\lambda^2\mu^2(\lambda^2+\mu^2) + 2E\lambda^2\mu^2 + 2F(\lambda^2+\mu^2)\},\tag{3.13}$$

$$d_{13} = -\Phi\mu^2 + \Psi\mu^2(\mu^2-\lambda^2) + p + 2\lambda^2\mu^2\{A + B\mu^2(\mu^2+\lambda^2) + C\lambda^2\mu^6 + D\mu^4(3\lambda^2+\mu^2) + E\mu^2(\lambda^2+\mu^2) + F(\lambda^2+3\mu^2)\},\tag{3.14}$$

$$d_{33} = \sigma_{33} + 2\lambda^4\{A + 4B\mu^4 + C\mu^8 + 4D\mu^6 + 2E\mu^4 + 4F\mu^2\},\tag{3.15}$$

$$\left.\begin{aligned} d_{11} - d_{12} &= 2\mu^2(\Phi + \Psi\lambda^2),\\ d_{44} &= \lambda^2(\Phi + \Psi\mu^2),\\ d_{55} &= \mu^2(\Phi + \Psi\mu^2),\\ d_{31} - d_{13} &= d_{55} - d_{44} = \sigma_{11} - \sigma_{33}, \end{aligned}\right\}\tag{3.16}$$

and

$$\left.\begin{aligned} \omega_1 &= L\mu^2 + M\mu^2(\mu^2+\lambda^2) + N\mu^4\lambda^2,\\ \omega_3 &= L\lambda^2 + 2M\mu^2\lambda^2 + N\mu^4\lambda^2. \end{aligned}\right\}\tag{3.17}$$

From (2.12), (2.13), (2.14) and (3.1) to (3.4) it follows that

$$-R_1 = \epsilon\,r_1 T'_x, \qquad -R_2 = \epsilon\,r_1 T'_y, \qquad -R_3 = \epsilon\,r_3 T'_z,\tag{3.18}$$

where

$$\left.\begin{aligned} r_1 &= \mathscr{C}_1 + \tfrac{1}{2}\mathscr{C}_2(\mu^2-1) + \tfrac{1}{4}\mathscr{C}_3(\mu^2-1)^2,\\ r_3 &= \mathscr{C}_1 + \tfrac{1}{2}\mathscr{C}_2(\lambda^2-1) + \tfrac{1}{4}\mathscr{C}_3(\lambda^2-1)^2, \end{aligned}\right\}\tag{3.19}$$

$\mathscr{C}_1$, $\mathscr{C}_2$, $\mathscr{C}_3$ now being constants, so that r_1, r_3 are constants. Equation (2.15) then gives $r_1 \geqslant 0$, $r_3 \geqslant 0$. Finally, denoting the entropy by $S + \epsilon S'$, we see from (2.10), (2.11) and the formulae of the present Section that

$$S' = -\frac{\partial^2 W}{\partial T^2} T' - \mu^2 \lambda \left[\omega_1 (u_x + v_y) + \omega_3 w_z\right], \tag{3.20}$$

and

$$-\epsilon T \frac{\partial S'}{\partial t} = \mu^2 \lambda \left[\frac{\partial R_1}{\partial x} + \frac{\partial R_2}{\partial y} + \frac{\partial R_3}{\partial z}\right], \tag{3.21}$$

where $\partial/\partial t$ is partial differentiation with respect to t holding x, y, z fixed. In (3.20) $\partial^2 W/\partial T^2$ is evaluated at $\epsilon = 0$ and is therefore a constant. Eliminating S' from (3.20) and (3.21), and using (3.18), yields

$$r_1 \nabla_1^2 T' + r_3 T'_{zz} + T\left[\omega_1 (u_{xt} + v_{yt}) + \omega_3 w_{zt}\right] - mT'_t = 0, \tag{3.22}$$

where

$$m = -\frac{T}{\lambda\mu^2}\frac{\partial^2 W}{\partial T^2}, \qquad \nabla_1^2 T' = T'_{xx} + T'_{yy}, \tag{3.23}$$

and suffices again denote differentiation. The equations of the present Section reduce to those given by England and Green (1961) when conditions are steady so that time derivatives are zero.

The equations of motion follow from (2.8) and (2.9) if we recall that the stresses (3.9) are constants. Thus

$$\left.\begin{aligned} \frac{\partial \sigma'_{11}}{\partial x} + \frac{\partial \sigma'_{12}}{\partial y} + \frac{\partial \sigma'_{13}}{\partial z} &= \rho \frac{\partial^2 u}{\partial t^2}, \\ \frac{\partial \sigma'_{12}}{\partial x} + \frac{\partial \sigma'_{22}}{\partial y} + \frac{\partial \sigma'_{23}}{\partial z} &= \rho \frac{\partial^2 v}{\partial t^2}, \\ \frac{\partial \sigma'_{13}}{\partial x} + \frac{\partial \sigma'_{23}}{\partial y} + \frac{\partial \sigma'_{33}}{\partial z} &= \rho \frac{\partial^2 w}{\partial t^2}, \end{aligned}\right\} \tag{3.24}$$

where ρ now denotes the density of the body after the initial large deformation, so that

$$\rho = \rho_0/(\lambda^2 \mu). \tag{3.25}$$

When the body is incompressible some simplification occurs in the above theory and we record the final formulae which can be obtained by straightforward analysis from Sections 2 and 3, with the extra conditions

$$\lambda\mu^2 = 1, \qquad u_x + v_y + w_z = 0. \tag{3.26}$$

Formulae (3.9) still hold, except that Φ and Ψ are now given by (2.7), evaluated at $\epsilon = 0$, and p is an arbitrary function. Equations (3.10) are replaced by

$$\left.\begin{aligned} \sigma'_{11} &= p' + a u_x + b v_y + \omega_1 T', \\ \sigma'_{22} &= p' + b u_x + a v_y + \omega_1 T', \\ \sigma'_{33} &= p' + c w_z + \omega_3 T', \end{aligned}\right\} \tag{3.27}$$

where

$$\left.\begin{aligned} a &= 2\mu^2(\Phi + \mu^2 \Psi) + 2\mu^2(\mu^2 - \lambda^2)\left[A + B\mu^2(\mu^2 + \lambda^2) + F(2\mu^2 + \lambda^2)\right], \\ b &= 2\mu^2(\mu^2 - \lambda^2)\left[\Psi + A + B\mu^2(\mu^2 + \lambda^2) + F(2\mu^2 + \lambda^2)\right], \\ c &= 2\lambda^2(\Phi + \mu^2 \Psi) + 2\lambda^2(\lambda^2 - \mu^2)(A + 2B\mu^4 + 3F\mu^2), \\ \omega_1 &= L\mu^2 + M\mu^2(\mu^2 + \lambda^2), \qquad \omega_3 = L\lambda^2 + 2M\mu^2\lambda^2, \\ a - b &= 2\mu^2(\Phi + \lambda^2 \Psi). \end{aligned}\right\} \tag{3.28}$$

In (3.28), A, B, F are evaluated from (3.8) using $I_3 = 1$. The components σ'_{12}, σ'_{23}, σ'_{13} of the stress tensor are still given by (3.11) and (3.16). Equation (3.22) still holds although it can be simplified with the help of (3.26).

4. Plane Waves in a Compressible Body

The basic differential equations for our problem are given by (3.22) and (3.24), where the stress components σ'_{ij} are found from (3.10) and (3.11). It is convenient to use the notation*

$$\Lambda = u_x + v_y, \qquad \Omega = u_y - v_x, \qquad \Gamma = w_z. \tag{4.1}$$

The basic equations then take the form

$$\mu^2 (\Phi + \Psi \lambda^2) \nabla_1^2 \Omega + \lambda^2 (\Phi + \Psi \mu^2) \Omega_{zz} - \rho \Omega_{tt} = 0, \tag{4.2}$$

$$r_1 \nabla_1^2 T' + r_3 T'_{zz} + T (\omega_1 \Lambda_t + \omega_3 \Gamma_t) - m T'_t = 0, \tag{4.3}$$

$$d_{11} \nabla_1^2 \Lambda + d_{44} \Lambda_{zz} - \rho \Lambda_{tt} + (d_{13} + d_{55}) \nabla_1^2 \Gamma + \omega_1 \nabla_1^2 T' = 0, \tag{4.4}$$

$$d_{55} \nabla_1^2 \Gamma + d_{33} \Gamma_{zz} - \rho \Gamma_{tt} + (d_{13} + d_{55}) \Lambda_{zz} + \omega_3 T'_{zz} = 0. \tag{4.5}$$

The equation for Ω is independent of the other equations and can be considered separately. We put

$$\Omega = \Omega_0 \exp \{i [\eta (l_1 x + l_2 y + l_3 z) - \omega t]\} \tag{4.6}$$

which represents a plane wave. Since (x, y, z) are coordinates of points of the body after the initial large deformation, l_i are direction cosines of the wave normal referred to this deformed state. The wave velocity v_2 is given by

$$v_2^2 = \omega^2/\eta^2. \tag{4.7}$$

If we substitute (4.6) into (4.2) and use (4.7) we find that

$$\begin{aligned} v_2^2 &= [\Phi \{\mu^2 (1 - l^2) + \lambda^2 l^2\} + \Psi \lambda^2 \mu^2]/\rho \\ &= [\Phi \{\mu^2 (1 - l^2) + \lambda^2 l^2\} + \Psi \lambda^2 \mu^2] \lambda \mu^2/\rho_0, \end{aligned} \tag{4.8}$$

where

$$l_1^2 + l_2^2 + l_3^2 = 1, \qquad l \equiv l_3. \tag{4.9}$$

This represents a transverse wave transmitted under isothermal conditions, with vibrations in planes parallel to the (x, y) plane.

When the initial deformation is zero,

$$\lambda = \mu = 1, \qquad \Phi + \Psi \to \mu', \tag{4.10}$$

where μ' is the second Lamé constant. Equation (4.8) then reduces to

$$v_2^2 \to \mu'/\rho_0, \tag{4.11}$$

the usual result for transverse waves.

We now consider the remaining equations (4.3)–(4.5). Guided by the work of England and Green (1961) for thermostatic problems for the whole space, and for the half space, we put†

*A similar technique has been used by Buchwald (1959) in discussing wave propagation in transversely isotropic bodies in classical elasticity.

†These satisfy the condition that $\Omega = 0$ here.

$$u = \frac{\partial}{\partial x}(x_1 + x_2), \qquad v = \frac{\partial}{\partial y}(x_1 + x_2), \qquad w = \frac{\partial}{\partial z}(k_1 x_1 + k_2 x_2), \tag{4.12}$$

where ν_1, ν_2 are roots of the equation

$$d_{11} d_{55} \nu^2 + \{(d_{13} + d_{55})^2 - d_{11} d_{33} - d_{44} d_{55}\} \nu + d_{33} d_{44} = 0, \tag{4.13}$$

and k_1, k_2 are corresponding values of k given by

$$\frac{d_{11}\nu - d_{44}}{d_{13} + d_{55}} = \frac{(d_{13} + d_{55})\nu}{d_{33} - d_{55}\nu} = k. \tag{4.14}$$

For later use we observe that

$$\left.\begin{aligned} \frac{d_{44}}{d_{55}} &= k_1 k_2, \qquad \frac{d_{33} d_{44}}{d_{11} d_{55}} = \nu_1 \nu_2, \\ d_{11}\left(\frac{\nu_1}{k_1} - \frac{\nu_2}{k_2}\right) &= d_{55}(k_2 - k_1) = \frac{d_{11} d_{55}(\nu_2 - \nu_1)}{d_{13} + d_{55}}, \\ 2(d_{13} + d_{55}) &= d_{11}\left(\frac{\nu_1}{k_1} + \frac{\nu_2}{k_2}\right) - d_{55}(k_1 + k_2), \end{aligned}\right\} \tag{4.15}$$

and, for the present, we assume that ν_1, ν_2 are distinct (but not necessarily real). Using (4.12), equations (4.3)–(4.5) can, without loss of generality, be satisfied if

$$d_{11}\left(\nabla_1^2 + \nu_1 \frac{\partial^2}{\partial z^2}\right) x_1 - \rho \frac{\partial^2 x_1}{\partial t^2} + d_{11}\left(\nabla_1^2 + \nu_2 \frac{\partial^2}{\partial z^2}\right) x_2 - \\ - \rho \frac{\partial^2 x_2}{\partial t^2} + \omega_1 T' = 0, \tag{4.16}$$

$$\frac{\nu_2 d_{11}}{k_2}\left(\nabla_1^2 + \nu_1 \frac{\partial^2}{\partial z^2}\right) x_1 - \rho k_1 \frac{\partial^2 x_1}{\partial t^2} + \\ + \frac{\nu_1 d_{11}}{k_1}\left(\nabla_1^2 + \nu_2 \frac{\partial^2}{\partial z^2}\right) x_2 - \rho k_2 \frac{\partial^2 x_2}{\partial t^2} + \omega_3 T' = 0, \tag{4.17}$$

$$T \frac{\partial}{\partial t}\left[\left(\omega_1 \nabla_1^2 + \omega_3 k_1 \frac{\partial^2}{\partial z^2}\right) x_1 + \left(\omega_1 \nabla_1^2 + \omega_3 k_2 \frac{\partial^2}{\partial z^2}\right) x_2\right] \\ + r_1 \nabla_1^2 T' + r_3 \frac{\partial^2 T'}{\partial z^2} - m \frac{\partial T'}{\partial t} = 0. \tag{4.18}$$

Plane wave solutions of these equations in which x_1, x_2, T' are proportional to

$$\exp i\,[\eta(l_1 x + l_2 y + l_3 z) - \omega t] \tag{4.19}$$

are found in the usual way. If we put

$$\left.\begin{aligned} \omega^* &= m v_1^2 / r_1, \qquad \rho v_1^2 = d_{11}, \\ \theta &= \omega/\omega^*, \qquad \xi = v_1 \eta/\omega^*, \\ g_1 &= \omega_1/m, \qquad g_3 = \omega_3/m, \qquad h = Tm/d_{11}, \qquad n^2 = r_3/r_1, \end{aligned}\right\} \tag{4.20}$$

the condition for plane waves can be put in the form

$$\begin{vmatrix} P\,\xi^2 - \theta^2 & Q\,\xi^2 - \theta^2 & -g_1 \\ \dfrac{\nu_2 P\,\xi^2}{k_2} - k_1\theta^2 & \dfrac{\nu_1 Q\,\xi^2}{k_1} - k_2\theta^2 & -g_3 \\ -ih\xi^2\theta\left[g_1(1-l^2)+g_3 k_1 l^2\right] & -ih\xi^2\theta\left[g_1(1-l^2)+g_3 k_2 l^2\right] & R\xi^2 - i\theta \end{vmatrix} = 0, \tag{4.21}$$

where

$$P = 1 - l^2 + \nu_1 l^2, \qquad Q = 1 - l^2 + \nu_2 l^2, \qquad R = 1 - l^2 + n^2 l^2. \tag{4.22}$$

We examine the roots of (4.21) when $\theta \ll 1$. A straightforward calculation shows that one root is given by

$$\xi^2 = \frac{i}{R}(1+\alpha)\,\theta + O(\theta^2), \tag{4.23}$$

where

$$\alpha = \frac{h}{PQ}\left[l^2(1-l^2)\left(g_3 - \frac{\nu_1 g_1}{k_1}\right)\left(g_3 - \frac{\nu_2 g_1}{k_2}\right)\frac{d_{11}}{d_{55}} + \left\{g_1(1-l^2) + l^2 k_1 g_3\right\}\left\{g_1(1-l^2) + l^2 k_2 g_3\right\}\right], \tag{4.24}$$

and the remaining roots by

$$\xi^2 = \beta\,\theta^2 + O(\theta^3), \tag{4.25}$$

where

$$PQ(1+\alpha)\beta^2 - \left[1 - l^2(1 - k_1 k_2) + \frac{d_{11}}{d_{55}}\left\{(1+hg_1^2)(1-l^2) + \left(\frac{\nu_1\nu_2}{k_1 k_2} + hg_3^2\right)l^2\right\}\right]\beta + \frac{d_{11}}{d_{55}} = 0. \tag{4.26}$$

We observe that PQ is always real and $R > 0$.

In order to understand the meaning of (4.23) and (4.25) it is useful to see what happens in the limiting case of no initial finite deformation, when

$$\left.\begin{aligned} &\lambda \to \mu \to 1, \qquad d_{11} \to \lambda' + 2\mu', \qquad d_{55} \to \mu', \\ &k_1 \to k_2 \to 1, \qquad \nu_1 \to \nu_2 \to 1, \qquad g_1 \to g_3, \end{aligned}\right\} \tag{4.27}$$

λ', μ' being the Lamé constants of classical elasticity. It follows that $\alpha \to hg_1^2$ and the value of ξ^2 given by (4.23) reduces to

$$\xi^2 = i(1+hg_1^2)\,\theta + O(\theta^2). \tag{4.28}$$

Apart from notation this corresponds to what Chadwick (1960) called the quasi-thermal mode. It is therefore convenient to call the mode corresponding to (4.23) the quasi-thermal mode when there is an initial finite deformation. In general such a wave is dispersed, attenuated and modified.

Again, applying conditions (4.27) to (4.26) we find that the quadratic equation for β factorizes and gives

$$\beta = \frac{1}{1+hg_1^2} \qquad \text{or} \qquad \beta = \frac{\lambda' + 2\mu'}{\mu'}. \tag{4.29}$$

Hence, from (4.20), (4.25) and (4.29) we have

$$\frac{\omega}{\eta} = (1 + hg_1^2)^{\frac{1}{2}} \left(\frac{\lambda' + 2\mu'}{\rho}\right)^{\frac{1}{2}} \quad \text{or} \quad \left(\frac{\mu'}{\rho}\right)^{\frac{1}{2}} \tag{4.30}$$

neglecting $O(\omega/\omega^*)$. The first of these results corresponds to that given by CHADWICK and is the usual velocity of longitudinal waves obtained under the assumption of isentropic motion. The second result is the ordinary velocity of transverse waves. When there is an initial finite deformation we can show that plane wave motion under the assumption that the extra entropy S' in (3.20) is zero, leads to

$$\xi^2 = \beta\theta^2, \tag{4.31}$$

where β satisfies the equation (4.26). Thus, provided terms of $O(\theta^3)$ are neglected in (4.25), we obtain, in general, two waves under isentropic conditions. One of these waves is a modification of the classical longitudinal wave, and the other is a modification of the classical transverse wave. When terms of $O(\theta^3)$ are retained both waves are dispersed, attenuated and modified. The three waves corresponding to (4.23) and (4.25) are such that the particles vibrate in planes parallel to a plane containing the z-axis and the wave normal.

We return to the exact equation (4.21) and examine two special cases in which the results simplify. When the wave is propagated in the direction of the z-axis, $l = 1$, and (4.21) has an exact solution

$$\xi^2 = \theta^2 d_{11}/d_{44} \tag{4.32}$$

which corresponds to a transverse wave propagated with velocity

$$(d_{44}/\rho)^{\frac{1}{2}} = \left[\lambda^2(\Phi + \Psi\mu^2)/\rho\right]^{\frac{1}{2}} \tag{4.33}$$

without change in temperature. This velocity coincides with that given by (4.8) when $l = 1$. Difficulty, however, arises in finding the displacements from (4.16) to (4.18) and it is necessary to return to the basic differential equations in terms of (u, v, w) in order to obtain them. The remaining roots of (4.21), when $l = 1$, are

$$\xi^2 = \frac{\theta^2}{d_{33}/d_{11} + hg_3^2} + O(\theta^3), \tag{4.34}$$

and

$$\xi^2 = \frac{i}{\mu^2}\left(1 + \frac{h\, d_{11}\, g_3^2}{d_{33}}\right)\theta + O(\theta^2). \tag{4.35}$$

If the wave is propagated in planes parallel to the (x, y) plane then $l = 0$ and (4.21) has the exact solution

$$\xi^2 = \theta^2 d_{11}/d_{55}. \tag{4.36}$$

The corresponding wave velocity is

$$(d_{55}/\rho)^{\frac{1}{2}} = \left[\mu^2(\Phi + \Psi\mu^2)/\rho\right]^{\frac{1}{2}} \tag{4.37}$$

and the wave is propagated without change in temperature. Again there is difficulty in finding the actual displacements from (4.16) to (4.18) and to obtain these we return to the basic differential equations in terms of displacements. This wave

is a transverse wave and the particles vibrate in planes perpendicular to the (x, y) plane. In contrast, the transverse wave velocity given by (4.8) is, when $l = 0$, equal to

$$\left[\mu^2 (\Phi + \Psi \lambda^2)/\rho\right]^{\frac{1}{2}}, \tag{4.38}$$

and the vibrations are in planes parallel to the (x, y) plane (and perpendicular to the wave normal). The remaining roots of (4.21), when $l = 0$, are

$$\xi^2 = \frac{\theta^2}{1 + h g_1^2} + O(\theta^3), \tag{4.39}$$

and

$$\xi^2 = i (1 + h g_1^2)\, \theta + O(\theta^2). \tag{4.40}$$

Results for an incompressible body may be found from the above results by a limiting process but we obtain them otherwise in the next Section.

5. Plane Waves in an Incompressible Body

When the body is incompressible

$$\lambda \mu^2 = 1, \qquad \rho = \rho_0, \qquad A + \Gamma = 0, \tag{5.1}$$

where A, Γ are given by (4.1). Using the work of Section 3 we see that equations (4.2)–(4.5) are replaced by

$$\mu^2 (\Phi + \Psi \lambda^2) \nabla_1^2 \Omega + \lambda^2 (\Phi + \Psi \mu^2) \Omega_{zz} - \rho \Omega_{tt} = 0, \tag{5.2}$$

$$r_1 \nabla_1^2 T' + r_3 T'_{zz} + T (\omega_3 - \omega_1) \Gamma_t - m T'_t = 0, \tag{5.3}$$

$$(d_{55} - a) \nabla_1^2 \Gamma - d_{44} \Gamma_{zz} + \rho \Gamma_{tt} + \nabla_1^2 (p' + \omega_1 T') = 0, \tag{5.4}$$

$$d_{55} \nabla_1^2 \Gamma + (c - d_{44}) \Gamma_{zz} - \rho \Gamma_{tt} + (p' + \omega_3 T')_{zz} = 0. \tag{5.5}$$

The equation for Ω is the same as that for a compressible body, except that $\lambda \mu^2 = 1$ and Φ, Ψ are evaluated from (2.7) when $\epsilon = 0$. It follows that there are plane transverse waves, propagated under isothermal conditions, with velocity v_2 still given by (4.8). In particular, in a Mooney material for which

$$\left.\begin{aligned} W &= C_1 (I_1 - 3) + C_2 (I_2 - 3), \\ C_1 &= c_1 T, \qquad C_2 = c_2 T, \end{aligned}\right\} \tag{5.6}$$

c_1, c_2 being constants, it follows that

$$v_2^2 = 2 \left[C_1 \{(1 - l^2)/\lambda + \lambda^2 l^2\} + C_2 \lambda\right]/\rho_0. \tag{5.7}$$

If v_S is the classical velocity of transverse waves then

$$v_S^2 = 2 (C_1 + C_2)/\rho_0,$$

so that

$$\frac{v_2^2}{v_S^2} = \frac{C_1 \{(1 - l^2)/\lambda + \lambda^2 l^2\} + C_2 \lambda}{C_1 + C_2}, \tag{5.8}$$

For the neo-Hookean material in which $C_2 = 0$ this result reduces to

$$\frac{v_2^2}{v_S^2} = (1 - l^2)/\lambda + \lambda^2 l^2. \tag{5.9}$$

Plane wave solutions of the remaining equations (5.3)–(5.5) may be obtained in the usual way by assuming that Γ, p' and T' have the form (4.19) apart from multiplying constants. Here it is convenient to introduce the notation

$$\left.\begin{aligned} &\omega^* = mv_3^2/r_1, \qquad \rho v_3^2 = d_{55}, \\ &\theta = \omega/\omega^*, \qquad \xi = v_3\,\eta/\omega^*, \\ &g_1 = \omega_1/m, \qquad g_3 = \omega_3/m, \qquad h = Tm/d_{55}, \qquad n^2 = r_3/r_1. \end{aligned}\right\} \tag{5.10}$$

Plane wave solutions are then possible provided

$$\begin{vmatrix} \dfrac{\xi^2}{d_{55}}\left[(d_{55}-a)(1-l^2) - d_{44}\,l^2\right] + \theta^2 & (1-l^2)\,\xi^2 & g_1(1-l^2)\,\xi^2 \\ \dfrac{\xi^2}{d_{55}}\left[d_{55}(1-l^2) + (c-d_{44})\,l^2\right] - \theta^2 & l^2\,\xi^2 & g_3\,l^2\,\xi^2 \\ ih(g_3-g_1)\,\theta & 0 & \xi^2(1-l^2+n^2\,l^2) - i\theta \end{vmatrix} = 0.$$

With the help of (3.16) and (3.28) this can be reduced to $\xi = 0$ and to the equation

$$(J\,\xi^2 - \theta^2)(R\,\xi^2 - i\theta) - i\,\delta\,\xi^2\,\theta = 0, \tag{5.11}$$

where R is given by (4.22) and

$$\left.\begin{aligned} J &= 1 + (\lambda^3 - 1)\,l^2 + \frac{2l^2(1-l^2)(\lambda^2 - 1/\lambda)^2(A\lambda + B/\lambda + 2F)}{\Phi + \Psi/\lambda}, \\ \delta &= \frac{l^2(1-l^2)\,T\lambda(\lambda^2 - 1/\lambda)^2(L + M/\lambda)^2}{m(\Phi + \Psi/\lambda)}. \end{aligned}\right\} \tag{5.12}$$

We observe that mechanical and thermal effects are uncoupled when $\delta = 0$, i.e. when $\lambda = 1$ or when $l = 0$ or 1.

As expected, one wave velocity (corresponding to $\xi = 0$) is infinite. The remaining velocities can be found from (5.11) without difficulty. As in Section 4 we consider roots of (5.11) for small values of θ and we find

$$\xi^2 = \frac{i(J+\delta)}{RJ}\,\theta + O(\theta^2), \tag{5.13}$$

or

$$\xi^2 = \frac{\theta^2}{J+\delta} + O(\theta^3). \tag{5.14}$$

In general the modes corresponding to (5.13) and (5.14) are dispersed attenuated and modified. The result (5.13) is similar in character to (4.28) and the corresponding mode can be called quasi-thermal. If we retain only the first term in (5.14) and use (5.10), we have

$$\frac{\omega}{\eta} = v_3(J+\delta)^{\frac{1}{2}} = \{d_{55}(J+\delta)/\rho\}^{\frac{1}{2}}. \tag{5.15}$$

When there is no initial deformation this result reduces to

$$\frac{\omega}{\eta} = \left(\frac{\mu'}{\rho}\right)^{\frac{1}{2}}, \tag{5.16}$$

the usual velocity of transverse waves. If we consider wave motion under isentropic conditions in which the perturbed entropy S' is zero we recover the wave velocity (5.15).

When the wave is propagated in the direction of the z-axis, $l = 1$, and (5.11) has exact solutions

$$\xi^2 = \frac{\theta^2}{\lambda^3}, \qquad \xi^2 = \frac{i\theta}{n^2}. \tag{5.17}$$

The first of these corresponds to a transverse wave propagated with velocity given by (4.33), without change in temperature. This velocity coincides with that given by (4.8) when $l = 1$.

When the wave is propagated in planes parallel to the (x, y) plane then $l = 0$ and (5.11) has the exact solutions

$$\xi^2 = \theta^2, \qquad \xi^2 = i\theta. \tag{5.18}$$

The first of these corresponds to a transverse wave propagated with constant temperature and with velocity given by (4.37), the particles vibrating in planes perpendicular to the (x, y) plane. The transverse velocity in which vibrations are in planes parallel to the (x, y) plane is again given by (4.38).

Note added in proof: Mention should also be made of a paper by Y. Shimazu, *J. Earth Sci. Nagoya Univ.* **2**, 15 (1954) in which some aspects of wave propagation in pre-stressed media are considered, but without temperature effects and for a restricted class of strain energy functions.

References

Buchwald, T. V.	1959	*Proc. Roy. Soc.* A **253**, 563
Chadwick, P.	1960	*Progress in Solid Mechanics*, Vol. 1, p. 265. (North Holland Publishing Co., Amsterdam).
England, A. H. and Green, A. E.	1961	*Phil. Trans.* In press.
Green, A. E. and Adkins, J. E.	1960	*Large Elastic Deformations* (Clarendon Press, Oxford).
Hayes, M. and Rivlin, R. S.	1960	Brown University Report, C11–62.

J. Mech. Phys. Solids, 1961, Vol. 9, pp. 191 to 195. Pergamon Press Ltd., London. Printed in Great Britain

A NOTE ON THERMOELASTIC RAYLEIGH WAVES*

By H. Deresiewicz
Columbia University, New York

(*Received* 17*th March*, 1961)

Summary

The propagation of waves on the surface of an elastic thermally conducting medium, which has been the subject of two recent papers, is re-examined herein, and expressions are displayed which exhibit the frequency dependence of the phase velocity and amplitude attenuation. It is shown that the order of magnitude of the frequency dependence is a function of the heat-transfer coefficient at the boundary.

1. Introduction

The effect of thermal conductivity on the propagation of waves of plane strain along the surface of a traction-free elastic semi-space was studied recently by Lockett (1958) and Chadwick (1960). Each of these authors contented himself with extracting from the general, complex, secular equation the 'zero-order' approximation, valid for very small values of a certain dimensionless frequency, Ω, Chadwick pointing out that the terms neglected were of $O(\Omega^{\frac{1}{2}})$. To the order computed, the motion was shown to be non-dispersive and non-dissipative.

The present paper treats the 'first-order' approximation, exhibiting explicitly the frequency dependence of the phase velocity and the frequency-dependent amplitude attenuation. Moreover, it is shown that, for frequencies above a certain level (which depends on the value of the constant in the linear heat-transfer boundary condition), the frequency-dependent correction is no greater than of $O(\Omega)$, the solution being qualitatively identical with that for the case of a thermally insulated boundary.

2. Secular Equation: General Case

Specialized for waves of plane strain (in the xz plane) propagating in the x direction, the general solution (Deresiewicz 1958)† of the field equations of thermoelasticity for the displacement (u_x, u_y, u_z) and the temperature deviation (T) from equilibrium reduces to

$$\left.\begin{aligned} u_x &= -\left[i\gamma(\hat{\phi}_1 + \hat{\phi}_2) + \hat{\phi}_3'\right]\exp i(\omega t - \gamma x), \\ u_y &= 0 \\ u_z &= (\hat{\phi}_1' + \hat{\phi}_2' - i\gamma\hat{\phi}_3)\exp i(\omega t - \gamma x), \end{aligned}\right\} \tag{1}$$

*This work was performed while the author was a (U.S. Government) Fulbright Research Scholar in Rome, Italy.

†The notation of that paper is carried over except that, for convenience, the non-zero (y) component of the vector potential is herein denoted by ϕ_3.

$$T = f \sum_{n=1}^{2} (\delta_n^2 - \omega^2/c_T^2)\, \hat{\phi}_n \exp i(\omega t - \gamma x), \tag{2}$$

where γ is the wave number and ω the frequency of the disturbance, and $f = (1 - \nu)/\alpha(1 + \nu)$, ν being the isothermal Poisson's ratio and α the coefficient of thermal expansion. The functions $\hat{\phi}_j \equiv \hat{\phi}_j(z)$ must satisfy the ordinary differential equation

$$\hat{\phi}_j'' - \kappa_j^2 \hat{\phi}_j = 0, \qquad j = 1, 2, 3, \tag{3}$$

where

$$\left.\begin{aligned} &\kappa_j^2 = \gamma^2 - \delta_j^2, \qquad \delta_j^2 = (\omega^2/c_T^2)\, \Lambda_j, \\ &\Lambda_{1,2} = \tfrac{1}{2}\left[\left(1 - i\frac{1+\epsilon}{\Omega}\right) \pm \left[1 + \frac{2i(1-\epsilon)}{\Omega} - \left(\frac{1+\epsilon}{\Omega}\right)^2\right]^{\frac{1}{2}}\right], \\ &\Lambda_3 = c_T^2/c_2^2. \end{aligned}\right\} \tag{4}$$

$\epsilon = c_S^2/c_T^2 - 1$ is a measure of the thermoelastic coupling and $\Omega = a^2\,\omega/c_T^2$ is the dimensionless reference frequency (equal to the product of the frequency of motion and the relaxation time of thermal currents); a^2 denotes the thermal diffusivity, c_T and c_S, the phase velocity of plane irrotational body waves in a perfectly conducting and perfectly non-conducting medium, respectively, and c_2, the phase velocity of plane equivoluminal body waves.

By virtue of (1), and with the aid of the first of (4), the non-zero components of traction across any plane $z =$ constant may be written

$$\left.\begin{aligned} \tau_{zx} &= -\mu\left[2i\gamma(\hat{\phi}_1' + \hat{\phi}_2') + (\gamma^2 + \kappa_3^2)\,\hat{\phi}_3\right] \exp i(\omega t - \gamma x), \\ \sigma_z &= \mu\left[(\gamma^2 + \kappa_3^2)(\hat{\phi}_1 + \hat{\phi}_2) - 2i\gamma\,\hat{\phi}_3'\right] \exp i(\omega t - \gamma x), \end{aligned}\right\} \tag{5}$$

where μ denotes the shear modulus of the material.

If we now assume the plane boundary of the half-space to be traction-free and subject to the linearized heat transfer condition, i.e.

$$\tau_{zx} = \sigma_z = 0, \qquad \frac{\partial T}{\partial z} + hT = 0, \qquad \text{on } z = 0, \tag{6}$$

and require a rapid decay of the amplitude of the wave with distance into the solid, i.e. we choose solutions of (3) of the form

$$\hat{\phi}_j(z) = A_j \exp(-\kappa_j z), \qquad \mathrm{Re}(\kappa_j) > 0, \tag{7}$$

then, upon inserting (7) in (2) and (5) and these, in turn, into the boundary conditions (6), we find the set of homogeneous algebraic equations

$$\left.\begin{aligned} -2i\gamma\kappa_1 A_1 - 2i\gamma\kappa_2 A_2 + (\gamma^2 + \kappa_3^2) A_3 &= 0, \\ (2\gamma^2 - \delta_3^2)(A_1 + A_2) + 2i\gamma\kappa_3 A_3 &= 0, \\ (\delta_1^2 - \omega^2/c_T^2)(h - \kappa_1) A_1 + (\delta_2^2 - \omega^2/c_T^2)(h - \kappa_2) A_2 &= 0. \end{aligned}\right\} \tag{8}$$

The vanishing of the determinant of the system (8) yields the secular equation which, on setting

$$\theta = hc_T/\omega, \qquad q = \omega^2/c_T^2\,\gamma^2, \tag{9}$$

may be written

$$(2 - \Lambda_3 q)^2 \left[(\Lambda_2 - 1)(1 - \Lambda_2 q)^{\frac{1}{2}} - (\Lambda_1 - 1)(1 - \Lambda_1 q)^{\frac{1}{2}} - (\Lambda_2 - \Lambda_1)\theta q^{\frac{1}{2}}\right]$$
$$= 4(1 - \Lambda_3 q)^{\frac{1}{2}} \left\{(\Lambda_2 - 1)(1 - \Lambda_1 q)^{\frac{1}{2}} \left[(1 - \Lambda_2 q)^{\frac{1}{2}} - \theta q^{\frac{1}{2}}\right]\right. \tag{10}$$
$$\left. - (\Lambda_1 - 1)(1 - \Lambda_2 q)^{\frac{1}{2}} \left[(1 - \Lambda_1 q)^{\frac{1}{2}} - \theta q^{\frac{1}{2}}\right]\right\}.$$

Thus, for given values of the frequency, (10) yields values of the wave number, γ, which, on account of the form of $\Lambda_{1,2}$, are, in general, complex.

3. Secular Equation: Case $\Omega \ll 1$

We now make use of the fact that, for most materials of interest, $\Omega \ll 1$ for ω well into the megacycle range. Accordingly, we may replace the expressions for $\Lambda_{1,2}$, (4), by their approximate forms,

$$\left.\begin{aligned} \Lambda_1 &= \frac{1}{1+\epsilon}\left[1 - \frac{i\epsilon\Omega}{(1+\epsilon)^2}\right] + O(\Omega^2), \\ \Lambda_2 &= -\frac{i(1+\epsilon)}{\Omega}\left[1 + \frac{i\epsilon\Omega}{(1+\epsilon)^2} - \frac{\epsilon\Omega^2}{(1+\epsilon)^4}\right] + O(\Omega^2). \end{aligned}\right\} \tag{11}$$

Moreover, we set

$$\gamma = \gamma_r - i\gamma_i = \frac{\omega}{c}(1 - i\beta), \tag{12}$$

where c denotes the phase velocity and $4\pi\beta$ the specific energy loss*. Then, with

$$\left.\begin{aligned} \theta_0 &= \theta(1+\epsilon)^{\frac{1}{2}} = hc_S/\omega, \\ b &= c_2^2/c_S^2, \qquad q_0 = c^2/c_2^2, \end{aligned}\right\} \tag{13}$$

the secular equation, (10), to terms of $O(\Omega)$, may be replaced by the pair of coupled real equations for the unknown phase velocity and attenuation measure, as expressed by q_0 and β, respectively:

$$\left.\begin{aligned} &(2 - q_0)^2 \left[1 - \frac{\theta_0 \Omega^{\frac{1}{2}}}{(1+\epsilon)\sqrt{2}}(1 + \xi\beta) - a_1\beta^2\right] \\ &\quad = 4(1 - q_0)^{\frac{1}{2}}(1 - bq_0)^{\frac{1}{2}} \left[1 - \frac{\theta_0 \Omega^{\frac{1}{2}}}{(1+\epsilon)\sqrt{2}}(1 + \eta\beta) - a_2\beta^2\right], \\ &(2 - q_0)^2 \left[\xi\beta + \frac{\theta_0 \Omega^{\frac{1}{2}}}{(1+\epsilon)\sqrt{2}}(1 - \xi\beta) - \frac{\phi\Omega}{(1+\epsilon)^2}\right] \\ &\quad = 4(1 - q_0)^{\frac{1}{2}}(1 - bq_0)^{\frac{1}{2}} \left[\eta\beta + \frac{\theta_0 \Omega^{\frac{1}{2}}}{(1+\epsilon)\sqrt{2}}(1 - \eta\beta) - \frac{(\psi + \epsilon x\theta_0)\Omega}{(1+\epsilon)^2}\right], \end{aligned}\right\} \tag{14}$$

where

$$\left.\begin{aligned} \xi &= \frac{2 - 5q_0}{2 - q_0}, \qquad \eta = \frac{1 - 2(1+b)q_0 + 3bq_0^2}{(1 - q_0)(1 - bq_0)}, \\ \phi &= \frac{1 + (2 - \epsilon)bq_0}{2bq_0}, \qquad \psi = \frac{1 + (1 - 3\epsilon)bq_0 - 2(1 - \epsilon)b^2 q_0^2}{2bq_0(1 - bq_0)}, \\ x &= \left(\frac{bq_0}{1 - bq_0}\right)^{\frac{1}{2}}, \qquad a_1 = \frac{4 - 24q_0 + 15q_0^2}{(2 - q_0)^2}, \\ a_2 &= \frac{2 - 9(1+b)q_0 + 6(1 + 5b + b^2)q_0^2 - 19b(1+b)q_0^3 + 12b^2 q_0^4}{2(1 - q_0)(1 - bq_0)}. \end{aligned}\right\} \tag{15}$$

*We recall the relation of β to the admittance; i.e. $\beta = (2Q)^{-1}$.

Simplification of equations (14) and, in particular, the uncoupling of q_0 and β, depends on the order of magnitude of the frequency-dependent heat-transfer parameter θ_0. We consider two cases*:

(1) $\theta_0 \Omega^{\frac{1}{2}} \gg 1$, with the assumption $\theta_0 = O(\Omega^{-1})$. Equations (14) now reduce to

$$\left.\begin{aligned} \frac{(2-q_0)^2}{4(1-q_0)^{\frac{1}{2}}(1-bq_0)^{\frac{1}{2}}} &= 1 - \frac{\epsilon x \Omega^{\frac{1}{2}}}{(1+\epsilon)\sqrt{2}} - \frac{(\xi-\eta)(1+\epsilon)\sqrt{2}}{\theta_0 \Omega^{\frac{1}{2}}} + O(\Omega), \\ \beta &= \epsilon \zeta \Omega^{\frac{1}{2}} (1 + \epsilon \xi \zeta \Omega^{\frac{1}{2}}) + O(\Omega^{\frac{3}{2}}), \end{aligned}\right\} \tag{16}$$

where $\zeta = x/(\xi - \eta)(1 + \epsilon)\sqrt{2}$. This case corresponds to a thermal boundary condition which differs only slightly from an isothermal one; the first-order correction is, as expected, of $O(\Omega^{\frac{1}{2}})$. The corresponding correction for the isothermal boundary condition may be obtained from (16) by letting $\theta_0 \to \infty$.

(2) $\theta_0 \Omega^{\frac{1}{2}} \ll 1$; i.e. $\theta_0 \leqslant O(1)$. It may be shown that, in this case,

$$\left.\begin{aligned} \frac{(2-q_0)^2}{4(1-q_0)^{\frac{1}{2}}(1-bq_0)^{\frac{1}{2}}} &= 1 + (x_1 - x\theta_0)\frac{\epsilon\theta_0 \Omega^{\frac{1}{2}}}{(1+\epsilon)^2\sqrt{2}} + O(\Omega^2), \\ \beta &= \frac{x_1 - x\theta_0}{\xi - \eta} \cdot \frac{\epsilon\Omega}{(1+\epsilon)^2} + O(\Omega^{\frac{3}{2}}), \end{aligned}\right\} \tag{17}$$

where $x_1 = (2 - bq_0)/2(1 - bq_0)$. The situation here is one which, effectively, differs only slightly from that for the adiabatic boundary condition, and reduces to it for $\theta_0 = 0$. It is seen that, now, the amplitude attenuation and the phase velocity correction are no longer of the same order, being of $O(\Omega)$ and $O(\Omega^{\frac{3}{2}})$, respectively.

TABLE 1

Material	ω_1 (c/s)	λ_1 (m)
Granite	2150	0·37
Limestone	3070	0·25
Sandstone	1510	0·37
Aluminium	11·6	86·5
Copper	4·1	167·6
Lead	22·5	15·1

We conclude by listing, in Table 1, numerical values, appropriate to three rocks and three metallic elements, of the frequency for which $\theta_0 = 1$, i.e. $\omega_1 = hc_S$, and of the corresponding wave length, $\lambda_1 = h^{-1}$. The ambient temperature was taken as $T_0 = 20°C$. Both radiation and natural convection were accounted for in the computation of h; values of the surface emissivity were 0·80 for the rocks and 0·04 for the (polished) metals (CARSLAW and JAEGER 1959, p. 21). Values of the thermal conductivity and diffusivity were taken from CARSLAW and JAEGER (1959, p. 497). Values of the phase velocity of dilatational waves were those given by CHADWICK (1960, p. 279) for the metals and LANDOLT–BÖRNSTEIN (1952) for the rocks. The latter values, representing those near the middle of the range of observed values given in the reference, are (in km/sec): granite, 5; limestone, 4·75; sandstone, 3·5.

*In each of these, of course, we retain the condition $\Omega \ll 1$.

References

Carslaw, H. S. and Jaeger, J. C.	1959	*Conduction of Heat in Solids*, 2nd ed. (Oxford University Press).
Chadwick, P.	1960	*Progress in Solid Mechanics*, (North-Holland Publishing Co., Amsterdam). Vol. 1, pp. 263–328 ; in particular, pp. 307–312.
Deresiewicz, H.	1958	*Proc. 3rd U.S. Nat. Congr. Appl. Mech.*, p. 287.
Landolt–Börnstein	1952	*Zahlenwerte und Funktionen*, 6th ed., Vol. III. (Springer, Berlin).
Lockett, F. J.	1958	*J. Mech. Phys. Solids* **7**, 71.

J. Mech. Phys. Solids, 1961, Vol. 9, pp. 196 to 199. Pergamon Press Ltd., London. Printed in Great Britain

ON SIZE EFFECTS IN POLYCRYSTAL PLASTICITY

By R. W. Armstrong
Westinghouse Research Laboratories, Pittsburgh

(*Received* 15*th April*, 1961)

Summary

Two cumulative 'size' effects are responsible for the increased strength of a polycrystalline aggregate above the single crystal strength at low temperatures: a 'specimen size' effect and a 'grain size' effect. The 'specimen size' effect occurs when few grains are present in a specimen cross-section (say less than twenty), and this effect is due mainly to the orientation dependence of crystal plastic flow. The 'grain size' effect occurs when many grains are in a specimen cross-section (say more than twenty), and this effect results because, in addition to the orientation dependence of plastic flow within grains, internal concentrations of stress are necessary at grain boundaries to cause bulk yielding and subsequent plastic flow of the polycrystalline aggregate.

Two 'size' effects differentiate the plastic flow of polycrystals, and hence their stress–strain curves, from single crystal plasticity at temperatures and strain rates where diffusion does not play a large part in the deformation: a 'specimen size' effect and a 'grain size' effect. Both effects appear when strength or work hardening comparisons are made between specimens of different grain size and/or different number of grains per cross-section (usually at constant specimen dimensions). Both effects result in the bulk material strength increasing with a decrease in grain size or increase in number of grains per cross-section. Both size effects contribute to an increased polycrystal strength over the single crystal strength. However, the two effects should not be confused with each other because (i) they have different origins, (ii) they cause this strengthening for different reasons, and (iii) they are in fact additive contributions to the bulk material strength. Their genesis and distinguishing characteristics are described in the following discussion.

If we consider specimens of increasing number of grains per cross-section, starting with a single crystal, the 'specimen size' effect is the first of the two size effects to cause an increase in bulk material strength above the single crystal value. This effect is due to the variation in orientation of the active slip systems and the corresponding resolved shear stress on the slip systems among different grains in a polycrystal; i.e. this effect is due mainly to the orientation dependence of crystal plastic flow, and, therefore, is dependent on grain orientation. The flow stress of the aggregate is equal to or greater than the single crystal value according to the number and orientation of the grains in the specimen because two closely related orientation dependent factors must be taken into account: (a) the critical resolved shear stress must be achieved on the slip systems of all the grains contributing to bulk plastic flow, and (b) the choice of slip systems in adjacent grains is

affected by the relative orientation of the grains to each other, as well as to the applied stress, because strain continuity must be maintained at the grain boundaries (this second orientation factor may be considered as a constraining factor that in effect reduces the number of available slip systems able to contribute to plastic flow, as considered in the first orientation factor). As a result of this ' size ' effect, the specimen flow stress, σ_f, can vary in a range from twice the single crystal critical resolved shear stress, τ (for a ' bamboo ' structure containing at least one grain of appropriate orientation), through the average orientation factor, m_0, times the single crystal strength as described by Sachs (1928), to the grain accommodation factor, m, times the single crystal strength as described by Taylor (1934, 1938, 1956).

$$2\,\tau \leqslant \sigma_f \leqslant m\,\tau, \qquad m_0 < m.$$

The ' specimen size ' effect predominates when few grains (say less than twenty) are present in a specimen cross-section (Pell-Walpole 1943; Feltham and Meakin 1957). However, it is independent of grain size: when the flow stresses of specimens having a constant range of grain orientations and number of grains per cross-section are compared by varying the specimen cross-section dimensions, a constant flow stress is observed for different grain size specimens.

In the orientation sensitive range of grain sizes that characterize the ' specimen size ' effect, grain boundaries contribute little of their own strength to the strength of the small aggregate (as will be discussed) because insufficient boundaries are present to really harden the material overall (Pell-Walpole pointed out that the limit of increased bulk strength due to this orientation effect occurred when completely enclosed grains were present in a specimen cross-section). When the plastic flow of some grains is restricted, because their neighbouring grains and their own grain boundaries are obstacles to bulk deformation, flow occurs in other grains of more favourable orientation and/or position along the specimen gauge length. Unfortunately, measurement of bulk polycrystal flow stresses in this range of few grains per specimen cross-section is also subject to much experimental scatter, because, (i) the flow stress is sensitive to the effects of initiating deformation in surface grains, (ii) a variety of matrix constraints along the specimen gauge length leads to heterogeneous flow, and (iii) uncontrolled orientation variation occurs in different specimens. However, these factors, in addition to the grain size and orientation dependence, also serve to differentiate the ' specimen size ' effect from the ' grain size ' effect.

The ' grain size ' effect occurs in polycrystalline materials because grain boundaries are obstacles to the initiation of bulk yielding and the subsequent propagation of plastic flow, and these boundaries require internal stress concentrations proportional to the grain diameters from within the grain volumes to induce general yielding of the aggregate (Petch 1953; Armstrong *et al.* 1961). The requirement of an internal stress concentration is an additional factor to be considered after the orientation conditions described by Taylor [and modified by Kocks (1958, 1960) in that *multislip* system flow properties of a single crystal should really be compared with the plastic behaviour of a grain in a polycrystal] have been satisfied in all the specimen grains. Thus, the ' grain size ' effect comes into play when sufficient grain boundaries are present in the specimen volume to allow measurement of the combined effects of the statistical orientation constraints

on plastic flow and the average grain boundary barrier to flow from within the grains. The 'grain size' effect on the flow stress of a polycrystalline aggregate explains values of the flow stress greater than $m\,\tau$. This effect results in an explicit dependence of the flow stress on grain size, l, as determined by ARMSTRONG *et al.*,

$$\sigma_f = m\,\tau + m\,k_s\,l^{-\frac{1}{2}}.$$

The parameter, k_s, depends on the number of deformation systems and the stress required to cause plastic flow on them in the vicinity of a grain boundary. In PETCH's theory of the stress–'grain size' effect, an additional factor of $1/\sqrt{2}$ would be in the concentrated stress term, $k\,l^{-\frac{1}{2}}$ (see Fig. 1), if surface grains nucleate and continue to propagate plastic flow, because of the increased length of the average dislocation queue in a slip band. By its very nature the 'grain size' effect is independent of grain orientation in the sense under discussion. In addition, this effect has the following specimen and deformation characteristics: many grains per specimen cross-section (say more than twenty), a flow stress that is predictably dependent on grain size (varies as inverse square root of grain size according to PETCH), and deformation that is more homogeneous than that occurring with fewer grains per cross-section.

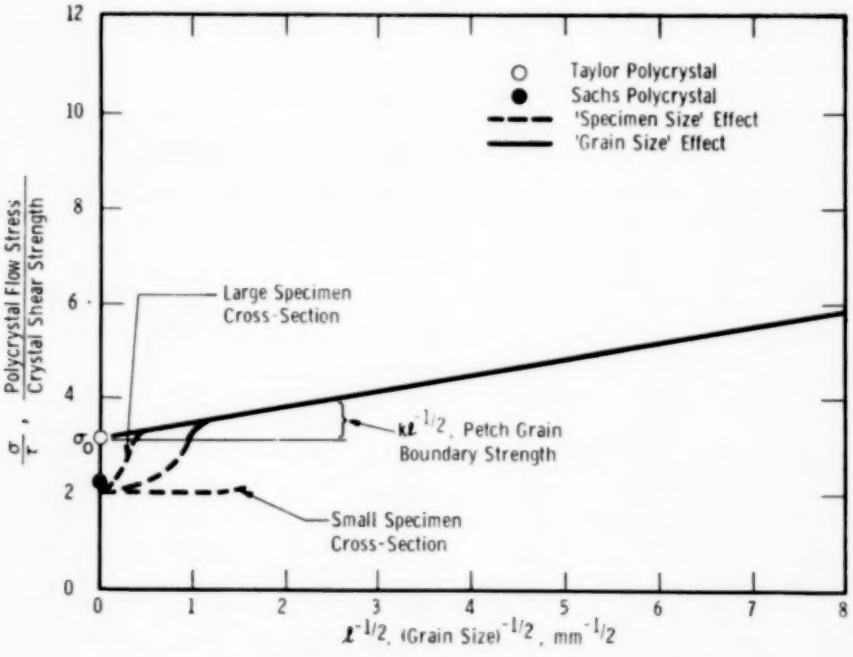

FIG. 1. Face-centred-cubic polycrystal flow stress as a function of grain size.

The Figure shows both 'size' effects plotted over a range of grain sizes for which we can differentiate the 'specimen size' effect and PETCH's 'grain size' effect for a typical face-centred-cubic metal. The 'specimen size' effect contributes only to σ_0 and we see its maximum contribution to the yield stress of an

aggregate at the limiting value $l^{-\frac{1}{2}} = 0$. The dashed curves for different specimen sizes indicate how the ' specimen size ' effect causes an increase in yield stress up to the value σ_0 with decreasing grain size. The solid extensions of the dashed curves above σ_0 to meet the curve predicted by the PETCH relation represent the transition regions where the ' grain size ' effect appears and adds on to the ' specimen size ' effect ; this stress interval obtains over a narrow range of grain size. The direct proportionality between the yield stress of the aggregate and the inverse square root of grain size at smaller grain sizes results from the direct effect of grain size on the internal concentrations of stress required to propagate plastic flow in the polycrystalline aggregate. Depending upon the specimen size and the grain size, achievement of TAYLOR's orientation constraint strengthening can occur very soon or very late as shown along the abscissa of the Figure. For different crystal structures, the relationship between the stress–' grain size ' effect intercept, σ_0, and the single crystal shear strength can be predicted (it is given by TAYLOR's analysis for the structure). The grain boundary strength parameter, $k\,l^{-\frac{1}{2}}$, can be separately correlated with slip anisotropy and dislocation interactions.

ACKNOWLEDGMENTS

The author acknowledges the valuable discussions contributed by Professor N. J. PETCH, King's College, Newcastle upon Tyne, Dr. R. L. FLEISCHER, General Electric Research Laboratories, Schenectady, New York, and members of the Metallurgy Department, Westinghouse Research Laboratories, Pittsburgh.

REFERENCES

ARMSTRONG, R. W., CODD, I., DOUTHWAITE, R. M. and PETCH, N. J. 1961 *Phil. Mag.* In press.

FELTHAM, P. and MEAKIN, J. D. 1957 *Phil. Mag.* **2**, 105.

KOCKS, U. F. 1958 *Acta Met.* **6**, 85.

1960 *Acta Met.* **8**, 345.

PELL-WALPOLE, W. T. 1943 *J. Inst. Met.* **69**, 131.

PETCH, N. J. 1953 *J. Iron St. Inst.* **174**, 25.

SACHS, G. 1928 *Z. Ver. Dtsch. Ing.* **72**, 734.

TAYLOR, G. I. 1934 *Proc. Roy. Soc.* A **145**, 362, 388.

1938 *J. Inst. Met.* **62**, 307.

1956 *Deformation and Flow of Solids*, p. 33 (Springer, Berlin).

J. Mech. Phys. Solids, 1961, Vol. 9, pp. 200 to 209. Pergamon Press Ltd., London. Printed in Great Britain

STRESS FIELD IN METALS AT INITIAL STAGE OF PLASTIC DEFORMATION

By T. H. Lin, S. Uchiyama and D. Martin
University of California, Los Angeles

(*Received 24th April*, 1961)

Summary

The initial stage of plastic deformation of a fine grained aggregate with slip occurring only in the most favourably oriented crystals is studied. The elastic modulus of the individual crystals is taken to be isotropic. The sliding crystals are assumed to be cubical in shape and located at the interior of the aggregate. Work-hardening in the sliding crystal is considered. The analogy of plastic strain gradient and body force in producing stress field in an elastic medium is developed. This analogy is applied to calculate the slip and stress fields caused by (1) one sliding crystal and (2) two sliding crystals spaced at a clear distance of half the crystal width. This shows the interaction effect of slips in two nearby crystals. From these stress fields, the residual stress may be easily obtained and the Bauschinger effect is clearly shown.

1. Introduction

Single crystal tests have shown that plastic strain is produced through the sliding of one plane of atoms over another. Taylor (1934) has shown that sliding is in such a way that perfect crystal structure is reformed after each atomic jump. The lattice structure of the bulk of the material is not changed. Hence the elastic constants of the crystals remain the same after the occurence of sliding.

Strain may be divided into two parts: the elastic part caused by the elastic deformation of the lattice structure and the plastic part caused by slips. With e_{ij} denoting the strain component referring to a set of rectangular coordinates x_i, and single prime and double prime denoting the elastic and plastic parts respectively

$$e_{ij} = e'_{ij} + e''_{ij}, \qquad i, j = 1, 2, 3. \tag{1}$$

The elastic behaviour of a single crystal is generally anisotropic. This anisotropy is small for face-centred cubic crystals and is neglected in the present study. Then the stress is related to the elastic strain as

$$\tau_{ij} = \delta_{ij} \lambda\theta' + 2\mu e'_{ij} \tag{2}$$

where δ_{ij} is the Kronecker delta, θ' is the elastic dilatation, μ and λ are Lamé's constants. The amount of slip vs. the resolved shear stress (shear stress along the slip direction on the slip plane) may be obtained from single crystal tests. From the slip, plastic strain is readily calculated. The stress-strain relation of a single crystal is hence completely determined (Bishop and Hill 1951; Lin 1957).

When an aggregate of these crystals with isotropic elastic constants is loaded within the elastic limit, the stress is uniform throughout the aggregate. Crystals

are differently oriented and hence have different resolved shear stresses. Those crystals with highest resolved shear stress are called most favourably oriented crystals, and first to reach the critical shear stress and slide. After sliding, should the aggregate be unloaded, the slips would remain and cause residual stress. If the aggregate is then loaded again, this residual stress plus the applied uniform stress gives the resultant stress field in the aggregate.

2. Analogy between Plastic Strain Gradient and Body Force

In order to calculate the residual stress due to localized slips, an analogy between the plastic strain gradient and body force in causing stresses in an elastic medium is derived. Considering the elastic strain as the difference between the total and the plastic strains:

$$\tau_{ij} = \delta_{ij}\,\lambda\,(\theta - \theta'') + 2\,\mu\,(e_{ij} - e''_{ij}) \tag{3}$$

where θ'' is the plastic dilatation.

The equation of equilibrium is written as

$$\tau_{ij,j} + F_i = 0 \tag{4}$$

where the subscript after comma denotes differentiation, the repetition of the subscript denotes summation from one to three, and F_i denotes the body force per unit volume along the x_i-axis. Substituting (2) into (4):

$$\delta_{ij}\,\lambda\theta_{,j} + 2\mu e_{ij,j} - (\delta_{ij}\,\lambda\theta''_{,i} + 2\mu e''_{ij,j}) + F_i = 0. \tag{5}$$

It is seen that the plastic strain gradient $-(\lambda\theta''_{,j} + 2\mu e''_{ij,j})$ is equivalent to F_i. This reduces the determination of the stress field in an elastic medium caused by plastic strain to that of the stresses caused by the equivalent body forces. For thermal stresses alone, the plastic strain due to thermal expansion with α as the coefficient of expansion and T as the temperature,

$$e''_{ij} = \delta_{ij}\,\alpha T, \qquad \theta'' = e''_{ii} = 3\alpha T.$$

Equation (5) reduces to

$$\delta_{ij}\,\lambda\theta_{,j} + 2\mu e_{ij,j} - (3\lambda + 2\mu)\,\alpha T_{,i} + F_i = 0. \tag{6}$$

This is the well-known analogy between the temperature gradient and the distributed body force in an elastic medium. For an inclusion with uniform plastic strain, the plastic strain gradient is zero within the inclusion and occurs only on the inclusion surface. The equivalent body force $-(\delta_{ij}\,\lambda\theta''_{,j} + 2\mu e''_{ij,j})$ reduces to surface traction $(\delta_{ij}\,\lambda\theta'' + 2\mu e''_{ij})\,n_j$ on the inclusion surface, where n_j is the outward normal to the surface. This same result has been obtained by Eshelby (1957) through a different approach in his noteworthy paper on ellipsoidal inclusions.

3. Stress Field Caused by Given Plastic Strains

The most favourably oriented crystal may be located near a free surface or at the interior of the aggregate. The stress field caused by a uniformly slid crystal at a free surface has been calculated by Lin and Tung (1961). The present study

is mainly concerned with sliding crystals located at the interior of a fine-grained aggregate. The equivalent body force caused by slips in this crystal may be considered as applied in an infinite elastic medium.

The displacement $u(x)$ in an infinite medium subject to body force $F_i(x')$ acting through a finite volume V' of finite size has been given by Kelvin (Sokolnikoff 1956) as

$$u_i(x) = A\int_{V'}\left[B\frac{F_i(x')}{r} - \left(\frac{1}{r}\right)_{,i}(x_j - x'_j)\,F_j(x')\right]dV' \tag{7}$$

where $A = \dfrac{\lambda+\mu}{8\pi\mu\,(\lambda+2\mu)}$; $B = \dfrac{\lambda+3\mu}{\lambda+\mu}$ and $r = [(x_i - x'_i)(x_i - x'_i)]^{\frac{1}{2}}$.

$F_i(x')$ are the components of the body force in terms of the variables of integration x_i'. The derivative of u_i with respect to x_k can be shown to converge uniformly both inside and outside of V', so the differentiation may be carried out under the integral sign giving

$$\frac{\partial u_i}{\partial x_k} = A\int_{V'}\left[BF_i(x')\left(\frac{1}{r}\right)_{,k} - \left(\frac{1}{r}\right)_{,ik}(x_j - x'_j)\,F_j(x') - \left(\frac{1}{r}\right)_{,i}F_k(x')\right]dV', \tag{8}$$

$$e_{ik} = \tfrac{1}{2}\left(\frac{\partial u_i}{\partial x_k} + \frac{\partial u_k}{\partial x_i}\right) =$$

$$= A\int_{V'}\left\{\frac{(B-1)}{2}\left[F_i(x')\left(\frac{1}{r}\right)_{,k} + F_k(x')\left(\frac{1}{r}\right)_{,i}\right] - \right.$$

$$\left. - \left(\frac{1}{r}\right)_{,ik}(x_j - x'_j)\,F_j(x')\right\}dV', \tag{9}$$

$$\theta = e_{ii} = \int_{V'} A\,(B-1)\,F_i(x')\left(\frac{1}{r}\right)_{,i}dV', \tag{10}$$

$$\tau_{ik} = \delta_{ik}\,\lambda\theta + 2\mu e_{ik} =$$

$$= \delta_{ik}\,\lambda A\,(B-1)\int_{V'}F_l(x')\left(\frac{1}{r}\right)_{,l}dV' + A\mu\int_{V'}\left\{(B-1)\left[F_i(x')\left(\frac{1}{r}\right)_{,k} + \right.\right.$$

$$\left.\left. + F_k(x')\left(\frac{1}{r}\right)_{,i}\right] - 2\left(\frac{1}{r}\right)_{,ik}(x_j - x'_j)\,F_j(x')\right\}dV'. \tag{11}$$

This gives the stress field caused by body forces F_i in an infinite elastic medium.

Let x_1 be normal to the sliding plane and x_2 be along the sliding direction of this most favourably orientated crystal. This sliding gives plastic strain e''_{12}. With e''_{12} expressed in terms of the x'-axes, the equivalent body forces caused by e''_{12} are

$$F_1 = -2\mu\frac{\partial e''_{12}}{\partial x'_2} \quad \text{and} \quad F_2 = -2\mu\frac{\partial e''_{12}}{\partial x'_1}. \tag{12}$$

Substituting these in (11),

$$\tau_{ik} = \frac{-\delta_{ik}\,\lambda\mu}{2\pi\,(\lambda+2\mu)}\int_{V'}\left[\frac{\partial e''_{12}}{\partial x'_2}\left(\frac{1}{r}\right)_{,1} + \frac{\partial e''_{12}}{\partial x'_1}\left(\frac{1}{r}\right)_{,2}\right]dV' -$$

$$- \frac{\mu^2}{2\pi\,(\lambda+2\mu)}\int_{V'}\left[\left(\delta_{i1}\frac{\partial e''_{12}}{\partial x'_2} + \delta_{i2}\frac{\partial e''_{12}}{\partial x'_1}\right)\left(\frac{1}{r}\right)_{,k} + \right.$$

$$+\left(\delta_{k1}\frac{\partial e''_{12}}{\partial x'_2}+\delta_{k2}\frac{\partial e''_{12}}{\partial x'_1}\right)\left(\frac{1}{r}\right)_{,i}\Bigg]dV'+$$

$$+\frac{(\lambda+\mu)\,\mu}{2\pi(\lambda+2\mu)}\int_{V'}\left(\frac{1}{r}\right)_{,ik}\left[(x_1-x'_1)\frac{\partial e''_{12}}{\partial x'_2}+(x_2-x'_2)\frac{\partial e''_{12}}{\partial x'_1}\right]dV'. \tag{13}$$

This gives the relation between stress field and the plastic strain distribution in an infinite medium.

4. Plastic Strain Distribution in the Sliding Crystal

The critical shear stress in the crystal is a function of slip as given by Taylor (1938). The initial portion of this function for single slip may be approximated by a linear relation

$$\tau_{12}=c_0+c_1 e''_{12} \tag{14}$$

where c_0 is the initial critical shear stress and c_1 is the initial rate of hardening per unit plastic strain. During sliding the resolved shear stress in the sliding region must be equal to the critical shear stress. From (13), the resolved shear stress caused by slips is

$$\tau_{12_s}=\int\frac{\partial e''_{12}}{\partial x'_2}\left[\alpha\frac{(x_1-x'_1)^2(x_2-x'_2)}{r^5}+\beta\frac{(x_2-x'_2)}{r^3}\right]dV'+$$

$$+\int\frac{\partial e''_{12}}{\partial x'_1}\left[\alpha\frac{(x_1-x'_1)(x_2-x'_2)^2}{r^5}+\beta\frac{(x_1-x'_1)}{r^3}\right]dV',$$

where $$\alpha=\frac{3\mu(\lambda+\mu)}{2\pi(\lambda+2\mu)} \quad \text{and} \quad \beta=\frac{\mu^2}{2\pi(\lambda+2\mu)}. \tag{15}$$

The total resolved shear stress is the sum of τ_{12_s} and τ_{12_0}, where τ_{12_0} is the applied resolved shear stress on the aggregate. In the sliding region,

$$\tau_{12_0}+\tau_{12_s}=c_0+c_1 e''_{12}. \tag{16}$$

At the start of plastic deformation in the aggregate, the sliding crystals are spaced far apart from one another so that the sliding of one causes negligible stress on the other. Eshelby has shown that a homogeneous plastic strain in an ellipsoidal crystal embedded in an infinite medium causes uniform stress in the crystal. This corresponds to constant τ_{12_s} and constant e''_{12}, so (16) is satisfied. Hence, if the most favourably oriented crystal is ellipsoidal in shape, the initial slip is uniform. Actually crystals exist in all shapes. They can not be all ellipsoidal since a three-dimensional continuum can not be composed of ellipsoids alone. In the present study sliding crystals of simple cubic shape are assumed. The stress field caused by a uniform sliding in a cubical crystal embedded in an infinite medium has been calculated and it has been found that the resolved shear stress within the crystal varies considerably. Uniform sliding requires uniform resolved shear stress. Hence the actual slip can not be uniform, and its distribution is here determined by (16).

This sliding cube is assumed to have side a. The reference axes x_1, x_2 and x_3 are taken to be parallel to the three perpendicular edges of the cube. The origin of the axes coincides with the centre of the cube. In the following calculation, an aggregate of pure aluminium is considered. Young's modulus and Poisson's

ratio are taken as 10^7 lb/in^2 and 0·3 respectively. From these, Lamé's constants λ and μ are calculated. c_1 in (14) and (16) is taken as 10^4 lb/in^2, which corresponds approximately to the initial slope of the critical shear stress vs. single slip curve from single crystal tests by Taylor and Elam (1923). Since this value of c_1 is much smaller than 2μ, the e''_{12}'s are very close to the case of zero hardening ($c_1 = 0$). The applied τ_{12_0} is taken to be $1{\cdot}10\, c_0$. With c_1 being negligible as compared to $2\,\mu$, (16) gives e''_{12} at different points in terms of $(\tau_{12_0} - c_0)$ and hence the stresses are directly proportional to $(\tau_{12_0} - c_0)$.

Equation (16) may be applied to a simply connected or multiply connected region embedded in an infinite medium. This equation is here applied to a single cube and is solved by the method of finite difference. This cube is divided into $8 \times 8 \times 8$ equal cubical elements by three perpendicular sets of equally spaced planes. There are $9 \times 9 \times 9$ intersecting points of these planes. The e''_{12} at each intersecting point is considered as one unknown, so there are $9 \times 9 \times 9$ unknown values of e''_{12}. Because of the symmetry of e''_{12} referring to three planes passing the origin and parallel to the three faces of the cube, and the two diagonal planes parallel to x_3-axis, these $9 \times 9 \times 9$ unknowns reduce to $5 \times 15 = 75$ independent unknowns. Equation (16) is written as seventy-five simultaneous equations of seventy-five unknown values of e''_{12}. The coefficients of these seventy-five equations and their solution were obtained by an IBM 709 computing machine. The e''_{12} distribution in the sliding crystal is shown in Fig. 1. It is seen that the slip e''_{12} is not uniform, being larger in the interior than at the boundary. The amount of slip e''_{12} required to relieve $0{\cdot}10\, c_0$ resolved shear stress is much greater than $0{\cdot}10\, c_0/2\,\mu$. This agrees with Eshelby's derivations applied to spherical inclusions (Budiansky *et al.* 1960).

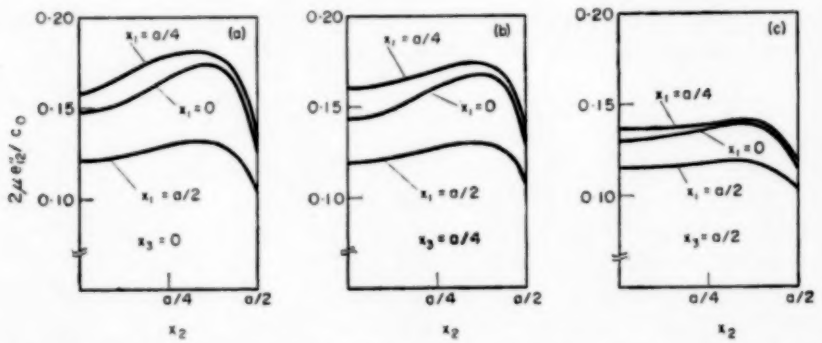

Fig. 1. Distribution of slips e''_{12}. Note: The ratio of the resolved shear stress τ_c to the critical shear stress c_0 is 1·10.

5. Stress Field Caused by the Non-Uniformly Slid Crystal

With e''_{12} at different points known, the plastic strain gradients at different points are computed. Then the stress components caused by these plastic strain gradients are obtained from (13). The sum of this stress and the uniformly applied stress τ_{12_0} gives the stress outside the sliding region. Inside this region this sum is reduced by the amount $2\mu e''_{12}$. The distribution of stress component τ_{12} with one sliding

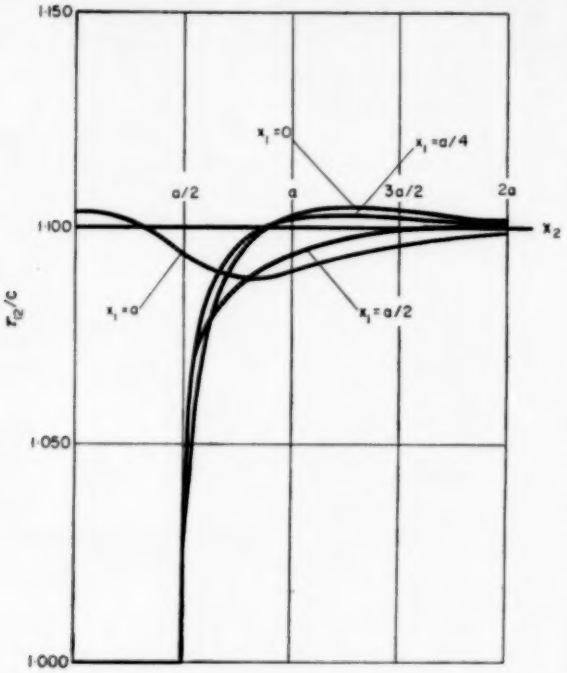

FIG. 2. Distribution of stress component τ_{12} near the sliding cube, $x_3 = 0$.

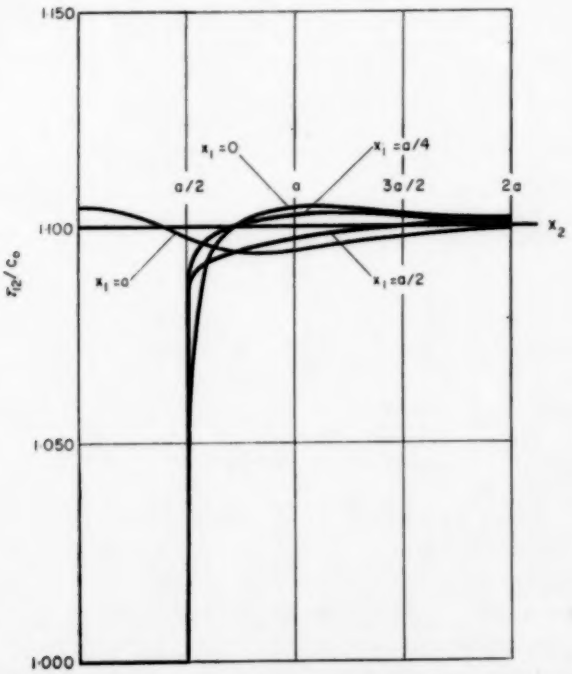

FIG. 3. Distribution of stress component τ_{12} near the sliding cube, $x_3 = 0{\cdot}50\,a$.

crystal is shown in Figs. 2–4.* It is seen that, within the sliding crystal, τ_{12} is nearly uniformly reduced by $0{\cdot}1\,c_0$ and the stress caused by the sliding fades rapidly with the distance from the sliding region. At a distance of three times the linear dimensions of the sliding crystal, the stress caused by slips practically vanishes. At the initial stage of plastic deformation, only a small percentage of crystals slide and the distance between two neighbouring sliding crystals is so large that the sliding of one has negligible effect on the other. The distribution of slips in a sliding crystal and its stress field are calculated by considering sliding in one crystal only as presently shown.

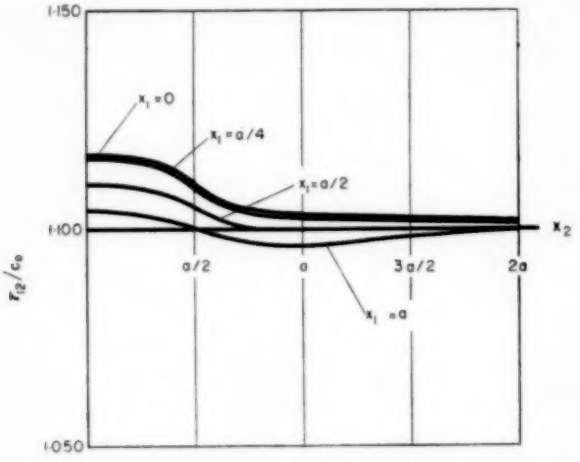

FIG. 4. Distribution of stress component τ_{12} near the sliding cube, $x_3 = 0{\cdot}75\,a$.

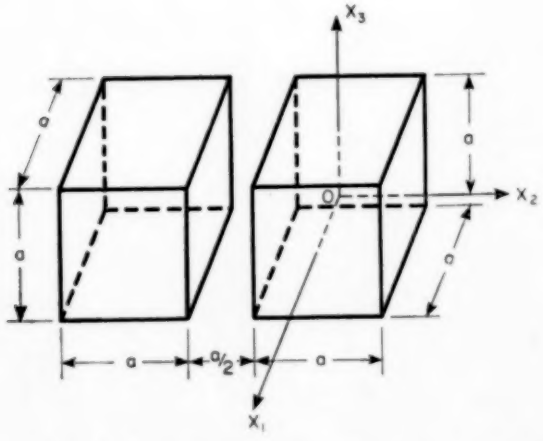

FIG. 5. The two cubical sliding cubes and the reference axes.

*The distributions of other stress components are shown in U.S. Air Force Tech. Note 60-1256, Report 60-44 by T. H. LIN and D. MARTIN, University of California, Los Angeles, November 1960.

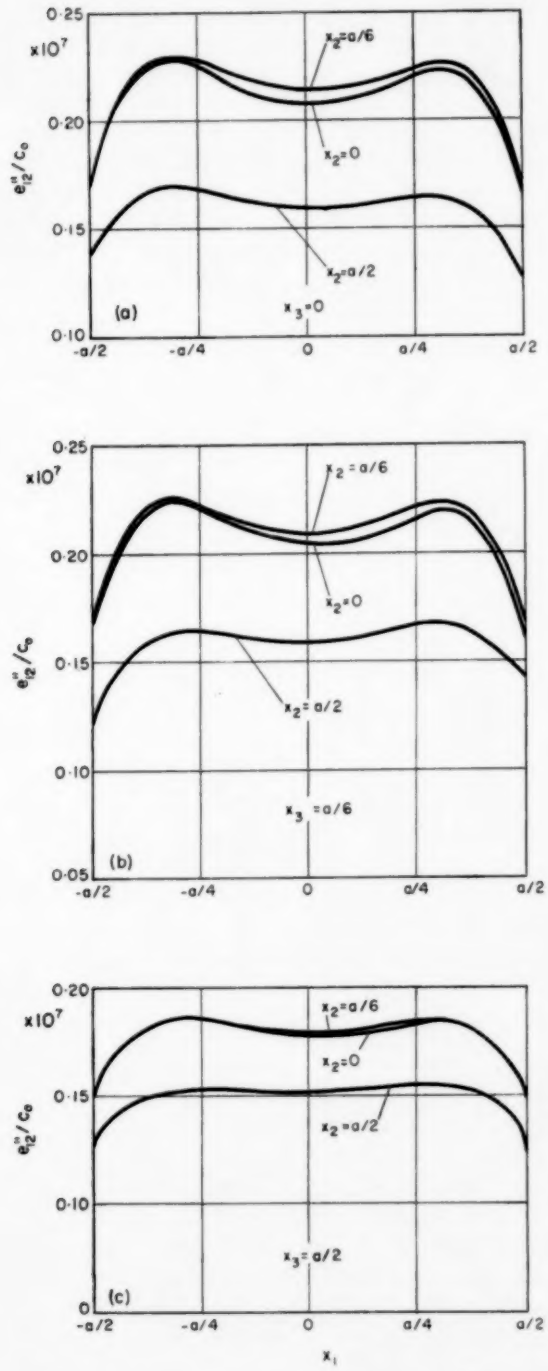

FIG. 6. Distribution of plastic slip in two nearby crystals at the interior of the aggregate.

6. Interaction of Two Neighbouring Sliding Crystals

In the previous Section the stress field caused by one sliding crystal has been shown. When the plastic deformation spreads in the aggregate, the distance between two sliding crystals decreases. The effect of the sliding of one on the other increases. In this Section two sliding crystals of cubical shape and of side a located side by side at a clear distance of $\frac{1}{2}a$ are considered (Fig. 5). The critical shear stress is taken to vary linearly as the amount of slip as shown in (14). The volume integral (15) is extended to two cubes. This integral equation is solved numerically by the method of finite difference. The resulting distribution of e''_{12} in these two cubes is shown in Fig. 6. The stress field has been similarly calculated. The stress component τ_{12} is shown in Fig. 7.

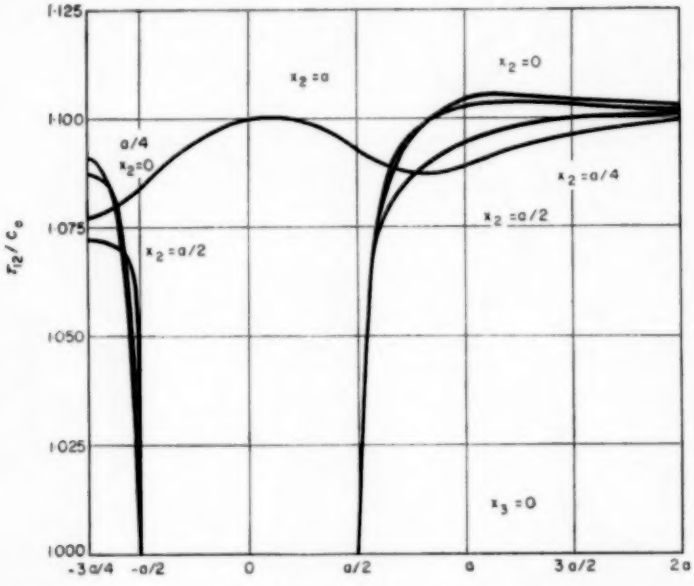

Fig. 7. Distribution of stress component τ_{12} caused by plastic slip in two neighbouring crystals embedded in an aggregate.

It is seen that the general forms of the slip distribution curves remain the same but the amount of slip near the other sliding cube is increased. Figs. 2, 3 and 7 show that, when the aggregate is unloaded, the sliding crystals have a residual stress τ_{12} of $-0{\cdot}10\,c_0$. Hence, upon reversed loading, these sliding crystals will start sliding at an applied aggregate stress τ_{12_0} of $-0{\cdot}90\,c_0$ instead of c_0. This clearly shows the Bauschinger effect.

With the stress field known, and with a given or assumed arrangement of crystals in an aggregate, the next crystal to slide can be found. The present calculations give the stress distribution caused by the sliding of one and two work-hardening crystals in an aggregate. The method shown can be extended to calculate the stress field caused by the sliding of a few more crystals under either single or reversed loadings.

Acknowledgments

This research was sponsored by the Solid State Science Branch, Office of Scientific Research, Air Research and Development Command, U.S. Air Force under Contract No. AF 49 (638)–20 between OSR and the University of California, Los Angles. The authors wish to express their thanks to Sir G. I. Taylor for his kind discussions and comments and to Western Data Processing Centre for the use of IBM 709 for calculations.

References

Barrett, C. S. 1952 *Structure of Metals*, p. 531 (McGraw-Hill, New York).

Bishop, J. F. W. and Hill, R. 1951 *Phil. Mag.* **42**, 414, 1298.

Budiansky, B., Hashin, Z. and Sanders, J. L. Jr. 1960 Harvard Univ. Tech. Rep. No. 7.

Eshelby, J. D. 1957 *Proc. Roy. Soc.* A **241**, 376.

Kochendörfer, A. 1941 *Plastische Eigenschaften von Kristallen* (Springer, Berlin).

Kochs, V. F. 1958 *Acta Met.* **6**, 85.

Lin, T. H. 1957 *J. Mech. Phys. Solids* **5**, 143.

Lin, T. H. and Tung, T. K. 1961 U.S. Air Force Tech. Note 60–1387, Univ. of California Report 60–98 (To be published in *J. Appl. Mech.*).

Taylor G. I. 1934 *Proc. Roy. Soc.* A **145**, 362.

1938 *J. Inst. Met.* **42**, 307.

Taylor, G. I. and Elam, C. F. 1923 *Proc. Roy. Soc.* A **102**, 643.

Sokolnikoff, I. S. 1956 *Mathematical Theory of Elasticity*, pp. 337, 359–360 (McGraw-Hill, New York).

BOOK REVIEWS

W. PRAGER: **Einführung in die Kontinuumsmechanik** (Lehr- und Handbücher der Ingenieurwissenschaften, Band 20). Birkhäuser Verlag, Basel und Stuttgart, 1961. 228 pp., DM 32.50.

THIS is a most attractive introduction to the mechanics of deformable solids and fluids. Its main aim is to provide a unified treatment of fundamentals, in order to avoid the duplication of effort that often occurs when students learn each separate specialism from different texts. The principal contributing factor to this is of course the variety of notations, above all the contrast between symbolic and tensor notations. In the former all quantities and differential operators are written in bold face without indicating components, together with a proliferation of symbols for various kinds of products; in the latter, all components are shown explicitly by subscripts or superscripts, the summation convention is used, and all products are simply indicated by juxtapositions. The relative merits of the two have often been passionately argued (for example in DUSCHEK-HOCHRAINER's book on tensor analysis); Professor PRAGER gives a balanced estimate with which the reviewer is in full accord. For instance, while symbolic notation is a perfect instrument for mechanics of rigid bodies or ideal fluids, it becomes cumbersome at quite an early stage in mechanics of viscous fluids and deformable solids, and is totally unworkable at an advanced level. The author has made the wise decision to present both notations in parallel at the beginning, wherever reasonable, but through most of the book suffix notation predominates. Only Cartesian tensors are used, however, and all the necessary apparatus is developed in an excellent introductory Chapter. (Curvilinear tensors are missed only at the end of the book, where certain results would have been illuminated and simplified by their use.)

There follow admirable Chapters on the stress and strain-rate tensors, and on the basic equations of motion and energy. The treatment is neat and businesslike, conducted with precision and dispatch, omitting no important detail or qualification. Above all, it *looks* and *reads* like applied mathematics, with well-spaced equations and plenty of verbal statement and explanation. Would that this could be said of most articles on continuum mechanics these days, but unfortunately there is a growing tendency to imagine that something can only be stated precisely, or somehow only becomes respectable or acquires a superiority, when it is all done with symbols, with frequent headings for lemmas, theorems, proofs, corollaries, etc. Yet it is perfectly possible – though not easy – to be readable as well as accurate and orderly, as Professor PRAGER so well demonstrates.

The last two-thirds of the book deals with ideal fluids, Newtonian viscous fluids, visco-elastic solids, hypo-elastic solids and classical elastic solids. Understandably the author touches on ideal plasticity only very briefly, in view of his other writings, though this is to be regretted (incidentally, the transition from the visco-plastic law might inadvertently suggest a generally valid physical picture, though it has the advantage of emphasizing the interplay of stress and velocity fields in plane plastic strain). The account of finite strain is especially noteworthy: in my view it is superior to any other I have seen, again primarily for its readability and clarity, as well as its completeness at this introductory level. The account of each constitutive law is taken far enough to include specific problems of real significance; it is remarkable how deep the author has succeeded in going in so short a space. Further developments, as well as routine exercises, appear in a very good and extensive collection of problems for solution.

There is, however, an omission surprising in a book of this kind, which is attempting to bring together separate disciplines (by unified notation and other means). This is a thoroughgoing use of analogies, for example Rayleigh's between the field equations for slow viscous flow and elastostatics. An even more effective use of structural analogy could have been made in proofs of uniqueness and extremum principles for various solids and fluids through the linking idea of convexity, so fruitful in current developments.

The reviewer has also two regrets in regard to terminology, to which Professor PRAGER has now lent the weight of his authority, namely the words hyper-elastic and hypo-elastic. It seems (if C. TRUESDELL's suggestion is to be adopted) that what we have all been learning for so many

years from Kirchhoff, Voigt, Love, Muskhelishvili and all the others, has not really been elasticity but hyper-elasticity ! Surely there is no need for a change in time-honoured usage here. And, in the other case, must we so far blur the far-reaching distinction between a holonomic and a non-holonomic constraint as to accept, in a pseudo-reversibility under special paths of loading or in first approximation, a justification for a nomenclature implying a kind of 'springiness' in a material defined by a non-integrable relation between stress-rate and strain-rate. I hope the author will re-consider this terminology in the next edition, all the more because he has given us a very welcome book that will exert great influence on the teaching of continuum mechanics.

R. HILL

R. E. D. BISHOP and D. C. JOHNSON: **The Mechanics of Vibration.** Cambridge University Press, 1960. 592 pp., 120s.

THIS BOOK is written primarily for engineers and engineering students who are specializing in the study of the vibration characteristics of mechanical systems. Receptances are used throughout, a receptance being defined as the ratio of the instantaneous displacement of a system to the instantaneous force causing that displacement. If the displacement is measured at the point of application of the force, the receptance is known as a direct receptance. If not, the receptance is termed a cross receptance.

The concept of a receptance is introduced and some of the properties and uses of receptances are given in Chapter 1. For example, it is shown that it is often possible to analyse a complex system into simpler parts whose receptances are known, either in graphical or algebraical form. This knowledge may be used to calculate natural frequencies and associated mode shapes of a complex system.

The terms generalized coordinate and generalized force are explained in Chapter 2, which ends with a derivation of Lagrange's equation of motion. This is followed, in Chapter 3, by a very enlightening discussion on the properties of receptances and the shapes of receptance and reciprocal receptance diagrams for lumped-parameter systems. Principal modes, principal coordinates, and the principle of orthogonality are then discussed at length. The principle of orthogonality is justified by considering the constancy of the total energy of a conservative system which is allowed to vibrate freely. Then, with the aid of a simple example, the physical basis of Rayleigh's principle is discussed, and a proof is given.

The reader is introduced to the problems associated with the vibration analysis of continuous systems in Chapter 4. The vibration characteristics of taut strings are considered, much the same pattern being adopted as for the lumped-parameter systems of Chapter 3, except that the equation of motion is set up by applying Newton's laws instead of the Lagrangian equations. It is also shown that the characteristic functions, that is, the functions describing the vibrating form of the string in each of its principal modes, may be used to represent any imposed deflection of the given string.

The possible discrepancies between the prediction from the highly-idealized systems considered in the book and the results from real systems are discussed in Chapter 5, which includes a lucid discussion on the application of Rayleigh's principle to continuous systems. Dunkerley's method and Southwell's theorem are also described. In Chapter 6 the vibration characteristics of uniform shafts in torsional and longitudinal vibration are examined, and a tabular method for calculating the receptances at the end of a chain of sub-systems is given. There is also a section in which consideration is given to the errors involved in replacing a uniform lumped-mass system by a continuous shaft, when torsional vibrations only are involved. Chapter 7, which takes up 120 pages, deals with the flexural vibration characteristics of uniform beams and shows clearly how to treat simple and composite systems. Tables of receptances, and characteristic functions and their derivatives are given for various end conditions. Transcendental functions, which arise in the receptances, are also tabulated. The major portion of this chapter has been published in the *Proceedings of the Institution of Mechanical Engineers* and will be well known by all practising Engineers interested in the solution of problems involving mechanical vibration. The tables were published separately by C.U.P. in 1956, and have proved very useful.

The vibration characteristics of systems in which there is viscous damping are examined in Chapter 8. The equations of motion for simple systems are set up by using Newton's Laws, and the complex receptances are derived. The variation with frequency of the real and imaginary parts of the receptances are illustrated by means of two and three dimensional curves. An expression for the dissipation function for use in Langrange's equations of motion is derived and receptances for systems having several degrees of freedom are obtained using the Lagrangian equations. Chapter 9 deals with hysteretic damping in much the same way as the previous chapter does with viscous damping. Hysteretic damping is put forward to account for the damping due to imperfect elasticity of the material of the spring. The damping force arising from this source is assumed to be in phase with the velocity and independent of frequency. However, the main justification for the inclusion of the chapter appears to be that the assumption of hysteretic damping leads to simpler algebra than does viscous damping. Nevertheless, the authors return to viscous damping in Chapter 10 and consider the free vibration of systems.

In the final Chapter non-harmonic and transient vibrations are discussed. The reader is reminded that a non-harmonic periodic force may be replaced by the sum of its Fourier components. The response of an undamped system may then be found by summing the product of each of the components and the corresponding receptance. The importance of these considerations to engineering designers is pointed out. The solution of problems involving the transient excitation of single degree of freedom systems using the Duhamel integral is considered. The impulsive excitation of multidegree of freedom systems is examined and impulsive receptances are derived; these are then used to solve problems involving the transient excitation of multidegree of freedom systems. The Chapter ends with a very interesting graphical solution to the transient response of single degree of freedom systems due to passage through resonance.

The layout of the book has been carefully thought out and the discussions, proofs, etc., are presented with exceptional clarity. There are examples at the end of each Chapter to which answers are given. Consequently the book should appeal to the reader who wishes to gain or develop the physical insight which is so valuable in this field. Matrix methods are not used but presumably they will feature in the second volume to which reference is made in the text. Other important items not included in the present book are numerical methods for the extraction of the roots of the frequency equation and the determination of the corresponding mode shapes, the vibration characteristics of rotating elastic systems, of gyroscopic systems and of non-linear and self-excited systems, instability, and experimental techniques. There is a real need for a book covering these items in the careful and logical manner of the present book and it is hoped that the authors will find time to undertake this task.

H. McCALLION

L. D. LANDAU and E. M. LIFSHITZ: **Mechanics** (Vol. 1 of 'Course of Theoretical Physics'). Translated from the Russian by J. B. SYKES and J. S. BELL. Pergamon Press, Oxford, 1960. 165 pp., 40s.

SEVERAL volumes of this remarkable tour-de-force in theoretical physics have already appeared in translation, but this one is the first in the actual sequence and deals with the foundations, namely classical mechanics. However, while containing plenty of elementary material, it is in no sense a conventional introduction to mechanics, but rather supplementary reading at a fairly advanced level, say for Final Honours mathematicians and physicists. It is quite short and covers only the indispensable minimum required for the succeeding volumes. On the other hand, some of the material is rarely found in books on mechanics, principally the Chapter on collisions and scattering of beams of particles. The other six Chapters, however, are for the most part concerned strictly with the classical basis, as their titles indicate: The Equations of Motion, Conservation Laws, Integration of the Equations of Motion, Small Oscillations, Motion of a Rigid Body, and The Canonical Equations.

There are many glimpses of really advanced topics, for instance resonance in non-linear oscillations. There are also frequent touches of individuality in treatment and emphasis, especially the reversal of the historical development from Newtonian to Lagrangian mechanics. Here the Least Action principle is assumed at the outset, together with postulated properties of inertial

frames of reference (so-called isotropy of space and homogeneity of space and time); from these are deduced the Lagrangian for a free particle and for a system, and hence Newton's laws. The logical structure could be criticized at various points from a philosophical standpoint, and in any event the reversal is highly undesirable for pedagogic purposes.

A number of problems (with solutions) are included, some of them developing the text. But too many are either trivial or do not test understanding, while a few are simply irrelevant (e.g. the elementary statics problems towards the end of the Chapter on Euler's equations and motion of tops).

Apart from this the book can be highly recommended as a tonic change from the ordinary run of texts on mechanics.

R. HILL

M. REDWOOD: **Mechanical Waveguides. The Propagation of Acoustic and Ultrasonic Waves in Fluids and Solids with Boundaries.** Pergamon Press, Oxford, 1960. 250 pp., 50*s*.

THE PAST TWO DECADES have brought considerable progress in the study of wave propagation in bounded media, and the appearance of a book devoted to this topic is very welcome. Dr. REDWOOD sets himself the task of making recent developments accessible to the non-specialist for whom guided mechanical waves are but a means to an end but who must, nevertheless, have some understanding of their behaviour. With this end in view the opening chapter is devoted to a brief account of the propagation of elastic waves in an infinite solid, with sound waves in fluids treated as a degenerate case, while the following chapter consists of an examination of the reflection and refraction of plane waves at an interface between various combinations of solid/fluid/vacuum.

The remaining eleven chapters are devoted to surveying the propagation of both continuous waves and pulses in fluid and solid waveguides. These range from comprehensive accounts for the infinite plate and circular cylinder (Chapters 3–7, 9, 10) to short reports on waveguides of miscellaneous cross-sections (Chapter 8), multilayered waveguides (Chapter 11), solid resonators (Chapter 12) and anisotropic media (Chapter 13). The main emphasis is on examining the dispersion (phase velocity–wavelength) relations and wherever possible interpreting these in terms of reflection at the boundaries. For continuous waves the methods of obtaining these dispersion relations are considered in some detail but for the more complex problem of pulses the specialist is generally referred to the original publications. As a result the mathematical standard required of the reader is not excessively high and unfamiliar topics are covered in four appendices. A fifth appendix is devoted to experimental techniques and the book contains a summary of the more important equations and results of the opening chapters, for ease of reference. Each chapter is followed by an excellent list of references, both directly cited and covering related topics. The result is a reference book of value not only to the non-specialist but also to the active research worker in this field.

W. A. GREEN

A. E. GREEN and J. E. ADKINS: **Large Elastic Deformations and Non-Linear Continuum Mechanics.** Clarendon Press, Oxford, 1960. xiii + 348 pp., 55*s*.

PRIMARILY, this is a sound and rather comprehensive treatment of non-linear elasto-statics, a subject in which both authors are expert. The breadth of the work is indicated by the Chapter titles. These are The Strain Energy Function, General Solutions of Problems, Finite Plane Strain, Theory of Elastic Membranes, Theory of Successive Approximations, Approximate Solution of Two-dimensional Problems, Reinforcement by Inextensible Cords, Thermodynamics of Deformation, Stability, Experimental Applications and Rheological Equations of State. The last named covers the formulation of nonlinear theories of viscoelasticity and hypoelasticity. There is essentially no coverage of non-linear dynamic elasticity theory.

While this work is reasonably self-contained, readers with rather slight acquaintance with the subject would do well to study related material in GREEN and ZERNA's *Theoretical Elasticity*

before tackling it. Those seriously interested in learning about this area of mechanics should find the book very helpful. A noteworthy feature is that considerable attention is given to anisotropic media.

The reviewer takes this opportunity to record a corrigendum communicated to him by the authors. In Chapter II, § 2.8 ff, the strain energy function W cannot be completely general, but should be restricted so that $\tau^{12} = \tau^{13} = 0$ in order that the equations of equilibrium be satisfied. Alternatively, W can be left general by allowing for the more general deformation mentioned on p. 71, with suitable modifications for the rectilinear cuboid.

J. L. ERICKSEN

NOTICE

WAVERLEY GOLD MEDAL ESSAY COMPETITION 1961

Research is this year sponsoring The Waverley Gold Medal Essay Competition for the ninth year in succession. The Competition is designed to encourage the scientist in the laboratory and the engineer in the production plant to express his views and translate his work into an essay that will be readily understood by other scientists, directors of industrial firms and others interested in science and technology.

The **Waverley Gold Medal**, named after and bearing the coat of arms of the late Lord Waverley, together with **£100** will be awarded for the best essay of about 3000 words describing a new project or practical development in pure or applied science, giving an outline of the scientific background, the experimental basis and the potential or actual application of the idea to industry or their importance to society. The essays will be judged for technical content by specialists in the subject, for clarity of presentation and for style. The entry should be written as an essay which should interest a well-informed layman. In assessing these essays particular attention will therefore be paid (a) to the logical presentation, (b) to the style, and (c) adherence to these terms of reference.

A second prize of **£50** will be awarded and also a special prize of **£50** for the best entry from a competitor under the age of thirty on 31 July 1961. If the first prize is awarded to a competitor under the age of thirty, the special prize will go to the next best entry. Entry Forms can be obtained from the Editor of *Research*, 88 Kingsway, W.C.2.

The last date of entry is 31 *July* 1961.

J. Mech. Phys. Solids, 1961, Vol. 9, pp. 215 to 229. Pergamon Press Ltd., London. Printed in Great Britain

INTERPRETATION OF MATHEMATICAL SOLUTIONS IN VISCOELASTICITY THEORY ILLUSTRATED BY A DYNAMIC SPHERICAL CAVITY PROBLEM

By F. J. Lockett
Armament Research and Development Establishment, Fort Halstead

(*Received* 24*th April*, 1961)

Summary

The purpose of this paper is to discuss the means by which physically meaningful results can be obtained from formal mathematical solutions to stress analysis problems in linear viscoelasticity theory. The discussion is illustrated by considering the effect produced by a rapid, but not discontinuous, change in pressure at the surface of a spherical cavity in an infinite medium. Results for the viscoelastic medium are compared with those for an elastic medium, and numerical solutions are presented graphically for typical cases.

1. Introduction

The mathematical theory of linear viscoelasticity is now well established, due to the work of authors such as Gross (1953, 1947), though it has received the attention of many authors in recent years. Perhaps the most notable recent contributions are a survey article on the propagation of viscoelastic waves by Hunter (1960a) and a textbook on the general theory of viscoelasticity by Bland (1960). The former topic has also been discussed by Kolsky (1960) and the subject of stress analysis in viscoelastic bodies has been treated by Lee (1960).

Despite this interest in the theory itself, far too little attention seems to have been given to the realistic application of the theory to problems of stress analysis. Too often general solutions are obtained in mathematical form (e.g. in terms of integral transforms) and are then specialized to the somewhat hypothetical spring-and-dashpot models of Voigt and Maxwell. The only real advantage of the use of these models is that they have an analytically simple form of complex modulus, and so in applications to simple problems they may lead to explicit analytic solutions. But in any but the most simple problems it is necessary to introduce some numerical procedure and these simple models do not then have a great advantage over more realistic models or the actual experimental curves representing the true mechanical behaviour. It has also been the practice of some writers to introduce into their mathematical treatment quantities which cannot be measured experimentally.

The problems considered to date are mainly of a one dimensional nature: see, for example, Berry and Hunter (1956), Kolsky (1956), Glauz and Lee (1954) and Lee (1953, 1956) – though three-dimensional problems have been considered by Hunter (1960b), Lee *et al.* (1959) and Bland (1957, 1960), and with the

increasing interest in the subject many more solutions will no doubt be derived from classical elasticity theory using the correspondence principle (see, for example, BLAND, 1960).

The aim of the present paper is to discuss the application of the mathematical theory to stress analysis problems, and to illustrate it by an application to a particular problem. Section 2 contains a discussion of the application of the basic theory and of the method of characterization of the material. In the following Sections the effect produced by a rapid, but not discontinuous, change in the normal pressure applied at the surface of a spherical cavity is considered. The analysis is made within the framework of the linear theory and the detailed numerical results are restricted to the immediate effects (of the order of ten times the rise-time of the loading) and not to the long-term effects. The solution obtained is compared with two elastic solutions which can be thought of as bounding cases to the viscoelastic representation.

In passing, it may be mentioned here that the problem of the dynamical expansion of spherical cavities in other types of material, especially ductile metals, has been surveyed by HOPKINS (1960). Particular mention should also be made of the work of HUNTER (1954) (although certain corrections due to GREEN (see HOPKINS 1960) should be carefully noted) and of the more general treatment of the spherical cavity problem in elastic materials by ERINGEN (1957).

2. PRACTICAL APPLICATION OF THE MATHEMATICAL THEORY OF LINEAR VISCOELASTICITY

There are several, albeit formally equivalent, forms in which the basic equations of linear viscoelasticity theory can be presented. In the complex modulus formulation, the equations are written in terms of complex Fourier transforms $\bar{f}(\mathbf{x}, \omega)$, viz.

$$\bar{f}(\mathbf{x}, \omega) = \int_{-\infty}^{\infty} f(\mathbf{x}, t)\, e^{-i\omega t}\, dt, \tag{2.1}$$

where the function $f(\mathbf{x}, t)$ is real and

$$f(\mathbf{x}, t) = \frac{1}{\pi} \operatorname{Re} \int_{0}^{\infty} \bar{f}(\mathbf{x}, \omega)\, e^{i\omega t}\, d\omega, \tag{2.2}$$

Re denoting the real part. In this form the basic equations of the linear theories of elasticity and viscoelasticity differ only in one respect, namely that the quantities expressing the material properties are constants in the elastic case (for example, the Lamé constants), whilst in viscoelasticity theory these quantities are complex functions of the transform variable ω. Thus, in problems that can be solved by the transform method, it is only in the interpretation of integrals like (2.2) that the elastic and viscoelastic solutions differ, the transforms of the unknown quantities having been found using the transformed basic equations and the transformed boundary conditions. It is with the interpetation or evaluation of these integral solutions that this paper is concerned.

In any particular solution expressions for the functions $\bar{f}(\mathbf{x}, \omega)$ appearing in (2.2) will contain the complex modulus functions $X(i\omega)$, $Y(i\omega)$ for shear and

bulk deformations. These functions are respectively the ratios of the transformed stress component to the transformed strain component for shear and bulk deformations. It is usual to write

$$X(i\omega) = X_1(\omega)\left[1 + i \tan \delta_x(\omega)\right], \tag{2.3}$$

with a similar representation for $Y(i\omega)$.

Thus, if the integral expressions are to be evaluated, then the functions $X(i\omega)$ and $Y(i\omega)$ must be specified, and since theoretical expressions are not available experimental data must be used. This can be done either by using the experimental data directly or by fitting some model to that data. It should be noted that the integral (2.2) is taken over an infinite range, whereas experimental data can only be available over a finite range of frequency. Thus the integrals can at best be approximated by finite integrals, and models can only be fitted over a finite range. However, the integrands $\bar{f}(\mathbf{x}, \omega)$ will in general be of such a form that the integrals have to be evaluated numerically, and therefore confined to a finite approximation for this reason also.

Most solutions to viscoelastic problems appearing in the literature are either left in the integral form or are specialized to some simple spring-and-dashpot representation for $X(i\omega)$ and $Y(i\omega)$. It has, however, been shown by KOLSKY and SHI (1958) that, in general, these simple models do not adequately represent the behaviour of real polymers. Thus, if only the solution to a particular problem is required, it would seem advisable to use the experimental data directly in the numerical integration. If it is desired to keep a number of parameters in the solution then mathematical models should be chosen which fit the experimental data well, even though they may not correspond to a simple spring-and-dashpot configuration. The simple forms of modulus corresponding to the simple spring-and-dashpot models only have an advantage in the solution of simple problems, when it may be possible to evaluate the integrals explicitly.

The basic theory of viscoelasticity requires that certain interrelations should be satisfied between the characterizing quantities, e.g. between $X_1(\omega)$ and $\tan \delta_x(\omega)$. Since the experimental values presumably satisfy these interrelations, models fitted separately to $X_1(\omega)$ and $\tan \delta_x(\omega)$ should not violate them too seriously. It is not possible to verify this accurately since the interrelations involve infinite integrations which cannot be evaluated exactly.

The choice of model to be used in the illustration below is based on the results of LETHERSICH (1950) for ebonite, polystyrene, polymethylmethacrylate and polythene at room temperature. The complete mathematical model chosen is

$$X(i\omega) = (\alpha \log_e \omega + \beta)(1 + i \tan \delta), \qquad Y(i\omega) = Y, \tag{2.4}$$

where α, β, $\tan \delta$ and Y are constants.

LETHERSICH's results for the real part of the complex modulus in shear are shown in Fig. 1. The logarithmic variation chosen in (2.4) is a good fit to these curves compared with the fit of the simple spring-and-dashpot models. KOLSKY and SHI (1958) noted from LETHERSICH's results that the assumption $\tan \delta_x =$ constant is much more accurate than the variation predicted by the simple spring-and-dashpot models. Experimental data for bulk deformation are available only over very restricted frequency ranges, and are insufficient to fit a reliable model.

However, such data as exist indicate that viscoelastic effects are small in bulk deformations in comparison with shear deformations. For these reasons the behaviour in bulk has been assumed to be adequately represented by a purely elastic behaviour.

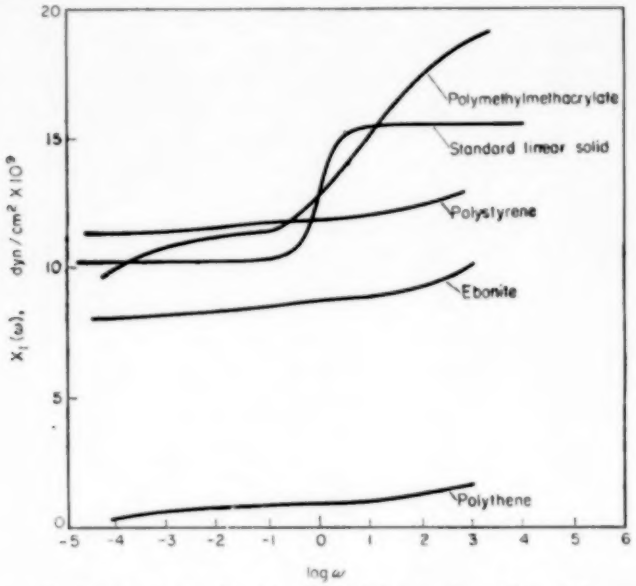

FIG. 1. Real part of complex (shear) modulus vs. logarithm of frequency.

A final point to be made relative to the interpretation of the integral solutions is the distinction between quantities which can and which cannot be measured experimentally. Certain quantities have been introduced into the general theory which cannot be measured experimentally, for example, the values of the moduli at zero and infinite frequencies. Since these quantities cannot be measured experimentally, and cannot be calculated accurately from the interrelations, they should not be retained in the final solutions, even when they are introduced for convenience in the analysis.

3. Dynamical Problem for a Spherical Cavity in an Infinite Medium

Consider now a spherical cavity of radius r_0 in an infinite viscoelastic material of the class discussed in the previous Section. It will be assumed that the cavity is not subjected to shear loading, but merely to a variation in the normal component of stress σ_r. Suppose, first, that this applied loading takes the form

$$\sigma_r = \sigma_{r0} = \begin{cases} -\tfrac{1}{2}P, & -\infty < t < 0 \\ \tfrac{1}{2}P, & 0 < t < \infty \end{cases} \quad \text{on} \quad r = r_0. \tag{3.1}$$

This loading involves a jump of amount P at $t = 0$ above a steady loading of amount $-\tfrac{1}{2}P$. The transform of σ_{r0} will then be

$$\bar{\sigma}_{r0} = \int_{-\infty}^{\infty} \sigma_{r0}(t)\, e^{-i\omega t}\, dt = \frac{P}{i\omega}, \tag{3.2}$$

where ω is real and the principal value of the integral is taken. In the actual loading considered later this specialization is not necessary.

It will be seen in the next Section that the solutions for the stresses and displacements due to the applied loading appear in the form of infinite integrals. These integrals, which include $\bar{\sigma}_{r\theta}$ as a factor in the integrand, also involve the function $X(i\omega)$. Since the model (2.4) is only valid in the experimental range, it would be necessary in the viscoelastic solution to approximate the infinite integral by a finite integral, the limits of integration being those of the experimental results. The effect of this approximation cannot be accurately assessed. The corresponding elastic problem (which corresponds to $X_1 =$ constant and which will be used for the purpose of comparison) can however be solved exactly. In making a comparison between the elastic and viscoelastic solutions it would then be difficult to say which differences were due to the approximation in the viscoelastic solution, and which were due to the difference in the nature of the materials.

This difficulty can be overcome by considering a slightly different problem. Instead of considering the loading (3.1) which has the transform (3.2), the loading $\sigma_{r\theta}$ is considered which has the transform

$$\bar{\sigma}_{r\theta} = \begin{cases} 0, & 0 \leqslant \omega < \omega_1 \\ P/i\omega, & \omega_1 \leqslant \omega \leqslant \omega_2 \\ 0, & \omega_2 < \omega \leqslant \infty \end{cases} \tag{3.3}$$

where the range (ω_1, ω_2) lies within the experimental range. The exact solution to both the elastic and the viscoelastic problem is then a finite integral over the range (ω_1, ω_2) and in each case $X(i\omega)$ is known over the whole range.

The loading corresponding to the transform (3.3) is given by the inversion formula (2.2) as

$$\frac{\pi\sigma_{r\theta}}{P} = \mathrm{Re}\int_{\omega_1}^{\omega_2} \frac{1}{i\omega}\, e^{i\omega t}\, d\omega = \int_{\omega_1}^{\omega_2} \omega^{-1} \sin \omega t\, d\omega = \mathrm{Si}(\omega_2 t) - \mathrm{Si}(\omega_1 t), \tag{3.4}$$

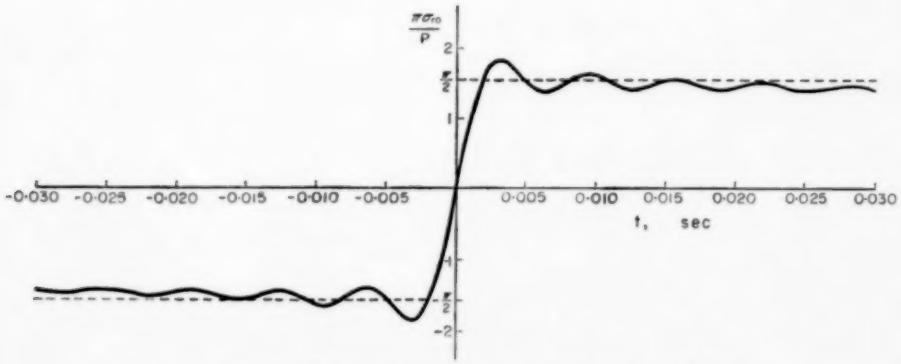

FIG. 2. Time variation of pressure applied to surface of cavity.

where $\mathrm{Si}(x)$ denotes the sine integral. For the numerical values $\omega_1 = 5\ \mathrm{sec}^{-1}$, $\omega_2 = 1000\ \mathrm{sec}^{-1}$ the loading (3.4) is the near-square function shown in Fig. 2. This loading is considered in its own right and not as an approximation to an exactly

square loading. The latter is not obtainable in practice, so the present loading is more realistic. Obviously the rise-time of the pulse can be made shorter by increasing ω_2 (up to the upper limit of the experimental range).

By this procedure exact solutions (within the limits set by the model) are obtained for both an elastic and a viscoelastic medium, so that an effective comparison may be made between the behaviour of the two types of material. Attention will be restricted to the immediate dynamic effects of the loading (i.e. times up to ten times the rise-time of the applied loading) and not to the long term effects.

4. Solution of the Basic Equations

Due to the type of loading considered the problem has spherical symmetry and there are therefore only two independent variables, viz. r and t. In terms of the radial displacement u, the components of strain may therefore be written

$$\left.\begin{aligned} &\epsilon_{rr} = \frac{\partial u}{\partial r}, \qquad \epsilon_{\theta\theta} = \epsilon_{\phi\phi} = \frac{u}{r}, \\ &\epsilon = \frac{\partial u}{\partial r} + \frac{2u}{r}, \qquad \epsilon_{r\phi} = \epsilon_{r\theta} = \epsilon_{\theta\phi} = 0. \end{aligned}\right\} \tag{4.1}$$

Thus the transformed stress–strain relations become

$$\left.\begin{aligned} &\bar{\sigma}_r = \lambda\left(\frac{\partial \bar{u}}{\partial r} + \frac{2\bar{u}}{r}\right) + 2\mu\frac{\partial \bar{u}}{\partial r}, \\ &\bar{\sigma}_\theta = \bar{\sigma}_\phi = \lambda\left(\frac{\partial \bar{u}}{\partial r} + \frac{2\bar{u}}{r}\right) + 2\mu\frac{\bar{u}}{r}, \\ &\bar{\sigma}_{r\phi} = \bar{\sigma}_{r\theta} = \bar{\sigma}_{\theta\phi} = 0, \end{aligned}\right\} \tag{4.2}$$

where $3\lambda = Y - X$ and $2\mu = X$.

The only non-trivial equation of motion is, in the absence of body forces,

$$\frac{\partial \sigma_r}{\partial r} + \frac{2}{r}(\sigma_r - \sigma_\theta) = \rho\frac{\partial^2 u}{\partial t^2}, \tag{4.3}$$

where ρ is the density of the material.

Applying the transform (2.1) to (4.3) and substituting from (4.2) gives the equation

$$\frac{\partial^2 \bar{u}}{\partial r^2} + \frac{2}{r}\frac{\partial \bar{u}}{\partial r} - \frac{2\bar{u}}{r^2} = -a^2\omega^2\bar{u}, \tag{4.4}$$

where $a^2 = \rho/(\lambda + 2\mu)$. This equation has the general solution

$$\bar{u} = \frac{\partial}{\partial r}\left[\frac{C(\omega)e^{ia\omega r} + D(\omega)e^{-ia\omega r}}{r}\right]. \tag{4.5}$$

Thus, restricting attention to outgoing waves only (due to the infinite extent of the homogeneous medium),

$$\bar{u} = -Dr^{-2}(1 + ia\omega r)e^{-ia\omega r}. \tag{4.6}$$

Equation (4.2) then yields the expressions

$$\left.\begin{aligned} &\bar{\sigma}_r = Dr^{-3}\left[4\mu(1 + ia\omega r) - \rho\omega^2 r^2\right]e^{-ia\omega r}, \\ &\bar{\sigma}_\theta = -Dr^{-3}\left[2\mu(1 + ia\omega r) + a^2\omega^2 r^2\lambda\right]e^{-ia\omega r}. \end{aligned}\right\} \tag{4.7}$$

Applying the boundary condition $\sigma_r = \sigma_{r0}$ on $r = r_0$, it is found that

$$D = r_0^3 \bar{\sigma}_{r0} e^{ia\omega r_0} \left[4\mu (1 + ia\omega r_0) - \rho\omega^2 r_0^2\right]^{-1}.$$

Therefore, by substituting this expression into (4.6) and (4.7) and applying the inversion formula (2.2), the values of u and σ_θ on the cavity surface (u_c and $\sigma_{\theta c}$) and σ_r can be written in the form

$$u_c(t) = -\frac{r_0}{\pi} \mathrm{Re} \int_0^\infty \frac{(1 + ia\omega r_0)\, \bar{\sigma}_{r0}\, e^{i\omega t}}{4\mu (1 + ia\omega r_0) - \rho\, \omega^2 r_0^2}\, d\omega, \tag{4.8}$$

$$\sigma_{\theta c}(t) = -\frac{1}{\pi} \mathrm{Re} \int_0^\infty \frac{2\mu (1 + ia\omega r_0) + a^2 \omega^2 r_0^2 \lambda}{4\mu (1 + ia\omega r_0) - \rho\omega^2 r_0^2}\, \bar{\sigma}_{r0}\, e^{i\omega t}\, d\omega, \tag{4.9}$$

$$\sigma_r(r, t) = \frac{r_0^3}{r^3} \frac{1}{\pi} \mathrm{Re} \int_0^\infty \frac{4\mu (1 + ia\omega r) - \rho\omega^2 r^2}{4\mu (1 + ia\omega r_0) - \rho\omega^2 r_0^2}\, \bar{\sigma}_{r0} \exp\left\{i\omega \left[t - a(r - r_0)\right]\right\} d\omega. \tag{4.10}$$

where $\bar{\sigma}_{r0}$ is, in the present analysis, given by (3.3).

5. Numerical Values: Importance of Inertia Terms

To illustrate the solutions obtained in the previous Section, typical numerical values are now substituted into the integrands and the solutions evaluated numerically. To characterize the viscoelastic material the following values are chosen:

$$\rho = 1\ \mathrm{g/cm^3}, \quad \alpha = 10^8\ \mathrm{dyn/cm^2}, \quad \beta = 10^9\ \mathrm{dyn/cm^2}, \quad \tan\delta = 10^{-1},$$

$$Y = 3k = 12 \times 10^{10}\ \mathrm{dyn/cm^2}. \tag{5.1}$$

These values are typical of the polymers investigated by Lethersich (1950) at temperatures where they are in the glass-like state. As introduced in Section 3 the values $\omega_1 = 5\ \mathrm{sec^{-1}}$, $\omega_2 = 1000\ \mathrm{sec^{-1}}$ are used, so that the applied loading is as shown in Fig. 2.

For the sake of comparison, two elastic solutions ($\alpha = \tan\delta = 0$) are also evaluated, the first solution with $\beta = 10^9\ \mathrm{dyn/cm^2}$, the second with $\beta = 2 \times 10^9\ \mathrm{dyn/cm^2}$. These solutions will be referred to as the first and second elastic solutions. The representations of $X_1(\omega)$ are shown in Fig. 3, and it will be noted that the elastic cases form an upper and a lower limit for the viscoelastic case over the relevant range of frequencies.

The radius of the cavity r_0 remains to be assigned. It may be noted that the solutions (4.8)–(4.10) take on a much simpler form if the terms

$$\rho\omega^2 r^2, \qquad \rho\omega^2 r_0^2, \qquad a^2 \omega^2 r_0^2 \lambda, \tag{5.2}$$

are small enough to be neglected in comparison with μ. By considering the two values $r_0 = 1$ cm and $r_0 = 100$ cm the two cases will be covered where these inertia terms are and are not negligible respectively. (Attention is confined to a finite region $r \leqslant 10\, r_0$ as this is sufficient to exhibit the results of interest). Presented in this way it appears that r_0, which is in fact the fundamental linear dimension, is the critical quantity in determining whether inertia terms are negligible. However it can also be seen that for a given cavity size in a given material it is the value of ω_2 which determines whether the terms (5.2) are small. Thus, if the rise-time of the loading is greater than a certain value, the terms (5.2) may be neglected, but for smaller values they must be taken into account. In fact it is, in general,

a combination of all the parameters which determines whether the inertial terms can be neglected. It should be noted that, in general, the case where these terms may be neglected does not correspond to a quasi-static solution since a is not neglected in the expression $(1 + ia\omega r)$.

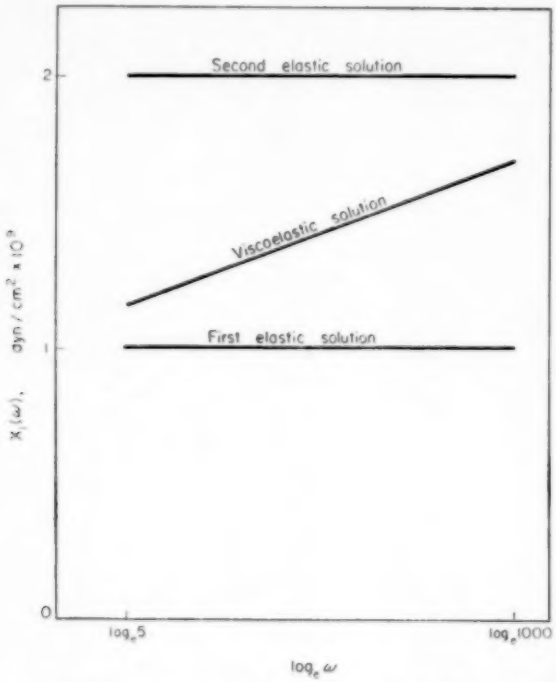

FIG. 3. Real part of complex shear modulus for the three solutions.

6. NUMERICAL SOLUTIONS: INERTIA TERMS SMALL

If, in the solutions (4.8)–(4.10), the terms (5.2) are neglected these solutions reduce to the forms

$$u_r(t) = -\frac{r_0}{4\pi}\,\mathrm{Re}\int_0^\infty \frac{\bar{\sigma}_{r0}}{\mu}\,e^{i\omega t}\,d\omega, \tag{6.1}$$

$$\sigma_{\theta r}(t) = -\frac{1}{2\pi}\,\mathrm{Re}\int_0^\infty \bar{\sigma}_{r0}\,e^{i\omega t}\,d\omega = -\tfrac{1}{2}\,\sigma_{r0}(t). \tag{6.2}$$

$$\sigma_r(r,t) = \frac{r_0^3}{r^3}\,\frac{1}{\pi}\,\mathrm{Re}\int_0^\infty \frac{1 + ia\omega r}{1 + ia\omega r_0}\,\bar{\sigma}_{r0}\exp\{i\omega[t - a(r - r_0)]\}\,d\omega. \tag{6.3}$$

Thus, in both the elastic and viscoelastic cases, the circumferential stress at the cavity is one-half the applied normal stress at that instant. In the elastic cases (6.1) can be written

$$u_r(t) = -\frac{r_0}{4\mu}\,\frac{1}{\pi}\,\mathrm{Re}\int_0^\infty \bar{\sigma}_{r0}\,e^{i\omega t}\,d\omega = -\frac{r_0}{4\mu}\,\sigma_{r0}(t), \tag{6.4}$$

which shows that, in these elastic solutions, the displacement at the boundary is a trivial solution, proportional to the applied loading. These solutions are shown in Fig. 4 for the two values of μ chosen in Section 5. As is obvious from the expression (6.4), the cavity displacement is greater in the material of smaller μ, and in both cases follows the applied loading exactly.

For the viscoelastic material (6.1) can be written

$$u_c(t) = \frac{Pr_0}{4\pi} \operatorname{Re} \int_{\omega_1}^{\omega_2} \frac{i\omega^{-1}}{\mu_1 + i\mu_2} e^{i\omega t}\, d\omega,$$

where μ has been decomposed into its real and imaginary parts, and the expression (3.3) substituted for $\bar{\sigma}_{rw}$. This expression is equivalent to

$$u_c(t) = \frac{Pr_0}{4\pi} \int_{\omega_1}^{\omega_2} \omega^{-1} (\mu_1^2 + \mu_2^2)^{-1} (\mu_2 \cos \omega t - \mu_1 \sin \omega t)\, d\omega, \tag{6.5}$$

and this function has also been plotted in Fig. 4 (denoted by a broken line) using the numerical values of Section 5 and remembering that $X = 2\mu$. It will be noted that the viscoelastic solution does not follow the applied loading exactly but tends to lag behind it by a small amount. At small times after the reversal of loading is applied, that is when large frequency components are most important, the viscoelastic solution behaves like the elastic material with the larger modulus. This is to be expected since at high-frequencies the modulus for the viscoelastic material agrees best with that for this elastic material (see Fig. 3). Conversely, as the time increases, and smaller values of frequency become more important, the viscoelastic solution departs from this elastic solution and tends towards the solution for the elastic material with the smaller modulus.

It may be noted that in all these solutions for the cavity displacement only the shear modulus is involved, the bulk modulus playing no part.

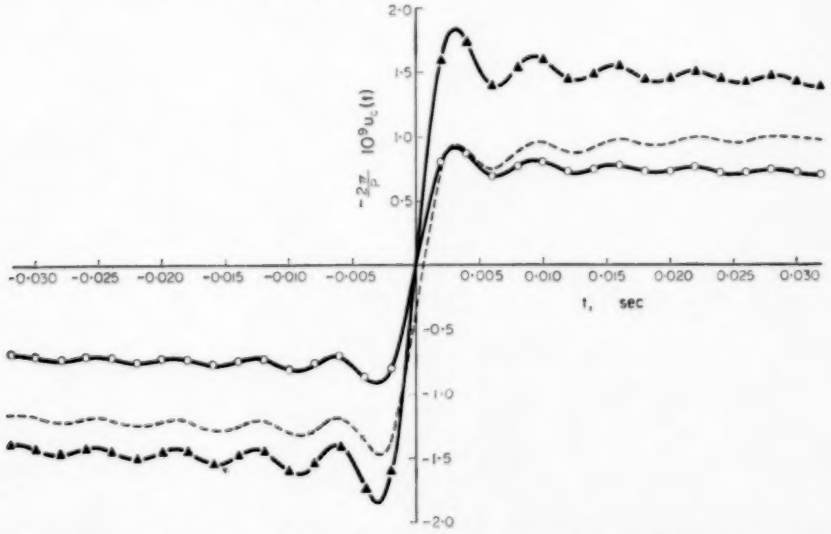

FIG. 4. Variation with time of surface displacement. Case (i) – Inertia negligible. ▲ First elastic solution, ○ Second elastic solution, – – – Viscoelastic solution.

From (6.3) the radial component of stress under the special loading condition (3.3) is

$$\sigma_r(r, t) = \frac{r_0^3}{r^3} \frac{P}{\pi} \operatorname{Re} \int_{\omega_1}^{\omega_2} \frac{1 + ia\omega r}{1 + ia\omega r_0} \frac{1}{i\omega} \exp\{i\omega [t - a(r - r_0)]\}\, d\omega,$$

which, upon setting $a = a_1 + ia_2$, becomes

$$\sigma_r(r, t) = \frac{r_0^3}{r^3} \frac{P}{\pi} \operatorname{Re} \int_{\omega_1}^{\omega_2} \frac{1 - a_2\,\omega r + ia_1\,\omega r}{1 - a_2\,\omega r_0 + ia_1\,\omega r_0} \frac{\exp[a_2\,\omega(r - r_0)]}{i\omega} \exp\{i\omega [t - a_1(r - r_0)]\}\, d\omega. \tag{6.6}$$

Now

$$a^2 = \frac{3\rho}{Y + 2X} = \frac{3\rho}{Y + 2X_1(1 + i \tan \delta)},$$

and remembering the magnitudes assigned to the various quantities in Section 5 it can be shown that

$$a_1 \sim \left(\frac{3\rho}{Y + 2X_1}\right)^{\frac{1}{2}}, \qquad a_2 \sim -\left(\frac{3\rho}{Y + 2X_1}\right)^{\frac{1}{2}} \frac{X_1 \tan \delta}{Y + 2X_1}, \tag{6.7}$$

In the expression for a_1 the values of Y and X_1 are such that neglect of the term $2X_1$ introduces an error of only 1 per cent. Thus in all three cases (two elastic and one viscoelastic) a_1 may be assigned the constant value

$$a_1 = (3\rho/Y)^{\frac{1}{2}} = \tfrac{1}{2} \cdot 10^{-5} \text{ sec/cm}. \tag{6.8}$$

Also the maximum values of r, a_2 and ω_2 are such that

$$a_2 \, \omega r \ll 1. \tag{6.9}$$

These remarks apply throughout the present analysis, including the next Section when inertia terms are relevant.

Equation (6.6) can now be simplified to the form

$$\sigma_r(r, t) = \frac{r_0^3}{r^3} \frac{P}{\pi} \operatorname{Re} \int_{\omega_1}^{\omega_2} \frac{1 + ia_1 \, \omega r}{1 + ia_1 \, \omega r_0} \frac{1}{i\omega} \exp\left\{ i\omega \left[t - a_1(r - r_0)\right]\right\} d\omega, \tag{6.10}$$

where a_1 is the constant (6.8), and (6.10) is the solution common to the elastic and viscoelastic problems. This solution may be written

$$\sigma_r(r, t) = \frac{r_0^3}{r^3} \frac{P}{\pi} \left\{ \int_{\omega_1}^{\omega_2} \frac{1 + a_1^2 \, \omega^2 \, rr_0}{\omega(1 + a_1^2 \, \omega^2 \, r_0^2)} \sin \omega t' \, d\omega + \int_{\omega_1}^{\omega_2} \frac{a_1(r - r_0)}{1 + a_1^2 \, \omega^2 \, r_0^2} \cos \omega t' \, d\omega \right\},$$

where $t' = t - a_1(r - r_0)$, and since $a_1^2 \, \omega^2 \, rr_0 \ll 1$ this approximates to

$$\sigma_r(r, t) = \frac{r_0^3}{r^3} \frac{P}{\pi} \left\{ \operatorname{Si}(\omega_2 t') - \operatorname{Si}(\omega_1 t') + \frac{a_1(r - r_0)}{t'} (\sin \omega_2 t' - \sin \omega_1 t') \right\}. \tag{6.11}$$

Reverting to (3.4) it is noted that

$$\sigma_{r0}(t) = \frac{P}{\pi} \left\{ \operatorname{Si}(\omega_2 t) - \operatorname{Si}(\omega_1 t) \right\}.$$

Thus

$$\sigma_r(r, t) \sim \frac{r_0^3}{r^3} \sigma_{r0} \left\{ t - a_1(r - r_0) \right\}, \tag{6.12}$$

the last term in (6.11) producing only a small correction and a delay of the nature found in the viscoelastic solution for the cavity displacement (see Fig. 4). Equation (6.12) shows that the radial stress at a station $r = r_1$ follows the applied loading after a time-delay equal to $a_1(r_1 - r_0)$ and has its amplitude reduced by the factor $(r_0/r_1)^3$.

It may be noted that in the quasi-static solution, when inertia terms are completely neglected (i.e. $\rho = 0$ and therefore $a = 0$) the radial stress becomes

$$\sigma_r(r, t) = \frac{r_0^3}{r^3} \frac{1}{\pi} \operatorname{Re} \int_0^{\infty} \bar{\sigma}_{r0} \, e^{i\omega t} \, d\omega = \frac{r_0^3}{r^3} \sigma_{r0}(t).$$

Thus the stress is propagated with an 'infinite' velocity. As can be seen from (6.7) and (6.12) the velocity of propagation in the present solution is equal to that of dilatational waves.

It has been shown that, for negligible inertia terms, the circumferential component of stress at the cavity $\sigma_{\theta c}(t)$ and the radial component of stress $\sigma_r(r, t)$ do not differ appreciably in the elastic and viscoelastic solutions. The former component is always exactly equal to one-half of the applied loading at that instant, whilst the latter approximately follows the applied loading with a small time-lag and with an amplitude which is inversely proportional to the cube of the radial coordinate. In both elastic solutions the cavity displacement is proportional to the applied loading, the constant of proportionality depending inversely on the shear modulus for the material. For small times after the reversal of loading the viscoelastic solution behaves like the elastic solution for which the agreement in the modulus is best at high-frequencies. Thereafter it departs from this elastic solution and tends towards the elastic solution for which the agreement in the modulus is best at low-frequencies.

7. Numerical Solutions: Inertia Terms Important

It is now assumed that $r_0 = 100$ cm, so that inertial effects become important. It can be seen that the statements (6.8) and (6.9) remain valid, so that the solutions (4.8)–(4.10) may be written

$$u_c(t) = \frac{Pr_0}{\pi} \operatorname{Re} \int_{\omega_1}^{\omega_2} \frac{(1 + ia_1\,\omega r_0)\, i\omega^{-1}\, e^{i\omega t}}{4\mu\,(1 + ia_1\,\omega r_0) - \rho\omega^2\, r_0^2}\, d\omega, \tag{7.1}$$

$$\sigma_{\theta c}(t) = \frac{P}{\pi} \operatorname{Re} \int_{\omega_1}^{\omega_2} \frac{2\mu\,(1 + ia_1\,\omega r_0) + (a_1^2 + 2ia_1\,a_2)\,\omega^2\, r_0^2\,\lambda}{4\mu\,(1 + ia_1\,\omega r_0) - \rho\omega^2\, r_0^2}\, i\omega^{-1}\, e^{i\omega t}\, d\omega, \tag{7.2}$$

$$\sigma_r(r, t) = \frac{r_0^3}{r^3}\frac{P}{\pi} \operatorname{Re} \int_{\omega_1}^{\omega_2} \frac{4\mu\,(1 + ia_1\,\omega r) - \rho\omega^2 r^2}{4\mu\,(1 + ia_1\,\omega r_0) - \rho\omega^2\, r_0^2}\frac{1}{i\,\omega} \exp\left\{i\omega\left[t - a_1\,(r - r_0)\right]\right\} d\omega. \tag{7.3}$$

In (7.2) the fact that $a_2^2 \ll a_1^2$ has also been used.

Remembering that in the elastic cases μ is real, while in the viscoelastic solution $\mu = \mu_1 + i\mu_2$, the real parts of the integrands of (7.1)–(7.3) may be taken and the solutions evaluated numerically using the values cited previously. The results for the cavity displacement are shown in Fig. 5. It is seen that for negative times,

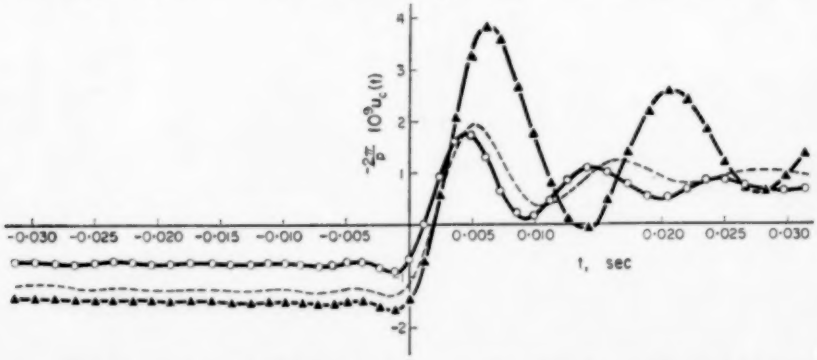

Fig. 5. Variation with time of surface displacement. Case (ii) – Inertia important. ▲ First elastic solution, ○ Second elastic solution, – – – Viscoelastic solution.

when the loading is steady apart from small oscillations, the cavity displacement is also steady. When the reversal of loading occurs the cavity displacement does not change in phase with the loading, as occurs with negligible inertia, but is

delayed due to the fact that the inertia of the material is now relevant. Once in motion, the cavity surface displacement overshoots its ' equilibrium ' value and performs damped oscillations. These oscillations are entirely due to inertia and not to the slight fluctuations in the applied loading which have a different (higher) frequency. As with negligible inertia the viscoelastic solution behaves at small times like the second elastic solution, but thereafter diverges from this solution towards the first. The frequency of the inertial oscillations in the viscoelastic case lies between the frequencies of the elastic solutions. The damping of these oscillations is, in the elastic cases, entirely due to spherical divergence. In the viscoelastic case the material itself produces some additional damping, and this is easily confirmed by examination of Fig. 5 where the viscoelastic solution is damped more rapidly than both of the elastic solutions.

If the variation of σ_r with $R = r/r_0$ is plotted for several constant values of t, it is found that for negative times, when conditions are approximately steady, the distribution of σ_r is also approximately steady, having the value $-\frac{1}{2}P$ at the cavity surface and varying like R^{-3} with distance from the origin. For large positive

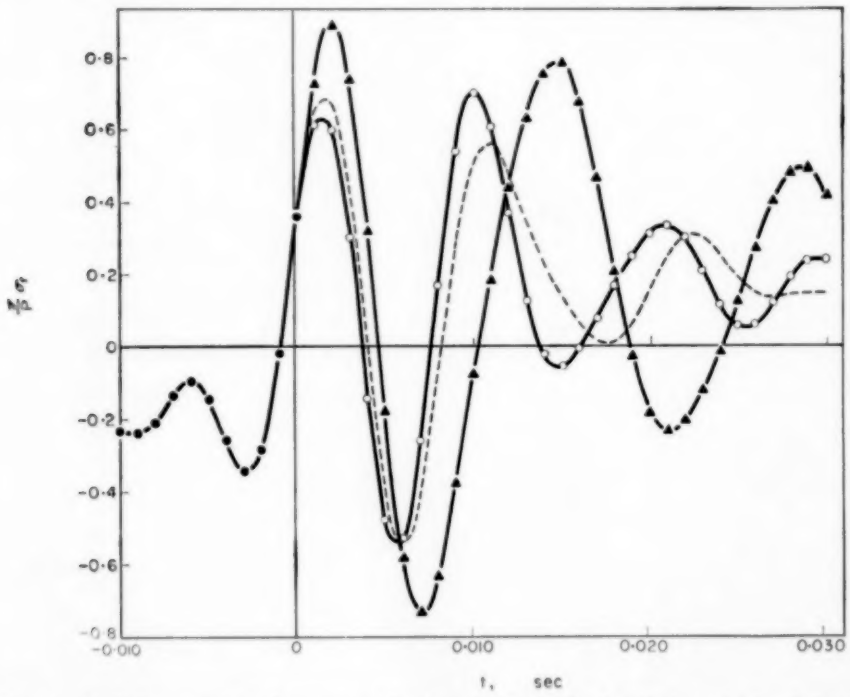

FIG. 6. Radial component of stress vs. t for $R = 2$. Case (ii) – Inertia important. ▲ First elastic solution, ○ Second elastic solution, – – – Viscoelastic solution, ● Points common to all three solutions.

times, after the inertial oscillations have been damped out, the radial stress distribution reaches an equilibrium state which is the ' mirror-image ' of that for negative times. That is, it has the value $+\frac{1}{2}P$ at the cavity surface and is proportional to R^{-3}. For intermediate times the stress at the cavity surface follows

the applied loading, but the distribution of σ_r with R follows a complicated pattern due to the propagation of the applied stress and to the oscillations of the material which induce fluctuations in the values of the stress components. Due to the different frequencies of these inertial oscillations in the different media, examination of the curves σ_r versus R for fixed values of t is not an instructive way of comparing the elastic and viscoelastic solutions. The comparison is best made by studying the time variation of stress for a fixed value of R. Fig. 6 shows these variations for the station $R = 2$. For negative times the fluctuations in loading are only small, so it is not surprising that, in common with the negligible inertia case, the three solutions are approximately identical. Thereafter the conclusions are similar to those drawn from the cavity displacement results. That is, all three solutions perform damped oscillations, the viscoelastic case being damped most rapidly and having a frequency intermediate to those of the elastic solutions. For small times the viscoelastic solution agrees best with the second elastic solution but thereafter diverges from that solution towards the first elastic solution. These remarks also apply to the circumferential component of stress at the cavity $\sigma_{\theta c}$ which has been plotted in Fig. 7.

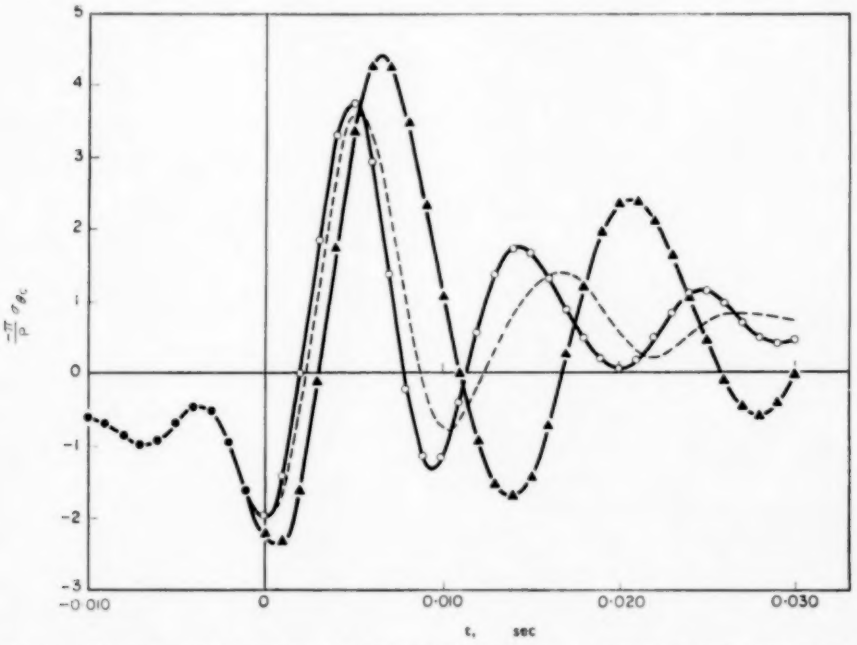

Fig. 7. Circumferential component of stress at the cavity vs. t. Case (ii) – Inertia important. ▲ First elastic solution, ○ Second elastic solution, – – – Viscoelastic solution, ● Points common to all three solutions.

The results of this section are now summarized. The rapid change of loading on the boundary induces a spherically-attenuated stress wave to travel radially outward from the cavity. This wave is, however, soon obscured by the fluctuations in stress caused by the oscillation of the material. These oscillations, and the fluctuations of stress which they produce, are damped most rapidly in the viscoelastic

material, and the frequency of oscillation in that material lies between the frequencies obtained in the two elastic solutions. At small times the viscoelastic solution agrees best with the solution for the elastic material with the larger rigidity modulus, but tends towards the other elastic solution as time increases.

8. Summary of Results

Two situations have been considered, corresponding to negligibly small inertia terms ($\mu_1 \gg \rho\,\omega_2^2\,r^2$) and to inertia terms of important magnitude. In the former it is found that, within the range of times considered, the solutions for the stress components are almost identical in the elastic and viscoelastic analyses. This is due mainly to the relative magnitude of the bulk and shear moduli. The displacement of the cavity is delayed slightly in the viscoelastic material in contrast to the elastic solutions which follow the applied loading exactly. For small times the amplitude of the displacement in the viscoelastic material agrees with that for the elastic material with the larger rigidity modulus, but thereafter diverges from that solution and approaches the other elastic solution. This last statement is true also for all the solutions (stresses and displacements) where inertia is important. The solutions then exhibit damped inertial oscillations, the damping being most rapid in the viscoelastic material, and the frequency of the oscillations in that material lying between the frequencies for the two elastic solutions.

In conclusion it can be stated that the viscoelastic material behaves, for the problem and the range of times considered, qualitatively similarly to an elastic material, and in many ways may be considered as an average of the two limiting elastic solutions. The amplitude of the oscillations of stress or displacement behaves initially like the one elastic solution and then tends towards the other. Also the frequency of these oscillations lies between the frequencies for the elastic solutions. The only way in which it may not be considered as an average is that the oscillations are damped more rapidly than either elastic oscillation.

Acknowledgment

The author is indebted to Dr. H. G. Hopkins and Dr. H. Kolsky for discussion and helpful criticism of the work reported in this paper. Crown copyright reserved. Reproduced with the permission of the Controller, H.M.S.O.

References

Berry, D. S. and Hunter, S. C. 1956 *J. Mech. Phys. Solids* **4**, 72.

Bland, D. R. 1957 Conference on Properties of Materials at High Rates of Strain. Inst. Mech. Engrs., London.

1960 *The Theory of Linear Viscoelasticity* (Pergamon Press, Oxford).

Eringen, A. C. 1957 *Quart. J. Mech.* **10**, 257.

Glauz, R. D. and Lee, E. H. 1954 *J. Appl. Phys.* **25**, 947.

Gross, B. 1947 *J. Appl. Phys.* **18**, 212.

1953 *Mathematical Structure of the Theories of Viscoelasticity* (Herman, Paris).

Hopkins, H. G.	1960	*Progress in Solid Mechanics* (Ed. by I. N. Sneddon and R. Hill), Vol. I, Ch. III. (North Holland Publ. Co., Amsterdam).
Hunter, S. C.	1954	Unpublished Ministry of Supply Report.
	1960a	*Progress in Solid Mechanics* (Ed. by I. N. Sneddon and R. Hill), Vol. I, Ch. I. (North Holland Publ. Co., Amsterdam).
	1960b	*J. Mech. Phys. Solids* **8**, 219.
Kolsky, H.	1956	*Phil. Mag.* **8**, 693.
	1960	Proc. Conf. Stress Propagation, Penna. State Univ., 1959 (Interscience, New York).
Kolsky, H. and Shi, Y. Y.	1958	Brown University Report No. 562 (14)/8.
Lee, E. H.	1953	*J. Appl. Phys.* **24**, 1115.
	1956	*Ibid.* **27**, 665.
	1960	*Viscoelastiticy: Phenomenological Aspects* (Ed. by J. T. Bergen) p. 1. (Academic Press, New York).
Lee E. H., Radok, J. R. M. and Woodward, W. B.	1959	*Trans. Soc. Rheol.* **3**, 41.
Lethersich, W.	1950	*Brit. J. Appl. Phys.* **1**, 294.

J. Mech. Phys. Solids, 1961, Vol. 9, pp. 230 to 241. Pergamon Press Ltd., London. Printed in Great Britain

BENDING OF UNIFORMLY LOADED SECTORIAL PLATES

By W. A. Bassali
Faculty of Science, University of Alexandria

and E. Halim
Faculty of Science, University of Khartoum, Sudan

(*Received 15th June*, 1961)

Summary

This paper deals with the deflexions of uniformly loaded plates in the form of a semi-circle or a quadrant of a circle whose boundary is clamped along the two radii and elastically restrained along the circular edge. The boundary conditions around the circular edge and the condition of zero slope on the straight edge are exactly satisfied. Good approximations to the accurate values of the deflexions for a certain value of the restraining parameter (simply supported circular edge) are obtained and judged by the closeness with which these approximate solutions satisfy the remaining boundary condition of zero deflexion on the bounding radii. Positions and magnitudes of maximum deflexions are determined.

1. Introduction

The study of the behaviour of normally loaded thin sectorial plates has attracted the attention of many researchers. The problem of analysing the deflexions in a uniformly loaded and clamped semi-circular plate was first treated by Kuno (1934). A method credited to Weinstein (1937) was applied to the same problem by Hassé (1950). Two methods of superposition on the elementary solution for a uniformly loaded and clamped circular plate have been used by Conway and Huang (1952) who applied one of their methods to a quadrant of a circle. Using curvilinear co-ordinates, Woinowsky-Krieger (1955) obtained an exact solution in the form of a definite integral which is not convenient for computation. The theorem of minimum potential energy was used by Ben-Amoz (1959) to obtain approximate and useful results concerning the bending of clamped sectorial plates. Displacements and stresses of a laterally loaded semi-circular plate with clamped edges have also been recently studied by Jurney (1959).

An approximate solution for a uniformly loaded semi-circular plate clamped around the curved edge and free along the diameter was given by Grinberg (1953). Using classical plate theory, Muster and Sadowsky (1956) have employed standard residual problem technique to obtain a series solution for a semi-circular plate simply supported around the curved edge and free along the diameter. Plates in the form of circular sectors, the straight edges of which are simply supported, have been analysed by Nadai (1915), whose results are quoted by Timoshenko (1940, p. 272). Problems dealing with plates bounded by two radii and two circular arcs have been discussed by Carrier (1944) and Bassali and Gorgui (1960).

This paper is concerned with the transverse flexure of a thin plate having the shape of a semi-circle, or a quadrant of a circle, where the straight part of the edge is clamped and the circular part is subject to a general boundary condition (including the clamped and simply supported edges as special cases), the plate being subject to the loading

$$p = p_0 r^{2n-2} \qquad (n \geqslant 1).$$

A method of superposition on the solution for a symmetrically loaded circular plate with an elastically restrained edge is used. Approximate expressions for the deflexions are given for a simply supported circular boundary (Poisson's ratio $= \frac{1}{3}$) with uniform load over the entire plate. By interpolation the positions and magnitudes of maximum deflexions are found. The technique could be extended to analyse other circular sectors for the same loading (or a different type) and for various values of the restraining parameter.

2. Elastically Restrained Circular Plate under Overall Symmetrical Pressure or Isolated Load

Let C denote the boundary of a thin circular plate of centre O, radius c and flexural rigidity D. We assume that the plate is subject to symmetrical loading of transverse intensity $p(r)$ at a distance r from O. The deflexion w_1, measured positively downwards, at any point (r, θ) of the mid-plane of the plate may be expressed as

$$w_1 = A + B r^2 + W(r), \tag{1}$$

where $W(r)$ is a particular integral of the partial differential equation

$$\nabla^4 w = \left(\frac{\partial^2}{\partial r^2} + \frac{1}{r}\frac{\partial}{\partial r}\right)^2 w = \frac{p(r)}{D}, \tag{2}$$

and A, B are real constants to be determined from the boundary conditions. These will be taken in the form

$$w_1 = 0, \qquad \frac{\partial^2 w_1}{\partial r^2} + \frac{\nu}{c}\frac{\partial w_1}{\partial r} = 0 \text{ along } C, \tag{3}$$

where ν is a restraining parameter. With

$$\nu = (1 + \lambda)/(1 - \lambda), \tag{4}$$

it was shown (Bassali and Dawoud 1956) that the boundary C is rigidly clamped or simply supported according as $\nu = \infty$, $\lambda = 1$ or $\nu = \eta$, $\lambda = (\eta - 1)/(\eta + 1)$, respectively, η being Poisson's ratio for the material of the plate. Assuming that

$$p(r) = p_0 r^{2n-2} \qquad (n \geqslant 1), \tag{5}$$

it is easily seen that $W(r)$ may be taken as

$$W(r) = p_0 r^{2n+2} \Big/ 16n^2 (n + 1)^2 D. \tag{6}$$

With this expression introduced in (1) the boundary conditions (3) are satisfied if

$$\left.\begin{aligned} A &= \frac{P_0\, c^2}{16n\,(n+1)\,\pi\, D}\left(n+1-n\,\lambda-\frac{1}{n+1}\right), \\ B &= \frac{P_0}{16n\,(n+1)\,\pi\, D}\left(n\,\lambda-n-1\right), \end{aligned}\right\} \tag{7}$$

where $P_0 = p_0\, c^2\, n/n$ is the total load on the plate. Substituting from (6) and (7) in (1) we obtain

$$w_1 = \frac{P_0\, c^2}{16n\,(n+1)\,\pi\, D}\left[(1-\rho^2)\,(n+1-n\,\lambda)-\frac{1-\rho^{2n+2}}{n+1}\right], \tag{8}$$

where $\rho = r/c$.

For uniform lateral pressure on the plate $n = 1$ and (8) reduces to

$$w_1 = \frac{p_0\, c^4}{64D}\,(1-\rho^2)\,(3-2\,\lambda-\rho^2), \tag{9}$$

in agreement with the solutions (62) and (67) of Timoshenko (1940), corresponding to clamped and simply supported edges, respectively.

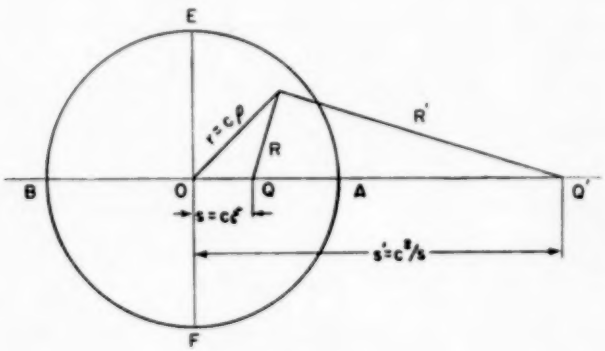

Fig. 1.

Another solution required is that due to a concentrated load P at a point $(s, 0)$, the plate being subject to the boundary conditions (3). With the notations of Fig. 1, the deflexion was derived (Bassali and Dawoud 1956, p. 147) in the form

$$w_2 = \frac{Pc^2}{16\pi D}\left[\frac{R^2}{c^2}\log\frac{R^2}{\xi^2\,R'^2}+(1-\xi^2)\,(1-\rho^2)\left\{\lambda+2\sum_{k=0}^{\infty}\frac{(\xi\rho)^k}{k+m}\cos k\,\theta\right\}\right], \tag{10}$$

where

$$\xi = s/c,\ R^2 = (\rho^2+\xi^2-2\xi\rho\cos\theta)\,c^2,\ \xi^2\,R'^2 = (1+\xi^2\,\rho^2-2\xi\rho\cos\theta)\,c^2, \tag{11}$$

and

$$m = \tfrac{1}{2}\,(1+\nu) = (1-\lambda)^{-1}. \tag{12}$$

For a clamped boundary $\lambda = 1$ and the solution (10) simplifies to the well-known solution of Michell obtained by the method of inversion.

3. Semi-circular Plate Elastically Restrained along the Circular Edge and Clamped along the Diameter

We now assume that the circular plate subject to the downward normal pressure (5) is also acted by a line distribution of upward loading extending along the diameter AOB of the plate (see Fig. 1). Let $f(\xi)$ be the intensity (force per unit length) of this line loading at a distance $s\ (= c\xi)$ from O, where $f(-\xi) = f(+\xi)$. Replacing P in (10) by $c f(\xi)\, d\xi$ and applying the principle of superposition, we find that the deflexion w at the point (r, θ) due to the combined effect of the load (5) distributed over the entire circular plate and the line loading $f(\xi)$ along AB is furnished by

$$w(\rho, \theta) = w_1 - \frac{c^3}{16\pi D}\int_{-1}^{1}\left[(\rho^2 + \xi^2 - 2\xi\rho\cos\theta)\log\frac{\rho + \xi^2 - 2\xi\rho\cos\theta}{1 + \xi^2\rho^2 - 2\xi\cos\theta} + \right.$$
$$\left. + (1 - \xi^2)(1 - \rho^2)\left\{\lambda + 2\sum_{k=0}^{\infty}\frac{(\xi\rho)^k}{k + m}\cos k\theta\right\}\right] f(\xi)\, d\xi. \qquad (13)$$

On making use of the relation $f(-\xi) = f(\xi)$, the expression (13) may be written as

$$w(\rho, \theta) = w_1 - \frac{c^3}{16\pi D}\int_{0}^{1}\left[(\rho^2 + \xi^2 - 2\xi\rho\cos\theta)\log\left(\frac{\rho^2 + \xi^2 - 2\xi\rho\cos\theta}{1 + \xi^2\rho^2 - 2\xi\rho\cos\theta}\right) + \right.$$
$$+ (\rho^2 + \xi^2 + 2\xi\rho\cos\theta)\log\left(\frac{\rho^2 + \xi^2 + 2\xi\rho\cos\theta}{1 + \xi^2\rho^2 + 2\xi\rho\cos\theta}\right) +$$
$$\left. + 2(1 - \xi^2)(1 - \rho^2)\left\{\lambda + 2\sum_{k=0}^{\infty}\frac{(\xi\rho)^{2k}}{2k + m}\cos 2k\theta\right\}\right] f(\xi)\, d\xi. \qquad (14)$$

We can easily verify that (14) satisfies the boundary conditions (3) along the semi-circle AEB and the condition $\partial w/\partial\theta = 0$ on the diameter AOB.

It is now desired to determine the distributed load $f(\xi)$ along the diameter AB that will produce zero displacement at every point of it. This is accomplished by equating to zero the displacement of equation (14) corresponding to $\theta = 0$. Since the deflexion vanishes for $\xi = \pm 1$, it is assumed that $f(\xi)$ tends to zero as ξ tends to ± 1. Substituting for w_1 from (8) and introducing for convenience

$$g(\xi) = 2n(n + 1)\, c f(\xi)/P_0, \qquad (15)$$

we are led to the integral equation

$$(1 - \rho^2)(n + 1 - n\lambda) - \frac{1 - \rho^{2n+2}}{n + 1} = \int_0^1\left[(\rho - \xi)^2\log\left|\frac{\rho - \xi}{1 - \xi\rho}\right| + \right.$$
$$\left. + (\rho + \xi)^2\log\left(\frac{\rho + \xi}{1 + \xi\rho}\right) + (1 - \xi^2)(1 - \rho^2)\left\{\lambda + 2\sum_{k=0}^{\infty}\frac{(\xi\rho)^{2k}}{2k + m}\right\}\right] g(\xi)\, d\xi. \qquad (16)$$

Solving (16) with respect to the unknown function $g(\xi)$, and inserting the result in (15) and then in (14), we obtain the deflected form of the semi-circular plate.

For uniform load ($n = 1$) and a clamped circular boundary ($\lambda = 1$) equation (16) reduces to equation (8) of Jurney (1959).

For uniform load and a simply supported circular boundary ($\eta = \frac{1}{3}$, $\lambda = -\frac{1}{2}$, $m = \frac{2}{3}$) equation (16) may be written as

$$\tfrac{1}{8} P_0(1 - \rho^2)(4 - \rho^2) = c\int_0^1 H(\rho, \xi) f(\xi)\, d\xi, \qquad (17)$$

where

$$H(\rho, \xi) = (\rho - \xi)^2 \log\left|\frac{\rho - \xi}{1 - \xi\rho}\right| + (\rho + \xi)^2 \log\left(\frac{\rho + \xi}{1 + \rho\xi}\right) + \\ + (1 - \xi^2)(1 - \rho^2)\left\{\tfrac{5}{2} + 3\sum_{k=1}^{\infty} \frac{(\xi\rho)^{2k}}{3k + 1}\right\}. \qquad (18)$$

Since no exact solution of this integral equation could be found, an approximate solution is here attempted. Equation (17) is replaced by a system of linear algebraic equations in $f(\xi_i)$

$$\tfrac{1}{8} P_0 (1 - \xi_j^2)(4 - \xi_j^2) = c \sum_i \delta_{ij} H(\xi_j, \xi_i) f(\xi_i) \; (\rho = \xi_j, j = 0, 1, 2, \ldots), \qquad (19)$$

where the ξ_i and δ_{ij} are determined by the form of the mean value method adopted. These can be taken from the Newton–Cotes formula or the Gauss formula of numerical integration (Whittaker and Robinson 1942). For the purpose of the present work we apply the trapezoidal rule. We divide the range of integration into N equal intervals by the points

$$\xi_i = i/N \; (i = 0, 1, 2, \ldots, \quad N - 1),$$

and take

$$\rho = \xi_j = j/N \; (j = 0, 1, 2, \ldots, \quad N - 1).$$

We obtain the following simultaneous linear equations for the determination of the $f(\xi_i)$ – values:

$$\left[\xi_j^2 \log \xi_j + \tfrac{5}{4}(1 - \xi_j^2)\right] f(0) + \sum_{i=1}^{N-1} \left[(\xi_j - \xi_i)^2 \log\left|\frac{\xi_j - \xi_i}{1 - \xi_i \xi_j}\right| + \right.$$

$$\left. + (\xi_j + \xi_i)^2 \log \frac{\xi_j + \xi_i}{1 + \xi_i \xi_j} + (1 - \xi_i^2)(1 - \xi_j^2)\left\{\tfrac{5}{2} + 3\sum_{k=1}^{\infty} \frac{(\xi_i \xi_j)^{2k}}{3k + 1}\right\}\right] f(\xi_i) =$$

$$= \frac{N P_0}{8c}(1 - \xi_j^2)(4 - \xi_j^2) \; (j = 0, 1, 2, \ldots, \; N - 1). \qquad (20)$$

For the sake of checking accuracy three values of N are used. The solutions of the three systems of N linear equations (20) corresponding to $N = 4$, 5 and 6 are presented in Table 1.

Table 1

$N = 4$		$N = 5$		$N = 6$	
ξ_i	$cf(\xi_i)/P_0$	ξ_i	$cf(\xi_i)/P_0$	ξ_i	$cf(\xi_i)/P_0$
0	0·3948844	0	0·3949180	0	0·3949278
1/4	0·3793574	1/5	0·3850078	1/6	0·3880687
1/2	0·3292807	2/5	0·3541175	1/3	0·3669257
3/4	0·2333855	3/5	0·2973666	1/2	0·3295594
		4/5	0·2045553	2/3	0·2712101
				5/6	0·1826957

The graph showing the variation of the load intensity $f(\xi)$ along the radius OA is plotted from the results of Table 1 in Fig. 2.

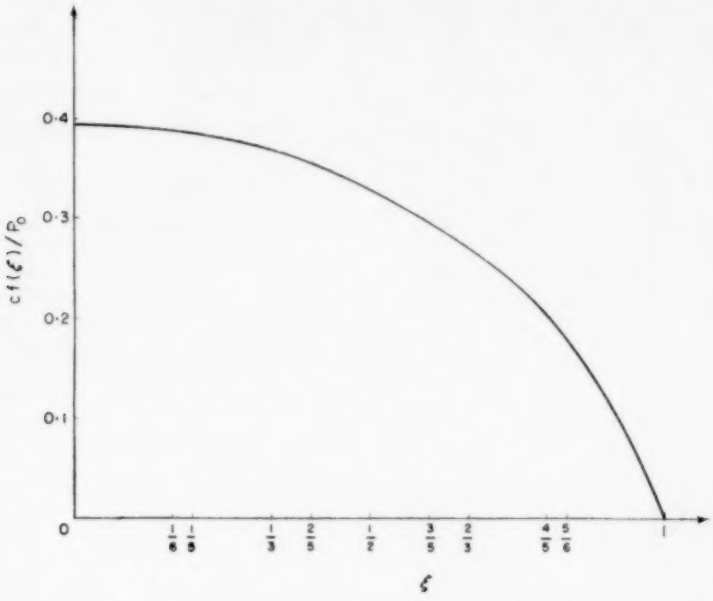

FIG. 2. Variation of the load intensity $f(\xi)$ along the radius OA of the semi-circular plate.

The deflexion at any point of the semi-circular plate is obtained by substituting from (9) in (14) and setting $\lambda = -\frac{1}{2}$, $m = \frac{2}{3}$, whence

$$w(\rho, \theta) = \frac{p_0 c^4}{64D}(1-\rho^2)(4-\rho^2) -$$

$$- \frac{c^3}{16\pi D}\int_0^1 \left[(\rho^2+\xi^2-2\xi\rho\cos\theta)\log\left(\frac{\rho^2+\xi^2-2\xi\rho\cos\theta}{1+\xi^2\rho^2-2\xi\rho\cos\theta}\right)+\right.$$

$$+(\rho^2+\xi^2+2\xi\rho\cos)\log\left(\frac{\rho^2+\xi^2+2\xi\rho\cos\theta)}{1+\xi^2\rho^2+2\xi\rho\cos\theta}\right)+$$

$$\left.+2(1-\xi^2)(1-\rho^2)\left\{\frac{5}{2}+3\sum_{k=1}^{\infty}\frac{(\xi\rho)^{2k}}{3k+1}\cos 2k\theta\right\}\right] f(\xi)\,d\xi. \qquad (21)$$

Approximate values for the deflexion at any point can then be calculated by applying the trapezoidal rule and using the $f(\xi_i)$–values obtained above.

It is clear that, as N increases, the solution will be more exact and the values of w on the diameter AOB of Fig. 1 should approach zero. To test the accuracy of the solutions, values of w on this diameter are calculated, from equation (21) with $\theta = 0$, for the points $\rho = \xi_i' = (2i+1)/2N$ $(i = 0, 1, 2, \ldots, N-1;$ $N = 4, 5, 6)$ and are listed in Table 2.

The deflexion at any point of the radius of symmetry OE is now given by putting $\theta = \frac{1}{2}\pi$ in (21). For $\lambda = -\frac{1}{2}$, $m = \frac{2}{3}$ the result is

$$\frac{8\pi D}{c^2} w(\rho, \tfrac{1}{2}\pi) = \tfrac{1}{8} P_0 (1-\rho^2)(4-\rho^2) - c \int_0^1 \left[(\rho^2+\xi^2) \log \left(\frac{\rho^2+\xi^2}{1+\xi^2\rho^2} \right) + \right.$$

$$\left. + (1-\xi^2)(1-\rho^2) \left\{ \tfrac{5}{2} + 3 \sum_{k=1}^{\infty} \frac{(-1)^k (\xi\rho)^{2k}}{3k+1} \right\} \right] f(\xi)\, d\xi. \qquad (22)$$

Table 2

$N = 4$		$N = 5$		$N = 6$	
ξ_i'	$D w/p_0 c^4$	ξ_i'	$D w/p_0 c^4$	ξ_i'	$D w/p_0 c^4$
1/8	0·0000823	1/10	0·0000421	1/12	0·0000244
3/8	0·0000758	3/10	0·0000400	1/4	0·0000235
5/8	0·0000615	1/2	0·0000356	5/12	0·0000217
7/8	0·0000384	7/10	0·0000279	7/12	0·0000189
		9/10	0·0000167	3/4	0·0000146
				11/12	0·0000085

Table 3 provides the values of the deflexion coefficients along OE as calculated from (22), using the values of $f(\xi)$ given in Table 1, corresponding to $N = 5$, 6 and carrying out the integration numerically in each case.

Table 3

$N = 5$		$N = 6$	
ρ	$D w/p_0 c^4$	ρ	$D w/p_0 c^4$
1/5	0·001457	1/6	0·001086
2/5	0·003503	1/3	0·002905
3/5	0·004117	1/2	0·004048
4/5	0·002738	2/3	0·003865
		5/6	0·002342

The deflexion profile of the semi-circular plate along the radius OE is shown in Fig. 3. From this graph of equation (22), and using interpolation methods, the maximum deflexion was found to be 0·004149 $p_0 c^4/D$ at a radius $r = 0{\cdot}562362\, c$. This is to be compared with the value 0·002021 $p_0 c^4/D$ at a radius $r = 0{\cdot}486$ in a uniformly loaded semi-circular plate clamped along the entire boundary (Woinowsky-Krieger 1955).

4. Quadrant with Fixed Radial Edges and an Elastically Restrained Circular Edge

A plate in the form of a quadrant of a circle will now be considered. In addition to the symmetrical load over the entire plate we superpose two upward line distributions of normal thrust extending along the two perpendicular diameters AOB and

EOF of Fig. 1, the intensity of loading at a distance $c\,\xi$ from O being $f(\xi)$, where, as before, we assume that $f(-\xi) = f(\xi)$, $f(1) = 0$. Proceeding along the same lines as before, and noting that the deflexion due to the upward line loading along *EOF* can be deduced from that due to the same distribution along *AOB* by replacing θ by $\theta - \frac{1}{2}\pi$, we find that the deflexion at any point is

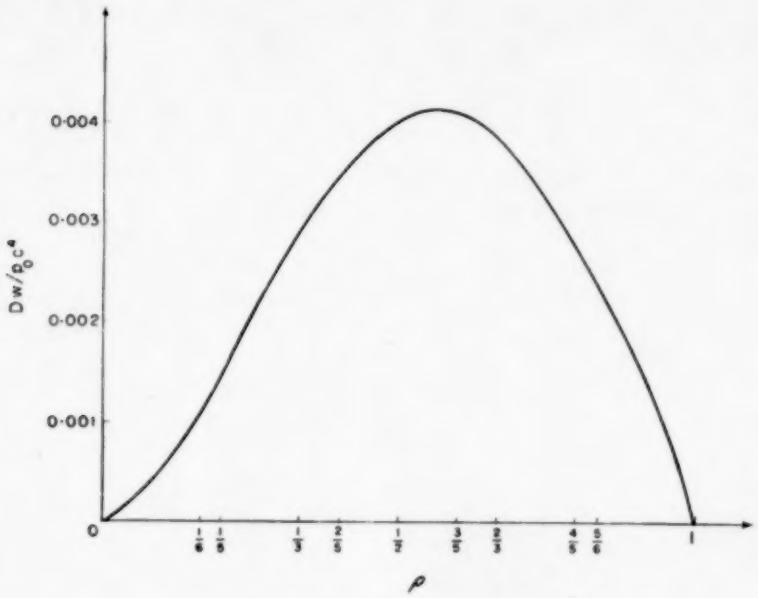

Fig. 3. Deflexion profile along the radius of symmetry *OE* of the semi-circular plate.

$$w = w_1 - \frac{c^3}{16\pi D}\int_0^1 \Bigg[(\rho^2+\xi^2-2\xi\rho\cos\theta)\log\left(\frac{\rho^2+\xi^2-2\xi\rho\cos\theta}{1+\xi^2\rho^2-2\xi\rho\cos\theta}\right) +$$
$$+(\rho^2+\xi^2+2\xi\rho\cos\theta)\log\left(\frac{\rho^2+\xi^2+2\xi\rho\cos\theta}{1+\xi^2\rho^2+2\xi\rho\cos\theta}\right) +$$
$$+(\rho^2+\xi^2-2\xi\rho\sin\theta)\log\left(\frac{\rho^2+\xi^2-2\xi\rho\sin\theta}{1+\xi^2\rho^2-2\xi\rho\sin\theta}\right) +$$
$$+(\rho^2+\xi^2+2\xi\rho\sin\theta)\log\left(\frac{\rho^2+\xi^2+2\xi\rho\sin\theta}{1+\xi^2\rho^2+2\xi\rho\sin\theta}\right) +$$
$$+4(1-\xi^2)(1-\rho^2)\left\{\lambda+2\sum_{k=0}^{\infty}\frac{(\xi\rho)^{4k}}{4k+m}\cos 4k\theta\right\}\Bigg] f(\xi)\,d\xi. \qquad (23)$$

The integral equation for the determination of the required loading is obtained as

$$(1-\rho^2)(n+1-n\lambda) - \frac{1-\rho^{2n+2}}{n+1} = \int_0^1 \Bigg[(\rho-\xi)^2\log\left|\frac{\rho-\xi}{1-\xi\rho}\right| +$$
$$+(\rho+\xi)^2\log\left(\frac{\rho+\xi}{1+\xi\rho}\right)+(\rho^2+\xi^2)\log\left(\frac{\rho^2+\xi^2}{1+\xi^2\rho^2}\right)+$$

$$+ 2(1-\xi^2)(1-\rho^2)\left\{\lambda + 2\sum_{k=0}^{\infty}\frac{(\xi\rho)^{4k}}{4k+m}\right\}\Big] g(\xi)\, d\xi, \qquad (24)$$

where the same relation (15) holds between the two functions $f(\xi)$ and $g(\xi)$.

For a uniformly loaded and clamped plate equations (15) and (24) yield the same integral equation (17), where now

$$H(\rho, \xi) = (\rho-\xi)^2 \log\left|\frac{\rho-\xi}{1-\xi\rho}\right| + (\rho+\xi)^2 \log\left(\frac{\rho+\xi}{1+\xi\rho}\right) +$$

$$+ (\rho^2+\xi^2)\log\left(\frac{\rho^2+\xi^2}{1+\xi^2\rho^2}\right) + 2(1-\xi^2)(1-\rho^2). \qquad (25)$$

This integral equation may be solved numerically for $f(\xi)$ by the same methods as in the previous Section. An approximate solution to the same problem was given by Conway and Huang (1952). Instead of applying line distributions of loading along the two perpendicular diameters *AOB* and *EOF* of Fig. 1, several concentrated loads were applied and the magnitudes of these loads adjusted so that the resultant deflexions under these loads vanish. The maximum deflexion was obtained as 0·00071655 $p_0 c^4/D$ at a radius $r = 0{\cdot}594\, c$.

When a uniformly loaded plate in the form of a quadrant of a circle is clamped along the straight edges and simply supported along the circular edge ($\eta = \frac{1}{3}$, $\lambda = -\frac{1}{2}$, $m = \frac{2}{3}$), we obtain the same integral equation (17) but with the kernel

$$H(\rho, \xi) = (\rho-\xi)^2 \log\left|\frac{\rho-\xi}{1-\xi\rho}\right| + (\rho+\xi)^2 \log\left(\frac{\rho+\xi}{1+\xi\rho}\right) +$$

$$+ (\rho^2+\xi^2)\log\left(\frac{\rho^2+\xi^2}{1+\xi^2\rho^2}\right) + (1-\xi^2)(1-\rho^2)\left\{5 + 6\sum_{k=1}^{\infty}\frac{(\xi\rho)^{4k}}{6k+1}\right\}. \qquad (26)$$

Table 4

$N = 5$		$N = 6$	
ξ_i	$c f(\xi_i)/P_0$	ξ_i	$c f(\xi_i)/P_0$
0	− 0·0143500	0	− 0·0218123
1/5	0·1372812	1/6	0·1047758
2/5	0·2713625	1/3	0·2464872
3/5	0·2756829	1/2	0·2835224
4/5	0·2053237	2/3	0·2603441
		5/6	0·1847750

By dividing the range of integration and following the same procedure of the foregoing section the sets of equations to determine the $f(\xi_i)$-values will be

$$2\left[\xi_j^2 \log \xi_j + \tfrac{5}{4}(1-\xi_j^2)\right] f(0) +$$

$$+ \sum_{i=1}^{N-1}\left[(\xi_j-\xi_i)^2 \log\left|\frac{\xi_j-\xi_i}{1-\xi_i\xi_j}\right| + (\xi_j+\xi_i)^2 \log\frac{\xi_j+\xi_i}{1+\xi_i\xi_j} +\right.$$

$$+ (\xi_j^2 + \xi_i^2) \log \frac{\xi_j^2 + \xi_i^2}{1 + \xi_i^2 \xi_j^2} + (1 - \xi_i^2)(1 - \xi_j^2) \left\{ 5 + 6 \sum_{k=1}^{\infty} \frac{(\xi_i \xi_j)^{4k}}{6k + 1} \right\} f(\xi_i) =$$

$$= \frac{NP_0}{8c} (1 - \xi_j^2)(4 - \xi_j^2), \tag{27}$$

where $\xi_i = i/N$, $\rho = \xi_j = j/N$ $(j = 0, 1, 2, \ldots, N - 1)$. Values of $f(\xi_i)$ corresponding to $N = 5$, 6 are calculated and presented in Table 4. Fig. 4 shows the variation of the function $f(\xi)$ along any of the two bounding radii OA or OE.

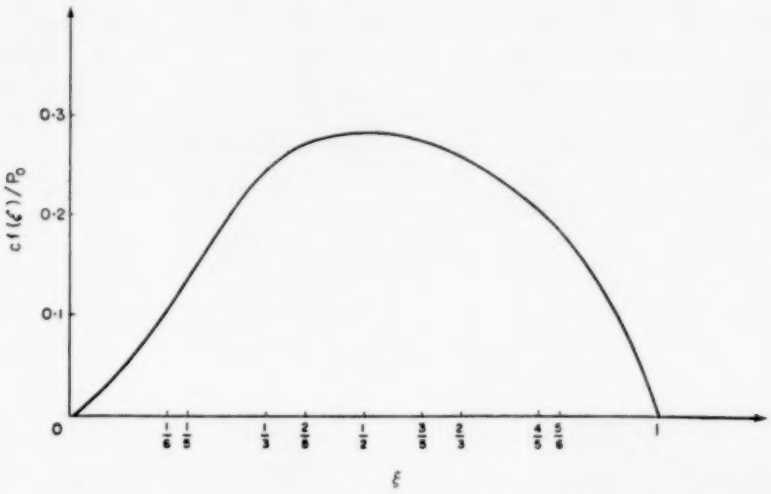

Fig. 4. Variation of the load intensity $f(\xi)$ along any of the two bounding radii of the quadrantal plate.

From equations (9) and (23), with $\lambda = -\frac{1}{2}$, $m = \frac{2}{3}$, the deflexion at any point of the plate is given by

$$w(\rho, \theta) = \frac{p_0 c^4}{64D} (1 - \rho^2)(4 - \rho^2) -$$

$$- \frac{c^3}{16\pi D} \int_0^1 \left[(\rho^2 + \xi^2 - 2\xi\rho \cos\theta) \log \left(\frac{\rho^2 + \xi^2 - 2\xi\rho \cos\theta}{1 + \xi^2 \rho^2 - 2\xi\rho \cos\theta} \right) + \right.$$

$$+ (\rho^2 + \xi^2 + 2\xi\rho \cos\theta) \log \left(\frac{\rho^2 + \xi^2 + 2\xi\rho \cos\theta}{1 + \xi^2 \rho^2 + 2\xi\rho \cos\theta} \right) +$$

$$+ (\rho^2 + \xi^2 - 2\xi\rho \sin\theta) \log \left(\frac{\rho^2 + \xi^2 - 2\xi\rho \sin\theta}{1 + \xi^2 \rho^2 - 2\xi\rho \sin\theta} \right) +$$

$$+ (\rho^2 + \xi^2 + 2\xi\rho \sin\theta) \log \left(\frac{\rho^2 + \xi^2 + 2\xi\rho \sin\theta}{1 + \xi^2 \rho^2 + 2\xi\rho \sin\theta} \right) +$$

$$\left. + 2(1 - \xi^2)(1 - \rho^2) \left\{ 5 + 6 \sum_{k=1}^{\infty} \frac{(\xi\rho)^{4k}}{6k + 1} \cos 4k\theta \right\} \right] f(\xi)\, d\xi. \tag{28}$$

The maximum deflexion occurs on the line bisecting the quadrant, and from (28) the deflexion at any point on that bisector is

$$\frac{8\pi D}{c^2}\, w\left(\rho, \frac{\pi}{4}\right) = \tfrac{1}{8} P_0 (1-\rho^2)(4-\rho^2) - c \int_0^1 \Bigg[(\rho^2 + \xi^2 - \sqrt{2}\,\xi\rho) \times$$

$$\times \log\left(\frac{\rho^2 + \xi^2 - \sqrt{2}\,\xi\rho}{1 + \xi^2\rho^2 - \sqrt{2}\,\xi\rho}\right) + (\rho^2 + \xi^2 + \sqrt{2}\,\xi\rho) \log\left(\frac{\rho^2 + \xi^2 + \sqrt{2}\,\xi\rho}{1 + \xi^2\rho^2 + \sqrt{2}\,\xi\rho}\right) +$$

$$+ (1-\xi^2)(1-\rho^2)\left\{5 + 6 \sum_{k=1}^{\infty} \frac{(-1)^k (\xi\rho)^{4k}}{6k+1}\right\}\Bigg] f(\xi)\, d\xi. \qquad (29)$$

Numerical values of the deflexion coefficients at points on the bisector are provided in Table 5. These are calculated from equation (29) for the cases $N = 5$ and $N = 6$ by using the results of Table 4, and the graph representing them is drawn in Fig. 5. From this curve and by interpolation the maximum deflexion was obtained as 0·001158 $p_0 c^4/D$ at a radius $r = 0{\cdot}661396\, c$.

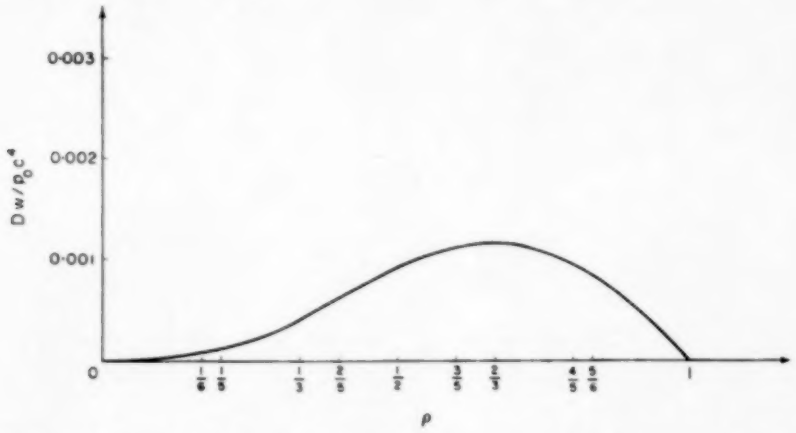

Fig. 5. Deflexion profile along the radius of symmetry of the quadrantal plate.

Table 5

$N = 5$		$N = 6$	
ρ	$D\,w/p_0 c^4$	ρ	$D\,w/p_0 c^4$
1/5	0·000100	1/6	0·000062
2/5	0·000619	1/3	0·000409
3/5	0·001125	1/2	0·000914
4/5	0·000946	2/3	0·001158
		5/6	0·000827

References

Bassali, W. A. and Dawoud, R. H. 1956 *Mathematika* **3**, 144.

Bassali, W. A. and Gorgui, M. A. 1960 *Proc. Camb. Phil. Soc.* **56**, 75 and 414.

Ben-amoz, M. 1959 *J. Appl. Mech.* **26**, 136.

Carrier, G. F.	1944	*J. Appl. Mech.* **11**, 134.
Conway, H. D. and Huang, M. K.	1952	*J. Appl. Mech.* **19**, 5.
Grinberg, G. A.	1953	*Prikl. Mat. Mekh.* **17**, 211.
Hassé, H. R.	1950	*Quart. J. Mech.* **3**, 271.
Jurney, W. R.	1959	*J. Appl. Mech.* **26**, 224.
Kuno, R.	1934	*J. Soc. Mech. Engrs.* **37**, 101.
Muster, D. F. and Sadowsky, M. A.	1956	*J. Appl. Mech.* **23**, 329.
Nadai, A.	1915	*Z. Ver. Dtsch. Ing.* **59**, 169.
Timoshenko, S.	1940	*Theory of Plates and Shells* (McGraw-Hill, New York).
Weinstein, A.	1937	*Mémor. Sci. Math.* **88**, 1.
Whittaker, E. T. and Robinson, G.	1942	*The Calculus of Observations* (Blackie, London).
Woinowsky-Krieger, S.	1955	*J. Appl. Mech.* **22**, 129.

J. Mech. Phys. Solids, 1961, Vol. 9, pp. 242 to 260. Pergamon Press Ltd., London. Printed in Great Britain

ON THE MECHANICAL BEHAVIOUR OF FIBRE-REINFORCED CRYSTALLINE MATERIALS

By E. Z. Stowell and T. S. Liu*
Southwest Research Institute, San Antonio, Texas

(*Received 26th June*, 1961)

Summary

A theoretical analysis of the mechanical behaviour of fibre-reinforced crystalline materials is presented in terms of the elastic and plastic properties of the components. Certain room temperature mechanical behaviour of fibre-reinforced composites is predicted using an 'inclusion' concept and from geometric, elastic, statistical distribution and plastic strength considerations. Certain elevated temperature mechanical behaviour of fibre-reinforced composites is predicted using a universal viscoelastic concept.

1. Introduction

It is the purpose of this paper to present the results of a theoretical study of certain expected mechanical behaviour of fibre-reinforced crystalline materials. The results serve to define the potentials one can expect of this type of composite materials.

In predicting the mechanical behaviour of crystalline materials in general, and reinforced crystalline materials designed for elevated temperatures in particular, there are two distinct areas of temperature environment to be considered. These are:

(1) A temperature range in which the fibre reinforcement and the matrix material retain their respective characteristics, generally represented by temperatures below one-half of the respective melting points (°K); and

(2) Temperature above one-half of the melting point (°K) where all materials become viscoelastic, and where, as far as their mechanical behaviour is concerned, the materials of reinforcement and that of the matrix lose their identities. It is obvious that the mechanical behaviour of materials in these environments are quite different.

2. Room Temperature Mechanical Behaviour of Fibre-reinforced Materials

1. *General consideration*

The fibre reinforcements, which may be of finite length, are considered for the present purpose to be of the nature of perfectly bonded inclusions in the matrix material. The theoretical study of such inclusions furnishes a clue to the probable behaviour of the composite material.

*Now at Research Center, Minneapolis-Honeywell Regulator Co., Hopkins, Minnesota.

One of the important objects of the fibres is to enable the composite material to withstand tension without rupture. Consider a flat plate made entirely of the matrix material except for a single inclusion of small dimensions, far removed from the edge of the plate. Let the elastic modulus of the matrix be E and that of the inclusion be E'. The value of Poisson's ratio is considered to be in the neighbourhood of 0·3 for both materials. Suppose the plate to be under a tensile stress σ_∞ applied to the edges of the plate far away from the inclusion.

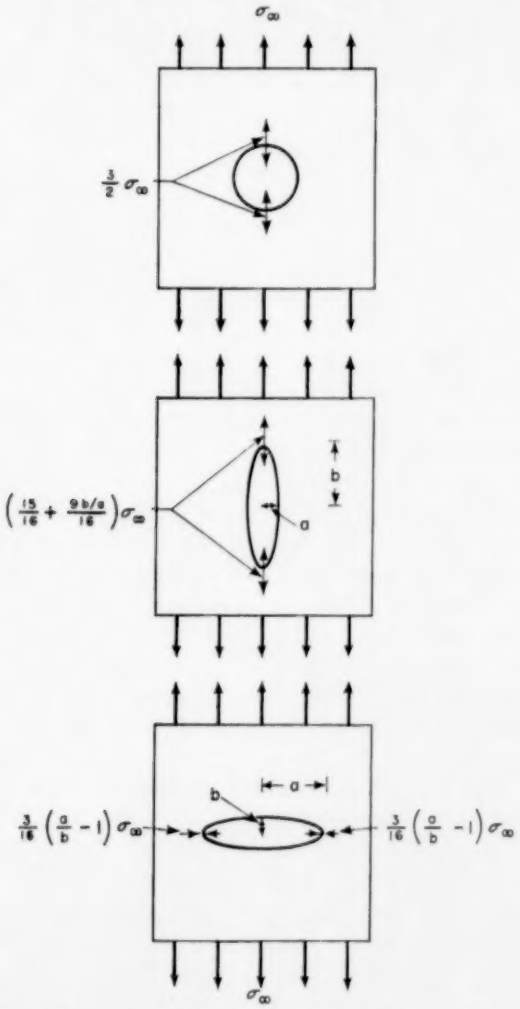

FIG. 1. Stresses at points indicated in inclusion when $E'/E = \infty$.

Theory indicates an important parameter to be the ratio E'/E. When $E'/E < 1$ the inclusion constitutes a weak spot in the plate, the extreme case being an empty hole at the location of the inclusion. Obviously, if the inclusion cannot carry its share of the tension, the matrix must bear the burden and must carry more

than its natural share. This situation defeats the purpose of introducing the inclusion. When $E'/E = 1$ the stress is carried in the plate as though the inclusion was not present. The inclusion serves no purpose. When $E'/E > 1$ the inclusion relieves the surrounding matrix of load by carrying an extra portion itself. The extra load carried varies from zero (when $E'/E = 1$) to a maximum (when $E'/E = \infty$).

Fig. 1 shows the effect of a single inclusion of circular and elliptical shapes when the ratio E'/E is large. The top figure shows the effect of a circular inclusion. The stress at opposite ends is 3/2 times the applied stress and this is approximately the stress throughout the inclusion. The surrounding matrix is relieved of the necessity of carrying this load.

The middle figure shows the effect of an elliptical inclusion when the longitudinal axis of the ellipse is lined up with direction of the tension. The stress at opposite ends of the longitudinal axis is

$$\left(\frac{15}{16} + \frac{9}{16}\frac{b}{a}\right)\sigma_\infty$$

where b and a are the dimensions of the ellipse as indicated. For a long narrow ellipse (b/a large), the inclusion will carry much of the stress that otherwise would be taken by the surrounding matrix.

The bottom figure shows an elliptical inclusion oriented at right angles to the applied tension. Here the inclusion is under large compression at right angles to the tension. Furthermore, because of the small value of b/a, the advantage of the inclusion is lost; its ability to carry tensile stress is not much different from that of the surrounding matrix.

To describe the stress-carrying ability of an inclusion, Fig. 2, after Saleme (1958), shows the stress distribution in the neighbourhood of a circular inclusion ($b/a = 1$, $E'/E = 2$) which is located at a distance of one diameter from one edge of the plate. In spite of this dissymmetry, however, the resulting stress distribution is seen to be very nearly as symmetrical as though the left hand edge of the plate was removed to infinity. This Figure shows that the stress in the matrix decreases from σ_∞ at a distance from the inclusion to a value of about $0{\cdot}6\ \sigma_\infty$ at the edges to about $1{\cdot}80\ \sigma_\infty$ near the middle. Thus, if one compares the load carried by portions of the plate between $x/r_0 = 0$ and $x/r_0 = 6$, it is found that although the inclusion occupies only $\frac{1}{3}$ the distance, it carries about $\frac{1}{2}$ the entire load.

2. *Theoretical strength of a matrix reinforced with fibres*

For a composite material, composed of a matrix interspersed with reinforcing fibres, the question arises as to what strength can be expected from the composite material due to the presence of the added fibres.

The fibres may be of different lengths but are taken to be perfectly bonded to the surrounding matrix. As a first approximation the problem may be considered to be one of perfect elasticity. Because the elastic modulus of the fibres differs from that of the matrix and is the larger of the two, the fibres carry more load in proportion to their area than the matrix. The problem is complicated by the breakage of individual fibres whenever their breaking strength – considered as a material property – is reached. The broken fibres are presumably largely ineffective

in carrying further load and the load that they formerly carried is probably transferred to shorter fibres.

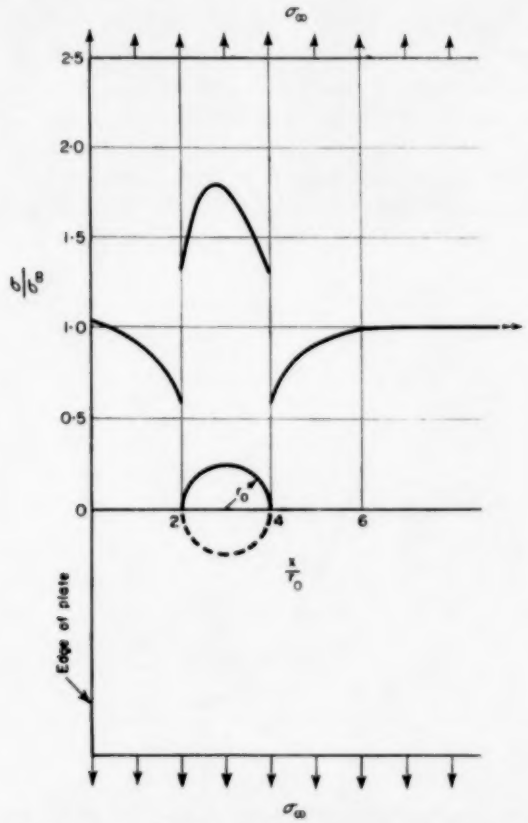

FIG. 2. Stress distribution in the vicinity of a circular inclusion located near the edge of a plate, when $E'/E = 2$, from SALEME (1958).

An attempt has been made to estimate the strength of such a composite material on the basis of perfect elasticity. The analysis is necessarily of a qualitative character, but it is hoped that the main features to be expected from a corporate material are revealed. The simplifying assumptions required to carry out the analysis are listed below :

(1) The reinforcing fibres may be considered as inclusions which are perfectly bonded to the matrix and which suffer the same strains as the matrix.

(2) The fibres all have the same diameter and the same breaking stress σ_f. In physical dimension they differ only in length.

(3) The fibres are aligned in the direction of the applied tension.

(4) The elastic modulus of the fibres is greater than the matrix modulus.

(5) The stress inside a fibre is taken to be uniform and equal to the stress implied by the stress concentration factor. This is known to be approximately true.

(6) The spacing of the fibres is assumed to be large enough so that each fibre acts individually. This will be true if they are a few diameters apart, as discussed previously.

(7) When a fibre breaks under a stress σ_f, it becomes completely ineffective.

(8) The matrix is assumed not to break before the fibres break.

With these assumptions a qualitative physical picture may be constructed which will permit use of the theory of inclusions.

Assume a block of the composite material in which the fibres have been aligned in the same direction in which tension is to be applied. A cut made through any typical cross section would disclose fibres all of the same diameter but of varying lengths distributed about a mean value in accordance with the curve of Fig. 3.

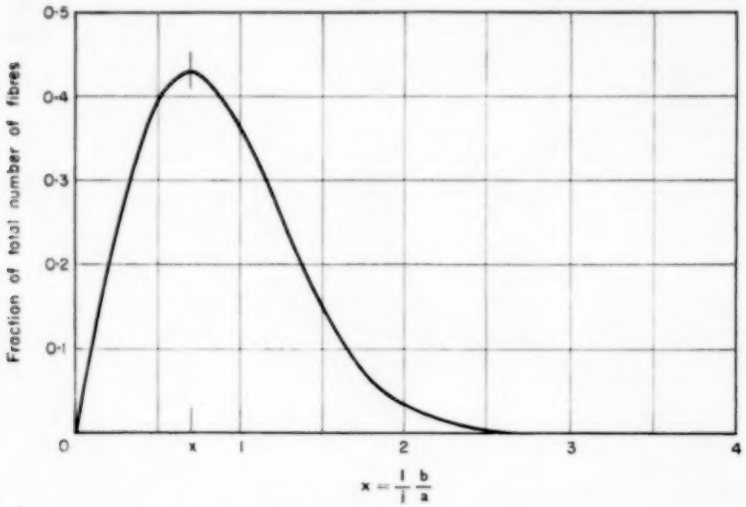

Fig. 3. Assumed distribution of fibre shapes about the mean shape $b/a = j/\sqrt{2}$.

Consider a fibre to be an ellipse of major axis b and minor axis a. The ratio of b/a thus is a measure of the slenderness or length of the fibre. The abscissa of Fig. 3 is

$$x = \frac{1}{j}\frac{b}{a} \tag{1}$$

where j is an adjustable constant. Since a is considered to be a constant [assumption (2)], the abscissa may be considered a measure of length b and so the curve may be considered as a chart giving the distribution of lengths.

The number of fibres included between x and $x + dx$ is

$$dn = 2Nxe^{-x^2}\,dx \tag{2}$$

where N is the total number of fibres present in the cross section.

From the theory of stress concentration in inclusion, the stress in any fibre of a given shape x is of the form

$$\sigma_x = \sigma_\infty (r + sx) \tag{3}$$

where r and s are constants, and σ_∞ is the uniform stress applied at a great distance from the inclusion. The curves of stress concentrations in inclusions presented in Fig. 4 show that equation (3) is approximately true for $b/a > 5$. These curves were computed from the two-dimensional solution given by DONNELL (1941). The three-dimensional solution by EDWARDS (1951) is of the same type with somewhat higher values of r and s.

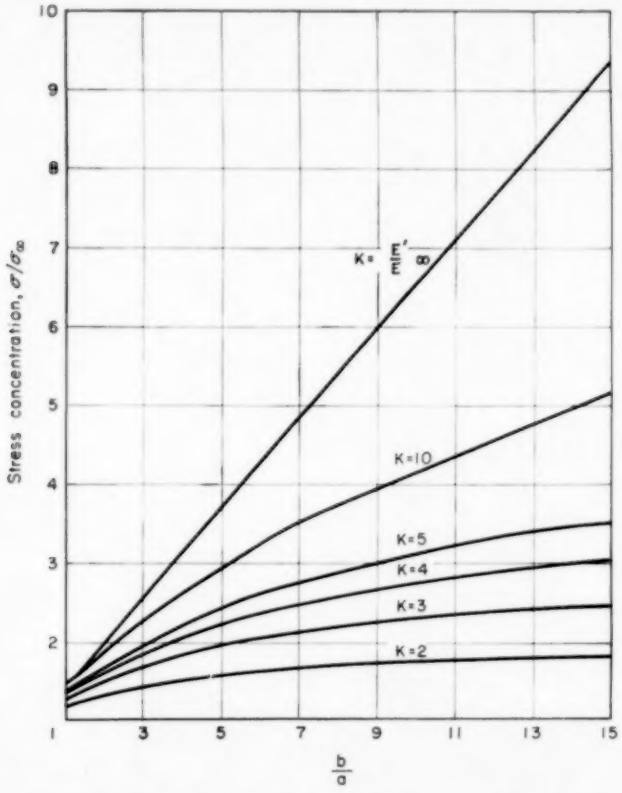

FIG. 4. Stress concentration in elliptical inclusions. b = major axis; a = minor axis; E' = modulus of inclusion; E = modulus of matrix, from DONNELL (1941).

The load carried by all the fibres having shapes between that given by x and that given by $x + dx$ is

$$dP_f = \sigma_x A dn \tag{4}$$

where A is the cross-sectional area of each fibre, taken as a constant. Substitution of the expressions for σ_x and dn in equation (4) gives

$$dP_f = 2\sigma_\infty AN(r + sx)xe^{-x^2}dx. \tag{5}$$

This expression could presumably be integrated to give the total load P_f carried by all the fibres. However, such a value of P_f would be unrealistic, because from equation (3), σ_x would become indefinitely large for large values of x. Actually,

what probably happens is that the fibres break whenever σ_x rises to achieve a value equal to σ_f, the breaking stress for the material of the fibres. The broken fibres from then on are ineffective for purposes of carrying load.

Consequently, the upper integration limit should not be $x \to \infty$ but a value of x equal to x_0 given by the relation

$$\sigma_f = \sigma_\infty (r + sx_0). \tag{6}$$

Thus

$$P_f = 2\sigma_\infty AN \int_0^{x_0} (r + sx)\, xe^{-x^2}\, dx$$

$$= \sigma_\infty AN \left[r + s \int_0^{x_0} e^{-x^2}\, dx - (r + sx_0)\, e^{-x_0^2} \right]. \tag{7}$$

The stress σ_∞ applied at the remote ends of the block can be interpreted as

$$\sigma_\infty = \frac{P}{A_{\text{total}}} \tag{8}$$

where P is the total impressed load and A_{total} is the total area of the composite block.

Perhaps a more satisfactory estimate of the ability of the fibres to carry stress may be obtained by relating the load carried by the fibres to the breaking stress directly. This may be done by combining equations (6) and (7) to give

$$P_f = \sigma_f AN \left[\frac{r + s \int_0^{x_0} e^{-x^2}\, dx}{r + sx_0} - e^{-x_0^2} \right]. \tag{9}$$

The quantity of $\sigma_f AN$ is the load that would be carried if all fibres operated at the breaking stress at the same time.

As a practical matter, an important question is how the load carried by the fibres varies with the applied load. That there will be a variation is seen from the following argument:

(1) For a small applied load (low σ_∞), many fibres are capable of carrying the load without breaking, but the load carried in each is small.

(2) For a large applied load (high σ_∞), the load in each fibre is large, but many fibres have been rendered inoperative because the stress in them has reached the fixed breaking stress σ_f. The load is again small.

(3) Hence, there must be some intermediate applied load where not too many fibres have been broken, giving a maximum load carried by all the fibres still effective.

Equation (9) gives the variation of the fibre load P_f with x_0. In order to show the variation with the applied load instead, x_0 may be replaced by σ_∞ through the relation (6):

$$\frac{\sigma_\infty}{\sigma_f} = (r_0 + sx_0)^{-1}.$$

Fig. 5 shows the variation of fibre load plotted against σ_∞/σ_f in this way where the values of r and s were selected from Fig. 4. (*Note*: since σ_f occurs in the denominator of both ordinate and abscissa of Fig. 5, the plot may be considered as a plot of P_f/AN, the average load per fibre, against σ_∞ = total load/total area). If the material were not composite but homogeneous, the plot would be the 45° line as shown. But because the material is composite, with the fibres carrying more load than the matrix, the curves go up more steeply than the 45° line at first.

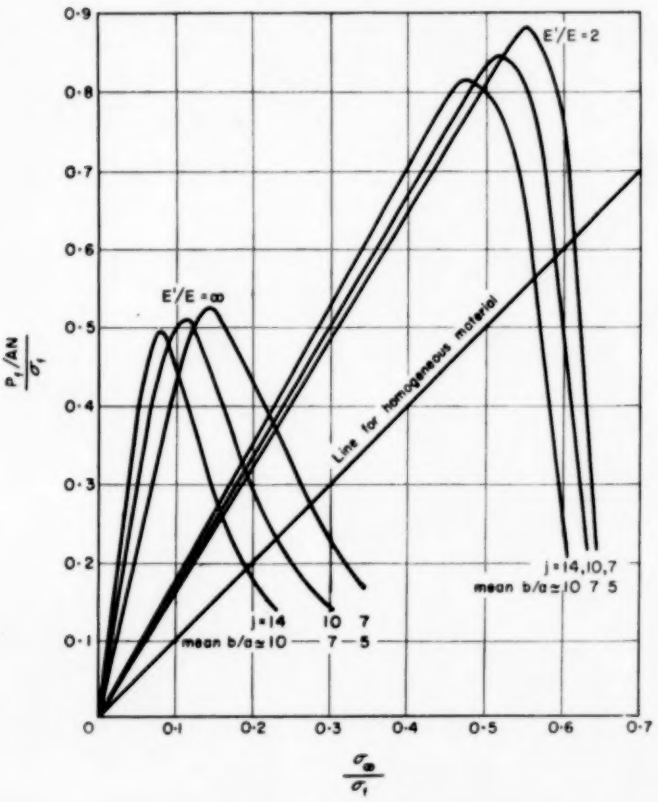

FIG. 5. Variation of fibre load with applied load (broken fibres ineffective).

As the applied load (σ_∞) increases, more and more fibres break and go out of action. Eventually so many fibres break that the total load cannot increase farther and the load has reached a maximum. If the applied load is carried still higher, the load carried by the fibres falls off rather sharply due to a lack of fibres available for carrying load.

With a perfectly rigid inclusion ($E'/E = \infty$) the maximum is reached fairly early, for low applied loads. For an elastic inclusion with $E'/E = 2$, the maximum is delayed and occurs for higher values of the applied load. The exact position of the peak in any case depends on the mean shape $\bar{b}/a$, which is $j/\sqrt{2}$.

Actually, when a fibre breaks, its ability to carry load is probably not lost completely. Suppose that when one breaks, it simply becomes two new fibres of shorter length and therefore of lower load-carrying ability. Suppose that these newly created fibres are absorbed into the original group in accordance with the distribution of Fig. 3 and that they may be treated as now fully effective – obviously an over-optimistic assumption. The number of new fibres is readily obtained from equation (2). The number of working fibres when the cut-off value of $x = x_0$ is

$$2N\int_0^{x_0} xe^{-x^2}\,dx = N(1 - e^{-x_0^2}).$$

The number of broken fibres must be therefore be $Ne^{-x_0^2}$. The number of new fibres must therefore be $2Ne^{-x_0^2}$. Hence, when $x = x_0$, the total number of working fibres is no longer N but $N(1 + e^{-x_0^2})$. If the new fibres carry stress precisely like the original fibres in accordance with the over-optimistic assumption, then the

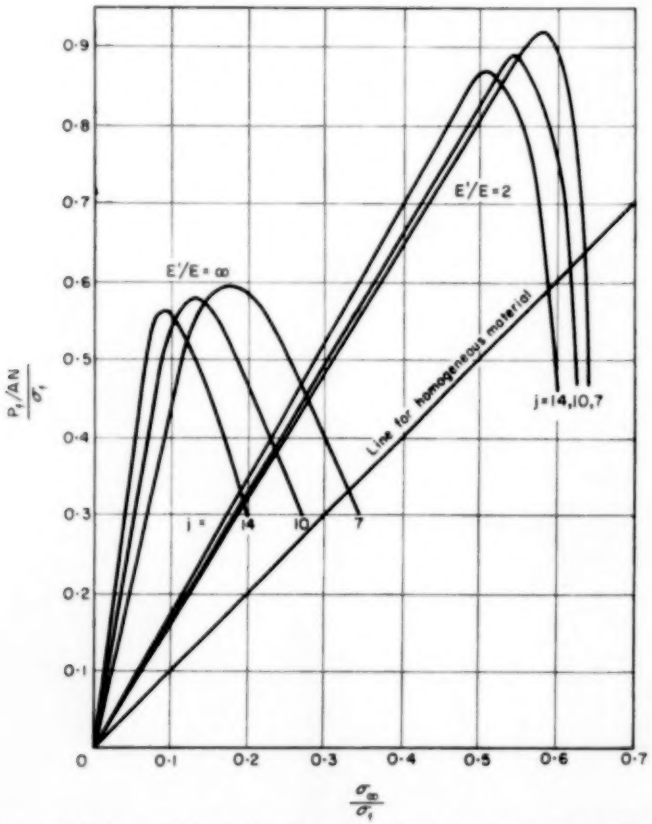

Fig. 6. Variation of fibre load with applied load (broken fibres effective).

effect of the creation of new fibres may be estimated by multiplying the ordinates of Fig. 5 by the factor $1 + e^{-x_0^2}$. The result is shown in Fig. 6. It is seen that the ordinates are all increased because more fibres are available to carry load and that the peaks are shifted slightly to higher loads.

The true behaviour is probably somewhere between the curves of Figs. 5 and 6, because a broken fibre is probably partially effective in carrying load but not as much as Fig. 6 would indicate.

3. *Estimated strength of composite material when stressed at an angle to the fibres*

A. *One set of fibres.* Fig. 7 shows a sheet of the composite material with one set of fibres aligned in the x direction.

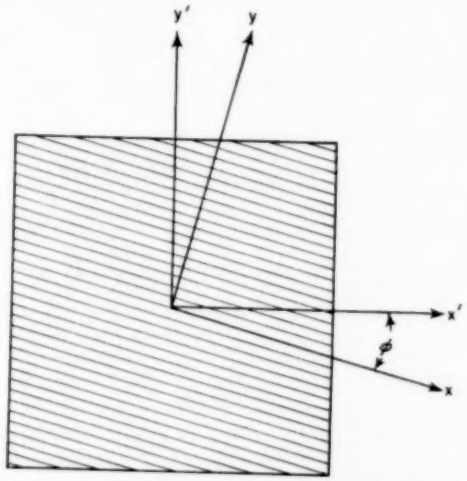

FIG. 7. One set of fibres in the x direction. Sheet of composite material.

The relations between stresses in the x' and y' directions (positive in tension) and those along and perpendicular to the fibres are

$$\left.\begin{aligned} \sigma_x &= \sigma_{x'} \cos^2 \phi + \sigma_{y'} \sin^2 \phi - \tau_{x'y'} \sin 2\phi, \\ \sigma_y &= \sigma_{x'} \sin^2 \phi + \sigma_{y'} \cos^2 \phi + \tau_{x'y'} \sin 2\phi, \\ \tau_{xy} &= \tfrac{1}{2}(\sigma_{x'} - \sigma_{y'}) \sin 2\phi + \tau_{x'y'} \cos 2\phi. \end{aligned}\right\} \qquad (10)$$

Equations (10) give the stresses along the fibre direction and perpendicular to it when the material is loaded in the x' and y' directions. These relations will hold up to the moment of failure, which may occur whenever σ_x, σ_y or τ_{xy} reaches some limiting value.

Suppose, for example, that a tensile stress $\sigma_{x'}$ is applied in the x' direction. Then up to the moment of failure

$$\sigma_x = \sigma_{x'} \cos^2 \phi, \qquad \sigma_y = \sigma_{x'} \sin^2 \phi, \qquad \tau_{xy} = \tfrac{1}{2} \sigma_{x'} \sin 2\phi.$$

Inspection of Fig. 5 shows that there is a maximum value of σ_x along the fibres which cannot be exceeded; call this $(\sigma_x)_f$. There are no fibres in the direction of y to supply tensile strength; consequently, the resistance to tension in that direction must be borne by the matrix material. Call the maximum value σ_y can achieve $(\sigma_y)_m$. Similarly, the fibres contribute nothing to the shear strength which again is supplied by the matrix. Call the maximum shear stress τ_{xy} which can be achieved $(\tau_{xy})_m$. Thus $\sigma_{x'}$ will be a maximum when either

$$\sigma_{x'} = \frac{(\sigma_x)_f}{\cos^2\phi}, \qquad \sigma_{x'} = \frac{(\sigma_y)_m}{\sin^2\phi}, \qquad \text{or when } \sigma_{x'} = \frac{2(\tau_{xy})_m}{\sin 2\phi},$$

whichever limit is reached first as $\sigma_{x'}$ is increased. This limit may be called the tensile strength in the x' direction for the given angle ϕ.

Similarly for an applied stress $\sigma_{y'}$, the limiting strengths will be either

$$\sigma_{y'} = \frac{(\sigma_x)_f}{\sin^2\phi}, \qquad \sigma_{y'} = \frac{(\sigma_y)_m}{\cos^2\phi}, \qquad \text{or } \sigma_{y'} = -\frac{2(\tau_{xy})_m}{\sin 2\phi},$$

whichever is reached first as $\sigma_{y'}$ is increased.

For an applied shear stress $\sigma_{x'y'}$ the limiting strengths are correspondingly

$$\tau_{x'y'} = \frac{(\sigma_x)_f}{\sin 2\phi}, \qquad \tau_{x'y'} = \frac{(\sigma_y)_m}{\sin 2\phi}, \qquad \tau_{x'y'} = \frac{(\tau_{xy})_m}{\cos 2\phi},$$

whichever is reached first as $\tau_{x'y'}$ is increased. However, since $-\sigma_x$ is a compressive stress, and since all compression is assumed to be borne by the matrix, the first relation should read

$$\tau_{x'y'} = \frac{(\sigma_x)_m}{\sin 2\phi}$$

where $(\sigma_x)_m$ is the maximum stress that can be achieved by σ_x in compression.

If $\sigma_{x'}$ and $\sigma_{y'}$ are compressive instead of tensile stresses, the same relations still hold, except that $(\sigma_{x'})_f$ must be replaced by $(\sigma_{x'})_m$ in the expressions for limiting values of $\sigma_{x'}$ and $\sigma_{y'}$.

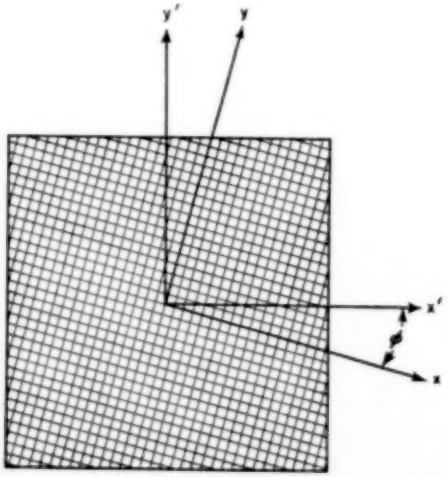

Fig. 8. Two sets of fibres in the x and y directions. Sheet of composite material.

B. *Two sets of fibres at right angles.* Fig. 8 shows a sheet of the composite material with one set of fibres aligned in the x direction and another in the y direction. The relations of equations (10) still hold up to the moment of failure. However, the tensile strength in the y direction is now supplied by the new set of fibres and has a value $(\sigma_y)_f$.

Thus, for an applied stress $\sigma_{x'}$ the maximum value which can be achieved is either

$$\sigma_{x'} = \frac{(\sigma_x)_f}{\cos^2\phi}, \qquad \sigma_{x'} = \frac{(\sigma_y)_f}{\sin^2\phi}, \qquad \text{or} \quad \sigma_{x'} = \frac{2\,(\tau_{xy})_m}{\sin 2\phi},$$

and for an applied stress $\sigma_{y'}$ the corresponding expressions are

$$\sigma_{y'} = \frac{(\sigma_x)_f}{\sin^2\phi}, \qquad \sigma_{y'} = \frac{(\sigma_y)_f}{\cos^2\phi}, \qquad \text{or} \quad \sigma_{y'} = \frac{-2\,(\tau_{xy})_m}{\sin 2\phi}.$$

The expressions for applied shear stress $\tau_{x'y'}$ are

$$\tau_{x'y'} = \frac{(\sigma_x)_m}{\sin 2\phi}, \qquad \tau_{x'y'} = \frac{(\sigma_y)_f}{\sin 2\phi}, \qquad \tau_{x'y} = \frac{(\tau_{xy})_m}{\cos 2\phi}.$$

The relations when $\sigma_{x'}$ and $\sigma_{y'}$ are compressive are unchanged.

3. Elevated Temperature Mechanical Behaviour of Fibre-reinforced Composite Materials

1. *General considerations*

From a designer's standpoint, assuming a given fibre-matrix combination is not chemically affected by the high temperature and other environments to which it is subjected, a basic knowledge of creep and rupture characteristics of the composite material is needed for the prediction of high temperature stress distribution and expected life of fibre reinforced components.

In pursuing along this line, it is noticed that both theoretical considerations and experimental data are lacking on the creep and rupture characteristics of fibre-reinforced bodies. One is then forced to look into the creep and rupture behaviour of the component materials to obtain clues. The component materials under consideration can generally be represented by either metals, or alloys, and refractory compounds. Since, at least from a phenomenological standpoint, the mechanical behaviour of metals at elevated temperatures has been well documented, it is considered adequate to direct our attention on the mechanical behaviour of ceramic materials at elevated temperatures. With the knowledge of the elevated temperature behaviour of ceramic materials and of metals, it is then possible to describe, based on certain reasonable assumptions, the behaviour of fibre-reinforced crystalline materials at elevated temperatures.

2. *Mechanical properties of ceramic materials*

A. *Creep characteristics.* Recent careful work by Chang (1960) on the creep of aluminium oxide single crystals demonstrated that such a material obeys the same laws as a metal at homologous elevated temperatures. It is thus apparent that, at temperatures above approximately one-half of the melting point, the viscosity of the ceramic material will play a major role in determining its high temperature strength.

For example, if we obtain the conventional stress-strain curve for a metal at elevated temperatures where the viscosity is important, it has been shown by Stowell (1957a) that the maximum stress obtainable from the material is given by the phenomenological relationship

$$\sigma_{max} = \sigma_0 \left[\frac{\Delta H}{RT} + \ln \frac{\dot{\epsilon}_0}{sT} \right] \tag{11}$$

where

$\dot{\epsilon}_0$ = strain-rate used in obtaining the stress–strain curves, per hour

s = a material constant, per hour per °K

T = temperature, °K

ΔH = activation energy, calories per mole

R = gas constant, taken as 2 cal/mole/°K

σ_0 = a material constant.

The activation energy, ΔH, and the material constants σ_0 and s can be determined experimentally by measurements of steady creep rate at a constant stress and temperature over a significantly wide range. Thus, since in equation (11) $\sigma_{max} \gg \sigma_0$, $\dot{\epsilon}_0$ can be expressed as below.

$$\dot{\epsilon}_0 = 2sTe^{-\frac{\Delta H}{RT}} \sinh \frac{\sigma_{max}}{\sigma_0}. \tag{12}$$

Here $\dot{\epsilon}_0$ is the measured steady creep rate.

The constant in equation (12) which characterize the viscous behaviour have been determined for a number of metals (Stowell 1957a, b; Stowell and Heimerl 1960).

Apparently, at a temperature above approximately one-half the melting point, both metals and ceramic materials lose their distinguishing characteristics and their individualities and become viscoelastic materials obeying identical laws. Since these laws can be mathematically formulated, the behaviour of a viscoelastic material is more predictable than when the material is in the ' cold ' state.

Among the predictable properties found for metals are:

(1) Steady creep at any temperature and stress;

(2) Stress-strain curve at any temperature and strain rate;

(3) Strain at any stress and linear temperature rate;

(4) Thermal stress at any linear temperature rate;

(5) Time to rupture at any temperature.

It is thus seen that with the concept of uniform viscoelastic behaviour of materials at elevated temperatures and the initial experimental verification on ceramic materials, it is likewise possible to predict the previously listed behaviours for fibre-reinforced crystalline components.

B. *Rupture time.* It was established experimentally by Monkman and Grant (1956) that, if a metal creeps at a constant rate $\dot{\epsilon}_0$ under a simple tensile stress, it will rupture at a time τ given by

$$\dot{\epsilon}_0 \tau \simeq \text{constant}. \tag{13}$$

A relationship of this type may also be obtained theoretically if some elementary assumptions are made concerning tertiary creep.

The final or tertiary phase of creep that precedes rupture is characterized by a rapidly increasing creep rate. Consideration of this change in creep rate suggests the reason why the product of steady creep rate and rupture life should be nearly constant. Suppose the creep rate in the tertiary region is of the form

$$\dot{\epsilon} = \dot{\epsilon}_0 f\left(\frac{\epsilon}{\epsilon_0}\right)$$

where $\dot{\epsilon}_0$ is the known secondary, or steady creep rate, ϵ is the creep strain, at time t, and ϵ_0 is some constant creep strain. This relation may be written as

$$\frac{d\,(\epsilon/\epsilon_0)}{f\,(\epsilon/\epsilon_0)} = \frac{\dot{\epsilon}_0}{\epsilon_0}\,dt.$$

This may be integrated to give

$$\int_0^{\epsilon/\epsilon_0} \frac{d\,(\epsilon/\epsilon_0)}{f\,(\epsilon/\epsilon_0)} = \frac{\dot{\epsilon}_0}{\epsilon_0}\,t.$$

The material will rupture at a time τ when ϵ/ϵ_0 reaches some large value. The function f is of the general type e^{ϵ/ϵ_0}. Thus

$$\frac{\dot{\epsilon}_0\,t}{\epsilon_0} = \int_0^{\epsilon/\epsilon_0} e^{-\epsilon/\epsilon_0}\,d\left(\frac{\epsilon}{\epsilon_0}\right) = 1 - e^{-\epsilon/\epsilon_0}.$$

Value of ϵ/ϵ_0 *at time* $t = \tau$ *when rupture occurs*	$e^{-\epsilon/\epsilon_0}$	$\frac{\dot{\epsilon}_0\tau}{\epsilon_0}$
3	0·05	0·95
4	0·018	0·982
5	0·007	0·993
6	0·0025	0·9975
∞	0	1·000

It is seen that the value of $\dot{\epsilon}_0\,\tau/\epsilon_0$ changes very little for large changes in ϵ/ϵ_0. The product $\dot{\epsilon}_0\,\tau$ would thus appear to be a constant when determined experimentally.

This relationship is of great practical interest because it permits the useful lifetime of a creeping metal component to be computed provided one can calculate the steady creep rate $\dot{\epsilon}_0$ at the given temperature and stress. This is possible, as pointed out earlier in (12), from steady creep data. The constant in (13) can be experimentally determined without difficulty. That this particular relationship of (12) is equally applicable to ceramic materials is indicated for Al_2O_3 by CHANG's work (1960).

Whether fibre-reinforced crystalline material behaves similarly can be verified in the steady creep rate experiments, as discussed in the previous Section. Alternatively, it can be checked experimentally against the relationship spelled out in

(13). To our knowledge, there is no experimental information on the validity of (13) when applied to fibre-reinforced crystalline materials. If this relationship is verified, a computation of the lifetime of fibre-reinforced crystalline compositites under creep conditions will be made possible.

3. *Stress distribution in a fibre-reinforced beam under constant bending moment*

Discussions in previous Sections indicated that at a temperature above one-half of the melting point, viscosity played an increasingly important role. Hence both metals and ceramic materials would lose their distinguishing characteristics as far as their mechanical behaviours were concerned. At this temperature range all materials behave as viscoelastic materials. Based on this concept, a calculation was made to determine the stress distribution at elevated temperatures in a fibre-reinforced beam under a constant bending moment.

At the elevated temperatures where it is to be used, a fibre-reinforced material will almost certainly become viscoelastic. The presence of the viscous element in the behaviour of the material will introduce time effects and will give rise to substantial changes in the stress distribution with time.

As an example of the effect of viscoelastic material properties on the distribution of stress in a structure, consider the case of a uniform beam of width b and depth h, under a constant bending moment M_0 applied at the ends. The law of material behaviour is taken to be

$$\frac{d\epsilon}{dt} = \frac{1}{E}\frac{d\sigma}{dt} + C \sinh \frac{\sigma}{\sigma_0} \tag{14}$$

where $d\epsilon/dt$ is the strain rate due to a stress σ; E, C and σ_0 are constants.

At time $t = 0$ the moment M_0 is applied. The instantaneous response of the beam is elastic; it immediately assumes a curvature

$$\varkappa_0 = \frac{M_0}{EI} \tag{15}$$

where $I = bh^3/12$ is the moment of inertia. The strain in any fibre at a distance z from the neutral axis is $\epsilon = \varkappa_0 z$. Since the material is still elastic, the initial stress σ in any fibre is proportional to this strain so that $\sigma = E\varkappa_0 z$.

Because of the law of material behaviour assumed in (14), the material along each fibre will immediately start to creep at a rate depending upon the initial stress prevailing in that fibre. The extreme fibre stresses will be reduced and the curvature of the beam will slowly increase to keep the stresses in equilibrium with the constant bending moment M_0.

We are interested only in the final stress distribution. After a sufficiently long time when the stress distribution has reached a steady state, we have, on integrating (14):

$$\epsilon = \frac{\sigma}{E} + Ct \sinh \frac{\sigma}{\sigma_0} =$$

$$= \left[\frac{\sigma_0}{E} + Ct\right]\left(\frac{\sigma}{\sigma_0}\right) + \frac{Ct}{3!}\left(\frac{\sigma}{\sigma_0}\right)^3 + \frac{Ct}{5!}\left(\frac{\sigma}{\sigma_0}\right)^5 + \cdots$$

or

$$\frac{\epsilon}{\sigma_0/E + Ct} = \frac{\sigma}{\sigma_0} + \frac{Ct}{\sigma_0/E + Ct}\frac{1}{3!}\left(\frac{\sigma}{\sigma_0}\right)^3 + \frac{Ct}{\sigma_0/E + Ct}\frac{1}{5!}\left(\frac{\sigma}{\sigma_0}\right)^5 + \cdots. \tag{16}$$

This series may be inverted to give

$$\frac{\sigma}{\sigma_0} = \left[\frac{\epsilon}{\sigma_0/E + Ct}\right] - \frac{Ct}{\sigma_0/E + Ct}\frac{1}{3!}\left[\frac{\epsilon}{\sigma_0/E + Ct}\right]^3 -$$

$$- \left[\frac{1}{5!}\frac{Ct}{\sigma_0/E + Ct} + \frac{3}{(3!)^2}\frac{(Ct)^2}{(\sigma_0/E + Ct)^2}\right]\left[\frac{\epsilon}{\sigma_0/E + Ct}\right]^5 - \cdots. \tag{17}$$

The strain in any fibre is still proportional to its distance z from the neutral axis:

$$\epsilon = xz$$

where x is now the curvature of the beam at a time t after equilibrium is established. Thus, the relation between stress and curvature is

$$\frac{\sigma}{\sigma_0} = \frac{xz}{\sigma_0/E + Ct} - \frac{Ct}{\sigma_0/E + Ct}\frac{1}{3!}\left[\frac{xz}{\sigma_0/E + Ct}\right]^3 -$$

$$- \left[\frac{1}{5!}\frac{Ct}{\sigma_0/E + Ct} + \frac{3}{(3!)^2}\frac{(Ct)^2}{(\sigma_0/E + Ct)^2}\right]\left[\frac{xz}{\sigma_0/E + Ct}\right]^5 - - - - - . \tag{18}$$

The stress distribution must satisfy two conditions:

$$\int_{-h/2}^{h/2} \sigma dz = 0 \text{ since there is no longitudinal force,} \tag{19}$$

$$b\int_{-h/2}^{h/2} \sigma z dz = M_0, \text{ the applied moment.} \tag{20}$$

Equation (19) is automatically satisfied since only odd powers of z appear in the expression (18) for σ. Relation (20) gives

$$M_0 = \frac{EIx}{1 + \dfrac{Ct}{\sigma_0/E}}\left\{1 - \frac{Ct}{\sigma_0/E + Ct}\frac{1}{40}\left(\frac{hx}{\sigma_0/E + Ct}\right)^2 -\right.$$

$$\left. - \left[\frac{1}{4480}\frac{Ct}{\sigma_0/E + Ct} + \frac{1}{448}\frac{(Ct)^2}{(\sigma_0/E + Ct)^2}\right]\left(\frac{hx}{\sigma_0/E + Ct}\right)^4 - - - -\right\}. \tag{21}$$

When $t = 0$, $M_0 = EIx_0$ from (15). Hence

$$x_0 = \frac{x}{1 + \dfrac{Ct}{\sigma_0/E}}\left\{1 - \frac{\dfrac{Ct}{\sigma_0/E}}{1 + \dfrac{Ct}{\sigma_0/E}} \cdot \frac{1}{40}\left(\frac{\dfrac{hx}{\sigma_0/E}}{1 + \dfrac{Ct}{\sigma_0/E}}\right)^2 -\right.$$

$$\left. - \left[\frac{1}{4480}\frac{\dfrac{Ct}{\sigma_0/E}}{1 + \dfrac{Ct}{\sigma_0/E}} + \frac{1}{448}\frac{\left(\dfrac{Ct}{\sigma_0/E}\right)^2}{\left(1 + \dfrac{Ct}{\sigma_0/E}\right)^2}\right]\left(\frac{\dfrac{hx}{\sigma_0/E}}{1 + \dfrac{Ct}{\sigma_0/E}}\right)^4 - - - -\right\}.$$

This series may be inverted to give

$$x = x_0\left(1 + \frac{Ct}{\sigma_0/E}\right)\left\{1 + \frac{\dfrac{Ct}{\sigma_0/E}}{1 + \dfrac{Ct}{\sigma_0/E}}\frac{1}{40}\left(\frac{hx_0}{\sigma_0/E}\right)^2 +\right.$$

$$\left. + \left[\frac{1}{4480}\frac{\dfrac{Ct}{\sigma_0/E}}{1 + \dfrac{Ct}{\sigma_0/E}} + \frac{203}{9760}\frac{\left(\dfrac{Ct}{\sigma_0/E}\right)}{\left(1 + \dfrac{Ct}{\sigma_0/E}\right)^2}\right]\left(\frac{hx_0}{\sigma_0/E}\right)^4 + - - -\right\}.$$

After a long time ($Ct \gg \sigma_0/E$) we have

$$x = x_0\left(1 + \frac{Ct}{\sigma_0/E}\right)\left\{1 + \frac{1}{40}\left(\frac{hx_0}{\sigma_0/E}\right)^2 + \left[\frac{1}{4480} + \frac{203}{9760}\right]\left(\frac{hx_0}{\sigma_0/E}\right)^4 + - - -\right\}$$

and

$$\frac{\sigma}{\sigma_0} = \sinh^{-1}\left(\frac{\epsilon}{Ct}\right) = \sinh^{-1}\left(\frac{xz}{Ct}\right) \text{ from (14)}$$

so that the final stress distribution is

$$\frac{\sigma}{\sigma_0} = \sinh^{-1}\left\{\frac{x_0 z}{Ct}\left(1 + \frac{Ct}{\sigma_0/E}\right)\left[1 + \frac{1}{40}\left(\frac{hx_0}{\sigma_0/E}\right)^2 + \left\{\frac{1}{4480} + \frac{203}{9760}\right\}\left(\frac{hx_0}{\sigma_0/E}\right)^4 + - - -\right]\right\}. \quad (22)$$

If hx_0 is not too large compared with σ_0/E we have

$$\frac{\sigma}{\sigma_0} = \sinh^{-1}\left(\frac{x_0 z}{\sigma_0/E}\right). \quad (23)$$

Near the neutral axis where z is small, $\frac{\sigma}{\sigma_0} = \frac{x_0 z}{\sigma_0/E}$ or $\sigma = Ex_0 z = E\epsilon$, the elastic value.

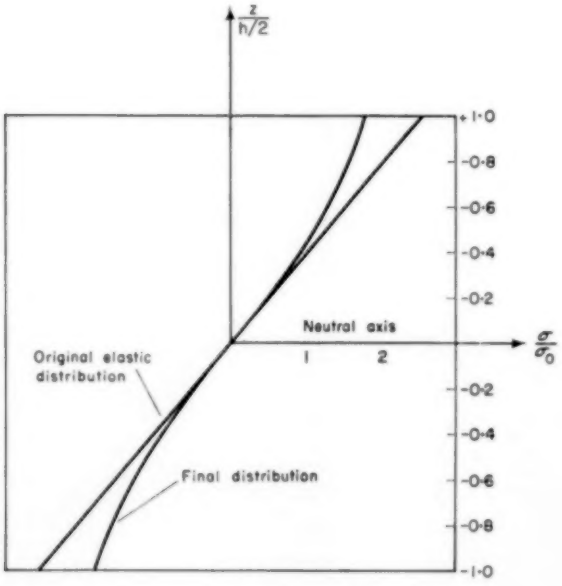

Fig. 9. Stress distribution in a bent beam of solid rectangular section under constant bending moment (for $x_0\, h/2 = 2{\cdot}13\, \sigma_0/E$).

Fig. 9 shows the nature of the stress distribution in the viscoelastic beam as it was initially at $t = 0$ and also after a sufficiently long time ($t > \sigma_0/EC$) for the distribution to become steady. The Figure shows that the stresses along the fibres farthest removed from the neutral axis are reduced from the initial values due to creep of the material.

4. Summary and Conclusions

From the foregoing considerations a number of conclusions can be reached. These conclusions, on the basis of the assumptions made, describe the potential

capacilities of *ideal* fibre-reinforced crystalline materials. It is believed that this information is of importance in designing fibre-reinforced composite crystalline materials.

The conclusions are summarized as follows:

(1) If the composite material is to carry tension, the fibres should be aligned in the direction of the tension. The resulting composite material will, of course, be orthotropic.

(2) The ratio E'/E should be as large as possible. A ratio of 2 would be desirable and is possible of achievement. For example, a mullite–tungsten combination would yield a ratio of $E'/E = 2{\cdot}3$ approximately.

(3) The curves of stress distribution indicate that the fibres may be fairly closely spaced without impairing their stress-carrying power too heavily. They may probably be spaced a distance apart of the order of the fibre diameter.

(4) An isotropic material can be achieved by a random orientation of metallic fibres, but probably at a sacrifice of the exceptional ability to carry unidirectional tension which results when the fibres are aligned.

(5) As the tensile load applied in the direction of the fibres to a composite block of material is increased, the fibres will carry more load in proportion to their area than will the matrix. The amount of the extra load depends chiefly on the modulus ratio E'/E and on the mean shape ratio b/a, as shown by Fig. 5.

(6) Although the longest fibres start breaking from the moment the load is applied, their number is so few initially that for a considerable time the load carried by the fibres appears to increase linearly with the applied load (see Fig. 5).

(7) The effect of breakage does not become evident until the peaks of the curves of Fig. 5 are approached. Near these peaks, and beyond, the breakage becomes rapid and the fibres as a group may no longer be considered useful for carrying tensile load.

(8) The picture as given by Fig. 5 is probably slightly conservative since a broken fibre can very likely carry a small load which is difficult to estimate. However, it is not believed that the results of Fig. 5 will be changed in any essential way by this small extra load-carrying ability. For example, when the modulus of the fibres is twice that of the matrix, it is probably unsafe to apply a stress to the composite material greater than $0{\cdot}45\,\sigma_f$.

(9) When the stress is lined up in the direction of a set of fibres, the strength of the material is obviously governed by the strength of that set.

(10) When the stress is applied at a small angle to a set of fibres, the strength of these probably still controls the strength of the material up to a certain angle. Beyond this angle, when shear stresses become appreciable, it is quite possible that failure may occur by excessive shear stress. As the angle of application of the stress is further increased and approaches 90° away from the first direction, the shear stresses again become unimportant and the strength of the material is now once more controlled by the strength of the fibres (if any) in the new direction at right angles to the first.

(11) By introducing a uniform viscoelastic concept, the elevated temperature behaviour of fibre-reinforced composite material can be predicted.

(12) The stress distribution at elevated temperature in a fibre-reinforced beam under constant bending moment is described.

Acknowledgments

The authors are grateful to the United States Navy, Bureau of Weapons for sponsoring this investigation.

References

Chang, R.	1960	*J. Appl. Phys.* **31**, 484.
Donnell, L. H.	1941	Von Kármán Anniversary Volume, p. 293.
Edwards, R. H.	1951	*J. Appl. Mech.* **18**, 19.
Monkman, F. C. and Grant, N. J.	1956	*Proc. Amer. Soc. Test. Mater.* **56**, 593.
Saleme, E. M.	1958	*J. Appl. Mech.* **25**, 129.
Stowell, E. Z.	1957a	N.A.C.A. T.N. 4,000.
	1957b	*J. Aero. Sci.* **24**, 922.
Stowell, E. Z. and Heimeri, G. J.	1960	N.A.S.A. Tech. Rep. R-59.

J. Mech. Phys. Solids, 1961, Vol. 9, pp. 261 to 278. Pergamon Press Ltd., London. Printed in Great Britain

FURTHER EXPERIMENTAL STUDY OF THE UNLOADING PHENOMENON IN CONSTANT VELOCITY IMPACT

By J. F. Bell
The Johns Hopkins University, Baltimore

(*Received 29th June*, 1961)

Summary

A further experimental study is presented of the unloading phenomenon for the constant velocity axial impact of identical annealed aluminium cylindrical rods. Measurements are made of stress–time behaviour at the impact face, displacement–time behaviour at several distances from the impact face as well as at the free end, and strain–time measurements in the vicinity of the free end. A linear equivalent approximation based upon the secant modulus is introduced, from which these experimental data may be predicted. The author's earlier determination of times of contact and coefficients of restitution from the characteristic of half the maximum stress is shown to be consistent with this linear approximation.

1. Introduction

This paper presents a continuation of the experimental study of the unloading phenomenon reported upon in a recent issue of this Journal (Bell 1961a; hereafter referred to as I). In that paper (I), it was found possible to predict the time of contact and the coefficient of restitution from a simple interpretation of the characteristics of the Lagrangian diagram, using the strain-rate independent theory of plastic wave propagation. It was shown that the time of contact was given by the summation of the time required for propagation along the characteristic associated with half the maximum stress from the impact face to the free end of the specimen, plus the time for an unloading wave to travel with an elastic velocity back to the impact face. The coefficient of restitution was obtained by assuming that the final velocity could be determined from the elastic unloading of the static stress–strain curve by half the maximum stress. Over the entire range of impact velocities, experimental times of contact were in excellent agreement with values predicted from the static stress–strain curve. The coefficient of restitution was in agreement only above an impact velocity of approximately 400 in/sec.

It has been shown (Bell 1961b) that the actual governing stress–strain curve is a parabola. This parabolic stress–strain relation may be determined by introducing static single crystal measurements into the theory of the polycrystalline aggregate of Taylor (1942) and of Bishop and Hill (1951). In that paper (Bell 1961b) it is shown further that, when cognizance is taken of the role of the initial elastic front, the coefficient of restitution is in as close an experimental agreement as the time of contact with the theoretical prediction referred to above.

The actual plastic strains associated with the characteristic of half the maximum stress obviously do not reach the end of the specimen ; hence, it seemed to be of some interest to carry out a further investigation of the observed role of the characteristics on the Lagrangian diagram. In the present paper a new series of experiments are discussed. These include the measurement of the stress–time history at the impact face, the displacement–time history at the free end of the specimen, the longitudinal displacement–time behaviour at several positions along the rod, and the strain–time behaviour at seven, eight, nine and ten diameters in ten diameter specimens, i.e. at three, two and one diameters from the free end of the rod, and the strain–time behaviour on the face of the free end of the rod.

From these experiments, and using an extension of essentially the same ideas as those contained in my previous paper (I), one may relate the displacement and velocity behaviour at the free end of the rod to the displacement and stress behaviour at, or in the vicinity of, the impact face, and one may determine in addition the largest distance of penetration of the maximum strain.

2. Experimental Data

The experimental situation under consideration is that of the free flight axial impact of two identical aluminium rods. The hitter specimen is shot from a smooth bore air gun, the last foot of which is ported so that a constant velocity impact may be obtained. The impact velocity is half the hitter velocity. All specimens are optically aligned prior to impact.

The unloading behaviour, wherein the characteristic of half the maximum stress governs the time of contact and the coefficient of restitution, suggests that in the unloading process the identity of the plastic front is maintained in some manner throughout the interval of interaction. In order to examine the type of strain–time behaviour which is present near the free end of the specimen, measurements were made at 7, 8 and 9 in. from the impact face in 10 in. long, 1 in. diameter specimens. These experimental results are shown in Figs. 1 and 2, together with the measurements at six diameters which were shown in the previous paper (I), and measurements made from wire resistance strain-gauges located at the centre of the face of the free end of the specimen itself.

All these measurements were made with wire resistance strain-gauges. The plastic strains and rise times are below those which involve the wire resistance strain-gauge errors observed for larger plastic strains (Bell and Gillich, unpublished).

The initial elastic unloading front in the previous paper (I) was shown to be absorbed between four and five diameters from the impact face, as had been predicted theoretically by Lee (1953). In the 10 in. specimens this front arrives at 6 in. at 70 μsec, 7 in. at 65 μsec, 8 in. at 60 μsec, and 9 in. at 55 μsec. As may be seen in Figs. 1 and 2, unloading is observed, in each instance, at the time specified. At 9 in. at a time of 270 μsec, the final unloading occurs from the maximum strain of 800 μin/in. The amount of decrease is exactly that of the elastic unloading of the static stress–strain curve from a strain of 800 μin/in, and the time of 270 μsec is also that predicted by the characteristic of half the maximum stress. The subsequent elastic behaviour, shown in the test at 9 in. has a period of approximately 100 μsec, which is the time to be expected for a 10 in. rod of aluminium.

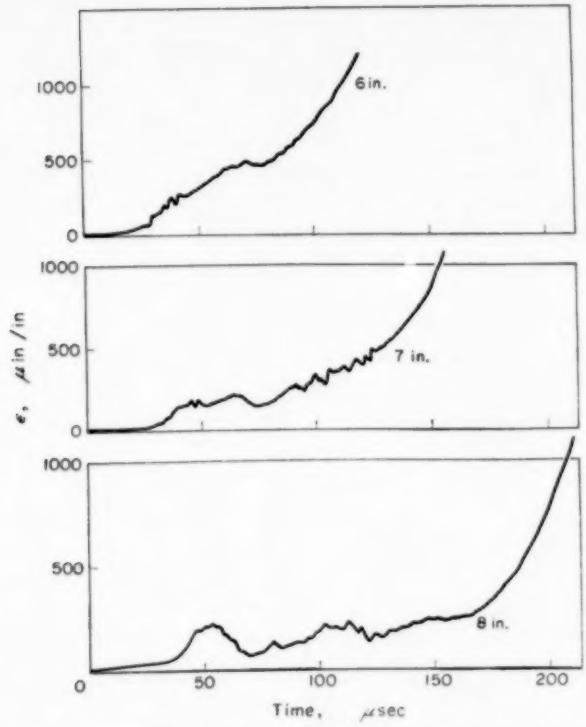

FIG. 1. Strain–time at 6, 7 and 8 in. from the impact face for 10 in. specimens.

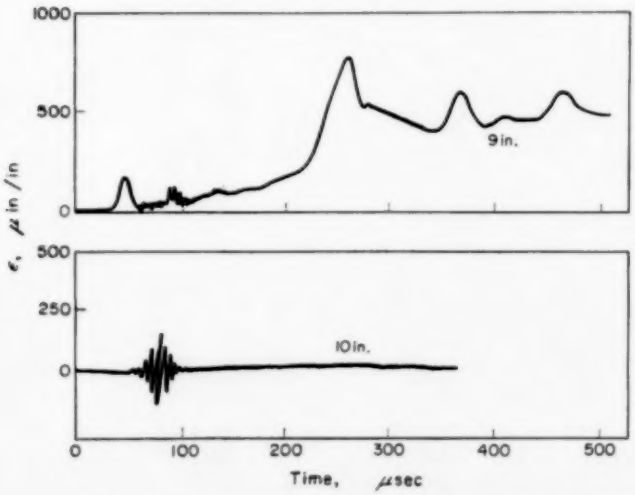

FIG. 2. Strain–time at 9 in. from impact face, and at 10 in., or the centre of the free face.

The hitter and struck specimens have separated during this time and the struck specimen, upon which the measurements are made, is in free flight.

An interesting aspect of these measurements is the high frequency oscillation present in these data. No such oscillations are found at four or fewer diameters from the impact face. The measurement on the free end (shown in Fig. 2 as that at 10 in.) suggests that the high frequency ripple is a radial oscillation in the vicinity of the free end. This radial oscillation is rapidly eliminated by the oncoming plastic wave as it propagates from the free end toward the impact face. The presence of what appears to be beating at 6 and 7 in., suggests that these oscillations may be reflected from the oncoming plastic front in a manner similar to that discussed earlier (I) for the initial elastic front.

These data of Figs. 1 and 2 may be summarized in a modified Lagrangian diagram shown in Fig. 3. The characteristics determined from strain measurements at 4 in. from the impact face are compared with experimental results between 4 and 9 in. from the impact face. All these data are for an impact velocity of 960 in/sec, for which the theoretical maximum strain is 0·028 in/in. Experimental maxima for 800 in/sec, are shown in Fig. 3 as triangles, and it is seen that the theoretical maximum penetrates to 4 in. from the impact face, following which lower values are obtained.

It is obvious from Fig. 3 that the strains in the vicinity of the free end of the specimen are not necessarily simply related to the characteristics of the plastic wave, although the unloading phenomenon is such as to indicate that the arrival time of these characteristics at the free end of the specimen do govern the process. As has been pointed out earlier (I), the maximum strains at five, six and seven diameters do occur at times which agree with the characteristics of each maximum strain level.

To examine this unloading effect further, displacement–time measurements for different impact velocities were made at one, two, four and six diameters from the impact face, and at the free end of the specimen. The experimental technique used was a modification of that reported upon earlier (I) for the determination of the time of contact. For the measurement of displacement–time at the free end of the specimen, the free end itself was allowed to interrupt a narrow rectilinear uniform light beam between a light source on one side of the specimen and a 5 in. photomultiplier tube on the opposite side of the specimen. Calibration was effected by the use of precision spacers, as reported upon earlier (I), and also by shooting specimens at known velocities through the light field. Longitudinal displacement–time measurements were made at intermediate positions along the specimen by painting one side of the point of interest with a non-reflecting black paint, and the other side with a reflecting white paint. The rectilineal, uniform, light field falls upon the specimen on either side of the intersection of the two painted surfaces. In this instance both the light source and the photomultiplier tube are located on the same side of the specimen. The calibration is obtained by shooting the specimen at a known velocity through the light field.

In Fig. 4 four tests of the above described type are shown at a distance of 2 in. from the impact face. The solid line in Fig. 4 is the theoretical displacement–time curve given by the strain-rate independent, finite amplitude, wave theory using the slopes of the static stress–strain curve.

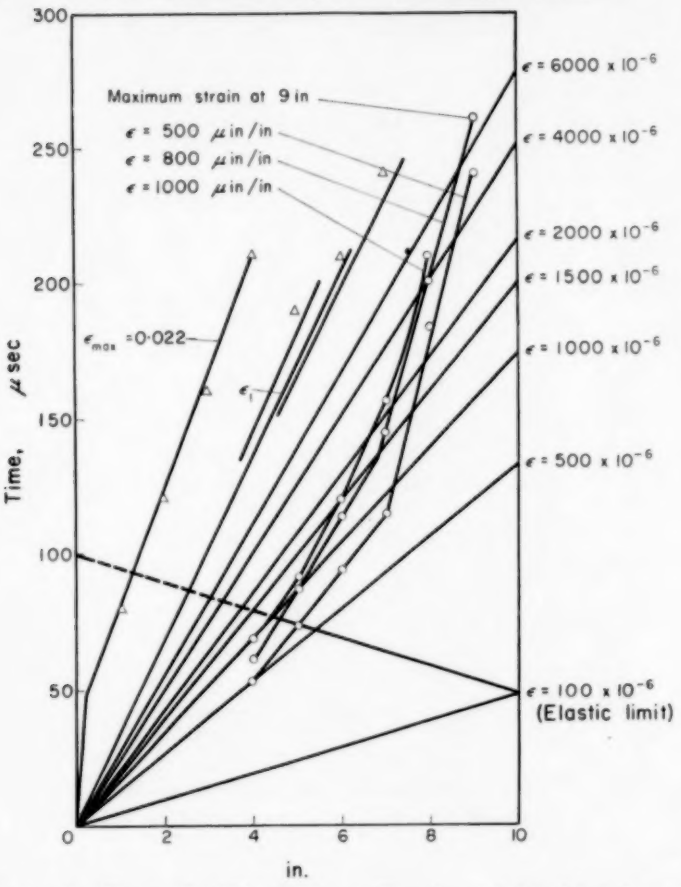

FIG. 3. Lagrangian diagram for 10 in. specimen. Experimental data (circles) are compared with characteristics. Triangles designate experimental maximum strain at location shown.

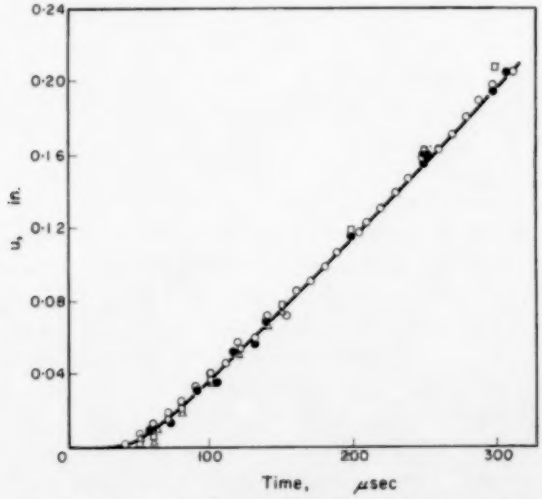

FIG. 4. Experimental displacement–time behaviour at two diameters from impact face (four tests) compared with theoretical curve (solid line). Impact velocity is 66·5 ft/sec.

In Fig. 5 are shown the experimental averages of tests at 1, 2, 4 and 6 in. from the impact face. These data provide a check, independent of the earlier diffraction grating experiments (BELL 1960a), for the applicability of the finite amplitude wave theory of VON KARMAN (1942), TAYLOR (1942), RAKHMATULIN (1945) and WHITE and GRIFFIS (1942).

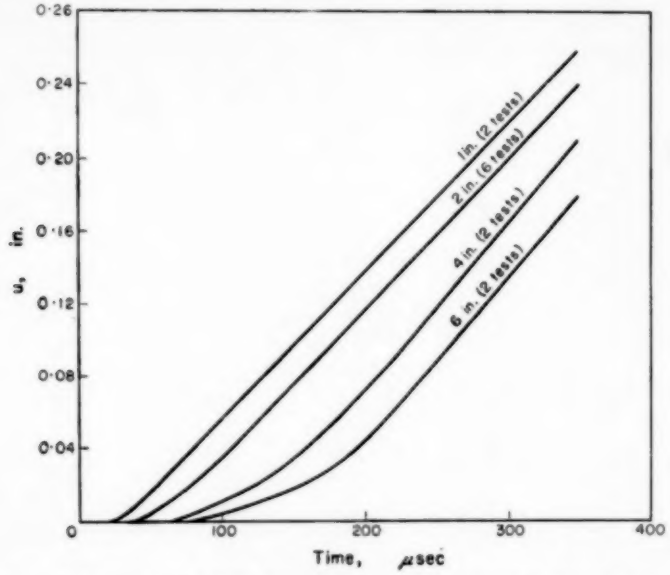

FIG. 5. Averaged experimental displacement–time behaviour at indicated distances from impact face for impact velocity of 66·5 ft/sec.

A very interesting aspect of Figs. 4 and 5 is that the displacement–time behaviour shown at 1, 2 and 4 in. is that of a semi-infinite rod. The entire plastic loading is developed without any visible unloading effects.

Fig. 6 shows typical displacement–time curves at the free end of the specimen for three different impact velocities. In each situation the final velocity is in agreement with the coefficients of restitution given earlier (I). For each of the specified impact velocities, the final straight lines, indicating uniform velocity, begin at times which are in agreement with the arrival of the characteristic of half the maximum stress at the free end of the specimen. For impact velocities below the KARMAN critical velocity of 581 in/sec, the earlier arrival times of the low displacement levels at the free end had been predicted (BELL 1961b) as being related to differences in the plastic wave development in the first diameter. Such predicted arrival times, it should be noted are for these lower impact velocities. By the time of final unloading, the displacement–time curve at 378 in/sec is nearly the same as that for impact velocities above the KARMAN critical velocity, and thus one obtains times of contact and coefficients of restitution in agreement with earlier observations (BELL 1961a, b).

A third type of experiment carried out by the present writer for the purpose of examining the unloading phenomenon is the measurement of stress at the impact

face. These experiments, which are similar to those of JOHNSON, WOOD and CLARK (1953) and CAMPBELL (1953), consist of allowing a specimen of annealed aluminium to be shot from an air gun and collide axially with a 5 ft rod of the same diameter of hard aluminium. The response of the hard rod is elastic, and measurements of the strain–time behaviour following impact are made at different distances from the impact face. These measurements from the different positions are, in accordance with elastic theory, extrapolated to the impact face itself, and interpreted as a measure of the stress history at the impact face.

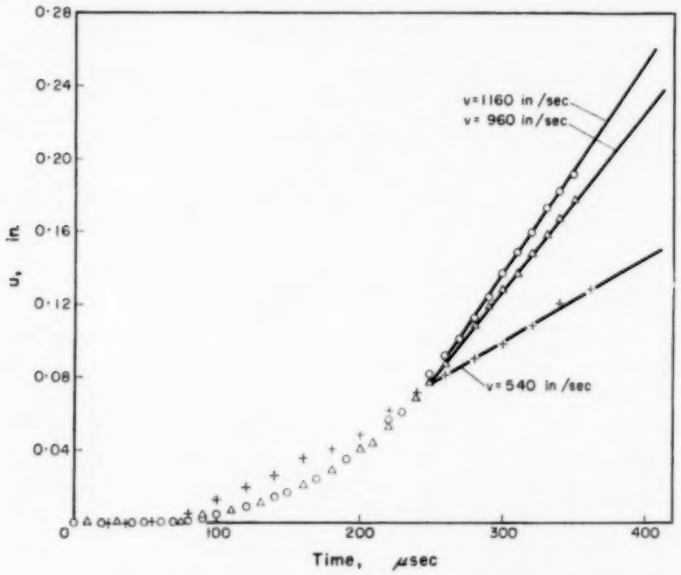

FIG. 6. Experimental displacement–time behaviour at free end of 10 in. specimen for indicated impact velocity. Impact velocity 948 in/sec (○), 800 in/sec (△), 378 in/sec (+).

As a check that stresses calculated from such a test are actually those present at the impact face, J. SPERRAZZA of the U.S. Army Ballistics Research Laboratories, Aberdeen Proving Ground (private communication) has conducted tests in specimens supplied by the present writer, using piezzo crystals at the interface. He has obtained results essentially in agreement with those shown here using the load bar technique.

In Fig. 7 typical load bar tests are shown for two different impact velocities. The annealed specimens used in the tests of Fig. 7 are 10 in. long. The initial stresses are in agreement with those given earlier by JOHNSON *et al.* (1953) for annealed aluminium which are shown in Fig. 7 as either P_v or P_s depending upon which method of measuring strain one chooses in their earlier measurements. The σ_{max} shown in Fig. 7 is that given by the finite amplitude wave theory for the impact velocity in question. The time of contact is shown as T_c, which, for the situation of 66·5 ft/sec, is in very good agreement with values obtained earlier (I), using an optical technique. As will be shown subsequently, the point at which

the measured stress-time curve crosses σ_{max} also may be determined from a consideration of the arrival of characteristics of the plastic wave at the free end of the specimen.

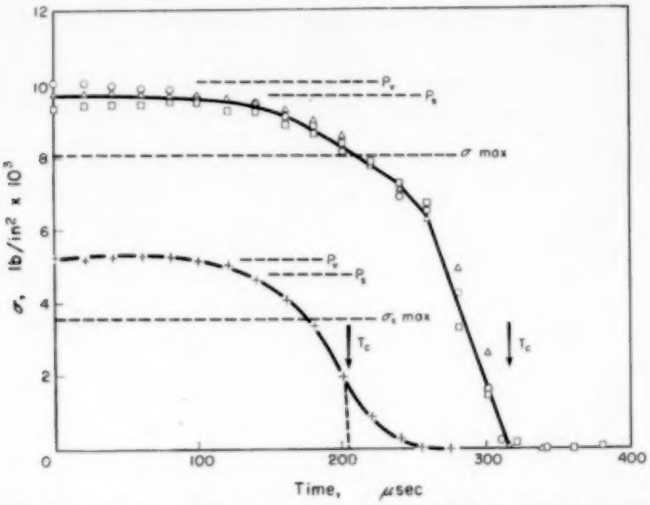

FIG. 7. Load bar measurement of stress at impact face for 10 in. long specimens for indicated impact velocities. Impact velocity: 66·5 ft/sec, unlubricated (○); 66·5 ft/sec, unlubricated (△); 66·5 ft/sec, stearic acid (□); 17·9 ft/sec, unlubricated (+).

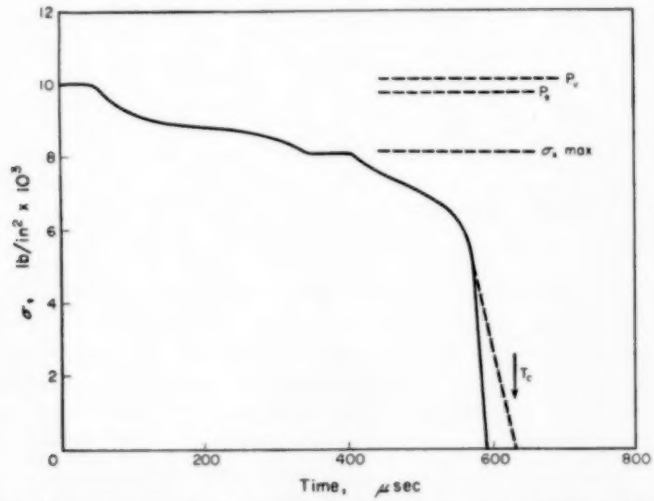

FIG. 8. Load bar measurement of stress at impact face for 20 in. long specimen. Impact velocity, 66·5 ft/sec. Test 389.

As was shown in an earlier paper (BELL 1960b), these initial dynamic stresses may be predicted from the static stress–strain curve from the theoretical assumption that dispersive plastic waves develop in the immediate vicinity of the impact face from initial non-dispersive shock fronts. It is interesting to observe that these initial stress levels, while maintained from between 80 and 100 μsec, gradually

decrease until final unloading takes place. In what follows it is presumed that the decrease of these higher stress associated with the plastic wave development in the first diameter is not part of the unloading process which develops from the free end of the specimen, unless the specimen is shorter than a specified length.

As a first indication that this hypothesis is correct, a test is shown (Fig. 8) for a 20 in. annealed aluminium, specimen striking a 5 ft long, hard aluminium, bar. In this situation the dynamic stresses fall to the theoretical maximum before the theoretical maximum itself begins to unload at what will be shown to be the predicted time of slightly in excess of 400 μsec. The time of contact could not be measured in this test since it was longer than the time for an elastic wave to traverse the hard load bar to its free end and return.

3. Discussion of Experimental Results

In the finite amplitude wave theory the stress is assumed to be a function of strain only. For wave propagation in a cylindrical rod approximating uniaxial stress conditions, the one-dimensional equation of motion is

$$\rho \frac{\partial^2 u}{\partial \tau^2} = \frac{\partial \sigma}{\partial \epsilon} \frac{\partial \epsilon}{\partial x} \tag{1}$$

or

$$\rho \frac{\partial^2 u}{\partial \tau^2} = \frac{\partial \sigma}{\partial \epsilon} \frac{\partial^2 u}{\partial x^2} \tag{2}$$

since

$$\epsilon = \frac{\partial u}{\partial x}.$$

Solutions in either Eulerian or Lagrangian terms for the situation of constant velocity impact have been given (Kolsky 1953). The velocities of propagation of each level of strain are found to be constant and equal to

$$c_p = \sqrt{\frac{\partial \sigma / \partial \epsilon}{\rho}} = \frac{x}{\tau} \tag{3}$$

and a relation is obtained between impact velocity and maximum strain:

$$v_0 = \int_0^{\epsilon_{max}} c_p \, d\epsilon. \tag{4}$$

Equations (3) and (4) presume that a single stress–strain curve governs the motion at all positions and times. The theory does not require that this stress–strain curve should necessarily be the static stress–strain curve of the material. The presence of higher stresses alone does not imply that other effects such as strain rate need be included unless it is shown that either or both of equations (3) and (4) are not satisfied experimentally. It has been found by the present writer (Bell 1960a) in annealed aluminium, and confirmed by his students (Werner 1960; Sperrazza 1961) in annealed copper and pure lead, that a single stress–strain curve *does* govern the motion. For strains up to approximately 3 per cent, this curve approximates the static stress–strain curve of the material. For annealed aluminium it has been shown further (Bell 1961b) that the governing stress–strain curve is actually a parabola which, for strains up to 2 or 3 per cent quite closely

approximates the static stress–strain curve. Such a parabola has been found also for annealed copper and for lead (BELL, unpublished manuscript). This parabola, which has been experimentally determined from dynamic diffraction grating measurements (BELL 1961b), may be predicted theoretically from the theory of TAYLOR (1958) for the polycrystalline aggregate, using experimental information obtained from compression tests on single crystals of the same metals.

The polycrystalline stress–strain curve, then, is

$$\sigma = \beta\epsilon^{\frac{1}{2}} \tag{5}$$

where, for polycrystalline annealed aluminium, β is $5{\cdot}60 \times 10^4$ lb/in^2. In using this parabola in the region of low strain proper account must be taken of the fact that allowance must be made for the initial elastic stresses. Thus, below strains of 2 per cent the static stress–strain curve is somewhat higher than the parabola, whereas, over 2 per cent, the parabola becomes increasingly above the static stress–strain curve. In the region over 2 per cent, as has been shown (BELL 1961b), the dynamic results follow the parabola rather than the static stress–strain curve. Below 2 per cent, however, the coefficient of restitution and dynamic stress calculations suggest (BELL 1961b) that the differences between the two curves are caused by the higher stress levels associated with the elastic region.

A propos of the above, the calculations which follow are based upon the static stress–strain curve itself, since the strain maxima are all below 3 per cent for the data reported upon here. Experiments in progress at the present time, for velocities up to 500 ft/sec, do suggest, however, that at strain maxima above 2·5–3 per cent one may no longer use the static stress–strain curve. At the higher strain maxima the motion is governed by the parabolic stress–strain curve.

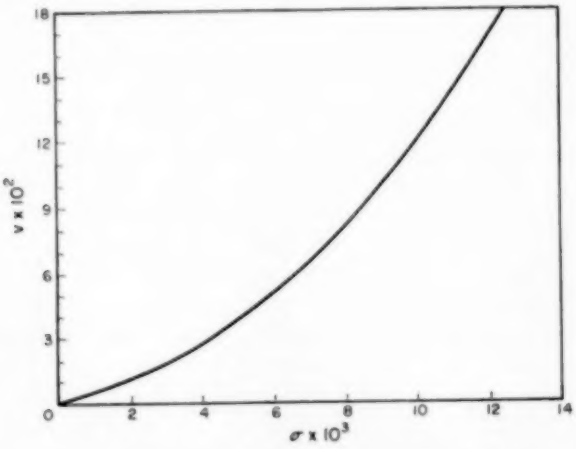

FIG. 9. Impact velocity vs. maximum stress.

For either the static stress–strain curve or the parabola, equation (4) results in an upward turning curve when the impact velocity is plotted against the maximum stress. This is shown in Fig. 9, which has been calculated from the slopes of the static stress–strain curve, Fig. 10.

In a paper on plastic wave propagation LEE (1953) obtained an expression [equation (6)] from a consideration of the properties of the characteristics. As LEE indicated, this describes the initial unloading phase of plastic wave propagation in finite specimens:

$$\sigma_a - \sigma_b = -\left[Y - \tfrac{1}{2}(\rho c_0 v_b - \sigma_b)\right] \tag{6}$$

where σ_b is the strain from the finite amplitude wave theory prior to unloading, and v_b is the corresponding particle velocity prior to unloading, given by equation (4); σ_a is the stress following the arrival of the unloading wave; Y is the elastic limit of the material; and ρ and c_0 are the mass density and elastic velocity $c_0 = \sqrt{(E/\rho)}$, respectively.

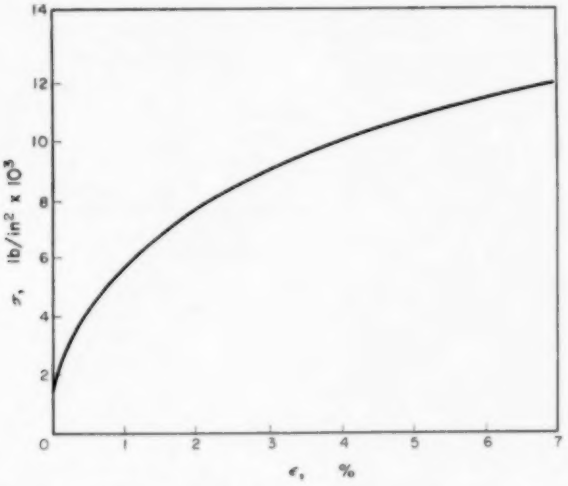

FIG. 10. Static stress–strain curve for annealed aluminium.

As LEE pointed out, the numerator of the right-hand side of equation (6) must approach zero as the impact velocity, v, is increased when the relation between impact velocity and stress is upward turning, as is shown for annealed aluminium in Fig. 9. If the right-hand side of equation (6) is zero, then $\sigma_a = \sigma_b$ and the elastic unloading wave has been absorbed or reflected back to the free end. For annealed aluminium Y is approximately 1100 lb/in² and the velocity for which the right-hand side of equation (6) is zero is approximately 80 in/sec.

For an impact velocity in excess of 80 in/sec, the complete absorption of the initial elastic front, i.e. $\sigma_a = \sigma_b$, occurs at some distance from the impact face. For 10 in. long and 1 in. diameter specimens of annealed aluminium, this occurs between four and five diameters from the impact face. This prediction was experimentally verified in the earlier paper (I). The discussion which follows presumes that this reflected initial elastic strain level, and the higher strain levels which follow, are progressively reflected in a fashion similar to that of the initial front. This is true until unloading levels are reached which are sufficiently high to begin the unloading of the maximum stress itself, following which the stresses in the vicinity of the impact face are quickly unloaded and the specimens separate.

The following proposed model is an approximation which gives results consistent with the above interpretation, with the experimental data, and with a modified version of equation (6).

If one were considering the unloading phenomenon associated with an elastic wave produced by constant velocity impact, one could introduce the mass and momentum equations:

$$\sigma = \rho c_0 v_0, \tag{7}$$

$$\epsilon = \frac{v_0}{c_0}, \tag{8}$$

where c_0 is the same in both equations, and the kinetic energy per unit volume, $\frac{1}{2}\rho v_0^2$, is equal to the deformation energy per unit volume, $\frac{1}{2}\sigma\epsilon$. For the nonlinear plastic wave the energy of deformation is always greater than the initial kinetic energy. It may be shown for a parabolic stress–strain curve that the energy of deformation per unit volume is equal to 3/2 × the kinetic energy per unit volume for any impact velocity.

Since the plastic wave propagation is non-linear, one would not expect to find an equivalent linear wave satisfying equations (7) and (8) from which an assumption of zero stress at the free end would permit of a determination of the unloading phenomenon. However, since the stress, strain and impact velocity are known from the finite amplitude wave theory, one might obtain an equivalent step front satisfying the stresss velocity condition of equation (7), where c_0 would be replaced by some other effective c_p. Similarly, an effective c_p might be found for the mass equation (8). The effective c_p of equations (7) and (8) would not be the same. It is interesting, though, that if one takes the average between these two equivalent effective velocities for a given impact velocity, this average, c_p^*, is in very close agreement with the velocity of the characteristic associated with half the maximum stress. As will be shown below from the relation of the parabola, by replacing the dispersive plastic front with a step front of equations (7) and (8) which has a wave velocity, c_p^*, the maximum error introduced is 6 per cent, and for maximum strains in the vicinity of 2 per cent, the errors are much less than that.

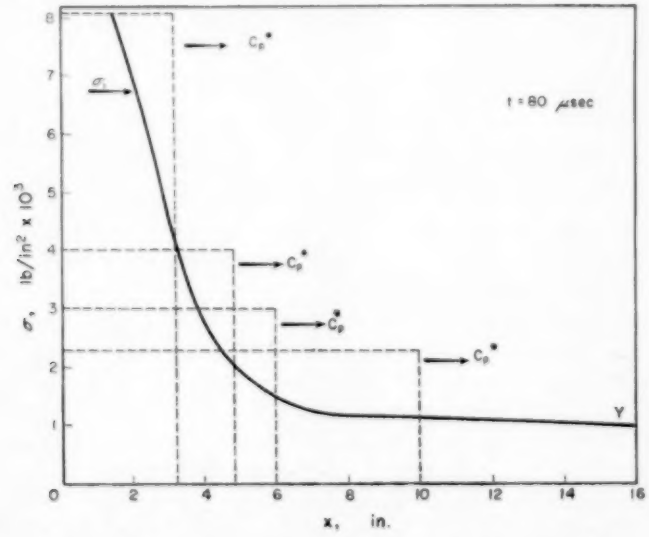

FIG. 11. Equivalent fronts at indicated stress, compared with stress–distance curve at 80 μsec, from finite amplitude wave theory.

In Fig. 11 equivalent elastic fronts are shown for various stress levels. The stress is plotted against distance at the particular time of 80 μsec, and the c_p^* of 8100, 4000, 3000 and 2250

lb/in^2 are indicated. The stress level σ_1 is that associated with the mean energy. As was shown earlier (BELL 1961a, b), propagation details up to this mean are essentially those generated from an infinite step at the impact face, whereas stresses and strains above σ_1 are considerably delayed in traversing the first half-diameter.

From Fig. 11, then, any given stress level may be represented by an equivalent linear front for which the energy integral $\int_0^\epsilon \sigma \, d\epsilon$ is approximated by $\frac{1}{2} \sigma \epsilon$. For the linear elastic situation we have the energy balance.

$$\tfrac{1}{2} \rho v^2{}_0 = \tfrac{1}{2} \sigma \epsilon. \tag{9}$$

By substituting the parabolic stress–strain law of (5) into (8) and (4), one obtains

$$c_p = \sqrt{(\beta/2\rho)}\, \epsilon^{-\frac{1}{2}}, \tag{10}$$

$$v^2{}_0 = \frac{8}{9} \frac{\beta}{\rho} \epsilon^{\frac{3}{2}}. \tag{11}$$

If one determines the $c_p{}^*$ from (10) at half the level of maximum stress,

$$c_p{}^* = \sqrt{(\beta/\rho)}\, \epsilon^{-\frac{1}{2}}. \tag{12}$$

Multiplying (11) by $\frac{1}{2}\rho$,

$$\tfrac{1}{2} \rho v^2{}_0 = \frac{4}{9} \beta \epsilon^{\frac{3}{2}} = \frac{4}{9} \sigma \epsilon. \tag{13}$$

Examining (12) and (13) in the light of (9), then, one finds that (9) is exactly satisfied for an equivalent impact velocity, v'_0, where $v'_0 = 1{\cdot}06\, v_0$, and where v_0 is the actual impact velocity. If v'_0 is introduced into (9), the corresponding maximum stress and maximum strain are those from the finite amplitude wave theory. It should be pointed out that this difference of 6 per cent was obtained from the parabola, which omits the small contribution from the initial elastic portion of the wave. The inclusion of the small elastic contribution will increase v_0 so that the difference between v_0 and v'_0, at least for small maximum strains, will be considerably less than 6 per cent.

In the elastic wave satisfying (9), the velocity is c_0 where $c_0 = \sqrt{(E/\rho)}$. The elastic modulus, E, is given by $E = \sigma/\epsilon$ and is the slope of the stress–strain relation. In the equivalent plastic front, with secant modulus $E_1 = \sigma/\epsilon$, it may be shown for a parabolic stress–strain relation that E_1 is parallel to the tangent modulus $\rho\, c_p{}^{*2}$ at half the maximum stress. Thus, in determining the time of contact, etc., the role of the characteristic associated with half the maximum stress is equivalent to that of a propagation velocity determined from the secant modulus of the stress level in question. This latter is then an approximation of the dispersive front, with the substitution of the somewhat larger $v_0{}'$ for v_0.

If the linear equivalent front is used to satisfy the zero stress condition at the free end of the specimen, in a manner shown in Fig. 12, then the elastic unloading wave (shown as the dotted step front on the lower right-hand portion of Fig. 12) necessary to maintain a zero stress at the free end may be determined from any portion of the incoming plastic wave. To reach the free end of the specimen, the stress σ_b at an instant of time must travel a distance $L - c_p{}^* T$ at a propagation velocity $c_p{}^*$. The particle velocity of this equivalent front is v_b. The unloading wave required to produce a zero stress at the free end has a stress level $-\sigma_b$ travelling with the velocity c_0, with a particle velocity $v = \sigma/\rho c_0$. At the time shown in Fig. 12 this unloading front is at a distance, $Z = c_0\, T$ from the free end of the specimen.

Since the time for each wave to reach the free end of the specimen is the same,

$$\frac{L - c_p{}^* T}{c_p{}^*} = \frac{Z}{c_0}. \tag{14}$$

Thus, when these two fronts cancel at the free end of the specimen,

$$T = \frac{L}{c_p{}^*}. \tag{15}$$

The unloading at the impact face will take place at a time greater than this by the amount required for an elastic wave to travel from the free end of the specimen to the impact face. The particle velocity at the free end following the arrival and interaction of the two fronts will be

$$v_u = v_b + \frac{\sigma_b}{\rho C_0}. \tag{16}$$

If one calculates as a function of time the velocity, v_u, at the free end, by considering each stress level as shown in Fig. 11 in a manner shown in Fig. 12, the solid line of Fig. 13 is obtained. Here the propagation velocities c_p^* for each stress level have been determined from the slopes of the static stress–strain curve.

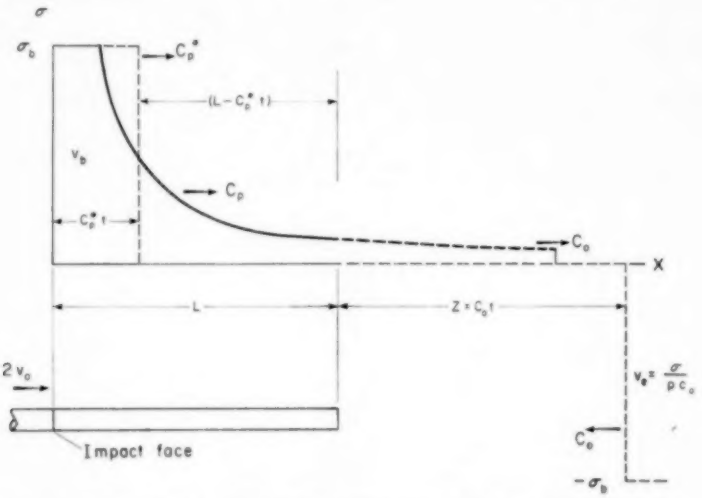

FIG. 12. The equivalent front and the corresponding elastic unloading front.

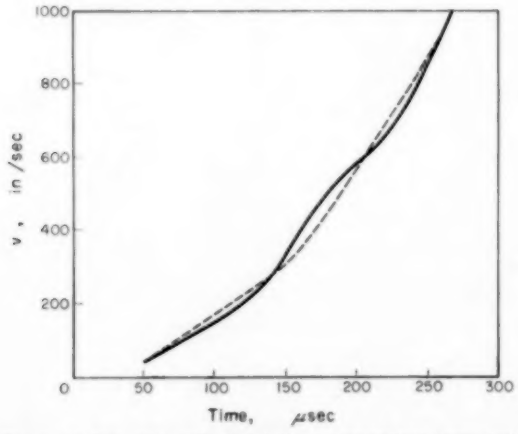

FIG. 13. The velocity v_u at free end, calculated from equivalent front (solid line) and from slopes of experimental displacement–time measurements (dashed line).

Integration of the velocity–time curve of Fig. 13 gives the solid line of Fig. 14. The circles of Fig. 14 are the average of several displacement–time tests of the type described above at an impact velocity of 66·5 ft/sec. The dotted line of Fig. 13 is a velocity–time curve obtained from measuring the slopes of the experimental data of Fig. 14. Hence, in considering the unloading

phenomenon, one may start with either the experimental data or the equivalent linear approximation.

Equation (16) is identical with (6) of LEE (1953) when σ_a – or the stress after the unloading wave has arrived – is set equal to zero, and for $2Y$ one substitutes $\rho c_0 v_u$ or the elastic unloading level necessary to completely unload the theoretical maximum stress level σ_b. Thus, (6) becomes

$$\sigma_a - \sigma_b = -\tfrac{1}{2}\left[\rho c_0 v_u - (\rho c_0 v_b - \sigma_b)\right]. \tag{17}$$

The v_u of (17) necessary to make $\sigma_a = 0$ may be introduced either from the experimental data or in terms of the linear equivalent front. For $\sigma_a = 0$ we have $v_u = v_b + \sigma_b/\rho c_0$ which is the same as (16). If one determines this velocity v_u, let us say from the experimental data, for an impact velocity of 66·5 ft/sec which occurs at a time $L/c_p{}^*$, then, 50 μsec later, the stress at the impact face would be unloaded. A calculation of this type predicts complete unloading at the impact face at approximately 308 μsec for an impact velocity of 66·5 ft/sec in annealed aluminium. As may be seen in Fig. 7 the stress at the impact face does completely unload at the predicted time. From optical experiments in the earlier paper (I), too, this was shown to be the time in which the specimens separated.

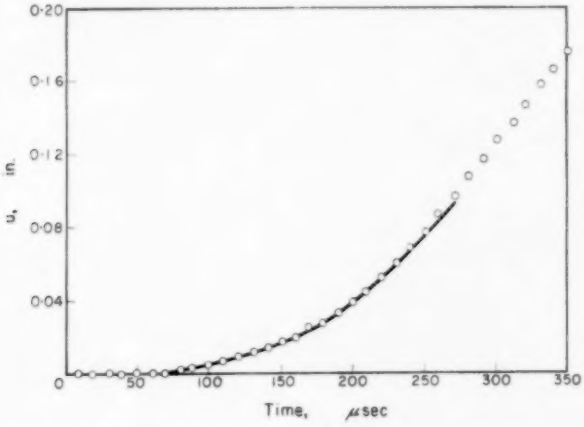

FIG. 14. Experimental displacement–time behaviour at free end (circles) compared with behaviour computed from linear equivalent approximation (solid line). Impact velocity, 66·5 ft/sec.

Since the situation considered is that of the impact of two identical specimens, a consideration of the boundary condition at the impact face following the arrival of the unloading front will result in a final specimen velocity in excess of the mass centre velocity of half the second term of the right-hand side of (16). A coefficient of restitution is thus obtained which is in excellent agreement with experimental values, provided, as was pointed out above, provision is made for the contribution of the initial elastic front.

If the specimen is 5 in. or less in length, the initial dynamic stress levels are not reduced to the theoretical value, σ_{max}, of Fig. 7 or Fig. 8 when the unloading wave arrives at the impact face. Correspondingly longer times of contact are to be expected for short specimens. In my earlier paper (I), for a specimen length of 5 in., an experimental contact time of 170 μsec was compared with a theoretical value predicted from the characteristic of half the maximum stress of 159 μsec. If one computes the dynamic stress level in accordance with the nondispersive wave front, as was proposed by this writer (BELL 1960b), or from measured values such as those of Fig. 7, and if one determines the characteristic of half this dynamic stress rather than the theoretical maximum, σ_{max}, then for an impact velocity of 66·5 ft/sec, 168 μsec is obtained as the time of contact. This is obviously in very good agreement with the reported experimental time of 170 μsec. Thus, as the unloading wave does arrive at the impact face prior to the time at

which the maximum stress has dropped to the value given from the finite amplitude wave theory, longer contact times should be measured.

As was shown above, the initial elastic unloading front is progressively absorbed or reflected by the oncoming plastic wave front. Upon its re-arrival at the free end of the specimen it produces a continuously increasing particle velocity. If this new particle velocity at the free end is considered as an unloading front, one might expect from (6) that the substitution for Y of an unloading stress given by $\rho c_0 v_u$ would result in the determination of a particle velocity at the free end. This particle velocity would have to be reached before the unloading of any particular stress level could begin, as, for example, the maximum stress level for which $\sigma_a = \sigma_b$. As long as progressive absorption is taking place, the elastic unloading waves will be continuously reflected to the free end. This will no longer be the situation after an unloading level of sufficient height has been reached so that the maximum stress is being unloaded. For this reason, in (17) the factor 2, in the first term of the right-hand side, is found to be present up to the point where unloading the maximum stress begins, but not after this time. If $\sigma_a = \sigma_b$ in (17), where $Y = \rho c_0 v_u$, then

$$v_u = -\tfrac{1}{2}(v_b - \sigma/\rho c_0). \tag{18}$$

For 66·5 ft/sec this corresponds to a velocity at the free end of the specimen of 320 in/sec, which, from Fig. 13, may be seen to occur at the free end of the specimen at a time of approximately 150 μsec. Thus, the theoretical maximum stress at the impact face should begin to unload at a time of 150 μsec plus the elastic time (50 μsec) required for the unloading wave to travel from the free end of the specimen to the impact face. This time of 200 μsec of the beginning of the unloading of the maximum theoretical stress, σ_{max}, at the impact face may be compared with the experimental value of 210 μsec of Fig. 7 for a 10 in. specimen, or the theoretical value of 400 μsec for the 20 in. specimen of Fig. 8. In this latter situation the unloading of the theoretical maximum stress is more obvious since the dynamic stress levels of the first diameter have decreased to the theoretical maximum before the unloading arrives from the free end of the specimen.

Thus, the phenomenon of progressive absorption and re-reflection permits the maximum plastic strain to proceed into the specimen a distance much longer than would be expected if the first elastic reflection front and subsequent plastic reflected strains were to arrive in the vicinity of the impact face with their higher velocities of propagation. As a matter of fact, for the situation of 66·5 ft/sec, where a time of over 200 μsec is involved, the maximum strain may propagate to over 4 in. from the impact face in a 10 in. long specimen. As was shown earlier (I), the maximum arrives at 4 in. from the impact face at a time of approximately 200 μsec, and the maximum strain at 4·5 in. is less than the theoretical value.

The displacement–time curves (Figs. 4 and 5) at 1, 2 and 4 in. from the impact face are found to be those predicted by the finite amplitude wave theory for the situation of a semi-infinite rod. If the unloading waves are prevented from penetrating into this first four diameters until after the maximum strain has been reached, one would expect that this displacement–time behaviour, as well as the strain–time behaviour reported upon earlier (Bell 1960a), would be that of the semi-infinite rod. On the other hand, in the region in which unloading is affected by the reflections of the lower strain levels, i.e. that from 4·5 to ten diameters, the behaviour would not be expected to be that of the semi-infinite rod. The experimental measurements bear this out, as may be seen from an examination of the displacement–time curve at 6 in. of Fig. 5, and the strain–time curves of Figs. 1 and 2.

4. Summary and Conclusions

In this paper it has been shown that one may correlate displacement–time experimental results at the free end of identical specimens in constant velocity impact with some aspects of the stress–time behaviour at the impact face. This interrelation between behaviour at the two ends of the specimen is found to be consistent with an approximation developed from the earlier observed (I) experimental fact that times of contact and coefficients of restitution may be determined from the propagation velocities of half the maximum stress given by the finite amplitude wave theory for the impact velocity in question.

Following the constant velocity impact, upon being reflected from the free end of the specimen, the initial elastic front is progressively absorbed, as are the plastic strain levels above the elastic limit. This progressive absorption and re-reflection builds up the particle velocity in the vicinity of the free end of the specimen until unloading levels are reached which are sufficiently high to begin the unloading of the maximum stress. By this time the maximum plastic strain has penetrated to a distance somewhat less than half the specimen length. For an impact velocity of 66·5 ft/sec, the maximum plastic strain penetrates to a distance of between $0{\cdot}4\,L$ and $0{\cdot}45\,L$ at a time which is approximately the equivalent of that required for an elastic wave to travel a distance of $4\,L$.

In the region between the impact face and the distance of largest penetration of maximum strain, strain–time and displacement–time are those which would be obtained if the finite rod were considered semi-infinite. The dynamic stress levels found in the first diameter decrease until they reach the levels of maximum theoretical stress. As has been shown, when the specimen is sufficiently long, these dynamic stresses drop to the theoretical value prior to unloading.

It should be mentioned that piezzo crystal measurements are superior to load bar measurements in demonstrating the existence of a flat at the theoretical maximum stress. Such flats are observed in piezzo crystal measurements for 10 in. long specimens, whereas in load bar measurements they are observed only in the 20 in. long specimens, such as that of Fig. 8.

Within the limits of the approximation described, it has not been possible to predict the strain–time behaviour shown in Figs. 1–3. Efforts are in progress at the present time to develop more exact relations along the lines of the above approximation, from which one may describe the strain–time and displacement–time behaviour in that section of the rod in which the unloading phenomenon is in process.

In this paper a linear approximation is introduced which is based upon propagation velocities determined from the secant modulus at the maximum stress and strain of the finite amplitude wave theory. From this approximation, predictions of time of contact, coefficients of restitution, largest distance of penetration of maximum strain, and some aspects of the stress behaviour at the impact face are in very close agreement with experimental results. The secant modulus at stress and strain maxima is shown for a parabolic stress–strain relation to be parallel to the tangent modulus of the stress–strain curve at half the maximum stress.

Acknowledgments

The author would like to express his appreciation to his assistant, Mr. John Suckling. This work was conducted under a Grant provided by the United States Army Research Office.

References

Bell, J. F.	1960a	*J. Appl. Phys.* **31**, 2.
	1960b	*J. Appl. Phys.* **31**, 12.
	1961a	*J. Mech. Phys. Solids* **9**, 1.
	1961b	*J. Appl. Phys.* In press.
Bishop, J. F. W. and Hill, R.	1951	*Phil. Mag.* **42**, 414, 1298.

CAMPBELL, J. D.	1953	*J. Mech. Phys. Solids* **1**, 113.
JOHNSON, J. E., WOOD, D. S. and CLARK, D. S.	1953	*J. Appl. Mech.* **20**, 4.
KARMAN, T. VON	1942	N.D.R.C. Report A 29, O.S.R.D. 365.
KOLSKY, H.	1953	*Stress Waves in Solids* (Clarendon Press, Oxford).
LEE, E. H.	1953	*Quart. Appl. Math.* **10**, 4.
RAKHMATULIN, K. A.	1945	*Prikl. Mat. Mekh.* **9**, 19.
SPERRAZZA, J.	1961	Dr. Eng. Thesis, The Johns Hopkins University.
TAYLOR, G. I.	1942	British Official Report R.C. 329.
	1958	*The Scientific Papers of Sir Geoffrey Ingram Taylor*, Vol. 1, Nos. 21, 22, 27, 41 (Cambridge University Press).
WERNER, W. M.	1960	Master's Essay, The Johns Hopkins University.
WHITE, M. P. and GRIFFIS, L.	1942	N.D.R.C. Report A72, O.S.R.D. 742.

J. Mech. Phys. Solids, 1961, Vol. 9, pp. 279 to 288. Pergamon Press Ltd., London. Printed in Great Britain

PERTURBATION METHODS IN PLASTICITY—I PLANE STRAIN OF NON-HOMOGENEOUS PLASTIC SOLIDS

By A. J. M. Spencer
Department of Theoretical Mechanics, University of Nottingham

(*Received 6th July*, 1961)

Summary

Perturbation methods can be applied to a number of problems in the plane strain of ideal plastic materials when the boundary conditions are such that exact analytical solution is not possible, and of materials which differ from the ideal plastic solid in that the governing equations contain additional terms which may be regarded as small. This paper is concerned with inhomogeneous rigid/plastic bodies whose yield stress $k(x, y)$ has the form $k^0 + \epsilon k'(x, y)$, where k^0 is constant and ϵ is small. A perturbation method of solving the equations for such a material is described; in this, approximate solutions for the inhomogeneous material are obtained as perturbations of corresponding solutions for a homogeneous material with yield stress k^0. The method is illustrated by application to the problem of punch identation, and the perturbed stress, velocity and slip-line fields are obtained for this problem.

1. Introduction

Although various approximate methods have been developed for the solution of problems in plasticity, relatively little use has been made of perturbation methods. As far as problems of plane strain are concerned, this is somewhat surprising, since these methods have been applied extensively in other branches of continuum mechanics, particularly to supersonic flow theory (see, for example, Ward 1955), in which the governing equations are hyperbolic. In view of this success in other fields, it seems possible that perturbation methods, if successfully developed, could be usefully added to the methods available for solving problems in plasticity, both for obtaining approximate solutions to problems in ideal plasticity which would otherwise require numerical solution, and as an approach to problems in the deformation of materials which differ slightly in their physical properties from the ideal plastic solid.

Among authors who have used perturbation methods in plasticity are Hodge (1953), in the treatment of elastic/plastic problems with axial symmetry, Ivlev (1957), in relation to bodies which depart slightly from axial symmetry, Kuznetsov (1958), for non-homogeneous materials, and Onat (1959), who has employed what amounts to a perturbation technique in investigating the behaviour of strain-hardening bodies beyond the yield point. Of these, all except Kuznetsov base their methods on the equations of plasticity in rectangular or polar coordinates; Kuznetsov utilizes the slip-line field to some extent, but eventually derives his solution from a stress function.

In a previous paper (Spencer 1960) an approximate method of solution of problems of dynamic plane plastic strain has been described. In this, the solution

of a dynamic problem is treated as a perturbation of a related quasi-static problem; an essential feature of the method is that the slip-line field is regarded as the basic element to be perturbed, and the method leads directly to the construction of the perturbed slip-line field. This approach can be applied to a number of other types of problem, which will be described in this and subsequent papers.

We will consider two classes of problem to which perturbation methods may be applied. The first concerns problems in which the equations are those of ideal plasticity, but the boundary conditions or geometry make an analytical solution impossible. A problem of this class, that of a body of slightly irregular shape, will be described in Part II. In the other class of problem, the equations themselves contain additional terms which do not appear in the equations of ideal plasticity, and solutions are sought on the assumption that the additional terms are small. Examples are the dynamic problems mentioned above, non-homogeneous solids, which form the subject of this paper, and ideal plastic solids and ideal soils with body forces, to be described in Part III. Some possible future applications are to workhardening solids, to visco-plastic solids and to problems of axial symmetry.

In this paper we consider the plane strain of a non-homogeneous rigid/plastic solid. While this is the same problem as that treated by KUZNETSOV (1958), the formulation is different, being based on the slip-line field rather than on the stress function used by KUZNETSOV. Among other advantages the slip-line formulation includes a method of applying continuity conditions between different parts of the plastic region which seems more satisfactory than that used by KUZNETSOV. This problem illustrates most of the features which will recur in connexion with other problems.

The general theory of non-homogeneous plane plastic strain is summarized in Section 2; in Section 3 the perturbation method of solution is described; and in Section 4 the method is applied to the problem of indentation of a semi-infinite solid by a smooth flat rigid punch, stress and velocity fields and the perturbed slip-line field being determined for this problem.

2. THEORY OF PLANE STRAIN OF INHOMOGENEOUS RIGID/PLASTIC SOLIDS

We consider isotropic rigid/plastic materials which differ from the homogeneous ideal plastic solid in that the shear yield stress k is a function $k(x, y)$ of position and, possibly, also of time. It is assumed that k, $\partial k/\partial x$, and $\partial k/\partial y$ are continuous. A review of plastic non-homogeneity has been given by OLSZAK and URBANOWSKI (1959); the theory of plane strain of a rigid/plastic inhomogeneous solid is described by KUZNETSOV (1958).

The notation used is, in the main, that of HILL (1950). If (x, y) are rectangular Cartesian coordinates, in plastic regions the stress components σ_x, σ_y, τ_{xy} satisfy the yield condition

$$(\sigma_x - \sigma_y)^2 + 4\,\tau_{xy}^2 = 4\,k^2(x, y), \tag{1}$$

and can be expressed in the form

$$\left.\begin{aligned} \sigma_x &= -p - k(x, y)\sin 2\phi, \\ \sigma_y &= -p + k(x, y)\sin 2\phi, \\ \tau_{xy} &= k(x, y)\cos 2\phi, \end{aligned}\right\} \tag{2}$$

where $\phi + \frac{1}{4}\pi$ is the angle (measured anti-clockwise) between the x-axis and the line of action of the algebraically greatest principal stress. Then, as is well known (1), (2) and the equations of equilibrium are equivalent to the equations*

$$\left.\begin{aligned} \partial p/\partial s_\alpha + 2k\partial\phi/\partial s_\alpha - \partial k/\partial s_\beta = 0, \\ \partial p/\partial s_\beta - 2k\partial\phi/\partial s_\beta - \partial k/\partial s_\alpha = 0, \end{aligned}\right\} \tag{3}$$

where $\partial/\partial s_\alpha$, $\partial/\partial s_\beta$ denote differentiation along the slip-lines

$$dy/dx = \tan\phi, \qquad dy/dx = -\cot\phi, \tag{4}$$

respectively. The families of curves defined by the first and second of (4) are termed α- and β-lines respectively. Equations (3) reduce to Hencky's equations for an ideal plastic solid when k is a constant.

The form of the velocity equations is not affected by the inhomogeneity. If v_α, v_β denote components of velocity in the directions of the α- and β-lines, then the velocity equations may be expressed in the form

$$\partial v_\alpha/\partial s_\alpha - v_\beta\,\partial\phi/\partial s_\alpha = 0, \qquad \partial v_\beta/\partial s_\beta + v_\alpha\,\partial\phi/\partial s_\beta = 0. \tag{5}$$

Equations (3) and (5), when solved subject to suitable boundary conditions, determine the stress and velocity fields in the plastic regions of a rigid/plastic solid in plane strain.

3. Perturbation Method of Solution

Kuznetsov (1958) also considered the case in which $k(x, y)$ can be expressed in the form

$$k(x, y) = k^0 + \epsilon k'(x, y), \tag{6}$$

where k^0 is constant and $\epsilon k'(x, y)$ and its first derivatives are continuous, and are such that $\epsilon k'$ is small in relation to k^0, and $\epsilon\partial k'/\partial x$ and $\epsilon\partial k'/\partial y$ are small in relation to k^0/a, where a is a typical length. In effect, by neglecting ϵ^2 and higher powers of ϵ, he derived a linear second-order partial differential equation for a stress function, from which the perturbed stress-field can be determined. We will formulate the perturbation problem in a rather different way, in that we regard the slip-line field as the basic element to be perturbed. This approach is possibly preferable in that it leads directly to the determination of the perturbed slip-line field, and the application of continuity conditions at boundaries between different parts of the field is thereby facilitated. Also, the equations for the perturbed velocity field are more easily included in this formulation.

We express k in the form (6), and seek solutions of (3) and (5) of the form

$$\left.\begin{aligned} p &= p^0 + \epsilon p' + \epsilon^2 p'' + \ldots\ldots\ldots, \\ \phi &= \phi^0 + \epsilon\phi' + \epsilon^2\phi'' + \ldots\ldots\ldots, \\ v_\alpha &= v_\alpha{}^0 + \epsilon v_\alpha{}' + \epsilon^2 v_\alpha{}'' + \ldots\ldots\ldots \\ v_\beta &= v_\beta{}^0 + \epsilon v_\beta{}' + \epsilon^2 v_\beta{}'' + \ldots\ldots\ldots \end{aligned}\right\} \tag{7}$$

*The earliest references seem to be Christopherson, Oxley and Palmer (1958) and Kuznetsov (1958), but the result was widely known some years earlier and has undoubtedly been derived independently many times.

The solution will be referred to the systems of curves

$$dy/dx = \tan \phi^0, \qquad dy/dx = -\cot \phi^0, \tag{8}$$

as coordinates, and these will be called initial α- and β-lines respectively. If $\partial/\partial s_\alpha{}^0$, $\partial/\partial s_\beta{}^0$ denote differentiation along the initial α- and β-lines respectively, then

$$\left.\begin{aligned} \partial/\partial s_\alpha &= \cos(\phi - \phi^0)\,\partial/\partial s_\alpha{}^0 + \sin(\phi - \phi^0)\,\partial/\partial s_\beta{}^0, \\ \partial/\partial s_\beta &= -\sin(\phi - \phi^0)\,\partial/\partial s_\alpha{}^0 + \cos(\phi - \phi^0)\,\partial/\partial s_\beta{}^0. \end{aligned}\right\} \tag{9}$$

A solution incorporating terms up to order ϵ^n in (7) will be called an nth order perturbation solution, and the families of curves (4), when ϕ is given by two or more terms of (7), will be called perturbed α- and β-lines.

Sets of linear equations for successive perturbation solutions are obtained by substituting (6), (7) and (9) into equations (3) and (5). The terms in the resulting equations are expressed as series of powers of ϵ and the coefficients of successive powers of ϵ in each equation are equated to zero. Equating to zero the terms independent of ϵ in each equation gives the following:

$$\partial p^0/\partial s_\alpha{}^0 + 2k^0\,\partial\phi^0/\partial s_\alpha{}^0 = 0, \qquad \partial p^0/ds_\beta{}^0 - 2k^0\,\partial\phi^0/\partial s_\beta{}^0 = 0, \tag{10}$$

$$\partial v_\alpha{}^0/\partial s_\alpha{}^0 - v_\beta{}^0\,\partial\phi^0/\partial s_\alpha{}^0 = 0, \qquad \partial v_\beta{}^0/\partial s_\beta{}^0 + v_\alpha{}^0\,\partial\phi^0/\partial s_\beta{}^0 = 0. \tag{11}$$

A solution of (10) and (11), with (8), will be called an initial solution. Note that (10) and (11) are simply the equations for the stress and velocity fields in a homogeneous solid with yield stress k^0. Thus a solution of a problem for a homogeneous material can be used as an initial solution for a related problem for an inhomogeneous material, and perturbation solutions can be developed on the basis of an initial solution derived in this way.

The equations for the first-order perturbation solution are obtained by equating to zero the terms of order ϵ in (3) and (5), after having made the substitutions (6), (7) and (9). The equations are

$$\left.\begin{aligned} &\partial(p' + 2k^0\phi')/\partial s_\alpha{}^0 + \phi'\,\partial(p^0 + 2k^0\phi^0)/\partial s_\beta{}^0 + 2k'\,\partial\phi^0/\partial s_\alpha{}^0 - \partial k'/\partial s_\beta{}^0 = 0, \\ &\partial(p' - 2k^0\phi')/\partial s_\beta{}^0 - \phi'\,\partial(p^0 - 2k^0\phi^0)/\partial s_\alpha{}^0 - 2k'\,\partial\phi^0/\partial s_\beta{}^0 - \partial k'/\partial s_\alpha{}^0 = 0, \end{aligned}\right\} \tag{12}$$

$$\left.\begin{aligned} &\partial v_\alpha{}'/\partial s_\alpha{}^0 - v_\beta{}'\,\partial\phi^0/\partial s_\alpha{}^0 - v_\beta{}^0\,\partial\phi'/\partial s_\alpha{}^0 + \phi'(\partial v_\alpha{}^0/\partial s_\beta{}^0 - v_\beta{}^0\,\partial\phi^0/\partial s_\beta{}^0) = 0, \\ &\partial v_\beta{}'/\partial s_\beta{}^0 + v_\alpha{}'\,\partial\phi^0/\partial s_\beta{}^0 + v_\alpha{}^0\,\partial\phi'/\partial s_\beta{}^0 - \phi'(\partial v_\beta{}^0/\partial s_\alpha{}^0 + v_\alpha{}^0\,\partial\phi^0/\partial s_\alpha{}^0) = 0. \end{aligned}\right\} \tag{13}$$

These equations determine the first-order perturbation terms ϕ', p', $v_\alpha{}'$ and $v_\beta{}'$. The equations for higher-order perturbation solutions are readily formulated, but will not be used in this paper.

In solving special problems, equations (12) and (13) are solved subject to boundary conditions on p', ϕ', $v_\alpha{}'$ and $v_\beta{}'$. It is of course, essential to choose the initial solution in such a way that boundary conditions for the perturbed solution can be formulated in terms of these quantities; that is, the initial solution must be chosen so that in it the boundary values of p^0, ϕ^0, $v_\alpha{}^0$ and $v_\beta{}^0$ differ by quantities at most of order ϵ from the prescribed values of p, ϕ, v_α and v_β which the perturbation solution is to satisfy.

The equilibrium conditions show that p and ϕ must be continuous, or have specifiable discontinuities, throughout any plastic region. We consider only cases

in which p and ϕ are continuous. Then, in the perturbed field, $p^0 + \epsilon p'$ and $\phi^0 + \epsilon\phi'$ must be continuous. When these conditions are applied across a slip-line separating different regions of a stress field, the slip-line must be a slip-line of the perturbed field, rather than of the initial field. Similarly, the conditions that v_α is continuous across any β-line, and v_β is continuous across any α-line, must always be applied across perturbed slip-lines.

4. Indentation of an Inhomogeneous Body by a Rigid Punch

As an illustration of the theory we consider the indentation, in plane strain, of a semi-infinite rigid/plastic solid by a smooth flat rigid punch, the yield stress being of the form (6). The solid occupies the region $y \leqslant 0$. The punch applies normal pressure $Q(x)$ but no tangential force to the surface $y = 0, |x| \leqslant a$ and moves downwards with velocity V. The surface $|x| > a$ is stress free.

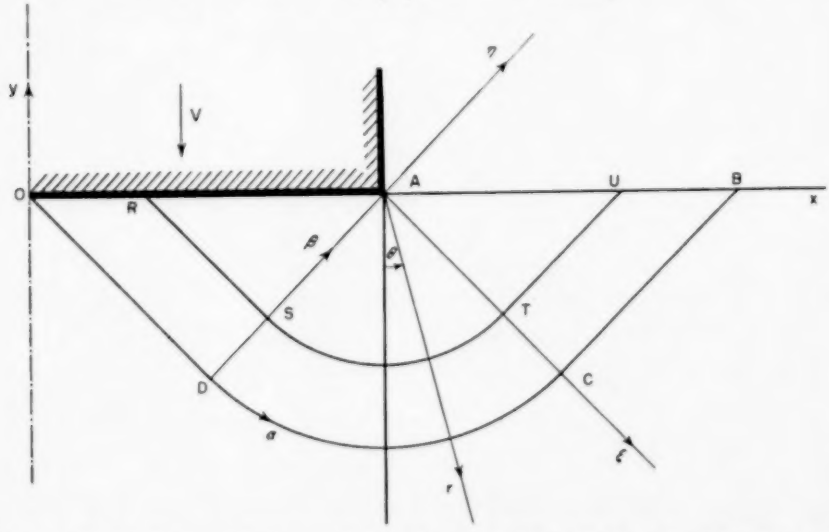

Fig. 1. Initial slip-line field for punch indentation. Only the field on the right of the axis of symmetry is shown.

For the initial field we choose that proposed by Hill (1949). This field is illustrated in Fig. 1. Since the configuration is symmetrical about $x = 0$, we consider the region $x \geqslant 0$ only. In this region, with the notation of Fig. 1, the initial solution corresponding to the assumed field is

$$p^0 = k^0(1 + \pi), \qquad \phi^0 = -\tfrac{1}{4}\pi, \qquad v_\alpha{}^0 = \sqrt{2}\,V, \qquad v_\beta{}^0 = 0, \qquad \text{in } OAD. \tag{14}$$

$$p^0 = k^0(1 + \tfrac{1}{2}\pi - 2\theta), \qquad \phi^0 = \theta, \qquad v_\alpha{}^0 = \sqrt{2}\,V, \qquad v_\beta{}^0 = 0, \qquad \text{in } ACD. \tag{15}$$

$$p^0 = k^0, \qquad \phi^0 = \tfrac{1}{4}\pi, \qquad v_\alpha{}^0 = \sqrt{2}\,V, \qquad v_\beta{}^0 = 0, \qquad \text{in } ABC. \tag{16}$$

These values satisfy (10) and (11) for the initial solution. In this initial solution the punch moves downwards with velocity V, AB is stress free, and the traction on OA is a normal pressure

$$Q^0 = k^0(2 + \pi). \tag{17}$$

In the perturbed field, let the α-line through O be a curve $OD'\,C'\,B'$, where B' lies on $y = 0$ and AD', AC' are β-lines which bound the fan of β-lines through A. The configuration is shown, for a special case to be described later, in Fig. 2.

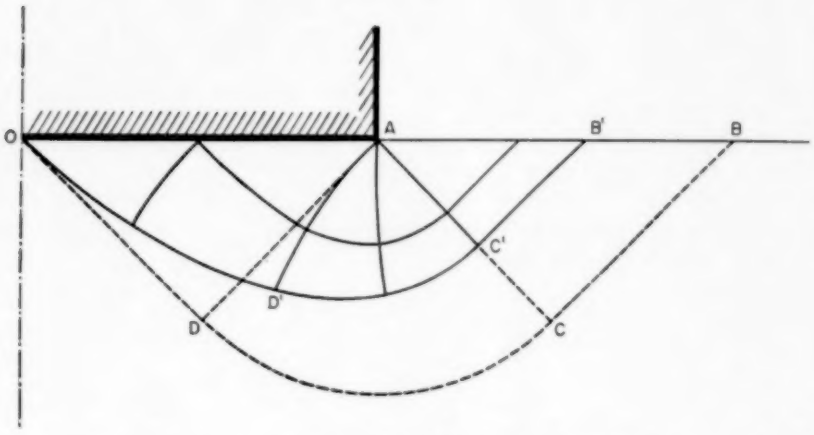

FIG. 2. Perturbed slip-line field for punch indentation when $\epsilon a = 0{\cdot}35\sqrt{2}\,k^0$. Only the field on the right of the axis of symmetry is shown. Perturbed slip-lines are denoted by continuous curves, initial slip-lines by broken curves.

The fields (14), (15), (16) are taken as initial solutions in the regions OAD', $AC'D'$, $AB'\,C'$ respectively, and the first-order perturbation solutions are to be superposed on these. The boundary conditions for the inhomogeneous solid are

$$p + k(x, 0) = Q(x), \qquad \phi = -\tfrac{1}{4}\pi, \qquad v_\alpha - v_\beta = \sqrt{2}\,V, \quad \text{on } OA. \tag{18}$$

$$p - k(x, 0) = 0, \qquad \phi = \tfrac{1}{4}\pi, \qquad \text{on } AB'. \tag{19}$$

To order ϵ, these conditions can be expressed in terms of p', ϕ', v_α' and v_β', by means of (6), (7), (14) and (16), and they then become

$$\epsilon\left[p' + k'(x, 0)\right] = Q(x) - Q^0, \qquad \phi' = 0, \qquad v_\alpha' - v_\beta^0 = 0, \qquad \text{on } OA. \tag{20}$$

$$p' - k'(x, 0) = 0, \qquad \phi' = 0, \qquad \text{on } AB'. \tag{21}$$

In addition, the condition that the region exterior to $OD'\,C'\,B'$ is rigid implies that $v_\beta = 0$ on $OD'\,C'\,B'$. Since $v_\beta^0 = 0$ everywhere, it follows that

$$v_\beta' = 0 \text{ on } OD'\,C'\,B'. \tag{22}$$

In this particular problem it is possible to determine the indentation pressure $Q(x)$ without obtaining a complete solution. We note from (14), (15) and (16) that the expression $p^0 + 2k^0\phi^0$ is constant throughout $OAB'\,C'\,D'$, and so is continuous across AD' and AC' (p^0 and ϕ^0 are not separately continuous across AD' and AC' unless these curves happen to coincide with AD and AC; this can be seen by comparing, for example, the values of p^0 and ϕ^0 on AD' as given by (14) and (15)). Since p and ϕ are everywhere continuous, it follows that $p' + 2k^0\phi'$ is continuous across AD' and AC'. To the required order in ϵ, this condition

may be applied on the initial β-lines AD and AC. The indentation pressure is obtained by integrating the first of equations (12) along a typical initial α-line, such as the α-line $RSTU$ illustrated in Fig. 1. Since p^0 and ϕ^0 are constant on every initial β-line the first of (12) becomes

$$\partial\,(p' + 2k^0\,\phi')/\partial s_\alpha{}^0 + 2k'\,\partial\phi^0/\partial s_\alpha{}^0 - \partial k'/\partial s_\beta{}^0 = 0. \tag{23}$$

Since $p' + 2k^0\,\phi'$ is continuous at S and T, equation (23), when integrated along $RSTU$, gives

$$(p'_R + 2k^0\,\phi'_R) - (p'_U + 2k^0\,\phi'_U) = \int_{RSTU} (2k'\,\partial\phi^0/\partial s_\alpha{}^0 - \partial k'/\partial s_\beta{}^0)\,ds_\alpha{}^0, \tag{24}$$

where p'_R, ϕ'_R, p'_U, ϕ'_U denote values of p', ϕ' at R, U respectively, and the integral along $RSTU$ is the sum of the integrals of $(2k'\,\partial\phi^0/\partial s_\alpha{}^0 - \partial k'/\partial s_\beta{}^0)$ along the α-line segments RS, ST and TU. With the boundary conditions (20) and (21), equation (24) becomes

$$Q\,(x_R) = Q^0 + \epsilon\,[k'\,(x_R, 0) + k'\,(x_U, 0) + \int_{RSTU} (2k'\,\partial\phi^0/\partial s_\alpha{}^0 - \partial k'/\partial s_\beta{}^0)\,ds_\alpha{}^0], \tag{25}$$

where x_R and x_U are the values of x at R and U. Thus $Q\,(x_R)$ can be evaluated if k' is specified. For example, suppose that the yield stress increases linearly with depth into the medium, so that

$$k' = -cy \tag{26}$$

where c is constant. This is the example considered by KUZNETSOV (1958). Then

$$\partial k'/\partial s_\beta{}^0 = \begin{cases} -c/\sqrt{2}, & \text{on } RS \\ -c\cos\theta, & \text{on } ST \\ -c/\sqrt{2}, & \text{on } TU \end{cases} \tag{27}$$

where (r, θ) are the polar coordinates illustrated in Fig. 1. When these values, with the values (14), (15) and (16) of ϕ^0, are inserted in (25), and the integrals evaluated, we obtain

$$Q\,(x_R) = Q^0 + 4\,\epsilon c\,(a - x_R), \tag{28}$$

which agrees with the numerical results given by KUZNETSOV for a particular value of ϵc.

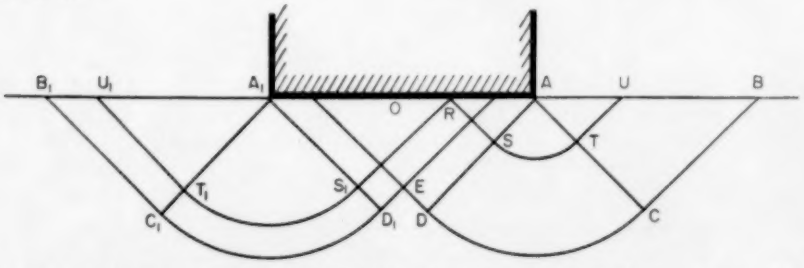

FIG. 2. Alternative initial slip-line field which is inadmissible if the entire region $OABCDED_1C_1B_1A_1$ is plastic.

It is interesting to note that for this problem an initial field of the type illustrated in Fig. 3, with the whole of the region $OABCDED_1C_1B_1A_1$ plastic, is not possible,

for in such a case integrations along say $RSTU$ and $RS_1T_1U_1$ lead to different values of p' at R. Also, any asymmetrical field, such as that illustrated in Fig. 4, leads to a greater mean indentation pressure than the symmetrical field of Fig. 1.

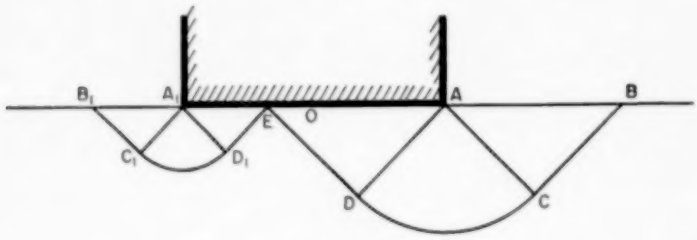

FIG. 4. Asymmetrical initial slip-line field.

In order to determine the perturbed velocity field a complete solution of the perturbed stress field is necessary; there is also some interest in finding the form of the perturbed slip-line field. For this we consider the case in which k' is given by (26) and introduce, in addition to the polar coordinates (r, θ), Cartesian coordinates (ξ, η) defined by

$$\xi = (x - a - y)/\sqrt{2}, \qquad \eta = (x - a + y)/\sqrt{2}. \tag{29}$$

The axes of ξ and η are shown in Fig. 1. The derivatives with respect to the initial system of α- and β-lines can now be expressed as follows:

$$\left.\begin{aligned} &\partial/\partial s_\alpha{}^0 = \partial/\partial\xi, && \partial/\partial s_\beta{}^0 = \partial/\partial\eta, && \text{in } OAD', \\ &\partial/\partial s_\alpha{}^0 = \partial/r\partial\theta, && \partial/\partial s_\beta{}^0 = -\partial/\partial r, && \text{in } AC'D', \\ &\partial/\partial s_\alpha{}^0 = \partial/\partial\eta, && \partial/\partial s_\beta{}^0 = -\partial/\partial\xi, && \text{in } AB'C'. \end{aligned}\right\} \tag{30}$$

With (14), (15), (16), (26), (29) and (30), the equations (12) for the initial stress field in the various regions become

$$\left.\begin{aligned} &\partial(p' + 2k^0\phi')/\partial\xi + c/\sqrt{2} = 0, \\ &\partial(p' - 2k^0\phi')/\partial\eta - c/\sqrt{2} = 0, \end{aligned}\right\} \quad \text{in } OAD'. \tag{31}$$

$$\left.\begin{aligned} &\partial(p' + 2k^0\phi')/\partial\theta + 3cr\cos\theta = 0, \\ &r\,\partial(p' - 2k^0\phi')/\partial r - 4k^0\phi' - cr\sin\theta = 0, \end{aligned}\right\} \quad \text{in } AC'D'. \tag{32}$$

$$\left.\begin{aligned} &\partial(p' + 2k^0\phi')/\partial\eta + c/\sqrt{2} = 0, \\ &\partial(p' - 2k^0\phi')/\partial\xi - c/\sqrt{2} = 0, \end{aligned}\right\} \quad \text{in } AB'C'. \tag{33}$$

The solution is begun in $AB'C'$. Integrating equations (33) and applying the conditions (21) on AB', and noting that $k' = 0$ on AB when k' has the form (26), we obtain

$$p' = c(\xi - \eta)/\sqrt{2}, \qquad \phi' = 0, \tag{34}$$

in $AB'C'$. In this region the initial and the perturbed slip-line fields coincide, and in particular AC' coincides with AC.

The stress-field in $AC'D'$ is obtained by integrating (32), the arbitrary functions which occur in the integration being determined by the conditions that $p^0 + \epsilon p'$, $\phi^0 + \epsilon\phi'$ are continuous across AC'. Since AC' coincides with AC, and p^0, ϕ^0 are continuous across AC, it is sufficient to make p', ϕ' continuous across AC. The solution of (32) which satisfies these conditions is

$$p' = cr(3 - 2\sqrt{2}\sin\theta)/\sqrt{2}, \qquad 2k^0\phi' = cr(1 - \sqrt{2}\sin\theta)/\sqrt{2}. \tag{35}$$

In the region OAD' (31) give

$$p' = -\tfrac{1}{2}\{c(\xi - \eta) + F(\eta) + G(\xi)\}/\sqrt{2},$$

$$2k^0\phi' = -\tfrac{1}{2}\{c(\xi + \eta) + F(\eta) - G(\xi)\}/\sqrt{2},$$

where F and G are functions to be determined. Since, from (20), $\phi' = 0$ when $\xi = \eta$ we have

$$G(\xi) = F(\xi) + 2c\xi,$$

and thus

$$\left.\begin{aligned} p' &= -\tfrac{1}{2}\{c(3\xi - \eta) + F(\eta) + F(\xi)\}/\sqrt{2}, \\ 2k^0\phi' &= -\tfrac{1}{2}\{c(\eta - \xi) + F(\eta) - F(\xi)\}/\sqrt{2}. \end{aligned}\right\} \tag{36}$$

The function F must be chosen so that $p^0 + \epsilon p'$, $\phi^0 + \epsilon\phi'$ are continuous across AD'. The equation of AD' is, to order ϵ

$$r\,d\theta/dr = \epsilon\phi',$$

where ϕ' is given by (35), and $\theta = -\tfrac{1}{4}\pi$ when $r = 0$. Hence the equation of AD' is

$$\theta = -\tfrac{1}{4}\pi + \sqrt{2}\,\epsilon cr/(2k^0), \tag{37}$$

to order ϵ. Also on AD', to order ϵ

$$r = -\eta, \qquad r(\theta + \tfrac{1}{4}\pi) = \xi = \sqrt{2}\,\epsilon c\eta^2/(2k^0). \tag{38}$$

From (15), (35) and (37), the values of $p^0 + \epsilon p'$ and $2k^0(\phi^0 + \epsilon\phi')$ on AD' are

$$\left.\begin{aligned} p^0 + \epsilon p' &= k^0(1 + \pi) + 3\,\epsilon cr/\sqrt{2}, \\ 2k^0(\phi^0 + \epsilon\phi') &= -\tfrac{1}{2}\pi k^0 + 2\sqrt{2}\,\epsilon cr. \end{aligned}\right\} \tag{39}$$

Also, from (14) and (36), the values of $p^0 + \epsilon p'$ and $2k^0(\phi^0 + \epsilon\phi')$ on AD' are

$$\left.\begin{aligned} p^0 + \epsilon p' &= k^0(1 + \pi) - \tfrac{1}{2}\epsilon\{-c\eta + F(\eta) + F(0)\}/\sqrt{2}, \\ 2k^0(\phi^0 + \epsilon\phi') &= -\tfrac{1}{2}\pi k^0 - \tfrac{1}{2}\epsilon\{c\eta + F(\eta) - F(0)\}/\sqrt{2}. \end{aligned}\right\} \tag{40}$$

Using (38), we find that (39) and (40) give the same values of $p^0 + \epsilon p'$ and $\phi^0 + \epsilon\phi'$ on AD' if

$$F(\eta) = 7c\eta.$$

When this value is substituted in (36), we have

$$p' = -c(5\xi + 3\eta)/\sqrt{2}, \qquad 2k^0\phi' = 4c(\xi - \eta)/\sqrt{2}, \tag{41}$$

in OAD'. At a point R on OA, $\xi = \eta = -(a - x_R)/\sqrt{2}$, and the expression (28) for the surface pressure is again obtained from (20) when these values for ξ and η are inserted in (41).

The equations for the perturbed velocity field are the equations (13). With the initial solution (14), (15), (16), and the values of ϕ' given by (34), (35), (41), these equations become

$$\partial v_\alpha'/\partial\xi = 0, \qquad \partial v_\beta'/\partial\eta - 2\,Vc/k^0 = 0, \tag{42}$$

in OAD';

$$\partial v_\alpha'/\partial\theta - v_\beta' = 0, \qquad \partial v_\beta'/\partial r + Vc(1 - \sqrt{2}\sin\theta)/k^0 = 0, \tag{43}$$

in $AC'D'$; and

$$\partial v_\alpha'/\partial\eta = 0, \qquad \partial v_\beta'/\partial\xi = 0, \tag{44}$$

in $AB'C'$. These have to be solved subject to the boundary conditions (20) and (22), and the condition that $v_\alpha^0 + \epsilon v_\alpha'$ is continuous across AC' and AD'. Since v_α^0 is constant, the latter condition is satisfied to the required order in ϵ if v_α' is made continuous across AC and AD. The solutions of (42), (43) and (44) which satisfy these conditions are

$$\left.\begin{aligned} v_\alpha' &= 2\,Vc(a/\sqrt{2} + \eta)/k^0, \\ v_\beta' &= 2\,Vc(a/\sqrt{2} + \eta)/k^0, \end{aligned}\right\} \quad \text{in } OAD', \tag{45}$$

$$\left.\begin{aligned} v_\alpha' &= Vc(a/\sqrt{2} - r)(\theta + \tfrac{1}{4}\pi + 1 + \sqrt{2}\cos\theta)/k^0, \\ v_\beta' &= Vc(a/\sqrt{2} - r)(1 - \sqrt{2}\sin\theta)/k^0, \end{aligned}\right\} \quad \text{in } AC'D', \tag{46}$$

$$\left.\begin{aligned} v_\alpha' &= Vc\,(2 + \tfrac{1}{2}\pi)\,(a/\sqrt{2} - \xi)/k^0, \\ v_\beta' &= 0, \end{aligned}\right\} \quad \text{in } AB'C'. \tag{47}$$

The equations of the perturbed slip-lines are readily found to order ϵ from the expressions (34), (35) and (41) for ϕ'. They are:

$$\left.\begin{aligned} &\alpha\text{-lines}: \quad \eta = \eta_0 + \epsilon c\,(\xi^2 - 2\xi\eta_0)/(\sqrt{2}\,k^0), \\ &\beta\text{-lines}: \quad \xi = \xi_0 + \epsilon c\,(\eta^2 - 2\xi_0\,\eta)/(\sqrt{2}\,k^0), \end{aligned}\right\} \quad \text{in } OAD',$$

$$\left.\begin{aligned} &\alpha\text{-lines}: \quad r = r_0 - \epsilon c r_0^2\,(\theta + \sqrt{2}\cos\theta - \sqrt{2})/(2\sqrt{2}\,k^0), \\ &\beta\text{-lines}: \quad \theta = \theta_0 + \epsilon c r\,(1 - \sqrt{2}\sin\theta)/(2\sqrt{2}\,k^0), \end{aligned}\right\} \quad \text{in } AC'D',$$

where $\xi_0, \eta_0, r_0, \theta_0$ are parameters which characterize the various families of slip-lines. As we have seen, in $AB'C'$ the perturbed slip-lines coincide with the initial slip-lines. The perturbed slip-line field is shown in Fig. 2 for the case $\epsilon c = 0{\cdot}35\sqrt{2}\,k^0/a$. This is the case which was considered by KUZNETSOV (1958). Comparison of Fig. 2 with Fig. 4 of KUZNETSOV's paper shows that there is a discrepancy, in that KUZNETSOV's solution contains discontinuities in p', ϕ' and v_α' across the initial β-line AD. These appear to arise because continuity conditions have been applied across the initial β-line AD, instead of across the perturbed β-line AD', as is required for a correct solution. This error does not affect the calculated value of the surface identation pressure, but it apparently leads to incorrect values of the surface velocity on AB, the correct values being given by (47).

The solution obtained in this Section is still incomplete in the sense that it has not been proved that it is possible for the rigid region to support the tractions across $OD'C'B'$. This problem may be investigated by seeking to extend the stress field in $OD'C'B'$ into the rigid region in such a way that the equilibrium equations are satisfied and the yield condition is not violated. BISHOP (1953) has shown how the extension can be made for indentation of a homogeneous body ; from the manner in which his solution was derived it seems probable that the field can be extended in a similar way for the inhomogeneous body provided that the variation from the homogeneous body is not too great. Intuitively, it seems likely that when the yield stress increases with depth into the medium, as in the present example, then the rigid region of the inhomogeneous body will support the tractions on it at least as well as the corresponding rigid region of the homogeneous body ; this however, is not certain, because although in such a case the inhomogeneous body has the greater resistance to deformation, it also has to support the greater load, because of the higher value of the indentation pressure.

REFERENCES

BISHOP, J. F. W.	1953	*J. Mech. Phys. Solids* **2**, 43.
CHRISTOPHERSON, D. E., OXLEY, P. L. B. and PALMER, W. B.	1958	*Engineering* **186**, 113.
HILL, R.	1949	*Quart. J. Mech.* **2**, 40.
	1950	*The Mathematical Theory of Plasticity* (Clarendon Press, Oxford).
HODGE, P. G.	1953	*J. Appl. Mech.* **20**, 183.
IVLEV, D. D.	1957	*Vestn. Moscov Univ.* (*Ser. Mat. Mekh. Astr. Fiz. Khim.*) **12**, 17.
KUZNETSOV, A. I.	1958	*Arch. Mech. Stos.* **10**, 447.
OLSZAK, W. and URBANOWSKI, W.	1959	*Non-homogeneity in Elasticity and Plasticity* (Ed. by W. OLSZAK), p. 259 (Pergamon Press, London).
ONAT, E. T.	1959	*Non-homogeneity in Elasticity and Plasticity* (Ed. by W. OLSZAK), p. 171 (Pergamon Press, London).
SPENCER, A. J. M.	1960	*J. Mech. Phys. Solids* **8**, 262.
WARD, G. N.	1955	*Linearised Theory of Steady High-speed Flow* (Cambridge University Press).

BOOK REVIEWS

Plasticity: E. H. Lee and P. S. Symonds (Editors). Proceedings of the Second Symposium on Naval Structural Mechanics, Brown University, 1960. Pergamon Press, Oxford, 1961. 672 pp., 70s.

The first symposium, reviewed in this Journal (vol. 9, p. 140), ranged over the whole field of continuum mechanics. In this second symposium the emphasis is on plastic deformation, mainly from the macroscopic viewpoint. There is good coverage of most topics of current interest, and a high standard is reached by nearly all the thirty contributors. Only two of these are commented on here, as being of general fundamental significance as well as controversial.

V. S. Lensky gives a valuable and detailed account of recent experimental work in Russia, bearing on some novel ideas of A. A. Ilyushin in regard to constitutive laws for elastic/plastic behaviour of metals at small strains. One such idea is that the Lévy-Mises flow rule sometimes operates *exactly* after a certain definite amount of strain, in circumstances where the Prandtl–Reuss theory would predict an asymptotic approach to the rule (though often in exponential fashion). There is nothing intrinsically impossible in such a finite delay period (as it is called) but there is, on the other hand, a strong probability that the observations simply reflect the degree of sensivity of the apparatus. Unfortunately, no judgment can be formed from Lensky's report.

A. Phillips describes his experimental work on combined tension and torsion of aluminium tubes, which he believes demonstrates the existence of pointed (or sharply rounded) vertices on the yield surface. To my mind, all that the results tend to show is a dependence of the direction (α) of the strain-rate vector on the direction (β) of the stress-rate vector, and this may perfectly well occur along with a smooth point of the surface. (The author's computation of the supposed vertex angle in a subsequent report rests on a number of unproved theoretical assumptions). Even the dependence itself is not too convincingly established: admittedly the angle α jumps often when β does (though not always), but it jumps almost as often when β does not. It is to be hoped that the author will succeed in improving the technique of these interesting and important experiments. In particular, other materials should be studied, since aluminium is a notoriously difficult subject because of creep.

Finally, a general observation on the theoretical basis of plasticity seems relevant. It is invariably assumed, when interpreting data on polycrystals in circumstances where the elastic and plastic components of strain-rate are comparable, that the whole of the plastic component will be governed by a constitutive law structurally similar to that experimentally observed when the elastic component is negligible: for example, there exists a plastic potential, this is identical with the yield function and is convex, etc. It seems to me that the constitutive law is likely to comprise two parts, of which the primary one will indeed embody such concepts; but the secondary one may not and will be comparatively sensitive to such things as mild annealing and structural details at a microscopic level, and will disappear quite soon under monotonic straining. It would follow from such a standpoint, for example, that an observed yield surface showing a generalized Bauschinger effect would not necessarily be the plastic potential for the primary part of the plastic strain-rate; rather that such a role would be played by a 'hidden' or 'latent' surface, which would become actual only under suitable paths of deformation. In other words, I suggest that (in the circumstances mentioned) observed deviations from the classical ideal should be thought of as *superimposed* effects subject to laws probably quite different in structure, 8$.

R. Hill

R. R. Long: **Mechanics of Solids and Fluids.** Prentice–Hall, Englewood Cliffs, New Jersey, 1961. x + 156 pp, 8$.

This book is designed to meet a need of which the author became aware when looking for a text to use with his one-term course given to final year American engineering science undergraduates. Its aim is to present a short, unified treatment of continuous media in which tensors play a vital,

but not 'too sophisticated,' role. Accordingly, the first Chapter contains a clear account of the main properties of Cartesian tensors; these are then used with balanced emphasis in the remaining 110 pages.

The book is of some interest because of its attempt to present an unusually wide scope in so short a space; this is a welcome viewpoint at this level. The Cartesian tensor specifications of infinitesimal strain and of rate of strain are developed side by side. Although repetitive mathematically, such a treatment, when (as here) followed up by applications to real solids and fluids, can assist the student in a first course to an intuitive grasp of the differences and similarities between various materials.

A brief account is given of the microstructure and mechanical behaviour of some real materials. This helps to set in perspective the second half of the book, in which the mathematical theories of linear elasticity and fluid mechanics are carefully developed, again side by side, to the point where some very simple problems can be solved. For a proper appreciation of the more typical problems in these fields the student will need to move on to the separate standard texts. This is not to imply that the present book is not successful as far as it goes, but it is perhaps the price that has to be paid for the adoption of a unified viewpoint in a one term course. As a case in point, problems requiring Green's integral transformation are inaccessible; but from the generalized Hooke's Law a deduction of the stress–strain law for a homogeneous, isotropic elastic solid is followed by a parallel deduction of the equations defining a Newtonian fluid. Emphasis is placed on a rigorous development of the field equations in these subjects.

M. J. SEWELL

N. G. CHETAYEV: **The Stability of Motion** (translated from the Russian by M. NADLER). Pergamon Press, Oxford, 1961. 200 pp. 60s.

THIS is an excellent and very welcome translation of the second, and slightly revised, edition of 1955 (the first edition appeared in 1946). It is almost superfluous to recommend this classic exposition of LYAPUNOV's methods, except regrettably in this country where his work (and that of pupils such as CHETAYEV himself) is even nowadays little known to engineers and still less used. It is true that there has been available for some years the really fine treatise by I. G. MALKIN: *Theory of Stability of Motion* (German edition 1959, Oldenbourg, Munich). This covers the same ground in greater detail and also recent advances. Still, CHETAYEV's account is the more readable and remains the closest in spirit to LYAPUNOV's own. In the author's own words the book describes 'those investigations of LYAPUNOV's which appear to have the most bearing on applied problems' and tries 'to present LYAPUNOV's results in a simple manner, without false modernizations.'

R. HILL

W. G. BICKLEY and A. TALBOT: **An Introduction to the Theory of Vibrating Systems.** Clarendon Press, Oxford, 1961. xiv + 238 pp., 30s.

WHEN the penalty to be paid for unduly violent vibration is exceptionally heavy, then great effort is put into the formulation of general solutions of the vibration problem concerned and something is done about the matter at the design stage. Care is taken, for instance, in the design of diesel engine installations to guard against torsional oscillations of large amplitude, while tremendous effort is devoted to the prevention of flutter in aircraft. But the fact remains that the number of problems of this sort, where there is a body of accepted standard procedures, is very limited. It is also true that vibration problems are liable to crop up in a surprisingly large number of forms. How then should one go about teaching the subject? This is, of course, a particular case of the far wider question of the form that engineering teaching in general should take.

One way of teaching engineering is to start with a relentless treatment of theory and principles. The experienced teacher can keep the interest of his class by frequent allusions to practical aspects – though it must be admitted that teachers who are capable of this are rare and incredibly difficult to lure on to a teaching staff. The less experienced teacher (in the practical engineering

sense) who adopts this approach has at least got the assurance that his material will be useful in the long run unless – as is too often the case – his students are allowed to cease to think about that material after graduation. At least, this point of view is an arguable one and the teacher who adopts it will welcome the book under review. Here is a well-written, lucid book that is concerned almost exclusively with elementary mathematical background.

In this reviewer's estimation, this book should prove most useful to the teacher who remembers that it is not even intended to tell the whole story. There is far more to engineering than elementary mathematics. The teacher – and reviewer – who does not remember this may not be very happy with the book.

The selection of theory that is dealt with by the authors is a fairly common one, though it does include Lagrange's equations, electro-mechanical analogues, elementary wave theory and theory of sound and also the elements of non-linear analysis. Two omissions, on the other hand, are matrices and a proper exploitation of impedance methods. The book is thoroughly readable and dependable and could well be 'required reading' for an honours degree candidate.

R. E. D. BISHOP

Selected Papers on Stress Analysis, Presented at The Institute of Physics Stress Analysis Group Conference, Delft, 1959. The Institute of Physics, London, 1961. 114 pp, 50*s*.

THE FIRST International Conference on Experimental Stress Analysis, initiated and organized by the Stress Analysis Group of the Institute of Physics with the help of T.N.O. of Holland, was held in Delft in April 1959. This slim volume represents its proceedings in a sadly mutilated form. The selection of eighteen papers published in full, out of fifty-one offered at the Conference, follows no recognizable guiding line in subject matter, quality or originality. Six German and two French contributions are presented in their original language, one Russian, one French, four Dutch and four English contributions are given in English. Each contribution is preceded by an author's summary in English, French and German. The papers not published in full are described in a survey so shortened as to be meaningless in places. Publication has taken just short of 2 years from the date of the Conference and in the meantime several contributions have been published elsewhere in amended form.

Of the papers given in full, seven deal with photoelasticity, three with extensometry, five with electrical ancillaries to strain measurement, one with analogue applications of the Moiré method, one with load analysis by destructive testing and one with brittle fracture. The following are perhaps of outstanding interest: a determination of stresses in complicated Francis turbine components by means of composite perspex and epoxy resin models investigated with strain gauges, extensometers and various photoelastic methods (PRIGOROWSKI); a new electric-screening displacement transducer with a small aluminium plate attached to the moving part and displaced between fixed primary and secondary electromagnets, giving full-scale deflexions between 1 and 10^4 μ with unlimited override (NOLTINGK); complete analysis of loads carried by the single welds in a fully welded joist–upright connection by simple fracture of fifty-four selected test pieces (LIGTENBERG); survey of the potentialities of magnetic tape recording (BOITEN); strain gauge calibration at temperatures up to 700 deg. C (MASLEN and CORBIN). Amongst the thirty-three unpublished papers, at least the investigation by strain gauges into the stresses in internal strands of wire ropes (DARNAULT) would have been of equal merit and interest.

Make-up and presentation are excellent. The full addresses of all the fifty-one authors are given, a feature thoroughly recommended for all proceedings of all conferences.

Details of the Second International Conference in Paris, 10–14 April 1962 are obtainable from M. ROLET, Secretary, C.P.A.C., 10 rue Vauquelin Paris 5^e, or from The Secretary, Joint British Committee for Stress Analysis, 1 Birdcage Walk, London S.W 1.

M. L. MEYER

R. F. S. HEARMON: **An Introduction to Applied Anisotropic Elasticity.** Clarendon Press, Oxford, 1961. viii + 136 pp., 35*s*.

THIS book has three aspects: it will indeed serve as a useful introduction for newcomers to linear anisotropic elasticity, it is also, in part, an extended survey article, with a valuable bibliography,

and it considers in some detail topics in which the author is particularly interested. Being addressed primarily to physicists and engineers it does not consider such questions as uniqueness and completeness, and it omits such mathematical preliminaries as are to be found in books on isotropic elasticity.

The first two chapters deal adequately with the properties of the basic equations and with the effects of all the classes of crystal symmetry: curvilinear aeolotropy is not considered. A short chapter is devoted to the measurement of the elastic constants of crystals, sheet materials and polycrystalline aggregates.

There is a brief discussion of some simple stress systems, including torsion. The chapter on more general stress fields seems to have been compressed too much to be very useful except for its references. The general plane problem receives only two pages (in which the parameters appearing in the solution are insufficiently defined) with no description of the general methods available for solving boundary-value problems. ELLIOTT's three-dimensional solution for hexagonal materials is given, but LODGE's more general solution is not mentioned (although the relevant paper is listed in the bibliography) and no consideration is given to known methods of solving some classes of problems for these materials.

Wave propagation is considered at some length, but the longest chapter is devoted to plates. The emphasis here is on approximation methods and prominence is given to discussions of stability and vibration.

The book is well furnished with tables and diagrams. It should be useful to all interested in the subject, but a fuller treatment of some topics would have increased its value.

D. S. BERRY

NOTICES

THE INTERNATIONAL CONFERENCE ON CRYSTAL LATTICE DEFECTS

An International Conference on Crystal Lattice Defects will be held in Kyoto, Japan, on 7–12 September 1962. The Conference is being organized by the Physical Society of Japan. The International Union of Pure and Applied Physics is considering sponsorship of the Conference.

The aim of the Conference is to obtain clearer understanding of lattice defects. In order to maintain a high scientific standard throughout the Conference, the attendance will be limited to active research workers in the field of lattice defects, and others who may be preparing to enter work in this field. The meeting will be arranged to reserve ample time for discussions. The language used will be English.

The Conference will cover point defects in metals, semiconductors and ionic crystals, as well as extended defects closely related to point defects. Suggested items of discussion are, for instance, electronic processes in imperfect crystals, properties of single and multiple point defects, radiation damage, association, dissociation and diffusion of point defects. Purely phenomenological studies will not be included, nor work that is ambiguous from the viewpoint of lattice defects.

Chairman of the Organizing Committee:
Dr. T. Fujiwara, Professor of Physics, Hiroshima University.

Chairman of the Executive Committee:
Dr. R. R. Hasiguti, Professor of Metal Physics, University of Tokyo.

Vice-Chairmen of the Executive Committee:
Dr. T. Suzuki, Professor of Physics, University of Tokyo.
Dr. Y. Uchida, Professor of Physics, Kyoto University.

All correspondense should be addressed to:
Lattice Defects Conference Secretariat,
c/o Prof. R. R. Hasiguti, Department of Metallurgy,
University of Tokyo, Bunkyo-ku, Tokyo, Japan.

SCHOOL OF MINES AND METALLURGY, INSTITUTE OF TECHNOLOGY, UNIVERSITY OF MINNESOTA, MINNEAPOLIS 14

Preliminary Announcement

The Fifth Rock Mechanics Symposium will be held at the University of Minnesota, 3–5 May, 1962, jointly sponsored by the mining departments of the Colorado School of Mines, the Missouri School of Mines and Metallurgy, the Pennsylvania State University, and the University of Minnesota. The Symposium will deal primarily with problems of 'dynamic' rock mechanics, although significant advances in other areas will also be included. It is tentatively proposed to hold five technical sessions in the 2½ day meeting devoted to the following topics:

1. Drilling.
2. Blasting.
3. Comminution.
4. 'Dynamic' physical properties of rocks.
5. Theories of rock failure and 'static' physical properties of rock.
6. General (important contributions, as determined from papers submitted for consideration).

Publisher's notice to subscribers and request to renew your subscription to this important journal

This is the last issue in Volume 9; the title page, contents list and author index will be published loose with the first issue in Volume 10. I hope you have already renewed your subscription. If not, please take positive steps to renew it in time to ensure the receipt of the next issue immediately on publication and thus maintain an uninterrupted set of this journal in your library.

END OF VOL.